OFFICE OF CIVILIAN RADIOACTIVE WASTE MANAGEMENT
ANALYSIS/MODEL COVER SHEET
COMPLETE ONLY APPLICABLE ITEMS

1. QA: QA AZB 1-22-02
Page: 1 of: 156 ~~158~~

2. ☒ Analysis — Check all that apply

Type of Analysis	☐ Engineering ☐ Performance Assessment ☒ Scientific
Intended Use of Analysis	☐ Input to Calculation ☒ Input to another Analysis or Model ☐ Input to Technical Document

Describe use: Documents availability and use of geochemical and isotopic data to derive bounds on geochemical characteristics of unsaturated-zone waters and gases, local infiltration rates, and flow paths and rates, including occurrence of fracture flow. Summarizes geochemical and isotopic data available for developing and testing site-scale flow and transport models of the unsaturated zone.

3. ☐ Model — Check all that apply

Type of Model	☐ Conceptual Model ☐ Abstraction Model ☐ Mathematical ☐ System Model ☐ Process Model
Intended Use of Model	☐ Input to Calculation ☐ Input to another Model or Analysis ☐ Input to Technical Document

Describe use: N/A

4. Title: Analysis of Geochemical Data for the Unsaturated Zone

5. Document Identifier (including Rev. No. and Change No., if applicable): ANL-NBS-HS-000017, Rev. 00, ICN 02

6. Total Attachments: 2

6. Attachment Numbers - No. of Pages in Each:
Attachment I (51 p.); Attachment II (77 pp.)

	Printed Name	Signature	Date
8. Originator	Arend Meijer	SIGNATURE ON FILE	12/19/01
9. Checker	Norma Biggar	SIGNATURE ON FILE	12/20/01
10. Lead/Supervisor	J. E. Houseworth	SIGNATURE ON FILE	12/20/01
11. Responsible Manager	G. S. Bodvarsson	SIGNATURE ON FILE	12/19/01

12. Remarks:

a. Rev. 00 of this report was prepared by June Fabryka-Martin (Los Alamos National Laboratory), Arend Meijer (GCX, Inc.), Brian Marshall, Leonid Neymark, Jim Paces, Joe Whelan, and Al Yang (U.S. Geological Survey). It was technically reviewed by John Apps.

b. Tables and figures are included in attachments I and II, respectively. Figures 42 and 43 have color-coded data points and should not be read in a black-and-white version. Figures 2, 3, 41 and 46 are location maps that use grey tones to distinguish physical features in the landscape such that photocopy versions may not be very legible.

c. Deficiency Report LVMO-00-D-039, Inaccurate Documentation And Validation of Software Routines And/or Macros, identified software issues that are addressed in MOL.20010910.0169 (Meijer 2001), additional software documentation. The information in the record will be integrated into the AMR as part of the next revision or ICN.

OFFICE OF CIVILIAN RADIOACTIVE WASTE MANAGEMENT
ANALYSIS/MODEL REVISION RECORD

Complete Only Applicable Items

2. Analysis or Model Title: Analysis of Geochemical Data for the Unsaturated Zone

3. Document Identifier (including Rev. No. and Change No., if applicable): ANL-NBS-HS-000017, Rev. 00, ICN 02

4. Revision/Change No.	5. Description of Revision/Change
00	Initial issue
Rev. 00, ICN 1	Modified to reflect changes in qualification status of direct input data. Minor changes have been made in Section 1. References to data sets have been revised in Sections 4 and 6, as well as Attachments 1 and 4. The DIRS has been updated to reflect those changes.
Rev. 00, ICN 2	Modified to reflect supercession and change in qualification status of DTNs GS980108312322.003 and GS960908315215.013. Superceding DTNs GS010808312322.004, GS010808312322.005, GS010608315215.002, and GS980708315215.012 were added and changes in qualification status addressed. Changes are indicated with change bars in the right margin. These changes affect Section 1, (p. 14, 15), Section 2, (p. 15), Section 4.1.12, (p. 22), Section 6.6.7 (p. 78), Section 7 (p.121), Section 8.1 (p. 128, 130, 135), Section 8.2 (p. 145), Section 8.4 (p. 145, 149, 151, 152), Table 2 (p. I-8), Table 9 (p. I-23), Table 21 (p. I-42), Table 23 (p. I-44), Figure 41 (p. II-43), Figure 42 (p.II-44), and Figure 43 (p. II-45).

CONTENTS

Page

TABLES

Page

FIGURES

Page

ABBREVIATIONS AND ACRONYMS

AMR	Analysis Modeling Report
ATDT	Automated Technical Data Tracking System
CMB	Chloride Mass Balance
DIRS	Document Input Reference System
DOE	Department of Energy
DRI	Desert Research Institute
DTN	Data Tracking Number
ESF	Exploratory Studies Facility
ICN	Interim Change Number
ka	thousand years
Ma	million years
NADP/NTN	National Atmospheric Deposition Program/National Trends Network
OCWRM	Office of Civilian Radioactive Waste Management
ORP	Oxidation/Reduction Potential
pmc	percent modern carbon
ppmv	parts per million on volume basis
QARD	Quality Assurance Requirements and Description
SEP	Site and Engineering Properties
TAMS	tandem accelerator mass spectrometry
TBV	to be verified
TDMS	Technical Data Management System
TU	Tritium Units
UNLV	University of Nevada – Las Vegas
USGS	U.S. Geological Survey
VPDB	Vienna Pee Dee Belemnite
VSMOW	Vienna Standard Mean Ocean Water
YMP	Yucca Mountain Site Characterization Project

1. PURPOSE

Geochemical data and models that are important for site characterization purposes and for evaluations of site performance are discussed in this report. Geochemical and isotopic data for present-day fluids and for fracture minerals which reflect past water chemistries at the site are reviewed and evaluated with respect to the development and testing of models to explain variations in water chemistry and their implications for the development and testing of site-scale hydrologic flow models for the unsaturated zone. Such models are required to derive bounds on future variations in the chemical compositions of waters in the Yucca Mountain flow system. These bounds are required to model the transport behavior of radionuclides in the flow system.

More specifically, this report:

- Identifies fluid geochemical parameters that are relevant to site characterization and repository evaluations (Section 6.1).
- Reviews the methods that were used in investigating fluid geochemistry (Section 6.2).
- Discusses available data on the geochemical and isotopic compositions of local precipitation (Section 6.3) and surface water (Section 6.4). The compositions of these waters define the starting point for the geochemical evolution of water in the unsaturated zone.
- Discusses available data on the geochemical and isotopic compositions of unsaturated-zone pore waters and perched water (Sections 6.5 and 6.6), unsaturated-zone gases (Section 6.7), secondary fracture minerals (Section 6.10), and fluid inclusions (Section 6.11).
- Discusses relevant geochemical data for saturated-zone groundwaters (Section 6.8) because the similarity between geochemical compositions of local perched water and waters from the saturated zone suggests common controls.
- Provides overviews of processes that control fluid compositions and the limitations of the existing data for each category (throughout Section 6).
- Summarizes a conceptual model for the evolution of fluid geochemistry in Yucca Mountain (Section 7.1).
- Discusses how these data bear on site characterization and repository performance issues (Section 7).

Constraints, caveats, and limitations associated with the analyses and models in this report are identified within the sections that discuss the analyses and models themselves.

Planning efforts for this report were outlined in the Analysis and Modeling Report (AMR) Development Plan TDP-NBS-HS-000040, "*U0085 Analysis of Geochemistry Data, Rev 00*"

(CRWMS M&O 1999a). The Interim Change Notice (ICN), ICN 01, of this AMR was prepared as part of activities being conducted under Technical Work Plan, TWP-NBS-HS-000001, "*Technical Work Plan for Unsaturated Zone (UZ) Flow and Transport Process Model Report*" (CRWMS M&O 2000a). The planning document for the technical scope, content, and management of Interim Change Notice (ICN) 02 to this AMR is Technical Work Plan (TWP), *Technical Work Plan for Unsaturated Zone (UZ) Flow and Transport Process Model Report* (BSC 2001a). The scope for the data qualification issues addressed in ICN 02 are described in *Technical Work Plan for: Integrated Management of Technical Product Input Department* (BSC 2001b, Addendum B, Section 4.1).

2. QUALITY ASSURANCE

The activities documented in Rev. 00 of this AMR were evaluated in accordance with QAP-2-0, *Conduct of Activities*, and were determined to be subject to the requirements of the U.S. Department of Energy (DOE) Office of Civilian Radioactive Waste Management (OCRWM) *Quality Assurance Requirements and Description* (QARD) (DOE 2000). This evaluation is documented in CRWMS M&O (1999b), and Wemheuer (1999, activity evaluation for work package WP 140123UM1). The Activity Evaluation for ICN 02 is contained in (BSC 2001a). This AMR has been prepared in accordance with the current version of procedures identified in the technical work plan.

3. COMPUTER SOFTWARE AND MODEL USAGE

Standard spreadsheet and visual display graphics programs were used to prepare this report, as listed below, but they are not subject to software quality assurance requirements.

Microsoft Excel 97 (Version SR-1, for Windows 95 and Windows NT 4.0) is a standard spreadsheet program that was used to organize and sort data, calculate averages and standard deviations, and to perform linear regressions on specific geochemical data sets using standard built-in Excel functions available with the software on a PC. In addition, the following visual display graphical programs were used to plot and illustrate the results of data analyses shown in this report. These programs were not used to develop data used in quality affecting work.

- Plotchem–Win, Version 7.9, for Windows 95, is a graphical program used to prepare trilinear (Piper) diagrams of dissolved ion concentrations of water samples
- Adobe Illustrator, Version 7.0, for Windows 95 and Windows NT 4.0
- Corel Draw 9, Version 9.337, for Windows 95 and Windows NT

All plots and figures were compared against the original data or other sources for correctness.

4. INPUTS

4.1 DATA AND PARAMETERS

This document is a compilation and synthesis of data and other information collected under various activities and reported in publications, YMP reports, the YMP Technical Data Management System (TDMS), and other databases. The qualification status of input data used in this report is tracked in the electronic YMP Document Input Reference System (DIRS) database.

The primary input data used in this report are geochemical and isotopic analyses of pore waters, perched water, gases and fracture minerals collected from the unsaturated zone at Yucca Mountain; and analytical data for surface waters and groundwaters in the area. Section 6.2 lists the major chemical and isotopic parameters used as input to the analyses in this report and provides an overview discussion of their appropriateness and relevance for these analyses. The data listed below are considered qualified for use on the YMP and are appropriate to be used as input for this report because they directly bear on values of these parameters applicable to the Yucca Mountain site.

Data used in this report that were acquired or developed as part of the Yucca Mountain Program are contained in data packages with unique Data Tracking Numbers (DTNs) that permit the data to be tracked in the YMP Automated Technical Data Tracking (ATDT) Database. Data sources are listed in the reference section (Section 8.3).

4.1.1 Precipitation Geochemical Data Inputs

Chloride concentrations in local and regional precipitation, along with associated precipitation quantities, are considered to be primary input data, and provide the basis for estimating infiltration rates by the chloride mass balance method (sections 6.3.2, 6.3.3, and 6.9.2).

LA0003JF12213U.001	Precipitation-weighted average monthly concentrations (mg/l) of precipitation in Red Rock Canyon, Nevada, 1985 to 1998
MO0005CL3SPRGS.000	3 Springs Basin, Precipitation water quality October 1984 to September 1991
MO0005CLESTWRT.000	East Stewart Basin precipitation water quality, dissolved chloride, October 1984 to September 1991
MO0005CLKAWICH.000	Kawich Peak precipitation water quality, dissolved chloride, October 1988 to September 1991
GS930108315214.004	Chemical analysis of surface water, spring, and precipitation samples collected from Kawich and Stewart Creek Basins from May, 1989, to September, 1991
GS930908315214.030	Chemical analysis of surface water, spring, and precipitation samples collected from Kawich and Stewart Creek Basins from February, 1992, to September, 1992.

LAJF831222AQ95.003 Halide analyses of rainwater from Yucca Mountain

All other precipitation chemistry data are used in a corroborative manner, to characterize local and regional precipitation chemistry in terms of average concentrations and relative ion ratios. These precipitation trend data provide a baseline against which to compare and contrast chemical compositions of the various sources of water at Yucca Mountain, and to illustrate general trends of relative enrichment or depletion of one element compared to another (sections 6.3.2 and 6.3.3).

4.1.2 Surface-water Geochemical Data Inputs

None of the surface-water geochemical and isotopic data used in this report are considered to be primary input data. Surface-water data presented in this report are used solely to characterize local and regional surface water chemistry in terms of concentration averages and ranges, relative ion ratios, and isotopic characteristics. These calculations provide a means to compare chemical compositions of surface water and runoff at Yucca Mountain to those of unsaturated-zone pore waters and perched water, so as to illustrate general trends of relative enrichment or depletion of one element compared to another (section 6.4.3).

4.1.3 Pore-water Geochemical Data Inputs

The following primary input data are used in Section 6.5.3 to characterize pore-water chemistry:

GS950608312272.001	Chemical Data For Pore Water From Tuff Cores Of USW NRG-6, NRG7/7a, UZ-14 and UZ-N55, and UE-25 UZ#16
GS961108312261.006	Gas Chemistry, ESF Alcoves 2 And 3, 11/95 - 4/96; Water Chemistry, Alcove 2 (Tritium), Alcove 3, And ESF Tunnel; And Pneumatic Pressure Response From Boreholes In Exploratory Studies Facility Alcoves 2 and 3, 10/95 - 5/96
GS961108312271.002	Chemical And Isotopic Composition Of Pore Water And Pore Gas, 1994-96, From Boreholes USW UZ-1, USW UZ-14, UE-25 UZ#16, USW NRG-6, USW NRG-7a, USW SD-7 USW SD-9, ESF-AL#3-RBT#1, And ESF-AL#3-RBT#4, And ESF Rubble
GS000608312271.001	Pore-Water Hydrochemistry and Isotopic Data for Boreholes USW NRG-6, USW NRG-7a, USW SD-7, USW SD-9, USW SD-12, USW UZ-14 and UE-25 UZ#16 from 10/1/96 to 1/31/97
GS970908312271.003	Unsaturated Zone Hydrochemistry Data, 2-1-97 to 8-31-97, Including Chemical Composition and Carbon, Oxygen, And Hydrogen Isotopic Composition: porewater from USW NRG-7A, SD-7, SD-9, SD-12 and UZ-14; and gas from USW UZ-14
GS981008312272.004	Analysis for Chemical Composition of Porewater from Boreholes USW UZ-7A, WT-24, SD-6, SD-7, and SD-12 during FY 1997 and 1998.

GS990208312272.001	Analysis for chemical composition of pore water from borehole USW UZ-14 and groundwater from USW UZ-16
LA9909JF831222.004	Chloride, bromide, and sulfate analyses of Busted Butte and Cross Drift tunnel porewaters in FY99
LA9909JF831222.010	Chloride, bromide, sulfate and chlorine-36 analyses of ESF porewaters
LA9909JF831222.012	Chloride, bromide, and sulfate analyses of porewater extracted from ESF Niche 3566 (Niche #1) and ESF 3650 (Niche #2) drillcore

4.1.4 Perched-water Geochemical Data Inputs

The following primary input data are used in Section 6.5.3 to characterize perched-water chemistry:

MO0012WTRIONCO.000	Water chemistry data
LAJF831222AQ98.011	Chloride, bromide, sulfate and chlorine-36 analyses of springs, groundwater, porewater, perched water and surface runoff

4.1.5 Tritium Data Inputs

The following primary input data are used in Section 6.6.2 to characterize the distribution of tritium in surface water, porewater, perched water and groundwater:

GS940308312133.002	Water quality data for samples taken in Fortymile Wash, Nevada, during the 1993 water year
GS960308312133.001	Water quality data from samples collected in the Fortymile Wash Watershed, Yucca Mountain area, Nevada, Water year 1995
GS961108312261.006	Gas Chemistry, ESF Alcoves 2 And 3, 11/95 - 4/96; Water Chemistry, Alcove 2 (Tritium), Alcove 3, And ESF Tunnel; And Pneumatic Pressure Response From Boreholes In Exploratory Studies Facility Alcoves 2 And 3, 10/95 - 5/96
GS961108312271.002	Chemical And Isotopic Composition Of Pore Water And Pore Gas, 1994-96, From Boreholes USW UZ-1, USW UZ-14, UE-25 UZ#16, USW NRG-6, USW NRG-7a, USW SD-7 USW SD-9, ESF-AL#3-RBT#1, And ESF-AL#3-RBT#4, And ESF Rubble
GS970108312232.001	Sulfur hexafluoride gas chemistry data and shut-in pressure monitoring data from the radial boreholes in Alcove 1 of the ESF, 4/95; and tritium data from borehole ESF-AL#2-HPF#1 in alcove 2
GS000608312271.001	Pore-Water Hydrochemistry and Isotopic Data for Boreholes USW NRG-6, USW NRG-7a, USW SD-7, USW SD-9, USW SD-12, USW UZ-14 and UE-25 UZ#16 from 10/1/96 to 1/31/97

GS970283122410.002	Gas and water chemistry data from samples collected at boreholes UE-25 NRG#5 and USW SD-7 on Yucca Mountain, Alcove 5, and borehole ESF-NAD-GTB#1a in Alcove 6, ESF, between 8-11-96 and 1-14-97
GS970608312272.005	Tritium Data From ESF Alcove #5 Cores For Single Heater Test
GS970908312271.003	Unsaturated Zone Hydrochemistry Data, 2-1-97 to 8-31-97, Including Chemical Composition and Carbon, Oxygen, And Hydrogen Isotopic Composition: porewater from USW NRG-7A, SD-7, SD-9, SD-12 and UZ-14; and gas from USW UZ-14
MO0012MAJIONIS.000	Water – Major ion and isotope data Field, Chemical, And Isotopic Data From A Precipitation Sample Collected Behind The Service Station In Area 25 And Ground Water Samples Collected At Boreholes UE-25 C #2, UE-25 C #3, USW UZ-14, UE-25 WT #3, UE-25 WT #17 And USW WT-24, Between 10/06/97 And 07/01/98
GS991108312272.004	Tritium analyses for porewater samples from UZ-14, WT-24, SD-12, SD-6, SD-7, SD-9, UZ-7A and NRG-7A

4.1.6 Chlorine-36 Data Inputs

The following primary input data are used in Section 6.6.3 to characterize the distribution of chlorine-36 in precipitation (using fossil packrat urine samples), surface water, soil, porewater, borehole cuttings and drillcore, perched water and groundwater:

LA9909JF831222.001	Chloride, bromide, sulfate and chlorine-36 analyses of groundwater and runoff in FY99
LA9909JF831222.005	Chlorine-36 analyses of ESF and Busted Butte porewaters in FY99
LA9909JF831222.010	Chloride, bromide, sulfate and chlorine-36 analyses of ESF porewaters
LAJF831222AQ95.005	Halide and chlorine-36 analyses of soils from the UE25 NRG#5 drillpad.
LAJF831222AQ95.006	Halide and chlorine-36 analyses of soils from Midway Valley pits and trenches.
LAJF831222AQ96.005	Halide and 36Cl analyses of cuttings from boreholes NRG-4, NRG-6, and NRG 7/7A
LAJF831222AQ96.006	Halide and 36Cl analyses of soil from Midway Valley Pit MWV-P2
LAJF831222AQ96.008	Halide and 36Cl analyses of cuttings from boreholes UZ-N15, UZ-N16, UZ-N17, UZ-N36, UZ-N38, UZ-N39, UZ-N61, UZ-N62, and UZ-N64
LAJF831222AQ96.009	Halide and 36Cl analyses of cuttings from borehole UZ-N11

LAJF831222AQ96.010	Halide and 36Cl analyses of cuttings from borehole UZ-N37
LAJF831222AQ96.011	Halide and 36Cl analyses of cuttings from borehole UZ-N53
LAJF831222AQ96.012	Halide and 36Cl analyses of cuttings from borehole UZ-N54
LAJF831222AQ96.013	Halide and 36Cl analyses of cuttings from borehole UZ-N55
LAJF831222AQ96.014	Halide and 36Cl analyses of cuttings from borehole UZ#16
LAJF831222AQ96.015	Halide and 36Cl analyses of cuttings from borehole UZ-14
LAJF831222AQ97.002	Chlorine-36 analyses of packrat urine
LAJF831222AQ97.006	Halide, sulfate and chlorine-36 analyses of soils from Midway Valley soil pits MWV-P31 and NRSF-TP-19
LAJF831222AQ97.007	Halide, sulfate and chlorine-36 analyses of cuttings from borehole SD-12
LAJF831222AQ98.004	Chloride, bromide, sulfate and chlorine-36 analyses of salts leached from ESF rock samples
LAJF831222AQ98.009	Chlorine-36 analyses of salts leached from ESF Niche 3566 (Niche #1) drillcore
LAJF831222AQ98.011	Chloride, bromide, sulfate and chlorine-36 analyses of springs, groundwater, porewater, perched water and surface runoff
LA9909JF831222.010	Chloride, bromide, sulfate and chlorine-36 analyses of ESF porewaters
LA9912JF831222.001	Halide and chlorine-36 analyses of drillcore from USW UZ-N55

4.1.7 Carbon-14 and Carbon-13 Data Inputs for Unsaturated-zone Water

The following primary input data are used in Section 6.6.4 to characterize the distribution of carbon isotopes in pore water and perched water:

GS961108312261.006	Gas Chemistry, ESF Alcoves 2 And 3, 11/95 - 4/96; Water Chemistry, Alcove 2 (Tritium), Alcove 3, And ESF Tunnel; And Pneumatic Pressure Response From Boreholes In Exploratory Studies Facility Alcoves 2 And 3, 10/95 - 5/96
GS961108312271.002	Chemical And Isotopic Composition Of Pore Water And Pore Gas, 1994-96, From Boreholes USW UZ-1, USW UZ-14, UE-25 UZ#16, USW NRG-6, USW NRG-7a, USW SD-7 USW SD-9, ESF-AL#3-RBT#1, And ESF-AL#3-RBT#4, And ESF Rubble
MO0012CARB1314.001	Water – Carbon 13 and Carbon 14 Isotope Abundance
MO0012CARBON13.000	Water - Carbon 13 Isotope Ratio

4.1.8 Carbon-14 and Carbon-13 Data Inputs for Gases from Open Boreholes

None of the data collected for samples from open boreholes are considered primary input data for characterization of the chemical composition of gas at Yucca Mountain. These data are discussed in Sections 6.6.4 and 6.7.2 but are only used to corroborate interpretations based on isotopic data for instrumented borehole samples (section 4.1.9).

4.1.9 Carbon-14 and Carbon-13 Data Inputs for Gases from Instrumented Boreholes

The following primary input data are used in Sections 6.6.4 and/or 6.7.2 to characterize the distribution of carbon isotopes in borehole gas from instrumented boreholes:

GS961108312271.002	Chemical And Isotopic Composition Of Pore Water And Pore Gas, 1994-96, From Boreholes USW UZ-1, USW UZ-14, UE-25 UZ#16, USW NRG-6, USW NRG-7a, USW SD-7, USW SD-9, ESF-AL#3-RBT#1, And ESF-AL#3-RBT#4, And ESF Rubble
MO0012CARBON14.000	Carbon 14 Isotope Ratio
GS940408312271.005	Laboratory results of carbon 14 analysis of gas samples from borehole USW UZ-1 collected 12/3/93 - 12/7/93
MO0012CARB1314.000	Water - Carbon 13 and Carbon 14 Abundance

4.1.10 Stable Hydrogen and Oxygen Isotopic Data Inputs

None of the stable hydrogen and oxygen isotopic data used in this report are considered to be primary input data. These data are used solely to corroborate interpretations of water flow paths and the timing of recharge that are based on other geochemical and isotopic signatures.

4.1.11 Strontium Isotopic Data Inputs for Waters, Rocks, and Minerals

The following primary input data are used in Sections 6.6.6 and 6.10 to characterize the distribution of strontium isotopes in soils, borehole cuttings, porewaters, perched water, and groundwater, and associated mineralogic analyses:

GS910508315215.005	Strontium isotope ratios and isotope dilution data for rubidium and strontium collected 5/3/89 to 5/9/91
GS920208315215.008	Strontium isotope ratios and isotope dilution data for rubidium and strontium collected 5/10/91 to 2/28/92
GS930908315215.027	Strontium isotope ratios and isotope dilution data for rubidium and strontium collected 3/2/92 to 11/18/92
GS931008315215.029	Strontium isotope ratios and isotope dilution data for rubidium and strontium collected 11/19/92 to 12/3/93
GS941108315215.010	Strontium isotope ratios and isotope dilution data for rubidium and strontium collected 12/6/93 to 8/17/94
GS950608315215.002	Strontium isotope ratios and isotope dilution data for rubidium and strontium collected 9/7/94 to 5/4/95

GS970908315215.011	Strontium isotope ratios and strontium concentrations in USW SD-7 rocks and soils, and ESF calcite
GS980108312322.004	Strontium Isotope Ratios And Strontium Concentrations In Water Samples From USW WT-24 And UE-25 J-13 Collected In October 1997
GS990308315215.003	X-ray fluorescence elemental compositions of rock core samples from USW SD-9 and USW SD-12
GS990308315215.004	Strontium isotope ratios and strontium concentrations in rock core samples and leachates from USW SD-9 and USW SD-12
MO0012STRIONIS.000	Water – Concentrations of Strontium Ions and Isotopes

4.1.12 Uranium Isotopic Data Inputs for Waters

The following primary input data are used in Section 6.6.7 to characterize the distribution of uranium isotopes in soils, borehole cuttings, porewaters, perched water, and groundwater:

GS010608315215.002	Uranium and Thorium Isotope Data for Waters Analyzed Between January 18, 1994 and September 14, 1996.
GS930108315213.004	Uranium isotopic analyses of groundwaters from SW Nevada – SE California.
GS970508312272.001	Uranium Isotopic Data From ESF Alcove 5 Pore-Water Leaches And UZ Heater-Test Water Collected Between April And May, 1997.
GS010808312322.004	Uranium and Uranium Isotope Data for Water Samples from Wells and Springs in The Yucca Mountain Vicinity Collected Between December 1996 And December 1997.
GS980208312322.006	Uranium isotopic data for saturated- and unsaturated-zone waters collected by non-YMP personnel between May 1989 and August 1997
GS980908312322.009	Uranium concentrations and 234U/238U ratios from spring, well, runoff, and rain waters collected from the Nevada Test Site and Death Valley vicinities and analyzed between 01/15/98 And 08/15/98.
MO0012URANISOT.000	Water – Selected Uranium Abundance and Isotope Ratios

4.1.13 Chemical Data Inputs for Gases from Open Boreholes

None of the data collected for samples from open boreholes are considered primary input data for characterization of the chemical composition of gas at Yucca Mountain. These data are only used to corroborate interpretations based on other gas chemical data.

4.1.14 Chemical Data Inputs for Gases from Instrumented Boreholes

None of the data collected for samples from instrumented boreholes are considered primary input

data for characterization of the chemical composition of gas at Yucca Mountain. These data are only used to corroborate interpretations based on other gas chemical data.

4.1.15 Groundwater Geochemical and Isotopic Data Inputs

Uranium activity ratios in local groundwater are considered to be primary input data, and provide the technical basis for identifying the presence of local recharge beneath Yucca Mountain (section 6.6.8). These input data are listed in section 4.1.12.

Carbon-14 activities in groundwater beneath Yucca Mountain are primary input data used to establish the boundary condition at the water table for the unsaturated-zone gas diffusion model cited in section 6.7.2. These input data are reported in the following DTN:

MO0012MAJIONIS.000	Water – Major ion and isotope data Field, Chemical, And Isotopic Data From A Precipitation Sample Collected Behind The Service Station In Area 25 And Ground Water Samples Collected At Boreholes UE-25 C #2, UE-25 C #3, USW UZ-14, UE-25 WT #3, UE-25 WT #17 And USW WT-24, Between 10/06/97 And 07/01/98

All other groundwater chemistry and isotopic data are used in a corroborative manner, to characterize local groundwater chemistry in terms of average concentrations and relative ion ratios. These groundwater trend data provide a baseline against which to compare and contrast chemical compositions of the various sources of water at Yucca Mountain, and to illustrate general trends of relative enrichment or depletion of one element compared to another (sections 6.8.2 and 6.8.3).

4.1.16 Data Inputs Used for Chloride Mass Balance Calculations

Precipitation data used in Section 6.9.2 to estimate bounds on present-day average chloride deposition rates at Yucca Mountain are listed in section 4.1.1. Pore-water chloride data analyzed by the chloride mass balance analysis are listed in section 4.1.3. Determination of the background $^{36}Cl/Cl$ ratio for the Yucca Mountain vicinity, which is used to estimate the long-term average chloride deposition rate at Yucca Mountain, uses the following input data:

LAJF831222AQ95.006	Halide and chlorine-36 analyses of soils from Midway Valley pits and trenches.
LAJF831222AQ96.006	Halide and 36Cl analyses of soil from Midway Valley Pit MWV-P2
LAJF831222AQ96.008	Halide and 36Cl analyses of cuttings from boreholes UZ-N15, UZ-N16, UZ-N17, UZ-N36, UZ-N38, UZ-N39, UZ-N61, UZ-N62, and UZ-N64
LAJF831222AQ96.010	Halide and 36Cl analyses of cuttings from borehole UZ-N37
LAJF831222AQ96.012	Halide and 36Cl analyses of cuttings from borehole UZ-N54
LAJF831222AQ96.014	Halide and 36Cl analyses of cuttings from borehole UZ#16

LAJF831222AQ96.015	Halide and 36Cl analyses of cuttings from borehole UZ-14
LAJF831222AQ97.002	Chlorine-36 analyses of packrat urine
LAJF831222AQ97.006	Halide, sulfate and chlorine-36 analyses of soils from Midway Valley soil pits MWV-P31 and NRSF-TP-19
GS960308315131.001	Woodrat midden radiocarbon (C14)

4.1.17 Uranium, Thorium and Lead Isotopic Data Inputs for Minerals

The following primary input data are used in Section 6.10 to characterize the uranium, thorium, and lead isotopic compositions of subsurface secondary mineral deposits from ESF and drill hole locations:

GS960208315215.001	Uranium and thorium isotope data determined by mass spectrometry for dating subsurface secondary deposits from ESF and drill hole locations, 8/1/95 to 2/15/96
GS960908315215.014	Uranium and thorium isotope data for ESF secondary minerals collected between 3/96 and 7/96.
GS970208315215.001	Uranium and thorium isotope data collected between 9/96 and 2/97 from secondary minerals in the ESF
GS970208315215.002	U-Pb isotope data for ESF secondary minerals, 9/12/96 – 2/15/97
GS970808315215.012	Uranium and thorium isotope data from secondary minerals in the ESF collected between 2/15/97 and 9/15/97
GS970908315215.013	U-Pb isotope data for ESF secondary minerals, 7/12/97 - 8/24/97
GS980908315215.015	Uranium and thorium isotope data including calculated 230Th/U ages and initial 234U/238U activity ratios for in situ microdigestions of outermost opal-rich mineral coatings from the Exploratory Studies Facility analyzed between 12/01/97 and 09/15/98.
GS980908315215.016	Uranium and thorium isotope data determined at the Royal Ontario Museum between 07/12/97 and 01/29/98 and calculated 230Th/U ages and initial 234U/238U ratios for secondary silica from the exploratory studies facility
MO0012WTRSAMPC.000	Sample Coordinates

4.1.18 Data Inputs for Abundances of Subsurface Secondary Minerals

The following primary input data are used in Section 6.10 to characterize the abundances of subsurface secondary minerals in ESF and drill hole locations:

GS971108314224.020	Revision 1 of detailed line survey data, station 0+60 to station 4+00, north ramp starter tunnel, Exploratory Studies Facility.
GS971108314224.021	Revision 1 of detailed line survey data, station 4+00 to station 8+00, north ramp, Exploratory Studies Facility.

GS971108314224.022	Revision 1 of detailed line survey data, station 8+00 to station 10+00, north ramp, Exploratory Studies Facility.
GS971108314224.023	Revision 1 of detailed line survey data, station 10+00 to station 18+00, north ramp, Exploratory Studies Facility.
GS971108314224.024	Revision 1 of detailed line survey data, station 18+00 to station 26+00, north ramp, Exploratory Studies Facility.
GS971108314224.025	Revision 1 of detailed line survey data, station 26+00 to station 30+00, north ramp and main drift, Exploratory Studies Facility.
GS971108314224.026	Revision 1 of detailed line survey data, station 45+00 to station 50+00, main drift, Exploratory Studies Facility.
GS971108314224.028	Revision 1 of detailed line survey data, station 55+00 to station 60+00, main drift and south ramp, Exploratory Studies Facility.
MO0012WTRCAC02.000	Water – Calcite and Carbon Dioxide Abundance
GS980308315215.008	Line survey information from the Exploratory Studies Facility obtained to estimate secondary mineral abundance

4.1.19 Carbon and Oxygen Isotopic Data Inputs for Minerals

The following primary input data are used in Section 6.11 to characterize the carbon-14, stable carbon, and stable oxygen isotopic compositions of calcite minerals from soil, ESF and drill hole locations:

GS931008315215.030	Carbon and oxygen isotope analyses of cavity- and fracture-coating calcite and soil carbonate from drill holes and outcrops, May '89 - Oct. '93.
GS931108315215.035	Oxygen stable isotope analyses of opal from drill holes and outcrops, June 92 - Aug. 92.
GS940608315215.006	Oxygen stable isotope analyses of opal from drill holes and outcrop, June 1994
GS950708315215.005	Delta 13C and delta 18O stable isotope data from the Yucca Mountain region, July 1992 to September 1994
GS960408315215.002	Carbon and oxygen stable isotope analyses of calcite from drill holes and the Exploratory Studies Facility (ESF), February 1995 to April 1996
GS960408315215.003	Oxygen stable isotope analyses of opal from drill holes, the Exploratory Studies Facility (ESF), and outcrop, April 1996.
GS960808315215.006	14-C analyses of calcite from ESF, 12/95 - 2/96
GS960908315215.010	C and O stable isotope KIEL analyses of calcite from ESF and USW-G2; 10/27/94 - 6/22/96

GS970208315215.003	14-C analyses of calcite from ESF fracture coatings, 12/2/96 - 2/13/97
GS970208315215.004	C and O stable isotope 252 analyses of calcite from ESF and USW G-2, SD-7, UE-25 a#7; 11/19/96 - 1/27/97
GS970208315215.005	C and O stable isotope KIEL analyses of calcite from ESF and USW G-2, G-2, G-4, UE-25 a#1, USW NRG-6, NRG-7/7a, UE-25 UZ#16; 4/8/96 - 1/17/97
GS970808315215.010	Carbon and oxygen stable isotope analyses of calcite from the ESF and USW G-1, G-2, and G-3/GU-3, from 01 /16/97 to 07/18/97
GS980408315215.010	Corrected data for carbon and oxygen isotope analyses of cavity- and fracture-coating calcite for one sample from drill hole USW G-2.
GS980908315213.002	Carbon and oxygen stable isotopic compositions of Exploratory Studies Facility secondary calcite occurrences, 10/1/97 to 8/15/98
GS990908315213.001	Stable carbon and oxygen isotope data for calcite from the ESF and analyzed, 2/96 – 5/99

4.1.20 Other Data Inputs for Minerals

The following primary input data are used in Section 6.11 to characterize the uranium, thorium, and lead isotopic compositions of subsurface secondary mineral deposits from ESF and drill hole locations:

GS931108315215.033	Fluid inclusion temperatures from drill holes USW G-1 and G-2, Oct. 92 – Sept. 93.

4.1.21 Other Data Inputs

The following data are used to establish the range of temperatures in the unsaturated zone at Yucca Mountain:

GS980408312232.001	Deep unsaturated zone surface-based borehole instrumentation program data from boreholes USW NRG-7a, UE-25 UZ#4, USW NRG-6, UE-25 UZ#5, USW UZ-7a and USW SD-12 for the time period 10/01/97 – 03/31/98

Accepted data used in this report are atomic masses of elements, and radioactive half-lives of radionuclides such as tritium, carbon-14, chlorine-36, rubidium-87, uranium isotopes, and thorium isotopes. These data are tabulated in numerous readily available sources (e.g. Parrington et al. 1996, pp. 18, 19, 22, 46 to 49, and 61).

4.2 CRITERIA

This AMR complies with the DOE interim guidance (Dyer 1999). Subparts of the interim guidance that apply to this analysis or modeling activity are those pertaining to the characterization of the Yucca Mountain site (Subpart B, Section 15), the compilation of

information regarding geochemistry and hydrology of the site in support of the License Application (Subpart B, Section 21(c)(1)(ii)), and the definition of hydrologic and geologic parameters and conceptual models used in performance assessment (Subpart E, Section 114(a)).

4.3 CODES AND STANDARDS

No specific formally established codes or standards have been identified as applying to this analysis and modeling activity. This activity does not directly support License Application design.

5. ASSUMPTIONS

Underlying assumptions used to perform the analyses of fluid and mineral geochemical and isotopic data are listed in Table 2, together with the rationale for accepting them. Assumptions that are indicated as To Be Verified (TBV) in Table 2 are also identified as such in the locations of the report where they are used.

6. ANALYSIS AND MODELS

The figures and tables cited in this section contain direct input and corroborative data.

6.1 GEOGRAPHIC AND GEOLOGIC SETTING

Yucca Mountain is in the northern Mojave Desert and lies 150 km northwest of Las Vegas in southern Nevada (Figure 1). It consists of a series of fault-bounded blocks of ash-flow and ash-fall tuffs and a smaller volume of lava deposited between 14 and 11 Ma (million years before present) from a series of calderas located a few to several tens of kilometers to the north (Table 1 and Figure 1 in Sawyer et al. 1994). Yucca Mountain itself extends northward to the southern end of the Claim Canyon caldera and southward toward U.S. Highway 95 where the tuffs thin and pinch out beneath the alluvium in the northern Amargosa Desert (Figure 2). The tuffs dip 5 to 10 degrees to the east over most of Yucca Mountain. Crater Flat is west of Yucca Mountain and separated from it by Solitario Canyon, which is the surface expression of the Solitario Canyon Fault - a steeply dipping scissors fault with down-to-the-west displacement of as much as 500 m in southern Yucca Mountain (Day et al. 1998, pp. 6 to 7). Underlying Crater Flat is a thick sequence of alluvium, lavas and tuffs that have been locally cut by faults and subvolcanic dikes. East of Yucca Mountain and separated from it by Fortymile Wash is Jackass Flats, which is underlain by a thick sequence of alluvium and volcanic rocks. Timber Mountain, approximately 25 km to the north of the potential repository area, is a resurgent dome within the larger caldera complex that erupted the tuffs at Yucca Mountain.

The central block of Yucca Mountain, into which waste would be emplaced if the site were licensed, is bounded by Drill Hole Wash on the north, the Solitario Canyon Fault on the west, and the Bow Ridge Fault on the east, and is dissected by the Ghost Dance and Dune Wash Faults. Topography is pronounced and, north of the central block, is dominated by long, northwest-

trending, fault-controlled washes (Figure 3). Within and south of the central block, washes are shorter and trend eastward. Topography in the southern part of Yucca Mountain is dominated by south-trending faults (Figure 4).

6.2 GEOCHEMICAL PARAMETERS AND METHODS

Fluid geochemical parameters of importance to site characterization and repository evaluations include the following, although not necessarily in order of importance:

- Major, minor and trace species
- Redox-sensitive elements
- Oxidation/reduction potential (ORP, usually expressed as Eh, for Electrode potential, on the hydrogen scale)
- Colloids and particulates
- Dissolved organic carbon
- Microbial populations
- Gases (dissolved in aqueous phase as well as present in gas phase)
- Stable isotopes (hydrogen, carbon and oxygen)
- Cosmogenic and atmospheric radionuclides (tritium, carbon-14, chlorine-36)
- Radiogenic isotopes (isotopes of strontium, uranium, and uranium decay products)
- Temperature and pressure
- Ages of fracture minerals

Some of the parameters on this list are primarily pertinent to site characterization issues, others are primarily pertinent to radionuclide transport issues, and some are pertinent to both sets of issues. Data on stable isotopes, cosmogenic and atmospheric radionuclides, and radiogenic isotopes are used primarily for site characterization purposes. More specifically, data for these isotopes have been used to develop and calibrate models for the hydrologic flow system. Most of the remaining parameters are primarily used in repository performance evaluations of radionuclide dissolution, mobilization and transport. The major constituent and trace-element concentration data are used in both areas. These parameters are discussed in this report.

The parameters pertinent to repository performance evaluations are used in various ways. For example, data on oxidation/reduction potentials, pH, major constituents, major species, gas concentrations, redox-sensitive elements, dissolved organic carbon, and microbial populations are all used to constrain predictions of the corrosion behavior of the waste packages and the solubility

of the waste forms. Most of these parameters are also used to constrain predictions for the sorption behavior of the radionuclides released from the waste forms.

The rest of this section reviews the sampling or measurement locations and collection methods for the different types of fluid samples analyzed in Yucca Mountain studies including precipitation, surface waters, pore waters, gases from the unsaturated zone, and perched water. Also reviewed are collection and analysis methods used for secondary fracture minerals at Yucca Mountain. For detailed descriptions of sampling or measurement locations and collection methods, the original publications cited in the discussion below should be consulted.

6.2.1 Sampling Locations

A summary of the types of unsaturated-zone geochemical and isotopic data available from boreholes at Yucca Mountain is provided in Table 3. Surface-based boreholes from which water and gas samples were collected in the Yucca Mountain area are shown in Figure 3. Lithostratigraphy of the samples that were collected was determined using the sources listed in Table 4. For subsurface-based boreholes, hydrochemical sampling was conducted in the Busted Butte Field Test facility (Figure 2); niches, alcoves and drifts in the Exploratory Studies Facility (ESF); and the East-West Cross Drift (Figures 3 and 4). The alcoves from which samples were collected include the Upper Tiva Canyon Alcove (ESF Alcove 1), the Bow Ridge Fault Alcove (ESF Alcove 2), the Upper Paintbrush Contact Alcove (ESF Alcove 3), the Thermal Test Facility (Alcove 5) and the Northern Ghost Dance Fault Access Drift (ESF Alcove 6) (Figure 4).

6.2.2 Gas Samples

Gas samples have been collected from a limited set of surface-based boreholes at Yucca Mountain. Borehole UZ-1 was instrumented for temperature and other probes at 33 levels, which allowed sampling of gas compositions from 15 distinct intervals (Montazer et al. 1985, p. 439). Additional boreholes were cased from the surface down to some depth and are open below this depth. These included UZ-6, UZ-6S, UZ#16, NRG-6, NRG-7a, SD-7, SD-9 and SD-12 (Thorstenson et al. 1990, p. 256; Yang et al. 1996, p. 11; Yang, Yu et al. 1998, p. 6). In boreholes UZ#16, NRG-6, SD-7, SD-9 and SD-12, packers were installed to isolate specified intervals for gas sampling. In addition, gases were collected from radial and horizontal boreholes drilled from alcoves driven from the Main Drift of the ESF (LeCain and Patterson 1997, p. 3).

Sulfur hexafluoride, SF_6, was used in each of these boreholes as a gaseous tracer to identify drilling-air contamination of the rock gas (Yang et al. 1996, pp. 9 to 11). Based on ten years of records and the stabilized value in borehole UZ-1, the tracer (SF_6) concentration of less than 0.1 ppmv (parts per million on a volume basis) in the borehole air is used to define uncontaminated rock gas. In some instances, such as boreholes in Alcoves 2 and 3, SF_6 tracer concentrations did not decrease even after several days of gas pumping (LeCain et al. 1997, p. 38; LeCain and Patterson 1997, p. 3). These residual tracer concentrations are believed to reflect the propensity of SF_6 to adsorb onto clays and zeolites in nonwelded units (Rattray et al. 1995, p. 1). Gas samples were collected from surface-based boreholes using a 500 cm^3-per-min peristaltic pump connected through short silicone tubing to within hole gas-sampling tubes (Yang et al. 1996, p. 8). Sampling tubes were pumped overnight to purge any atmospheric air.

Two different methods were used to collect CO_2 for isotopic analysis (Yang et al. 1996, pp. 8 to 11). A molecular-sieve method was used from 1984 to 1991, and involved passing the gas stream through a silica-gel tower to remove moisture, then through an anhydrous 50-nm molecular sieve to trap to CO_2 gas. Starting in 1991, a whole-gas method was used for batch sampling, which involved collection of the gas in a flow-through glass container (or in a Mylar balloon). Separation of CO_2 from the air sample took place in the laboratory using a trap cooled with dry-ice alcohol to trap water vapor, followed by a liquid-nitrogen trap to trap the CO_2. The whole-gas method is the preferred technique because the molecular-sieve method depletes ^{13}C relative to ^{12}C, such that $\delta^{13}C$ values reported for gas samples collected by this method represent depleted samples and are not representative of *in-situ* conditions (DTN: GS970908312271.003, footnote for SEP Table S97576.018). Consequently, $\delta^{13}C$ data obtained for molecular-sieve samples are not included in this report.

Investigations in the ESF alcoves were intended to provide a better understanding of gas flow in the upper part of the unsaturated zone; provide evidence of gas flow direction, gas flux, and travel time; determine the degree of fracture connectivity in the rocks; and support conceptual models of fluid flow in the unsaturated zone (LeCain et al. 1997, pp. 18 to 20). In general, stable CO_2 concentrations, at levels significantly higher than atmospheric or alcove (350 ppmv) concentrations, were an indication that the gas being pumped from the borehole was representative of rock gas. Gas samples for CO_2 and SF_6 concentrations were collected in glass syringes with three-way stopcocks so that the syringes could be filled and purged a minimum of three times before the actual sample was obtained. Three duplicate samples were collected from each borehole interval and then transported to the laboratory for analysis by gas chromatograph. Gas samples for ^{14}C analysis were collected by pumping the borehole gas through molecular sieves designed to collect the CO_2. Gas samples for $\delta^{13}C$ analysis were collected in Mylar balloons.

In addition to the analysis of C isotopes in CO_2, other isotopic analyses sometimes included O isotopes in CO_2 (as an indicator of the degree of isotopic exchange with pore water), and H and O isotopes in water vapor. Geochemical and isotopic data for gases are presented in section 6.7.

6.2.3 Pore-water Samples

For drillcore samples intended for pore-water analysis, each core was wrapped in plastic, placed in a Lexan liner, sealed inside an aluminum foil bag, and stored under cool conditions (6 to 9° C) until ready for analysis (Yang et al. 1996, p. 6). Despite all subsequent precaution to preserve the integrity of these samples for pore-water characterization, some geochemical and isotopic characteristics of these fluids may have been perturbed due to the fact that drilling was conducted using air and the cores were exposed to ambient atmospheric conditions for some time before they were hermetically sealed (Assumptions 2 (TBV), 4, 9 (TBV), 12 and 14 in Table 2). Thus, pore-water analyses should be used with appropriate caution in subsequent interpretations.

Water samples were extracted from drillcore using one of three methods: compression, ultracentrifugation, or vacuum distillation (for analysis of tritium and stable isotopes of hydrogen and oxygen). In many cases, following extraction of pore water by compression or high-speed

centrifugation, residual water was extracted from the core by vacuum distillation and analyzed for tritium and stable isotopes of hydrogen and oxygen.

The advantages and disadvantages of different compression methods for extracting pore water from drillcore, and of the effects of each on the major-ion chemistry of the extracted water, was investigated by Mower et al. (1994, pp. 1 to 7, 60 to 62). The method used to extract most of the pore-water samples obtained from surface-based boreholes was high-pressure uni-axial compression, applying an initial pressure of 103.4 MPa which was gradually increased to a final pressure of 827 MPa (Yang, Yu et al. 1998, pp. 6 to 7). To protect against atmospheric contamination, particularly with regard to carbonate species, the system is air tight throughout the extraction process. Additional pore water was extracted in some cases by injecting dry nitrogen gas into the porespace and by forcing out pore water at the end of the compression. The compression extraction technique was applied to core samples recovered from several dry-drilled boreholes (LeCain et al. 1997, p. 14; Yang et al. 1988, pp. 29 to 30, 33 to 34; Yang et al. 1996, p. 12; Yang, Yu et al. 1998, p. 6).

Extracted pore waters were filtered through Nucleopore filters (0.45 μm) before chemical analysis (Yang, Yu et al. 1998, p. 7). Cation concentrations were measured using inductively coupled plasma emission spectroscopy, and anion concentrations were measured using ion chromatography. Analytical errors were "5% (one-sigma) for all major ions except sulfate, for which the error was "10%. Reported aluminum values reflect the presence of both dissolved and particulate components less than 0.45 :m. Yang et al. (1988, pp. 38 to 41) determined that the chemical composition of extracted water changed under increasing stress in a triaxial compression cell operating with an axial stress between 41 and 190 MPa and a lateral confining stress between 34 and 69 MPa. However, with a few exceptions, the range of variation was generally less than 20% for calcium, sodium, magnesium, potassium, chloride, sulfate and silica (DTN: GS90090123344G.001).

Analyses of chloride, bromide and sulfate were performed on pore waters extracted from ESF and Cross Drift drill core by ultracentrifugation (Fabryka-Martin, Wolfsberg, Roach et al. 1998, pp. 264 to 265). Centrifugation methods were also used on some samples to test whether a compression method modified the chemistry of the pore-water samples. Yang et al. (1990, p. 250) analyzed pore waters extracted from adjacent samples of nonwelded tuff using a triaxial compression system (operating up to 152 MPa axial stress and 62 MPa confining stress) and a high-speed centrifuge (operating up to 18,000 rpm). These authors concluded that both methods produced reliable data, with similar results from each under the operating conditions used in the test. In general, differences in chemical concentrations of the major ions (calcium, sodium, magnesium, chloride, and sulfate) within each pair were less than 15% (Yang et al. 1990, p. 258). However, other chemical species were not analyzed in the study. For example, it is likely that *in-situ* concentrations of bicarbonate and carbonate would be influenced to different extents by the extraction methods used. However, these concerns do not affect the conclusions in this report that are based on general geochemical trends, although they are an important consideration for interpretation of carbon isotopic data for pore waters.

Pore-water data are discussed in Section 6.5.3 (geochemistry) and 6.6 (isotopes). For densely welded tuff core samples, which generally have moisture contents less than 5% by weight, only a

few samples produced sufficient pore water by the compression or centrifugation methods to permit a complete chemical analysis. For these samples, vacuum distillation was used to extract water (as vapor) for analyses of tritium and stable isotopes of hydrogen and oxygen (Yang et al. 1996, p. 6). This method was applied to core from some of the surface-based boreholes. In addition, in the Bow Ridge Fault Alcove (Alcove 2), water samples were extracted from cores of boreholes HPF#1 and HPF#2 by vacuum distillation and analyzed for tritium to assess the rate of infiltration of water from the land surface (LeCain et al. 1997, p. 40). In the Upper Paintbrush Contact Alcove, water samples were obtained by vacuum distillation from cores of boreholes RBT#1 and RBT#4 (Alcove 3) (LeCain and Patterson, 1997, p. 15). These water samples were analyzed for tritium to provide an indication of the spatial distribution of percolation flux near the PTn-TSw contact between the Paintbrush nonwelded (PTn) and underlying Topopah Spring welded (TSw) hydrogeologic units (LeCain and Patterson, 1997, p. 17) (unit stratigraphy shown in Table 1).

6.2.4 Perched Water and Groundwater Samples

Samples of perched waters were obtained from deep surface-based boreholes UZ-14, NRG-7a, SD-7, and SD-9 (Yang et al. 1996, pp. 34 to 37) as well as from WT-24 (DTNs: GS980108312322.004 and GS991108312272.004). These samples were collected with a bailer or from the surface output of a downhole pump. As with the pore-water extraction methods, these methods of sampling perched water make it very difficult to derive reliable values for some parameters of interest such as pH, ORP/Eh, and the major species of redox-sensitive elements such as ferrous and total iron. Geochemical and isotopic analyses of perched waters are discussed in Sections 6.5 and 6.6, respectively.

Groundwater samples from the saturated zone were generally obtained either with a downhole pump or a bailer (Ogard and Kerrisk 1984, pp. 5 and 7; Benson and McKinley 1985, p. 1). Geochemical data for these samples are discussed in Section 6.8, and isotopic data are discussed in Section 6.7.

6.2.5 Fracture Minerals

Fracture minerals consisting primarily of calcite and opal were extracted from surface-based and ESF drillcore, as well as being collected directly from rocks exposed along the ESF tunnels and alcoves. Analyses conducted on these minerals included stable isotopes of carbon, oxygen, and strontium, as well as ^{14}C and members of the uranium and thorium α–decay chains. These data are presented in sections 6.6.6, 6.10 and 6.11, in which they are interpreted in terms of evidence for paleoclimatic and paleohydrologic conditions in the unsaturated zone.

6.2.6 Sample Processing for Isotopic Analyses

Methods of processing samples for isotopic analyses include leaching salts from unsaturated rock cores or cuttings for ^{36}Cl and Sr isotopic analysis, distillation or compression of core to extract water for analysis of tritium or stable isotopes of hydrogen and oxygen, compression of core to extract water for carbon isotopic analysis, and digestion of mineral samples for analyses of Sr isotope ratios or of U series nuclides. Centrifugation of core has also been used to extract water

for some of these isotopic analyses. All uncertainties quoted below are one standard deviation unless stated otherwise.

Tritium—Hydrogen-3 (tritium) was analyzed by liquid scintillation counting, with an uncertainty of "4 tritium units (TU) (one-sigma) (Yang, Yu et al. 1998, p. 7). Section 6.6.2 provides a statistical evaluation of the tritium data to show that only results above 25 TU can be interpreted unambiguously as containing a component of bomb-pulse tritium. When sufficient water was available, some samples from ESF boreholes were isotopically enriched prior to analysis by liquid scintillation, a method with an uncertainty of ±0.7 TU or better (Clark and Fritz 1997, p. 17).

Stable hydrogen and oxygen isotope ratios—Ratios of hydrogen-2 to hydrogen-1 ($^{2}H/^{1}H$) and of oxygen-18 to oxygen-17 ($^{18}O/^{16}O$) were measured by gas source mass spectrometry. These data are reported as delta (δ) ^{2}H and $\delta^{18}O$, which express the sample's degree of enrichment or depletion of the heavy isotope relative to the Vienna Standard Mean Ocean Water (VSMOW) standard (Clark and Fritz 1997, pp. 6 to 8). Uncertainties were ±0.2 per mil (‰) for $\delta^{18}O$ and ±1.0 ‰ for $\delta^{2}H$ (Yang et al. 1996, p. 8).

Stable carbon isotope ratio—The ratio of carbon-13 to carbon-12 ($^{13}C/^{12}C$) was measured by conventional mass spectrometry. It is reported as $\delta^{13}C$ with a precision of about 0.2‰ (Yang, Yu et al. 1998, p. 7). $\delta^{13}C$ is measured relative to the Vienna Pee Dee Belemnite (VPDB) standard ($^{13}C/^{12}C = 0.011237$) (Clark and Fritz 1997, pp. 6 and 9).

Carbon-14—Carbon-14 was analyzed either by conventional liquid scintillation or tandem accelerator mass spectrometry (TAMS) (Yang, Yu et al. 1998, p. 7). Both methods have analytical uncertainties on the order of ±0.7 percent modern carbon (pmc). The advantage of TAMS, however, is its capability to analyze extremely small samples (less than 5 mg of carbon), whereas conventional scintillation counting requires between 1 and 3 g of carbon, depending upon the sample's age (Clark and Fritz 1997, p. 19).

Chlorine-36—Chlorine-36 was analyzed by accelerator mass spectrometry (as $^{36}Cl/Cl$), with typical uncertainties of 5% (Sharma et al. 1990, p. 410).

Stable strontium isotope ratio—The ratio of strontium-87 to strontium-86 ($^{87}Sr/^{86}Sr$) was measured using solid-source thermal ionization mass spectrometry. The ratios are commonly expressed as $\delta^{87}Sr$ relative to the ratio of reference seawater strontium ($^{87}Sr/^{86}Sr = 0.7092$) (Paces, Marshall et al. 1997, p. C-1).

Uranium, thorium and lead isotope ratios—Solid-source thermal ionization mass spectrometry with isotope dilution was used to obtain $^{234}U/^{238}U$, $^{230}Th/U$, $^{207}Pb/^{235}U$ and $^{206}Pb/^{238}U$ ratios (Paces, Neymark et al. 1996, p. 16; Paces, Marshall, Whelan and Neymark 1997, p. E-2).

Sections 6.6, 6.10 and 6.11 provide additional details on sample processing methods for specific isotopes.

6.3 CHEMICAL COMPOSITION OF PRECIPITATION

Chloride concentrations in local and regional precipitation, along with associated precipitation quantities, are considered to be primary input data, and provide the basis for estimating infiltration rates by the chloride mass balance method (sections 6.3.2 and 6.9.2). These input data are listed in section 4.1.1. All other precipitation chemistry data are used in a corroborative manner, to characterize local and regional precipitation chemistry in terms of average concentrations and relative ion ratios. These precipitation trend data provide a baseline against which to compare and contrast chemical compositions of the various sources of water at Yucca Mountain, and to illustrate general trends of relative enrichment or depletion of one element compared to another (sections 6.3.2 and 6.3.3).

6.3.1 Processes Controlling Precipitation Chemistry

The initial chemical and isotopic composition of Yucca Mountain groundwater is largely established by that of local precipitation and dry fallout. Once the precipitation enters the soil zone, absolute and relative concentrations of the various constituents are shifted to varying degrees by evapotranspiration and by interactions with minerals, organic matter, and the gas phase. The effects of these latter processes are described in subsequent sections. Isotopic data for precipitation are discussed in Section 6.6.

Several processes control the initial composition of precipitation or fallout. Some examples are:

- Salts from marine and terrestrial sources. For example, ions such as Na and Cl in precipitation derive predominantly from the ocean, whereas terrestrial sources contribute to Ca and Mg concentrations.

- Anthropogenic sources. Acid rain resulting from industrial releases of sulfur is an example of an anthropogenic source that impacts the chemical reactivity of precipitation. Other examples of anthropogenic sources are freons and fallout of radioactivity from above-ground nuclear tests. Global fallout nuclides (tritium, ^{14}C, and ^{36}Cl) in precipitation are discussed in Section 6.6.2, 6.6.3 and 6.6.4.

- Wet and dry deposition processes. For example, between one-third and two-thirds of the Cl deposition in Southern Nevada is from dry deposition of aerosols and particulates, a process also known as dry fallout (Eriksson 1960, p. 82; Dettinger 1989, p. 62).

- Atmospheric processes (for example, chemical transformation of molecular species). Different chemical species can be present as inorganic or organic gases or as aerosols, with each species having different average residence times in the atmosphere.

- Season, frequency and cycles of precipitation events.

- Evaporation prior to deposition will concentrate many solutes, as well as affect the fractionation of hydrogen and oxygen isotopes in moisture.

- Air temperature affects H and O isotopic fractionation, with the greatest fractionation observed for cold temperatures. Air temperature also controls gas solubilities.

Many problems complicate the collection and analysis of precipitation data. These include evaporation of rain or sublimation of snow in the collector, bacterial modification, and CO_2 uptake or loss. Even major elements may be below instrumental detection limits, and the charge imbalance for these analyses often exceeds 10%.

6.3.2 Present-Day Regional Characteristics

The largest database available for characterizing regional precipitation chemistry is that maintained by the National Atmospheric Deposition Program/National Trends Network (NADP/NTN), which was established in 1978 (National Atmospheric Deposition Program 1996, pp. 1 to 4). The network is a cooperative effort between many different groups, including the State Agricultural Experiment Stations, U.S. Geological Survey, U.S. Department of Agriculture, and numerous other governmental and private entities. This network presently consists of 200 rural stations throughout the United States that monitor wet-only deposition. A limited number of stations also monitor dry deposition, but none of these stations are in Nevada. Chemical analyses on weekly precipitation samples are conducted by the Central Analytical Laboratory operated by the Illinois State Water Survey. Summary records are available for annual, quarterly, and monthly periods. The data are subject to the quality assurance program of the NADP/NTN.

Within the YMP, the NADP/NTN regional database has been used to characterize Cl deposition rates in the Southwestern United States. Cl is the most conservative dissolved chemical species in Yucca Mountain groundwaters, insofar as its origin is strongly dominated by atmospheric sources and the contribution from water-rock interactions generally appears to be negligible. Increases in its subsurface concentrations relative to that in precipitation (including dry fallout of aerosols and particulates) are attributed to evapotranspiration in the soil zone, including sublimation of snow. Because of this characteristic, various pore-water constituents are commonly plotted as a function of Cl concentration to assess the direction and magnitude of rock-water interactions in the subsurface (Section 6.5.3).

Chloride pore-water concentrations have also been used as a surrogate measure of infiltration rates, an approach called the chloride mass-balance method (Scanlon 1991, p. 138). Total Cl deposition is a key parameter in the Cl mass-balance method. In general, Cl concentrations in precipitation decrease with increasing distance from the ocean (Eriksson 1960, p. 87). However, dry deposition of Cl is quite variable, showing no clear trend, possibly because dry fallout is largely dependent upon local sources of Cl in addition to distance from the ocean and wind patterns, which control the regional distribution of aerosol particles and their deposition rates (Winchester and Duce 1967, p. 110; Eriksson 1960, p. 88). Eriksson (1960, p. 82) studied the ratio of Cl concentrations in runoff to those in precipitation and suggested that, as a rule of thumb, precipitation chloride constitutes about one third of the total chloride deposition, with dry fallout accounting for the remaining two-thirds. In a local study of the Great Basin of Nevada and Utah, Dettinger (1989, p. 62) calculated an average bulk-precipitation concentration of 0.6 mg/L (for 8 sites) and an average wet-precipitation concentration of 0.4 mg/L (for 66 sites), implying that dry deposition comprises about 33 percent of the total Cl input in this region. A crude

estimate of the contribution of dry fallout to total Cl deposition rates in Southern Nevada can also be derived by comparing the average annual Cl concentration in wet fallout at Red Rock Canyon (0.16 mg/L, unweighted average calculated from Cl data in DTN: LA0003JF12213U.001) to the average annual Cl concentration in precipitation at 3 Springs Basin, which includes both wet and dry fallout (0.51 mg/L, calculated from data in DTN: MO0005CL3SPRGS.000, MO0005CLESTWRT.000, MO0005CLKAWICH.000, GS930108315214.004, and GS930908315214.030). This comparison indicates that dry fallout comprises about 70 percent of the total fallout in this area.

6.3.3 Present-Day Site Characteristics

The isotopic and chemical composition of precipitation at the Yucca Mountain site is largely inferred from measurements made at other local sites. Seven years of record (1984 to 1992) are available for precipitation chemistry in the semiarid 3 Springs Basin located east of Kawich Peak in the Kawich Range east of Tonopah, Nevada, and about 130 km due north of Yucca Mountain (McKinley and Oliver 1994, pp. 1 to 3; 1995, pp. 1 to 3) (Figure 1). Major ion chemistries of precipitation for the two precipitation chemistry monitoring stations at this location (3 Springs Basin and Kawich Peak) were used to derive average annual weighted concentrations for major constituents and regression lines for these constituents relative to Cl concentrations (Table 5). The regression lines are used in Sections 6.4 and 6.5 to illustrate subsequent changes in water chemistry as it flows through the subsurface.

Chemical data for precipitation are also available for Red Rock Canyon, the desert observation station closest to Yucca Mountain in the NADP/NTN network (Figure 1). This site is about 120 km southeast of Yucca Mountain. The record used for the analysis in this report spans 12 years, from 1985 to 1997, which includes two El Niño episodes, one in 1986 to 1987, and a long episode from autumn 1989 through the summer of 1995 (chemistry data in DTN: LA0003JF12213U.001; Fabryka-Martin, Turin et al. 1996, section 4.1.2.2). Neither alkalinity nor carbonate species are reported in this database.

The chemistry of precipitation is important for modeling the composition of waters at Yucca Mountain because precipitation represents the starting point in the evolution of groundwater chemistry. Subsequent changes in the water chemistry as it enters the subsurface are illustrated by three types of diagrams:

- *Trilinear (Piper) diagrams* show the relative concentrations of major ionic species. Figure 5 is a trilinear diagram for the precipitation samples from 3 Springs Basin, to be compared against other trilinear diagrams for surface waters and subsurface waters in later sections. Because bicarbonate concentrations are not available for the Red Rock Canyon data (DTN: LA0003JF12213U.001), these data are not presented on a trilinear diagram. Bicarbonate concentrations could be estimated for these samples based on charge-balance calculations although the uncertainties in relative anion proportions would probably be large for these dilute fluids.

- *Frequency distributions (histograms)* of major elements are used to contrast the distributions of specific dissolved species in different parts of the hydrologic system.

Frequency distributions for precipitation data have been included on the figures in Section 6.5.3, so that they can be directly compared to analogous data for surface and subsurface waters.

- *Scatterplots* of various major constituents as a function of some conservative species are a common method for evaluating the role of water-rock interactions in changing concentrations along a flow path. Chloride is usually considered to be the most conservative species, and a common assumption is that its concentration in surface and subsurface pore waters reflects increases due solely to evapotranspiration (Assumption 3 in Table 2). Figure 6 presents a set of plots of sodium, calcium, sulfate, bicarbonate, and silica as a function of Cl. Only samples with less than 1 mg/L Cl have been included. The regression lines plotted for each constituent on this figure represent least-squares fits to the precipitation data from the two 3 Springs Basin sites. These lines have also been plotted on analogous figures in Section 6.5.3 (chemistry of waters from the unsaturated zone) as a basis for a discussion of the direction and magnitude of rock-water interactions in the subsurface.

Other than the monitoring studies at 3 Springs Basin and Red Rock Canyon, only a few studies of Yucca Mountain precipitation chemistry have been conducted, and the coverage of these studies was limited in time, space, and/or analytical data. Chloride, bromide and sulfate were measured in a suite of about 100 samples collected from rain gauges at several neutron-monitoring boreholes at Yucca Mountain in the spring of 1995 (DTN: LAJF831222AQ95.003 and LAJF831222AQ97.009). The purpose of these analyses was to provide independent corroboration for estimates of the Cl deposition rate, a parameter used in the Cl mass-balance method (Section 6.9.2), and to characterize the Cl/Br and SO_4/Cl ratios of precipitation. These ratios can be useful qualitative tracers of groundwater origins and flow paths. Histograms showing the frequency distributions of Cl and SO_4 from this work are presented in Section 6.5.3 (Figures 18 and 19), in which they are compared to the concentrations of these species in waters from the unsaturated and saturated zones.

6.3.4 Representativeness of the Available Data

An important issue to address is the extent to which these precipitation data are representative of precipitation at Yucca Mountain, both past and present. Monitoring at the site at the present time may not produce valid data because it may not be possible to separate out the effects of site disturbance from natural conditions. Present-day compositions may also not be representative of past (pre-industrial) compositions, for example, because of the widespread effects of air pollution. This raises the question, then, of which of the two available data sets is more representative of natural conditions at Yucca Mountain. The compositions differ in both absolute as well as relative concentrations of major ions (for example, compare annual average values for Na/Cl, SO_4/Cl, and Ca/Cl in Figure 6). The Red Rock Canyon data have the advantage of providing a comparatively long (12-year) record, with details available for individual storms if desired. However, the proximity of Las Vegas may influence dust loadings and chemical compositions, and the lack of alkalinity analyses is a significant shortcoming that also makes it impossible to calculate a charge balance. In addition, only wet deposition chemistry is measured. The 3 Springs Basin data, although further removed from Yucca Mountain and representing a shorter

period of time (seven years), have the advantages of a reduced influence from urban activities associated with Las Vegas and of the inclusion of both wet and dry deposition data.

These precipitation data are considered adequate for the purposes for which they are used, i.e., as input data for simple correlation plots and as corroborative data to support independent estimates of the chloride deposition rate at Yucca Mountain. For the saturated zone, the geochemical evolution of the water is not very sensitive to uncertainties in the precipitation chemistry. However, for the unsaturated zone, the dominant input function is the composition of precipitation following evapotranspiration, and hence, predictions of the unsaturated-zone pore-water compositions based on precipitation inputs can be more sensitive to the precipitation uncertainties because errors may be magnified as the water becomes more concentrated.

6.4 CHEMICAL COMPOSITION OF SURFACE WATERS

This section describes the data available on the chemistry of surface water in the region. Three types of surface-water chemistry exist, depending on the source of the water:

- Relatively dilute waters from runoff during precipitation or snowmelt
- Relatively saline waters from groundwater discharge at springs
- A mixture of the two preceding types.

After an overview of the occurrence of surface water in the basin, the following discussion focuses on the chemical composition of the first category of surface waters, and particularly on surface waters from potential recharge areas and along flow paths through the Yucca Mountain area. Isotopic data for surface waters are discussed in Section 6.6.

None of the surface-water geochemical and isotopic data used in this report are considered to be primary input data. The surface-water data are used solely to characterize local and regional surface water chemistry in terms of concentration averages and ranges, relative ion ratios, and isotopic characteristics. These calculations provide a means to compare chemical compositions of surface water and runoff at Yucca Mountain to those of unsaturated-zone pore waters and perched water, so as to illustrate general trends of relative enrichment or depletion of one element compared to another (section 6.4.3).

6.4.1 Overview of Regional and Local Surface-Water Bodies and Drainage Areas

Local drainages on Yucca Mountain ultimately enter the Amargosa River. The eastern slope drains via Yucca Wash, Drill Hole Wash, and Dune Wash to Fortymile Wash; Fortymile Wash spreads out into a distributary system in the Amargosa Desert, joining the Amargosa River about 18 km north of Death Valley Junction, California (Figure 2). An unnamed ephemeral channel in Crater Flat collects drainage from the western and southern slopes of Yucca Mountain, draining to the Amargosa River near its confluence with Fortymile Wash. In addition, the tributary Carson Slough enters the Amargosa River as it flows southward through the Amargosa Desert. Carson Slough drains spring flow from the Ash Meadows regional groundwater discharge area in the eastern portion of the Franklin Lake Playa (also known as Alkali Flat), a discharge area for Yucca Mountain regional groundwater. However, the Amargosa River and its tributaries are ephemeral streams except for short distances where spring discharges enter the channel system; flow

throughout its entire reach occurs rarely (Malmberg and Eakin 1962, p. 7; Walker and Eakin 1963, pp. 14 to 15) because of losses to infiltration and evaporation from the streambed.

Savard (1995, p. F241; 1998, pp. 9 and 24) and Grasso (1996, pp. 11 to 13) discuss climatic and weather patterns responsible for Yucca Mountain area streamflow and associated flooding. Winter/spring stream flow occurs during El Niño events when the track of Pacific cyclonic fronts crosses the Yucca Mountain area. Summer streamflow occurs from thunderstorms, often when the summer monsoon in the southwestern United States extends into the Yucca Mountain area. Occasionally, remnant hurricanes from the Pacific Ocean move into the Yucca Mountain area, causing stream flow in the late summer and fall. These climatic factors influence the initial chemical and isotopic composition of the local precipitation.

Once the water contacts the ground, the chemistry of ephemeral surface waters evolves based upon the type of geologic materials with which the water comes into contact and the length of time of the contact period. Factors that influence the chemistry of ephemeral surface waters include:

- Site topography (for example, slope, ridgetop, terrace, sideslope, channel),
- Soil development (for example, depth of regolith, porosity, soil stratification/profile development, infiltration rates),
- Soil mineralogy and chemistry,
- Biota and vegetative coverage, and
- Evaporative concentration of solutes during flow.

In addition to ephemeral flows following precipitation events, perennial surface water in the Amargosa River drainage basin is associated with springs (Malmberg and Eakin 1962, p. 8). Flowing water occurs in the Oasis Valley, Ash Meadows, Tecopa, and Badwater areas after infrequent precipitation/runoff events, as well as during winter months when evapotranspiration is at a minimum. Some of these areas dry up almost entirely during high evapotranspiration periods during the summer. Perennial surface waters are found at the following locations:

- Numerous permanent or nearly permanent springs discharge along or near the Amargosa River channel in Oasis Valley. Although the flow in the channel is ephemeral through the Amargosa Desert, short reaches of persistent flow occur between the desert and the location at which the channel enters Death Valley. Wet playas occur in the eastern (Amargosa or Peters Playa) and southernmost (Franklin Lake Playa or Alkali Flat) parts of Amargosa Desert.
- The Ash Meadows regional groundwater system, which drains the region east of Yucca Mountain, discharges at several perennial springs that sustain small pools at Ash Meadows in southeastern Amargosa Desert. Crystal Reservoir, a man-made structure,

captures discharge from Crystal Spring and several springs in the Point of Rocks area and drains to the Amargosa River by Carson Slough.

- Four small perennial ponds occur in the Amargosa Desert in former clay mining pits.
- Badwater is a spring discharge pool in the terminal area of the Amargosa River in Death Valley.

The following section presents chemical data only for ephemeral surface waters (runoff).

6.4.2 Relevance of Surface-Water Chemistry to Flow and Transport Models

Chemical and isotopic compositions of some of the surface waters described above may be relevant to flow and transport modeling for two major reasons. First, infiltration of surface runoff into the beds of large channels such as Fortymile Wash may contribute significantly to local recharge and may thereby influence the chemistry of saturated-zone fluids. Although such fluids do not have the potential to contact waste packages and are, furthermore, unlikely to lie along the direct flow path between the potential repository and the accessible environment, characterizing their chemical and isotopic compositions is nonetheless necessary in order to be able to use these constituents as groundwater tracers for the regional flow system. Secondly, infiltration from runoff events collected from small channels above the potential repository, at locations where soil cover is negligible, may contribute to seeps that have the potential to directly contact the repository backfill and the waste canisters. Runoff water chemistry is discussed in Section 6.4.3.

6.4.3 Surface-Water Chemistry Data

Samples have been collected to document stream flow chemistry during the occasional runoff event as part of Yucca Mountain site characterization studies. Sampling locations are plotted on the map in Figure 7. Water-quality data are also taken from a compilation of hydrochemical data collected in the Death Valley region during the period from 1910 to 1990, including baseline data from rivers and playas in addition to springs and wells (Perfect et al. 1995, pp. 1 and 3). Although the main objective of the Perfect et al. (1995) report was to document groundwater quality in the Yucca Mountain area, surface-water quality was also documented. The chemical analyses in the compilation by Perfect et al. are taken from four general sources: USGS unpublished data files, USGS National Water Information System database, published reports from Federal and State agency investigations, and unpublished data.

The following general observations are made from the chemical data for channel flow and surface runoff. Major ion chemistry for these samples is plotted in the trilinear diagram in Figure 8. The sampling sites fall into three general categories: channel flow fed by springs and seeps, channel flow from runoff events and surface runoff, and overland runoff mixed with spring discharge.

Nineteen samples were analyzed for major and minor ions between 1984 and 1995 from 15 locations within 15 km of Yucca Mountain along its eastern side. These data were collected during three series of runoff events:

- Surface water samples collected in Fortymile Wash, Drill Hole Wash, and Busted Butte Wash in August 1984 were the first surface-water samples collected during site characterization studies in the Yucca Mountain area (Perfect et al., 1995, attached file dataedit.wk1).

- Emett et al. (1994, p. 550) document analyses from dip samples of surface water in the Amargosa River drainage basin from six sampling sites during stream flow conditions in January and February 1993. Two of the sites—Stockade Wash at Airport Road and Yucca Wash near its mouth—represent local overland runoff during precipitation. (Note: Three of the other sites—Amargosa River near Beatty, Carson Slough at Stateline Road, and Amargosa River near Eagle Mountain—represent spring discharge from groundwater or mixing of overland runoff and spring discharge and are not relevant to this discussion. The remaining sample of runoff is from Cane Spring Wash below Skull Mountain but is not included here because it is not representative of runoff in the vicinity of Yucca Mountain.)

- During periods of stream flow in 1994 and 1995, surface-water quality samples were collected on Yucca Mountain and in Fortymile Canyon during overland runoff and channel flow following precipitation (DTN: GS940308312133.002 and GS960308312133.001; the latter data are also presented in Savard 1996, p. 28). Some of the overland runoff from the hillslopes in the drainage basins infiltrated soil and volcanic rock layers and then re-emerged as overland runoff. Some of the overland runoff also originated from disturbed areas in the drainage basins such as roads and drill pads where compaction of the surface material reduced infiltration and increased overland runoff. Some of the surface-water quality samples in Fortymile Canyon were taken during overland runoff of precipitation and or snowmelt, whereas others were taken during the recession period after peak discharge. All samples probably represent a mixing of overland runoff and shallow infiltration waters that discharge along the hillslopes.

Among the dilute runoff samples described above, total dissolved solids range from 45 to 122 mg/L. These waters have similar ionic chemistries when plotted on a trilinear diagram (Figure 8). The cation field is dominated by calcium, which accounts for 50 to 60 percent of the cation charge, whereas the anion field is dominated by carbonate species, which account for 70 to 90 percent of the total anion charge. The average Cl content of these local runoff waters is 3.5 mg/L.

In addition to surface-water samples from the general vicinity of Yucca Mountain, water quality data are also available for 3 Springs Basin and East Stewart Basin, sites that are considered representative of potential recharge areas in central Nevada (Figure 1) (McKinley and Oliver 1994, pp. 1 to 3; 1995, pp. 1 to 3). The 3 Springs Basin is a semiarid basin in the Kawich Range east of Tonopah; sampling locations are at elevations of 7,070 to 9,040 feet. East Stewart Basin is a subalpine basin in the Toiyabe Range north of Tonopah with sampling occurring at elevations of 9,455 to 10,240 feet. The two basins were studied as analog sites to Yucca Mountain during wetter and cooler periods (Section 6.4.1). Water quality samples were collected from precipitation, springs, and other surface waters during the period 1986 to 1992. Chemical data for precipitation at the 3 Springs Basin sites were discussed previously in Section 6.3.3. Springs

in the basins are probably above the regional groundwater system and do not represent discharge from large groundwater basins, in contrast to springs at Ash Meadows in the Amargosa Desert. The water chemistry of the spring discharges does reflect modification due to movement of water through unsaturated volcanic rock layers in the basins. Surface-water samples can represent overland runoff from precipitation or snow melt and also mixing of spring discharge with overland runoff.

Major ion compositions of some of the 3 Springs Basin and Stewart Basin samples are plotted in the trilinear diagram shown in Figure 9, and the major constituents are plotted versus chloride concentrations in Figure 10. These waters are very similar to the Yucca Mountain runoff samples with respect to their relative proportions of the major ions; that is, they are Ca-bicarbonate waters with a significant component of Na. However, the central Nevada samples have slightly higher proportions of Na and Cl, and lower proportions of Ca and carbonate species, than the Yucca Mountain waters.

Figure 10 shows various major constituents plotted against Cl concentrations for channel flow and surface runoff at Yucca Mountain and for surface waters from 3 Springs Basin and Stewart Basin. Also shown on the plots are the regression lines obtained for 3 Springs Basin precipitation chemistry from Table 5 in Section 6.3.3. The surface-water plots illustrate the direction and magnitude of changes in water chemistry in response to evaporation, dissolution of dry-fall salts accumulated since the last infiltration event, and water-rock interactions. Sulfate in these waters increases to a similar extent as does Cl, as shown by the fact that the surface-water compositions cluster about the regression line shown for these two anions on Figure 10. This observation suggests that sulfate concentrations in these waters are fairly conservative and are mostly a function of evaporative concentration and dissolution of dry-fall salts. In contrast, both Na and Ca concentrations plot considerably above the precipitation regression lines, suggesting that their concentrations are increased by dissolution of carbonate minerals and weathering reactions of soil minerals. Dissolution of carbonate minerals also leads to a large gain in bicarbonate concentrations, which is also apparent in a comparison of the trilinear plot of Figure 5 (precipitation) with those in Figures 8 (Yucca Mountain runoff) and 9 (surface waters from 3 Springs Basin and Stewart Basin). Finally, the most dramatic constituent increase is observed for silica, which increases by two orders of magnitude over its concentration in precipitation due to fast dissolution of opaline silica in the soil (Chadwick et al. 1987, p. 977).

Another source of chemical data for surface-water samples is the compilation of analyses of springs and tunnel seeps from Rainier Mesa (location shown on Figure 2) (McKinley et al. 1991, Tables 5 and 6 on pp. 26 to 33). Because of the similarity in geologic settings for Yucca Mountain and Rainier Mesa, these samples expand the database used to develop a conceptual model for the early stages of the geochemical evolution of waters contacting tuff. A trilinear plot of these data is presented in Figure 11, in which some of the tunnel seeps (points 8, 9, A) are observed to have similar compositions to those of perched waters at Yucca Mountain (Figure 17).

These surface-water chemical data are also included in the discussion on the geochemical evolution of Yucca Mountain waters (Section 6.5.3.2) in which frequency histograms for some of the major ion species are presented (Figures 18 to 23).

6.4.4 Representativeness of the Data

A key question is, to what extent are the Yucca Mountain runoff samples representative of surface water at this location? Surface waters under current climatic conditions at Yucca Mountain are an infrequent occurrence, thereby making it difficult to build a chemical database. Re-aeration of surface water as it proceeds down the channel may also affect the chemistry of the collected samples. Some samples were analyzed for bicarbonate in the laboratory instead of at the site during collection, such that the reported bicarbonate concentrations may not represent field conditions.

Some of the samples may also be affected by site activities because man-made disturbances influence sediment concentrations in surface water. For example, runoff from the ESF pad and tunnel waste piles during light precipitation events goes down the Drill Hole Wash channel. During some periods of runoff from the ESF pad, no other runoff was noted in the area, leading to the hypothesis that the ESF pad and tunnel waste piles were influencing water quality and runoff. Fine sediment probably originating from the ESF pad and tunnel waste piles has been transported down the channel system and has clogged infiltration pathways in the channel alluvial material. Because of greatly reduced infiltration in the channel bottom, surface-water runoff and sediment were both transported much greater distances than they would have been under natural conditions.

However, none of these concerns affect the conclusions in this report that are based on general geochemical trends. These surface-water data are considered adequate for the purposes for which they are used, i.e., as input data for simple correlation plots and histograms for comparison against the chemistry of water in the unsaturated zone. Including the more extensive data from the 3 Springs Basin is useful to develop and test concepts about geochemical evolution in this environment. The surface geology at the two central Nevada sites is similar to that at Yucca Mountain insofar as both are dominated by silicic volcanic rocks, and the precipitation chemistry is also expected to be similar. The prevailing climatic regime at the central Nevada sites differs from that at Yucca Mountain, leading to differences in soil chemistry, in particular less calcic soils. The central Nevada sites also have higher precipitation rates and higher infiltration rates, such that ionic concentrations should be slightly lower for these surface waters than for the Yucca Mountain samples. Nonetheless, general geochemical trends should be the same. These data are used in the following section as corroborative evidence that the description of geochemical evolution of subsurface waters is consistent with general trends observed in surface waters.

6.5 CHEMICAL COMPOSITION OF PORE WATERS AND PERCHED WATER

Primary input data for the chemical compositions of unsaturated-zone waters at Yucca Mountain are listed in sections 4.1.3 (pore water) and 4.1.4 (perched water). Primary input data for subsurface temperatures are listed in section 4.1.21. Boreholes for which chemical data are available for pore waters and perched water are listed in Table 3. Assumptions 1, 2 (TBV) and 3 in Table 2 apply to discussions in this section.

6.5.1 Processes Controlling the Chemistry of Unsaturated-Zone Waters

The major processes that could influence the chemistry of waters in the unsaturated zone, including perched water, include the following:

- Dry and wet deposition (precipitation). This refers to the compositions of rain, snow, and dust deposited on the surface of Yucca Mountain. These compositions provide the starting point (that is, input composition) for unsaturated-zone water chemistry. Chemical data available for wet and dry deposition were discussed in Section 6.3.

- Surface-water chemistry. Under some conditions, surface waters may be a significant source of recharge to the unsaturated zone in the Yucca Mountain region (see Section 6.4). Therefore, the chemistry of surface waters is potentially an important factor in the control of unsaturated-zone water compositions. Chemical data available for surface waters were discussed in Section 6.4.3.

- Soil-zone processes. Soil-zone processes of importance to unsaturated-zone water chemistry include evapotranspiration, deposition of pedogenic mineral horizons, reaction of infiltrating precipitation waters with soil minerals, and biogenic processes.

- Infiltration paths and rates. The pathways by which waters infiltrate Yucca Mountain impact water chemistry not only because they determine the rock/mineral types that the waters contact but also because they determine the contact times for waters with the various rock/mineral types. These contact times in turn determine the extent of reaction between the waters and the rocks/minerals. Particularly significant to solute transport rates is the distribution of flow between fractures and matrices in each lithologic unit.

- Rock-water interactions. The extent to which infiltrating waters react with the rocks/minerals with which they come into contact will have a major impact on water chemistry. These interactions can include rock/mineral-dissolution reactions, ion-exchange reactions, hydrolysis reactions, precipitation reactions, and possibly other alteration reactions.

- Mineral-substrate-water interactions. These interactions are a subset of rock/mineral interactions but are separated out here because of their potential significance with respect to radionuclide retardation reactions (for example, sorption).

- Water-air interactions. The composition of the gas phase in the unsaturated zone is an important factor in the control of unsaturated-zone water chemistry. For example, the carbon-dioxide partial pressure influences the carbonic-acid system and the oxygen partial pressure influences the oxidation state of redox-sensitive elements such as carbon, sulfur, iron, and manganese.

- Microbial influences. The existence of various microbial populations in the unsaturated zone implies that water chemistry could be altered by microbial activity. For example,

microbial metabolic activity could influence pH, the concentrations of redox-sensitive species, and the concentrations of organic acids in unsaturated-zone waters.

- Temperature. Variations in temperature can influence the composition of unsaturated-zone waters by increasing or decreasing the rates of important reactions (for example, dissolution or precipitation reactions) and by changing the composition of the equilibrium assemblage in the system. Temperature variations beneath Yucca Mountain between depths of about 40 feet to the top of the water table range from about 18°C to 34°C (based on data for NRG-6, NRG-7a, UZ#4, UZ#5 and SD-12 in DTN: GS980408312232.001; corroborated by data for H-1, H-3, H-4, H-5, G-4, UE-25 b#1, UZ-1, WT-2, and WT#4 reported in DTN: GS950408318523.001) and likely have only small although measurable impacts on water chemistry.

- Pressure. Pressure variations will have a minor effect on water chemistry through its effect on the dissolution of gases such as CO_2 in water. More significant, however, is its effect on gas flow patterns, including water vapor transport.

6.5.2 Significance and Occurrence of Perched Water

6.5.2.1 Significance

Perched water is a zone in which the rocks are locally saturated above the regional water table. The presence of perched water implies that, at least at some time in the past, the percolation rate through the unsaturated zone has exceeded the saturated hydraulic conductivity of the perching layer. The perched-water reservoir may be a remnant from a time during which percolation rates were higher or may reflect long-term steady-state conditions. Perched-water reservoirs of large volume could indicate that structural or stratigraphic traps are present that allow infiltrating waters to accumulate. Perched water in proximity to the waste-emplacement tunnels in a repository is a potential source of water—in addition to pore water—that may become mobilized as vapor resulting from waste-generated heat, a fact that needs to be considered when attempting to analyze the impact of that mobilized water on repository performance.

6.5.2.2 Perched Water Occurrences

Perched water has been identified below the potential repository horizon in six boreholes in the Yucca Mountain Site area: UZ-1, UZ-14, and NRG-7a in Drill Hole Wash; and SD-7, SD-9, and SD-12 along the ESF Main Drift (Rousseau et al. 1999, pp. 170 to 171; O'Brien 1997, p. 23; Rautman and Engstrom 1996a, p. 32; Rautman and Engstrom 1996b, p. 8 and 32). The perched-water bodies identified are at elevations significantly below (100 to 200 m) the potential repository horizon. Although other boreholes in the site area did not detect perched water, this may be because they were not drilled to sufficient depth to intercept the geologic units where perched water has been identified or because they were drilled with water or foam that obscured the perched water when it was encountered. In all cases, accumulation of perched water seems to be caused by either the basal vitrophyre of the Topopah Spring Tuff or the vitric-zeolitic boundary in the Calico Hills Formation acting in concert with a lateral structural barrier (Rousseau et al. 1999, pp. 171 to 172). Although not detected in all boreholes, based on field observations and

the apparent prerequisite conditions, perched water beneath the site area seems to be a common occurrence and is probably nearly everywhere near the base of the Topopah Spring Tuff in the vicinity of the North Ramp (Rousseau et al. 1999, p. 170).

The following discussion summarizes aspects of the perched water occurrences relevant to interpretation of their geochemical and isotopic constituents.

UZ-1 and UZ-14—These two boreholes penetrate perched water in Drillhole Wash about 190 m above the water table (Rousseau et al. 1999, pp. 170 to 171). The top of the perched water is within the lower nonlithophysal zone of the Topopah Spring Tuff (Tptpln) about 8 m (for UZ-1) and 9 m (for UZ-14) above the contact with the crystal-poor vitric zone (Tptpv). Chemical analysis of the water showed that it was contaminated by water used to drill G-1, a borehole located about 305 m to the southeast (Whitfield et al. 1990, p. 6). During the drilling of G-1, approximately 8.7 million liters of drilling fluid was lost into the rock (Whitfield 1986, p. 418). Pumping tests of UZ-14 indicated that this perched-water reservoir may be extensive (Rousseau et al. 1999, pp. 170 to 171).

NRG-7a—This borehole is located in Drill Hole Wash. Water was first noticed in the borehole at a depth of 461.3 m (Rousseau et al. 1999, p. 171), below the contact between the bedded tuff (Tpbt1) and the crystal-poor vitric zone (Tptpv) at the base of the Topopah Spring Tuff. The water level in the borehole then rose about 30 m to stand at a depth of 428 m (elevation of 855 m), which is 4 m above the base of the lower nonlithophysal zone (Tptpln). The perched water was initially detected about 91 m above the predicted water table at this borehole (Ervin et al. 1994, Plate 1). The perched water was encountered near the contact of a series of highly fractured welded tuffs overlying relatively unfractured, nonwelded tuffs. This is similar to the situation at boreholes UZ-1 and UZ-14 where perched water may be entrapped in fractures while slowly imbibing into the matrix of the less fractured, underlying rock unit.

SD-7—This borehole is located on the eastern slope of Yucca Mountain near the ESF Main Drift and near the southern extent of the potential repository area. Water was first observed during coring at a depth of 488 m in the bedded tuffs (Tacbt) at the base of the Calico Hills Tuff (O'Brien 1997, p. 23). This level is 4.5 m above the top of the Prow Pass Tuff and about 150 m above the regional water table. The perched-water level subsequently rose 8 m, apparently having been confined by the low-permeability zeolitic materials in this interval (Rautman and Engstrom 1996b, p. 32). The stratigraphically complex bedded-tuff zone is a well-sorted volcanic sandstone layer with argillically altered pumice in all layers, predominantly horizontal fractures, and some lamination below 487 m (Rautman and Engstrom 1996b, p. 60).

SD-9¾ This borehole is located in Drillhole Wash. Standing water was first noticed at a depth of about 449 m (Rousseau et al. 1999, p. 171). Television logs revealed that water was seeping through a fracture into borehole SD-9 at a depth of 413 m (elevation of 890 m), which is 3 m above the contact between the lower nonlithophysal unit (Tptpln) and the crystal-poor vitric unit (Tptpv) of the Topopah Spring Tuff and about 157 m above the predicted regional water table (Ervin et al. 1994, Plate 1). The perched-water reservoir is in fractured welded tuff (Tptpv) underlain by less-fractured nonwelded and bedded tuffs that comprise the uppermost part of the

CHn. Because no pumping tests have been conducted on this perched-water reservoir, its areal extent is uncertain.

SD-12—Although no perched-water reservoir of sufficient magnitude to cause standing water in the borehole was detected during the drilling of SD-12 (Rautman and Engstrom 1996a, p. 8), the video-camera log of this borehole indicates that a perched-water zone of limited extent probably is present in the densely welded vitric unit (Tptpv3) of the Topopah Spring Tuff, extending from the top of this unit down to the base of the moderately welded vitric unit of the CHn (Rousseau et al. 1997, p. 21). Perched water over this interval is also indicated by the *in-situ* pneumatic-pressure responses observed in the instrument station immediately below this zone. Fracture densities measured for the core indicate intense fracturing within the lower nonlithophysal unit (Tptpln) and sparse fracturing in the underlying crystal-poor vitric unit (Tptpv) (Rautman and Engstrom 1996a, p. 25).

WT-24—This borehole is north of the repository block, approximately 1.5 km north of UZ-14. Based on saturation data, water appeared to be perched above either the moderately welded base of the Topopah Spring Tuff (Tptpv2, depth to top of unit is 512 m) or the basal vitrophyre of the Topopah Spring Tuff (Tptpv3, depth to top of unit is 524.5 m) (DTN: GS980708312242.011). The perching layer was difficult to determine with more precision because of inadequate core preservation for moisture analysis. The regional water table was encountered at a depth of 670 m. No published reports have discussed the nature of the apparent perched layer.

6.5.3 Major Constituents in Unsaturated-Zone Pore Waters and Perched Waters

This section discusses the data available on the major ion chemistry of pore waters and perched waters in the unsaturated zone. Interpretation of the chemical data in a geochemical framework is based largely on the groundwater chemistry discussion in Triay et al. (1997, Section II).

The compositions of pore waters above the potential repository horizon are of significance to transport modeling because they represent the types of waters that could enter the near field of the potential repository. They are also significant because they can be used to constrain models for the rock/mineral-water-gas interactions that occur in the soil zone and the unsaturated zone above the potential repository horizon. Such models can be used to derive estimates of future variations in unsaturated zone water chemistry. Data on major constituents can also be used to evaluate potential flow paths for flow modeling.

Trilinear (Piper) diagrams are used to characterize the relative distributions of major cations and anions in these waters as a function of their stratigraphic depths. Figures 12 through 16 present such plots for pore waters from the PTn, TSw, and CHn hydrogeologic units, as well as from the combined Prow Pass (Tcp), Bullfrog (Tcb) and Tram (Tct) lithostratigraphic units. Figure 17 presents a trilinear plot for perched-water samples. These plots are referenced in the subsequent discussion of the geochemical evolution of pore fluids in the unsaturated zone.

Frequency histograms of chloride concentration data are plotted in Figure 18 for pore waters from the Tiva Canyon welded (TCw), PTn, CHn, TCw and TSw hydrogeologic units. These

concentrations are compared against data for precipitation, surface waters, perched waters, and saturated-zone waters in order to elucidate general trends.

6.5.3.1 Major-Ion Chemistry

PTn Pore-water Chemistry—Pore waters extracted from bedded tuff of the PTn are calcium-chloride or calcium-sulfate-type waters, i.e. samples plot near the top part of the diamond in a trilinear diagram (Figure 12). This characteristic becomes more pronounced for samples collected deepest within the PTn. Pore-water samples near the top of the PTn have not yet acquired the calcium-chloride or calcium-sulfate signature (e.g., point H from UZ-14 and point Y from UZ#16, on Figure 12).

TSw Pore-water Chemistry—Data for TSw pore waters are sparse due to the difficulty of extracting sufficient water for analysis from densely welded core. In general, the waters have equal quantities of Na and Ca, with negligible Mg; the dominant anion is bicarbonate, with a much smaller proportion of sulfate than is typical of PTn waters (Figure 13). In terms of relative proportions of anions, the chemical composition of TSw waters is intermediate between those of the PTn and CHn. The fields occupied by PTn, TSw, and CHn pore waters on a trilinear diagram are distinctly different with only slight overlaps.

CHn Pore-water Chemistry—Pore waters extracted from the Calico Hills nonwelded unit are sodium carbonate-bicarbonate-type waters that plot near the lower part of a trilinear diagram (Figures 14, 15 and 16). Waters become more strongly sodium carbonate-bicarbonate types with increasing depth within the Calico Hills Formation (compare Figure 14 to Figure 16).

Total Dissolved Solids—The total concentration of constituents in pore waters as shown by total dissolved solid contents (Table 6) is highly variable, and is often greater near contacts than in the middle of stratigraphic units (Yang et al. 1996, p. 24). Unsaturated-zone pore waters from surface-based boreholes have significantly larger concentrations of total dissolved solids than either perched water (Tables 7 and 8) or saturated-zone water (Benson and McKinley 1985, p. 5). The larger concentrations suggest either a greater degree of evapotranspiration near the surface (e.g., for PTn pore-water samples from UZ-14), or a greater degree of rock-water interaction which could indicate a prolonged contact of percolating water with silicate rocks.

Chloride and Sulfate Concentrations—Chloride and sulfate are generally conservative constituents in oxidizing groundwater and hence are commonly used as indicators of water origins, flow paths, and mixing. The concentrations of chloride and sulfate in many pore-water samples from surface-based boreholes are one to two orders of magnitude greater than those of either perched water or saturated-zone water. For example, chloride concentrations of deep perched waters lie between 4.1 and 15.5 mg/L (Table 8) with a mean of 6.8 mg/L, which is similar to that of the saturated zone water from the volcanic rocks beneath Yucca Mountain (9.5 mg/L). In contrast, the chloride concentration of matrix pore water from surface-based boreholes ranges from 10 to 245 mg/L with a mean of 49 mg/L (calculated from data in Table 6). If matrix pore water had contributed significantly to the perched-water bodies, the chloride concentration of perched water should be similar to that of the pore water. The smaller concentration of chloride in perched water implies that pore waters and perched waters have distinctly different histories of

geochemical evolution, undergoing different degrees of evaporation and/or of water-rock interactions.

Figure 19 shows that sulfate concentrations are similarly elevated in PTn pore waters relative to those for the other waters plotted. The higher proportions of chloride and sulfate concentrations in PTn pore waters relative to the other waters at the site are also evident by comparing the trilinear plot in Figure 12 to the trilinear plots in Figure 14 (upper Calico Hills pore waters), Figure 15 (lower Calico Hills pore waters), Figure 16 (Prow Pass pore waters), and Figure 17 (perched waters).

Silica Concentrations—The frequency distribution for silica shown in Figure 20 indicates that silica is low in precipitation but substantially higher in surface waters. By the time precipitation and surface waters infiltrate into the unsaturated zone, the silica concentrations have reached a limit. This limit is presumably the result of saturation with a silica phase as discussed further in Section 6.5.3.2.

Major Cation Concentrations—The concentrations of sodium and calcium are also elevated in pore waters relative to other waters at the site as shown in Figures 21 and 22. Sodium is elevated in most of the pore-water samples whereas calcium is elevated only in the PTn and TSw samples. The trilinear diagram for PTn pore waters (Figure 12) shows that PTn pore-water compositions extend to higher calcium proportions than observed in either precipitation compositions (Figure 5) or surface-water compositions (Figures 8 and 9). This enhancement presumably reflects water-soil/rock reactions that release calcium to solution preferentially to the release of sodium and magnesium. The pore waters in the Calico Hills and Prow Pass units show high proportions of sodium (Figures 14, 15 and 16). This shift in dominance from divalent to monovalent cations primarily reflects the ion-exchange reactions with zeolites in the CHn unit. The zeolites preferentially take up calcium and magnesium while releasing sodium to the water.

Vertical Trends in Ion Concentrations—The chemical composition of pore waters within the nonwelded units does not change in a simple or predictable fashion in a given borehole. Chloride and sulfate show large concentration changes within the CHn, even by as much as a factor of two for samples separated by less than 0.5 m (e.g., compare two SD-7 samples from 791 m, three UZ-14 samples at 477 m, two WT-24 samples from 532 m, all in Table 6). Similar large contrasts are noted for sodium and total carbonate within the PTn. If flow within these units were dominated by vertical percolation of pore water, a monotonic increase in sodium and a monotonic decrease in calcium should be noted in the CHn because of cation exchange by zeolites (replacement of Na with Ca or Mg on ion-exchange sites). Although pore waters for SD-9 show a continual increase in the sodium content with depth, the data set is limited to only four samples. Data for UZ#16 show a decrease in calcium with depth, but changes are fairly erratic and the concentration of calcium rebounds sharply at the top of the Prow Pass Tuff. The data, therefore, suggest at least some component of lateral flow within the nonwelded units.

6.5.3.2 Geochemical Evolution

A convenient method for assessing the magnitude and direction of rock/mineral-water interactions experienced by percolating infiltration waters transported through the soil and unsaturated zones

is to plot the concentrations of the major constituents in these waters relative to a conservative constituent (that is, a highly soluble and nonsorbing constituent), such as chloride, in an *x-y* plot. In the absence of other geochemical processes, evaporation or transpiration of a given water sample will result in proportional increases in all constituent concentrations, describing a linear trend in this plot starting at the origin. If processes other than evapotranspiration significantly influence the concentration of a particular constituent, the resulting data point will lie off the evapotranspiration trend. The selection of chloride as the normalizing constituent for such a plot assumes that its concentration is not affected significantly by leakage from fluid inclusions or by geochemical reactions along the flow path (Assumption 3 in Table 2).

Calcium and Bicarbonate—Plots showing the concentrations of calcium and bicarbonate versus chloride for various pore-water, perched-water, and saturated-zone samples are presented as Figures 24 and 25, respectively. Included on each plot is a regression line representing a least-squares fit to the weighted annual precipitation data from the 3 Springs Basin monitoring sites (regression lines from Table 5). These plots show that both calcium and bicarbonate concentrations in PTn pore waters generally plot on or below the evapotranspiration lines (Figures 24a and 25a). This observation implies that calcium and bicarbonate were lost from these waters relative to chloride. Given the fact that soils on Yucca Mountain contain abundant caliche horizons, this loss likely reflects the precipitation of calcite as the result of evapotranspiration and possibly other reactions in the soil zone.

Pore waters from the Calico Hills and Prow Pass units show even greater depletions of calcium relative to the precipitation trend (Figures 24b and 24c). These greater depletions likely reflect ion-exchange processes in which sodium in the ion-exchanger phase (for example, zeolite or clay) was replaced by calcium from the water and vice versa. Unlike the PTn pore waters, many of the Calico Hills and Prow Pass pore waters are enriched in bicarbonate relative to the precipitation trend (Figures 25b and 25c). This fact most likely reflects carbonic acid weathering reactions which start with the dissociation of carbonic acid in the water as follows:

$$H_2CO_3 \Leftrightarrow H^+ + HCO_3^- . \qquad \text{(Eqn 1)}$$

Sodium—In the weathering of aluminosilicate rocks and minerals, weathering reactions include the exchange of the hydrogen ions produced in the carbonic acid reaction with sodium or other cations on the rock or mineral. This step leads to an increase in sodium as well as bicarbonate concentrations in the water. The overall reaction is approximated as follows:

$$>SO–Na + H_2CO_3 \Leftrightarrow >SO–H + Na^+ + HCO_3^- , \qquad \text{(Eqn 2)}$$

where >SO is a mineral substrate with a surface-complexation site at which ions can be exchanged. As shown in Figures 26b and 26c, sodium concentrations in pore waters from the Calico Hills and Prow Pass units generally plot well above the precipitation trendline. This result is attributed to the sodium/hydrogen ion-exchange reaction and to ion-exchange reactions involving calcium, magnesium, and sodium ion exchange on zeolites and clays. Assuming the sodium/hydrogen ion-exchange reaction is accompanied by the formation of an equimolar amount

of bicarbonate, the increase in bicarbonate levels over and above the amount predicted by the precipitation trend line (Figure 25b and 25c) would imply a large proportion of the increase in sodium concentrations shown in Figure 26 is due to the sodium/hydrogen ion reaction.

In contrast to the increase in sodium relative to the precipitation trend line for the Calico Hills and Prow Pass units, data for PTn pore waters (Figure 26a) plot below the regression line calculated from the 3 Springs Basin precipitation data. As explained previously, sodium is generally leached from minerals and rocks during low-temperature weathering reactions. Such leaching would lead to compositions that plot above the evapotranspiration line, not below it. Furthermore, the PTn pore waters also have low values of bicarbonate relative to chloride (Figure 25a). These trends would seem to preclude reactions similar to that proposed above for the Calico Hills and Prow Pass units to explain the geochemistry of pore waters for the PTn. Analytical error is not considered a likely explanation for the Na vs. Cl trend because of quality-control measures and because nearly all the samples plot below the line, implying they would all have to be in error, and because the charge balances for the analyses generally agree within ±10% (Table 6, last column).

Several explanations could account for the observed Na versus Cl trend in the PTn pore waters.

- The average Na/Cl ratios in precipitation may have been lower in the past (i.e., closer to the halite line) than those measured in the 3 Springs Basin samples at the present day. This possibility is supported by the fact that the weighted-average Na/Cl ratio in precipitation at the Red Rock site near Las Vegas (1.1 molar ratio) is about half of that for the 3 Springs Basin data (2.4 molar ratio). (The Red Rock Na/Cl ratio is calculated from precipitation-weighted average annual Na and Cl concentrations using data reported in DTN: LA0003JF12213U.001. The 3 Springs Basin Na/Cl ratio is calculated from precipitation-weighted average annual Na and Cl concentrations using summary data shown in Table 5.)

- Sodium may be taken up by some sort of rock-water interaction not generally considered. However, smectites in the PTn are generally low in sodium and high in potassium and calcium. Although present in the PTn, zeolites do not appear to be particularly common in this unit, and limited analytical data also show them to be calcium-rich.

- Sodium may have been sequestered in the soil zone as some other sodium salt such as sodium sulfate.

The last hypothesis is the preferred one, insofar as it also accounts for the observed depletion in sulfate relative to chloride for PTn pore waters (Figure 27a).

Sulfate—Like chloride, sulfate is considered to be a generally conservative constituent in dilute oxidizing waters such as the unsaturated-zone pore waters in Yucca Mountain. However, as shown in Figures 27a, 27b, and 27c, unsaturated-zone pore waters show sulfate-to-chloride ratios consistently lower than the ratios observed in recent precipitation. Because all the unsaturated-zone pore-water analyses are grossly undersaturated with chloride phases and with gypsum and other possible sulfate phases involving the major cations, it is unlikely that solid chloride or sulfate phases are precipitated in the unsaturated zone (Triay et al. 1997, p. 29). Although anthropogenic sulfate may have elevated the modern-day SO_4/Cl ratio in precipitation, the data used to calculate

parameters of the precipitation regression line do not appear to have been significantly influenced by this source because perched waters and saturated-zone waters plot near the precipitation regression line (Figure 27d).

Drever and Smith (1978, p. 1452) presented a model that offers one potential explanation for the low sulfate-to-chloride ratios in the unsaturated-zone pore waters (Triay et al. 1997, p. 29). Their model involves drying and wetting cycles in the soil zone. During the drying phase, concentrations of dissolved solutes are increased in soil waters by evapotranspiration to the degree that phases such as calcite, gypsum, silica, and the more soluble salts precipitate. During occasional heavy rains, the phases precipitated during the drying phase are partially redissolved. Because the dissolution rates for highly soluble salts, such as sodium chloride, are higher than the rates for less-soluble salts, such as calcite, gypsum, and silica, a portion of the less-soluble salts may remain undissolved after the occasional heavy rains infiltrate through the soil zone. In terms of sulfate and chloride concentrations, this process could lead to soil waters with lower sulfate-to-chloride ratios than those observed in precipitation. The actual concentrations of sulfate and chloride in these waters would depend on the details of the processes involved, including the dissolution kinetics of the sulfate and chloride phases, the residence time of the waters in the soil zone, and the original masses of sulfate and chloride in the soil zone.

An alternative hypothesis to account for the low sulfate-to-chloride ratio is the microbial reduction of sulfate ions in the soil (e.g., initially to hydrogen sulfide, or more likely to a mixture of organic sulfides such as methyl disulfide and dimethyl disulfide). These volatile compounds are commonly produced in soils and are readily lost to the atmosphere. However, decreased SO_4/Cl are not observed in up-gradient saturated-zone waters. Because up-gradient waters recharge in regions with more vegetation and wetter soils, one might expect the likelihood of microbial reduction of sulfate to be even greater for those waters than for infiltrating waters at Yucca Mountain. Hence, this hypothesis is considered improbable for the Yucca Mountain site.

Although differences in the dissolution kinetics of sulfate and chloride salts may be part of the explanation for the low sulfate-to-chloride ratios in pore waters from the unsaturated zone at Yucca Mountain, these differences are likely augmented, and perhaps even dominated, by crystallization-sequence effects. For example, it is possible that minerals (such as calcite and gypsum) that precipitate from evaporating soil pore waters early in a crystallization sequence, are partially or completely sequestered by minerals that precipitate later in the sequence (such as being coated by opal-A). Alternatively, early crystallized phases may completely fill smaller pores in the rocks and, therefore, be less accessible to infiltrating waters than minerals crystallized later in the sequence in larger pores (for example, Chadwick et al. 1987, p. 975). During subsequent infiltration events, the latest-formed phases in pores accessible to infiltrating waters would preferentially dissolve, leading to soil solutions enriched in the more soluble salts relative to the less soluble salts.

Silica—A plot of silica versus chloride concentrations in pore waters, perched waters, and saturated-zone waters is shown in Figure 28. Most of the water samples from the Yucca Mountain area plot above the precipitation trend line. This result suggests that a process other than evapotranspiration is contributing to the increase in silica concentrations in these waters. According to Gifford and Frugoli (1964, pp. 386 to 388) and Chadwick et al. (1987, p. 977),

silica is added to soil waters as a result of the dissolution of opaline silica in soil horizons in arid regions. This explanation would be consistent with the presence of opal in the soils of Yucca Mountain and opal deposits on fracture surfaces exposed in the ESF (section 6.11.1). It is also consistent with the fact that surface waters have much higher silica concentrations than precipitation compositions (Figure 20).

Perched Water—Perched-water compositions are generally distinct from the compositions of pore waters although they are very similar to saturated-zone water compositions (Section 6.8). These relationships are readily seen by comparing the trilinear plots of each category of water: perched water (Figure 17), unsaturated-zone pore waters (Figures 12 to 16), and groundwater from the saturated zone (Figure 48). The similarity of perched and saturated-zone water compositions suggests that these waters are subject to similar water-rock interactions. As discussed in Section 6.8, these reactions predominantly involve mineral/rock dissolution and ion exchange.

pH—pH values shift from slightly acidic values for precipitation (pH 6), to increasingly basic values with depth in the unsaturated zone (pH 9 for the deepest pore-water samples, Table 6) (Figure 23). Controls on pH in ambient unsaturated-zone pore waters and perched waters are dominated by the carbonic-acid system and the interaction of hydrogen ions with the host rock/mineral. As discussed above, hydrogen ions can replace sodium ions in the host rock/mineral (for example, volcanic glass, feldspar) under most conditions. As hydrogen ions are used up, carbonic-acid dissociation produces additional hydrogen ions and bicarbonate ions. If hydrogen/sodium exchange is inhibited, the pH of a given pore-water sample will depend primarily on the partial pressure of carbon dioxide in the gas phase in contact with the water and on whether or not the gas phase has equilibrated with the water phase. This process will buffer the pH of the (dilute) pore waters at near-neutral levels. If both the carbonic-acid dissociation and hydrogen/sodium exchange reactions are important, the control of pH becomes a kinetic problem. For example, if the rate at which hydrogen ions react with the host rock is fast relative to the rate at which the carbon-dioxide partial pressure changes or the rate at which the carbon dioxide in the gas phase equilibrates with the water phase, the pH of the water phase could increase above the equilibrium level for the carbon-dioxide partial pressure of interest. Conversely, if the hydrogen reaction rate is slow relative to the carbon-dioxide equilibration rate, the pH of the water phase would more directly reflect the carbon-dioxide partial-pressure variations.

Because the sodium-versus-chloride concentration data for pore waters from units above the Calico Hills nonwelded (CHn) unit (Figure 26) suggest little or no evidence for the hydrogen/sodium ion-exchange reaction, the pH of these pore waters likely is controlled in part by the carbon-dioxide partial pressure with which they are in contact. Measured pH values in PTn pore waters average 7.2. In contrast, the CHn pore waters and perched waters show clear evidence of sodium/hydrogen ion exchange. The average pH values for these waters are 8.1 for perched water, 8.3 for pore waters from the CHn unit above the Prow Pass Tuff, and 9.0 for pore waters from the Prow Pass Tuff and below. Analytical uncertainties in pH measurements are about "0.2 to "0.3 pH units. Whether the higher pH values for deeper samples reflect the cation/hydrogen-ion exchange rate or simply a lower partial pressure of carbon dioxide in the gas phase has not yet been resolved although there may be sufficient CO_2 gas data available to do so.

However, it is also possible that the pore-water pH changes when it is exposed to air during sample collection, or that it is affected by the compression of the rock during the pore-water extraction process; both processes could vary according to rock type.

Redox State—The oxidation/reduction state of unsaturated-zone waters is likely dominated by the presence of oxygen in the unsaturated-zone gas phase. At the two locations where such measurements have been made, the unsaturated-zone gas phase has atmospheric levels of oxygen: 21% reported for UZ-6S gas in Thorstenson et al. (1990, p. 256); and 18.5 to 21.1% reported for UZ-1 gas (DTN: MO0102UNSZHYCM.000; also Yang et al. 1996, p. 42). These results confirm that unsaturated-zone pore waters would generally be oxidizing. Measured Eh would typically be high (400 to 600 mV) even though in low-temperature natural systems this value does not always indicate equilibrium insofar as some oxidation/reduction reactions may not have gone to completion. It is possible that lower oxidation/reduction potentials could be present locally (that is, in microenvironments) as a result of microbial activity or the presence of a reducing compound (for example, pyrite).

Microbial Activity—The influence of microbes on the chemistry of waters in the unsaturated zone is not well defined. At a minimum, microbes could produce organic acids and locally alter pH and oxidation/reduction states. Microbial activity could also affect concentrations of sulfate, bromide, and other dissolved species, as well as fractionate isotopes of light elements such as carbon. According to Kieft et al. (1997, p. 3128), microbial cell counts and microbial biomasses were low at all the locations sampled in the ESF. Kieft et al. (1997, p. 3128) suggest that this result was likely due to low water contents and low nutrient availability. However, they note that the potential for microbial activity was high. That is, microbial populations were present but not active. They concluded that if sufficient water and nutrients were added to the system, microbial populations could increase dramatically.

6.5.4 Representativeness of Available Data

The data available on pore-water and perched-water chemistry are limited in several ways. First, complete pore-water analyses are available mainly for those horizons in Yucca Mountain that contain nonwelded tuffs with relatively high porosities. Very few complete pore-water analyses are available for well-indurated, low-porosity rocks (for example, welded tuffs in the repository horizon). Second, pore-water and perched-water analyses are only available for samples from a limited number of boreholes (Table 3). Third, the procedure for extraction of water from the pores may have an impact on the water chemistry. For example, the release of carbon dioxide from pore-water samples could change the pH of the samples. Similarly, the pH of perched-water samples could shift due to degassing as the bailer is brought to the surface or at the pump outlet.

Despite these restrictions, the major ion chemistry of the pore waters is sufficiently consistent and the controls on this chemistry are sufficiently well understood that bounds can be placed on the likely range of variations to be expected. An important parameter in estimation of these bounds is the net infiltration rate (that is, the degree of evapotranspiration) over the period of interest. Bounds on the pH of the pore waters are more difficult to derive because the variations in carbon-dioxide partial pressures within the unsaturated-zone gas phase are not well defined at the present time. However, model calculations assuming saturation with calcite would allow this parameter

to be bounded. Lower bounds on the oxidation/reduction state cannot be derived without additional field data.

The compositional variations of pore waters and perched waters in the unsaturated zone at Yucca Mountain reflect a variety of infiltration rates, rock-water interactions, gas-water interactions, and other effects. The range of these processes and effects will likely not change greatly within the potential range of climatic regimes likely to affect Yucca Mountain. What may change is the relative importance of these processes and effects. For example, under climatic regimes involving higher infiltration rates, the ion-exchange processes represented by pore waters from the Calico Hills nonwelded unit and by the perched waters may become more dominant. This scenario would result in more dilute pore waters with higher proportions of sodium ions and possibly higher pH. However, as these types of waters are present in the ambient system, they do not present an unanticipated change in water chemistry.

6.6 ISOTOPIC COMPOSITION OF FLUIDS

The purpose of this section is to summarize available aqueous-phase isotopic data for precipitation, surface waters, pore waters and perched waters recovered from the unsaturated zone, and groundwaters. These data provide constraints for water and solute transport rates and mechanisms. Examples of specific issues addressed by these data include spatial and temporal variability in net fluxes, lateral diversion in specific stratigraphic units, role of faults in controlling flow paths, fracture-matrix interactions, and distribution of water travel times.

The types of isotopic data available for borehole samples from the unsaturated zone are presented in Table 3. Borehole and tunnel alcove locations are plotted in Figures 3 and 4.

6.6.1 Overview of Isotopic Methods

Isotopes measured in unsaturated-zone fluids as part of YMP site characterization activities fall into five general categories as described below. It would be incorrect to assume that the various methods in each category provide redundant information. Rather, each method yields very different types of information (see reviews of isotopic methods in IAEA 1983, sections 5 to 8, 10, 11 and 13; Davis and Murphy 1987, pp. 4 to 9; Clark and Fritz 1997, Chapters 1, 7 and 8). Hence, a large suite of different approaches has been critical to the development and testing of conceptual models for flow and transport through the unsaturated zone at Yucca Mountain.

Anthropogenic Material—This category of environmental tracers includes radioactive species present in global fallout from nuclear weapons testing and from releases from nuclear-fuel reprocessing plants. Tritium, ^{14}C, and ^{36}Cl produced in the atmosphere during above-ground nuclear testing activities, primarily between 1952 and 1963, have been widely used in hydrologic studies. The presence of these nuclides above background levels in subsurface fluids is generally accepted as a clear indication that some proportion of the water was transported to that depth in less than 50 years. If the sampled depth is more than a few meters in an arid environment, the presence of global fallout nuclides implies a component of fracture flow. Hence, these isotopic data provide a means for constraining the extent to which solute transport is retarded by diffusion from fractures into the adjacent matrix. Fission products ^{99}Tc and ^{129}I in a subsurface sample

(above natural background) would also provide a clear indication of a component of recent water. However, a robust analytical protocol for these species in unsaturated-zone fluids has not yet been developed. Other radionuclides in global fallout, such as ^{137}Cs and plutonium isotopes, sorb strongly onto most mineral surfaces and hence are largely immobilized in the near-surface soil. Tritium, ^{36}Cl, and ^{14}C data acquired as part of the YMP site characterization activities are discussed in Sections 6.6.2, 6.6.3, and 6.6.4, respectively. Fluorocarbon compounds have also been used as tracers of gas movement at Yucca Mountain but are not discussed in this report because their primary use is to characterize how the presence of boreholes can alter natural gas flow patterns and rates (Thorstenson et al. 1998, p. 1507).

Atmospheric Radionuclides—Tritium, ^{36}Cl, and ^{14}C also exist naturally in the atmosphere as the result of the interactions of cosmic rays with atmospheric gases. To the extent that the original concentrations at the surface can be reconstructed, these nuclides are useful indicators of water residence times, with water ages based on the extent of radioactive decay of the atmospheric component. As part of YMP site characterization activities, ^{14}C and ^{36}Cl have been used to constrain water age estimates. Chlorine-36 and ^{14}C data acquired as part of the YMP site characterization activities are discussed in Sections 6.6.3 and 6.6.4, respectively.

Climatic Reconstruction—Stable isotopic compositions of hydrogen and oxygen can be used to infer paleoclimatic conditions. Hydrogen and oxygen isotopic analyses of water samples acquired under Yucca Mountain site characterization activities are summarized in Section 6.6.5. Noble gases are another indicator of the paleotemperature of recharge waters but are relevant mostly to saturated-zone water and have not been measured in YMP site characterization activities.

Water-Rock Interactions—Groundwater is commonly out of chemical and isotopic equilibrium with the rocks through which it moves (Davis and Murphy 1986, Section 8). The extent of disequilibrium provides a qualitative method for establishing flow paths and flow chronologies. Furthermore, if the kinetics of chemical or isotopic exchange between the water and minerals along its flow path are sufficiently well known, then semi-quantitative estimates of water travel times may be possible. Sections 6.6.6 and 6.6.7 address the hydrologic implications of trends observed in isotopic ratios for strontium and uranium in pore waters.

Dating of Secondary Fracture Minerals—Waters percolating through the unsaturated zone at Yucca Mountain deposit secondary minerals in areas where solutions exceed chemical saturation with respect to various mineral phases, most commonly calcite and opal (Paces, Neymark et al. 1998, p. 36). These minerals provide evidence of past percolation flow paths and preserve physical and isotopic records related to fracture solutions). As part of site characterization activities, measurements of ^{14}C activities, $^{230}Th/U$ activity ratios, and $^{207}Pb/^{235}U$ ratios were obtained to provide the basis for estimating mineral formation ages. These age data, combined with the physical and isotopic data, can be used to derive constraints on water flow through the mountain (Section 6.10.3).

6.6.2 Tritium

Primary input data used to characterize the distribution of tritium in the unsaturated zone at Yucca Mountain, which provide a basis for water travel time estimates, are listed in section 4.1.5.

Assumption 4 in Table 2 applies to discussions in this section.

6.6.2.1 Background

Natural tritium (^{3}H or T) is produced in the upper atmosphere by the bombardment of nitrogen by the flux of neutrons in cosmic radiation (Clark and Fritz, 1997, p. 174):

$$ {}^{14}_{7}N + {}^{1}_{0}n \Rightarrow {}^{12}_{6}C + {}^{3}_{1}H \qquad \text{(Eqn 3)} $$

where n is a neutron. Once produced, tritium oxidizes rapidly to tritiated water (HTO). Transfer of tritium to the troposphere occurs during spring in mid-latitude zones. Tritiated water has a short residence time in the troposphere (less than one year) and is eventually removed from the atmosphere in precipitation or through isotopic exchange. Historical concentrations in rain water in the middle latitudes have been estimated to be on the order of 10 tritium units (TU) with one TU being equal to one tritium atom per 10^{18} atoms of ^{1}H and corresponding to 3.19 pCi/L (IAEA 1983, p. 58). Tritium values in precipitation prior to the 1950's were between 2 and 25 TU (Yang et al. 1996, p. 51). Because of the relatively short half-life of tritium (12.3 yr, Parrington et al. 1996, p. 18), groundwater infiltrating prior to 1952 with an initial tritium content of 10 TU would have a present-day tritium content of 0.7 TU or less.

Above-ground testing of nuclear devices in the Northern Hemisphere between 1952 and 1963 produced significant amounts of tritium in the Earth's atmosphere. Tritium from powerful thermonuclear blasts was injected into the stratosphere during that time. Bomb-pulse tritium overwhelmed natural background levels by as much as several orders of magnitude (Figure 29). Peak concentrations in precipitation, expressed as annual precipitation-weighted averages, were reached in 1963 when the annual average measured values at Albuquerque, NM, and Salt Lake City, UT—the two stations probably most representative of fallout at Yucca Mountain—were about 1,900 TU and 3,600 TU, respectively (IAEA 1981, pp. 134 and 154). Seasonal variations in post-bomb tritium concentrations in precipitation are quite significant (Davis and Murphy 1987, pp. 36 to 37; Clark and Fritz 1997, pp. 177 to 178). These variations are caused by changes in atmospheric circulation between the troposphere and the stratosphere, which is a major reservoir of tritium. During the early 1960's in the Northern Hemisphere, early summer maxima at many monitoring locations were ten times as large as the winter minima. Even in the early 1980's, 20 years after the cessation of atmospheric nuclear tests, summer maxima were still more than twice winter minima at many stations. Consequently, the seasonal timing of precipitation is a critical determinant of the magnitude of the tritium signal introduced into the subsurface.

A nuclear-test ban treaty signed in 1963 largely stopped further nuclear testing activity in the atmosphere, although some small atmospheric releases of tritium continued from nuclear reactors and testing by countries that had not signed the treaty (Carter and Moghissi 1977, p. 58). Tritium concentrations have gradually decreased since 1963 to about 10 to 40 TU measured in precipitation at the Nevada Test Site between November 1983 to June 1985 (DTN: GS920908315214.032). Precipitation samples from 3 Springs Basin in Central Nevada, slightly north of the Nevada Test Site, showed slightly lower tritium concentrations in samples collected between 1985 and 1991, ranging from 19 to 71 pCi/L (6 to 22 TU) (McKinley and Oliver 1994, pp. 27 and 74). Annual mean values and monthly maximum values for monitoring stations in states surrounding Nevada likewise were in this range (i.e., still elevated above pre-1952

background levels) during 1988 to 1993 (Yang et al. 1996, p. 51). In the winter of 1992, the tritium content of surface runoff collected from several sites in the vicinity of Yucca Mountain ranged from 19 to 33 pCi/L (6 to 10 TU) (Emett et al. 1994, p. 550; Savard 1996, p. 28); values of tritium during the winter are typically the lowest of the year.

It is possible that venting of tritium from subsurface nuclear detonations on the Nevada Test Site may also have contributed to tritium in precipitation at Yucca Mountain. For example, the Project Plowshare Schooner event on December 8, 1968, was a shallow cratering experiment conducted in Area 20 (Pahute Mesa, shown on Figure 2) of the Nevada Test Site, about 40 km due north of Yucca Mountain, and was known to have vented tritium to the atmosphere (EPA 1971, pp. i, ii, 34 and 42). Immediately following the event, tritium concentrations of 5,200 to 10,000 pCi/L (1,630 to 3,135 TU) were reported for snow samples from three sites in Nevada. However, trajectories for this particular event were mostly northerly and northeasterly, such that Yucca Mountain precipitation was unlikely to have been influenced by it.

The extent to which detectable quantities of tritium enter the subsurface is dependent upon the spatial and temporal variations in precipitation. If precipitation is insufficient to lead to net infiltration following a storm event, then the tritium is lost back to the atmosphere by evapotranspiration. Consequently, because 1958 to 1964 experienced below-average levels of precipitation at Yucca Mountain (Precipitation Station 4JA) (French 1985, pp. 52 to 56), it is entirely possible that much of the peak tritium concentrations were never transported into the bedrock at Yucca Mountain. In this regard, the behavior of tritium as a tracer of modern water differs substantially from that of ^{36}Cl. In the latter case, all global fallout ^{36}Cl eventually is carried into the subsurface.

6.6.2.2 Statistical Analysis of Tritium Data

As part of YMP site-characterization activities, tritium has been analyzed in over 800 pore-water fluids extracted from unconsolidated material in shallow surface-based boreholes, from drill core from deep surface-based boreholes, and from ESF drillholes. Analyses are also available for water samples bailed and pumped from perched-water bodies (Table 9) and from the saturated zone. Detectable levels of tritium have been observed in the Bow Ridge fault zone in ESF Alcove 2 and in pore waters extracted from core samples from surface-based boreholes. These detections occur within the TCw, PTn and TSw, and also in some samples from the CHn, as deep as the Prow Pass member of the Crater Flat Tuff.

Because of the implications of post-bomb tritium for the presence of fast transport paths and large fracture fluxes, it is important to define the threshold at which a given signal can be considered as being above background. Although the analytical uncertainty is 4 TU (for 1-sigma) based on counting statistics, other factors contribute to a larger uncertainty in the measured value. For this analysis report, Chauvenet's criterion for identifying outliers was the basis of the statistical test used to establish the cutoff tritium value above which a sample result is considered to be elevated over background (Bevington and Robinson 1992, p. 58), i.e., the minimum tritium activity that would indicate the presence of bomb-pulse water in a sample. The approach taken in this report is to rank the tritium data from lowest to highest value and to calculate a cumulative average and standard deviation for each step of the ranking. One then calculates the number of standard

deviations that the highest-value data point lies above the mean as each new data point is included in the cumulative average. These standard deviations are plotted in Figure 30, in which they are compared against Chauvenet's criterion for identifying outliers (solid line) as a function of ranking. This criterion states that a data point is an outlier of a Gaussian (normal) distribution if the probability of such a value being that far from the cumulative mean of the ranked data set is less than 0.5% (Bevington and Robinson 1992, p. 58). The plot of sample standard deviations versus sample rank (Figure 30) varies smoothly within the region of background. Sample 730, with 25.7 TU, exceeds the cumulative mean of 5.3 by 3.4 standard deviations, which exceeds Chauvenet's criterion for identifying statistical outliers for a population of this size. Hence, all values above 25 TU (the value for the preceding sample) are considered to lie outside the range of the population of background samples. The limitation of this approach is that "background" in this case includes post-bomb waters which have returned to pre-bomb tritium levels. A more appropriate statistical analysis would compare the sample data against the results obtained for analytical blanks since the objective is to identify the presence of any tritium with non-zero concentrations as indicative of any component of water less than 50 years old, post-bomb as well as bomb-pulse.

Following this simple statistical analysis, Table 10 summarizes the distribution of pore-water samples in each borehole, according to the total number of samples analyzed for each hydrogeologic unit and the number that exceeded the threshold of 25 TU. Of the 718 samples included in this summary table, 51 had tritium contents above 25 TU. These individual samples are listed in Table 11. These tritium results are summarized below.

6.6.2.3 Summary of Tritium Data

The following discussion summarizes tritium data for drillcore samples from surface-based and ESF boreholes, with respect to the identification of samples containing bomb-pulse tritium (Tables 10, 11 and 12).

TCw samples—Some of the highest tritium concentrations at Yucca Mountain were in TCw samples from the vicinity of the Bow Ridge fault zone. Samples were collected from drillhole HPF#1, which was drilled into the fault zone from the ESF Bow Ridge Fault Alcove (Alcove #2). A concentration of 155 TU was measured for pore water 3.4 m west of the fault within the pre-Rainier Mesa Tuff (LeCain et al. 1997, p. 40). Values of 118 and 128 TU were found in pore waters within the fault breccia. The high values indicate minimal mixing of the percolating fluids with older fluids and may be a consequence of the width of the fault zone at the surface, the lack of alluvium up-slope from the fault, and the shallow depth of the fault where sampled (approximately 20 to 30 m).

None of the 40 TCw samples from seven surface-based boreholes included in the Table 10 summary showed tritium levels above 25 TU.

In UZ#5, a zone of samples with levels above 30 TU occurred in the interval of 28.3 to 36.7 m, at the base of the Tiva Canyon unit, with a peak of 75 TU (corroborative data, Table 12). Collection of these data preceded the establishment of the YMP quality assurance program.

PTn samples—Bomb-pulse tritium was detected in PTn samples from two out of 10 surface-based boreholes. One UZ#16 sample from the Tpcpv2 (48 m), near the top of the PTn, contained 148.5 TU. Five of the 13 PTn samples from NRG-6 contained tritium above 25 TU; these were from the Tpp and Tpbt2 units and spanned a 55-ft interval. In UZ-14, one out of 35 PTn samples contained tritium above the threshold (32 TU in a Tpp sample).

No bomb-pulse tritium was detected in the 104 PTn samples from NRG-7a, UZ-7a, SD-6, SD-7, SD-9, SD-12, or UZ-1, nor in the 3 PTn samples from ESF Alcove 3. PTn samples from three ESF South Ramp drillholes (at stations 6720, 6721 and 6679) also were below the threshold (corroborative data in DTN: GS990183122410.001).

A cluster of four PTn samples with levels of 38 to 45 TU occurred in the interval of 44.8 to 49.5 m in UZ#4, within and below the Yucca Mountain unit (corroborative data, Table 12). Collection of these data preceded the establishment of the YMP quality assurance program.

TSw samples—Bomb-pulse tritium was detected in TSw samples from five out of 10 surface-based boreholes, representing nearly 10% of the 244 samples from this unit. Half of the bomb-pulse results were in UZ#16 samples, in which tritium peaks were observed at several depths: 80 m, 204 m, and the interval of 317 to 357 m. Seven out of 10 WT-24 samples from the Tptpv3 unit contained 26 to 50 TU (depth interval, 1689 to 1703 ft). SD-6, which is located in the bottom of a small wash, had a cluster of elevated tritium values (27 to 30 TU) from a 3-ft interval in the Tptpln at a depth of about 1440 ft. Single occurrences of bomb-pulse tritium were detected in UZ-1 (28 TU at 621 ft) and NRG-7a (47 TU at the top of the TSw at 357 ft).

No bomb-pulse tritium was detected in 7 TSw samples from the drillhole transecting the Ghost Dance fault in the Northern Ghost Dance Fault Access Drift (Alcove 6) (DTN: GS970283122410.002), despite the fact that elevated levels of ^{36}Cl were measured in Alcove 6 (see section 6.6.3). This negative result is corroborated by analyses of 9 other samples from this drillhole (DTN: GS9901083122410.001).

Seventeen samples from ESF boreholes were analyzed following isotope enrichment, resulting in analytical uncertainties of ±0.2 TU or less, more than an order of magnitude lower than analytical uncertainties for conventional counting without enrichment. Of this set, the highest tritium activity was 1 TU in ESF-SR-MOISTSTDY#7; other samples were from ESF Alcove #6, ESF-NDR-MF#1, South Ramp holes #1, 2, 5, 6, and 7, and North Ramp holes #4, 13 and 16 (DTN: GS990183122410.004). Because of the potential for isotopic exchange with tunnel air, this result is not considered to indicate the presence of bomb-pulse or post-bomb tritium

CHn unit above the Prow Pass—Of 144 CHn samples above the Prow Pass from seven surface-based holes, bomb-pulse tritium was detected in two samples from UZ#16 (about 43 and 104 TU), separated by 37 ft.

Prow Pass Tuff—In the Prow Pass portion of the CHn at about 1752 ft (30 to 43 TU). One sample from the Prow Pass in SD-12 contained 39 TU (Table 11). All tritium analyses from SD-7 and SD-9 are less than 25 TU.

Perched water— Isotopic compositions have been measured in perched water from four Yucca Mountain boreholes (Table 9). None of the tritium analyses were above the 25 TU threshold indicating the presence of bomb-pulse tritium.

Summary—Tritium data for some of the unsaturated-zone boreholes show several inversions in which samples with larger tritium concentrations occur below background values in a vertical profile (Yang et al. 1996, p. 31). These inversions suggest that vertical water percolation through the rock matrix is not the predominant flow mechanism in the unsaturated zone for all stratigraphic units at Yucca Mountain. The occurrence of detectable tritium in waters below non-tritium-bearing water (and hence older water) in a vertical profile is strong evidence for the occurrence of fracture and lateral flow at Yucca Mountain.

6.6.3 Chlorine-36

Primary input data used to characterize the distribution of chlorine-36 at Yucca Mountain, which provides a basis for water travel time estimates, are listed in section 4.1.6. Assumptions 5, 6 and 7 in Table 2 apply to discussions in this section.

6.6.3.1 Background

Measurements of chloride (Cl^-) concentrations and $^{36}Cl/Cl$ for salts extracted from water, soil, and rocks have been used to provide information on characteristics of water movement and solute transport through the unsaturated zone at Yucca Mountain (Fabryka-Martin, Wolfsberg et al. 1997, pp. 75, 77 to 79; Fabryka-Martin, Wolfsberg, Levy, Roach et al. 1998, p. 93; Fabryka-Martin, Wolfsberg, Roach et al. 1998, p. 264; Wolfsberg et al. 1998, p. 81). Chlorine-36 is a radioactive isotope of chlorine, with a half-life of 3.01×10^5 years (Parrington et al. 1996, p. 22), and in nature, it occurs primarily as the chloride anion. As such, it is relatively inert in the subsurface environment and behaves conservatively. This radionuclide is present in infiltrating waters as a natural tracer produced mainly in the upper atmosphere by the bombardment of argon gas by cosmic radiation (Clark and Fritz, 1997, p. 232):

$$\begin{aligned} {}^{40}Ar + p &\Rightarrow {}^{36}Cl + n + a \\ {}^{36}Ar + n &\Rightarrow {}^{36}Cl + p \end{aligned} \qquad \text{(Eqn 4)}$$

where n = neutron, p = proton, and " = alpha particle. Common Cl in the atmosphere is also irradiated by the atmospheric neutron flux to produce Cl and gamma radiation:

$$^{35}Cl + n \Rightarrow {}^{36}Cl + g \qquad \text{(Eqn 5)}$$

The relatively long half-life of ^{36}Cl theoretically permits the detection of travel times up to several hundred-thousand years. To normalize the data for the variable effects of evapotranspiration, the ^{36}Cl concentration is generally reported relative to that of stable Cl^-. Expressed in this manner, the present-day background level of $^{36}Cl/Cl$ is 502 ($\pm$ 53) x 10^{-15} (Table 25, discussed in Section 6.9.2.3).

Global fallout from thermonuclear tests conducted primarily in the Pacific Proving Grounds resulted in a ^{36}Cl "bomb pulse" with maximum meteoric ratios in excess of 200,000 x 10^{-15} (Figure 29). These extremely high values were diluted by mixing processes in the soil zone and subsurface and are not observable today. Nevertheless, high $^{36}Cl/Cl$ (those greater than about 1250 x 10^{-15}) indicate some bomb-pulse component, and their appearance in an environmental sample signals the presence of at least a small component of bomb-pulse ^{36}Cl. Present day $^{36}Cl/Cl$ in surface soils at Yucca Mountain are generally in the range of 1500 x 10^{-15} to 3000 x 10^{-15} (CRWMS M&O 1998, p. 3-5). In subsurface water, high ratios suggest travel times from the ground surface of 50 years or less.

Although the existence of bomb-pulse ^{36}Cl enables the study of solute transport with travel times of 50 years or less, the natural cosmogenic background permits analysis of much longer-term transport processes. However, the use of $^{36}Cl/Cl$ for dating older waters is not as straightforward as the case for bomb-pulse signals due to the time-varying input signal. Both theoretical considerations as well as measurements of soil profiles and fossil urine from ancient pack-rat middens support the hypothesis that the present-day background ratio has remained relatively constant during the Holocene (last 10 ka) (Plummer et al. 1997, Figure 3B). Expected lower rates of stable Cl deposition during the Pleistocene (10 ka to 2 Ma), in combination with higher rates of cosmogenic ^{36}Cl deposition as a result of Southern shifts in the jet stream, would have led to higher local meteoric $^{36}Cl/Cl$, relative to those that were present throughout the Holocene (Plummer et al. 1997, p. 540). Superimposed on this effect are varying atmospheric ^{36}Cl production rates caused by variations in the Earth's geomagnetic field. Based on these two factors, the meteoric $^{36}Cl/Cl$ at Yucca Mountain has been reconstructed for the last 1.8 Ma (Fabryka-Martin, Wolfsberg et al. 1997, pp. 4 to 5). Analyses of $^{36}Cl/Cl$ in pack-rat midden samples dated by the ^{14}C technique are generally consistent with the reconstruction, although these data can only cover the last 40 ka due to the comparatively short half-life of ^{14}C (Figure 31).

Chlorine-36 is also produced in rocks due to a low but ubiquitous neutron flux resulting from the decay of uranium and thorium isotopes and their daughters, but these background levels are low relative to those that have been measured in Yucca Mountain water samples (Fabryka-Martin, Wolfsberg et al. 1997, pp. 8 and 13, and Table 5-3). Although uranium concentrations reach several hundred ppm in some silica deposits lining fractures in the unsaturated zone at Yucca Mountain, such concentrations do not elevate the local neutron flux (or ^{36}Cl production rates) because the flux is determined by uranium and thorium concentrations averaged on a much larger scale (e.g., 10^4 cm^3).

Together the bomb-pulse record and the long-term reconstruction allow $^{36}Cl/Cl$ observations in subsurface fluids at Yucca Mountain to be divided into four classes:

- Ratios over 1250 x 10^{-15} provide clear evidence of bomb-pulse influence, and indicate the presence of some rapid transport pathways (Fabryka-Martin, Wolfsberg et al. 1997, p. 18).

- Ratios near the present-day value of 500 x 10^{-15} suggest Holocene precipitation of pre-nuclear-age (from 1950, extending back to about 10 ka before the present) (Figure 31a). A value of 500 x 10^{-15} is very unlikely to indicate extremely young (post-1980)

precipitation because bomb-pulse ^{36}Cl is still widely prevalent in surface soils at Yucca Mountain, based on analyses of surface soils and surface runoff.

- Ratios that are elevated above present-day background but less than 1250×10^{-15} cannot be interpreted unambiguously in terms of water travel time, in the absence of additional geochemical or isotopic information. These may be attributed to Pleistocene-aged water that is not so old as to unequivocally demonstrate radioactive decay (note elevated ratios at the end of the Pleistocene in Figure 31b; Fabryka-Martin, Wolfsberg et al. 1997, pp. 4 to 5). Alternatively, these ratios may reflect the presence of a small component of bomb-pulse ^{36}Cl, possibly as low as a percent of the total flow.

- Ratios significantly less than 350×10^{-15} clearly show the effects of radioactive decay of ^{36}Cl. Actual estimates of water age will depend on the past meteoric ratios, which must be considered highly speculative for the period before the earliest packrat data (40 ka). However, based on the current reconstruction, these ratios imply ages in excess of 200 ka.

Unfortunately, the interpretation of a given sample in one of the above categories is not always clear-cut. Only interpretation of the highest ratios (indicating bomb-pulse water) and the lowest ratios (indicating radioactively decayed ancient water) may usually be considered relatively unequivocal. Intermediate ratios may represent Holocene or Pleistocene input with corresponding travel times or may represent mixtures of waters of different ages. Nonetheless, the intermediate ratios shed light on the interpretation of water ages when considered in conjunction with other independent lines of evidence, such as other isotopic measurements and infiltration studies and results of flow and transport simulations of alternative conceptual models.

Over 900 ^{36}Cl measurements have been conducted thus far for the Yucca Mountain Project. Analyzed samples include surface soils and soil profiles; rock samples collected from surface-based boreholes, the ESF, and the Cross Drift; water samples including surface runoff, unsaturated-zone pore water, perched water, and saturated-zone water; and fossilized urine from pack-rat middens. Observations from these sample analyses are summarized in Table 13 and discussed below.

6.6.3.2 Chlorine-36 in Shallow Samples

Analyses of bomb-pulse ^{36}Cl and Cl profiles in soil and alluvial profiles show that thick alluvium is generally effective at reducing net infiltration to levels less than 1 mm/yr (Fabryka-Martin, Turin et al. 1996, section 5.1.2) (e.g., see data for soil from pits and trenches in DTN: LAJF831222AQ95.006 and LAJF831222AQ96.006). An exception to this generalization may be in channels and at the base of sideslopes, as illustrated by the penetration of bomb-pulse ^{36}Cl into the soil exposed at the NRG#5 drill pad (DTN: LAJF831222AQ95.005) and in samples as deep as 3.3 m in the soil-test pit NRSF-TP-19 at the North Portal (DTN: LAJF831222AQ97.006).

Similarly, borehole samples collected from the PTn when this rock unit is overlain by thick alluvium do not show any evidence for the presence of bomb-pulse ^{36}Cl (e.g., data for UZ-N37,

UZ-N54, UZ#16, and UZ-14 in DTN: LAJF831222AQ96.010, LAJF831222AQ96.012, LAJF831222AQ96.014, and LAJF831222AQ96.015, respectively).

In contrast, where alluvial cover is thin (for example, less than a few meters thick) or missing, water is able to readily enter fractures of the bedrock, as shown by the detection of bomb-pulse ^{36}Cl measurements in samples from such locations (e.g., see data for neutron boreholes in DTN: LAJF831222AQ96.008, LAJF831222AQ96.009, LAJF831222AQ96.011 and LAJF831222AQ96.013). For example, fast transport through the welded Tiva Canyon (TCw) is indicated by bomb-pulse ^{36}Cl/Cl ratios measured in several boreholes that intersect the nonwelded Paintbrush Tuff (PTn), which lies below the TCw. Bomb-pulse levels of ^{36}Cl were also observed in drillcore samples from the top of the Calico Hills unit in the shallow Busted Butte Field Transport Facility (DTN: LA9909JF831222.005).

6.6.3.3 Bomb-Pulse ^{36}Cl in the Exploratory Studies Facility and Cross Drift

Evidence for fast pathways that persist into the TSw is provided by bomb-pulse ^{36}Cl/Cl ratios measured at locations in the ESF and Cross Drift (Figure 32 and Table 14). Over 250 samples have been analyzed from the 8-km ESF tunnel including two of its niches and alcoves. Of these, more than 40 had ^{36}Cl levels sufficiently elevated as to be interpreted as unambiguous evidence for the presence of bomb-pulse ^{36}Cl (DTN: LAJF831222AQ98.004, LAJF831222AQ98.009 and LA9909JF831222.010). For example, bomb-pulse ^{36}Cl was detected in the Drillhole Wash fault zone, in the vicinity of the Sundance fault zone in the Main Drift and ESF Niche #1, and near the Sundance fault zone and the Ghost Dance fault zone where they were intersected by the Northern Ghost Dance Fault Access Drift (Alcove 6). Similar to the ESF results, five out of 15 Cross Drift samples had ratios above 1250 x 10^{-15}, and nine were above 1000 x 10^{-15} (DTN: LA9909JF831222.003).

The correlation of the elevated ^{36}Cl measurements with the surface expression of faulting indicates that the pathway and travel time may involve locally modified PTn fracture properties (Fabryka-Martin, Wolfsberg et al. 1997, p. 78; Fabryka-Martin, Flint et al. 1997, pp. 6-22 and 8-18). These data support the hypothesis that faulting or other disturbances increase PTn fracture permeability, thereby generating a local environment in the PTn that supports fracture flow and hence rapid transport of solutes. Once through the PTn, flux distributions favor fracture flow in the TSw, thereby providing a continuous pathway to the sampled depths.

6.6.3.4 Non-Bomb-Pulse ^{36}Cl in the Exploratory Studies Facility

Most of the ESF sample analyses had ratios less than the threshold for indicating bomb-pulse ^{36}Cl (Figure 32). In the southern part of the ESF, beyond station 45+00, most samples had ^{36}Cl/Cl ratios typical of Holocene water, which could suggest travel times less than 10 ka to this depth. (Averages of water with greater and lesser values provide a less likely explanation because the mixing proportions would have to be the same for the large number of samples). A number of samples from this part of the system also had ^{36}Cl signals that were significantly below the present-day background value, suggesting the possible presence of zones of relatively stagnant water.

Many of the samples from the northern part of the ESF, up to station 45+00, had $^{36}Cl/Cl$ ratios variably above the present-day background and provide a striking contrast to the nearly-constant ratios measured in the southern part of the ESF (Figure 32). The largest signals–those above a ratio of $1250x10^{-15}$–are attributed to global fallout ^{36}Cl. Fabryka-Martin, Wolfsberg et al. (1997, pp. 19 and 21) discuss alternative hypotheses to account for these highly elevated signals and rule out sample contamination as well as *in-situ* production of ^{36}Cl either at the surface or deeper in the profile. The favored hypothesis is that fast hydrologic paths capable of conducting bomb-pulse ^{36}Cl to the level of the ESF are more prevalent in the northern part of the ESF than in the southern part, due to a greater number of faults in the north that cut through the comparatively unfractured PTn where it overlies the ESF. With regard to those intermediate samples with ratios greater than present-day background but less than 1250×10^{-15}, it is not presently possible to assess whether or not these intermediate signals indicate the presence of a very small component of bomb-pulse ^{36}Cl or whether the elevated signals reflect travel times exceeding 10 ka, the most recent time when the signal in infiltrating water would have been high enough to provide the $^{36}Cl/Cl$ signatures found in water from this area.

6.6.3.5 Chlorine-36 in Deep Boreholes

Measured $^{36}Cl/Cl$ ratios for samples of moderately to densely welded tuff from boreholes are systematically lower than the values for ESF samples. This apparent discrepancy is probably attributable to differences in the sample collection techniques (Fabryka-Martin, Turin et al. 1996, section 6.2). Borehole samples are obtained from ream cuttings. Rock Cl is released to the cuttings during drilling and, subsequently, is leached together with the pore-water Cl during sample preparation for ^{36}Cl analysis. This source of Cl has a $^{36}Cl/Cl$ ratio on the order of 40×10^{-15}. The extent to which rock Cl contributes to the total amount of Cl leached from the rock can be estimated from its Br/Cl ratio (Fabryka-Martin, Wolfsberg et al. 1997, pp. 30 to 32; Fabryka-Martin, Turin et al. 1996, section 6.2.1). Because of the low $^{36}Cl/Cl$ of the rock Cl, the $^{36}Cl/Cl$ calculated for the meteoric component of Cl in the borehole samples is always equal to or higher than the measured ratio. Samples collected from tunnel walls are not as greatly affected by rock Cl as are borehole samples because the manual method of collection used in the tunnel does not pulverize the rock as does the ream bit. Borehole samples from nonwelded units (PTn, CHn, Prow Pass) also do not appear to be greatly affected by the release of rock Cl, probably because the concentration of leachable rock Cl in these particular units is negligibly small relative to that in the pore-water fluids. Differences between uncorrected $^{36}Cl/Cl$ ratios for borehole samples from welded units and those from the ESF demonstrate the importance of recognizing the magnitude of the influence of rock Cl to the $^{36}Cl/Cl$ values measured for borehole samples. After correcting for this effect, the two sets of analyses are consistent (Fabryka-Martin, Wolfsberg et al. 1997, p. 33). None of the few $^{36}Cl/Cl$ measurements available for samples collected below the potential repository horizon are sufficiently high as to indicate the unambiguous presence of bomb-pulse ^{36}Cl (Table 13, Observations for TSw and CHn samples). The maximum ratio measured for a surface-based borehole sample in or below the Tptpul unit was 843×10^{-15} for SD-12 (1940 to 1941 ft, Tcp2 unit; LAJF831222AQ97.007).

6.6.3.6 Chlorine-36 in Perched Water

The variation of input signal for $^{36}Cl/Cl$ over time enables $^{36}Cl/Cl$ measurements in perched water (Table 9) to be interpreted in support of ^{14}C ages. Figure 31b shows that co-variation of ^{14}C and $^{36}Cl/Cl$ is irregular but can be smoothed as a "meteoric water curve" (Figure 33). This co-variation can be used as corroborative data to support interpreted ^{14}C ages as being less than or greater than about 10,000 years. For example, ^{14}C activity is plotted against $^{36}Cl/Cl$ for perched water samples on the same curve (Figure 33). The data match the meteoric water curve well and the ages of the perched water can be estimated by interpolation along the meteoric water curve. Chlorine-36 and other isotopic analyses of perched water provide a consistent estimate of the age of the perched water bodies. Ages of the perched water can be estimated by interpolation along a characteristic curve based on a predicted correlation between reconstructed ^{14}C and ^{36}Cl input functions for the past 25 ka. By this approach, the ^{36}Cl analyses indicate ages ranging from 2 to 12 ka for the different perched-water bodies sampled, which is in general agreement with ^{14}C-based ages. However, there is substantial uncertainty in attributing $^{36}Cl/Cl$ data to particular ages above 10,000 years, as well as uncertainty in the quantitative interpretation of ages from ^{14}C data.

6.6.3.7 Consistency of Data with Site-Scale Flow and Transport Models

A flow and transport model using the FEHM code was used to simulate transport of ^{36}Cl into the ESF tunnel (Fabryka-Martin, Wolfsberg et al. 1997, pp. 78 to 79). Modeling results show that observed ^{36}Cl signals are consistent with the above site-scale conceptual model and with reasonable parameter estimates. The overall picture from these studies is that:

- Infiltration is spatially variable and, on the average, exceeds 1 mm/year over the potential repository block.
- Fracture transport can be critical, permitting rapid transport through otherwise low-conductivity materials.
- Isolated fast paths associated with faults and fractures may penetrate deep into the mountain.

These modeling studies showed that the arrival of even small (1 percent of the input flux) amounts of bomb-pulse ^{36}Cl at the ESF and Cross Drift horizon in under 50 years generally required percolation fluxes of at least 1 to 10 mm/year, depending on the characteristics of the secondary permeability assumed for the model layers corresponding to the PTn (Fabryka-Martin, Wolfsberg et al. 1997, Tables 8-4 to 8-6). This modeling study considered the stratigraphy at two locations within the ESF, one where the thickness of the PTn was large (ESF station 35+00) and one where the PTn was relatively thin (ESF station 59+00). Conclusions drawn from the one-dimensional modeling study included the following (Fabryka-Martin, Flint et al. 1997, section 8.3):

- Generally, fracture flow through the PTn could be sustained more readily with increases in percolation flux and secondary permeability, and when fractures contributing to the secondary permeability were assumed to be sparse (thereby minimizing fracture-matrix interactions) and have large apertures.

- Increases to the assumed water retention capacity of the fractures by adjusting poorly constrained parameters that described the fracture's capillary properties also resulted in more sustained fracture or fault flow through the PTn at lower fluxes.

- Fluxes insufficient to sustain fracture flow in the densely welded Tiva Canyon and Topopah Spring Tuffs resulted in water samples at the ESF that were very old, with predicted ^{36}Cl/Cl ratios that indicated significant decay (approximately 300 x 10^{-15} to 600 x 10^{-15}) and which were generally too small relative to those obtained for what were considered to be non-bomb-pulse samples (500 x 10^{-15} to 1,500 x 10^{-15}).

- The predicted ratios for non-bomb-pulse samples were generally consistent with those predicted using assumed percolation fluxes of 1 to 10 mm/year. Just as fluxes on the order 0.1 mm/year led to ^{36}Cl/Cl ratios at the ESF horizon that displayed considerable decay of the meteoric signal, fluxes greater than 10 mm/year resulted in short travel times that led to introduction of Holocene water with ^{36}Cl/Cl ratios lower (500 x 10^{-15}) than observed for the non-bomb-pulse samples.

6.6.4 Carbon Isotopes

Primary input data used to characterize the distribution of carbon-14 at Yucca Mountain, which provides a basis for water and gas travel time estimates, are listed in section 4.1.7 (pore water and perched water), 4.1.8 (gas from open boreholes), 4.1.9 (gas from instrumented boreholes), and 4.1.15 (groundwater). Table 3 lists the locations for which these data are available. Relevant assumptions that apply to discussions in this section are Assumptions 8, 9 (TBV) and 10 in Table 2.

6.6.4.1 Background

The best-developed isotopic method for dating groundwater is that using ^{14}C, an application that began with Munnich's study in 1957 (Davis and Murphy 1987, pp. 29 to 34; Clark and Fritz 1997, pp. 200 to 231). Carbon-14 is produced naturally in the upper atmosphere by bombardment of nitrogen by the secondary neutron flux (Clark and Fritz 1997, p. 202):

$$ {}^{14}_{7}N + {}^{1}_{0}n \Rightarrow {}^{14}_{6}C + {}^{1}_{1}p \qquad \text{(Eqn 6)} $$

The modern atmospheric activity of ^{14}C is set by convention to 13.56 decays per minute per gram of carbon in the year A.D. 1950, which is considered to have an activity of 100 Percent Modern Carbon (pmc) (Clark and Fritz 1997, p. 18). Based on a half-life of 5,715 years (Parrington 1996, p. 19), this specific activity corresponds to a ^{14}C/C ratio of about 1.2 x 10^{-12}. The effect of above-ground testing of nuclear devices was to temporarily increase the ^{14}C content by as much as a factor of two (Figure 29). The decrease since 1964 is due to the exchange of ^{14}C for nonradioactive carbon from the biosphere and hydrosphere, predominantly the ocean. Other secondary influences on the atmospheric ^{14}C inventory are releases of ^{14}C from nuclear fuel reprocessing plants and dilution by releases of nonradioactive carbon from the burning of fossil fuels.

Despite its extensive use in hydrologic studies, numerous processes related to carbon geochemical reactions complicate the interpretation of ^{14}C analyses in water. These processes involve the isotopic exchange between carbonate species dissolved in pore water, and carbonates in soil and fracture minerals along the flow path, as well as with CO_2 in the gas phase. Hence, the successful use of ^{14}C to date groundwater is dependent upon a thorough understanding of geochemical reactions involving carbon species in the hydrologic system. This stipulation is even more important in the case of unsaturated-zone fluids. Stable carbon isotope ratios ($\delta^{13}C$ values) are invaluable for evaluating the likelihood and magnitude of subsurface reactions involving carbon. Delta ^{18}O has been measured in CO_2 gases in YMP studies for a similar reason. Detailed discussions of geochemical modeling of carbon reactions, which clearly have implications for ^{14}C ages of Yucca Mountain pore waters, are provided in numerous publications (Davis and Murphy 1987, pp. 29 to 34; Clark and Fritz 1997, pp. 200 to 231).

6.6.4.2 Carbon-14 in Pore-water Samples

As is the case for tritium, post-bomb levels of ^{14}C have been observed in a few samples collected above and within the PTn unit. None of the pore-water samples from surface-based boreholes have shown post-bomb levels of ^{14}C, that is, activities above 100 pmc (Table 15; corroborative data in Table 16). However, it is possible that the presence of a relatively small volume of post-bomb water could be obscured by mixing with a large volume of old water, such that the resulting mixture would have an activity less than 100 pmc. For the 14 pore-water samples extracted from the PTn unit, ^{14}C activities range from 74 pmc (NRG-7a and SD-7) to 96 pmc (UZ-14) (Table 15). The 33 samples extracted from the CHn unit range from 53 pmc (UZ#16) to 98 pmc (UZ#16) (Table 15). A histogram of the data from these two hydrogeologic units (Figure 34) shows that the PTn values cluster tightly about the range of 80 to 90 pmc, whereas the CHn values spread more evenly across the range, presumably reflecting a larger spread in groundwater travel times to this depth as would be expected if fracture flow were mixing to variable extents with slower matrix flow. Stable carbon isotope ratios for these same pore waters show a wide range in both hydrogeologic units (Figure 34), which may be a consequence of a variety of processes but which is also consistent with spatially and temporally variable infiltration rates and mixing between fast fracture flow and slow matrix flow. The extent of contamination with drilling air for some of the samples has not yet been resolved (see discussion below).

The ^{14}C pore-water data do not show any trend with stratigraphic depth, with larger ^{14}C activities interspersed among smaller ^{14}C activities in a vertical profile (Tables 15). These irregular profiles are consistent with a conceptual model in which fracture flow and perhaps lateral flow occur in some of the stratigraphic units at Yucca Mountain (Yang et al. 1996, p. 32; Yang, Yu et al. 1998, p. 23). In general, ^{14}C activities in pore waters from both the PTn and CHn suggest apparent ages that are less than 6,000 years. Apparent ages are based on the assumption that the initial ^{14}C activity is 100 pmc, and that the carbon isotopic composition of the sample has not been significantly altered by any geochemical processes such that changes relative to the initial atmospheric activity are solely the result of radioactive decay (Assumption 10 in Table 2). This assumption is supported by the high ^{14}C activities measured in the annulus of shallow boreholes (Table 17).

Detailed evaluations of the various processes that could affect ^{14}C activities and stable carbon isotope ratios in Yucca Mountain pore waters are presented in Yang et al. (1996, pp. 31 to 34) and in Yang, Yu et al. (1998, pp. 21 and 23). These processes include:

- Atmospheric contamination of pore-water samples during drilling could shift ^{14}C activities to higher values.
- $^{14}CO_2$ in the gaseous phase may exchange with bicarbonate species in the groundwater.
- Seasonal variations in $\delta^{13}C$ in soil gas as a function of the stage of vegetative growth affect the isotopic signature in infiltrating waters.
- Dissolution of caliche and calcites in fractures, with their wide variations in ^{14}C ages, can dilute the initial ^{14}C activity of infiltrating pore water and shift its $\delta^{13}C$ value.

To some extent, the significance of these processes can be evaluated by examining the $\delta^{13}C$ and ^{14}C data for trends as a function of borehole, depth, and stratigraphic unit and by comparing pore-water data to those for the gas phase, perched water and groundwaters for which some of the above processes can be assumed to be negligible. Figure 35 plots $\delta^{13}C$ versus ^{14}C for these different categories. This plot suggests the idea that some of the high ^{14}C pmc values and young apparent ages may be the result of contamination from $^{14}CO_2$ in the drilling air (about 120 pmc, $\delta^{13}C$ about -8 ‰). Although the total mass of carbon in pore water is orders of magnitude higher than that in subsurface air, it is possible that the injection of large volumes of drilling air may alter the carbon isotopic composition of pore waters under some conditions.

6.6.4.3 Carbon-14 in Gas Samples

Gas samples were collected from open surface-based boreholes following overnight pumping to remove atmospheric air from the well bore (Tables 18 and 19). Gas samples have also been collected from two instrumented surface-based boreholes, with records available from 1984 to 1995 for UZ-1, and for 1996 for SD-12 (Table 20). Finally, gas samples from ESF drillholes were collected after CO_2 and SF_6 concentrations had stabilized (Table 21) (section 6.2.2).

The carbon isotope data for gas samples are discussed in greater detail in Section 6.7.2. The observed distribution can be summarized as follows:

Gas samples in open surface-based boreholes (Tables 18 and 19)—Uncorrected radiocarbon ages range from modern to 2600 years in the TCw, modern to 3100 years in the PTn, 650 to 7200 years in the Tptpul and Tptpmn, and modern to 11,200 years in the CHn. Radiocarbon profiles generally do not show any clear trend, with apparently younger gas often underlying older gas. However, for gas collected from open boreholes, it is often difficult to discern a clear trend with respect to the spatial distribution of ^{14}C activities in unsaturated-zone gases. The downhole packer system did not completely seal against the borehole wall for all of these samples. Thus trends are obscured by the inclusion of data that probably show the effects of atmospheric contamination. Although $\delta^{13}C$ and CO_2 concentrations can often be used to identify such contamination, there is no simple rule by which to identify which ^{14}C activities represent *in-situ*

conditions because $\delta^{13}C$ and CO_2 also vary in the subsurface as a function of surface conditions (e.g., soil thickness and vegetative activity). Nor are ^{14}C activities in nearby pore waters a good guide. If the CO_2 in the gas phase were in isotopic equilibrium with CO_2 in the aqueous phase of the pore water, then the ^{14}C activities in the two phases should be comparable; however, the pore waters themselves may have been contaminated by the drilling air. Because of these various unresolved issues, Yang et al. (1996, p. 32) conclude "it would be difficult to make a good age correction. However, a possible range of ages with some uncertainty can be assigned in the future when more data become available. At present, apparent ages will be used to make preliminary interpretation."

Gas samples in instrumented surface-based boreholes (Table 20)—Carbon-14 data from samples from the two instrumented boreholes are the most reliable indicators of *in-situ* conditions. Uncorrected radiocarbon ages for UZ-1 are modern at the probe near the top of the PTn (62 ft), about 3600 years at the probe closest to the base of the PTn (266 ft), about 7000 years at a depth of 621 ft in the Tptpmn, and about 7800 and 16,000 years at the bottom two probes, in the Tptpll (1100 and 1207 ft). Uncorrected ages for SD-12 of similar magnitude although the profile is not as smooth. The gas age is about 1000 years at the top of the PTn and about 2100 years at its base. The age increases to nearly 8000 years in the Tptpul, and to about 11,000 years at probe B near the top of the CHn.

Gas samples from instrumented boreholes in ESF alcoves (Table 21)—Carbon-14 isotope results are available for gases from boreholes in ESF Alcove 1 and 6. Samples from three boreholes in Alcove 1, all tapping intervals within the TCw unit, contained 93, 101 and 107 pmc indicating the presence of young CO_2. Ten samples from the Alcove 6 borehole, which penetrated the Ghost Dance fault zone in the TSw unit, ranged from 75.1 to 58.1 pmc, corresponding to uncorrected ^{14}C ages of 2400 to 4500 years, somewhat younger than those obtained for similar stratigraphic depths in UZ-1 and SD-12. Activities measured for gas samples from boreholes ESF-NDR-MF#1 and ESF-NDR-MF#2 ranged from 73.8 to 64.8 pmc, corresponding to ages of 2500 to 3600 years (DTN: GS981283122410.006, corroborative data).

6.6.4.4 Carbon-14 and d^{13}C in Perched Waters

Carbon-14 activities and $\delta^{13}C$ values of perched waters are shown in Table 9. The ^{14}C values range from 67 to 27 pmc, corresponding to apparent ^{14}C residence times of about 3300 to 11,000 years (Yang et al. 1996, p. 34). Water ^{14}C ages can be affected by the dissolution of older carbon in the carbonate minerals, which would result in anomalously old apparent ages. Reaction with or incorporation of gas-phase CO_2 from deep in the unsaturated zone can also result in an anomalous apparent age. Recent input of post-bomb ^{14}C is expected to be minor because all perched-water samples contain background tritium concentrations. If post-bomb water is present in the perched bodies, the component is too small to be detectable.

The $\delta^{13}C$ values measured for perched water are quite variable, ranging from -9.2 to -16.6 ‰ (Table 9). A weak correlation is observed between these values and the surface material in which the drillhole is located. Perched water in SD-7, a borehole that is essentially started in bedrock, has heavy values of about -9.5 ‰, only slightly lighter than atmospheric CO_2. In contrast, perched water from NRG-7a, which was drilled through soil, has the lightest value of -16.6 ‰,

presumably reflective of the isotopic composition of soil CO_2 gas. This observation is similar to that made for strontium isotopic data, which show a less radiogenic input for bedrock and fracture coatings where there is no soil and for pore waters from a drillhole that was started in bedrock (Section 6.6.6). In summary, $\delta^{13}C$ data show that most of the bicarbonate in unsaturated-zone matrix pore fluids originated in the soil zone. In contrast, most of the perched-water bodies and groundwater in the Yucca Mountain area have heavier (less negative) $\delta^{13}C$ values that do not show the same degree of soil influence as do the unsaturated-zone pore waters (Figure 35).

6.6.5 Stable Hydrogen and Oxygen Isotopes

None of the stable hydrogen and oxygen isotopic data used in this report are considered to be primary input data. These data are used solely to corroborate interpretations of water flow paths and the timing of recharge that are based on other geochemical and isotopic signatures. Table 3 lists the locations for which stable isotope data are available. Assumptions 11, 12, 13 and 14 from Table 2 apply to discussions in this section.

6.6.5.1 Background

Large differences in hydrogen and oxygen isotopic ratios ($\delta^{2}H$ and $\delta^{18}O$) in water arise from phase changes that do not go to completion, that is, partial evaporation, condensation, crystallization, or melting (Davis and Murphy 1987, p. 119). Such incomplete processes are typical of rainfall, snowfall, evapotranspiration, and sublimation of snow and ice. As a consequence, regional differences arise in surface waters as a function of elevation, distance from water sources (such as the ocean), orographic (rain shadow) effects, degree of evaporation, and air temperature during precipitation. If the first four of these factors stay relatively constant for a given location, then variations in $\delta^{2}H$ and $\delta^{18}O$ in infiltrating water may be related to temperature variations during precipitation events. Factors that might complicate simple interpretations of such data at Yucca Mountain include shifts in $\delta^{18}O$ in pore waters due to: alteration, dissolution, or precipitation of minerals containing oxygen; isotopic exchange; and sorption of water by clays and zeolites (Yang, Yu et al. 1998, p. 24).

6.6.5.2 Isotopic Characteristics of Precipitation, Surface Waters, Perched Water and Groundwater

The standard method for presenting stable isotope data is by plotting $\delta^{2}H$ versus $\delta^{18}O$, as has been done in Figure 36 for precipitation, surface waters, perched water, and regional groundwater. The following observations are made from this figure:

- Precipitation data from 3 Springs Basin and Stewart Basin are plotted in Figure 36a. These data illustrate how fractionation of oxygen and hydrogen isotopes in atmospheric moisture results in a well-defined correlation line, called the “meteoric water line.” Interpretations of isotopic data for other waters are all based upon the extent to which their compositions shift along or away from this line. Based on its lower elevation and warmer temperatures, modern precipitation at Yucca Mountain is generally expected to fall along the upper end of the range shown, with heavier (less negative) compositions as demonstrated by four local precipitation samples plotted in Figure 36.

- Surface water data from 3 Springs Basin and Stewart Basin (Figure 36b) illustrate how stable isotopes reflect average climatic conditions prevailing during infiltration events. The cooler climate at Stewart Basin results in lighter (more negative) isotopic compositions. These surface waters have not undergone much evaporation, based on the fact that the isotopic data plot on the meteoric line. Such a conclusion is supported by the dilute chemical compositions of these waters (Section 6.4.3). Data for two Yucca Mountain surface runoff samples, both collected in February 1993, also show negligible evaporation. Their heavy isotopic signatures overlap with those of the four precipitation samples collected at Yucca Mountain in 1984 (Figure 36a).

- Stable isotopic data of the perched-water samples also lie close to the meteoric water line, indicating little evaporation occurred before infiltration (Figure 36c).

- Groundwaters beneath Fortymile Wash (Figure 36d) have stable isotope values similar to those for perched water beneath Yucca Mountain. Both of these data sets are consistent with recharge during the Holocene (that is, post-glacial climate), as suggested by the ^{14}C data for these waters (Section 6.6.4; Figures 35c and 35d).

- Among the groundwaters in the Yucca Mountain area, the lightest waters are from wells in the southwestern most portion of the site (for example, VH-1, WT#10, H-3). Local groundwaters with the heaviest isotopic values overlap with the values measured for perched waters and for wells in Fortymile Wash.

- Groundwaters from Pahute Mesa have lighter isotopic values than do the perched waters and groundwaters from Fortymile Wash. This difference is consistent with recharge of the Pahute Mesa waters under colder climatic conditions than those that prevailed for the perched waters and samples from Fortymile Wash, and subsequent modification of the Pahute Mesa waters by water-rock interactions that shift $\delta^{18}O$ to heavier values. Although isotopic shifts due to evaporative loss cannot be altogether ruled out, this process seems unlikely to be significant for the Pahute Mesa recharge waters.

6.6.5.3 Isotopic Characteristics of Pore Waters

Extraction of Pore Waters for Isotopic Analysis—In contrast with the above types of samples, hydrogen and oxygen isotope data for unsaturated-zone pore waters are more difficult to interpret, presumably due to complications related to the methods used to extract the fluids for analysis. Vacuum distillation and compression extraction ("squeezing") were the two methods of pore-water extraction for stable-isotope analysis of $\delta^{2}H$ and $\delta^{18}O$ used in the site-characterization investigation (Yang, Yu et al. 1998, pp. 25 to 27). Vacuum distillation involves heating the rock sample under vacuum in a distillation apparatus and collecting and condensing the evolved water vapor in a separate flask. Compression extraction is similar to the procedures described previously for pore-water extraction for chemical compositions and ^{14}C analyses. Water samples were collected in glass syringes attached to the compression cell. For both extraction methods, stable isotope ratios are determined by mass spectrometer.

Testing for isotopic effects resulting from the two different water-extraction procedures was accomplished by analyzing adjacent core samples (Yang, Yu et al. 1998, pp. 30 to 33). The two methods yielded comparable results for samples from the PTn. However, isotopic compositions of water obtained by vacuum distillation are more depleted in δ^2H and $\delta^{18}O$ than water obtained by the compression method for cores containing clay or zeolite minerals, particularly for samples from CHn, Prow Pass Tuff, and Bull Frog Tuff (Yang, Yu et al. 1998, Figures 15 and 16). Subsequent tests have shown that vacuum distillation of pore waters for stable isotope analysis produced reliable results from tuffs free of clay and zeolite minerals but not for tuffs with large contents of hydrated minerals (Yang, Yu et al. 1998, p. 44). The compression-extraction process only extracts pore water, whereas the vacuum-distillation process extracts both pore water as well as water held by zeolites or clays. Percolating water can replace the water in the large pore spaces as well as undergo isotopic exchange with water in zeolites. Isotopic exchange rates range from days to months. Pore waters extracted from zeolitic core by compression may, therefore, reflect the most recently infiltrated water but may lose the record of past percolating water.

Interpretation of Isotopic Characteristics of Pore Waters—The oxygen and hydrogen isotopic compositions of pore waters can yield information about infiltrating waters, provided that sampling has not disturbed the original compositions. Significant amounts of drilling air were injected into the formation during borehole drilling that could cause drying of the core samples. The potential magnitude of this effect can be examined by plotting the stable isotope compositions of the pore water on the δ^2H versus $\delta^{18}O$ diagram, as has been done for UZ-14 in Figure 37. Data for unsaturated-zone pore-water samples obtained by squeezing the core, plot on or slightly below the meteoric precipitation line, indicating minor evaporative loss (Figure 37b). This evaporation may have occurred either prior to recharge or during drilling. Alternatively, the shift away from the meteoric water line may reflect oxygen isotopic exchange with the host rock.

In contrast, the composition of the CHn pore waters extracted by distillation is significantly lighter than that of the PTn pore waters (Figure 37a). The lighter values for CHn pore waters do not result from incomplete recovery by the distillation method because more than 96% of the water was recovered by vacuum distillation in laboratory tests in which tap water of known mass and isotopic composition was imbibed into an oven-dried core (Yang, Yu et al. 1998, Table 13). On the basis of these experiments, Yang, Yu et al. (1998, pp. 41 to 43) concluded that these extremely light oxygen isotopic signatures are not representative of *in-situ* pore waters but rather are caused by isotopic fractionation induced by the distillation technique.

Comparison of isotopic compositions of unsaturated-zone pore waters (Figures 37b) with those of the saturated-zone groundwaters (Figures 36d) beneath Yucca Mountain show that the CHn pore waters are similar to the heaviest (least negative isotopic values) groundwaters in the Yucca Mountain area, whereas the PTn pore waters are significantly heavier (less negative) than either of these data sets. Again, this difference is consistent with recharge of the CHn pore waters and Yucca Mountain groundwaters occurring under colder climatic conditions than recharge for the PTn pore waters. In the TSw basal vitrophyre, δ^2H values in pore water from three boreholes (SD-7, SD-9, SD-12) are consistently shifted to more negative values, implying that waters were infiltrated during the colder climate of the last ice age (Yang, Rattray et al. 1998, p. 27 and Figure 2). The δ^2H values in pore waters from the underlying CHn are heavier than those for pore

waters from the basal vitrophyre and similar to those for waters above the basal vitrophyre zone, indicating post-ice-age water.

Isotopic Characteristics of Pore Waters with Large Concentrations of Dissolved Solids—A few pore-water samples have very large dissolved-solid concentrations, exceeding 800 ppm and indicating very large evapotranspirative losses. The isotopic compositions of pore waters for three of these samples plot to the right of the Yucca Mountain precipitation line, which would also indicate evaporation after precipitation (Yang, Yu et al. 1998, p. 51). The extent of evaporation for sample NRG-6 (256 feet), which has the largest apparent loss of moisture by evaporation, can be approximated assuming a temperature of 20°C for evaporation, equilibrium Rayleigh fractionation, and an initial starting isotopic composition equal to that of the average winter precipitation. However, the results of this latter calculation suggest that the pore waters were subjected to a maximum evaporation of only 12 percent. The different estimates obtained for evaporative losses from salt content and from isotopic characteristics reflect the fact that the two measures apply to different period of time. The salt concentration in infiltrating water reflects evaporative losses integrated over all precipitation events that occurred since the last event that resulted in infiltration below the soil zone. In contrast, the isotopic ratios of infiltrating water reflect the evaporative losses for the particular storm event that resulted in the net infiltration.

Diffusion Controls on Isotopic Exchange Rates—Water within tuffs at Yucca Mountain undergoes isotopic exchange, particularly between pore water and percolating infiltration. Isotopic exchange appears to be diffusion controlled and the equilibration time is dependent on the mean travel distance and the diffusion coefficient (Yang, Yu et al. 1998, pp. 38 to 43). Zeolites contain loosely held water which is referred to as channel water, and as noted above, its presence can contribute to analytical results for pore water. The channel water of pure clinoptilolite powder exchanges with the water percolating through laboratory columns within several hours to days. For ground tuffs from Yucca Mountain, the exchange rate is also several hours to days, whereas exchange for zeolites within intact cores take longer, depending on the core size and grain size of the zeolites within the core. The exchange processes for zeolite-bearing core can be divided into two steps: the exchange between the pore water and the percolating water, and the exchange between the pore water and channel water. If the system reaches equilibrium, the stable isotopic compositions of pore water should equal those of percolating water, and those of channel water will differ from pore water by a fractionation factor. The second mechanism is still unknown, but the reaction is fast, as shown by column experiments. Therefore, the equilibration time is determined by the first process (Yang, Yu et al. 1998, p. 54). For Topopah Spring Tuff, which bears no zeolites, the stable isotope composition of pore water will be controlled by exchange occurring through diffusion mechanisms.

6.6.5.4 Isotopic Characteristics of Perched Waters

Stable isotopic data of the perched water are generally between -12.8 ‰ and -13.8 ‰ for $\delta^{18}O$ and -94 ‰ and -99.8 ‰ for $\delta^{2}H$ (Table 9). These values are slightly greater than those for the saturated-zone values and similar to values for pore waters. They are generally close to the Yucca Mountain precipitation line, indicating little evaporation before infiltration (Figure 36c). All stable-isotopic values are similar to modern precipitation and are, therefore, consistent with

recharge during the Holocene as suggested by the ^{14}C data for the perched waters and consistent with the ^{36}Cl data for these samples.

6.6.6 Strontium Isotopes

Primary input data used to characterize the distribution of strontium isotopes in rocks, minerals, pore waters, and groundwater are listed in section 4.1.11. Assumptions 15 and 16 from Table 2 apply to discussions in this section.

Background—Calcite is ubiquitous at Yucca Mountain, occurring in soils and as fracture and cavity coatings within the volcanic tuff section. Strontium is a trace element in calcite, with concentrations generally at the tens to hundreds of ppm level. Decay of rubidium-87 (^{87}Rb) is the source of stable ^{87}Sr. Because calcite contains very little rubidium and the half-life of the ^{87}Rb parent is 4.9×10^{10} years (Parrington et al. 1996, p. 29), $^{87}Sr/^{86}Sr$ ratios of calcite record the ratio in the water from which the calcite precipitated. Dissolution and reprecipitation do not alter strontium isotopic compositions. Thus, in the absence of other sources of strontium, one would expect the strontium ratios along a flow path to preserve variations inherited from strontium in the soil zone (Marshall, Futa et al. 1998, pp. 55 to 56).

Strontium isotope compositions of calcites from various settings in the Yucca Mountain region have contributed to our understanding of the unsaturated zone, especially in distinguishing unsaturated zone calcite from saturated zone calcite. Different populations of calcite have been compared, either to group them together or distinguish them from each other in terms of their strontium isotope compositions. Ground water and perched water have also been analyzed. This section focuses on strontium isotope data obtained from pore water.

Methods—Although pore water can be squeezed from the nonwelded tuffs at Yucca Mountain, the volumes recovered from reasonable lengths of drill core are small (Marshall, Futa et al. 1998, pp. 55 to 56). We have used dry-drilled core samples that have dried during storage, as repositories of pore water salts that can be carefully leached with deionized water for analysis of strontium isotope ratios. Crushed core is sieved to obtain a coarse sand (30-60 mesh) fraction that is then leached for less than an hour with deionized water to redissolve the pore-water salts. This water sample is then centrifuged and filtered; strontium is separated by standard techniques for analysis by thermal ionization mass spectrometry (TIMS). Strontium isotope ratios are reported as differences from modern seawater in parts per thousand using

$$\delta^{87}Sr = [((^{87}Sr/^{86}Sr) / 0.7092) - 1] \times 1000 \qquad \text{(Eqn 7)}$$

A single comparison between $\delta^{87}Sr$ from water-leached pore-water salts and that of water squeezed in adjacent core from UZ-14 suggests that the extraction method is valid, at least for non-welded samples.

Results for SD-7—Strontium isotope compositions in the host volcanic rocks differ significantly from those of the pore waters, indicating that pore water has not reached equilibrium with the tuffs. Core was sampled from SD-7, excluding core containing macroscopic calcite coatings. The

pore water strontium data obtained from SD-7 (Figure 38) are remarkable in their systematic variation with depth and their distinction from whole rock compositions. At the top of the core, the $\delta^{87}Sr$ in the pore water is 3.6 ‰, matching the $\delta^{87}Sr$ found in surface coatings of calcite at the drill pad. Delta-^{87}Sr increases with depth; this increase is especially evident within the nonwelded units of the Paintbrush Tuff (PTn) and is only slightly discernible in the underlying welded Topopah Spring Tuff (TSw).

Interpretation—Although the data preclude local equilibrium between pore-water and rock, the rock data can predict the strontium isotope composition of the pore water if recalculated as a down-hole cumulative value weighted according to strontium content of the rock samples and the associated depth interval. An additional weighting factor that takes into account the higher reactivity of the PTn provides a close match to observed pore-water strontium values throughout most of the TSw. Deviations of the pore-water $\delta^{87}Sr$ from the predicted values are likely due to the presence of clays or zeolites which may contain a long-lived record of pore-water strontium compositions and could have been partially leached in the laboratory.

A working model assumes that strontium is added to infiltrating water by dissolution of calcite in the soil zone (Marshall, Futa et al. 1998, pp. 55 to 56). During times of increased surface vegetation, soil waters are more acidic and volcanic detritus in the soil zone can contribute radiogenic strontium into infiltrating water, thus increasing the $^{87}Sr/^{86}Sr$ ratio in the thick calcretes formed during these times. There are two separate populations of soil carbonate that can contribute strontium to infiltrating water; one is dominated by eolian carbonate with a $\delta^{87}Sr = 3.6$ ‰ and the other is dominated by calcretes in thick alluvial soils with $\delta^{87}Sr = 4.5$ ‰ (Marshall and Mahan 1994, Figure 7). Although the eolian signal, represented by soil A/B horizons and calcite coatings on bedrock surfaces, exists throughout the Yucca Mountain region, the strontium signal from calcretes may dominate over the eolian component the strontium when both sources are present.

Water infiltrating into welded tuff (Tiva Canyon Tuff or Topopah Spring Tuff) tends to retain the strontium isotope composition of the overlying soil. However, the pore-water data indicate that water infiltrating into or percolating through nonwelded tuff (PTn) reacts readily and acquires a strontium isotope signature reflecting interaction with this unit. The strontium isotope composition of the volcanic rocks changes systematically over millions of years due to the decay of ^{87}Rb. As a result, pore waters interacting with these rocks would have $\delta^{87}Sr$ values that decrease linearly with age. Delta-^{87}Sr of pore waters in the TSw unit are predicted to change from a modern value of 4.9 ‰ to about 0.4 ‰ at the time of TSw emplacement (12.7 Ma). The observation that $\delta^{87}Sr$ varies with microstratigraphic position within thick calcite coatings that occur in the TSw and the match between these ratios and the predicted values strongly suggests that the calcite coatings derive their strontium from the same source as the pore waters; in other words, both pore water and the fracture water leading to calcite deposition within the TSw derive strontium from water-rock interaction in the overlying section, dominantly in the nonwelded units. This model indicates that pore waters in the PTn are redistributed between pore and fracture water that subsequently percolates through the TSw.

6.6.7 Uranium Isotopes

Primary input data used to characterize the distribution of uranium isotopes in rocks, minerals, pore waters, and groundwater are listed in section 4.1.12. No assumptions are listed in Table 2 that apply to discussions in this section.

Background—Uranium isotopic ratios have been used to address the question of local recharge to the water table through the unsaturated zone at Yucca Mountain, and the prevalence and frequency of fracture flow. The presence of calcite and opal lining fractures and cavities in the lowest units of the TSw exposed in the East-West Cross Drift and in core from underlying unsaturated-zone units suggests that water moving through fractures has reached these depths. Flow through the matrix also accounts for some portion of the total infiltration. However, the fraction of the shallow ground water beneath Yucca Mountain that is locally versus regionally derived, and the ratio of fracture flow versus matrix flow contributing to local recharge, are poorly known. Uranium isotopic compositions of unsaturated-zone fracture minerals, pore water, perched water, and shallow ground water contribute to the conceptualization of these issues (Paces, Ludwig et al. 1998, pp. 187 and 188; Paces and Peterman 1999, pp. 134 to 138), which is summarized in this section.

Unlike oxygen-, carbon-, and strontium-isotope signatures that are largely inherited during infiltration through soils, uranium isotopic compositions of percolating water are significantly modified from values observed in soil- and surface-water, which usually have $^{234}U/^{238}U$ activity ratios of 1.4 to 1.8 (Table 24; Figure 3 of Muhs et al. 1990; Paces et al. 1994, p. 2400; Figures 9, 10, 13, 16, 17, 20, 21, 25, 26, 27, 32, 36, 39, 42, 45, 46, and 53 of Paces et al. 1995), to $^{234}U/^{238}U$ activity ratios as large as 9 at the potential repository horizon (Figure 66, discussed in section 6.10.2) (Figure 3.7 of Paces, Neymark et al. 1996; Figure D3 of Paces, Marshall et al. 1997). As a consequence of radioactive decay, ^{234}U is preferentially enriched relative to ^{238}U in migrating ground water (Figure 9.1 of Osmond and Cowart 1992). The primary causes for this enrichment are the greater solubility of ^{234}U due to radiation-damage of crystal lattice sites containing ^{234}U atoms (Szilard-Chalmers effect) and the greater probability that these ^{234}U atoms have been converted to the more soluble uranyl ion due to the effects of radiation-induced ionization (Section 2.5.1 in Gascoyne 1992). In addition, decay of ^{238}U can cause the displacement of the intermediate ^{234}Th daughter (which rapidly decays to ^{234}U) off of crystal surfaces into the adjacent water by alpha-recoil processes. The amount of excess ^{234}U relative to ^{238}U is controlled by ^{234}U decay, water/rock ratios, flow path length, and the amount of bulk-rock dissolution in the aquifer.

Meteoric water that interacts with readily soluble soil components results in infiltration containing relatively large amounts of both ^{234}U and ^{238}U derived by bulk dissolution (Table 23). As infiltrating water descends through the fracture network, small amounts of ^{234}U that have become available from radioactive decay will be incorporated into these solutions. If water fluxes are large relative to the amount of ^{234}U produced along fracture surfaces, then the $^{234}U/^{238}U$ ratio will remain relatively unchanged from its initial infiltration value. If water fluxes are small and only occur infrequently, ^{234}U can build up in sufficient amounts along the fracture surface between infiltration events such that the $^{234}U/^{238}U$ activity ratio in the water becomes elevated. The large

$^{234}U/^{238}U$ ratios in unsaturated fracture flow at Yucca Mountain imply that volumes of percolation are small relative to shallow environments that receive larger amounts of percolation.

It should be noted that some data used in this analysis have been qualified with some limitations that affect the precision, accuracy, and representativeness of some data (e.g., DTN: GS980208312322.006, see CRWMS M&O 2000b, Section 3.2). These concerns should not alter the regional patterns shown on Figure 42 but should be considered when evaluating individual points.

Results—Data supporting this conceptual model of $^{234}U/^{238}U$ evolution were obtained from water samples collected during the single heater test conducted in the Thermal Test Facility (ESF alcove 5) (Figure 39). Water derived from the welded tuffs proximal to the heater was mobilized and flowed through a connected fracture network for several months into a nearby borehole. Uranium concentrations decreased from about 0.1 to 0.03 ppb between late November 1996 and late May 1997. In the same samples, $^{234}U/^{238}U$ activity ratios dropped from a value of 8.03 in the first water collected, to values of 4.56 and 4.13 in the two subsequent collections. These data are interpreted as evidence that the fracture pathways used by mobilized water during the test had not experienced recent natural flow, and had built up substantial amounts of ^{234}U on their surfaces. Fracture water mobilized during the early stages of the test incorporated the more labile *^{234}U en route* to the collection site. Once the most reactive components were dissolved, later water flowing along the same flow paths incorporated less total uranium as well as less ^{234}U, resulting in smaller uranium concentrations and $^{234}U/^{238}U$ activity ratios with time. A longer duration test would presumably have resulted in water with $^{234}U/^{238}U$ activity ratios approaching either secular equilibrium ($^{234}U/^{238}U$ activity ratio of 1.0) or values that are characteristic of readily exchangeable pore water ($^{234}U/^{238}U$ activity ratio between 1 and 4). Although large $^{234}U/^{238}U$ activity ratios were not observed in early water from the much larger and more complex Drift Scale Heater Test, a similar pattern of decreasing values with time is present in water mobilized from volumes of rock much larger than the Single Heater Test (Figure 40). This pattern illustrates, in a qualitative sense, the likelihood that frequent flushing of fracture surfaces may not allow sufficient accumulation of ^{234}U on fracture surfaces to substantially alter the $^{234}U/^{238}U$ ratios in fracture water.

Uranium isotope data from other areas of the Nevada Test Site that receive recharge sufficient to support small-volume spring discharge can also be interpreted to indicate that small fluxes and infrequent flux events are required to attain the large $^{234}U/^{238}U$ ratios observed at Yucca Mountain. Springs and seeps discharging from perched water zones at Comb Peak, Shoshone Mountain, Skull Mountain and Rainier Mesa have $^{234}U/^{238}U$ activity ratios ranging between 1.9 and 3.8 (Figure 41). These values are larger than those associated with surface water and pedogenic minerals (Paces et al. 1995, Figures 9, 10, 13, 16, 17, 20, 21, 25, 26, 27, 32, 36, 39, 42, 45, 46, and 53), but are lower than $^{234}U/^{238}U$ ratios in most of the perched water at Yucca Mountain (Table 9) as well as the initial $^{234}U/^{238}U$ ratios in young calcite and opal in the deep unsaturated zone (Paces, Neymark et al. 1996, Figure 3.6). Water discharging from NTS springs have relatively large volume to path-length ratios and either continuous or frequent flow that does not permit accumulation of substantial excess ^{234}U on solid surfaces along flow paths. As a result, uranium in water from these systems has isotopic compositions that are only slightly greater than values observed in the infiltrating water. In contrast, waters perched within the welded TSw at

Yucca Mountain (boreholes WT-24, UZ-14, NRG-7a) have larger $^{234}U/^{238}U$ activity ratios (Table 9). These values (5.2 to 8.4) are in the range of initial $^{234}U/^{238}U$ activity ratios observed for young calcite and opal from the potential repository horizon in the ESF.

Ground water from the saturated zone beneath Yucca Mountain also has elevated $^{234}U/^{238}U$ ratios compared to well water in adjacent areas (compare Figure 42 to Figure 43) (Ludwig et al. 1993, Figure 2; Paces, Ludwig et al. 1998, p. 185). Regional saturated-zone ground water in carbonate-rock, alluvial, and Precambrian-rock aquifers from Oasis Valley, Amargosa Valley, Spring Mountains, and the easternmost Nevada Test Site have $^{234}U/^{238}U$ activity ratios between 1.5 and 4. Ground water $^{234}U/^{238}U$ activity ratios from volcanic-rock aquifers in the region are commonly between 4 and 6; however, shallow saturated-zone ground water beneath Yucca Mountain has anomalously large $^{234}U/^{238}U$ activity ratios between 6 and 8.5. Groundwater obtained from Paleozoic carbonate rocks at depth beneath Yucca Mountain (UE-25 p#1) has a much smaller $^{234}U/^{238}U$ ratio of 2.32, typical of the regional carbonate aquifer and indicative of the stratification of shallow and deep aquifers at the site. Up-gradient regions including Timber Mountain, Pahute Mesa, and Rainier Mesa (locations shown on Figures 1 and 2) are at higher topographic elevations and receive greater amounts of recharge. Although the number of analyzed wells in these areas is relatively small, observed $^{234}U/^{238}U$ activity ratios are equal to or less than about 5. Smaller $^{234}U/^{238}U$ ratios (activity ratios less than 6) are also characteristic of ground water in the volcanic-rock aquifer in the Fortymile Wash and Crater Flat areas east and west of Yucca Mountain, and in down-gradient water wells along Highway 95 and in the Amargosa Valley. Uranium concentrations in ground waters from most of these areas range from about 0.5 to 3 ppb.

The anomalous uranium isotopic compositions of shallow saturated-zone water beneath Yucca Mountain are similar to the elevated initial $^{234}U/^{238}U$ compositions measured for deep unsaturated-zone minerals and perched water bodies within the welded TSw. The similarity of the unsaturated and saturated-zone uranium reservoirs at Yucca Mountain is interpreted as an indication of a genetic linkage between the two. Therefore, some component of recharge through the thick unsaturated zone at Yucca Mountain is required. If this recharge made up only a small proportion of the saturated-zone ground water beneath Yucca Mountain, a $^{234}U/^{238}U$ value that is only slightly larger than the presumed up-gradient signature would be expected. Instead, the observed value is near the upper end of the range observed in the unsaturated-zone materials, implying that the local recharge has not been highly diluted by through-flow from the north. Likewise, ground water down-gradient from Yucca Mountain should have a relatively large $^{234}U/^{238}U$ signature if the local recharge contributed significantly to the uranium budget. Groundwater containing elevated $^{234}U/^{238}U$ ratios is not observed in either Fortymile Wash (with the exception of J-13, the main supply well for activities in NTS Area 25) or along the southern margin of Yucca Mountain at Highway 95. More-or-less uniform U concentrations in waters throughout this area indicate that the different ground waters should have roughly equal weighting when mixed on a volume basis. Because of this similarity, small volumes of ground water in adjacent areas should not rapidly mask the uranium isotopic contributions of Yucca Mountain saturated-zone ground water. Therefore, local recharge is considered an important component to the saturated zone immediately below Yucca Mountain; however, this component does not contribute significantly to the regional water budget in the Fortymile or Crater Flat hydrologic flow systems. These conclusions are consistent with major ion data, as well as $\delta^{2}H$, $\delta^{18}O$, and $\delta^{87}Sr$ data from the shallow groundwaters at Yucca Mountain that are interpreted to indicate km-scale heterogeneities

over the same areas (Peterman and Patterson 1998, pp. 277 to 278; Paces and Peterman 1999, p. 137).

Preliminary uranium isotopic data from pore water extracted by centrifugation may indicate that most of the local recharge flows through fracture pathways rather than through the matrix. Several samples of pore water (1.5 to 3.0 mL) have been extracted from the upper lithophysal unit of the welded Tpt. Pore water has uranium concentrations of about 1 ppb and $^{234}U/^{238}U$ activity ratios of 2.5 to 3.0. These ratios are slightly larger than most of the pore water squeezed from nonwelded tuff near the top of the PTn ($^{234}U/^{238}U$ activity ratios of 1.5 to 2.5), but are smaller than water collected from boreholes associated with *in-situ* heater tests ($^{234}U/^{238}U$ activity ratios of 2.5 to 5.6). Larger values approaching those that are indicative of fracture water (initial $^{234}U/^{238}U$ in fracture minerals as well as water perched within the Tpt) or characteristic of shallow saturated-zone ground water have not been observed. Substantial differences in $^{234}U/^{238}U$ compositions between pore water and fracture water indicate a general lack of equilibration between the two unsaturated-zone water sources and implies minimal liquid exchange. These differences also indicate that fracture water is likely the most dominant contributor to recharge of the shallow saturated zone beneath Yucca Mountain.

6.7 CHEMICAL AND ISOTOPIC COMPOSITION OF GASES

Only chemical and isotopic data collected for gas samples from instrumented boreholes are considered primary input data for characterization of the chemical composition of gas at Yucca Mountain. These data are listed in sections 4.1.14 (gas chemistry) and 4.1.9 (carbon isotopes). Chemical and isotopic data for gas samples collected from open boreholes are only used to corroborate interpretations based on data for instrumented borehole samples. Table 3 lists locations for which gas chemical data are available. Assumptions 17 and 18 from Table 2 apply to discussions in this section.

6.7.1 Processes Controlling Gas Chemistry

The major processes that control the chemistry of the gas phase include:

- Atmospheric gas chemistry. The composition of air is the primary control on unsaturated-zone gas chemistry.

- Soil-zone processes. Soil-zone processes such as plant respiration can alter the chemistry of the gases that diffuse into the unsaturated zone. Carbon-dioxide partial pressures are particularly susceptible to modification by these processes.

- Water-air interactions. Once gases diffuse from the soil zone into the unsaturated zone, the gas-phase composition will tend to equilibrate with the waters present in the unsaturated zone. For example, CO_2 will tend to dissolve or exsolve from the waters depending on the partial pressures of CO_2 in the soil zone versus the upper unsaturated zone.

- Upward gas flow. Gases can migrate upward through the unsaturated zone along various gradients including concentration gradients and temperature and pressure gradients. The

gases migrating along these gradients may have a nonatmospheric composition. Therefore, as they mix with the indigenous gases in the unsaturated zone, they alter the overall gas composition in the unsaturated zone.

- Matrix, fractures, and fault structures. Because gas permeabilities of matrix, fractures, and faults are very different, the composition of the gas phase in a certain part of Yucca Mountain at a given time may deviate from the average composition.

- Microbial influences. Microbial metabolic activity may locally influence the composition of the gas phase in the unsaturated zone.

- Temperature. Temperature can influence the composition of the gas phase in the unsaturated zone primarily through its influence on the kinetics of the various reactions involved controlling the composition of the gas phase. In addition, temperature controls the equilibrium fractionation of light stable isotopes, particularly oxygen. A summary of temperature data available for the unsaturated zone at Yucca Mountain is presented in Section 6.5.1.

- Pressure. Variations in total gas pressure can influence the composition of unsaturated-zone waters through their effect on the partial pressures of separate gases in the gas phase. For example, the partial pressure of carbon dioxide in the gas phase varies directly with total gas pressure. Such variations in the CO_2 partial pressure directly affect the concentration of CO_2 in water, which in turn, affects the dissociation of carbonic acid and, thereby, the pH. More significant, however, is its effect on gas flow patterns, including water vapor transport.

6.7.2 Site Characteristics

6.7.2.1 Gas Compositions

Data exist on the abundances of the major atmospheric gases in the unsaturated-zone gas phase at Yucca Mountain, including data obtained from the instrumented borehole UZ-1 (Yang et al. 1996, Table 8) as well as from other boreholes. To a depth of 368 m in UZ-1, the concentrations of oxygen, nitrogen, and argon are within analytical error of atmospheric compositions (DTN: MO0102UNSZHYCM.000 for O_2 and N_2, corroborated by data in DTN: MO0102UNSZHYCM.000). According to Thorstenson et al. (1990, p. 260), samples of gases from UZ-6S, UZ-6, and the neutron boreholes also showed concentrations of O_2, N_2, and Ar that were identical to the concentrations of these gases in atmospheric air to the limits of precision of the analyses. The authors report that soil gases sampled on and near Yucca Mountain showed methane concentrations that were depleted relative to the atmospheric value of about 1.7 ppm by volume (ppmv), but still greater than 0.5 ppmv (Thorstenson et al. 1990, p. 267). In contrast, neutron hole and UZ-6S gases generally showed methane concentrations near zero, ranging up to a maximum value of 0.5 (± 0.1) ppmv, suggesting that methane consumption occurs in the subsurface, even below the soil zone (Figure 4 of Thorstenson et al. 1990).

CO_2 concentrations are generally larger in the rock gas (about 0.1 percent) than in air (0.035 percent) (UZ-1 gas data from DTN: GS930408312271.014 for 1989, MO0012CO2UNSZO.001 for 1991, MO0012CO2UNSZO.002 and MO0012CO2UNSZO.003 for 1993, and MO0012CO2UNSZ0.004 for 1995). CO_2 gas concentrations in boreholes ranged from 0.01 to 1.3 percent by volume (Thorstenson et al. 1990, Figure 4; Yang et al. 1996, Table 8) compared to an atmospheric value of approximately 0.035 percent by volume. The CO_2 concentration profiles as a function of time in UZ-1 show that relatively low CO_2 concentrations were measured in 1983 shortly after completion of the borehole, and that, except for probe 13, concentrations steadily increased until 1987 (Yang et al. 1996, Table 8 and Figure 18). Thus the early CO_2 samples were probably diluted by drilling air (Yang et al. 1996, p. 40). As the semiannual gas sampling process proceeded, most of the drilling air was removed from the hole. Halfway down the hole in the 1994 data set, carbon dioxide dropped to 0.08 percent by volume but increased with increasing depth to 0.36 percent by volume at the lowest sampling point in the hole (367.9 m). The more recent samples probably represent uncontaminated rock gas. This conclusion is supported by data collected from 1986 through 1994, which show CO_2 concentration from 100 m to 360 m changed very little (Yang et al. 1996, Figure 18).

The CO_2 concentrations on the upper portions of UZ-1 are elevated due to their proximity to the soil zone where biologic activity increases CO_2 concentrations (Yang et al. 1996, p. 40). The increased CO_2 concentrations at the bottom of the borehole probably represent breakdown of organic polymers from drilling fluids. The consistently low values for CO_2 concentrations at Probe 13 cannot be explained by currently available data. If probe 13 is sensing a fracture connected to the atmosphere, the concentrations would indeed be anomalously low, but the $\delta^{13}C$ composition would also be anomalously heavy, which is not the case (Figure 19 in Yang et al. 1996).

Essentially all gas data indicate that the partial pressure of CO_2 in the unsaturated-zone gas phase is higher by factors of three or more than that in the atmosphere. This conclusion is based on analyses of CO_2 concentrations in open boreholes NRG#4, NRG#5, NRG-6, NRG-7A, SD-9, SD-12, UZ-7, UZ#16, WT-4, WT-18, UZ-6, and UZ-6s as well as in instrumented borehole UZ-1 (DTN: GS941208312261.008, GS950808312261.004). Some of these data are listed in Tables 18 and 20.

6.7.2.2 Carbon Isotopes in Gases

Carbon isotopes were monitored at the different sampling depths in UZ-1 starting in 1984 (Yang et al. 1996, Figures 19 and 20). Early data show the effects of contamination by drilling air, as evidenced by shifts in the radiocarbon profile from one sampling period to the next (DTN: GS930508312271.021 for 1984 and 1985, MO0102UNSZHYCM.000, for 1988, 1986 and 1987). The ^{14}C activities have stabilized since 1989 (top part of Figure 44) and these more recent data sets are more representative of *in situ* conditions, although some of the $\delta\ ^{13}C$ values still show fluctuations at a given sampling depth that lie outside the range of analytical uncertainty (e.g., Probe 11 in the bottom part of Figure 44). Most values for $\delta\ ^{13}C$ lie within the range of -16 ‰ to -22 ‰ (Table 20 and Figure 44). SD-12 gases are lighter, ranging from –20 ‰ to –25 ‰ (two samples with values of –16 ‰ and –17 ‰ are believed to have been contaminated with atmospheric air, based on their ^{14}C activities) (Table 20). Slightly heavier $\delta\ ^{13}C$ values ranging from -13.5 ‰ to -16.5 ‰ were obtained for gas samples from boreholes in ESF alcoves 1 and 6

(Table 21). There is very little overlap between the $\delta^{13}C$ values for UZ-1 and SD-12 gases and those obtained for the gases from the ESF boreholes. However, the slightly heavier $\delta^{13}C$ values observed in the ESF alcoves are likely to be due to contamination by atmospheric CO_2 as a result of ESF ventilation through highly fractured TSw tuff. Hence, the UZ-1 $\delta^{13}C$ values that were obtained before the excavation of the ESF are considered to be more representative of *in-situ* rock gas $\delta^{13}C$ values.

The ^{14}C data for UZ-1 have been very consistent for the last seven years of monitoring, with a gradual decrease in ^{14}C activity with depth to about 23 pmc at 368 m (Figure 44). The ^{14}C profile shows an abrupt change in the slope within the Pah Canyon interval of the PTn. The gas transport velocity (^{14}C concentration gradient over distance) within the PTn unit is smaller than the transport velocity in the TSw unit (Yang et al. 1993, p. 404). The smaller transport velocity may be due to a greater degree of water saturation in this unit. An estimate of the minimum travel time of gas in the TSw unit based on the apparent ^{14}C ages and depths in the borehole yields gas movement of 3.26 cm/year. This rate, as well as results of gas-transport modeling (Yang et al. 1996, pp. 47 and 49), is nominally consistent with downward movement of atmospheric CO_2 by simple Fickian diffusion. The fact that the ^{14}C values of rock gas in the closed (i.e., instrumented) borehole decrease steadily with depth indicates that inhalation and exhalation of gases in response to changes in atmospheric pressure, as observed in open boreholes, is not a significant process under undisturbed conditions. If such a topographic effect were to be significant, then ^{14}C values would not decrease steadily as seen in UZ-6 and UZ-6s. Although diffusion may not be the only mechanism for gas movement in the TSw unit at UZ-1, it seems to be the dominant mechanism and can account for the observed distribution of gaseous ^{14}C with depth.

The extent to which rock gas is in isotopic equilibrium with the pore waters is not clear. The isotopic composition of pore waters is highly variable, with $\delta^{13}C$ ranging from -9 ‰ to -27 ‰ (Table 15, Figure 34). Unsaturated-zone gases show a nearly identical range, with $\delta^{13}C$ ranging from –8 ‰ to -26 ‰ (Tables 18 to 21). At equilibrium, carbon in bicarbonate in water should be about 8.5 ‰ heavier than carbon in CO_2 in the gas phase at 25°C (Clark and Fritz 1997, Figure 5-4 on p. 120). For the example shown in this reference, $\delta^{13}C$ would be -15.1 ‰ for aqueous-phase HCO_3 in equilibrium with gas-phase CO_2 with $\delta^{13}C$ of -23 ‰. Although no data exist for gas and pore water extracted from the same sample, Table 22 compares samples that were collected from the same general depth ranges in Yucca Mountain boreholes. These samples show apparent disequilibrium insofar as the differences for $\delta^{13}C$ in gas and pore water are much less than 8.5 ‰ for all but a couple samples from the CHn unit in UZ-14. After coexisting for hundreds or even thousands of years, CO_2 gas in pore spaces would have to be in isotopic equilibrium with inorganic carbon species in the pore water. Therefore, the apparent disequilibrium between the two phases is probably not representative of *in situ* conditions, but rather a consequence of the drilling or sampling technique; e.g., in a fractured rock, the pore water may have been contaminated by drilling air, or the sampled gas may not derive from the immediate vicinity of the packed-off-interval.

Although the data sets are less extensive, data for NRG-6 and NRG-7a (Table 15) yield different results from those for UZ-1 and SD-12 (Table 20). In these drillholes, ^{14}C activity does not appear to decrease with depth, and in fact, all three gas analyses from NRG-7a show post-bomb

carbon. However, leakage of air through poor sealing of the packer system against the borehole wall could account for these large ^{14}C activities.

The ^{14}C activity of gas in borehole SD-12 is similar to that of UZ-1 in that there is a decrease from surface to depth, but with some irregularly large deviations from the trend (Table 20). Another striking difference is the markedly lighter carbon in SD-12 and the strong correlation between $\delta^{13}C$ and ^{14}C activities. Rousseau et al. (1997, p. 64) noted that the pneumatic pressures in the two deepest stations of SD-12 (both within the CHn) were lower than predicted by extrapolation of the static-pressure profile developed across the overlying TSw. This "gas-pressure deficiency" could be due to the presence of hydrocarbons, perhaps breakdown organic products from the drilling operation. The oxidation of hydrocarbons, such as methane, could account for the anomalously light carbon in the drillhole. Assuming that the methane is older than 50,000 years, this source would also account for the low ^{14}C activity of the sample at 407 m. Because the postulated methane would be affecting both carbon isotopes, the two isotopic compositions would tend to be correlated.

The smooth ^{14}C trends observed in the SD-12 data are consistent with the data obtained from UZ-1, supporting the concept of gas transport by a diffusion mechanism as previously concluded. However, the large fluctuations towards greater percentages of modern carbon at a couple of the SD-12 stations probably represent a fracture-flow component. Alternatively, the component in the bottom of the hole could be modern atmospheric carbon, given the sharp increase in both $\delta^{13}C$ and ^{14}C (Table 20). Tests conducted on SD-12 instrument stations in January 1997 revealed a leak between one of the monitoring stations (Station C at a depth of 385.6 m in the Tptplnc unit) and the open fiberglass support pipe (Rousseau et al. 1997, p. 21), which probably allowed gas samples from this station to be contaminated with atmospheric air (Yang, Yu et al. 1998, p. 21). Monitoring data suggest that atmospheric contamination of the lowest station (A) may have occurred prior to instrumentation and sealing of the borehole (Yang, Yu et al. 1998, p. 21).

6.7.3 Representativeness of Available Data

Gas chemical and isotopic data reported for boreholes UZ-1 and SD-12 are considered to be representative of *in-situ* conditions at specific depths. Data obtained in annual sampling events of borehole UZ-1 for gas compositions over a decade have established that variability in gas compositions (that is, CO_2 partial pressure and isotopic compositions) tends to decrease with time in instrumented boreholes. This fact suggests that reported gas compositions reflect distinct zones in the borehole and that the compositions reflect *in-situ* (that is, natural) compositions.

Data for samples collected from open boreholes are less useful because the gas samples are subject to contamination from atmospheric gas as a result of drilling and because most of these gas samples were obtained from open boreholes and thus reflect an averaging of gas characteristics over large depth intervals. This approach makes it difficult to associate a given gas analysis with a pore water from a specific depth interval.

The number of boreholes for which gas data are available is limited in terms of both areal coverage and depth. This fact makes it difficult to evaluate the $\delta^{13}C$ variations in gas compositions in the unsaturated zone of Yucca Mountain.

6.8 CHEMICAL AND ISOTOPIC COMPOSITION OF SATURATED-ZONE GROUNDWATER

Uranium activity ratios in local groundwater are considered to be primary input data, and provide the technical basis for identifying the presence of local recharge beneath Yucca Mountain (section 6.6.8). These input data are listed in section 4.1.12 and are discussed in section 6.6.7. All other groundwater chemistry and isotopic data are used in a corroborative manner, to characterize local and regional groundwater chemistry in terms of average concentrations and relative ion ratios. These groundwater trend data provide a baseline against which to compare and contrast chemical compositions of the various sources of water at Yucca Mountain, and to illustrate general trends of relative enrichment or depletion of one element compared to another (sections 6.8.2 and 6.8.3). No assumptions are listed in Table 2 that apply to discussions in this section.

6.8.1 Processes That Control Saturated-Zone Water Chemistry

The chemistry of saturated-zone waters is determined by a series of processes that are linked in space and time. In this section, the primary focus will be on processes that control the chemistry of groundwaters along flow paths from recharge areas north of Yucca Mountain, through Yucca Mountain, and downgradient from Yucca Mountain to the accessible environment. A discussion of saturated-zone geochemistry has been included in this report on unsaturated-zone geochemistry because the similarities in compositions between groundwater and perched water suggest that similar geochemical processes control their compositions, and that these processes differ from those controlling the geochemistry of unsaturated-zone pore waters. The chemistry of local saturated-zone water is compared to that of perched waters in section 6.8.3.

The main processes that determine groundwater chemistry along its flowpaths are:

- Precipitation quantities and compositions (Section 6.3)
- Surface-water quantities and compositions at recharge areas and along flow paths between recharge areas and the accessible environment (Section 6.4)
- Soil-zone processes at recharge areas and along flow paths between recharge areas and the accessible environment, including the effects of evapotranspiration
- Rock-water-gas interactions in the unsaturated zone at recharge areas
- Rock-water-gas interactions in the unsaturated zone (Section 6.7)
- Rock-water interactions in the saturated zone along flowpaths between the recharge areas and the accessible environment
- Temperature and pressure along flow paths between recharge areas and the accessible environment
- Mixing of groundwaters from different flow systems

Recharge areas for saturated-zone waters in Yucca Mountain are located to the north of Yucca Mountain in the direction of Buckboard Mesa, Rainier Mesa, and Pahute Mesa (Figure 2). The rock types dominating the recharge areas are silicic and basaltic volcanic units (Byers et al. 1976, pp. 6, 7, and 19). Although Paleozoic limestones and other sedimentary units are present at great depth, they do not appear to influence the compositions of waters that occur in the volcanic units in the saturated zone beneath Yucca Mountain.

Climatic conditions in the recharge areas are somewhat different from those that prevail at Yucca Mountain. Specifically, they receive more precipitation and are cooler on average than the Yucca Mountain area and support a greater abundance of vegetation. Accordingly, infiltration rates on Pahute Mesa are also expected to be higher on average than infiltration rates on Yucca Mountain. Higher infiltration rates imply that dissolved salts and other constituents that may accumulate in the soil zone as a result of evapotranspiration of infiltrating waters (that is, precipitation) have shorter residence times in this zone. This process is likely the reason that soils on Pahute Mesa and adjacent areas contain much less pedogenic calcite and/or silica than is the case at Yucca Mountain. The higher infiltration rates also imply that waters infiltrating into the saturated zone will have lower salt and silica concentrations than is the case at Yucca Mountain. This dilute composition makes these waters more reactive with respect to the rock units through which they may subsequently migrate.

As discussed in Section 6.5, water-rock reactions that occur in the soil zone or the unsaturated zone include mineral dissolution, mineral precipitation, mineral alteration, and ion exchange on charged surfaces. Because the waters percolating downward from the soil zones in recharge areas are likely more reactive than soil waters percolating into the unsaturated zone in Yucca Mountain, dissolution reactions are likely more important in the unsaturated zones of the recharge areas. The dominant changes to the water compositions that result from these reactions are major increases in silica, sodium, and bicarbonate (White et al. 1980, pp. Q15 to Q17).

Once the water has undergone the initial dissolution reactions, the rate of change in water composition would likely decrease. This decrease is because the rate of dissolution is a function of the degree to which the water has approached thermodynamic equilibrium with the rock units with which it is in contact. The closer the water is to thermodynamic equilibrium with the host rock, the slower the rate of reaction.

Actual calculation of the degree to which the reaction approaches thermodynamic equilibrium is difficult because the reactions involved are commonly incongruent. For example, in the case of feldspar equilibration with a given water composition, the feldspar crystals do not simply dissolve into the solution. It appears that the cation/hydrogen ion-exchange reaction discussed previously (Section 6.5.3.2) causes the feldspar surface layers to be converted (that is, hydrolyzed) into a poorly structured hydrogen aluminosilicate solid “phase.” Sodium, potassium and calcium are the major cations that participate in this exchange. The solubility of this solid “phase” would then control the rate of disappearance of the feldspar crystal (Brantley and Stillings 1996, p. 101). Unfortunately, the thermodynamic properties of this solid “phase” are not well defined. The same situation occurs with the hydrolysis of volcanic glass at ambient temperatures.

The dominant water-rock reactions that impact the water chemistry after the initial dissolution reactions are silica precipitation and ion exchange involving minerals such as zeolites and clays. The cation/hydrogen ion-exchange reaction will also continue to be of significance. The ion-exchange reactions will tend to lead to increased sodium concentrations and decreased calcium, magnesium, and potassium concentrations in the waters. However, changes in the concentrations of these ions will only occur if zeolites and/or clays are present in adequate quantities in rock units through which the waters migrate. The sodium/hydrogen ion-exchange reaction will continue to increase the sodium content of the waters until thermodynamic equilibrium is achieved with the host rock (although the formation of metastable phases may cause the approach to equilibrium to be very slow).

The degree to which alteration reactions involving silicates and aluminosilicates in the host rock control water compositions is unclear. For example, volcanic glass is thermodynamically unstable in contact with water at ambient conditions, and given enough time, it will alter to secondary minerals such as clays, zeolites, silica polymorphs, and other minerals. However, glass is still present in great abundance in the volcanic units that make up Pahute Mesa and Rainier Mesa (Byers et al. 1976, pp. 6, 7 and 19). Although glass alteration reactions are taking place at some rate, this rate appears to be much slower than the rate of the initial dissolution reactions and ion-exchange reactions. For purposes of predicting water compositions, restricting the discussion to the latter reaction is probably adequate given the current state of knowledge.

Controls on the pH of groundwaters in the saturated zone are similar to those discussed in Section 6.5.3.2. In brief, the primary controls on pH are the partial pressure of CO_2 and the rate at which hydrogen ions are consumed by the rock/mineral matrix. In the saturated zone, access to the CO_2 reservoir in the gas phase of the unsaturated zone becomes progressively more difficult with depth. Therefore, unless a secondary source of carbonic acid or another source of acidity (for example, sulfide minerals) exist in the saturated zone, the reaction of hydrogen ions with the rock/mineral matrix will eventually consume the available acidity, leading to increased pH. The high pH value observed in H-3 (pH 9.4) (Ogard and Kerrisk 1984, p. 9) likely reflects this process.

Controls on reduction/oxidation (redox) states in the saturated zone are more difficult to define. Potential redox reactions in the saturated zone include various redox couples such as oxygen/water, ferrous/ferric iron, sulfide/sulfate, nitrite/nitrate, and other couples. The methane/CO_2 couple is not likely to be of significance where methane abundances are very low because this redox couple only becomes active at low temperatures if it is microbially mediated. If dissolved oxygen is higher than approximately 0.1 mg/L, it could produce a relatively high redox potential (Eh > 600 mV). The redox state of saturated-zone waters as calculated from the concentrations or activities for respective couples may or may not be at equilibrium. Lindberg and Runnels (1984, p. 925) have argued that ground and surface waters are rarely in equilibrium in terms of redox couples and that different couples may give different redox potentials (that is, Eh). However, this conclusion is based primarily on measurements on young groundwaters. Deep groundwaters such as those in the saturated zone at Yucca Mountain have had longer residence times during which to reach equilibrium.

In summary, the dominant processes that are likely to control water compositions along the flow paths from recharge areas to the saturated zone beneath Yucca Mountain are dissolution reactions, silica and calcite precipitation reactions, and ion-exchange reactions. The pH of these waters will be controlled primarily by the partial pressure of CO_2 and the rate at which the rocks consume hydrogen ions. Controls on the redox state in the saturated zone are poorly defined at the present time.

6.8.2 Present-Day Regional Characteristics

This section summarizes the available data for groundwater chemistry in volcanic aquifers and tuffaceous valley fill in the saturated zone in the Yucca Mountain region extending from recharge areas north of Yucca Mountain along flow paths through Yucca Mountain and to the accessible environment boundary south of Yucca Mountain.

Figure 45 shows the locations of several wells on Pahute Mesa from which water samples have been obtained. All of these wells were completed in Tertiary volcanic rocks (McKinley et al. 1991, Table 5). Full identifiers for these wells are shown in Figure 47. Based on regional flow models, only those wells in the eastern part of Pahute Mesa are likely to lie along flow paths that pass through the Yucca Mountain area. Those wells located in the western part of Pahute Mesa apparently lie along flow paths that pass through Oasis Valley. Water samples from springs located in the area of Rainier Mesa may reflect the compositions of waters recharging the saturated zone in the Pahute Mesa area.

The available data on saturated-zone waters from the recharge areas consist primarily of analyses of the major constituents, although a limited number of isotopic analyses have been reported. A trilinear plot of relative major-ion abundances in saturated-zone waters from eastern Pahute Mesa and southern Rainier Mesa is shown in Figure 47. The data indicate that the waters are dominated by sodium bicarbonate. These waters have pH values ranging from 7.4 to 8.2 and total dissolved solids ranging from 169 to 578 mg/L. Claassen (1985, p. F13) noted that these waters are chemically relatively evolved. By this he was apparently referring to the fact that the ratio of sodium to other major cations was high. Because these waters occur in the recharge area (that is, they are the youngest waters in the flow system), this is an important observation.

The locations of wells in the vicinity of Yucca Mountain from which groundwater samples were taken to obtain geochemical data are shown in Figure 46. Physical data for these wells are listed in Table 24. The relative abundances of major ionic constituents in saturated-zone waters from wells in the vicinity of Yucca Mountain are plotted in Figure 48. Comparison of Figures 47 to 48 shows saturated-zone waters from volcanic aquifers to be very similar in both areas. Data for down-gradient waters were not plotted in the cations/anions versus chloride plots (Figures 24 to 28) because they directly overlap data points for Yucca Mountain area saturated-zone waters. The down-gradient waters show a pH range from 7.5 to 8.2 and a range in total dissolved solids from 217 to 233 mg/L, depending on where the southern boundary is placed (Excel file yucca.xls in Oliver and Root 1997). The fact that the down-gradient waters are even farther from the recharge areas than those in the Yucca Mountain area again suggests these waters are close to equilibrium with their host rocks.

6.8.3 Present-Day Characteristics of Groundwaters in the Yucca Mountain Area

As pointed out in the last section, saturated-zone waters from volcanic aquifers in the recharge area are compositionally very similar to saturated-zone waters from the Yucca Mountain area (compare Figures 47 and 48). Analyses of groundwater from drillholes that penetrate the host rock and other volcanic units in the area of the exploration block indicate that they are principally sodium-bicarbonate waters (Figure 48) with low contents of total dissolved solids (200 to 400 mg/L, based on data in DTN: GS930308312323.001, MO0012MAJIONIS.000, GS990608312133.001 and Excel file yucca.xls in Oliver and Root 1997). Compared to waters in the recharge areas, the Yucca Mountain area waters show a greater range in pH values from 6.6 to 9.2 and total dissolved solids ranging from 181 to 887 mg/L (DTN: GS930308312323.001, MO0012MAJIONIS.000, GS990608312133.001 and Excel file yucca.xls in Oliver and Root 1997).

Plots of the major cations versus chloride show that saturated-zone waters (as well as perched waters, based on data from Sections 6.5.3 and 6.6.5) are generally distinct from unsaturated-zone pore waters in the Yucca Mountain area in several ways:

- First, saturated-zone waters and perched waters have much lower chloride concentrations than the pore waters (Figure 18). This result suggests the saturated-zone and perched waters were subject to less evapotranspiration than the pore waters. An alternative explanation, loss of chloride from solution by reactions with glass or hydroxyl phases in tuff, is improbable for unsaturated-zone pore waters at Yucca Mountain.

- Second, saturated-zone waters are either on or above the precipitation trend line in a sulfate versus chloride plot suggesting they gained sulfate, perhaps by dissolving some sulfate mineral(s) such as gypsum (Figure 27). Among the unsaturated-zone pore waters, only some samples from the PTn unit show a similarly high SO_4/Cl ratio. The vast majority of pore waters plot well below the trend line.

- Third, unlike unsaturated-zone waters, all of the perched waters and a significant proportion of the saturated-zone waters plot above the precipitation trend line in a calcium-versus-chloride plot (Figure 24). This result suggests some of these waters gained calcium while others lost calcium. The fact that nearly all of these waters gained bicarbonate (Figure 25) suggests the calcium gained may have come from the dissolution of calcite. The loss of calcium likely reflects ion-exchange reactions on clays and zeolites. This possibility is supported by the fact that these waters have all gained sodium (Figure 26).

- Finally, silica concentrations in these waters are slightly lower than those measured in most pore waters. However, nearly all waters are oversaturated with alpha-cristobalite (Figure 28), suggesting that a different silica phase may control their concentrations.

On trilinear diagrams, local groundwater and perched waters show distributions of major ions that are quite similar to one another (Figures 17 and 48), and considerably different from those of unsaturated-zone pore waters. The relative abundances of cations in saturated-zone waters show

considerable variation from east to west across Yucca Mountain, with perched water being most like groundwater from wells in Fortymile Wash (e.g., J-13). Wells on Yucca Mountain and just to the west (USW H-3, USW H-5, and USW H-6) plot nearest the sodium apex of Figure 48. Wells on the eastern slopes and washes (USW H-1, USW H-4, USW G-4, J-13, and UE-25 b#1) show increasing levels of calcium. The Na+K / Ca+Mg molar ratio increases from 3.8 in J-12 to 263 in H-3. This result most likely reflects ion-exchange reactions involving the zeolites and clays in the saturated-zone units beneath Yucca Mountain and the sodium/hydrogen ion-exchange reaction. The fact that bicarbonate concentrations also increase from east to west suggests a significant contribution from the latter reaction.

The anionic constituents of the Yucca Mountain groundwaters show a relatively uniform distribution in all the wells, with about 80 percent bicarbonate and the remainder as sulfate and chloride (usually present in nearly equal molar concentrations) and fluoride (in varying concentrations). Perched waters have a slightly higher molar proportion of bicarbonate (about 85% of total anions) and more than twice the proportion of sulfate relative to chloride (Figure 17).

6.8.4 Representativeness of Available Data

Because the analyses of major constituents in saturated-zone groundwaters from volcanic aquifers in the Yucca Mountain region show only limited variability (compare Figures 47 and 48), the available data are sufficiently representative for characterization and modeling purposes. For pH, bounds can be placed on the likely variability to be expected based on observations and hydrochemical models.

6.9 FLUID GEOCHEMICAL INDICATORS OF FLOW AND TRANSPORT PROCESSES

6.9.1 Chloride as a Hydrologic Tracer

Chloride pore-water concentrations obtained from unsaturated core samples serve several purposes within the Yucca Mountain investigation:

- *Infiltration estimates*. Cl concentrations provide independent corroboration of surface infiltration rates estimated by modeling. The Cl mass balance (CMB) method estimates infiltration as a proportion of precipitation based upon the enrichment of Cl in pore water relative to its concentration in precipitation.

- *Perched water origin*. The origin and age of perched water bodies underlying Yucca Mountain have been problematic because their Cl concentrations (4 to 10 mg/L) are generally considerably lower than those of pore waters from the unsaturated zone above the bodies. Expanding the spatial coverage of the pore-water data helps constrain the various hypotheses on the derivation of the perched water.

- *Mixing of waters*. Cl, Br, and SO_4 pore-water concentrations indicate the extent to which water geochemistry is homogenized as it percolates through the nonwelded

Paintbrush unit. Fracture-dominated flow in the overlying low-permeability, highly fractured TCw unit is expected to transition to matrix-dominated flow in the high-permeability, comparatively unfractured PTn (Wolfsberg et al. 1998, p. 82). The transition process from fracture to matrix flow in the PTn, as well as the transition from low to high matrix storage capacity, could damp out most of the seasonal, decadal, and secular variability in surface infiltration. This process could also result in the homogenization of the variable geochemical and isotopic characteristics of pore water entering the top of the PTn. In contrast, fault zones that provide continuous fracture pathways through the PTn may damp climatic and geochemical variability only slightly and may provide fast paths from the surface to the sampled depths, whether within the PTn or in underlying welded tuffs (Wolfsberg et al. 1998, p. 82 and Figure 2). If this concept can be validated, then it would suggest that repository design and performance assessment efforts can be based on fluxes that are uniform in time, except near fault zones.

- *Lateral diversion*. Variability in Cl, Br, and SO_4 pore-water concentrations can be used to assess the extent to which water may be laterally diverted due to contrasting hydrologic properties of the various stratigraphic units above the potential repository horizon (although it is recognized that this aspect may be obscured by climatic variability in the geochemistry of infiltrating fluids).

- *Model calibration*. To the extent that the Cl pore-water database can be extended to a wide spatial and stratigraphic coverage, it is an increasingly valuable data set for site-scale modelers to use in calibrating flow and transport models of Yucca Mountain.

6.9.2 Infiltration Estimates using the Chloride Mass Balance Method

Precipitation data used in Section 6.9.2 to estimate bounds on present-day average chloride deposition rates at Yucca Mountain are listed in section 4.1.1. Pore-water chloride data analyzed by the CMB analysis are listed in section 4.1.3. Determination of the background $^{36}Cl/Cl$ ratio for the Yucca Mountain vicinity, which is used to estimate the long-term average chloride deposition rate at Yucca Mountain, uses input data listed in section 4.1.16. Assumptions 1, 2 (TBV), 3, 19 (TBV), 20 (TBV), and 21 (TBV) from Table 2 apply to discussions in this section.

6.9.2.1 Chloride mass balance model

The CMB approach is based on the premise that the flux of Cl deposited at the surface equals the flux of Cl carried beneath the root zone by infiltrating water. With increasing depth, as water is extracted by evapotranspiration, Cl concentrations in pore waters increase and apparent infiltration rates decrease. Net infiltration is the flux of water moving below the zone of evapotranspiration, at which depth Cl concentrations remain relatively constant (Figure 49a). Infiltration rates can thus be estimated from measured Cl concentrations using the relationship:

$$I = (P\ C_0)/C_p, \qquad \text{(Eqn 8)}$$

where I is average net infiltration (mm/yr), P is average annual precipitation (mm/yr), C_0 is the effective average Cl concentration in precipitation (mg/L), including the contribution from dry

fallout, and C_p is the measured Cl concentration in pore water (mg/L).

This approach has been widely used to estimate water transport rates in alluvial profiles through the unsaturated zone and basin-wide recharge (e.g., see reviews by Dettinger 1989, pp. 57 to 61; Herczeg and Edmunds 2000, pp. 49 to 50; Phillips 1994, pp. 19 to 21; Scanlon et al. 1997, pp. 470 to 472). Estimates of recharge using the CMB technique for 15 groundwater basins in Nevada were found to be in fairly good agreement with estimates obtained by the Maxey-Eakin linear step function (Dettinger 1989, p. 75). Using a 6-year study of two upland basins selected as analog wetter climate sites for Yucca Mountain, Lichty and McKinley (1995, p. 1) showed the CMB method to be more robust than a water balance modeling approach using a deterministic watershed model for estimating basin-wide recharge for two comparatively wet sites in the Kawich Range north of Yucca Mountain. They attributed the robustness of the CMB method to the small number of measured parameters required as compared to the number of parameters needed for defining a deterministic watershed model. Point estimates of net infiltration or recharge using the CMB technique tend to be less robust than basin-wide estimates because of additional assumptions concerning vertical ground water flow and surface water flow.

6.9.2.2 Model assumptions

The CMB method is based on the following simplifying assumptions (Assumptions 19, 20, 21 in Table 2, all TBV):

- the average annual Cl deposition rate (the product of precipitation and Cl concentration in precipitation), is known and constant (or can be bounded) throughout the time period of interest,
- run-on or run-off is negligible,
- lateral subsurface flow, such as along the bedrock/alluvial contact, is negligible,
- precipitation (dry and wet fallout) is the only source of Cl,
- there is no sink for Cl,
- transport of Cl in soil can be approximated as piston flow (i.e., uniform downward movement of water without dispersion),
- preferential flow allowing a portion of dilute infiltrating water to bypass the root zone (e.g., via root channels or fractures) is negligible, and
- extracted pore water is representative of *in-situ* infiltrating water.

Applicability of the CMB method to the specific conditions at Yucca Mountain (e.g., shallow soil cover over fractured rock) is an assumption to be verified (TBV) (Assumption 19 in Table 2). It is possible that relatively dilute water that has infiltrated rapidly through fracture pathways may be inadequately represented by matrix pore water because of incomplete mixing. If this is the case, matrix pore-water samples might be biased toward the slower moving, more concentrated matrix

component of flow; and percolation estimates based on these samples would constitute lower bounds on the actual percolation rates. In the PTn, some component of the flux can bypass the matrix as fracture or fault flow, as evidenced by the presence of bomb-pulse tracers in the ESF. However, based on the discussion of these assumptions, the method appears to be valid for a first-approximation of infiltration at Yucca Mountain (Fabryka-Martin, Flint et al. 1997, section 6.3.1).

6.9.2.3 Model parameter values

Two approaches can be used to estimate the deposition rate of meteoric Cl onto the land surface at Yucca Mountain: (a) measuring Cl concentrations in precipitation and dry fallout, and (b) dividing the natural ^{36}Cl fallout at the site, which varies with latitude, by the prebomb $^{36}Cl/Cl$ ratio (Phillips 1994, pp. 22 to 23; Scanlon et al. 1997, p. 471). Both approaches have been taken for Yucca Mountain. Deposition is highly variable on short time scales, such that long-term monitoring records are needed that cover all seasons for several years or more. Section 6.3.2 summarizes the availability of precipitation records for the area:

- In his study of desert basins in Nevada, Dettinger (1989, p. 62) calculated an average bulk-precipitation concentration of 0.6 mg/L (using data from 8 sites). For his study of recharge in Las Vegas Valley, this author used an average concentration of 0.4 mg/L (for 74 sites) but noted that 66 of the sites only had wet fallout data (Dettinger 1989, pp. 63 and 66).

- At 3 Springs Basin north of Yucca Mountain (Figure 1), the average annual Cl concentration was 0.51 mg/L with an average annual precipitation rate of 335 mm (calculated from data in DTN: MO0005CL3SPRGS.000, MO0005CLKAWICH.000, GS930108315214.004, and GS930908315214.030; these data were also published in McKinley and Oliver 1994, pp. 23 to 27, 66 to 74, and McKinley and Oliver 1995, pp. 17, 18, 29 and 30).

- Cl data for the Red Rock Canyon site outside of Las Vegas (Figure 1) average 0.16 mg/L for an average annual precipitation of 162 mm, but only include wet fallout (data from DTN: LA0003JF12213U.001).

- The concentration of Cl in 111 samples collected from Yucca Mountain for the present study during the Spring of 1995 ranged from 0.3 to 1.8 mg/L, averaging 0.5 mg/L (DTN: LAJF831222AQ95.003).

A longer-term record is provided by the second approach in which the Cl deposition rate (D_{Cl}) is estimated from:

$$D_{Cl} = D_{36} / (^{36}Cl/Cl)_0, \qquad \text{(Eqn 9)}$$

where D_{36} is the deposition rate of prebomb ^{36}Cl, and $(^{36}Cl/Cl)_0$ is the prebomb $^{36}Cl/Cl$ ratio. The prebomb $^{36}Cl/Cl$ ratio is 502×10^{-15}, based on analyses of 41 samples of soil, alluvium and fossil packrat urine (Table 25). The data for radiocarbon-dated packrat samples indicate that this ratio has been fairly constant throughout the Holocene. For the latitude at which Yucca Mountain is located, Phillips (2000, Figure 10.2 on p. 308) presents an empirical equation for estimating ^{36}Cl deposition rate as a function of precipitation:

$$D_{36} = 0.047\ P + 8.09, \qquad \text{(Eqn 10)}$$

where D_{36} has units of atoms $m^{-2}\ s^{-1}$, and P is average annual precipitation in mm. The average annual precipitation over Yucca Mountain is 172 mm and ranges from 128 mm at the lower elevations (3000 ft) to over 231 mm at higher elevations (6000 ft) (Hevesi et al. 1992, p. 677 and equation 5 on p. 685). Using these precipitation bounds, estimates for D_{36} range from 14 atoms/m^2/s (for an average annual precipitation of 128 mm), to 19 atoms/m^2/s (for 231 mm), averaging 16 atoms/m^2/s for Yucca Mountain itself (172 mm). Estimates for D_{Cl} thus range from 52 to 70 mg/m^2/yr (for precipitation of 128 and 231 mm/yr, respectively), corresponding to effective Cl concentrations of 0.40 and 0.31 mg/L for these two precipitation rates. In general, however, the spatial distribution of precipitation directly over the repository site is fairly uniform, with high rates over the crest (e.g., 184 mm/yr at UZ-6), decreasing to 160 or 150 mm/yr in the lower washes (Hevesi et al. 1992, Table 3). Assuming an average precipitation of 170 mm/yr, the Cl deposition rate for Yucca Mountain is 60 mg/m^2/yr with an effective concentration of 0.35 mg/L.

From this discussion, the following is concluded:

- The rate of Cl deposition is proportional to the precipitation rate and is probably fairly constant on the timescales of interest for estimating infiltration at Yucca Mountain (i.e., hundreds or thousands of years).

- Estimates of average annual Cl concentrations in precipitation at Yucca Mountain range from 0.3 to 0.6 mg/L, with 0.35 mg/L being the best estimate for a long-term average.

The relationship between measured pore-water concentration and inferred infiltration rate is plotted in Figure 49b for this range of concentrations and a precipitation rate of 170 mm/yr.

6.9.2.4 Infiltration rates at Yucca Mountain

Values of net infiltration estimated at Yucca Mountain using the CMB technique range from less than 0.1 mm/yr to nearly 20 mm/year (Tables 26 and 27). Table 26 lists Cl pore-water concentrations for boreholes in the ESF, Cross Drift and Busted Butte, together with the associated apparent infiltration rates. Average concentrations for the Yucca Mountain samples are tabulated in Table 27. Average Cl concentrations for the North Ramp (23 mg/L) and Main Drift (20 mg/L) are similar to that for the Cross Drift (22 mg/L) and about a third of the average value for the South Ramp (64 mg/L). Assuming precipitation of 170 mm/yr with an average Cl concentration of 0.35 mg/L, these pore-water concentrations correspond to infiltration rates of 5 to 14 mm/yr above the North Ramp, Main Drift, and Cross Drift, and 1 to 2 mm/yr above the South Ramp. Despite variable Cl concentrations in the easternmost South Ramp samples, the corresponding infiltration rates calculated for individual samples cover a narrow range, 0.4 to 4 mm/yr (Table 26), because of the insensitivity of the CMB method to concentrations above about 20 mg/L (Figure 49b).

Table 27 lists average Cl pore-water concentrations for surface-based boreholes, together with the associated apparent infiltration rates. In the north part of the study area, Cl concentrations are

higher—and associated infiltration rates lower—for pore waters from these boreholes as compared to pore waters from tunnel boreholes. This difference is probably due to the location of the surface-based boreholes in washes with thick alluvial cover. On the basis of chloride concentration data from alluvium and from nonwelded PTn, along with supporting information from neutron moisture logging and ^{36}Cl analyses, the alluvium is, in most cases, a significant barrier to water movement and infiltration is indeed higher where alluvium is thin or absent. Some channel boreholes, as well as soil samples collected from sideslopes, display chloride profiles that suggest recent flushing of chloride from the soil profile (as evidenced by low concentrations in the surficial layers). Based on Cl concentrations, infiltration through the alluvium is less than 0.05 mm/year at UZ#16 and UZ-N54, which are located on alluvial terraces, and 0.4 to 0.8 mm/year at UZ-N37, which is located in a channel. Pore-water chloride concentrations from the PTn at UZ#16 yield an estimated percolation flux of 2 to 3 mm/year. Pore-water chloride concentrations from the top of the PTn at UZ-14 yield an estimated percolation flux of 0.2 to 0.4 mm/year. Estimates of percolation flux in the PTn using the CMB equation were 0.6 to 1.0 mm/year at UZ#4 and 1.4 to 2.4 mm/year at UZ#5.

6.9.3 Origin, Age and Continuity of Perched-Water Bodies

Hydrochemical and isotopic data are useful in the evaluation of alternative hypotheses for the origin of perched water at Yucca Mountain. Among possible alternative hypotheses are the following:

- They represent a transient rise in the water level in the saturated zone.
- They represent a remnant from a time during which percolation rates were higher and locally exceeded the hydraulic conductivity of the rock units in the unsaturated zone.
- They reflect long-term steady-state conditions.

Although analyses of major chemical constituents in perched water and saturated zone waters suggest a close similarity (Section 6.8.2), isotopic data generally do not. The $\delta^{13}C$ values, $\delta^{87}Sr$ values, and $^{234}U/^{238}U$ activity ratios for perched waters are generally distinct from those obtained for saturated zone waters (Section 6.6). Further, there are consistent trends in $\delta^{13}C$ values, $\delta^{87}Sr$ values, and $^{234}U/^{238}U$ activity ratios in water and secondary mineral samples from the soil zone down through the unsaturated zone and into the upper-most saturated zone (Sections 6.6 and 6.10). These observations strongly suggest that the water in the perched zones originated at the surface of Yucca Mountain and do not represent upwelling from the saturated zone.

Assuming the water in the perched-water bodies originated at the surface of Yucca Mountain, the next important question is how the water accumulated in the perched-water bodies. Did it accumulate in a steady-state process that may be on-going or did it accumulate during a transient period of increased infiltration at some time in the past? Analyses of major chemical constituents in perched water samples and pore waters squeezed from core samples indicate that these two water types are generally different in composition. The pore waters have much higher concentrations of most constituents compared to the perched water samples (Tables 6 and 8; Figures 18 to 20). This observation suggests that the infiltration mechanism for matrix pore water

is different from that feeding the perched water bodies. The higher ionic strength of the pore waters can be explained by higher rates of evapotranspiration at the infiltration points for these waters, as compared to the locations at which perched waters infiltrate the subsurface. Thus, perched waters appear, on average, to have spent less time in the near-surface zones than did unsaturated-zone pore waters.

The mechanism proposed to explain the chemical differences in pore waters and perched waters is one in which pore waters flow primarily through the rock matrix while perched waters accumulate from flow that occurred primarily through the fractures in the host rock. For perched waters, isotopic data suggest that the flux of water through fractures is likely episodic and of small volume compared to the hydraulic conductivity of the fracture. For example, $^{234}U/^{238}U$ activity ratios measured in perched water samples are much higher than the ratios in pore waters (Section 6.6.7). The high activity ratios in perched waters would be most readily produced when there are episodic fluxes through many small fractures. Under these conditions of rare episodic fracture flow, ^{234}U that has accumulated on the fracture surfaces between fracture flow events is preferentially leached into the water relative to ^{238}U. If the original concentration of uranium in the water is small or if the flux of water is small, a high $^{234}U/^{238}U$ activity ratio can be produced in the percolating water. Clearly, the higher the fracture surface area to water volume ratio, the higher the resulting $^{234}U/^{238}U$ activity ratio, assuming all other factors remain constant.

The identification of bomb-pulse constituents at depth within Yucca Mountain (Sections 6.6.2, 6.6.3 and 6.6.4 for tritium, ^{36}Cl and ^{14}C, respectively) suggests that flow along fractures can be rapid. However, the absence of a clear bomb-pulse signal for any of these radionuclides in perched water samples (Table 9, Section 6.6.3) indicates that the present-day flux of water from the surface downward through fractures to perched water bodies must be small.

In summary, the hydrochemical evidence suggests that pore waters and perched waters in the unsaturated zone at Yucca Mountain originated at the surface of the mountain. Perched waters appear to form as a result of episodic fracture flow involving small volumes of water. The travel time of waters percolating from the surface to the depth of the perched water bodies can be short (i.e., less than 40 years). The matrix pore waters apparently represent a more continuous percolation of water infiltrated at the surface and moving slowly downward after enough residence time in the soil zone to gain the major-ion constituent concentrations observed in the pore waters.

Data bearing on the age of perched water were discussed in Section 6.7.4. The ^{14}C values range from 67 to 27 pmc, corresponding to “residence times” of 3,500 to 11,000 years. These “residence times” have not been corrected for dead carbon that may have been gained by the waters due to the dissolution of carbonate minerals along flowpaths from the surface.

6.9.4 Ion Exchange in the Calico Hills Tuff

Data on major-ion concentrations in unsaturated-zone waters beneath the proposed repository horizon are of great significance as corroborative data for radionuclide transport calculations. For example, the fact that pore waters in the lower portions of the zeolitized Calico Hills tuff have negligibly low calcium and magnesium concentrations compared to pore waters in the overlying

units indicates that ion-exchange processes operate on the pore waters that percolate through the zeolitic tuffs. These processes tend to remove calcium and magnesium from the percolating waters, replacing them with equimolar concentrations of sodium. When combined with ^{14}C age data suggesting relatively young ages (up to 100 pmc) for CHn pore waters, these data indicate that ion-exchange processes operate on vertically migrating young pore waters in the CHn. This suggests ion-exchange processes would also operate on any radionuclides released from the potential repository into aqueous solutions that migrate vertically into the zeolitic CHn.

6.10 FRACTURE MINERALS

Calcite and opal are present as fracture and cavity coatings within the unsaturated zone at Yucca Mountain. These mineral coatings provide a record of past water percolation through the connected fracture network in areas where solutions exceed chemical saturation with respect to various mineral phases. Calcite and opal are typically present in the form of 0.1-cm to 6-cm-thick coatings in high- to low-angle fractures where apertures exceed several millimeters and on floors of lithophysal cavities intersected by fractures allowing the ingress of fracture flow. A small proportion of the calcite and opal deposits are present as cements coating breccia fragments in narrow rubble zones, or as thin (1-mm to 5-mm-thick) filled veins with low porosity.

The following sources of primary input data are used to support the conclusions in section 6.10:

- uranium, thorium and lead isotopic data for minerals (section 4.1.17),
- abundances of secondary minerals in the subsurface (section 4.1.18),
- carbon and oxygen isotopic data for minerals (section 4.1.19), and
- strontium isotopic data for minerals (section 4.1.11).

6.10.1 Occurrences of Mineral Coatings

6.10.1.1 Spatial Distribution of Mineral Coatings

The abundance of mineral coatings measured in the ESF ranges from zero to 0.65 percent (DTN: GS980308315215.008). In general, nonwelded tuffs (PTn) with large matrix permeability and few open fractures or cavities have small abundances compared to values in the overlying welded TCw and underlying welded TSw tuffs. Abundance data for all intervals in welded tuffs have an arithmetic mean of 0.084 percent; however, the frequency distribution is strongly skewed, as shown in Figure 50. The data are better represented by a lognormal distribution with a geometric mean of 0.034 percent. A number of factors may control the distribution of hydrogenic minerals in the subsurface, including topography, infiltration, fracture density, fault and shear frequency, and depth. None of these factors are highly correlated to the measured mineral abundances in Figure 51. Instead, abundances measured by visual examination in the ESF show an apparent decrease with increasing stratigraphic depth in Figure 52 and appear to be associated, at least qualitatively, with fault density (Figures 51C and 51D). Preferred estimates of mineral abundances grouped by stratigraphic position show an apparent decrease with depth in the welded tuffs of the Tpt-welded with log means of 0.14 percent for the crystal-rich nonlithophysal unit, 0.06 percent for the

crystal-poor upper lithophysal unit, and 0.03 percent for the crystal-poor middle nonlithophysal unit. Uncertainties for percentages in these groups have substantial overlap.

Preliminary calcite abundance data from WT-24 cuttings indicate large abundances in the near-surface welded TCw that decrease progressively downwards into the PTn (Figure 53). These data imply a progressively smaller amount of evaporation and CO_2 loss from the open fracture network with increasing depth in the TCw (see assumption 22 in Table 2). These data also indicate the likelihood of an inequality between estimates of net infiltration and the amount of recharge to the PTn. Abundances are uniformly low in the lower part of the PTn and shallow part of the underlying welded TSw, but increase with depth below the base of the PTn, especially in the upper and lower lithophysal units. These data will be used to help evaluate the 3-D model of fracture mineral distribution and will provide fundamental information to be used in modeling fracture fluxes based on mineral data.

Mineral coatings in fractures are generally restricted to depositional sites where apertures exceed several millimeters (Paces, Neymark et al. 1996, Section 2.1.1). Individual fractures that vary in aperture along their lengths commonly lack deposits in the narrow-aperture (typically less than 1 mm) portions but may contain coarse sparry calcite and opal in wide-aperture segments (typically greater than 5 mm). Calcite and opal deposits are present on both high-angle and low-angle fractures; however, the nature of the coatings differs between these two fracture settings. Coatings on high-angle fracture surfaces are generally less than 1 to 5 mm in thickness, whereas coatings on low-angle fracture surfaces may attain thicknesses up to several centimeters. Opal is most abundant in coatings on low-angle fractures and is commonly rare or absent in deposits on high-angle fracture surfaces. Fracture coatings are present almost exclusively on the footwalls (lower surface) of open-aperture fractures. Hanging wall (upper) surfaces of the same mineralized fracture, unless near vertical, are almost invariably barren of mineral deposits. Mineral coatings have outer surfaces that clearly grew into the open space. Completely filled fractures, typically between 1 mm and 5 mm in width, constitute a small volume of the total calcite deposited exposed in the ESF, in contrast to veins from the saturated zone that are commonly filled with coarse calcite.

Floors of lithophysal cavities (primary spheroidal cavities, typically 5 to 50 cm in diameter) in and subjacent to the upper lithophysal unit of the TSw can contain coatings of calcite and opal up to 5 to 6 cm thick (Paces, Neymark et al. 1996, Section 2.1.2). More commonly, coatings vary between 0.5 and 3 cm thick. Mineral coatings are present in only a small number of the total lithophysae. Unlike the vapor-phase minerals that cover all surfaces of these cavities, calcite and opal deposits are confined to the floors of the cavities. Walls and ceilings of lithophysal cavities are barren of calcite and opal deposits. Even though the coatings are topographically irregular, forming mound- and lump-like shapes rather than smooth, uniform layers, they typically follow the slope of the floor. In those cases with dipping floors, coatings do not extend up the walls or ceiling on the down-slope end of the cavity.

In most cases, lithophysae are intersected by thin-aperture fractures that could serve as fluid pathways (Paces, Neymark et al. 1996, Section 2.1.2). These can either be high-angle, fractures cutting the cavity ceiling, or bedding-plane partings that extend only short distances away from the lithophysae. In some cases, ridges or valleys preserved in the mineral coatings may correlate

with the lower extension of the fracture. Obvious connections to a fracture network are not always apparent; however fractures may have been removed by the tunneling process, or may remain unexposed. Determination of the actual mechanisms of seepage into the cavities remains as one of the significant uncertainties of these deposits.

In addition, most calcite and opal deposits do not completely fill lithophysal cavities (Paces, Neymark et al. 1996, Section 2.1.2). Typically the thickness of the mineral coating is small relative to the height of the lithophysae. In small or flattened lithophysae with heights of only several centimeters, bladed calcite may extend from the bottom to the top of the cavity. However, even in these instances, the voids between calcite blades remained unfilled and highly porous. Calcite from completely filled thin veins (typically less than several mm thick), which are scattered throughout the rockmass, constitutes only a small proportion of the total volume of fracture minerals.

6.10.1.2 Mineral Morphology

Calcite forms coarse, sparry crystals ranging from equant prisms to thin upright, blades commonly having flaring-upward overgrowths at the blade tips (scepter-head overgrowths) (Figures 2.3 and 2.8 and Section 2.3 of Paces, Neymark et al. 1996; Figures 3 and 4d and p. 8 of Whelan et al. 1998). Opal in post-cooling mineral coatings is present as thin sheets or lacey patchworks veneering calcite crystals or as small hemispheres present at the tips of calcite blades. Both opal and calcite are finely layered (micrometer or finer) and are commonly intergrown at very fine scales. These features contrast markedly with occurrences in the saturated zone where large-aperture fractures are typically completely filled with coarse, banded calcite, and opal is absent. The coatings are also distinct from the granular assemblage of tridymite/cristobalite and minor alkali feldspar and hematite that formed from a high-temperature vapor phase during cooling of the tuffs and uniformly coats floors, walls, and ceilings of lithophysal cavities.

Mineral coatings commonly show a systematic sequence of growth that involves changes in both mineral compositions and textures (Figure 2.8a and Section 2.4 of Paces, Neymark et al. 1996). The oldest parts of the coating commonly include an early silica phase with or without calcite and fluorite. The early silica phase commonly is represented by both chalcedony and euhedral prisms of quartz, which are restricted to basal positions within individual mineral coatings. Main-stage deposits consist of calcite that commonly has blocky to tabular textures in older parts of the coating and delicate thin-bladed textures in the later parts. Opal is the dominant silica phase throughout this main-stage sequence, and commonly is most abundant near outer surfaces.

6.10.1.3 Geochronological Observations

Outermost growth surfaces have been dated using radiocarbon (calcite), ^{230}Th/U (calcite and opal) and ^{207}Pb/^{235}U (opal) methods (Appendices 1 and 2 of Paces, Neymark et al. 1996; Tables B1, D1, and 3E of Paces, Marshall et al. 1997; Figures 2 and 3 of Neymark et al. 1998; Section IV of Paces, Neymark et al. 1998). Radiocarbon dates range from 44 to 16 ka whereas ^{230}Th/U ages range from greater than 500 ka to 28 ka (see assumptions 24 and 25 in Table 2) (Figure 54). Subsamples of opal at or near outer growth surfaces have ^{207}Pb/^{235}U ages that commonly range from about 100 ka to just over 1 Ma. Growth surfaces of mineral coatings show no systematic

^{230}Th/U age differences between calcite and opal regardless of the depositional setting of a mineral coating indicating that lithophysal cavities are just as likely to receive percolating water as the fractures. Mineral coatings from both settings have outer surfaces with ages that are young (typically less than 500 ka) compared to the age of the host rocks (12.7 Ma). However, there are systematic differences between younger radiocarbon ages, intermediate ^{230}Th/U, and older ^{207}Pb/^{235}U ages determined from outer surfaces of the same sample. It is also common for multiple subsamples from the same outer surfaces to have different rather than similar ages. Typically, the thinnest subsamples from a given surface tend to have the youngest ages. Where multiple ^{230}Th/U ages were obtained from different levels within the outer portions of a mineral coating, deeper layers have older ages indicating progressive, outward growth of minerals. At one site (sample HD2074 from ESF station 30+50.7), half-millimeter-radius hemispheres of opal showing distinct micrometer-scale layering have ^{230}Th/U ages of about 152 to 226 ka (Figure 55, Table 28). Microdigestions of the outer layers (10 to 50 µm thicknesses) of these hemispheres have distinctly younger ages between about 4 and 12 ka. Differences in age between the whole hemispheres and their outer layers indicate that deposition of these small opal hemispheres was not geologically instantaneous.

Uranium-lead isotopic systems can also be used to date older layers within mineral coatings (Neymark et al. 1998, p. 86). Opal layers within the interiors of mineral coatings have ^{207}Pb/^{235}U ages that range from about 2 to 8 Ma (Figure 56). Ages were calculated from ^{207}Pb/^{235}U ratios given in DTN: GS970208315215.002 and GS970908315215.013, using the following formula (Dickin 1995, p. 105):

$$\left(\frac{^{207}Pb^{*}}{^{235}U}\right)_{t} = e^{\lambda_{235} t} - 1 \qquad \text{(Eqn. 11)}$$

where ^{207}Pb* is radiogenic Pb resulting from the α-decay of ^{235}U and its daughters, and λ_{235} is the decay constant of ^{235}U, with a value of 9.8485 x 10^{-10} yr^{-1} (Steiger and Jager 1977, p. 359). Ages become progressively older with increasing depth below outer surfaces. Ages of opal near the base of mineral coatings are variable, typically from about 4 to 7 Ma implying that not all mineral coatings were initiated at the same time. Chalcedony has somewhat older ages than opal ranging between about 7.5 to 10 Ma. These results are consistent with paragenetic (depositional sequence) observations. Neither opal nor chalcedony has yielded ^{207}Pb/^{235}U ages older than about 10 Ma resulting in an apparent time gap of over two and a half million years between the deposition of the host tuffs and the oldest fracture mineral ages. It is not clear whether this time gap represents a real period of non-deposition, or whether it represents a thermal signature after which these silica phases were capable of remaining closed to the decay products of uranium. The latter explanation is supported by radiometric ages between 10 and 11 million years for illite/smectite clay minerals from boreholes G-2 and G-1 that formed at temperatures as high as 200 to 275 EC in the deep unsaturated and saturated zones beneath northern Yucca Mountain (Bish and Aronson 1993, p. 148).

6.10.2 Isotopic Compositions of Calcite and Opal

Oxygen, carbon, and strontium isotopic compositions of subsurface calcite were initially determined from fracture coatings in drill core both above and below the water table (Table 1 of Szabo and Kyser 1990; p. 930 and Figure 2 of Whelan and Stuckless 1990; Table 1 and Figure 3 of Whelan and Stuckless 1992; Table 1 of Marshall et al. 1992; p. 1583 and Figure 2 of Peterman et al. 1992; Marshall et al. 1993, p. 1949; Figure 3 of Whelan et al. 1994). Most of the reported $\delta^{18}O$ values vary systematically with depth from the surface (Figure 57) and are consistent with temperature-controlled water-calcite isotope fractionation factors responding to modern-day geothermal gradients of 30 to 40°C per kilometer measured at Yucca Mountain (Szabo and Kyser 1990, p. 1718) (see assumption 23 in Table 2). Variations of both $\delta^{13}C$ and $^{87}Sr/^{86}Sr$ values in drill hole calcite are limited within the unsaturated zone, overlapping the values observed in soil carbonate (Whelan et al. 1994, p. 2738; p. 1950 and Figure 5 of Marshall et al. 1993). However, $\delta^{13}C$ and $^{87}Sr/^{86}Sr$ values for unsaturated-zone calcites are distinct from values for calcites in the saturated zone, precluding an upwelling source of water in the unsaturated zone (Figures 58 and 68).

Calcites from mineral coatings in the ESF have a much wider range of $\delta^{13}C$, $\delta^{18}O$ and $\delta^{87}Sr$ values than those characterized from deposits sampled from drill core (Sections 4.1 and 4.2 of Paces, Neymark et al. 1996; Whelan et al. 1998, p. 13). Values of $\delta^{13}C$ vary from about -8.2 to +8.5 per mil and $\delta^{18}O$ vary from about 21 to less than 10 per mil (Figure 59). Compared to previous determinations of stable isotope compositions of drill core calcite, a larger percentage of ESF calcite analysis have $\delta^{13}C$ values greater than 0 per mil and $\delta^{18}O$ values less than 15 per mil. This difference is likely related to differences between the quality of the mineral coatings available for subsampling between the drilling and tunneling programs. Both $\delta^{13}C$ and $\delta^{18}O$ in calcite are negatively correlated such that subsamples with large $\delta^{13}C$ values tend to have small $\delta^{18}O$ values (Figure 60). Systematic microsampling across individual mineral coatings indicates that $\delta^{13}C$ values in calcite shifted from larger values (+2 ‰ to +9 ‰) early in the depositional history to intermediate values (-3 ‰ to 0 ‰) and finally to smaller values (-8 ‰ to -5 ‰) with time (Figure 61). Calcite microsamples show similar correlations between age and composition. Late calcite $\delta^{18}O$ values from coatings within the Tiva Canyon Tuff typically range from 18 ‰ to 21 ‰ whereas coatings from deeper in the Topopah Spring Tuff have $\delta^{18}O$ that varies from 16 ‰ to 18 ‰. Early calcite has $\delta^{18}O$ values less than 16 ‰, and even less than 10 ‰ for some of the earliest calcite from basal positions within mineral coatings.

Opal, quartz and chalcedony also show shifts in both abundance and $\delta^{18}O$ compositions with time (Figure 62: data from Moscati and Whelan 1996, Table 1; Whelan et al. 1998, Appendix 3). Massive chalcedony, deposited early in the depositional sequence, has the smallest $\delta^{18}O$ values (7.9 ‰ to 17.3 ‰). Quartz also formed early in the mineralization sequence although it is commonly deposited on top of, and slightly later than, chalcedony. Values for $\delta^{18}O$ in quartz are substantially larger than in chalcedony (16.8 ‰ to 22.8 ‰). Opal deposited throughout the intermediate and late stages of the depositional history of mineral coatings overlaps the values for early quartz but extends the range of $\delta^{18}O$ to even larger values (18.0 ‰ to 27.9 ‰).

Strontium isotope ratios from ESF calcite overlap the range reported previously from drill core samples, but extend the range to much smaller values (Figure 4.7 of Paces, Neymark et al. 1996). Variations in $^{87}Sr/^{86}Sr$ are crudely correlated with microstratigraphic positions within individual mineral coatings showing a general trend of decreasing ratios with relative age (Figure 63). Late calcite has $^{87}Sr/^{86}Sr$ values of 0.7115 to 0.7127 directly overlapping previously published values from pedogenic calcite deposits (Figure 5 of Marshall and Mahan 1994). Early calcite generally has the least radiogenic $^{87}Sr/^{86}Sr$ ratios between 0.7105 and 0.7120 whereas intermediate-aged calcite has $^{87}Sr/^{86}Sr$ between these two ranges. Strontium concentrations show a less well-defined variation with time; however, calcite from the early and intermediate groups typically has concentrations less than about 130 µg/g (Figure 63) whereas late calcite commonly has larger concentrations. Strontium isotope ratios from subsamples across mineral coatings show distinct correlations with carbon and oxygen isotopes that are probably related to a gradual evolution of isotopic compositions in water percolating through fractures (Figure 64). The relatively large amount of scatter observed in these correlations indicate that separate, time-dependent processes most likely control the resulting isotopic composition of fracture water.

An initial $^{234}U/^{238}U$ ratio can be calculated from the measured uranium isotopic composition and the $^{230}Th/U$ age of a given mineral, assuming the mineral has behaved as a closed isotopic system. This initial $^{234}U/^{238}U$ represents the isotopic composition of percolating waters at the time of mineral deposition. Values for initial $^{234}U/^{238}U$ activities in outermost opal and calcite span a wide range from about 1 to over 9. When plotted against their associated $^{230}Th/U$ age, initial $^{234}U/^{238}U$ ratios show a scattered but distinct negative correlation (Figure 65) indicating that older subsamples tend to have smaller initial ratios (section 3.2.3 of Paces, Neymark et al. 1996). This relation generally is true for both multiple subsamples from a single mineral coating as well as for the entire set of data. Taken at face value, this trend suggests that fracture water has become progressively enriched in ^{234}U over the last 500 ka; however, mechanisms causing this type of long-term trend are difficult to imagine. Other natural reservoirs of uranium, such as soil (Figure 2D and p. 2400 of Paces et al. 1994; Figures 9, 10, 13, 16, 17, 20, 21, 25, 26, 27, 32, 36, 39, 42, 45, 46, and 53 of Paces et al. 1995) and ground water (Figure 5 of Ludwig et al. 1992; Figure 20 of Paces, Forester et al. 1996; Figures 4, 11, and 13 of Paces, Whelan et al. 1997) have $^{234}U/^{238}U$ that appear to remain relatively uniform over similar time periods. The observed negative correlation between age and initial $^{234}U/^{238}U$ ratios has been explained using a constant $^{234}U/^{238}U$ in fracture water at a given depositional site but by the presence of both older layers with small present-day $^{234}U/^{238}U$ and younger layers with larger present-day $^{234}U/^{238}U$ in individual subsamples (section 3.4 of Paces, Neymark et al. 1996). The resulting initial $^{234}U/^{238}U$ in opal and calcite subsamples is therefore strongly influenced by the age of the oldest layer present in the analyzed subsample, and the proportion of older and younger materials mixed together.

Outermost calcite with ages less than 100 ka are minimally impacted by this analytical artifact. Initial $^{234}U/^{238}U$ activity ratios observed in these younger materials still span a large range from 4 to 9.5 implying isotopic heterogeneity of fracture water in different unsaturated-zone flow paths. In addition, available isotopic data indicates that $^{234}U/^{238}U$ in fracture water has varied systematically with depth in the unsaturated zone (Figure 66; also Figure 3 of Paces, Neymark et al. 1998). Calcite and opal within the shallow unsaturated zone (Tpc and PTn) have maximum initial $^{234}U/^{238}U$ ratios similar to those values observed in soils and surface runoff (about 1.5 to slightly greater than 2). In contrast, maximum initial $^{234}U/^{238}U$ ratios attained by calcite and opal

from below the PTn increase with depth in the TSw, reaching activity ratios up to 9 at the level of the potential repository (Figure 66). Therefore, ^{234}U-enrichment with depth is a function of the percolation process and contains information related to the history and mechanisms of unsaturated-zone flow. This issue is discussed in greater detail in section 6.6.7.

6.10.3 Interpretation of Isotopic Data for Fracture Minerals

Assumption 23 in Table 2 applies to discussions throughout this section.

6.10.3.1 Interpretation of Ages

Conventional age models (Ivanovich and Harmon 1992, p. 781) assume that mineral deposition occurs instantaneously and that the resulting deposit consists of a layer of finite thickness, constant age, and uniform initial isotopic compositions. However, even the finest scale of subsampling is unable to resolve this layering, and therefore, subsamples represent mixtures of both younger and older layers and the resulting measured isotopic ratios will be intermediate between the values of the end members. A depositional model that is more consistent with observed data is based on the observation of very thin layers at a micrometer scale that are likely added more or less continuously (Section 3.4 of Paces, Neymark et al. 1996). The model predicts many of the features observed in the geochronological data sets including subsample thickness and resulting age, wide-ranging ages from a single outer surface, the discordance between isotopic systems with different half-lives, the negative correlation between ^{230}Th/U age and initial ^{234}U/^{238}U ratios, and ages that are less than those at which secular equilibrium or complete decay is attained (Figures 3.13 and 3.14, and Table 1 of Paces, Neymark et al. 1996).

6.10.3.2 Growth Rates

Slow long-term rates of deposition (less than about 5 mm of mineral per million years) are inferred from subsamples of outermost calcite and opal. Measurements of ^{230}Th/U age and estimates of the thickness for subsample of individual opal hemispheres and microdigestions of their outermost surfaces yield estimated growth rates of between 0.4 and 6 mm/Ma (Table 28). Growth rates estimated from both millimeter and micrometer scales are similar. Rates of the same order of magnitude calculated assuming a continuous deposition model of mineral growth closely match the observed U and Th isotopic data (Section 3.4 of Paces, Neymark et al. 1996). In addition, similar rates are obtained for the generalized case assuming that the 0.5- to 3-cm-thick mineral coatings accumulated over a 12.7 million year period (Section 3.4 of Paces, Neymark et al. 1996).

Long-term growth rates over the last 8 million years can also be calculated from the U-Pb ages of interior opal layers within mineral coatings (Table 4E of Paces, Marshall et al. 1997; Neymark et al. 1998, p. 86). Average long-term growth rates of 1 to 4 mm/Ma are calculated using thicknesses measured between dated layers in mineral coatings within the Topopah Spring Tuff (Figure 67). Although this range of rates varies by only a factor of about 3 between different mineral coatings, rates calculated for different layers within individual coatings are even more uniform, typically within a factor of 40%, regardless of relative position within the coating. In contrast, mineral coatings from the Tiva Canyon Tuff have more complex depositional relations including more rapid growth rates and obvious depositional hiatuses (Neymark et al. 1998, p. 86).

Growth rates during the early stages of mineral deposition throughout the unsaturated zone remain uncertain because of the absence of opal with ages older than about 8 Ma as well as the smaller number and lower precision of chalcedony dates between 8 and 10 Ma. The similarity of mineral growth rates based on independent methods of $^{230}Th/U$ dating for outer layers and $^{207}Pb/^{235}U$ dating for interior layers, plus the uniformity of rates within and between mineral coatings over the last 8 million years, indicate that fracture flow systems in the deep unsaturated zone have been buffered from Neogene and Quaternary climate variations (see Section 6.10.3.7 on long-term isotopic shifts).

6.10.3.3 Source of Unsaturated-Zone Water

Isotopic data from unsaturated zone minerals strongly support a descending meteoric water source that has interacted with soil at Yucca Mountain, and refute a saturated-zone source. Textural gradations in the upper 10 to 30 meters of the unsaturated zone provide a genetic link between the fine-grained, detritus-rich pedogenic deposits, and the detritus-free, coarse calcite and opal present in the deeper unsaturated zone. Isotopic compositions of oxygen, carbon and strontium in late unsaturated-zone calcite also completely overlap the isotopic compositions of calcite observed within Yucca Mountain soils (Figure 5 of Marshall and Mahan 1994; Figure 4 of Vaniman and Whelan 1994; Figure 4.11 of Paces, Neymark et al. 1996; Whelan et al. 1998, p. 13). Values of $\delta^{13}C$ and $\delta^{18}O$ in late unsaturated-zone calcites are also consistent with the present-day carbon isotopic compositions of CO_2 and HCO_3^- in unsaturated-zone gas and PTn pore waters. Carbon dioxide gas in isotopic equilibrium with late calcite has calculated $\delta^{13}C$ compositions between about -5 ‰ to -18 ‰ (enrichment factor for low temperature $CO_{2(g)}$-calcite, from Clark and Fritz 1997, inside front cover), overlapping the heavy end of $\delta^{13}C$ values measured in unsaturated-zone gas (Figure 35b).

The amount of fractionation between oxygen isotopes is more sensitive to mineral formation temperature than are carbon isotopes. Temperature gradients calculated from $\delta^{18}O$ compositions of calcite and depth relations are similar to measured unsaturated-zone geothermal gradients in several boreholes at Yucca Mountain, yielding average values of about 35°C/km (Sass et al. 1980, 1988; Szabo and Kyser 1990, p. 1718). Water in equilibrium with late calcite in the Tiva Canyon Tuff (calcite $\delta^{18}O$ values of 18 ‰ to 21 ‰) at temperatures between 18 °C and 21°C should have $\delta^{18}O$ values of about -10 ‰ to -12 ‰. Warmer temperatures at the repository horizon (ESF main drift temperatures of about 27°C) result in similar estimates of water $\delta^{18}O$ values in equilibrium with calcite $\delta^{18}O$ values of +16.5 ‰ to +18 ‰. Conditions during pluvial episodes throughout the Quaternary would yield somewhat cooler subsurface temperatures and slightly more negative water $\delta^{18}O$ estimates (-11 ‰ to -14 ‰). Modern precipitation (individual rain events dropping more than 0.25 cm and snowfalls at Yucca Mountain) has $\delta^{18}O$ values ranging between about -9 ‰ and -18 ‰ (Figures 14 and 16 of Benson and Klieforth 1989) with mean $\delta^{18}O$ values of -8 ‰ to -10‰. Mean $\delta^{18}O$ values for precipitation during the cooler pluvial conditions of the Pleistocene were likely to be somewhat more negative. Unsaturated-zone pore waters distilled from the welded tuffs or squeezed from the non-welded tuffs have $\delta^{18}O$ values that generally range from -14 ‰ to -12‰ (Figure 37b), also suggesting a pluvial origin.

In contrast, carbon and oxygen isotope values in unsaturated-zone calcite are difficult to reconcile with a saturated-zone source of water. Ground water from the shallow part of the saturated zone beneath Yucca Mountain has dissolved inorganic carbon $\delta^{13}C$ values of about - 11 ‰ to - 7 ‰, and $\delta^{18}O$ values of - 13 ‰ to - 14 ‰ (Table 6 of Claassen 1985; Table 1a of Benson and Klieforth 1989; Table 1 of White and Chuma 1987). Although waters with these compositions would yield calcite with $\delta^{13}C$ similar to those observed in unsaturated-zone calcite, the $\delta^{18}O$ values of -13 ‰ to -14 ‰ and present-day ground water temperatures of 30° C would result in calcite with $\delta^{18}O$ values of +13 ‰ to +14 ‰.

Shallow ground water from the saturated zone beneath Yucca Mountain has $^{87}Sr/^{86}Sr$ ratios between 0.7093 and 0.7116 (Figure 2 of Peterman and Stuckless 1993; Peterman and Patterson 1998, p. 277 to 278). These values are less radiogenic than either late unsaturated-zone calcite or pedogenic calcite. In addition, saturated-zone ground water beneath Yucca Mountain is undersaturated with respect to calcite and would tend to dissolve rather than precipitate material in unsaturated-zone fractures (Section 6.2 of Paces, Neymark et al. 1996). Calcite-saturated ground water from the deeper Paleozoic-carbonate aquifer has the same problems with $\delta^{18}O$ and $^{87}Sr/^{86}Sr$, but also has a carbon isotopic composition that would result in $\delta^{13}C$ values that are much larger than those observed in the late unsaturated-zone calcite. Field, morphologic, chemical and isotopic arguments have been used previously to refute a saturated-zone water source for pedogenic calcite deposits (Muhs et al. 1990, p. 928 and Figure 3; Stuckless et al. 1991, p. 553; Stuckless 1991, p. 1429; National Research Council 1992, p. 5; Whelan and Stuckless 1992, p. 1580; Vaniman et al. 1994, p. 15; Vaniman and Whelan 1994, p. 2736; Taylor and Huckins 1995, Table 5 and pp. 19 to 24; Stuckless et al. 1998, p. 76). Strontium and calcium concentrations within the zeolitized Calico Hills formation above the modern water table vary vertically and also support a descending water source (Vaniman et al. 1999, p. S5). In addition, a defensible physical mechanism responsible for saturated-zone ground water upwelling more than a few meters above the static water table has not been identified (National Research Council 1992, pp. 136 to 139 and p. 212; Rojstaczer 1999, p. S4).

Although fracture water percolating through the unsaturated zone has not been sampled at Yucca Mountain, its major element composition is probably intermediate between runoff and perched water intercepted in boreholes at depth. Precipitation rapidly interacts with calcite- and opal-rich materials in surface deposits, typically reaching chemical saturation with respect to calcite and opal after only brief overland flow (Figure 6.2 of Paces, Neymark et al. 1996). Fracture water is likely to have compositions that are similar to or even more chemically evolved than runoff samples considering the interactions that take place during infiltration through calcite- and opal-rich soils and possible silicate/water interaction that occurs within the nonwelded tuffs of the PTn. Chemistries of perched-water bodies, presumably recharged largely by fracture flow, support this expectation. Therefore, descending fracture water is likely to be at or very near levels of saturation with respect to both calcite and opal. Chemical and textural arguments imply that once fracture water reaches mineral saturation, it is not likely to later become undersaturated during further descent through the unsaturated zone.

6.10.3.4 Mechanisms of Mineral Deposition

The process of unsaturated-zone mineral deposition is initiated during infiltration where meteoric water interacts with materials in the soil, after which a portion may then enter the bedrock fracture network. Fracture water is distributed into connected pathways in response to gravity-controlled downward percolation as thin films that do not require complete water saturation of the fractures within the welded tuff (Tokunaga and Wan 1997, p. 1287). Physical and textural evidence indicates that these coatings of calcite and opal must have formed in hydrologically unsaturated environments with the additional requirement of the presence of open space (Sections 2.1 and 2.5 of Paces, Neymark et al. 1996). Textures indicate that mineral growth commonly occurs at the tips of calcite blades and that a mechanism is required to transport dissolved ions to these sites where solutions reach supersaturation. Differences in textures between near-horizontal substrates and high-angle fractures indicate that slowing of downward-migrating water may play an important role.

These observations plus the presence of mineral coatings in open cavities imply a depositional mechanism involving liquid/gas exchange including loss of both CO_2 and water vapor. Other mechanisms of mineral precipitation do not provide adequate explanations of the observed textural and mineralogical features. Although an increase in temperature in response to the geothermal gradient may explain some of the calcite deposition, it does not account for the distribution of calcite with depth in either the ESF or WT-24 drill cuttings (Figures 52 and 53). It also does not provide an explanation for opal precipitation, which should be more soluble at greater temperatures. Silicate hydrolysis may provide an alternative mechanism for opal deposition; however, the devitrified welded tuffs consist of quartz and potassium feldspar which are not particularly reactive at low temperatures, and the calcite/opal coatings lack evidence of aluminosilicate phases required to balance the hydrolysis reactions. Both thermal and hydrolysis mechanisms would permit mineral precipitation in narrow aperture fractures and small pores which generally are not observed. Also, neither of these mechanisms readily explains the mineral textures observed in many of the open cavities (delicate calcite blades, opal concentrations at blade tips, fine-scale intergrowths of calcite and opal, and textural differences between steep and shallow fracture cavities).

A more likely depositional mechanism for calcite precipitation involves transport of both CO_2 and water vapor in an independently migrating gas phase (see assumption 22 in Table 2). Such a mechanism also accounts for simultaneous deposition of calcite and opal from a single solution. Rates of mass transfer of both water vapor and CO_2 from deeper parts of the unsaturated zone are likely to be small; however, operation over long time periods may explain the very slow growth rates observed in the calcite-opal coatings at the level of the potential repository. A depositional mechanism involving interactions between liquid and gas phases also offers possible explanations for the observed textural features. Because physical evidence indicates that the coatings formed in locally unsaturated environments, thin films of water seeping into fracture and lithophysal cavities are the likely source of solutions. Water films may only be present on some fraction of the total surface area at any given time. An uneven distribution of wetted surfaces likely contributes to the age heterogeneities observed for different subsamples of the same outer surfaces of a mineral coating. Thin water films must also be capable of wicking up the outside surfaces of elongated calcite blades by capillary processes similar to those that form anthoditic

speleothems. Water that moves out of cavities and back into the fracture network can form additional calcite and opal at sites deeper in the unsaturated zone by further losses of CO_2 and water vapor as the fracture water descends toward the water table.

6.10.3.5 Conceptualization of Seepage into Cavities from Secondary Calcite

Seepage of water into emplacement drifts is a major factor contributing to a calculated release of radionuclides, but estimates of seepage flux based on hydrologic parameters have large uncertainties. Densely welded Topopah Spring Tuff in the thick unsaturated zone at Yucca Mountain is the host rock for a potential high-level radioactive waste repository. Observations in the ESF show that the welded tuffs contain both large-aperture fractures and lithophysal cavities containing secondary calcite and opal deposited from downward-percolating water that has seeped into these openings in the past (DTN: GS980308315215.008). Uranium-lead dating indicates that these minerals formed throughout most of the timespan since the tuffs were emplaced 12.7 million years ago.

The percentage of lithophysae containing secondary minerals within the upper lithophysal zone of the Topopah Spring Tuff is variable, ranging from 1 to 40 percent per 30 m of tunnel length (DTN: GS980308315215.008). Because essentially all the cavities are intersected by fractures, the lack of secondary mineral coatings in some cavities is interpreted to indicate a lack of flow in some of the fractures. Calcite typically composes 90 percent of the low-temperature mineral assemblage. Calcite is abundant in the calcic soils at Yucca Mountain, leading to rapid saturation of infiltrating water with respect to calcite. The volcanic rocks are calcium (Ca)-poor so infiltrating water is essentially the only source of Ca available to form the calcite in the unsaturated zone. Therefore, the calcite that has formed in a cavity can be related directly to an amount of water required to transport that amount of Ca into the cavity (Marshall et al. 1999, p. S5; Marshall, Paces et al. 1998, pp. 127 to 129). The calculated amount of water would be a minimum estimate of the amount of water that actually seeped into the cavity unless the water evaporated completely within the cavity. However, calculation of the total seepage flux for the whole unsaturated zone based on measurements of total calcite abundance in the ESF indicates a flux of about 2 millimeters per year, which is within an order of magnitude of the estimated long-term infiltration flux at the surface.

Calculated rates of water flow into cavities over the past 10 million years, using 0.3 to 2-cm coating thicknesses in hypothetically spherical cavities ranging from 12 to 40 cm in diameter, would range from about 0.007 milliliters per year to about 20 milliliters per year. Scaling of detailed line survey data to the 5-meter diameter of the potential emplacement drifts, the estimated seepage rate per 5-m length of drift is 0.1 to 1000 milliliters per year.

Observations of calcite and opal in cavities in the unsaturated zone at Yucca Mountain indicate that: 1) seeps are not regularly spaced in underground workings and there has been no change in seepage locations over time, 2) not all fractures sustain flow, 3) there is no evidence (such as dripstone) for seepage dripping into cavities from their ceilings, and 4) an actively flowing fracture intersecting a 5-m diameter tunnel is not likely to produce more than about 1 liter of water per year based on calcite abundances observed in the ESF. This estimate of seepage is significantly lower than that used for performance assessment.

6.10.3.6 Thermal Evolution of the Unsaturated Zone

Patterns of $\delta^{18}O$ variations in both silica phases and calcite preserve a record of decreasing temperatures as deposition progressed with time in the unsaturated zone. Early chalcedony and quartz have $\delta^{18}O$ values that imply elevated unsaturated-zone temperatures (as high as about 80°C) with respect to the modern geothermal gradient. Heat sources included the cooling tuffs themselves during the first few thousands to hundreds of thousands of years, as well as the steeper geothermal gradients associated with regional magmatism during the first several million years after tuff emplacement. Small $\delta^{18}O$ values in early calcite also support the notion of higher temperatures as indicated by early silica phases. Larger $\delta^{18}O$ values in quartz and subsequent opal and calcite indicate that geothermal gradients reached near-modern values by the time that the bulk of the mineral coatings were deposited.

6.10.3.7 Long-Term Isotopic Shifts

Isotopic compositions of fluids continued to evolve after Yucca Mountain reached modern-like thermal gradients by the end of the episode of early chalcedony/quartz deposition between 8 and 10 million years ago. Carbon isotopic compositions are relatively enriched in ^{13}C in intermediate calcite with $\delta^{13}C$ values of about +3 ‰ to - 5 ‰ compared to late calcite with $\delta^{13}C$ values of about - 5 ‰ to - 9 ‰ (Figure 4.6 of Paces, Neymark et al. 1996; Figures 1 and 2 of Whelan and Moscati 1998). This shift in composition is presumably caused by changes in the composition of the corresponding plant communities at the surface, which are in turn a function of changes in climate, as discussed in Boutton (1996, pp. 50 to 57). Carbon isotopic data indicate that the earlier plant community was dominated by C_4 plants (using the Hatch-Slack photosynthetic pathway), which produced soil CO_2 gas enriched in ^{13}C. Water infiltrating through this soil deposited subsurface calcite with characteristic $\delta^{13}C$ compositions of - 3 ‰ to 0 ‰. Carbon isotopic compositions in the late calcite indicate that the plant community had evolved to one with a larger C_3 (using the Calvin photosynthetic pathway, Boutton 1996, pp. 50 to 57) component in more recent times. Dating by the U-Pb method indicates that this major shift in $\delta^{13}C$ values occurred between about 2 and 4 million years ago (p. 14 and Figure 3 of Whelan and Moscati 1998). During this same time, climate conditions were undergoing a major change from milder, wetter conditions characteristic of the Tertiary to the more severe, semi-arid conditions of the Quaternary. Despite this major shift from wetter to drier conditions, mineral growth rates in the deep unsaturated zone remained unchanged, suggesting that the deep fracture flow may be buffered from substantial variations in infiltration.

Strontium isotopic compositions of fracture water have also changed over the last 8 million years. Early calcite has $^{87}Sr/^{86}Sr$ ratios of about 0.7105 to 0.7120 whereas late calcite has more radiogenic values of 0.7118 to 0.7127. Two different factors may have affected this temporal shift in $^{87}Sr/^{86}Sr$ ratios. Large Rb/Sr ratios in the felsic tuffs cause the $^{87}Sr/^{86}Sr$ ratio of the wall rocks to evolve to larger values over time through decay of ^{87}Rb to ^{87}Sr. Strontium in fracture fluids that is derived from water/rock reaction in the more reactive portions of the flow paths (nonwelded tuffs of the PTn) will therefore have larger $^{87}Sr/^{86}Sr$ values in more recent calcite relative to early calcite. In addition, development of calcite-rich soils at Yucca Mountain in response to increased aridity during the Quaternary provides a large reservoir of readily leachable

Sr during infiltration. The similarity of $^{87}Sr/^{86}Sr$ compositions in late ESF calcite to values in pedogenic deposits (Figure 64) is probably not a coincidence.

6.10.3.8 Mineral Growth Rates and Quaternary Climate Variations

Geochronological and isotopic data show no strong evidence of the effects of pluvial-interpluvial climate variations during the last several glacial cycles (Section 7 of Paces, Neymark et al. 1996). Although evidence throughout the Great Basin suggests cooler conditions and greater amounts of precipitation were common during pluvial episodes (Haynes 1967, pp. 77 to 82; Mifflin and Wheat 1979, pp. 37 to 50; Spaulding 1985, pp. 27 to 45; Quade et al. 1995, pp. 213 to 228; Bradbury 1997, pp. 99 and 109 to 111), $^{230}Th/U$ ages of calcite and opal show neither an increase nor decrease in frequency during these intervals (see assumption 25 in Table 2) (Figure 54). Records of late calcite and opal show no obvious evidence of dissolution during periods of greater meteoric precipitation. Carbon and oxygen isotopes also show a range of two to three per mil in late calcite; similar to the entire range of variation seen in pluvial and interpluvial records from saturated-zone calcite at nearby Devils Hole (Figure 2 of Winograd et al. 1992; Figure 2 of Coplen et al. 1994). If deposition of unsaturated-zone calcite was affected by Quaternary climate variation, a more restricted range of $\delta^{13}C$ and $\delta^{18}O$ values at either the larger or smaller end of the range observed in late calcite might be expected. These observations are consistent with the concept that the average rate of deposition of unsaturated-zone opal and calcite at the potential repository horizon may be relatively constant over long periods of time

6.10.3.9 Implications of Mineral Data for Long-Term Unsaturated-Zone Hydrologic Behavior

Observations of slow, uniform, average growth rates over long periods of time imply that the unsaturated zone fracture network has maintained a large degree of hydrologic stability over time. Evidence from mineral coatings implies that fracture flow in the deep unsaturated zone is buffered from climate-induced variations in precipitation and infiltration. Buffering may be accomplished by a number of different processes that operate at different stratigraphic levels within the unsaturated zone as well as on a spectrum of magnitude scales. Because these processes are complex, the concept that net infiltration equates directly to recharge to the water table is probably an oversimplification at Yucca Mountain.

Numerous processes occurring in the near-surface environment are likely to damp net infiltration in response to climate-induced variations in meteoric precipitation. Long-term variations in mean annual precipitation result in changes to the plant community. Consequently, the plant biomass and its associated evapotranspiration may be able to utilize much of the mean annual effective moisture available during any given climate state. A proportion of shallow infiltration that is not capable of being utilized by plants is diverted down-slope along the tuff/colluvium interface. The presence of massive calcrete deposits in thicker colluvial or alluvial surface deposits on the down-thrown side of normal faults provides evidence of a greater accumulation of soil water at these sites. The large permeability contrast between colluvium and welded TCw over most of the site is likely sufficient to provide an effective mechanism for downslope lateral diversion. In addition, many of the near-surface fractures in the welded TCw are largely filled with pedogenic calcite and opal, and although their permeability may still be greater than the welded tuff, direct ingress into

the fracture network is likely to be further restricted. Surface runoff from the slopes into alluvial-filled drainages further diverts infiltration during extreme precipitation events.

Once net infiltration enters the subsurface fracture network, hydrogeologic processes may further dissipate, divert, or reduce downward fluxes. Calcite abundances show a systematic decrease with depth through the TCw in cuttings from borehole WT-24 (Figure 53), requiring a hydrologic process that results in a progressively smaller mass of Ca^{2+} at greater depths from the surface (see assumption 22 in Table 2). One way to achieve this result is through non-steady-state net infiltration that frequently provides fluxes to the shallowest bedrock fractures and only infrequently provides fluxes to deeper levels of the TCw. This process implies that not all net infiltration events ultimately result in local recharge to the saturated zone. The data could also be explained under a steady-state flux environment if the degree of gas loss decreased progressively within the TCw such that greater amounts of CO_2 and water vapor are removed from the shallowest levels within the bedrock. In the latter scenario, rates of mineral deposition are also likely to decrease with depth and may help explain the gradual transition of textures from microcrystalline calcite and turbid opal in near-surface veins to the coarse, sparry calcite and transparent, glassy opal observed at depths below about 10 to 20 meters. Both of these scenarios imply that the amount of percolation through the TCw fracture network contributing percolation to the PTn is less than the amount of net infiltration at the base of the root zone.

Most water flowing through fractures in the welded TCw is intercepted by nonwelded tuffs of the PTn where flow occurs dominantly through the high permeability matrix. The PTn decreases in thickness from north to south at Yucca Mountain (p. 8 and Figure 4 of Moyer et al. 1996) and has a large capacity to store water recharging through the TCw . Therefore, short-term variations in percolation flux are likely to be buffered by fluctuations in the degree of saturation within this unit. In addition, a portion of the matrix flow may be diverted down dip towards the east to structurally disturbed zones where greater amounts of vertical flow may be focused.

6.10.3.10 Comparisons of Fracture Minerals with $^{36}Cl/Cl$ Data

The concept of slow and more-or-less uniform growth of fracture minerals over long periods of time implies that the fracture flow system in the deep unsaturated zone tends to be sluggish in response to short-term variations in meteoric precipitation and infiltration. This conclusion appears to conflict with those based on elevated $^{36}Cl/Cl$ signals in the ESF that are interpreted as evidence of rapid (50 years or less) liquid flow through fractures to the level of the potential repository (Section 6.6.3). Possible explanations for this apparent discrepancy have been proposed in Fabryka-Martin, Flint et al. (1997, Section 6.2.4) including:

- The possibility that the two different methods have sampled two different flow networks.
- The possibility that fast paths transmit water that is unsaturated with respect to calcite or silica and leave no mineralogical records of this hydrologic activity.
- The possibility that youngest mineral ages record cessation of flow due to blocking or diversion of individual flow channels along the fracture surface as a result of mineral deposition.

- Slow, long-term mineral growth rates may not form deposits on time scales relevant to decade- to century-scale flow that are sufficiently thick for petrographic or geochronological resolution.

Although these reasons may represent possible explanations, the two interpretations may not be mutually exclusive. Both conceptual models imply that relatively small volumes of fracture fluid are responsible for the observed phenomena. The absence of elevated $^{36}Cl/Cl$ signatures in perched water or saturated-zone ground water beneath Yucca Mountain constrains the fast-path contribution to a very limited component of the total fracture flux. In addition, dating of calcite and opal places constraints on the time at which the solid phase became closed to mobilization of parent and daughter isotope. However, there is no inherent information on the unsaturated-zone travel times preserved in these analyses. Waters from which the minerals were deposited could have been 50 or 50,000 years old at the time of mineral formation, yet geochronological information would be the same in both cases. Large volumes of water or extremely rapid percolation are expected to yield consistently small $^{234}U/^{238}U$ ratios at the sampling site at depth. However, the uranium isotopic response to percolation of very small volumes of rapid flow might not be noticed if it is spatially restricted, and if the small amounts of ^{238}U inherited from the surface source are still able to be assimilate sufficient ^{234}U from flow-path surfaces.

In order to provide additional confirmation, work is currently underway to more thoroughly evaluate the distribution of $^{36}Cl/Cl$ across two structural zones within the ESF that exhibited bomb-pulse signatures in previous reports (Drill Hole Wash Fault and Sundance Fault) using a suite of bomb-pulse indicators including $^{36}Cl/Cl$, ^{3}H, ^{99}Tc and ^{129}I. In addition, samples of fracture surfaces are being analyzed for uranium isotopic disequilibrium for evidence of recent hydrologic activity.

6.11 THERMAL HISTORY OF THE UNSATURATED ZONE

The following sources of primary input data are used to support the conclusions in section 6.11:

- uranium, thorium and lead isotopic data for minerals (section 4.1.17),
- abundances of secondary minerals in the subsurface (section 4.1.18),
- carbon and oxygen isotopic data for minerals (section 4.1.19), and
- other input data for minerals (section 4.1.20).

6.11.1 Isotopic and Fluid Inclusion Evidence of Unsaturated-Zone Temperature

At present, models of future flow through the potential repository assume that this zone will remain, as it is today, well above the water table. This assumption is based in large part on evidence collected from deposits of calcite and opal found in cavities and open fractures of the unsaturated zone (Whelan et al. 1994, p. 2744; Whelan et al. 1999, p. S-8; Paces, Neymark et al. 1996, Section 2.1; Paces et al. 1999, p. S-4). Taken in its entirety, this evidence argues strongly that the water table has always remained well below the level of the potential repository and that the modern extent of the unsaturated zone is representative of past conditions, at least since uplift

and tilting of the volcanic sequence. This interpretation, however, has been disputed. Hill et al. (1995, p. 86), Dublyansky et al. (1996, pp. 38 to 39), Dublyansky (1999, p. S-4), and Dublyansky and Reutsky (1998, p. A-79) have suggested that most, perhaps all, of this calcite and opal was deposited by repeated, and possibly recent, flooding of the potential repository by heated fluids upwelling from below.

The upwelling hypothesis is based, in part, on a limited amount of data from calcite-hosted fluid inclusions. Minimum formation temperatures estimated from calcite-hosted fluid inclusions cluster between 35 and 55°C but locally range up to 70 to 85°C (Dublyansky et al. 1996, pp. 38 to 39; Dublyansky 1999, p. S-4; Dublyansky and Reutsky 1998, p. A-79). The position of these inclusions within the respective calcite samples, that is, whether they represent old or recent depositional conditions, is generally not described although the warmest temperatures (70 to 80°C) are ascribed to the oldest portion of that sample. Calcite $\delta^{18}O$ values, coupled with paragenetic and age relations, provide independent evidence of past temperatures in the unsaturated zone. This evidence indicates that the tuffs experienced an episode of elevated temperature (perhaps up to about 100°C) during the earliest stage of calcite formation.

6.11.2 Paragenetic Relations and Sampling Protocols

Previous studies (e.g., Whelan et al. 1994, p. 2738) have shown that the unsaturated-zone calcite $\delta^{13}C$ and $\delta^{18}O$ coincide with those of pedogenic carbonate in the overlying soils (Figure 68). Inasmuch as the $\delta^{13}C$ of soil carbonate is a function of the types of plants present, and thus of the climate, the $\delta^{13}C$ of the unsaturated zone calcite is a record of climate at the time of infiltration. The steady decrease of calcite $\delta^{18}O$ with depth is a reflection of the depositional temperature.

The fractionation of oxygen isotopes between calcite and water is temperature sensitive. Figure 69 plots this fractionation against temperature and shows, for low temperatures, a change of about 0.18‰/°C (O'Neil et al. 1969, p. 5552; Kim and O'Neil 1997, p. 3467). If any two of the variables—$\delta^{18}O$ of calcite, $\delta^{18}O$ of water, or temperature—are known, then the third can be estimated. This relation permits some useful inferences to be made from the calcite $\delta^{18}O$ values. It also explains the gradual decrease of calcite $\delta^{18}O$ with depth as a reflection of warming of the calcite-depositing water down the local geothermal gradient.

Roughly 300 samples of calcite and opal deposits have been collected from ESF exposures by the Environmental Science Team of the USGS; input data resulting from these samples are listed in Sections 4.1.17 and 4.1.19. Mineralization sequences (parageneses) exhibited by these samples define the following generalized paragenesis for post-cooling mineral deposition. Calcite is found throughout the paragenesis. Earliest calcite is typically found underlying or associated with chalcedony and (or) drusy quartz; the end of the early stage is tentatively placed at the end of chalcedony/quartz deposition. Both intermediate- and late-stage deposition consist mainly of calcite and opal. Whereas intermediate-stage calcite may be riddled with tiny liquid and solid inclusions and is, hence, often murky, late-stage calcite contains fewer inclusions and often forms clear, sparry overgrowths. Such textural distinctions, however, are often lacking and distinguishing between intermediate and late stages on their basis is frequently impractical. As discussed in section 6.11.3, the intermediate- to late-stage boundary is best defined by a shift in $\delta^{13}C$ values.

Most ESF samples were sampled to determine the range of calcite stable-isotope compositions. Moreover, those occurrences that display a simple paragenesis were also the object of detailed microsampling to determine the time/space $\delta^{13}C$ and $\delta^{18}O$ systematics of the calcite. Microsamples were milled from the polished surface of samples at magnifications of 30-40x. For each sample, the oldest calcite (closest to the tuff host rock) was designated "early" and the youngest calcite (usually free-growing crystal faces) was designated "late." Intermediate-stage boundaries were based on changes in mineralogy or texture. This approach led to some misclassification of calcite stage (e.g., those samples missing a stage) but ensured objectivity.

6.11.3 ESF Calcite $\delta^{13}C$ and $\delta^{18}O$ Values

Calcite $\delta^{13}C$ values decrease markedly during the paragenetic sequence, from nearly +10‰ in the early stage to less than -9‰ in the late stage. Frequency diagrams of early, intermediate, and late calcite $\delta^{13}C$ values display this time dependence (Figure 61) and show that calcite $\delta^{13}C$ values provide a coarse indication of relative age. Figure 70, a plot of calcite $\delta^{13}C$ vs. age, shows a sharp decrease of $\delta^{13}C$ between 3 and 4 Ma that defines the boundary between the late and intermediate stages. This shift probably reflects a change in the $\delta^{13}C$ of plant organic matter in the overlying soils caused by a change in regional climate. The higher $\delta^{13}C$ values of the intermediate-stage calcite suggest a greater dominance by C4 plants such as grasses, perhaps indicating a prairie or savanna climate, in contrast to the high desert to pygmy conifer climate zones of the late stage (e.g. Quade et al. 1989, p. 467).

Calcite $\delta^{18}O$ values also change with time. A plot of $\delta^{13}C$ vs. $\delta^{18}O$ for the microsamples (Figure 71) shows late-stage $\delta^{18}O$ was fairly constant between 16 and about 20‰, but gradually decreasing values during the intermediate and early stages. A small subset of the early-stage calcite displays anomalously low $\delta^{18}O$ values.

6.11.3.1 Late-Stage Calcite $\delta^{18}O$ Variations

Three important observations can be made from the distribution of late stage calcite $\delta^{18}O$ values. First, when plotted versus age based on $^{207}Pb/^{235}U$ or $^{230}Th/^{238}U$ (Figure 72), late-stage deposits (roughly the last 4 million years) from the Tiva Canyon Tuff and the Topopah Spring Tuff both display ranges of 1.5 to 2.0‰. These ranges are comparable to that of the 500 thousand year (ky) record from Devils Hole in southwestern Nevada (Winograd et al. 1992, p. 256). At Devils Hole, where calcite deposits provide a detailed record of groundwater $\delta^{18}O$ and regional climate during the last 500 ky, a similar range of values is observed. This similarity indicates that the scatter shown by late-stage calcite $\delta^{18}O$ values is probably also a reflection of regional climate variability. Second, plotting late-stage calcite $\delta^{18}O$ versus depth below surface shows two distinct trends (Figure 73). In the Tiva Canyon Tuff, calcite $\delta^{18}O$ decreases steeply, at a rate of about 2.5‰/100m. Assuming that calcite $\delta^{18}O$ changes by about 0.18‰/°C, this decrease is equivalent to an unreasonably high geothermal gradient of nearly 140°C/km. However, because the Tiva Canyon Tuff is highly fractured and open to the atmosphere, it seems likely that evaporation, not a high geothermal gradient, increased the $\delta^{18}O$ of the water and, hence, of the calcite. Evaporation enriches the remaining water in ^{18}O, and the $\delta^{18}O$ values increase towards the surface where evaporative loss would be greatest. Topopah Spring Tuff calcite deposits, on the other hand, are

beneath the PTn which would at least limit evaporation rates. Although there is some scatter to the data, late-stage calcite $\delta^{18}O$ values in the Topopah Spring Tuff have a best-fit slope of about 36°C/km with an r^2 of 0.48, in relatively good agreement with geothermal gradients measured in the unsaturated zone which range between 15 and 60°C/km (Sass et al. 1988, p. 38). If some percolation water $\delta^{18}O$ values were less than -11 ‰, the calculated geothermal gradients would be lower.

6.11.3.2 Intermediate Through Early-Stage d^{18}O Decrease

Although intermediate and early-stage calcite $\delta^{18}O$ values scatter somewhat more than the late stage, they tend to cluster within a similar overall range of about 3‰. This similarity suggests that the scatter of $\delta^{18}O$ in the older stages is also a reflection of climate variability. Nonetheless, a gradual decrease of calcite $\delta^{18}O$ with age is apparent in Figure 72. Plotting only data from the middle non-lithophysal unit of the Topopah Spring Tuff (Tptpmn) (Figure 74) clarifies the relation by restricting the depth interval (i.e., limiting the temperature variable). The calcite of the older stages must reflect either water with lower $\delta^{18}O$ values, warmer temperatures, or both. Lowering the water $\delta^{18}O$ to produce the decrease requires a more or less monotonic shift in climate between 3 and 10+ my. A reasonable average $\delta^{18}O$ for waters in the unsaturated zone and at Devils Hole is –11±1‰. Ascribing the 4‰ lowering of past $\delta^{18}O$ entirely to a climate change indicates meteoric waters with $\delta^{18}O$ of -15±1‰ at 10 Ma. Meteoric waters with this range of $\delta^{18}O$ today are characteristic of southern Canada. Even though Quaternary climates in the region may have hit such extremes during glacial maxima, no published regional climate records indicate such a long-term shift to such colder conditions.

The long history of volcanism in the region suggests that past geothermal gradients may have been higher than today and that higher geothermal gradients may have caused the lower $\delta^{18}O$ values of the intermediate and early-stage calcite. Intermediate and early stage percolation-water $\delta^{18}O$ values are presently unconstrained. However, assuming that they have remained within the same range as for the late stage, and that calcite $\delta^{18}O$ values decrease about 0.18‰/°C, the 4‰ lower values found in the early stage equate to a temperature increase to about 46°C at the level of the Tptpmn. If we assume a depth of ~300 meters to the Tptpmn and a surface mean annual temperature of 15°C, this indicates geothermal gradients of around 100°C/km during the early stage and perhaps around 60°C/km at the beginning of the intermediate stage.

6.11.3.3 Possible Early Stage Thermal Event

Oxygen isotopic evidence from drill core samples indicating warmer temperatures of deposition during formation of the earliest calcite was reported in a milestone report to DOE in 1996 (Whelan et al. 1998, p. 21). Although the number of occurrences in the ESF displaying low $\delta^{18}O$ values of early-stage calcite is small, detailed study has revealed some stratigraphic and paragenetic controls on their distribution. Figure 75 plots data from the different stages against distance in the ESF from the North Portal. Early-stage calcite with low $\delta^{18}O$ values occurs exclusively in the North and South Ramp portions of the tunnel. Stratigraphically, it is restricted to the Tiva Canyon Tuff and upper part of the Topopah Spring Tuff. Although the early-stage calcite $\delta^{18}O$ values are lower in the lower part of the Topopah Spring Tuff (Tptpmn), none are

lower than about 12‰. Furthermore, these low $\delta^{18}O$ calcite occurrences are typically associated with, but older than, the early-stage silica stage of chalcedony and (or) quartz in those samples. They do not compose the entire early stage but typically represent only a thin layer near the base of the early calcite stage.

Nothing is known about the $\delta^{18}O$ of the early-stage water. Nonetheless, we have argued that late stage $^{*18}O$ was relatively constant around -11‰ and that, in concert with a change in geothermal gradient in the past, meteoric waters may have remained in that range for the last 10 my or more. Recognizing beforehand that it is a long-range extrapolation, assuming a value of -11‰ for the water does, however, provide an initial constraint on the maximum temperature during the early stage.

Early-stage calcite $\delta^{18}O$ values range down to 3.2‰. This calcite would form from -11‰ water at a temperature of about 114°C (O'Neil et al. 1969, p. 5552). The fact that this estimate is above the boiling temperature, and there is no evidence from fluid inclusion observations for boiling during calcite deposition (as discussed in section 6.11.4), indicates that the $\delta^{18}O$ of the depositing water was at least 1 to 2‰ less than –11‰. So, assuming a water $\delta^{18}O$ of –12.5‰ yields an estimated temperature of about 102°C for formation of the calcite with the lowest $\delta^{18}O$ value (3.2‰) and a temperature of 55°C for calcite with a $\delta^{18}O$ of 10‰. Temperatures of 55 to 100°C are significantly warmer than those estimated for normal early-stage calcite and represent a thermal anomaly. The stratigraphic distribution of calcite with low $\delta^{18}O$ values may provide a clue to the heat source for this thermal pulse.

So far, calcite with low values of $\delta^{18}O$ has been found only sporadically, only in the Tiva Canyon Tuff or the top of the Topopah Spring Tuff, only in volumetrically minor amounts, and only in the earliest part of the early stage. These conditions are all consistent the hypothesis that deposition of the Tiva Canyon Tuff caused conductive heating of the underlying tuffs. These conditions do not appear to be consistent with a heat source at depth or with upwelling of heated fluids. However, fluid inclusion evidence of warmer depositional temperatures, which appears to be at least in partial accord with the distribution of calcite with low values of $\delta^{18}O$, has been interpreted as proof of the upwelling of heated groundwater (Dublyansky et al. 1996, pp. 38 to 39; Dublyansky 1999, p. S-4; Dublyansky and Reutsky 1998, p. A-79).

6.11.4 Fluid Inclusion Studies of Unsaturated-Zone Calcite

Fluid inclusions are tiny (generally ≤100 micrometers) cavities in minerals that trap samples of the liquids and (or) gases (i.e., fluids) present at the time the cavity was sealed by subsequent mineral growth. They may form in many ways (Roedder 1984, pp. 12 to 25; Goldstein and Reynolds 1994, pp. 5 to 9), but most commonly by ongoing mineral precipitation sealing imperfections in the surface of mineral grains (primary fluid inclusions) or by trapping of fluids present during healing of microfractures in mineral grains (secondary fluid inclusions). The contents of fluid inclusions are as variable as the multitude of geologic settings in which minerals may form. Several common inclusion types are germane to the origin of unsaturated zone calcite.

Inclusions formed in a vadose setting (i.e., the unsaturated zone) may trap the gas phase (typically dominated by atmospheric gases), the liquid (dominantly water), or mixtures of the two in varying

proportions. Inclusions formed in saturated settings will trap the liquid phase present (e.g., groundwater, hydrothermal fluid, or brine). If this trapping occurs at near-ambient temperatures, a single-phase, all-liquid inclusion will result. However, if trapping occurs at elevated temperatures, the fluid density will increase during cooling and the fluid will shrink. If it shrinks enough, a vapor bubble will nucleate in the inclusion to offset the decrease in fluid volume. These are termed two-phase inclusions and are particularly useful because they permit estimates of the temperature of mineral formation. However, any fluid inclusion must meet many petrographic criteria (too numerous to discuss here but listed in Chapter 2 of Roedder 1984, pp. 43 to 45) before it can be considered a reliable source of temperature data.

Estimates of mineral formation temperatures from two-phase fluid inclusions are made by gradually heating the two-phase inclusion and observing the temperature at which vapor and liquid re-homogenize to a single phase. If the inclusion was trapped at atmospheric pressure, this temperature of homogenization (T_h) is essentially the temperature of trapping; to the extent that the inclusion was formed at >1 atmosphere (i.e., at depth), T_h is an underestimate of the formation temperature and must be corrected for the hydrostatic or lithostatic pressure on the fluid. Calcite formed in an unsaturated zone setting would require no pressure correction and that formed in a shallow saturated zone, <200 m below the water table, a trivial correction of only several degrees.

6.11.4.1 Fluid Inclusion Evidence for the Origin of Unsaturated Zone Calcite

Several researchers have examined the fluid inclusions present in the calcite from the unsaturated zone of Yucca Mountain (Bish and Aronson 1993, pp. 152 to 154; Roedder et al. 1993, p. A-184; 1994, pp. 1854 to 1860; Roedder and Whelan 1998, p. 56; Dublyansky et al. 1996, pp. 38 to 39; Dublyansky 1999, p. S-4; Dublyansky and Reutsky 1998, p. A-79) and, in general, all have reported three types of inclusions: liquid-filled or vapor-filled single phase, and two phase, consisting of varying proportions of liquid plus vapor. They have not, however, agreed on the genetic implications of those observations.

Liquid-Filled and Small Vapor-Liquid Ratio Two-Phase Inclusions—Unsaturated-zone calcite from Yucca Mountain contains numerous fluid inclusions. The majority of these are liquid filled and indicative of relatively low formation temperatures, although how low is uncertain. Ideally, only inclusions trapped at room temperature or less, would be all liquid at room temperature. In reality, many all-liquid inclusions formed at 60-70°C or less will fail to nucleate a shrinkage bubble but will metastably remain a single, liquid, phase. This behavior by low-temperature inclusions is caused by the small decrease of internal pressure during cooling being insufficient to overcome the surface tension of the liquid. Failure to nucleate a vapor bubble is most common for small inclusions, trapped at low temperature, and containing low-salinity fluids–typical attributes of the unsaturated zone calcite all-liquid inclusions.

The unsaturated-zone calcite also contains two-phase inclusions consisting of liquid plus vapor. The vapor:liquid ratios in these inclusions range from nearly all liquid to all vapor, but can be divided into two types: (1) small groups of inclusions with small, but consistent, vapor:liquid ratios, and (2) scattered vapor-dominated inclusions with large and highly variable vapor:liquid ratios. The first type provides evidence of the formation temperatures of the calcite; the second,

through estimates of internal pressure and gas composition, can permit inferences regarding the depositional setting.

Fluid inclusion studies of secondary calcite occurrences sampled from drill core by YMP scientists revealed many two-phase inclusions with large and variable vapor:liquid ratios and many all-vapor inclusions but very few two-phase inclusions that met the petrographic requirements to yield reliable temperature data (Roedder et al. 1994, pp. 1857 to 1858). Roedder and Whelan (1998, p. 56) reported T_h ranging from about 50 to 100°C for seven calcite-hosted inclusions from four occurrences sampled from the unsaturated zone of boreholes USW G-1 and USW G-2 (data are in DTN: GS931108315215.033). It now appears that this sample set may have been adversely affected by core and sample handling procedures. Core from these boreholes was not always protected from extremes of temperature (e.g., core sometimes remained at the drill site during the summer when temperatures may have exceeded 40°C). Also, procedures used to prepare the sections could have inadvertently heated the samples to temperatures of 40 to 50 °C. Just as fluid inclusions that trapped only a liquid phase may metastably fail to nucleate a vapor bubble on cooling, low-temperature two-phase inclusions with small vapor:liquid ratios will homogenize to a single phase if accidentally heated above their T_h and then fail to renucleate the vapor bubble on cooling. Thus, accidental heating can erase evidence of formation conditions below the maximum temperature reached.

Subsequent studies of calcite samples from the ESF have described the limited occurrence of two-phase inclusions with T_h ranging from 35 to 55°C, and the rare existence of fluid inclusions with T_h up to at least 80°C (Dublyansky et al. 1996, pp. 38 to 39; Dublyansky 1999, p. S-4; Dublyansky and Reutsky 1998, p. A-79). The scarcity of similar fluid inclusions in drill core samples examined by Roedder et al. (1993, p. A-184; 1994, pp. 1857 to 1858), suggests that thermal mishandling could have rehomogenized the previously two-phase inclusions that had been trapped at <50°C. Why the higher T_h's were not observed is uncertain although, if their distribution is restricted like that of the calcite with low values of $\delta^{18}O$, reconnaissance sampling of drill core could have easily missed them.

Vapor-Filled or Large Vapor-Liquid Ratio Inclusions—Although not as abundant as all-liquid inclusions, vapor-filled or vapor-rich inclusions are common. The most common depositional settings that produce minerals having inclusions of widely-ranging vapor:liquid ratios are where the depositing fluids have boiled, or where mineral deposition took place in an unsaturated (vadose) environment. Inclusions formed in these two settings are, however, easily distinguished by their internal pressures. Vapor-rich inclusions formed in a boiling environment that trap steam or a mixture of steam and fluid will, when cooled to room temperature, have an internal pressure that is a near vacuum (unless they contain large amounts of CO_2). Inclusions formed in a vadose setting trap a mixture of the gases present (dominated by atmospheric gases) and the liquid; these inclusions should have internal pressures near or just slightly less than atmospheric pressure (depending on the trapping temperature). Dublyansky (1999, p. S-4) has offered a third explanation for the vapor-rich inclusions: exsolution of gases from a fluid in a saturated zone (i.e., sub-water-table) setting. In this case, the inclusions should have an internal pressure equivalent to the height of the overlying water column and which would be considerably greater than atmospheric pressure.

Fortunately, a simple device called a crushing stage permits qualitative estimates of the internal pressure of fluid inclusions (Roedder 1970, pp. 41 to 42). A mineral grain containing an inclusion of interest is placed in an immersion medium (oil, glycerol, etc.) between two glass plates on a microscope stage. Squeezing of the mineral chip between the two plates generates fractures which ultimately rupture the fluid inclusion. If the internal pressure is much less than atmospheric, as in a high-temperature or boiling inclusion, the immersion fluid will be sucked into and fill the inclusion. If the internal pressure is near atmospheric, as in vadose zone mineral formation, little or no immersion fluid will enter the inclusion. Lastly, if the internal pressure is greater than atmospheric, the inclusion gases will expand into and form a bubble in the immersion fluid.

Analysis of the vapor-rich inclusions in the unsaturated zone calcite fluid inclusions has produced conflicting results. Roedder et al. (1993, p. A-184) reported that small amounts of immersion oil entered the vapor-rich fluid inclusions when they were crushed. Subsequent qualitative analyses of the gases released during crushing (Roedder et al. 1994, p. 1859), however, indicated large quantities of CH_4 and CO_2, with N_2 and O_2 in roughly atmospheric proportions. These results lead to a re-evaluation of the initial crushing experiments because CH_4, which is locally present in concentrations of tens of percent, is readily soluble in the immersion oil used in the experiment. Solution of the CH_4 into the immersion oil at the time of inclusion rupture would lower the internal pressure in the inclusion and result in oil entering the inclusion cavity. The crushing test was therefore repeated using glycerol as the immersion fluid, in which CH_4 is insoluble. In these tests no glycerol entered the inclusions and they appeared to have ~atmospheric internal pressure, indicating that they had likely formed in the same vadose setting that they are found in today.

Again, however, Dublyansky (1999, p. S-4) has reported crushing and gas composition results from the vapor-rich inclusions that are at odds with those of Roedder et al. (1994, p. 1859). He reported that immersion fluids, including glycerol, entered the inclusions during crushing tests, thus indicating a less-than-atmospheric internal pressure. Furthermore, although he reported qualitative gas compositions that were similarly rich in CH_4, CO_2, and N_2 he found no O_2; and he inferred the presence of traces of aromatic hydrocarbons, based on Raman spectroscopy.

6.11.4.2 Percolation vs. Upwelling Origins for Unsaturated-Zone Calcite

Not surprisingly, these two research groups have come to distinctly different conclusions regarding the formation of the secondary calcite deposits in the unsaturated zone.

Roedder et al. (1994, pp. 1859 to 1860) concluded that the calcite and associated silica mineralization (early chalcedony/quartz, intermediate and late opal) had formed from meteoric water. This water infiltrated through the soil zone, picking up its C, Sr, and U geochemical signatures, and then percolated through the unsaturated zone depositing calcite and silica along its fracture and cavity flowpath. Roedder et al's (1994, pp. 1859 to 1860) and Roedder and Whelan's (1998, p. 56) interpretations were based largely on the following observations:

- The majority of fluid inclusions are liquid-filled, indicating low formation temperature.

- The liquid-filled inclusions are closely associated with vapor-rich inclusions in which crushing tests have indicated near atmospheric pressure and quadrupole mass spectrometry has revealed atmosphere-like N_2/O_2 ratios.

- As discussed in Section 6.10, all stages of calcite-silica deposition are largely restricted to the footwalls of fractures or the floors of lithophysal cavities and typically mineralize only a small percentage of suitable fracture or lithophysal surfaces. This arrangement of occurrences is more compatible with deposition controlled by the distribution of discrete flowpaths in the unsaturated zone than with the pervasive mineralization that would be expected from wholesale flooding of the tuffs.

Dublyansky (1999, p. S-4) disputed these conclusions and argued that the calcite and silica deposits have formed from the upwelling of relatively low-temperature, but deep-seated, thermal fluids. These fluids, he contended, have repeatedly invaded the UZ, possibly recently, depositing calcite and silica. His conclusions are based primarily on the following observations:

- The common occurrence of two-phase inclusions that have T_h typically of 35 to 55°C but which range up to ~80°C in some of the early stage calcite. Dublyansky insists that these temperatures, which are well above the present-day ambient temperature, require upwelling of heated fluids and flooding of the unsaturated zone to form the calcite.

- Vapor-rich inclusions from which crushing tests have indicated less than atmospheric internal pressure and in which other analytical studies have suggested the presence of traces of aromatic hydrocarbons. Again, this evidence is presented as conclusive proof of the upwelling hypothesis.

6.11.4.3 Alternative Interpretations of Fluid Inclusion Data

The possibility that thermal water has flooded the unsaturated zone in the past and might do so again in the future, no matter how unlikely, must be evaluated carefully. Independent but parallel studies of the occurrence and paragenetic distribution of two-phase fluid inclusions, and of the timing of deposition of the host calcite, were begun in April 1999 by the US Geological Survey (USGS) and the University of Nevada at Las Vegas (UNLV). These studies will be based on a comprehensive set of approximately 200 samples jointly collected by the participants from the underground workings, and are scheduled for completion in the Spring of 2001.

Sample collection for the parallel studies is nearly complete. Preliminary reviews of the existing data by representatives of the USGS, the UNLV, and the State of Nevada, coupled with observations of the new samples appear to support the following inferences:

- Primary two-phase inclusions are more common than originally reported by Roedder et al. (1994, pp. 1857 to 1858). This may reflect the uncertain storage history and sample preparation procedures of the drill core samples used in that study.

- Fluid inclusion T_h measurements indicate temperatures of 35 to 55°C may have been common, and temperatures up to 80°C occur at least locally in the early stage paragenesis. These temperatures are consistent with those inferred from calcite $\delta^{18}O$ values (Whelan et al. 1999, p. S-8) which record a thermal event in the oldest calcite and a progressive decline of the geothermal temperature gradient with time. Geochronologic studies in conjunction with the fluid inclusion T_h measurements will test the thermal history of the unsaturated zone inferred from calcite $\delta^{18}O$ values.

- Warmer temperature does not, in and of itself, necessitate upwelling fluids or saturated conditions. Early stage calcite is still restricted to fracture footwalls and cavity floors. Calcite of unquestioned hydrothermal origin formed in tuffs deep below the water table about 10.4 Ma (Bish and Aronson 1993, p. 148) and it is isotopically, texturally, and chemically distinct from the unsaturated zone calcite (Whelan et al. 1994, pp. 2738 to 2739 and Figure 3). As long as temperatures were below 100°C, unsaturated-zone fluids were liquid, and inclusion T_h measurements do not necessitate a saturated environment.

7. SUMMARY AND CONCLUSIONS

An extensive database of geochemical and isotopic characteristics has been established for pore waters and gases from the unsaturated zone, perched water, and saturated-zone waters in the Yucca Mountain area. The analytical work has been driven by diverse needs of the YMP site characterization, process modeling and performance assessment communities. Water and gas chemistries influence the sorption behavior of radionuclides and the solubilities of the radionuclide compounds that form. The chemistry of waters that may infiltrate the potential repository will be determined in part by that of water present in the unsaturated zone above the potential repository horizon, while pore-water compositions beneath the potential repository horizon will influence the sorption behavior of the radionuclides transported towards the water table. However, more relevant to the discussion in this report, development and testing of conceptual flow and transport models for the Yucca Mountain hydrologic system are strengthened through the incorporation of natural environmental tracer data into the process. Chemical and isotopic data are used to establish bounds on key hydrologic parameters and to provide corroborative evidence for model assumptions and predictions. Examples of specific issues addressed by these data include spatial and temporal variability in net fluxes, lateral diversion in specific stratigraphic units, role of faults in controlling flow paths, fracture-matrix interactions, age and origin of perched water, and distribution of water travel times. This section summarizes the types of data available and their implications for key hydrologic processes at Yucca Mountain.

The following assumptions are identified as "to be verified:"

- Chemical data for pore waters extracted from drillcore are representative of *in situ* conditions (Assumption 2 in Table 5; impacts conclusions in Section 7.1, 7.3, 7.4, and 7.7).

- Carbon isotopic data for pore waters and gases are representative of *in situ* conditions, and have not been affected significantly by laboratory or field sources of contamination, including drilling air (Assumption 9 in Table 5; impacts conclusions in Section 7.2 and 7.3).

- The chloride mass balance (CMB) method is assumed to be applicable to the estimation of infiltration rates at Yucca Mountain, for samples obtained above the CHn (Assumption 19 in Table 5; impacts conclusions in Section 7.4).

- The estimated range of annual deposition rates for chloride at Yucca Mountain encompasses the present-day rate as well as the rates that prevailed when the sampled pore waters infiltrated below the soil zone (Assumption 20 in Table 5; impacts conclusions in Section 7.4).

- Pore-water samples that have been analyzed for chloride are representative of the full spectrum of significant flow paths in the unsaturated zone at Yucca Mountain (Assumption 21 in Table 5; impacts conclusions in Section 7.4).

For these reasons, quantitative values and bounds provided in this report and summarized below, are subject to change but the general trends are judged to be valid.

7.1 CHEMICAL COMPOSITION

Total Dissolved Solids and Chloride—Pore-water samples were extracted by tri-axial compression and by centrifugation from unsaturated core samples recovered from dry-drilled boreholes. Only nonwelded to poorly welded tuffs generally yield sufficient water for complete chemical analysis, and analyses of pore water from densely welded units are scarce. In general, unsaturated-zone pore waters have higher total dissolved solid concentrations than perched or saturated-zone waters, reflecting low surface infiltration rates. The variability in the dissolved-solids content of the shallow-most nonwelded unit (PTn) is a direct consequence of the spatial variability of surface infiltration rates. Chloride concentrations in this unit are highest beneath the terraces of large washes, and lower elsewhere. This inverse relationship between infiltration rates and pore-water chloride concentrations is reflected in the fact that infiltration rates calculated on the basis of the CMB method are generally consistent with rates calculated on the basis of physical methods.

Geochemical Evolution of Major Ion Chemistry—The relative concentrations of ions in pore-water samples also provide information about percolation processes. Most of the major chemical characteristics of the pore waters appear to be established by soil-zone processes—predominantly evapotranspiration and dissolution or precipitation of pedogenic calcite and amorphous silica—such that pore waters entering the bedrock are nearly always saturated with respect to these two phases. The infiltrating water compositions range from calcium-sodium bicarbonate type to calcium-sodium sulfate-chloride types, depending upon the residence time of the water in the soil zone. During large rainfall events that lead to percolation of soil waters directly into the unsaturated zone, the waters may be predominantly of the calcium-sodium bicarbonate type. During smaller rainfall or snowfall events, waters that percolate into the unsaturated zone may be closer to the calcium-sodium chloride-sulfate type.

Major-ion compositions of deeper pore waters indicate that water-rock reactions are very restricted during percolation through the unsaturated zone. Relative abundances of cations are altered through ion-exchange reactions with clays and zeolites along the flow paths. As a result of these reactions, pore waters extracted from the Calico Hills nonwelded (CHn) unit are sodium-

(carbonate+bicarbonate) type waters, a characteristic that becomes stronger with increasing depth. In contrast to PTn pore waters, chemical compositions in the CHn are generally similar within a given stratigraphic unit and markedly different between different host lithologies in any given borehole, implying significant lateral movement of water within the CHn unit.

Samples that deviate from this general geochemical evolution may provide insight into the role of other factors that can influence water chemistry, such as faults as pathways.

7.2 ISOTOPIC COMPOSITION

The isotopic data that are summarized in this section bear on the paleoclimatology of Yucca Mountain as well as on the details of the flow system. The paleoclimatic information is largely contained in the stable isotopes of hydrogen, oxygen, and carbon. Details of flow, in particular evidence for recent flow at depth, is provided by the tritium, carbon-14 and chlorine-36 data. In addition, evidence for the presence of local recharge is provided by uranium activity ratios. The Sr isotope data largely reflect water-rock interactions, and therefore is pertinent to discussion of transport processes.

Tritium—Tritium has been analyzed in over 800 pore-water fluids extracted from unconsolidated material in shallow surface-based boreholes, from drill core from deep surface-based boreholes, and from ESF drillholes. Analyses are also available for water samples bailed and pumped from perched-water bodies and from the saturated zone. Statistical analysis was used to define 25 tritium units (TU) as the threshold at which a given signal can be considered as being above background. (One of the limitations of this approach is that "background" in this case includes post-bomb waters which have returned to pre-bomb tritium levels.) By this criterion, detectable levels of tritium have been observed in the Bow Ridge fault zone in ESF Alcove 2 and in about 6% of the pore waters extracted from core samples from 11 surface-based boreholes. These detections occur predominantly within the TSw and the Prow Pass member of the Crater Flat Tuff. No bomb-pulse tritium was detected in TSw samples from the drillhole transecting the Ghost Dance fault in the Northern Ghost Dance Fault Access Drift (Alcove 6), despite the fact that elevated levels of ^{36}Cl were measured in Alcove 6. Bomb-pulse tritium was not detected in any of the perched-water samples, as all of these were well below 25 TU.

Tritium data for some of the unsaturated-zone boreholes show several inversions in which samples with larger tritium concentrations occur below samples with background values in a vertical profile. The occurrence of detectable tritium in waters below non-tritium-bearing water (and hence older water) in a vertical profile is strong evidence for the occurrence of fracture and lateral flow at Yucca Mountain.

Chlorine-36—Chlorine-36 analyses exist for several hundred rock samples from surface-based boreholes and the ESF. Bomb-pulse concentrations are present in the PTn at several locations and in the vicinity of some fault zones in the ESF. Bomb-pulse chlorine-36 is not present in perched water or groundwater from the site (other than in shallow recharge from UE-29 a#2 in Fortymile Wash).

Carbon-14—Uncorrected carbon-14 ages of unsaturated-zone pore waters range from modern to 5,200 years. These data do not show any trend with stratigraphic depth. In fact, larger ^{14}C activities are interspersed among smaller ^{14}C activities in a vertical profile. These irregular profiles are consistent with a conceptual model in which fracture flow and perhaps lateral flow occur in some of the units. Radiocarbon ages for PTn pore-water samples span a narrower range than for CHn pore waters, as expected if the CHn unit were fed by fracture flow mixing to variable extents with slower matrix flow.

For carbon isotopes in gases, samples collected from instrumented boreholes (UZ-1, SD-12, and drillholes in ESF Alcoves 1 and 6) are considered to be the most reliable indicators of *in-situ* conditions. Gas ages for these samples range from modern in the upper 100 feet, to 15,900 years near the water table in UZ-1. The measured gas profiles generally increase smoothly with depth and appear to be consistent with gas-transport modeling of downward movement of atmospheric CO_2 by simple diffusion. In the potential repository horizons, between the TSw upper lithophysal and lower lithophysal units, radiocarbon ages for gases range from 6,100 to 9,500 years in UZ-1 and SD-12. A slightly younger range of 2,400 to 4,500 years was obtained for gases from the Alcove 6 drillhole, which intersected the Ghost Dance fault zone.

Ages for perched waters are 3,300 years for the sample from NRG-7a, and between 7,200 and 10,700 years for samples from three other boreholes (SD-7, SD-9, UZ-14). If post-bomb water is present in the perched bodies, the component is too small to be detectable by any of the three bomb-pulse isotope signals (tritium, ^{14}C and ^{36}Cl).

Questions regarding corrections to the radiocarbon ages remain to be resolved. The extent of contamination of pore-water samples with drilling air has not been quantified; such contamination would shift the isotopic signature to apparently younger ages. Pore-water and perched-water ^{14}C activities can also be diluted by the dissolution of older carbon in the carbonate minerals, which would result in anomalously old apparent ages. Reaction with or incorporation of gas-phase CO_2 from deep in the unsaturated zone can also result in an anomalous apparent age. However, although questions can be raised about the representativeness of individual samples, the general trends shown by the samples support the conclusion that average travel times through the unsaturated zone are on the order of 5,000 to 10,000 years.

Carbon-13—Relative to stable carbon isotope ratios in the atmosphere, most pore-water samples are isotopically light. This signature indicates that these pore waters have been influenced by biogenic processes, and that most of the bicarbonate in unsaturated-zone matrix pore fluids originated in the soil zone. In contrast, most of the perched-water bodies and groundwater in the Yucca Mountain area have heavier (less negative) $\delta^{13}C$ values that do not show the same degree of soil influence as do the unsaturated-zone pore waters. Stable carbon isotope ratios for pore waters show a wide range in both the Ptn and CHn units, which may be a consequence of a variety of processes but which is also consistent with spatially and temporally variable infiltration rates and mixing between fast fracture flow and slow matrix flow.

Deuterium and oxygen-18—Stable isotopic compositions of hydrogen and oxygen reflect climatic conditions that prevailed when the pore water infiltrated below the root zone. Lighter isotopic values for CHn pore waters suggest that much of the water in this unit originated either

during winter precipitation or during a time of colder climate, as compared to the origin of pore water in the PTn. This timing may also be the explanation for the more dilute nature of the CHn pore waters, because waters are subject to less evapotranspiration during winter precipitation or during a colder climate. Spatial differences in Yucca Mountain groundwater samples from the saturated zone are not large, but the general trend is that groundwaters to the south of the site tend to be isotopically lighter than those farther to the north or east, suggesting that recharge occurred under cooler climatic conditions.

Strontium-87—Strontium isotope compositions in the host volcanic rocks differ significantly from those of the unsaturated-zone pore waters, indicating that pore water has not reached isotopic equilibrium with the tuffs. Near the top of borehole SD-7, the $\delta^{87}Sr$ in the pore water matches the $\delta^{87}Sr$ found in calcite surface coatings at the drillpad. Delta-^{87}Sr increases with depth; this increase is especially evident within the PTn and is only slightly discernible in the underlying TSw. A working model assumes that strontium is initially added to infiltrating water by dissolution of calcite in the soil zone. During subsequent percolation through the PTn, the pore water interacts with the rocks in this unit, which changes its strontium signature.

Uranium activity ratios— Uranium isotopic ratios have been used to address the prevalence and frequency of fracture flow through the unsaturated zone at Yucca Mountain and the issue of local recharge to the water table. Substantial differences in $^{234}U/^{238}U$ activity ratios between pore water and fracture water imply that, once water is entrained in fractures, there may be minimal liquid exchange between these two types of flow pathways. Anomalously large $^{234}U/^{238}U$ activity ratios in shallow saturated-zone water beneath Yucca Mountain are similar to the elevated initial $^{234}U/^{238}U$ ratios measured for deep unsaturated-zone minerals and perched water bodies at the site. The similarity of the signals for shallow groundwaters, fracture water, and perched waters supports the concept of recharge through the thick unsaturated zone at Yucca Mountain, and that much of the local recharge derives from flow through fracture pathways in the deep unsaturated zone rather than from percolation through the matrix column. Furthermore, the fact that the $^{234}U/^{238}U$ values in the groundwater are near the upper end of the range observed in the unsaturated-zone materials, implies that the local recharge has not been highly diluted by through-flow from the north.

7.3 FLOW PATHS

Geochemical and isotopic data in waters from the unsaturated and saturated zones at Yucca Mountain are consistent with a flow model in which all unsaturated-zone waters, including perched waters, originate at the surface of the mountain. Although flow paths appear to be predominantly vertical, there is evidence that suggests lateral flow in some units. For example, the observation that samples from the PTn with tritium values well above background are found beneath samples with tritium at background values is difficult to explain without calling upon some type of lateral flow mechanism. The isotopic data further provide evidence of water that has flowed rapidly to at least the depth of the ESF. This water presumably flowed along pathways that included fractures and/or faults. To account for the data, there must also be fractures and/or faults through the PTn. How much of the total percolation flux is due to this fracture flow is difficult to quantify. The available hydrochemical data, *in toto,* suggest the proportion is small. This implies that the bulk of water in the unsaturated zone moves through the matrix. However,

the fact that CHn pore waters are considerably more dilute than pore waters in the overlying tuffs suggests that the fracture flow component can dominate the chemistry of the deeper unsaturated-zone waters. Alternatively, the more dilute nature of the CHn fluids could reflect infiltration under cooler climates than the present climate at Yucca Mountain.

7.4 INFILTRATION RATES

Apparent infiltration rates were estimated by the CMB method, using chloride concentrations for pore-water samples from 11 surface-based boreholes, 53 ESF drillholes, and 24 Cross Drift drillholes. Alluvium in washes or forming terraces had apparent infiltration rates less than 0.5 mm/yr. Apparent infiltration rates in the PTn were generally higher than the rates estimated for alluvium, even for samples from the same boreholes, presumably due to lateral flow and mixing within this unit. Nonetheless, the rates appear to be roughly correlated with surface topography. PTn samples beneath deep alluvium had infiltration rates between 0.6 and 3.3 mm/yr. PTn and TSw pore waters beneath sideslopes and ridgetops, which have thin alluvial cover, had average infiltration rates between 5 and 8 mm/yr in the northern half of the study area (e.g., Cross Drift, North Ramp, main drift up to station 45+00), but only about 1 mm/yr in the southern half (ESF South Ramp). The overall average infiltration rate for pore-water samples collected along the Main Drift and Cross Drift (30 samples) is about 6 mm/yr.

7.5 PERCHED WATER

The existence of perched water bodies beneath Yucca Mountain is of interest because of potential implications for flow and transport in the unsaturated zone. With respect to flow issues, the existence of the perched water bodies could reflect an earlier period(s) of increased infiltration rates or it could reflect some sort of steady-state phenomenon. The fact that perched water samples appear to be up to 11,000 years old based on ^{14}C and ^{36}Cl ages favors the former explanation. Major ion concentrations and uranium isotope data suggest that these bodies were formed by water flowing through fractures in the unsaturated zone rather than through the matrix. The fact that these waters do not appear to have equilibrated with water in the matrix of units in which the perched water bodies are found also supports a distinct origin (e.g., fracture flow) for these waters and very slow exchange between fracture and matrix reservoirs.

7.6 PALEOHYDROLOGIC CONSTRAINTS ON FRACTURE FLOW

Deposits of calcite and opal lining fractures and cavities in the ESF contain spatial and temporal information on past migration of water through the unsaturated zone. Mineral textures, the fact that less than 10% of all fractures and open spaces contain coatings of calcite and opal, and restriction of minerals to fracture footwalls and cavity floors, are consistent with deposition from thin films of descending fracture water at sites where solutions lose carbon dioxide and water vapor. Carbon, oxygen, and strontium isotopic compositions of the unsaturated zone calcite and silica phases also support a source of water from downward-percolating meteoric water. Oxygen isotopic data on secondary fracture minerals indicate that geothermal gradients during the last eight million years have been relatively constant.

Geochronological data indicate that calcite and opal grew at extremely slow and relatively uniform rates for millions of years. Radiocarbon, uranium-thorium, and uranium-lead ages for outer (youngest) mineral surfaces range from less than ten thousand to about 1.5 million years. Uranium-lead ages for interior (older) layers of opal and chalcedony range from 0.5 to 10 million years and result in calculated long-term average deposition rates of about 1 to 5 mm/million years. These rates are consistent with estimates based on uranium-thorium ages for subsamples deposited over the last half million years.

Stable isotope compositions ($\delta^{13}C$ and $\delta^{18}O$) of calcite deposited over the last several million years span a wide range of values indicating deposition from water originating from both pluvial and interpluvial precipitation, consistent with climate fluctuations documented throughout the region. However, uniform mineral growth rates imply that fracture flow in the deep unsaturated zone at Yucca Mountain did not vary substantially despite these climate variations. In addition, $^{230}Th/U$ ages do not show clustering that can be correlated with cycles of pluvial-interpluvial climate over the last 200 ka. Initial $^{234}U/^{238}U$ ratios calculated for opal and calcite deposited within the potential repository horizon also imply that deep unsaturated zone fracture flow at Yucca Mountain was low volume and/or infrequent.

Hydrologic buffering of the deep fracture-flow system is attributed to a number of hydrogeologic factors including increased runoff and surface drainage in response to additional precipitation, downslope diversion along the colluvium-bedrock interface, increased vegetation during wetter climates leading to greater rates of evapotranspiration, and the presence of nonwelded tuffs with large matrix permeabilities in the PTn overlying the fractured, densely welded tuffs of the potential repository horizon. A combination of these factors has resulted in the long-term hydrologic stability of the fracture-flow system at the level of the potential repository horizon.

7.7 IMPLICATIONS FOR REPOSITORY PERFORMANCE

The chemistry of water is a potentially important factor in radionuclide transport because it influences the solubilities of radionuclide compounds that form and because it influences the sorption behavior of the radionuclides. In addition, the chemistry of waters that may infiltrate the potential repository will be determined largely by the chemistry of water present in the unsaturated zone above the potential repository horizon.

Variations expected in water compositions that intersect the near-field environment will be strongly dependent on the climatic regime and on flow paths. Because most flow paths that would produce water in the repository horizon will likely represent fracture flow paths, the water compositions may be more dilute than those of matrix pore waters extracted from welded and nonwelded tuffs. If infiltration rates increased in the site area as a result of a climatic shift, these compositions would likely become even more dilute, presumably more like the perched-water compositions.

Data on major ion concentrations in unsaturated zone waters beneath the proposed repository horizon are of great significance to radionuclide transport. For example, the fact that pore waters in the lower portions of the zeolitized Calico Hills tuff have very low calcium and magnesium concentrations compared to pore waters in the overlying units indicates that ion exchange

processes operate on the pore waters that percolate through the zeolitic tuffs. These processes tend to remove calcium and magnesium from the percolating waters replacing them with equivalent concentrations of sodium. When combined with ^{14}C age data suggesting relatively young ages (up to 100 pmc) for CHn pore waters, these data indicate ion exchange processes operate on vertically migrating young pore waters in the CHn. This suggests ion exchange processes would also operate on radionuclides released from the potential repository into aqueous solutions that subsequently migrated vertically into the zeolitic CHn.

8. REFERENCES

8.1 CITED REFERENCES

Benson, L. and Klieforth, H. 1989. "Stable Isotopes in Precipitation and Ground Water in the Yucca Mountain Region, Southern Nevada: Paleoclimatic Implications." *Geophysical Monograph, 55,* 41-59. Washington, D.C.: American Geophysical Union. TIC: 224413.

Benson, L.V. and McKinley, P.W. 1985. *Chemical Composition of Ground Water in the Yucca Mountain Area, Nevada, 1971-84.* Open-File Report 85-484. Denver, Colorado: U.S. Geological Survey. ACC: NNA.19900207.0281.

Bevington, P.R. and Robinson, D.K. 1992. *Data Reduction and Error Analysis for the Physical Sciences.* 2nd Edition. New York, New York: McGraw-Hill. TIC: 243514.

Bish, D.L. and Aronson, J.L. 1993. "Paleogeothermal and Paleohydrologic Conditions in Silicic Tuff from Yucca Mountain, Nevada." *Clays and Clay Minerals, 41,* (2), 148-161. Long Island City, New York: Pergamon Press. TIC: 224613.

BSC (Bechtel SAIC Company) 2001a. *Technical Work Plan for Unsaturated Zone (UZ) Flow and Transport Process Model Report.* TWP-NBS-HS-000001 REV 01. Las Vegas, Nevada: Bechtel SAIC Company. ACC: MOL.20010404.0007.

BSC 2001b. *Technical Work Plan for: Integrated Management of Technical Product Input Department.* TWP-MGR-MD-000004 REV 02. Las Vegas, Nevada: Bechtel SAIC Company. ACC: MOL.20010814.0324.

Boutton, T.W. 1996. "Stable Carbon Isotope Ratios of Soil Organic Matter and Their Use as Indicators of Vegetation and Climate Change." Chapter 2 of *Mass Spectrometry of Soils.* Boutton, T.W. and Yamasaki, S., eds. New York , New York : Marcel Dekker. TIC: 246834.

Bradbury, J.P. 1997. "A Diatom-Based Paleohydrologic Record of Climate Change for the Past 800 k.y. from Owens Lake, California." Chapter 9 of *An 800,000-Year Paleoclimatic Record from Core OL-92, Owens Lake, Southeast California.* Smith, G.I. and Bischoff, J.L., eds. Special Paper 317. Boulder, Colorado: Geological Society of America. TIC: 236857.

Brantley, S.L. and Stellings, L. 1996. "Feldspar Dissolution at 25ºC and Low pH." *American Journal of Science, 296,* (2), 101-127. New Haven, Connecticut: Yale University, Kline Geology Laboratory. TIC: 239822.

Buesch, D.C.; Spengler, R.W.; Moyer, T.C.; and Geslin, J.K. 1996. *Proposed Stratigraphic Nomenclature and Macroscopic Identification of Lithostratigraphic Units of the Paintbrush Group Exposed at Yucca Mountain, Nevada.* Open-File Report 94-469. Denver, Colorado: U.S. Geological Survey. ACC: MOL.19970205.0061.

Byers, F.M., Jr.; Carr, W.J.; Orkild, P.P.; Quinlivan, W.D.; and Sargent, K.A. 1976. *Volcanic Suites and Related Cauldrons of Timber Mountain-Oasis Valley Caldera Complex, Southern Nevada.* Professional Paper 919. Washington, D.C.: U.S. Geological Survey. TIC: 201146.

Carter, M.W. and Moghissi, A.A. 1977. "Three Decades of Nuclear Testing." *Health Physics, 33,* 55-71. New York, New York: Health Physics Society. TIC: 239141.

Chadwick, O.A.; Hendricks, D.M.; and Nettleton, W.D. 1987. "Division S-5—Soil Genesis, Morphology, and Classification, Silica in Duric Soils: I. A Depositional Model." *Soil Science Society of America Journal, 51,* 975-982. Madison, Wisconsin: Soil Science Society of America. TIC: 236964.

Claassen, H.C. 1985. *Sources and Mechanisms of Recharge for Ground Water in the West-Central Amargosa Desert, Nevada — A Geochemical Interpretation.* Professional Paper 712-F. Washington, D.C.: U.S. Geological Survey. TIC: 204574.

Clark, I.D. and Fritz, P. 1997. *Environmental Isotopes in Hydrogeology.* Boca Raton, Florida: Lewis Publishers. TIC: 233503.

Coplen, T.B.; Winograd, I.J.; Landwehr, J.M.; and Riggs, A.C. 1994. "500,000-Year Stable Carbon Isotopic Record from Devils Hole, Nevada." *Science, 263,* 361-365. Washington, D.C.: American Association for the Advancement of Science. TIC: 234269.

CRWMS M&O 1998. *Evaluation of Flow and Transport Models of Yucca Mountain, Based on Chlorine-36 and Chloride Studies for FY98.* BA0000000-01717-5700-00007 REV 00. Las Vegas, Nevada: CRWMS M&O. ACC: MOL.19981208.0119.

CRWMS M&O 1999a. *Analysis of Geochemistry Data.* TDP-NBS-HS-000040 REV 00. Las Vegas, Nevada: CRWMS M&O. ACC: MOL.19990824.0142.

CRWMS M&O 1999b. *M&O Site Investigations -- (Q).* Activity Evaluation, September 28, 1999. Las Vegas, Nevada: CRWMS M&O. ACC: MOL.19990928.0224.

CRWMS M&O 2000a. *Technical Work Plan for Unsaturated Zone (UZ) Flow and Transport Process Model Report*. TWP-NBS-HS-000001, REV 00, ICN 2. Las Vegas, Nevada. CRWMS M&O. ACC: MOL.20010115.0311.

CRWMS M&O 2000b. *Data Qualification Report: Water Chemistry and Infiltration Rate Data for Use on the Yucca Mountain Project.* TDR-NBS-GS-000023 REV 00. Las Vegas, Nevada: CRWMS M&O. ACC: MOL.20001208.0086.

Davis, S.N. and Murphy, E. 1987. *Dating Ground Water and the Evaluation of Repositories for Radioactive Waste.* NUREG/CR-4912. Washington, D.C.: U.S. Nuclear Regulatory Commission. ACC: NNA.19900522.0260.

Day, W.C.; Potter, C.J.; Sweetkind, D.S.; Dickerson, R.P.; and San Juan, C.A. 1998. *Bedrock Geologic Map of the Central Block Area, Yucca Mountain, Nye County, Nevada.* Miscellaneous Investigations Series Map I-2601. [Washington, D.C.]: U.S. Geological Survey. TIC: 237019.

Dettinger, M.D. 1989. "Reconnaissance Estimates of Natural Recharge to Desert Basins in Nevada, U.S.A., by Using Chloride-Balance Calculations." *Journal of Hydrology, 106,* 55-78. Amsterdam, The Netherlands: Elsevier Science. TIC: 236967.

Dickin, A.P. 1995. *Radiogenic Isotope Geology.* New York, New York: Cambridge University Press. TIC: 242869.

Drever, J.I. and Smith, C.L. 1978. "Cyclic Wetting and Drying of the Soil Zone as an Influence on the Chemistry of Ground Water in Arid Terrains." *American Journal of Science, 278,* 1448-1454. New Haven, Connecticut: Yale University, Kline Geology Laboratory. TIC: 237357.

Dublyansky, Y.; Reutsky, V.; and Shugurova, N. 1996. "Fluid Inclusions in Calcite from the Yucca Mountain Exploratory Tunnel." *Sixth Biennial Pan American Conference on Research in Fluid Inclusions, May 30 - June 1, 1996.* Brown, P.E. and Hagemann, S.G., eds. Madison, Wisconsin: Department of Geology, University of Wisconsin. TIC: 237704.

Dublyansky, Y.V. 1999. "Fluid Inclusions in Calcite from the ESF, Yucca Mountain, Nevada: Evidence of Saturated Environments and Elevated Temperatures." *EOS, Transactions, American Geophysical Union 1999 Spring Meeting.* S4. Washington, D.C.: American Geophysical Union. TIC: 246467.

Dublyansky, Y.V. and Reutsky, V.N. 1998. "Epigenetic Quartz-Opal-Calcite Crusts in the Yucca Mountain Subsurface: Fluid Inclusion and Stable Isotopic Evidence of Hydrothermal Origin." *Abstracts with Programs, Geological Society of America 1998 Annual Meeting, October 26-29, 1998, 30,* (7), A-79. Boulder, Colorado: Geological Society of America. TIC: 246483.

Dyer, J.R. 1999. "Revised Interim Guidance Pending Issuance of New U.S. Nuclear Regulatory Commission (NRC) Regulations (Revision 01, July 22, 1999), for Yucca Mountain, Nevada." Letter from J.R. Dyer (DOE/YMSCO) to D.R. Wilkins (CRWMS M&O), September 3, 1999, OL&RC:SB-1714, with enclosure, "Interim Guidance Pending Issuance of New NRC Regulations for Yucca Mountain (Revision 01)." ACC: MOL.19990910.0079.

Emett, D.C.; Hutchinson, D.D.; Jonson, N.A.; and O'Hair, K.L. 1994. *Water Resources Data, Nevada, Water Year 1993.* Water-Data Report NV-93-1. Carson City, Nevada: U.S. Geological Survey. TIC: 236836.

Engstrom, D.A. and Rautman, C.A. 1996. *Geology of the USW SD-9 Drill Hole, Yucca Mountain, Nevada.* SAND96-2030. Albuquerque, New Mexico: Sandia National Laboratories. ACC: MOL.19970508.0288.

EPA (Environmental Protection Agency) 1971. *Final Report of Off-Site Surveillance for Project Schooner.* PNE-524. Pages i, ii, 34, 42. Las Vegas, Nevada: Environmental Protection Agency. TIC: 246092.

Eriksson, E. 1960. "The Yearly Circulation of Chloride and Sulfur in Nature: Meteorological, Geochemical, and Pedalogical Implications. Part II." *Tellus, 12,* (1), 63-109. Stockholm, Sweden: Swedish Geophysical Society. TIC: 236893.

Ervin, E.M.; Luckey, R.R.; and Burkhardt, D.J. 1994. *Revised Potentiometric-Surface Map, Yucca Mountain and Vicinity, Nevada.* Water-Resources Investigations Report 93-4000. Denver, Colorado: U.S. Geological Survey. ACC: NNA.19930212.0018.

Fabryka-Martin, J.T.; Turin, H.J.; Wolfsberg, A.V.; Brenner, D.; Dixon, P.R.; and Musgrave, J.A. 1996. *Summary Report of Chlorine-36 Studies.* LA-CST-TIP-96-003. Draft. Los Alamos, New Mexico: Los Alamos National Laboratory. ACC: MOL.19970103.0037.

Fabryka-Martin, J.; Wolfsberg, A.V.; Dixon, P.R.; Levy, S.; Musgrave, J.; and Turin, H.J. 1996. *Summary Report of Chlorine-36 Studies: Sampling, Analysis and Simulation of Chlorine-36 in the Exploratory Studies Facility.* 3783M. Los Alamos, New Mexico: Los Alamos National Laboratory. ACC: MOL.19970103.0047.

Fabryka-Martin, J.T.; Flint, A.L.; Sweetkind, D.S.; Wolfsberg, A.V.; Levy, S.S.; Roemer, G.J.C.; Roach, J.L.; Wolfsberg, L.E.; and Duff, M.C. 1997. *Evaluation of Flow and Transport Models of Yucca Mountain, Based on Chlorine-36 Studies for FY97.* LA-CST-TIP-97-010. Los Alamos, New Mexico: Los Alamos National Laboratory. ACC: MOL.19980204.0916.

Fabryka-Martin, J.T.; Wolfsberg, A.V.; Dixon, P.R.; Levy, S.S.; Musgrave, J.A.; and Turin, H.J. 1997. *Summary Report of Chlorine-36 Studies: Sampling, Analysis, and Simulation of Chlorine-36 in the Exploratory Studies Facility.* LA-13352-MS. Los Alamos, New Mexico: Los Alamos National Laboratory. ACC: MOL.19980812.0254.

Fabryka-Martin, J.T.; Wolfsberg, A.V.; Levy, S.S.; Roach, J.L.; Winters, S.T.; Wolfsberg, L.E.; Elmore, D.; and Sharma, P. 1998. "Distribution of Fast Hydrologic Paths in the Unsaturated Zone at Yucca Mountain." *High-Level Radioactive Waste Management, Proceedings of the Eighth International Conference, Las Vegas, Nevada, May 11-14, 1998.* Pages 93-96. La Grange Park, Illinois: American Nuclear Society. TIC: 237082.

Fabryka-Martin, J.T.; Wolfsberg, A.V.; Roach, J.L.; Winters, S.T.; and Wolfsberg, L.E. 1998. "Using Chloride to Trace Water Movement in the Unsaturated Zone at Yucca Mountain." *High-Level Radioactive Waste Management, Proceedings of the Eighth International Conference, Las Vegas, Nevada, May 11-14, 1998.* Pages 264-268. La Grange Park, Illinois: American Nuclear Society. TIC: 237082.

Flint, A.L.; Hevesi, J.A.; and Flint, L.E. 1996. *Conceptual and Numerical Model of Infiltration for the Yucca Mountain Area, Nevada.* Milestone 3GUI623M. Denver, Colorado: U.S. Geological Survey. ACC: MOL.19970409.0087.

Flint, L.E. and Flint, A.L. 1995. *Shallow Infiltration Processes at Yucca Mountain, Nevada—Neutron Logging Data 1984-93.* Water-Resources Investigations Report 95-4035. Denver, Colorado: U.S. Geological Survey. ACC: MOL.19960924.0577.

French, R.H. 1985. *Daily, Seasonal, and Annual Precipitation at the Nevada Test Site, Nevada.* DOE/NV/10384-01. Las Vegas, Nevada: Desert Research Institute, Water Resources Center. TIC: 206773.

Gascoyne, M. 1992. "Geochemistry of the Actinides and Their Daughters." Chapter 2 of *Uranium-Series Disequilibrium: Applications to Earth, Marine, and Environmental Sciences.* Ivanovich, M. and Harmon, R.S. eds. 34-61. Oxford, England: Clarendon Press. TIC: 246658.

Geslin, J.K.; Moyer, T.C.; and Buesch, D.C. 1995. *Summary of Lithologic Logging of New and Existing Boreholes at Yucca Mountain, Nevada, August 1993 to February 1994.* Open-File Report 94-342. Denver, Colorado: U.S. Geological Survey. ACC: MOL.19940810.0011.

Gifford, R.O. and Frugoli, D.M. 1964. "Silica Source in Soil Solutions." *Science, 145,* 386-388. Washington, D.C.: American Association for the Advancement of Science. TIC: 239118.

Goldstein, R.H. and Reynolds, T.J., eds. 1994. "Fluid Inclusions and Their Origin." SEPM short Course 31 *Systematics of Fluid Inclusions in Diagenetic Minerals.* 5-9. Tulsa, Oklahoma: Society for Sedimentary Geology. TIC: 246523.

Grasso, D.N. 1996. *Hydrology of Modern and Late Holocene Lakes, Death Valley, California.* Water-Resources Investigations Report 95-4237. Denver, Colorado: U.S. Geological Survey. ACC: MOL.19970204.0218.

Haynes, C.V. 1967. "Quaternary Geology of the Tule Springs Area, Clark County Nevada." *Pleistocene Studies in Southern Nevada.* Anthropological Papers No. 13. Carson City, Nevada: Nevada State Museum. TIC: 225695.

Herczeg, A.L. and Edmunds, W.M. 2000. "Inorganic Ions as Tracers." Chapter 2 of *Environmental Tracers In Subsurface Hydrology.* Cook, P.G. and Herczeg, A.L., eds. Boston, Massachusetts: Kluwer Academic Publishers. TIC: 247093.

Hevesi, J.A.; Flint, A.L.; and Istok, J.D. 1992. "Precipitation Estimation in Mountainous Terrain Using Multivariate Geostatistics. Part II: Isohyetal Maps." *Journal of Applied Meteorology, 31,* (7), 677-688. Boston, Massachusetts: American Meteorological Society. TIC: 225248.

Hill, C.A.; Dublyansky, Y.V.; Harmon R.S.; and Schluter, C.M. 1995. "Overview of Calcite/Opal Deposits at or Near the Proposed High-Level Nuclear Waste Site, Yucca Mountain, Nevada, USA: Pedogenic, Hypogene, or Both?." *Environmental Geology, 26,* 69-88. New York, New York: Springer-Verlag. TIC: 222318.

IAEA (International Atomic Energy Agency) 1981. *Statistical Treatment of Environmental Isotope Data in Precipitation.* Technical Reports Series No. 206. Pages xi-xx, 2, 3, 134-137, 154, 155, and 245-255. Vienna, Austria: International Atomic Energy Agency. TIC: 246103.

IAEA (International Atomic Energy Agency) 1983. *Isotope Techniques in the Hydrogeological Assessment of Potential Sites for the Disposal of High-Level Radioactive Wastes.* Technical Report Series No. 228. Vienna, Austria: International Atomic Energy Agency. TIC: 238099.

Ivanovich, M. and Harmon, R.S. 1992. *Uranium-Series Disequilibrium: Applications to Earth, Marine, and Environmental Sciences.* New York, New York: Oxford University Press. TIC: 234680.

Kieft, T.L.; Kovacik, W.P., Jr.; Ringelberg, D.B.; White, D.C.; Haldeman, D.L.; Amy, P.S.; and Hersman, L.E. 1997. "Factors Limiting Microbial Growth and Activity at a Proposed High-Level Nuclear Repository, Yucca Mountain, Nevada." *Applied and Environmental Microbiology, 63,* (8), 3128-3133. Washington, D.C.: American Society for Microbiology. TIC: 236444.

Kim, S.T. and O'Neil, J.R. 1997. "Equilibrium and Nonequilibrium Isotope Effects in Synthetic Carbonates." *Geochimica et Cosmochimica Acta, 61,* (16), 3461-3475. New York, New York: Pergamon Press. TIC: 236999.

LeCain, G.D. and Patterson, G.L. 1997. "Milestones — Submittal of Milestone SPH35EM4." Memorandum from G.D. LeCain and G.L. Patterson (USGS) to R. Craig (USGS-TPO), March 11, 1997, with attachment. ACC: MOL.19980224.0146.

LeCain, G.D.; Patterson, G.L.; and Severson, G.R. 1997. *Results from Pneumatic Monitoring, Hydrochemistry Sampling, Air-Injection, and Tracer Testing in the Upper Tiva Canyon, and Bow Ridge Fault Alcoves, Yucca Mountain, Nevada, November,1994 to July,1996.* Milestone 3GUS619M-1996. Denver, Colorado: U.S. Geological Survey. ACC: MOL.19970415.0387.

Lichty, R.W. and McKinley, P.W. 1995. *Estimates of Ground-Water Recharge Rates for Two Small Basins in Central Nevada.* Water-Resources Investigations Report 94-4104. Denver, Colorado: U.S. Geological Survey. ACC: MOL.19960924.0524.

Lindberg, R.D. and Runnells, D.D. 1984. "Ground Water Redox Reactions: An Analysis of Equilibrium State Applied to Eh Measurements and Geochemical Modeling." *Science, 225,* 925-927. Washington, D.C.: American Association for the Advancement of Science. TIC: 224111.

Ludwig, K.R.; Peterman, Z.E.; Simmons, K.R.; and Gutentag, E.D. 1993. "234U/238U as a Ground-Water Tracer, SW Nevada-SE California." *High Level Radioactive Waste Management, Proceedings of the Fourth Annual International Conference, Las Vegas, Nevada, April 26-30, 1993.* 1567-1572. La Grange Park, Illinois: American Nuclear Society. TIC: 208542.

Ludwig, K.R.; Simmons, K.R.; Szabo, B.J.; Winograd, I.J.; Landwehr, J.M.; Riggs, A.C.; and Hoffman, R.J. 1992. "Mass-Spectrometric 230[Th]-234[U]-238[U] Dating of the Devils Hole Calcite Vein." *Science, 258,* 284-287. Washington, D.C.: American Association for the Advancement of Science. TIC: 237796.

Malmberg, G.T. and Eakin, T.E. 1962. *Ground-Water Appraisal of Sarcobatus Flat and Oasis Valley, Nye and Esmeralda Counties, Nevada.* Ground-Water Resources – Reconnaissance Series Report 10. Carson City, Nevada: State of Nevada, Department of Conservation and Natural Resources. TIC: 208666.

Marshall, B.D. and Mahan, S.A. 1994. "Strontium Isotope Geochemistry of Soil and Playa Deposits Near Yucca Mountain, Nevada." *High Level Radioactive Waste Management, Proceedings of the Fifth Annual International Conference, Las Vegas, Nevada, May 22-26, 1994. 4,* 2685-2691. La Grange Park, Illinois: American Nuclear Society. TIC: 210984.

Marshall, B.D.; Futa, K.; and Peterman, Z.E. 1998. "Hydrologic Inferences from Strontium Isotopes in Port Water from the Unsaturated Zone at Yucca Mountain, Nevada." *Proceedings of FTAM: Field Testing and Associated Modeling of Potential High-Level Nuclear Waste Geologic Disposal Sites, December 15-16, 1997.* Bodvarsson, G.S., ed. *LBNL-42520,* 55-56. Berkeley, California: Lawrence Berkeley National Laboratory. TIC: 243019.

Marshall, B.D.; Neymark, L.A.; Paces, J.B.; Peterman Z.E.; and Whelan, J.F. 1999. "Seepage Flux Conceptualized from Secondary Calcite in Lithophysal Cavities in the Topopah Spring Tuff, Yucca Mountain, Nevada." *EOS, Transactions, American Geophysical Union 1999 Spring Meeting.* S5. Washington, D.C.: American Geophysical Union. TIC: 246466.

Marshall, B.D.; Paces, J.B.; Neymark, L.A.; Whelan, J.F.; and Peterman, Z.E. 1998. "Secondary Minerals Record Past Percolation Flux at Yucca Mountain, Nevada." *High-Level Radioactive Waste Management, Proceedings of the Eighth International Conference, Las Vegas, Nevada, May 11-14, 1998.* Pages 127-129. La Grange Park, Illinois: American Nuclear Society. TIC: 237082.

Marshall, B.D.; Peterman, Z.E.; and Stuckless, J.S. 1993. "Strontium Isotopic Evidence for a Higher Water Table at Yucca Mountain." *High Level Radioactive Waste Management, Proceedings of the Fourth Annual International Conference, Las Vegas, Nevada, April 26-30, 1993. 2,* 1948-1952. La Grange Park, Illinois: American Nuclear Society. TIC: 208542.

Marshall, B.D.; Whelan, J.F.; Peterman, Z.E.; Futa, K.; Mahan, S.A.; and Stuckless, J.S. 1992. "Isotopic Studies of Fracture Coatings at Yucca Mountain, Nevada, USA." *Proceedings of the 7th International Symposium on Water-Rock Interaction, Park City, Utah, July 13-18, 1992.*

Kharaka, Y.K. and Maest, A.S., eds. *1,* 737-740. Rotterdam, The Netherlands: A.A. Balkema. TIC: 208527.

McKinley, P.W. and Oliver, T.A. 1994. *Meteorological, Stream-Discharge, and Water-Quality Data for 1986 through 1991 from Two Small Basins in Central Nevada.* Open-File Report 93-651. Denver, Colorado: U.S. Geological Survey. ACC: NNA.19940114.0099.

McKinley, P.W. and Oliver, T.A. 1995. *Meteorological, Stream-Discharge, and Water-Quality Data for Water Year 1992 from Two Basins in Central Nevada.* Open-File Report 94-456. Denver, Colorado: U.S. Geological Survey. ACC: MOL.19950124.0284.

McKinley, P.W.; Long, M.P.; and Benson, L.V. 1991. *Chemical Analyses of Water from Selected Wells and Springs in the Yucca Mountain Area, Nevada and Southeastern California.* Open-File Report 90-355. Denver, Colorado: U.S. Geological Survey. ACC: NNA.19901031.0004.

Meijer, A. 2001. *Stand Alone DR 39 Package for Analysis and Model Report: ANL-NBS-HS-000017, Rev 00, ICN 01, Analysis of Geochemical Data for the Unsaturated Zone.* Las Vegas, Nevada: Bechtel SAIC Company. ACC: MOL.20010910.0169.

Mifflin, M.D. and Wheat, M.M. 1979. *Pluvial Lakes and Estimated Pluvial Climates of Nevada.* Bulletin 94. Reno, Nevada: Nevada Bureau of Mines and Geology. TIC: 200724.

Montazer, P.; Weeks, E.P.; Thamir, F.; Yard, S.N.; and Hofrichter, P.B. 1985. "Monitoring the Vadose Zone in Fractured Tuff, Yucca Mountain, Nevada." *Proceedings of the NWWA Conference on Characterization and Monitoring of the Vadose (Unsaturated) Zone, November 19-21, 1985, Denver, Colorado.* Pages 439-469. Worthington, Ohio: National Water Well Association. TIC: 201366.

Moscati, R.J. and Whelan, J.F. 1996. *Origins of Secondary Silica Within Yucca Mountain, Nye County, Southwestern Nevada.* Open-File Report 95-289. Denver, Colorado: U.S. Geological Survey. TIC: 225888.

Mower, T.E.; Higgins, J.D.; Yang, I.C.; and Peters, C.A. 1994. *Pore-Water Extraction from Unsaturated Tuff by Triaxial and One-Dimensional Compression Methods, Nevada Test Site, Nevada.* Water-Resources Investigations Report 93-4144. Denver, Colorado: U.S. Geological Survey. ACC: NNA.19940621.0002.

Moyer, T.C. and Geslin, J.K. 1995. *Lithostratigraphy of the Calico Hills Formation and Prow Pass Tuff (Crater Flat Group) at Yucca Mountain, Nevada.* Open-File Report 94-460. Denver, Colorado: U.S. Geological Survey. ACC: MOL.19941208.0003.

Moyer, T.C.; Geslin, J.K.; and Flint, L.E. 1996. *Stratigraphic Relations and Hydrologic Properties of the Paintbrush Tuff Nonwelded (PTn) Hydrologic Unit, Yucca Mountain, Nevada.* Open-File Report 95-397. Denver, Colorado: U.S. Geological Survey. ACC: MOL.19970204.0216.

Muhs, D.R.; Whitney, J.W.; Shroba, R.R.; Taylor, E.M.; and Bush, C.A 1990. "Uranium-Series Dating of Secondary Carbonates near Yucca Mountain, Nevada: Application to Tectonic, Paleoclimatic, and Paleohydrologic Problems." *High Level Radioactive Waste Management, Proceedings of the International Topical Meeting, Las Vegas, Nevada, April 8-12, 1990. 2,* 924-929. La Grange Park, Illinois: American Nuclear Society. TIC: 202058.

National Atmospheric Deposition Program 1996. "National Atmospheric Deposition Program/National Trends Network: A Descriptive Summary." Fort Collins, Colorado: National Atmospheric Deposition Program. Accessed August 16, 1996. TIC: 246211. http://nadp.nrel.colostate.edu/NADP/ documentation/progdesc.txt.html

National Research Council 1992. *Ground Water at Yucca Mountain: How High Can It Rise?, Final Report of the Panel on Coupled Hydrologic/Tectonic/Hydrothermal Systems at Yucca Mountain.* Washington, D.C.: National Academy Press. TIC: 204931.

Neymark, L.A.; Amelin, Y.V.; Paces, J.B.; and Peterman, Z.E. 1998. "U-Pb Age Evidence for Long-Term Stability of the Unsaturated Zone at Yucca Mountain." *High-Level Radioactive Waste Management, Proceedings of the Eighth International Conference, Las Vegas, Nevada, May 11-14, 1998.* Pages 85-87. La Grange Park, Illinois: American Nuclear Society. TIC: 237082.

O'Brien, G.M. 1997. *Analysis of Aquifer Tests Conducted in Boreholes USW WT-10, UE-25 WT#12, and USW SD-7, 1995-96, Yucca Mountain, Nevada.* Water-Resources Investigations Report 96-4293. Denver, Colorado: U.S. Geological Survey. ACC: MOL.19980219.0822.

O'Neil, J.R.; Clayton, R.N.; and Mayeda, T.K. 1969. "Oxygen Isotope Fractionation in Divalent Metal Carbonates." *The Journal of Chemical Physics, 51,* (12), 5547-5558. New York, New York: American Institute of Physics. TIC: 216938.

Ogard, A.E. and Kerrisk, J.F. 1984. *Groundwater Chemistry Along Flow Paths Between a Proposed Repository Site and the Accessible Environment.* LA-10188-MS. Los Alamos, New Mexico: Los Alamos National Laboratory. ACC: HQS.19880517.2031.

Oliver, T. and Root, T. 1997. *Hydrochemical Database for the Yucca Mountain Area, Nye County, Nevada.* Denver, Colorado: U.S. Geological Survey. ACC: MOL.19980302.0367.

Osmond, J.K. and Cowart, J.B. 1992. "Ground Water." Chapter 9 of *Uranium-Series Disequilibrium: Applications to Earth, Marine, and Environmental Sciences.* Invanovich, M. and Harmon, R.S.; eds. 2nd Edition. New York, New York: Oxford University Press. TIC: 234680.

Paces, J.B. and Peterman, Z.E. 1999. "Isotope Hydrology of Ground-Water Flow Systems, Southern Nevada." *Proceedings of the International Symposium on Dynamics of Fluids in Fractured Rocks Concepts and Recent Advances held February 10-12, 1999, LBNL-42718.* Faybishenko, Boris, ed. 134-138. Berkeley, California: Lawrence Berkeley National Laboratory. TIC: 246681.

Paces, J.B.; Forester, R.M.; Whelan, J.F.; Mahan, S.A.; Bradbury, J.P.; Quade, J.; Neymark, L.A.; and Kwak, L.M. 1996. *Synthesis of Ground-Water Discharge Deposits Near Yucca Mountain.* Milestone 3GQH671M. Las Vegas, Nevada: U.S. Geological Survey. ACC: MOL.19970205.0007.

Paces, J.B.; Ludwig, K.R.; Peterman, Z.E.; Neymark, L.A.; and Kenneally, J.M. 1998. "Anomalous Groundwater 234U/238U Beneath Yucca Mountain: Evidence of Local Recharge?." *High-Level Radioactive Waste Management, Proceedings of the Eighth International Conference, Las Vegas, Nevada, May 11-14, 1998.* Pages 185-188. La Grange Park, Illinois: American Nuclear Society. TIC: 237082.

Paces, J.B.; Mahan, S.A.; Ludwig, K.R.; Kwak, L.M.; Neymark, L.A.; Simmons, K.R.; Nealey, L.D.; Marshall, B.D.; and Walker, A. 1995. *Progress Report on Dating Quaternary Surficial Deposits.* Milestone 3GCH510M. Final Draft. Denver, Colorado: U.S. Geological Survey. ACC: MOL.19960611.0220.

Paces, J.B.; Marshall, B.D.; Whelan, J.F.; and Neymark, L.A. 1997. "Submission of Milestone: SPC23FM4, Due March 14, 1997." Memorandum from J.B. Paces, B.D. Marshall, J.F. Whelan, and L.A. Neymark (USGS) to R.W. Craig, March 14, 1997, with attachment, "Progress Report on Unsaturated Zone Stable and Radiogenic Isotope Studies." ACC: MOL.19980224.0119.

Paces, J.B.; Marshall, B.D.; Whelan, J.F.; Neymark, L.A.; and Peterman, Z.E. 1998. *Summary of Subsurface Secondary Mineralization and Predictions of the Distribution and Isotopic Nature of Mineralization Along the East-West Cross Drift Alignment, Yucca Mountain, Nevada.* SPC237M4. Denver, Colorado: U.S. Geological Survey. Submit to RPC

Paces, J.B.; Menges, C.M.; Widmann, B.; Wesling, J.R.; Bush, C.A.; Futa, K.; Millard, H.T., Jr.; Maat, P.B.; and Whitney, J.W. 1994. "U-Series Disequilibrium and Thermoluminescence Ages of Paleosols Associated with Quaternary Faults, East Side of Yucca Mountain." *High Level Radioactive Waste Management, Proceedings of the Fifth Annual International Conference, Las Vegas, Nevada, May 22-26, 1994. 4,* 2391-2401. La Grange Park, Illinois: American Nuclear Society. TIC: 210984.

Paces, J.B.; Newmark, L.A.; Marshall, B.D.; Whelan, J.F.; and Peterman, Z.E. 1998. "Inferences for Yucca Mountain Unsaturated-Zone Hydrology from Secondary Minerals." *High-Level Radioactive Waste Management, Proceedings of the Eighth International Conference, Las Vegas, Nevada, May 11-14, 1998.* Pages 36-39. La Grange Park, Illinois: American Nuclear Society. TIC: 237082.

Paces, J.B.; Neymark, L.A.; Marshall, B.D.; Whelan, J.F.; and Peterman, Z.E. 1996. *Letter Report: Ages and Origins of Subsurface Secondary Minerals in the Exploratory Studies Facility (ESF).* Milestone 3GQH450M. Las Vegas, Nevada: U.S. Geological Survey. ACC: MOL.19970324.0052.

Paces, J.B.; Neymark, L.A.; Whelan, J.F.; Marshall, B.D.; and Amelin, Y.V. 1999. "Characteristics of Unsaturated-Zone Fracture Flow Interpreted from Calcite and Opal Deposits at Yucca Mountain, Nevada." *EOS, Transactions, American Geophysical Union 1999 Spring Meeting.* S4. Washington, D.C.: American Geophysical Union. TIC: 246468.

Paces, J.B.; Whelan, J.F.; Forester, R.M.; Bradbury, J.P.; Marshall, B.D.; and Mahan, S.A. 1997. *Summary of Discharge Deposits in the Amargosa Valley.* Milestone SPC333M4 . Denver, Colorado: U.S. Geological Survey. ACC: MOL.19981104.0151.

Parrington, J.R.; Knox, H.D.; Breneman, S.L.; Baum, E.M.; and Feiner, F. 1996. *Nuclides and Isotopes, Chart of the Nuclides.* 15th Edition. San Jose, California: General Electric Company and KAPL, Inc. TIC: 233705.

Perfect, D.L.; Faunt, C.C.; Steinkampf, W.C.; and Turner, A.K. 1995. *Hydrochemical Data Base for the Death Valley Region, California and Nevada.* Open-File Report 94-305. Denver, Colorado: U.S. Geological Survey. ACC: MOL.19940718.0001.

Peterman, Z.E. and Patterson, G. 1998. "Isotopes Aid in Understanding the Yucca Mountain Flow System." *High-Level Radioactive Waste Management, Proceedings of the Eighth International Conference, Las Vegas, Nevada, May 11-14, 1998.* Pages 182-184. La Grange Park, Illinois: American Nuclear Society. TIC: 237082.

Peterman, Z.E. and Stuckless, J.S. 1993. "Isotopic Evidence of Complex Ground-Water Flow at Yucca Mountain, Nevada, USA." *High Level Radioactive Waste Management, Proceedings of the Fourth Annual International Conference, Las Vegas, Nevada, April 26-30, 1993. 2,* 1559-1566. La Grange Park, Illinois: American Nuclear Society. TIC: 208542.

Peterman, Z.E.; Stuckless, J.S.; Marshall, B.D.; Mahan, S.A.; and Futa, K. 1992. "Strontium Isotope Geochemistry of Calcite Fracture Fillings in Deep Core, Yucca Mountain, Nevada -- A Progress Report." *High Level Radioactive Waste Management, Proceedings of the Third International Conference, Las Vegas, Nevada, April 12-16, 1992. 2,* 1582-1586. La Grange Park, Illinois: American Nuclear Society. TIC: 204231.

Phillips, F.M. 1994. "Environmental Tracers for Water Movement in Desert Soils of the American Southwest." *Soil Science Society of America Journal, 58,* 15-24. Madison, Wisconsin: Soil Science Society of America. TIC: 240651.

Phillips, F.M. 2000. "Chlorine-36." Chapter 10 of *Environmental Tracers In Subsurface Hydrology.* Cook, P.G. and Herczeg, A.L. eds. Norwell, Massachusetts: Kluwer Academic Publishers. TIC: 247021.

Plummer, M.A.; Phillips, F.M.; Fabryka-Martin, J.; Turin, H.J.; Wigand, P.E.; and Sharma, P. 1997. "Chlorine-36 in Fossil Rat Urine: An Archive of Cosmogenic Nuclide Deposition During the Past 40,000 Years." *Science, 277,* 538-541. Washington, D.C.: American Association for the Advancement of Science. TIC: 237425.

Quade, J.; Cerling, T.E.; and Bowman, J.R. 1989. "Systematic Variations in the Carbon and Oxygen Isotopic Composition of Pedogenic Carbonate Along Elevation Transects in the Southern Great Basin, United States." *Geological Society of America Bulletin, 101,* 464-475. Boulder, Colorado: Geological Society of America. TIC: 224797.

Quade, J.; Mifflin, M.D.; Pratt, W.L.; McCoy, W.; and Burckle, L. 1995. "Fossil Spring Deposits in the Southern Great Basin and Their Implications for Changes in Water-Table Levels Near Yucca Mountain, Nevada, During Quaternary Time." *Geological Society of America Bulletin, 107,* (2), 213-230. Boulder, Colorado: Geological Society of America. TIC: 234256.

Rattray, G.W.; Striegl, R.G.; and Yang, I.C. 1995. *Adsorption of Sulfur Hexafluoride onto Crushed Tuffs from the Yucca Mountain Area, Nye County, Nevada.* Water-Resources Investigations Report 95-4057. Denver, Colorado: U.S. Geological Survey. ACC: MOL.19970331.0042.

Rautman, C.A. and Engstrom, D.A. 1996. *Geology of the USW SD-12 Drill Hole Yucca Mountain, Nevada.* SAND96-1368. Albuquerque, New Mexico: Sandia National Laboratories. ACC: MOL.19970613.0101.

Rautman, C.A. and Engstrom, D.A. 1996. *Geology of the USW SD-7 Drill Hole Yucca Mountain, Nevada.* SAND96-1474. Albuquerque, New Mexico: Sandia National Laboratories. ACC: MOL.19971218.0442.

Roedder, E. 1970. "Application of an Improved Crushing Microscope Stage to Studies of the Gases in Fluid Inclusions." *Schweizerische Mineralogische und Petrographische Mitteilungen, 50,* (1), 41-58. Zurich, Switzerland: Institut fur Mineralogie und Petrographie. TIC: 243697.

Roedder, E. 1984. *Fluid Inclusions.* Reviews in Mineralogy, Volume 12. Washington, D.C.: Mineralogical Society of America. TIC: 236874.

Roedder, E. and Whelan, J.F. 1998. "Ascending or Descending Water Flow Through Yucca Mountain Tuffs? - Fluid Inclusion Evidence." *PACROFI VII, Pan-American Conference on Research On Fluid Inclusions, Las Vegas, Nevada, June 1-4, 1998. Open-File Report 98-4,* 56. Reno, Nevada: Nevada Bureau of Mines and Geology. TIC: 247943.

Roedder, E.; Whelan, J.F.; and Vaniman, D.T. 1993. "Environment of Formation of Calcite Veins from Yucca Mountain, Nevada, Tuffs as Evidenced by Fluid Inclusion Crushing Studies." *Abstracts with Programs, Geological Society of America, 25,* (6), A-184. Boulder, Colorado: Geological Society of America. On Order Library Tracking Number-248233

Roedder, E.; Whelan, J.F.; and Vaniman, D.T. 1994. "Fluid Inclusion Studies of Calcite Veins from Yucca Mountain, Nevada, Tuffs: Environment of Formation." *High Level Radioactive Waste Management, Proceedings of the Fifth Annual International Conference, Las Vegas, Nevada, May 22-26, 1994.* 4. 1854-1860. La Grange Park, Illinois: American Nuclear Society. TIC: 210984.

Rojstaczer, S. 1999. "Stress Dependent Permeability and Its Political Consequences at Yucca Mountain." *EOS, Transactions, American Geophysical Union 1999 Spring Meeting. 80,* S4. Washington, D.C.: American Geophysical Union. TIC: 246513.

Rousseau, J.P.; Kwicklis, E.M.; and Gillies, D.C., eds. 1999. *Hydrogeology of the Unsaturated Zone, North Ramp Area of the Exploratory Studies Facility, Yucca Mountain, Nevada.* Water-Resources Investigations Report 98-4050. Denver, Colorado: U.S. Geological Survey. ACC: MOL.19990419.0335.

Rousseau, J.P.; Loskot, C.L.; Thamir, F.; and Lu, N. 1997. *Results of Borehole Monitoring in the Unsaturated Zone Within the Main Drift Area of the Exploratory Studies Facility, Yucca Mountain, Nevada.* Milestone SPH22M3. Denver, Colorado: U.S. Geological Survey. ACC: MOL.19970626.0351.

Sass, J.H.; Lachenbruch, A.H.; and Mase, C.W. 1980. *Analysis of Thermal Data from Drill Holes UE25a-3 and UE25a-1, Calico Hills and Yucca Mountain, Nevada Test Site.* Open-File Report 80-826. Denver, Colorado: U.S. Geological Survey. ACC: HQS.19880517.1429.

Sass, J.H.; Lachenbruch, A.H.; Dudley, W.W., Jr.; Priest, S.S.; and Munroe, R.J. 1988. *Temperature, Thermal Conductivity, and Heat Flow Near Yucca Mountain, Nevada: Some Tectonic and Hydrologic Implications.* Open-File Report 87-649. Denver, Colorado: U.S. Geological Survey. ACC: MOL.19971027.0303.

Savard, C.S. 1995. "Ground-Water Recharge from Small to Large Streamflow Events During El Niño Periods Under Fortymile Wash near Yucca Mountain, Nevada." *American Geophysical Union 1995 Fall Meeting December 11-15, 1995 San Francisco, California.* F241. Washington, D.C.: American Geophysical Union. TIC: 237433.

Savard, C.S. 1996. *Selected Hydrologic Data from Fortymile Wash in the Yucca Mountain Area, Nevada, Water Years 1993-94.* Open-File Report 95-709. Denver, Colorado: U.S. Geological Survey. ACC: MOL.19980226.0548.

Savard, C.S. 1998. *Estimated Ground-Water Recharge from Streamflow in Fortymile Wash Near Yucca Mountain, Nevada.* Water-Resources Investigations Report 97-4273. Denver, Colorado: U.S. Geological Survey. TIC: 236848.

Sawyer, D.A.; Fleck, R.J.; Lanphere, M.A.; Warren, R.G.; Broxton, D.E.; and Hudson, M.R. 1994. "Episodic Caldera Volcanism in the Miocene Southwestern Nevada Volcanic Field: Revised Stratigraphic Framework, 40Ar/39Ar Geochronology, and Implications for Magmatism and Extension." *Geological Society of America Bulletin, 106,* (10), 1304-1318. Boulder, Colorado: Geological Society of America. TIC: 222523.

Scanlon, B.R. 1991. "Evaluation of Moisture Flux from Chloride Data in Desert Soils." *Journal of Hydrology, 128,* 137-156. Amsterdam, The Netherlands: Elsevier Science. TIC: 224126.

Scanlon, B.R.; Tyler, S.W.; and Wierenga, P.J. 1997. "Hydrologic Issues In Arid, Unsaturated Systems and Implications for Contaminant Transport." *Reviews of Geophysics, 35,* (4), 461-490. Washington, D.C.: American Geophysical Union. TIC: 246881.

Sharma, P.; Kubik, P.W.; Fehn, U.; Gove, H.E.; Nishiizumi, K.; and Elmore, D. 1990. "Development of (36)Cl Standards for AMS." *Nuclear Instruments and Methods in Physics Research, B52,* 410-415. Amsterdam, The Netherlands: Elsevier Science Publishers. TIC: 224755.

Spaulding, W.G. 1985. *Vegetation and Climates of the Last 45,000 Years in the Vicinity of the Nevada Test Site, South-Central Nevada.* Professional Paper 1329. Washington, D.C.: U.S. Geological Survey. TIC: 203210.

Steiger, R.H. and Jager, E. 1977. "Subcommission on Geochronology: Convention on the Use of Decay Constants in Geo- and Cosmochronology." *Earth and Planetary Science Letters, 36,* 359-362. Amsterdam, The Netherlands: Elsevier Scientific Publishing Company. TIC: 236817.

Stuckless, J.S. 1991. "An Evaluation of Evidence Pertaining to the Origin of Vein Deposits Exposed in Trench 14, Nevada Test Site, Nevada." *High Level Radioactive Waste Management, Proceedings of the Second Annual International Conference, Las Vegas, Nevada, April 28-May 3, 1991. 2,* 1429-1438. La Grange Park, Illinois: American Nuclear Society. TIC: 204272.

Stuckless, J.S.; Marshall, B.D.; Vaniman, D.T.; Dudley, W.W.; Peterman, Z.E.; Paces, J.B.; Whelan, J.F.; Taylor, E.M.; Forester, R.M.; and O'Leary, D.W. 1998. "Comments on 'Overview of Calcite/Opal Deposits at or Near the Proposed High-Level Nuclear Waste Site, Yucca Mountain, Nevada, USA: Pedogenic, Hypogene, or Both' by C.A. Hill, Y.V. Dublansky, R.S. Harmon, and C.M. Schluter." *Environmental Geology, 34,* (1), 70-78. New York, New York: Springer-Verlag. TIC: 238097.

Stuckless, J.S.; Peterman, Z.E.; and Muhs, D.R. 1991. "U and Sr Isotopes in Ground Water and Calcite, Yucca Mountain, Nevada: Evidence Against Upwelling Water." *Science, 254,* 551-554. Washington, D.C.: American Association for the Advancement of Science. TIC: 224423.
Szabo, B.J. and Kyser, T.K. 1990. "Ages and Stable-Isotope Compositions of Secondary Calcite and Opal in Drill Cores from Tertiary Volcanic Rocks of the Yucca Mountain Area, Nevada." *Geological Society of America Bulletin, 102,* 1714-1719. Boulder, Colorado: Geological Society of America. TIC: 221927.

Taylor, E.M. and Huckins, H.E. 1995. *Lithology, Fault Displacement, and Origin of Secondary Calcium Carbonate and Opaline Silica at Trenches 14 and 14d on the Bow Ridge Fault at Exile Hill, Nye County, Nevada.* Open-File Report 93-477. Denver, Colorado: U.S. Geological Survey. ACC: MOL.19940906.0001.

Thorstenson, D.C.; Weeks, E.P.; Haas, H.; Busenberg, E.; Plummer, L.N.; and Peters, C.A. 1998. "Chemistry of Unsaturated Zone Gases Sampled in Open Boreholes at the Crest of Yucca Mountain, Nevada: Data and Basic Concepts of Chemical and Physical Processes in the

Mountain." *Water Resources Research, 34,* (6), 1507-1529. Washington, D.C.: American Geophysical Union. TIC: 246315.

Thorstenson, D.C.; Weeks, E.P.; Hass, H.; and Woodward, J.C. 1990. "Physical and Chemical Characteristic of Topographically Affected Airflow in an Open Borehole at Yucca Mountain, Nevada." *Focus '89, Proceedings of the Topical Meeting on Nuclear Waste Isolation in the Unsaturated Zone, Las Vegas, Nevada, September 17-21, 1989.* 256-270. La Grange Park, Illinois: American Nuclear Society. TIC: 216833.

Tokunaga, T.K. and Wan, J. 1997. "Water Film Flow along Fracture Surfaces of Porous Rock." *Water Resources Research, 33,* (6), 1287-1295. Washington, D.C.: American Geophysical Union. TIC: 242739.

Triay, I.R.; Meijer, A.; Conca, J.L.; Kung, K.S.; Rundberg, R.S.; Strietelmeier, B.A.; Tait, C.D.; Clark, D.L.; Neu, M.P.; and Hobart, D.E. 1997. *Summary and Synthesis Report on Radionuclide Retardation for the Yucca Mountain Site Characterization Project.* LA-13262-MS. Los Alamos, New Mexico: Los Alamos National Laboratory. ACC: MOL.19971210.0177.

Vaniman, D.T. and Whelan, J.F. 1994. "Inferences of Paleoenvironment from Petrographic, Chemical and Stable-Isotope Studies of Calcretes and Fracture Calcites." *High Level Radioactive Waste Management, Proceedings of the Fifth Annual International Conference, Las Vegas, Nevada, May 22-26, 1994. 4,* 2730-2737. La Grange Park, Illinois: American Nuclear Society. TIC: 210984.

Vaniman, D.T.; Carey, J.W.; Bish, D.L.; and Chipera, S.J. 1999. "Cation Profiles Generated by Downward Transport Into Unsaturated Zeolitic Strata at Yucca Mountain, Nevada." *EOS, Transactions, American Geophysical Union 1999 Spring Meeting.* S5. Washington, D.C.: American Geophysical Union. TIC: 246464.

Vaniman, D.T.; Chipera, S.J.; and Bish, D.L. 1994. "Pedogenesis of Siliceous Calcretes at Yucca Mountain, Nevada." *Geoderma, 63,* 1-17. Amsterdam, The Netherlands: Elsevier Science B.V. TIC: 212060.

Walker, G.E. and Eakin, T.E. 1963. *Geology and Ground Water of Amargosa Desert, Nevada–California.* Ground-Water Resources – Reconnaissance Series Report 14. Carson City, Nevada: State of Nevada, Department of Conservation and Natural Resources. TIC: 208665.

Whelan, J.F. and Moscati, R.J. 1998. "9 M.Y. Record of Southern Nevada Climate from Yucca Mountain Secondary Minerals." *High-Level Radioactive Waste Management, Proceedings of the Eighth International Conference, Las Vegas, Nevada, May 11-14, 1998.* Pages 12-15. La Grange Park, Illinois: American Nuclear Society. TIC: 237082.

Whelan, J.F. and Stuckless, J.S. 1990. "Reconnaissance [Delta]13C and [Delta]18O Data from Trench 14, Busted Butte, and Drill Hole G-4, Yucca Mountain, Nevada Test Site." *High Level Radioactive Waste Management, Proceedings of the International Topical Meeting, Las Vegas,*

Nevada, April 8-12, 1990. 2, 930-933. La Grange Park, Illinois: American Nuclear Society. TIC: 202058.

Whelan, J.F. and Stuckless, J.S. 1992. "Paleohydrologic Implications of the Stable Isotopic Composition of Secondary Calcite Within the Tertiary Volcanic Rocks of Yucca Mountain, Nevada." *High Level Radioactive Waste Management, Proceedings of the Third Annual International Conference, Las Vegas, Nevada, April 12-16, 1992. 2,* 1572-1581. La Grange Park, Illinois: American Nuclear Society. TIC: 204231.

Whelan, J.F.; Moscati, R.J.; Allerton, S.B.M.; and Marshall, B.D. 1998. *Applications of Isotope Geochemistry to the Reconstruction of Yucca Mountain, Nevada, Paleohydrology—Status of Investigations: June 1996.* Open-File Report 98-83. Denver, Colorado: U.S. Geological Survey. ACC: MOL.19981012.0740.

Whelan, J.F.; Paces, J.B.; Moscati, R.J.; Neymark, L.A.; Marshall, B.D.; and Peterman, Z.E. 1999. "Paragenesis and Oxygen Isotopes of Calcite in the Unsaturated Zone of Yucca Mountain, Nevada: Evidence of an Early Thermal Event." *EOS, Transactions, American Geophysical Union 1999 Spring Meeting.* S8. Washington, D.C.: American Geophysical Union. TIC: 246462.

Whelan, J.F.; Vaniman, D.T.; Stuckless, J.S.; and Moscati, R.J. 1994. "Paleoclimatic and Paleohydrologic Records from Secondary Calcite: Yucca Mountain, Nevada." *High Level Radioactive Waste Management, Proceedings of the Fifth Annual International Conference, Las Vegas, Nevada, May 22-26, 1994. 4,* 2738–2745. La Grange Park, Illinois: American Nuclear Society. TIC: 210984.

White, A.F. and Chuma, N.J. 1987. "Carbon and Isotopic Mass Balance Models of Oasis Valley - Fortymile Canyon Groundwater Basin, Southern Nevada." *Water Resources Research , 23,* (4), 571-582. Washington, D.C.: American Geophysical Union. TIC: 237579.

White, A.F.; Claassen, H.C.; and Benson, L.V. 1980. "The Effect of Dissolution of Volcanic Glass on the Water Chemistry in a Tuffaceous Aquifer, Rainier Mesa, Nevada." *Geochemistry of Water.* Geologic Survey Water-Supply Paper 1535-Q. Washington, D.C.: U.S. Government Printing Office. TIC: 221391.

Whitfield, M.S. 1986. "Vacuum Drilling of Unsaturated Tuffs at a Potential Radioactive-Waste Repository, Yucca Mountain, Nevada." *Proceedings of the NWWA Conference on Characterization and Monitoring of the Vadose (Unsaturated) Zone, Denver, Colorado, November 19-21, 1985.* 413-423. Worthington, Ohio: National Water Well Association. TIC: 222624.

Whitfield, M.S.; Thordarson, W.; Hammermeister, D.P.; and Warner, J.B. 1990. *Drilling and Geohydrologic Data for Test Hole USW UZ-1, Yucca Mountain, Nye County, Nevada.* Open-File Report 90-354. Denver, Colorado: U.S. Geological Survey. ACC: NNA.19900622.0450.

Winchester, J.W. and Duce, R.A. 1967. "The Global Distribution of Iodine, Bromine, and Chlorine in Marine Aerosols." *Naturwissenschaften, 54,* (5), 110-113. New York, New York: Springer-Verlag. TIC: 226930.

Winograd, I.J.; Coplen, T.B.; Landwehr, J.M.; Riggs, A.C.; Ludwig, K.R.; Szabo, B.J.; Kolesar, P.T.; and Revesz, K.M. 1992. "Continuous 500,000-Year Climate Record from Vein Calcite in Devils Hole, Nevada." *Science, 258,* 255-260. Washington, D.C.: American Association for the Advancement of Science. TIC: 237563.

Wolfsberg, A.V.; Fabryka-Martin, J.T.; Roemer, G.J.C.; and Robinson, B.A. 1998. "Modeling Flow and Transport Pathways to the Potential Repository Horizon at Yucca Mountain." *High-Level Radioactive Waste Management, Proceedings of the Eighth International Conference, Las Vegas, Nevada May 11-14, 1998.* Pages 81-84. La Grange Park, Illinois: American Nuclear Society. TIC: 237082.

Yang, I.C. 1992. "Flow and Transport through Unsaturated Rock – Data from Two Test Holes, Yucca Mountain, Nevada." *High Level Radioactive Waste Management, Proceedings of the Third International Conference, Las Vegas, Nevada, April 12-16, 1992. 1,* 732-737. La Grange Park, Illinois: American Nuclear Society. TIC: 204231.

Yang, I.C.; Davis, G.S.; and Sayre, T.M. 1990. "Comparison of Pore-Water Extraction by Triaxial Compression and High-Speed Centrifugation Methods." *Proceedings of Conference on Minimizing Risk to the Hydrological Environment, American Institute of Hydrology.* Pages 250-259. Dubuque, Iowa: American Institute of Hydrology. TIC: 224435.

Yang, I.C.; Peters, C.A.; and Thorstenson, D.C. 1993. "Carbon Isotopic Data from Test Hole USW UZ-1 Yucca Mountain, Nevada." *High Level Radioactive Waste Management, Proceedings of the Fourth Annual International Conference, Las Vegas, Nevada, April 26-30, 1993.* 401-406. La Grange Park, Illinois: American Nuclear Society. TIC: 208542.

Yang, I.C.; Rattray, G.W.; and Scofield, K.M. 1998. "Carbon and Hydrogen Isotopic Compositions for Pore Water Extracted from Cores at Yucca Mountain, Nevada." *High Level Radioactive Waste Management, Proceedings of the Eighth International Conference, Las Vegas, Nevada, May 11-14, 1998.* Pages 27-32. La Grange Park, Illinois: American Nuclear Society. TIC: 237082.

Yang, I.C.; Rattray, G.W.; and Yu, P. 1996. *Interpretation of Chemical and Isotopic Data from Boreholes in the Unsaturated Zone at Yucca Mountain, Nevada.* Water-Resources Investigations Report 96-4058. Denver, Colorado: U.S. Geological Survey. ACC: MOL.19980528.0216.

Yang, I.C.; Turner, A.K.; Sayre, T.M.; and Montazer, P. 1988. *Triaxial-Compression Extraction of Pore Water from Unsaturated Tuff, Yucca Mountain, Nevada.* Water-Resources Investigations Report 88-4189. Denver, Colorado: U.S. Geological Survey. ACC: NNA.19890309.0161.

Yang, I.C.; Yu, P.; Rattray, G.W.; Ferarese, J.S.; and Ryan, J.N. 1998. *Hydrochemical Investigations in Characterizing the Unsaturated Zone at Yucca Mountain, Nevada.* Water-Resources Investigations Report 98-4132. Denver, Colorado: U.S. Geological Survey. ACC: MOL.19981012.0790.

8.2 CODES, STANDARDS, REGULATIONS AND PROCEDURES

DOE (U.S. Department of Energy) 2000. *Quality Assurance Requirements and Description.* DOE/RW-0333P, Rev. 10. Washington, D.C.: U.S. Department of Energy, Office of Civilian Radioactive Waste Management. ACC: MOL.20000427.0422.

QAP-2-0, Rev. 5. *Conduct of Activities*. Las Vegas, Nevada: CRWMS M&O. ACC: MOL.19980826.0209.

8.3 SOFTWARE

Reserved

8.4 SOURCE DATA, LISTED BY DATA TRACKING NUMBER (DTN)

GS010608315215.002. Uranium and Thorium Isotope Data for Waters Analyzed Between January 18, 1994 and September 14, 1996. Submittal date: 06/26/2001.

GS010808312322.004. Uranium and Uranium Isotopic Data for Water Samples from Wells and Springs in the Yucca Mountain Vicinity Collected Between December 1996 and December 1997. Submittal date: 08/29/2001.

GS010808312322.005. Uranium and Uranium Isotope Data for Water Samples from UE-25 J-12/J-13 Storage Tank Collected Between October 1996 and November 1997. Submittal date: 08/29/2001.

GS90090123344G.001. Triaxial-Compression Extraction of Pore Water From Unsaturated Tuff, Yucca Mountain, Nevada. Submittal date: 09/17/1990. Submit to RPC

GS910508315215.005. Strontium Isotope Ratios and Isotope Dilution Data for Rubidium and Strontium Collected 5/3/89 to 5/9/91. Submittal date: 05/15/1991.

GS920208315215.008. Strontium Isotope Ratios and Isotope Dilution Data for Rubidium and Strontium Collected 5/10/91 to 2/28/92. Submittal date: 02/28/1992.

GS920208315215.012. Strontium Isotope Ratios and Isotope Dilution Data for Rubidium and Strontium Collected 4/8/88 to 5/2/89. Submittal date: 02/28/1992.

GS920408312272.002. Preliminary Isotopic Data for Tritium, Chemical Composition, Carbon-14, Carbon-13, Oxygen-18, and Deuterium in Pore Water in Cores Obtained from Two Test Holes in Pagany Wash, a Dry Channel on the East Side of Yucca Mountain. Submittal date: 04/29/1992.

GS920708315215.017. Carbonate Carbon and Oxygen Isotope Analyses of Samples from Trench 14, Busted Butte, and Drill Hole USW G-4. Submittal date: 07/15/1992.

GS920908315214.032. Isotope Content and Temperature of Precipitation in Southern Nevada, August 1983 – August 1986. Submittal date: 01/07/1993.

GS930108315213.004. Uranium Isotopic Analyses of Groundwaters from SW Nevada – SE California. Submittal date: 01/21/1993.

GS930108315214.004. Chemical Analysis of Surface-Water, Spring, and Precipitation Samples Collected from Kawich and Stewart Creek Basins from May, 1989, to September, 1991. Submittal date: 11/18/1992.

GS930308312323.001. Chemical Composition of Groundwater and the Locations of Permeable Zones in the Yucca Mountain Area. Submittal date: 03/05/1993.

GS930408312271.014. Analysis Of CO2 Concentration Of Syringe Samples Taken During USW UZ-1 Borehole Gas Sampling, May, 1989, Thru Jan., 1991. Submittal date: 03/30/1993.

GS930508312271.021. Analysis of Gaseous-Phase Stable and Radioactive Isotopes in the Unsaturated Zone, Yucca Mountain, Nevada. Submittal date: 04/30/1993.

GS930908315214.030. Chemical Analysis of Surface-Water, Spring, and Precipitation Samples Collected from Kawich and Stewart Creek Basins from February, 1992, to September, 1992. Submittal date: 09/30/1993.

GS930908315215.027. Strontium Isotope Ratios and Isotope Dilution Data for Rubidium and Strontium Collected 3/2/92 to 11/18/92. Submittal date: 09/29/1993.

GS931008315215.029. Strontium Isotope Ratios and Isotope Dilution Data for Rubidium and Strontium Collected 11/19/92 to 12/3/93. Submittal date: 12/08/1993.

GS931008315215.030. Carbon and Oxygen Isotope Analyses of Cavity- and Fracture-Coating Calcite and Soil Carbonate from Drill Holes and Outcrops, May '89 - Oct. '93. Submittal date: 10/26/1993.

GS931108315215.033. Fluid Inclusion Temperatures from Drill Holes USW G-1 and G-2, Oct. 92 - Sept. 93. Submittal date: 11/17/1993.

GS931108315215.035. Oxygen Stable Isotope Analyses of Opal From Drill Holes and Outcrops, June 92 – Aug. 92. Submittal date: 11/17/1993.

GS940208314211.002. Table of Contacts in Boreholes USW UZ-N62. Submittal date: 02/01/1994.

GS940208314211.004. Table of Contacts in Borehole USW UZ-N27. Submittal date: 02/10/1994.

GS940208314211.008. Table of Contacts in Boreholes USW UZ-N57, UZ-N58, UZ-N59, and UZ-N61. Submittal date: 02/10/1994.

GS940308312133.002. Water Quality Data for Samples Taken in Fortymile Wash, Nevada, During the 1993 Water Year. Submittal date: 03/02/1994.

GS940308314211.011. Table of Contacts for the Tiva Canyon Tuff in Borehole USW UZ-N38. Submittal date: 03/10/1994.

GS940308314211.016. Table of Contacts for the Tiva Canyon Tuff in Borehole USW UZ-N64. Submittal date: 03/28/1994.

GS940308314211.018. Table of Contacts for the Tiva Canyon Tuff in Borehole USW UZ-N36. Submittal date: 03/28/1994.

GS940308314211.019. Table of Contacts for the Tiva Canyon Tuff in Boreholes USW UZ-N15, USW UZ-N16, and USW UZ-N17. Submittal date: 03/28/1994.

GS940408312271.005. Laboratory Results of Carbon 14 Analysis of Gas Samples from Borehole USW UZ-1 collected 12/3/93 – 12/8/93. Submittal date: 03/25/1994

GS940608315215.006. Oxygen Stable Isotope Analyses of Opal From Drill Holes and Outcrop, June 1994. Submittal date: 06/27/1994.

GS941108315215.010. Strontium Isotope Ratios and Isotope Dilution Data for Rubidium and Strontium Collected 12/6/93 to 8/17/94. Submittal date: 11/30/1994.

GS941208312261.008. Carbon Dioxide, Methane, Carbon 14, and Carbon 13/12 Data from USW NRG-6 and USW NRG-7 for May and June 1994; and Carbon 14 Data from USW Wells NRG#5, UZ-6S, UZ-N27, UZ-N62, UZ-N64, UZ-N93, UZ-N94, and UZ-N95 from March 1994. Submittal date: 12/16/1994.

GS950408318523.001. Temperature, Thermal Conductivity, and Heat Flow Near Yucca Mountain, Nevada. Submittal date: 04/21/1995.

GS950608312272.001. Chemical Data for Pore Water from Tuff Cores of USW NRG-6, NRG7/7a, UZ-14 and UZ-N55, and UE-25 UZ#16. Submittal date: 05/30/1995.

GS950608315215.002. Strontium Isotope Ratios and Isotope Dilution Data for Rubidium and Strontium Collected 9/7/94 to 5/4/95. Submittal date: 05/12/1995.

GS950708315131.001. Woodrat Midden and Pollen Core Radiocarbon (C14). Submittal date: 07/21/1995.

GS950708315131.002. Woodrat Midden Contents Comprised of Raw Counts of Plant Macrofossils from Northern and Southern Nevada. Submittal date: 07/21/1995.

GS950708315131.003. Woodrat Midden Age Data in Radiocarbon Years Before Present. Submittal date: 07/21/1995.

GS950708315215.005. Delta 13C and Delta 18O Stable Isotope Data From the Yucca Mountain Region, July 1992 to September 1994. Submittal date: 07/17/1995. Submit to RPC

GS950708315215.006. Delta 13C and Delta 18O Stable Isotope Data From Non-Qualified Borehole Core of the Yucca Mountain Region, July 1988 to September 1994. Submittal date: 07/17/1995.

GS950808312261.004. Carbon 14 Results from Gas Samples Collected in February and March 1995. Submittal date: 08/29/1995.

GS960208312261.002. Carbon-14 Results from Gas Samples Collected; Carbon Dioxide, Carbon 13/12, Oxygen 18/16, and Carbon-14 Results from Gas Samples Collected; and Carbon Dioxide, Methane, Carbon 13/12 and Oxygen 18/16 Results from Gas Samples Collected. Submittal date: 02/16/1996.

GS960208315215.001. Uranium and Thorium Isotope Data Determined by Mass Spectrometry for Dating Sub-Surface Secondary Deposits from ESF and Drill Hole Locations. Submittal date: 02/21/1996.

GS960308312133.001. Water Quality Data from Samples Collected in the Fortymile Wash Watershed, Yucca Mountain Area, Nevada, Water Year 1995. Submittal date: 03/27/1996.

GS960308315131.001. Woodrat Midden Radiocarbon (C14) . Submittal date: 03/07/1996.

GS960408315215.002. Carbon and Oxygen Stable Isotope Analyses of Calcite From Drill Holes and the Exploratory Studies Facility (ESF), February 1995 to April 1996. Submittal date: 04/18/1996.

GS960408315215.003. Oxygen Stable Isotope Analyses of Opal from Drill Holes, The Exploratory Studies Facility (ESF), and Outcrop, April 1996. Submittal date: 04/18/1996.

GS960708314224.008. Provisional Results: Geotechnical Data for Station 30 + 00 to Station 35 + 00, Main Drift of the ESF. Submittal date: 08/05/1996.

GS960708314224.010. Provisional Results: Geotechnical Data for Station 40 + 00 to Station 45 + 00, Main Drift of the ESF. Submittal date: 08/05/1996.

GS960808315215.006. 14-Carbon Analyses of Calcite from Exploratory Studies Facility (ESF) Fracture Coatings, 12/95 - 2/96. Submittal date: 08/21/1996.

GS960908312211.003. Conceptual and Numerical Model of Infiltration at Yucca Mountain, Nevada. Submittal date: 09/12/1996.

GS960908314224.014. Provisional Results - ESF Main Drift, Station 50+00 to Station 55+00. Submittal date: 09/09/1996.

GS960908315215.010. Carbon and Oxygen Stable Isotope KIEL Analyses of Calcite from the ESF and USW-G2, October 1994 to June 1996. Submittal date: September 13, 1996.

GS960908315215.014. Uranium and Thorium Isotope Data for ESF Secondary Minerals Collected Between March 1996 and July 1996. Submittal date: 09/25/1996.

GS961108312261.006. Gas Chemistry, ESF Alcoves 2 and 3, 11/95 – 4/96; Water Chemistry, Alcove 2 (Tritium), Alcove 3, and ESF Tunnel; and Pneumatic Pressure Response from Boreholes in Exploratory Studies Facility Alcoves 2 and 3, 10/95 – 5/96. Submittal date: 11/12/1996.

GS961108312271.002. Chemical and Isotopic Composition of Pore Water and Pore Gas, 1994–96, from Boreholes USW UZ-1, USW UZ-14, UE-25 UZ#16, USW NRG-6, USW NRG-7A, USW SD-7, USW SD-9, ESF-AL#3-RBT#1, and ESF-AL#3-RBT#4, and ESF Rubble. Submittal date: 12/04/1996.

GS970108312232.001. Sulfur Hexafluoride Gas Chemistry Data and Shut-in Pressure Monitoring Data from the Radial Boreholes in Alcove 1 of the ESF, 4/95; and Tritium Data from Borehole ESF-AL#2-HPF#1 in Alcove 2. Submittal date: 01/09/1997.

GS970208314224.003. Geotechnical Data for Station 60+00 to Station 65+00, South Ramp of the ESF. Submittal date: 02/12/1997.

GS970208315215.001. Uranium and Thorium Isotope Data Collected Between September 1996 and February 1997 from Secondary Minerals in the ESF. Submittal date: 03/06/1997.

GS970208315215.002. Uranium-Lead Isotope Data for ESF Secondary Minerals from Sep. 96 to Feb. 97. Submittal date: 03/06/1997.

GS970208315215.003. 14-Carbon Analyses of Calcite from ESF Fracture Coatings, February 1997. Submittal date: 02/27/1997.

GS970208315215.004. Carbon and Oxygen Stable Isotope 252 Analyses of Calcite from the ESF and USW G-2 and SD-7, and UE-25 A#7, November 1996 – January 1997. Submittal date: 02/27/1997.

GS970208315215.005. Carbon and Oxygen Stable Isotope Kiel Analyses of Calcite from the ESF and USW G-1, G-2 and G-4, UE-25 A#1, USW NRG-6 and NRG-7/7A, and UE-25 UZ#16, April 1996 – January 1997. Submittal date: 02/27/1997.

GS970283122410.002. Gas and Water Chemistry Data from Samples Collected at Boreholes UE-25 NRG#5 and USW SD-7 on Yucca Mountain, Alcove 5, and Borehole ESF-NAD-GTB#1A in Alcove 6, ESF, between 8-11-96 and 1-14-97. Submittal date: 02/21/1997.

GS970508312272.001. Uranium Isotopic Data from ESF Alcove 5 Pore-Water Leaches and UZ Heater-Test Water Collected Between April and May, 1997. Submittal date: 05/30/1997.

GS970608312272.005. Tritium Data from ESF Alcove #5 Cores for Single Heater Test. Submittal date: 06/06/1997.

GS970708312323.001. Delta 18-O and Delta D Stable Isotope Analyses of a Bore-Hole Waters from GEXA Well 4 and VH-2. Submittal date: 07/22/1997.

GS970808314224.008. Provisional Results: Geotechnical Data for Station 65+00 to Station 70+00, South Ramp of the ESF. Submittal date: 08/18/1997.

GS970808314224.010. Provisional Results: Geotechnical Data for Station 70+00 to Station 75+00, South Ramp of the ESF. Submittal date: 08/25/1997.

GS970808314224.012. Provisional Results: Geotechnical Data for Station 75+00 to Station 78+77, South Ramp of the ESF. Submittal date: 08/25/1997.

GS970808315215.010. Carbon and Oxygen Stable Isotope Analyses of Calcite from the ESF and USW G-1, G-2, and G-3/GU-3, from 01/16/97 to 07/18/97. Submittal date: 08/18/1997.

GS970808315215.012. Uranium and Thorium Isotope Data from Secondary Minerals in the ESF Collected Between 02/15/97 and 09/15/97. Submittal date: 09/17/1997.

GS970908312271.003. Unsaturated Zone Hydrochemistry Data, 2-1-97 to 8-31-97, Including Chemical Composition and Carbon, Oxygen, and Hydrogen Isotopic Composition: Porewater from USW NRG-7A, SD-7, SD-9, SD-12 and UZ-14; and Gas from USW UZ-14. Submittal date: 09/08/1997.

GS970908315215.011. Strontium Isotope Ratios and Strontium Concentrations in USW SD-7 Rock and Soils, and ESF Calcite. Submittal date: 09/11/1997.

GS970908315215.013. Uranium-Lead Isotope Data for ESF Secondary Minerals from July 12, 1997 to August 24, 1997. Submittal date: 09/17/1997.

GS971108314224.020. Revision 1 of Detailed Line Survey Data, Station 0+60 to Station 4+00, North Ramp Starter Tunnel, Exploratory Studies Facility. Submittal date: 12/03/1997.

GS971108314224.021. Revision 1 of Detailed Line Survey Data, Station 4+00 to Station 8+00, North Ramp, Exploratory Studies Facility. Submittal date: 12/03/1997.

GS971108314224.022. Revision 1 of Detailed Line Survey Data, Station 8+00 to Station 10+00, North Ramp, Exploratory Studies Facility. Submittal date: 12/03/1997.

GS971108314224.023. Revision 1 of Detailed Line Survey Data, Station 10 + 00 to Station 18 + 00, North Ramp, Exploratory Studies Facility. Submittal date: 12/03/1997.

GS971108314224.024. Revision 1 of Detailed Line Survey Data, Station 18+00 to Station 26+00, North Ramp, Exploratory Studies Facility. Submittal date: 12/03/1997.

GS971108314224.025. Revision 1 of Detailed Line Survey Data, Station 26+00 to Station 30+00, North Ramp and Main Drift, Exploratory Studies Facility. Submittal date: 12/03/1997.

GS971108314224.026. Revision 1 of Detailed Line Survey Data, Station 45+00 to Station 50+00, Main Drift, Exploratory Studies Facility. Submittal date: 12/03/1997.

GS971108314224.028. Revision 1 of Detailed Line Survey Data, Station 55+00 to Station 60+00, Main Drift and South Ramp, Exploratory Studies Facility. Submittal date: 12/03/1997.

GS980108312322.004. Strontium Isotope Ratios and Strontium Concentrations in Water Samples from USW WT-24 and UE-25 J-13 Collected in October 1997. Submittal date: 01/26/1998.

GS980208312322.006. Uranium Isotopic Data for Saturated- and Unsaturated-Zone Waters Collected by Non-YMP Personnel Between May 1989 and August 1997. Submittal date: 02/03/1998.

GS980308315215.008. Line Survey Information From the Exploratory Studies Facility Obtained to Estimate Secondary Mineral Abundance. Submittal date: 03/24/1998.

GS980408312232.001. Deep Unsaturated Zone Surface-Based Borehole Instrumentation Program Data from Boreholes USW NRG-7A, UE-25 UZ #4, USW NRG-6, UE-25 UZ #5, USW UZ-7A and USW SD-12 for the Time Period 10/01/97 - 03/31/98. Submittal date: 04/16/1998.

GS980408315215.010. Corrected Data for Carbon and Oxygen Isotope Analyses of Cavity- and Fracture-Coating Calcite for One Sample from Drill Hole USW G-2. Submittal date: 04/10/1998. Submit to RPC

GS980708312242.011. Physical Properties and Hydraulic Conductivity Measurements of Lexan-Sealed Samples from USW WT-24. Submittal date: 07/30/1998.

GS980708315215.012. Uranium and Thorium Isotope Data from UE-25 A#1 Altered Tuff, and UE-25 J-13 and UE-25 ONC#1 Waters Analyzed from 3/23/94 through 10/25/95. Submittal date: 07/17/1998.

GS980908312322.009. Uranium Concentrations and 234U/238U Ratios from Spring, Well, Runoff, and Rain Waters Collected from the Nevada Test Site and Death Valley Vicinities and Analyzed Between 01/15/1998 and 08/15/1998. Submittal date: 09/23/1998.

GS980908315213.002. Carbon and Oxygen Stable Isotopic Compositions of Exploratory Studies Facility Secondary Calcite Occurrences, 10/01/97 to 08/15/98. Submittal date: 09/16/1998.

GS980908315215.015. Uranium and Thorium Isotope Data Including Calculated 230TH/U Ages and Initial 234U/238U Activity Ratios for in Situ Microdigestions of Outermost Opal-Rich Mineral Coatings from the Exploratory Studies Facility Analyzed Between 12/01/97 and 09/15/98. Submittal date: 09/23/1998.

GS980908315215.016. Uranium and Thorium Isotope Data Determined at the Royal Ontario Museum Between 07/12/97 and 01/29/98 and Calculated 230TH/U Ages and Initial 234U/238U Ratios for Secondary Silica from the Exploratory Studies Facility. Submittal date: 09/23/1998.

GS981008312272.004. Analysis for Chemical Composition of Porewater from Boreholes USW UZ-7A, USW WT-24, USW SD-6, USW SD-7, and USW SD-12 during FY 1997 and 1998. Submittal date: 10/28/1998.

GS981108314224.005. Locations of Lithostratigraphic Contacts in the ECRB Cross Drift. Submittal date: 11/30/1998.

GS981283122410.006. Gas Chemistry and Isotope Data from 3 ESF Boreholes. Submittal date: 12/28/1998.

GS990183122410.001. Tritium Data from Pore Water from ESF Borehole Cores, 1997 Analyses by USGS. Submittal date: 01/06/1999.

GS990183122410.004. Tritium Data from Pore Water from ESF Borehole Cores, 1998 Analyses by University of Miami. Submittal date: 10/14/1999.

GS990208312272.001. Analysis for Chemical Composition of Pore Water from Borehole USW UZ-14 and UE-25 UZ#16 and Groundwater from UE-25 UZ#16. Submittal date: 02/23/1999.

GS990308315215.003. X-ray Fluorescence Elemental Compositions of Rock Core Samples from USW SD-9 and USW SD-12. Submittal date: 03/25/1999.

GS990308315215.004. Strontium Isotope Ratios and Strontium Concentrations in Rock Core Samples and Leachates from USW SD-9 and USW SD-12. Submittal date: 03/25/1999.

GS990608312133.001. Ground-Water Quality Data. Submittal date: 06/09/1999.

GS990908315213.001. Stable Carbon and Oxygen Isotope Data for Calcite from the ESF and Analyzed 2/96 – 5/99. Submittal date: 10/28/1999.

GS990983122410.003. Carbon-14 Data from ESF/NAD/GTB#1A Gas. Submittal date: 09/30/1999.

GS991108312272.004. Analysis of Tritium Concentrations in Pore Water During FY98 and FY99. Submittal date: 11/24/1999.

GS000608312271.001. Pore-water Hydrochemistry and Isotopic Data for Boreholes USW NRG-6, USW NRG-7A, USW SD-7, USW SD-9, USW SD-12, USW UZ-14 and UE25 UZ # 16 from 10/1/96 to 1/31/97.

GS000608314224.004. Provisional Results: Geotechnical Data for Station 35+00 to Station 40+00, Main Drift of the ESF. Submittal date: 6/20/2000.

LA000000000062.002. Halide and Chlorine-36 Analyses of Cuttings from Borehole USW UZ-N27. Submittal date: 09/01/1993.

LA0001JF12213U.001. Reconstructed Annual Record of Tritium in Atmospheric Moisture for Albuquerque, New Mexico, 1946-1993. Submittal date: 01/07/2000.

LA0002JF831222.001. Apparent Infiltration Rates in Alluvium from USW UZ-N37, USW UZ-N54, USW UZ-14 and UE-25 UZ#16, Calculated by Chloride Mass Balance Method. Submittal date: 02/25/2000.

LA0002JF831222.002. Apparent Infiltration Rates in PTN Units from USW UZ-7A, USW UZ-N55, USW UZ-14, UE-25 UZ#16, USW NRG-6, USW NRG-7A, and USW SD-6, SD-7, SD-9 and SD-12 Calculated by the Chloride Mass Balance Method. Submittal date: 02/25/2000.

LA0003JF12213U.001. Precipitation-Weighted Average Monthly Concentrations (MG/L) of Precipitation in Red Rock Canyon, Nevada, 1985 to 1998. Submittal date: 03/13/2000.

LA9909JF831222.001. Chloride, Bromide, Sulfate and Chlorine-36 Analyses of Groundwater and Runoff in FY99. Submittal date: 09/29/1999.

LA9909JF831222.003. Chloride, Bromide, Sulfate and Chlorine-36 Analyses of Salts Leached from Cross Drift Rock Samples in FY99. Submittal date: 09/29/1999.

LA9909JF831222.004. Chloride, Bromide, and Sulfate Analyses of Busted Butte and Cross Drift Tunnel Porewaters in FY99. Submittal date: 09/29/1999.

LA9909JF831222.005. Chlorine-36 Analyses of ESF and Busted Butte Porewaters in FY99. Submittal date: 09/29/1999.

LA9909JF831222.010. Chloride, Bromide, Sulfate, and Chlorine-36 Analyses of ESF Porewaters. Submittal date: 09/29/1999.

LA9909JF831222.012. Chloride, Bromide, and Sulfate Analyses of Porewater Extracted from ESF Niche 3566 (Niche #1) and ESF 3650 (Niche #2) Drillcore. Submittal date: 09/29/1999.

LA9912JF831222.001. Halide and Chlorine-36 Analyses of Drillcore from USW UZ-N55. Submittal date: 12/16/1999.

LAJF831222AN97.008. Halide, Sulfate and 36CL Analyses of Cuttings from Borehole ONC#1. Submittal date: 09/26/1997.

LAJF831222AN97.012. Halide, Sulfate and 36CL Analyses of Surface Soils. Submittal date: 09/26/1997.

LAJF831222AN98.013. Chloride, Bromide, Sulfate, and Chlorine-36 Analyses of Groundwater from USW UZ-1, UE#25-p1, UE25 UZN#2, and USW VH-1. Submittal date: 09/09/1998.

LAJF831222AQ95.003. Halide Analyses of Rainwater from Yucca Mountain. Submittal date: 09/26/1995.

LAJF831222AQ95.005. Halide and Chlorine-36 Analyses of Soils from the UE25 NRG#5 Drillpad. Submittal date: 09/26/1995.

LAJF831222AQ95.006. Halide and Chlorine-36 Analyses of Soils Collected from Midway Valley Pits and Trenches. Submittal date: 09/26/1995.

LAJF831222AQ95.007. Halide and Chlorine-36 Analyses of Soils from Test Cell C, NTS Area 25. Submittal date: 09/26/1995.

LAJF831222AQ96.005. Halide and Chlorine-36 Analyses of Cuttings from Boreholes UE25 NRG -4, USW NRG -6, and USW NRG-7A. Submittal date: 09/30/1996.

LAJF831222AQ96.006. Halide and Chlorine-36 Analyses of Soil From Midway Valley Pit MWV-P2. Submittal date: 09/30/1996.

LAJF831222AQ96.008. Halide and Chlorine-36 Analyses of Cuttings from Boreholes USW UZ-N15, USW UZ-N16, USW UZ-N17, USW UZ-N36, USW UZ-N38, UE25 UZ-N39, USW UZ-N61, USW UZ-N62, and USW UZ-N64. Submittal date: 09/30/1996.

LAJF831222AQ96.009. Halide and Chlorine-36 Analyses of Cuttings from Borehole USW UZ-N11. Submittal date: 09/30/1996.

LAJF831222AQ96.010. Halide and Chlorine-36 Analyses of Cuttings from Borehole USW UZ-N37. Submittal date: 09/30/1996.

LAJF831222AQ96.011. Halide and Chlorine-36 Analyses of Cuttings from Borehole USW UZ-N53. Submittal date: 09/30/1996.

LAJF831222AQ96.012. Halide and Chlorine-36 Analyses of Cuttings from Borehole USW UZ-N54. Submittal date: 09/30/1996.

LAJF831222AQ96.013. Halide and Chlorine-36 Analyses of Cuttings from Borehole USW UZ-N55. Submittal date: 09/30/1996.

LAJF831222AQ96.014. Halide and Chlorine-36 Analyses of Cuttings from Borehole UE25 UZ#16. Submittal date: 09/30/1996.

LAJF831222AQ96.015. Halide and Chlorine-36 Analyses of Cuttings from Borehole USW UZ-14. Submittal date: 09/30/1996.

LAJF831222AQ97.002. Chlorine-36 Analyses of Packrat Urine. Submittal date: 09/26/1997.

LAJF831222AQ97.006. Halide, Sulfate and Chlorine-36 Analyses of Soils from Midway Valley Soil Pits MWV-P31 and NRSF-TP-19. Submittal date: 09/26/1997.

LAJF831222AQ97.007. Halide, Sulfate and 36CL Analyses of Cuttings from Borehole SD-12. Submittal date: 09/26/1997.

LAJF831222AQ97.009. Sulfate Analyses of Yucca Mountain Precipitation. Submittal date: 08/26/1997.

LAJF831222AQ98.003. Chloride, Bromide, Sulfate, and Chlorine-36 Analysis of Construction Water. Submittal date: 09/09/1998.

LAJF831222AQ98.004. Chloride, Bromide, Sulfate, and Chlorine-36 Analyses of Salts Leached from ESF Rock Samples. Submittal date: 09/10/1998.

LAJF831222AQ98.005. Chloride, Bromide, Sulfate, and Chlorine-36 Analyses of Soils Collected Above the ESF South Ramp. Submittal date: 09/09/1998.

LAJF831222AQ98.009. Chlorine-36 Analyses of Salts Leached from ESF Niche 3566 (Niche #1) Drillcore. Submittal date: 09/09/1998.

LAJF831222AQ98.011. Chloride, Bromide, Sulfate and Chlorine-36 Analyses of Springs, Groundwater, Porewater, Perched Water and Surface Runoff. Submittal date: 09/10/1998.

MO0012CARB1314.000. Water – Carbon 13 and Carbon 14 Abundance. Submittal date: 12/01/2000.

MO0012CARB1314.001. Water – Carbon 13 and Carbon 14 Isotope Abundance. Submittal date: 12/01/2000.

MO0012CARBON13.000. Water - Carbon 13 Isotope Ratio. Submittal date: 12/01/2000.

MO0012CARBON14.000. Carbon 14 Isotope Ratio. Submittal date: 12/01/2000.

MO0012MAJIONIS.000. Water – Major Ion and Isotope Data. Submittal date: 12/01/2000.

MO0012STRIONIS.000. Water – Concentrations of Strontium Ions and Isotopes. Submittal date: 12/04/2000.

MO0012URANISOT.000. Water – Selected Uranium Abundance and Isotope Ratios. Submittal date: 12/06/2000.

MO0012WTRCACO2.000. Water – Calcite and Carbon Dioxide Abundance. Submittal date: 12/01/2000.

MO0012WTRIONCO.000. Water – Ionic Concentrations Water. Submittal date: 12/05/2000.

MO0012WTRSAMPC.000. Water – Sample Coordinates. Submittal date: 12/04/2000.

SNF40060198001.001. Unsaturated Zone Lithostratigraphic Contacts in Borehole USW WT-24. Submittal date: 10/15/1998.

SNF40060298001.001. Unsaturated Zone Lithostratigraphic Contacts in Borehole USW SD-6. Submittal date: 10/15/1998.

MO0012CO2UNSZO.001. Carbon Dioxide Abundance in Unsaturated Zone Borehole USW UZ-1 collected from 12/10/1991 to 12/16/1991. Submittal date: 12/22/2000

MO0012CO2UNSZO.002. Carbon Dioxide Abundance in Unsaturated Zone Borehole USW UZ-1 collected from 12/04/1993 to 12/06/1993. Submittal date: 12/22/2000.

MO0012CO2UNSZO.003. Carbon Dioxode Abundance in Unsaturated Zone Borehole USW UZ-1 collected from 01/25/1993 to 01/28/1993. Submittal date: 12/22/2000.

MO0012TRITUNSZ.000. Tritium data for Unsaturated Zone Borehole.

MO007GNDWTRIS.013. Isotopic Content of Perched Groundwater from Yucca Mountain Project Boreholes, extracted from ANL-NBS-HS-000021, *Geochemical and Isotopic Constraints on Groundwater Flow Directions, Mixing and Recharge at Yucca Mountain, Nevada*. Submittal date: 07/28/2000

MO0012CO13UNSZ.003. Carbon 13 Data for Unsaturated Zone Borehole USW UZ-1. Submittal date: 12/22/2000.

MO0012C013UNSZ.000. Carbon 13 Data for Unsaturated Zone Borehole. Submittal date: 12/21/2000.

MO0012CO13UNSZ.001. Carbon 13 Data for Unsaturated Zone Borehole. Submittal date: 12/21/2000.

MO0012CO14UNSZ.002. Carbon 14 Data for Unsaturated Zone Borehole. Submittal date: 12/21/2000.

MO0012CO13UNSZ.002. Carbon 13 Data for Unsaturated Zone Borehole. Submittal date: 12/21/2000.

MO0005CL3SPRGS.000. Dissolved Chloride, 3 Springs Basin. Submittal date: 05/22/2000.

MO0005CLESTWRT.000. Dissolved Chloride, East Stewart Basin. Submittal date: 05/22/2000.

MO0005CLKAWICH.000. Dissolved Chloride, Kawich Peak. Submittal date: 05/22/2000.

MO0102UNSZHYCM.000. Preliminary Unsaturated Zone Borehole Hydrochemistry Data. Submittal date: 02/02/2001.

MO9906GPS98410.000. Yucca Mountain Project (YMP) Borehole Locations. Submittal date: 06/23/1999.

MO0012CO2UNSZO.004. Carbon Dioxide Abundance in Unsaturated Zone Borehole, USW UZ-1, collected from 02/06/1995 to 02/10/1995. Submittal date: 12/22/2000.

Table 1. Correlation of Lithostratigraphic Units with Hydrogeologic Units

Lithostratigraphic Nomenclature[1]	Lithostratigraphic Abbreviations	Hydrogeologic Units
Alluvial and colluvial deposits (Quaternary)	QTac	Unconsolidated Surficial Materials (UO)
TIMBER MOUNTAIN GROUP (Tm)		
Rainier Mesa Tuff (Tmr)	Tmr	
PAINTBRUSH GROUP (Tp)		
Tiva Canyon Tuff (Tpc)		
Crystal-rich member	Tpcr	
Vitric zone	Tpcrv	
nonwelded	Tpcrv3	
moderately welded	Tpcrv2	
densely welded	Tpcrv1	Tiva Canyon Welded Hydrogeologic Unit (TCw)
Nonlithophysal zone	Tpcm	
Lithophysal zone	Tpcrl	
Crystal-poor member	Tpcp	
Upper lithophysal zone	Tpcpul	
Middle nonlithophysal zone	Tpcpmn	
Lower lithophysal zone	Tpcpll	
Lower nonlithophysal zone	Tpcpln	
Vitric zone	Tpcpv	
Densely welded	Tpcpv3	
Moderately welded	Tpcpv2	
nonwelded	Tpcpv1	Paintbrush Nonwelded Hydrogeologic Unit (PTn)
Pre-Yucca Mountain Tuff bedded tuff	Tpbt3	
Pah Canyon Tuff	Tpp	
Pre-Pah Canyon Tuff bedded tuff	Tpbt2	
Topopah Spring Tuff	Tpt	
Crystal-rich member	Tptr	
Vitric zone	Tptrv	
nonwelded	Tptrv3	
moderately welded	Tptrv2	
densely welded	Tptrv1	Topopah Spring Welded Hydrogeologic Unit (TSw)
Nonlithophysal zone	Tptrn	
Lithophysal zone	Tptrl	
Crystal-poor member	Tptp	
Upper lithophysal zone	Tptpul	
Middle nonlithophysal zone	Tptpmn	
Lower lithohysal zone	Tptpll	
Lower nonlithophysal zone	Tptpln	
Vitric zone	Tptpv	
Densely welded	Tptpv3	
moderately welded	Tptpv2	Calico Hills Nonwelded Hydrogeologic Unit (CHn)
Nonwelded	Tptpv1	
Pre-Topopah Spring Tuff bedded tuff	Tpbt1	
CALICO HILLS FORMATION	Tac	
Bedded tuff	Tacbt	
Basal sandstone	Tacbs	
CRATER FLAT GROUP (Tc)		
Prow PassTuff	Tcp	
Pre-Prow Pass bedded tuff	Tcpbt	
Bullfrog Tuff	Tcb	
Tram Tuff	Tct	Crater Flat Hydrogeologic unit (CFu)

Notes: Official Group and Formation names are shown in bold type. Member designations, zonal subdivisions, and unit abbreviations follow the usage of Buesch et al. (1996, Table 4) and Day et al. (1996, map sheet 2). Correlation of lithostratigraphic and hydrogeologic units from Buesch et al. (1996, Table 4).

Table 2. Assumptions Used in This Report

	Assumption	Rationale for considering assumption to be valid	Assumption to be verified (TBV)	Section in which assumption is used
1.	Reported chemical data for pore waters and perched waters are of sufficient quality (e.g., precision and accuracy) that meaningful inferences can be made regarding their variability in space.	Standard quality-control measures used by the laboratories producing the chemical data include analyses of blanks, standards, replicates. When analyses of all major ions are available, charge balances are used to verify consistency. In addition, the data are used in this report to define general qualitative trends, such that outliers if present can be clearly distinguished from the population.	No	Sections 6.5, 6.9.2; Tables 6, 8, 26, 27
2.	Chemical data for pore waters and perched waters can be considered to be representative of *in situ* conditions. When data are reported for more than one aliquot in a given DTN, it is assumed that the published values represent the ones considered to be most representative of *in situ* conditions (e.g., that the author(s) averaged the available data in an appropriate manner).	A laboratory study comparing pore water extracted from nonwelded tuff by the compression system to that extracted by a high-speed centrifuge found no significant difference in the major-ion chemistry (Yang et al. 1990, p. 250). No verification studies have been conducted for pH or minor elements but chemical analyses of these parameters are not directly used for calculations in this report. Caution about aluminum data, which may contain particulate aluminum that passed through the 0.45 :m filters, is noted in Section 6.2.3; this caution may also apply to silica concentrations but is expected to be negligible. The assumption of representativeness is TBV for pore-water data reported in Table 6 because it is not clear, when data are reported for multiple aliquots of the same pore-water sample, whether the value to be used should be the result for the first aliquot, the aliquot with the largest volume, a straight average of all aliquots, a volume-weighted average, or (in the case of pH) a geometric volume-weighted average. It also is not clear when the reported pH and conductivity values are "field" analyses (i.e., measured in the pore water immediately following its extraction) and when they are laboratory analyses (i.e., submitted to an outside laboratory). "Field" analyses are more likely to be representative of *in situ* conditions for these parameters. The assumption is also TBV because chloride pore-water concentrations are directly used for testing the flow and transport model. None of these concerns apply to perched water chemical analyses, for which this assumption is considered not TBV.	Yes for pore-water data No for perched water data	Sections 6.2.3, 6.5, 6.9.2, 7; Tables 6, 8, 26, 27
3.	Chloride concentrations in surface and subsurface pore waters and perched waters reflect increases due solely to evapotranspiration. Cl concentrations are not significantly affected significantly by leakage from fluid inclusions or by geochemical reactions along the flow path.	Chloride is a conservative anion, and minerals containing it are rare in the Yucca Mountain environment. Br/Cl ratios are available to evaluate this assumption for many samples.	No	Sections 6.3.3, 6.5, 6.9.2; Tables 26, 27
4.	Reported tritium data for pore waters and perched waters are of sufficient quality (e.g., precision and accuracy) that meaningful inferences can be made regarding their variability in space. Tritium values above a statistically-	Precision and accuracy have been monitored through the analysis of duplicate samples and standards, and background levels of contamination have been monitored through the analysis of blanks and duplicate samples. The threshold value is evaluated through statistical	No	Sections 6.2.3, 6.6.2; Tables 9, 10, 11, 12

Table 2. Assumptions Used in This Report

	Assumption	Rationale for considering assumption to be valid	Assumption to be verified (TBV)	Section in which assumption is used
	determined threshold are assumed to indicate a component of water less than 50 years old at the sampling location. Cross-contamination of samples in the field, in storage facilities and in the laboratory can be ruled out as an explanation for elevated tritium levels. Similarly, sampling, storage and analytical protocols minimize loss of tritium due to evaporation or isotopic exchange.	analysis. The interpretation of the tritium data is not very sensitive to the precise threshold value that is calculated.		
5.	Reported chlorine-36 data for surface waters, soils, pore waters, perched waters and groundwaters are of sufficient quality (e.g., precision and accuracy) that meaningful inferences can be made regarding their variability in space.	Precision and accuracy have been monitored through the analysis of blind duplicate samples and blind standards.	No	Section 6.6.3; Tables 9, 13, 14
6.	Chlorine-36 data can be considered to be representative of *in situ* conditions, unless a statement to the contrary accompanies the data. Samples used for direct input for this report have not been significantly affected by sources of contamination in the field, storage areas or laboratory.	Lack of any significant contamination has been verified through analysis of frequent blanks and replicates, and through the analysis of Cl/Br ratios.	No	Section 6.6.3; Tables 9, 13, 14
7.	$^{36}Cl/Cl$ ratios elevated above a threshold of about 1250 x 10^{-15} are attributable to the presence of bomb pulse fallout.	This threshold value is evaluated through statistical analysis. The interpretation of these data is not very sensitive to the precise threshold value that is calculated.	No	Section 6.6.3; Tables 9, 13, 14
8.	Reported carbon isotopic data for pore waters, perched waters and gases are of sufficient quality (e.g., precision and accuracy) that meaningful inferences can be made regarding their variability in space.	It is assumed that precision and accuracy have been monitored through the analysis of blind duplicate samples and blind standards.	No	Section 6.6.4, 6.7; Tables 9, 15, 16, 17, 18, 19, 20, 21, 22
9.	Carbon isotopic data for pore waters, perched waters and gases can be considered to be representative of *in situ* conditions, unless a statement to the contrary accompanies the data. These data have not been affected significantly by laboratory or field sources of contamination, including drilling air.	This assumption is considered not TBV for perched water analyses. However, this assumption may not be valid for all pore-water and gas samples, some of which may have been contaminated with drilling air. Although the total mass of carbon in pore water is orders of magnitude higher than that in subsurface air, it is possible that the injection of large volumes of drilling air may alter the carbon isotopic composition of pore waters under some conditions. In particular, gas data from open boreholes cannot be assumed to be representative of *in situ* conditions. Gas data from instrumented boreholes, however, appear to be reliable, with exceptions as noted in the text and tables.	Yes for pore-water and unsaturated-zone gas data from open boreholes No for gas data from instrumented boreholes, perched water and	Sections 6.2.3, 6.6.4, 6.7, 7; Tables 9, 15, 16, 17, 18, 19, 20, 21, 22

Table 2. Assumptions Used in This Report

	Assumption	Rationale for considering assumption to be valid	Assumption to be verified (TBV)	Section in which assumption is used
			atmospheric data	
10.	Lower limits on pore-water and gas ages can be calculated based on the assumption that the initial ^{14}C activity is 100 pmc, and that decreases relative to the initial atmospheric activity are solely the result of radioactive decay.	The assumption for an initial ^{14}C activity of 100 pmc is supported by the high ^{14}C activities measured in the annulus of shallow boreholes (Tables 17 and 19).	No	Section 6.6.4; Tables 9, 15, 16, 18, 19, 20
11.	Reported stable hydrogen isotopic data are of sufficient quality (e.g., precision and accuracy) that meaningful inferences can be made regarding their variability in space	Precision and accuracy have been monitored through the analysis of duplicate samples and standards.	No	Section 6.6.5; Table 9
12.	Stable hydrogen isotopic data for perched waters, pore waters, and groundwater can be considered to be representative of *in situ* conditions.	Stable hydrogen and oxygen isotopes are well-established as conservative tracers of water provenance and evaporative history. However, experiments reported in Yang, Yu et al. (1998, pp. 28 to 48) show the extent to which different methods of pore-water extraction can fractionate isotopes of these two elements, such as by incomplete extraction in the presence of hydrated minerals such as clays and zeolites. They concluded that different extraction methods should be used for different samples depending upon their mineral contents (Yang, Yu et al., 1998, p. 44). Vacuum distillation is appropriate for samples with few hydrated minerals, provided extraction is complete. For zeolite-bearing or clay-bearing samples, the compression method should be used. The method used for a given sample can be determined from its unique sample identifier.	No	Section 6.2.3, 6.6.5; Table 9
13.	Reported stable oxygen isotopic data are of sufficient quality (e.g., precision and accuracy) that meaningful inferences can be made regarding their variability in space	Precision and accuracy have been monitored through the analysis of duplicate samples and standards.	No	Section 6.6.5; Table 9
14.	Stable oxygen isotopic data for perched waters, pore waters, groundwater and minerals can be considered to be representative of *in situ* conditions.	See rationale for assumption 12.	No	Section 6.2.3, 6.6.5; Table 9
15.	Reported strontium isotopic data are of sufficient quality (e.g., precision and accuracy) that meaningful inferences can be made regarding their variability in space	Precision and accuracy have been monitored through the analysis of duplicate samples and standards.	No	Section 6.6.6; Table 9
16.	Strontium isotopic data for perched waters, pore waters, groundwater and minerals can be considered to be representative of *in situ* conditions.	Extraction and analysis of strontium isotopes from water, rock and mineral samples are well-established protocols.	No	Section 6.6.6; Table 9
17.	Reported chemical data for unsaturated-zone gases are of sufficient quality (e.g., precision and accuracy) that meaningful inferences can be made regarding their	Precision and accuracy have been monitored through the analysis of duplicate samples and standards.	No	Section 6.7; Tables 18 and 20

Table 2. Assumptions Used in This Report

	Assumption	Rationale for considering assumption to be valid	Assumption to be verified (TBV)	Section in which assumption is used
	variability in space			
18.	Chemical data for unsaturated-zone gases can be considered to be representative of *in situ* conditions, unless a statement to the contrary accompanies the data.	Unsaturated-zone gas chemical data are generally the same as that for the atmosphere, with the expected exception of CO_2, which is considerably elevated in the subsurface. These elevated CO_2 analyses cannot be attributed to contamination from the atmosphere or from drilling air. Stable carbon isotope ratios and ^{14}C activities can be used to evaluate whether the gas chemical data are reasonable for *in situ* conditions. A more difficult problem to address, however, is the interval which the gas sample represents if it has been collected from a fractured rock with low matrix permeability. However, gas chemical data in this report have only been used to define general qualitative trends and so this assumption is not TBV for this limited purpose.	No	Section 6.7; Tables 18 and 20
19.	The chloride mass balance (CMB) method is assumed to be applicable to the estimation of infiltration rates at Yucca Mountain, for samples obtained above the CHn. The CMB method assumes one-dimensional, downward piston flow, constant average annual precipitation rate, constant average annual Cl deposition rate, no run-on or run-off, no Cl source other than precipitation (e.g., it is assumed that the concentrations of Cl brought in by surface runoff and Cl released from weathering of surface rocks are negligible), and no Cl sink (e.g., it is assumed that removal of Cl through the formation of halite is negligible).	The CMB method is well-established for estimating recharge rates on a watershed scale and for estimating infiltration rates in deep soil profiles in which one-dimensional porous media flow can be assumed to apply. What has not been clearly established, however, is the validity of applying this method to an intermediate scale in which runon and runoff may not be negligible, and in an environment where water is known to percolate through fractured rock. Of particular concern is the apparent discrepancy between infiltration estimates obtained by the CMB method and those obtained by the numerical infiltration model of Flint et al. (1996, Fig. 39). The assumption is TBV because chloride pore-water concentrations are directly used for testing the flow and transport model.	Yes	Section 6.9.2, 7; Tables 26, 27
20.	The estimated range of annual deposition rates for chloride at Yucca Mountain encompasses the present-day rate as well as the rates that prevailed when the sampled pore waters infiltrated below the soil zone.	This assumption is supported by several independent lines of evidence. However, what is still needed is an estimate of the uncertainties in the deposition rates, and propagation of that uncertainty through the resulting estimates of infiltration obtained by the CMB method. The assumption is TBV because the chloride deposition rate is directly used in the CMB method for determining infiltration boundary conditions for the flow and transport model.	Yes	Section 6.9.2, 7; Tables 26, 27
21.	Pore-water samples that have been analyzed for chloride are representative of the full spectrum of significant flow paths in the unsaturated zone at Yucca Mountain.	It is possible that relatively dilute water that has infiltrated rapidly through fracture pathways may be inadequately represented by matrix pore water extracted for analysis because of incomplete mixing. If this is the case, matrix pore-water samples might be biased toward the slower moving, more concentrated matrix component of flow; and percolation estimates based on these samples would constitute lower bounds on the actual percolation rates. In the PTn, some component of the flux can bypass the matrix as fracture or fault flow, as evidenced by the presence of bomb-pulse tracers in the ESF.	Yes	Section 6.9.2, 7; Tables 26, 27

Table 2. Assumptions Used in This Report

	Assumption	Rationale for considering assumption to be valid	Assumption to be verified (TBV)	Section in which assumption is used
22.	Reported calcite concentrations for cuttings from borehole WT-24 are based on the assumption that the secondary calcite is the only source for Ca released from the rock and measured CO_2 amounts.	No significant source of CO_2 other than calcite is present in the volcanic rock section.	No	Sections 6.10.1.1, 6.10.3.4, Figure 53
23.	Calculated estimates of mineral formation temperatures or isotopic compositions of formation water are based on the assumption that the mineral deposition was an equilibrium process.	Typically these assumptions are clearly stated in text when made. They are not necessarily valid, but provide a means of comparing temperature conditions between mineralization stages or between variations in the isotopic compositions of formation waters at different depositional episodes.	No	Sections 6.10.2, 6.10.3
24.	Reported uncorrected ^{14}C ages for fracture minerals are ased on the law of radioactive decay and on the assumption that carbon initially incorporated into the mineral during its deposition contained 100 percent modern carbon.	Although this assumption is not strictly true, it allows comparisons of ^{14}C data in a geochronological framework that can be compared to $^{230}Th/U$ and U/Pb ages; and this simplification is considered acceptable for the limited purpose of such comparisons. Calculated ^{14}C ages are likely to be maximum ages due to incorporation of dead carbon at the surface and decay of ^{14}C in the percolating water during travel time to site of calcite formation.	No	Section 6.10.1.3, Figure 54
25.	Reported ages calculated from $^{230}Th/U$ and $^{207}Pb/^{235}U$ ratios are based on the law of radioactive decay and on the assumption that studied minerals behaved as closed systems with regard to uranium and its decay products.	U-Th-Pb isotope ratios rarely show disruption of the systematic evolution that allows ages to be calculated. Calculated $^{230}Th/U$ ages are particularly sensitive to U leaching resulting in $^{230}Th/^{238}U$ ratios greater than those allowed through closed-system decay. Lack of disturbed ratios supports the closed-system behavior of the U decay systems in calcite and opal.	No	Section 6.10.1.3, 6.10.3, Table 28, Figures 54, 55, 56, 65, 67, 70 and 72
26.	The uranium isotope data contained in DTNs GS010808312322.005 and GS980708315215.012 are assumed to be representative of the uranium isotope values in the vicinity of the UE-25 J-13 and UE-25 J-12 wells but do not contain specific information about isotope data for UE-25 J-13. The uranium and thorium isotope data for borehole UE-25 ONC#1 from DTN: GS980708315215.012 are also assumed to representative of the waters in that borehole.	When this revision of the AMR was prepared, the subject data were considered qualified and representative of uranium isotope concentrations in borehole UE-25 J-13 and UE-25 ONC#1. These results were therefore used in the analysis. A subsequent evaluation determined that the samples attributed to UE-25 J-13 may actually represent a mix of UE-25 J-13 and UE-25 J-12 waters in unknown proportions. Therefore, these data should be considered as providing only a general indication of uranium isotope abundance in the vicinity of these two boreholes. The data should be considered as corroborating the trends in the region and should not be used for detailed analyses. The data for UE-25 ONC#1 and UE-25 J-13 from DTN: GS980708315215.012 were also considered to be unqualified because	No	Figures 42, 43

Table 2. Assumptions Used in This Report

Assumption		Rationale for considering assumption to be valid	Assumption to be verified (TBV)	Section in which assumption is used
		sample collection records could not be located. This assumption does not significantly impact the contouring shown on Figure 42 since the concentration and ratio shown for UE-25 J-13 are supported by another qualified DTN (GS930108315213.004). A comparison between the data sets gives the following results for concentration/activity ratios: DTN: GS930108315213.004 0.6/6.96 DTN: GS010808312322.005 0.5/7.23 (range 7.18 – 7.33) DTN: GS980708315215.012 0.6/6.38 (range 5.76 – 7.07). These results indicate that the data sets can be considered mutually corroborating and are additionally corroborated by four boreholes immediately to the west with similar values, as indicated on Figure 42. ONC#1 is not used on Figure 42 but is shown on Figure 43. The activity ratio (5.73) is lower than that for the nearby UE-25 c#3 borehole but supports the pattern of generally high values in this area.		

Table 3. Types of Isotopic and Geochemical Data Collected for Unsaturated-zone Fluids at Yucca Mountain

Shorthand Identifier	Official Borehole Identifier (depth in m shown for surface-based holes)		Analyses of pore waters or leached salts						Gas and water vapor analyses	Perched-water analyses
			Chem	^{3}H	$^{13,14}C$ (pore)	^{2}H – ^{18}O	^{36}Cl	Other		
NRG#4	UE-25 NRG#4	221	—	—	—	—	•	—	—	—
NRG#5	UE-25 NRG#5	411	—	—	—	—	•	—	—	—
NRG-6	USW NRG-6	335	•	•	•	•	•	—	CO_2, CH_4, $^{13,14}C$, ^{18}O	—
NRG-7a	USW NRG-7a	461	•	•	•	•	•	$^{234,238}U$	CO_2, CH_4, $^{13.14}C$	Chem, ^{3}H, $^{13,14}C$, ^{2}H, ^{18}O, ^{36}Cl, ^{87}Sr, $^{234,238}U$
ONC#1	UE-25 ONC#1	469	—	—	—	—	•	—	—	—
SD-12	USW SD-12	660	•	•	•	•	•	—	CO_2, CH_4, $^{13,14}C$, ^{18}O	
SD-6	USW SD-6	774	•	•	•	•	—	^{87}Sr	—	—
SD-7	USW SD-7	815	•	•	•	•	—	^{87}Sr	$^{13,14}C$, CO_2, ^{18}O	Chem, ^{3}H, $^{13,14}C$, ^{2}H, ^{18}O, ^{36}Cl, $^{234,238}U$
SD-9	USW SD-9	678	•	•	•	•	—	$^{234,238}U$	CO_2, CH_4, $^{13,14}C$, ^{18}O	Chem, ^{3}H, $^{13,14}C$, ^{2}H, ^{18}O, ^{36}Cl, ^{87}Sr, $^{234,238}U$
UZ#16	UE-25 UZ#16	514	•	•	•	•	•	—	$^{13,14}C$, CO_2, CH_4, ^{18}O	—
UZ#4	UE-25 UZ#4	112	•	•	•	•	—	—	—	—
UZ#5	UE-25 UZ#5	111	•	•	•	•	—	—	—	—
UZ-1	USW UZ-1	387	—	•	—	—	—	—	CO_2, atm gases, $^{13,14}C$, ^{2}H, ^{18}O, ^{3}H	^{3}H, $^{13,14}C$, ^{2}H, ^{18}O, ^{36}Cl
UZ-13	USW UZ-13	18	—	—	—	—	—	—	CO_2, CH_4, $^{13,14}C$, ^{18}O	—
UZ-14	USW UZ-14	678	•	•	•	•	•	$^{234,238}U$	$^{13,14}C$, CO_2	Chem, ^{3}H, $^{13,14}C$, ^{2}H, ^{18}O, ^{36}Cl, ^{87}Sr, $^{234,238}U$
UZ-6	USW UZ-6	575	—	—	—	—	—	—	CO_2, CH_4, $^{13,14}C$, ^{18}O	—
UZ-6s	USW UZ-6s	158	—	—	—	—	—	—	CO_2, $^{13,14}C$, ^{18}O, atm gases	—
UZ-7a	USW UZ-7a	235	•	•	—	—	—	—	CO_2, CH_4, ^{13}C, ^{18}O	—
UZN#1	UE-25 UZN#1	15	—	•	—	—	—	—	—	—
UZN#2	UE-25 UZN#2	15	—	—	—	—	—	—	—	Chem, ^{36}Cl

Table 3. Types of Isotopic and Geochemical Data Collected for Unsaturated-zone Fluids at Yucca Mountain

Shorthand Identifier	Official Borehole Identifier (depth in m shown for surface-based holes)		Analyses of pore waters or leached salts						Gas and water vapor analyses	Perched-water analyses
			Chem	^{3}H	$^{13,14}C$ (pore)	^{2}H – ^{18}O	^{36}Cl	Other		
UZN#39	UE-25 UZN#39	18	—	—	—	—	•	—	—	—
UZN#8	UE-25 UZN#8	14	—	•	—	—	—	—	—	—
UZN#91	UE-29 UZN#91	29	—	—	—	—	—	—	—	^{36}Cl
UZ-N11	USW UZ-N11	26	—	—	—	—	•	—	—	—
UZ-N15	USW UZ-N15	18	—	—	—	—	•	—	—	—
UZ-N16	USW UZ-N16	18	—	—	—	—	•	—	—	—
UZ-N17	USW UZ-N17	18	—	—	—	—	•	—	—	—
UZ-N27	USW UZ-N27	62	—	—	—	—	•	—	$^{13,14}C$, ^{18}O	—
UZ-N36	USW UZ-N36	18	—	—	—	—	•	—	—	—
UZ-N37	USW UZ-N37	83	—	—	—	—	•	—	—	—
UZ-N38	USW UZ-N38	27	—	—	—	—	•	—	—	—
UZ-N43	USW UZ-N43	14	—	—	—	—	•	—	—	—
UZ-N46	USW UZ-N46	30	—	—	—	—	—	—	—	Chem
UZ-N53	USW UZ-N53	72	—	—	—	—	•	—	—	—
UZ-N54	USW UZ-N54	75	—	—	—	—	•	—	—	—
UZ-N55	USW UZ-N55	78	•	—	—	—	•	—	—	—
UZ-N61	USW UZ-N61	36	—	—	—	—	•	—	—	—
UZ-N62	USW UZ-N62	18	—	—	—	—	•	—	$^{13,14}C$, ^{18}O	—
UZ-N64	USW UZ-N64	18	—	—	—	—	•	—	$^{13,14}C$, ^{18}O	—
UZ-N90	USW UZ-N90	14	—	•	—	—	—	—	—	—
UZ-N93	USW UZ-N93	12	—	—	—	—	—	—	CO_2, CH_4, $^{13,14}C$, ^{18}O	—
UZ-N94	USW UZ-N94	9	—	—	—	—	—	—	CO_2, CH_4, $^{13,14}C$, ^{18}O	—
UZ-N95	USW UZ-N95	6	—	—	—	—	—	—	CO_2, CH_4, $^{13,14}C$, ^{18}O	—
WT#18	UE-25 WT#18	623	—	—	—	—	—	—	CO_2, CH_4, ^{13}C, ^{18}O	—
WT#4	UE-25 WT#4	482	—	—	—	—	—	—	CO_2, CH_4	—
WT-24	USW WT-24	Not avail.	•	•	—	—	—	—	—	Chem, ^{3}H, $^{13,14}C$, ^{2}H, ^{18}O, ^{36}Cl, ^{87}Sr, $^{234,238}U$
Busted Butte	UZTT-BB-PH1-2		•	—	—	—	•	—	—	—
Busted Butte	UZTT-BB-PH1-3		•	—	—	—	•	—	—	—
Busted Butte	UZTT-BB-PH1-4		•	—	—	—	•	—	—	—
Busted Butte	UZTT-BB-PH1-6		•	—	—	—	•	—	—	—
Busted Butte	UZTT-BB-PH1-7		•	—	—	—	—	—	—	—

Table 3. Types of Isotopic and Geochemical Data Collected for Unsaturated-zone Fluids at Yucca Mountain

Shorthand Identifier	Official Borehole Identifier (depth in m shown for surface-based holes)	Analyses of pore waters or leached salts						Gas and water vapor analyses	Perched-water analyses
		Chem	^{3}H	$^{13,14}C$ (pore)	^{2}H – ^{18}O	^{36}Cl	Other		
Cross Drift	Cross Drift samples collected from walls (manually or with dry excavation method)	—	—	—	—	•	—	—	—
Cross Drift	ECRB-SYS-CSnnnn holes, where nnnn is distance in meters	Cl, Br, SO_4	—	—	—	—	—	—	—
ESF	ESF samples collected from walls of Main Drift or alcoves (manually or with dry excavation method)	—	•	—	—	•	^{87}Sr	—	—
ESF Alcove #1	ESF-AL#1-RBT#1, #2, #3	—	—	—	—	—	—	$^{13,14}C$, ^{18}O	—
ESF Alcove #1	Seeps from infiltration test	Cl, Br, SO_4	—	—	—	•	—	—	—
ESF Alcove #2	ESF-AL#2-HPF#1	—	•	—	—	—	—	—	—
ESF Alcove #2	ESF-LPCA-MOISTSTDY#n	Cl, Br, SO_4	—	—	—	—	—	—	—
ESF Alcove #3	ESF-AL#3-RBT#1, #4	•	•	•	—	—	—	—	—
ESF Alcove #5	Single Heater Test (SHT) Hole 16	•	—	—	—	•	$^{234,238}U$	—	—
ESF Alcove #5	ESF-AL#5	Sr	•	—	—	—	^{87}Sr	—	—
ESF Alcove #5	ESF-HD-PERM-1, -3	Cl, Br, SO_4	•	—	•	—	^{87}Sr, $^{234,238}U$	—	—
ESF Alcove #5	ESF-TMA-NEU-2	—	•	—	—	—	—	—	—
ESF Alcove #5	Drift Scale Heater Test Holes, DST-60 and DST-186	—	—	—	—	—	$^{234,238}U$	—	—
ESF Alcove #6	ESF-NAD-GTB#1A	—	•	—	—	—	—	$^{13,14}C$, ^{18}O, CO_2	—
ESF Main Drift	ECRB-CWAT#1, #2, #3	Cl, Br, SO_4	•	—	•	—	^{87}Sr	—	—
ESF Main Drift	ESF-MD-WATMOV#nn	Cl, Br, SO_4	—	—	—	—	—	—	—
ESF Niche #1	ESF-MD-NICHE3566#1, #2, LT#1	Cl, Br, SO_4	—	—	—	•	—	—	—

Table 3. Types of Isotopic and Geochemical Data Collected for Unsaturated-zone Fluids at Yucca Mountain

Shorthand Identifier	Official Borehole Identifier (depth in m shown for surface-based holes)	Analyses of pore waters or leached salts						Gas and water vapor analyses	Perched-water analyses
		Chem	^{3}H	$^{13, 14}C$ (pore)	^{2}H – ^{18}O	^{36}Cl	Other		
ESF Niche #1	ESF-MD-NICHE3650#nn	Cl, Br, SO_4	—	—	—	—	—	—	—
ESF North Ramp	ESF-NR-MOISTSTDY#nn	Cl, Br, SO_4	—	•	—	•	—	—	—
ESF South Ramp	ESF-SR-MOISTSTDY#nn	Cl, Br, SO_4	—	—	—	•	—	—	—

Notes:

a. Data identified by this table include data that are directly used (listed in Section 4.1) as well as data used solely for corroborative purposes in this report. Not all data indicated in this table are discussed in this report; e.g., many data are not directly relevant to the discussions in this report.

b. Borehole depths are reported in feet in DTN: MO9906GPS98410.000 and have been converted to meters in the table above.

c. Abbreviations for types of analyses: Chem, pore-water chemistry; H, tritium, $^{13, 14}C$ (pore), carbon-13 and carbon-14 analyses for pore waters; ^{2}H—^{18}O, stable hydrogen and oxygen isotopes; ^{36}Cl, chlorine-36

Table 4. Sources of Stratigraphic Information Used to Classify Pore-water and Gas Samples in This Report

Borehole	Sources for stratigraphic information	Table or figure in which information is used
NRG#4	Moyer et al. (1996, Appendix 3)	Table 13
NRG#5	Geslin et al. (1994, Appendix 3) Rousseau et al. (1999, Figure 26)	Tables 13 and 18
NRG-6	Moyer et al. (1996, Appendix 3) for PTn Geslin et al. (1994, Appendix 3)	Tables 6, 10, 11, 15, 18 and 22
NRG-7a	Geslin et al. (1994, Appendix 2), for upper part Moyer et al. (1996, Appendix 3) for PTn Rousseau et al. (1999, Figure 25) for TSw	Tables 6, 10, 11, 13, 15 and 18
SD-12	Rautman and Engstrom (1996a, Table 3)	Tables 6, 10, 11, 13, 15, 18, 20 and 22
SD-6	DTN: SNF40060298001.001	Tables 6, 10 and 11
SD-7	Rautman and Engstrom (1996b, Table 3)	Tables 6, 10, 13, 15, 18 and 22
SD-9	Engstrom and Rautman (1996, Table 3)	Tables 6, 10, 13, 15, 18 and 22
UZ#16	Moyer et al. (1996, Appendix 3) for PTn Geslin et al. (1994, Appendix 3) Moyer and Geslin (1995, Tables 4 and 6) for CHn	Tables 6, 10, 11, 13, 15 and 18
UZ#4	Yang (1992, Figure 2)	Tables 12 and 16
UZ#5	Yang (1992, Figure 3)	Tables 12 and 16
UZ-1	Rousseau et al. (1999, Figure 92)	Tables 10, 20 and 22
UZ-14	Geslin et al. (1994, Appendix 2), for upper part of UZ-14 Moyer et al. (1996, Appendix 3) for PTn Moyer and Geslin (1995, Tables 4 and 6) for CHn	Tables 6, 10, 11, 13, 15, 18 and 22
UZ-6	Thorstenson et al. (1998, p. 1510)	Table 19
UZ-6s	Thorstenson et al. (1998, pp. 1509 to 1510)	Table 19
UZ-7a	Moyer et al. (1996, Appendix 3) for PTn	Tables 6 and 10
UZ-N11	Moyer et al. (1996, Appendix 3)	Table 13
UZ-N15	DTN: GS940308314211.019	Table 13
UZ-N16	DTN: GS940308314211.019	Table 13
UZ-N17	DTN: GS940308314211.019	Table 13
UZ-N27	DTN: GS940208314211.004	Table 13
UZ-N36	DTN: GS940308314211.018	Table 13
UZ-N37	Geslin et al. (1994, Appendix 2)	Table 13
UZ-N38	DTN: GS940308314211.011	Table 13
UZN#39	Flint and Flint (1995, p. 34)	Table 13
UZ-N53	Geslin et al. (1994, Appendix 2)	Table 13
UZ-N54	Geslin et al. (1994, Appendix 2)	Table 13
UZ-N55	Geslin et al. (1994, Appendix 2)	Tables 6 and 13
UZ-N61	DTN: GS940208314211.008	Table 13
UZ-N62	DTN: GS940208314211.002	Table 13
UZ-N64	DTN: GS940308314211.016	Table 13
WT-24	DTN: SNF40060198001.001	Tables 6, 10 and 11

Note: These sources for stratigraphic information are used as corroborative data. Stratigraphic misclassification of a sample would not be expected to change the interpretation of the data.

Table 5. Average Annual Weighted Concentrations for Precipitation, 3 Springs Basin, Nevada

Nominal Year	Start	End	Total precip. (cm)	Annual Weighted concentration (mg/L)								
				Alkalinity as $CaCO_3$	Equiv. HCO_3	Ca	Mg	Na	K	SO_4	Cl	SiO_2
3 Springs Creek												
1986	850924	860930	13.93	2.67	3.26	0.61	0.06	0.40	0.15	0.73	0.34	0.13
1987	860930	880109	15.58	2.04	2.49	0.46	0.04	0.34	0.13	0.63	0.31	0.08
1988	880109	890223	14.24	2.93	3.57	0.98	0.09	0.78	0.28	1.12	0.47	0.13
1989	890223	891108	5.85	4.30	5.25	1.06	0.18	1.03	0.15	1.41	0.59	0.19
1990	891108	910130	12.62	1.40	1.70	0.81	0.08	0.79	0.20	1.12	0.56	N/C
1991	910130	910925	11.65	N/C	N/C	0.73	0.08	0.46	0.17	1.13	0.25	N/C
1992	910925	920917	13.94	N/C	N/C	0.49	0.05	0.23	0.15	0.81	0.17	N/C
Kawich Peak												
1989	881001	891108	13.44	3.23	3.94	0.97	0.16	0.97	0.16	1.27	0.64	0.20
1990	891108	910130	15.07	1.83	2.23	0.73	0.07	0.62	0.64	0.96	0.39	N/C
1991	910130	920218	17.77	N/C	N/C	0.68	0.07	0.95	0.15	0.95	0.31	N/C
1992	920218	920917	6.8	N/C	N/C	0.66	0.07	0.32	0.21	1.25	0.31	N/C
Results of linear regression for Cl as the independent variable												
Y-intercept (assigned value of zero to force line through origin)				0	0	0	0	0	0	0	N/A	0
Standard error of y-intercept				0.91	1.11	0.15	0.03	0.18	0.16	0.30	N/A	0.02
R squared				0.13	0.13	0.38	0.65	0.63	-0.22	-0.49	N/A	0.88
No. Of observations				7	7	11	11	11	11	11	N/A	5
X coefficient				5.433	6.628	1.787	0.220	1.578	0.489	2.431	N/A	0.313
Standard error of X coefficient				0.707	0.863	0.111	0.019	0.127	0.116	0.213	N/A	0.016

Source data: The above values were calculated from data reported in DTN: MO0005CL3SPRGS.000, MO0005CLKAWICH.000, GS930108315214.004 and GS930908315214.030. The calculated regression lines are used solely to provide a way to graphically compare and contrast chemical compositions of the various sources of water at Yucca Mountain, and to illustrate general trends of relative enrichment or depletion of one element compared to another. Precipitation data reported in the original source DTNs in inches have been converted to centimeters in the table above.

Notes: "N/C" signifies not calculated; "N/A" signifies not applicable.

Table 6. Chemical Composition of Unsaturated-zone Pore-water Samples from Surface-based Boreholes at Yucca Mountain

Bore hole	Depth Interval (ft)	Hydro-Geologic unit[2]	Litho-stratigra-phic unit[2]	Ave. depth (m)	pH	Spec. cond. (:S/cm)	Concentration (mg/L)										Charge balance[1]
							Ca	Mg	Na	SiO_2	K	HCO_3	CO_3	Cl	NO_3	SO_4	
NRG-6	158.2–158.58	PTn	Tpbt4	48	6.4	1070	122	23.3	35.6	97.4	—	34	0	185	32	159	-0.2
NRG-6	160.8–161.2	PTn	Tpbt4	49	7.0	860	104	18	35.0	84.0	—	55	0	148	35	139	-2.0
NRG-6	171.0–171.3	PTn	Tpbt3	52	7.0	620	70.5	11.5	29.2	79.4	—	48	13	58	43	94	2.1
NRG-6	175.6–175.95	PTn	Tpp	54	6.6	520	49.2	8.6	29.4	78.1	—	60	0	47	42	64	1.4
NRG-6	219.9–220.2	PTn	Tpp	67	7.0	660	24.3	4.2	99.3	61.4	—	92	0	77	47	77	-1.4
NRG-6	244.6–245.0	PTn	Tpbt2	75	6.6	630	33	4.9	72.0	51.0	—	61	0	49	40	115	-2.2
NRG-6	255.9–256.1	PTn	Tptrv3	78	6.7	1910	176	19	215.0	68.0	—	61	0	115	35	840	-6.2
NRG-7A	165.75–166.0	PTn	Tpbt3	51	7.4	510	55.3	5.6	31.7	68.3	—	89	0	38.9	45.5	63.4	-0.1
NRG-7A	258.0–258.4	PTn	Tpp	79	8.2	600	43	3.7	82	68.9	—	128	0	53.6	43.7	65.5	2.9
NRG-7A	1483.5-1483.8	CHn	Tptpv1	452	7.9	580	61	0.6	94	48.6	—	323	0	33.1	16.7	24.4	1.3
NRG-7A	1492.7-1493.1	CHn	Tptpv1	455	7.9	580	30.6	0.3	74.7	71.5	—	104	34	39	18	23	1.0
NRG-7A	1498.6-1498.9	CHn	Tac	457	7.5	500	28.7	0.5	73.2	83.0	—	156	0	50	17	18	0.5
SD-6	430.3-430.6	PTn	Tpcpv1	131	7.4	430	46	9.4	56.8	81.7	2.8	109	0	43	69	43	5.7
SD-6	443.2-443.5	PTn	Tpbt4	135	7.3	580	55.2	11.2	53.2	94.8	1.4	134	0	27	64	73	4.5
SD-6	443.5-443.8	PTn	Tpbt4	135	7.2	630	62.4	12	51.6	92.8	1.8	95	0	33	57	101	7.4
SD-7	339.7–340.2	PTn	Tpbt3	104	7.4	690	110	15	20	82.8	—	220	0	77.2	1.5	76.7	1.3
SD-7	370.3–370.6	PTn	No core	113	6.7	1420	289	0.2	39	25.9	—	73	0	133	0.6	650	-6.7
SD-7	1498.4–1498.6	CHn	Tac2	457	7.2	440	31	0.6	67	63.5	—	171	0	28.9	13.6	14.1	4.4
SD-7	1524.6–1525.7	CHn	Tac1	465	7.2	490	38.7	0.9	57.6	68.6	7	203	0	30.1	12.4	15.9	-0.2
SD-7	1558.4–1558.6	CHn	Tac1	475	7.2	390	39	0.9	43	69.3	—	171	0	25.1	9.0	14.9	-0.9
SD-7	1600.1-1600.33	CHn	Tacbt	488	7.6	380	23	0.6	59	66.7	—	150	0	31	5.7	12	1.2
SD-7	1617.0–1617.2	CHn	Tacbs	493	7.2	570	40.2	< 1	79	62.2	—	194	< 1	65	11.0	14	-0.3
SD-7	1890.7-1891.1	CHn	Tcp1	576	8.7	850	0	0.2	206	67	—	334	78	18	4.8	10	0.6
SD-7	1952.4-1952.7	CHn	Tcp1	595	8.8	980	0	0.3	251	67.4	—	353	120	22	6.7	11	0.9
SD-7	2088.2-2088.5	CHn	Tcp1	636	9.2	710	0	0	173	54.4	—	157	101	15	4.0	25	4.0
SD-7	2170.1-2170.5	CHn	Tcpbt	661	9.2	670	0	0	164	55.4	—	100	103	18	3.8	18	8.5
SD-7	2596.1–2596.3	CHn	Tcbts	791	9.0	670	< 1	< 1	158	64.3	—	79	65	83	3.2	12	5.9
SD-7	2596.5-2596.9	CHn	Tcbts	791	9.0	680	0	0	148	53.3	—	95	71	46	2.2	12	7.8
SD-7	2598.3–2598.5	CHn	Tct	792	8.7	630	< 1	< 1	152	94.8	—	231	59	22	4.0	18	-1.5
SD-9	94.2–94.4	PTn	Tpbt4	29	5.5	1050	125	24	43	74	—	37	0	170	11	260	-4.3
SD-9	114.1-114.3	PTn	Tpy	35	6.8	920	95	18	55	62.3	—	31	0	138	10.9	181	1.6
SD-9	135.1-135.3	PTn	NR	41	8.5	890	91	15	66	60.1	—	37	0	144	12	162	2.5

Table 6. Chemical Composition of Unsaturated-zone Pore-water Samples from Surface-based Boreholes at Yucca Mountain

Bore hole	Depth Interval (ft)	Hydro-Geologic unit[2]	Litho-stratigra-phic unit[2]	Ave. depth (m)	pH	Spec. cond. (:S/cm)	Concentration (mg/L)										Charge balance[1]
							Ca	Mg	Na	SiO_2	K	HCO_3	CO_3	Cl	NO_3	SO_4	
SD-9	154.0–154.2	PTn	Tpbt3	47	6.8	650	72	13	36	55	—	90	0	93	4.7	106	-1.2
SD-9	176.2-176.4	PTn	Tpp	54	7.5	720	43	9.5	95	58.4	—	122	0	64	1.9	124	4.8
SD-9	251.8-252.0	PTn	Tpbt2	77	7.2	500	44	8	53	55.0	—	92	0	40	14.2	73	8.1
SD-9	1452.6–1452.8	CHn	Tptpv1	443	7.3	530	6.9	0	112	62.5	—	256	0	15.7	10.6	12.3	1.4
SD-9	1535.2–1535.35	CHn	Tac3	468	7.4	530	0.8	0.1	112	54.9	7	226	0	15.6	10.6	15.5	4.7
SD-9	1619.9–1661.4	CHn	Tac2	500	8.3	610	0.4	0	136.6	55.6	4	232	12	50.2	9.0	18.3	-0.7
SD-9	1661.1–1661.3	CHn	Tac2	506	8.1	660	0.7	0	164	48.8	—	317	0	42.0	8.2	18.9	1.8
SD-9	1741.0–1741.2	CHn	Tac1	531	8.7	520	0.2	0	125	52	—	185	41	19	4.4	10	2.2
SD-9	1741.7–1741.9	CHn	Tac1	531	8.4	310	0.2	0	74	53	—	113	12	15	3.8	8.7	5.0
SD-9	1800.7-1800.9	CHn	Tacbt1	549	9.3	790	0.8	0	180.7	59.6	6	137	106	32.3	4.6	20.9	5.6
SD-12	265.8–266.1	PTn	Tpbt4	81	7.2	470	48.9	7.6	28.6	62.7	3	107	0	49.6	15.9	47.5	-0.1
SD-12	278.6–278.8	PTn	Tpp	85	7.3	580	74	12.7	27	71.2	—	159	0	46	16.0	75	1.7
SD-12	296.1–296.6	PTn	Tpbt2	90	6.9	490	75	8.0	21	72.2	—	163	< 1	60	18.0	21	2.2
SD-12	1460.7–1461.0	CHn	Tac4	445	8.5	490	31	0	89	65.5	—	98	30	55.9	7.3	30.1	4.8
SD-12	1495.5–1495.8	CHn	Tac3	456	8.5	550	16	0.2	108	87.3	—	49	57	57	8.1	55	-0.7
SD-12	1517.0–1517.4	CHn	Tac3	462	7.6	660	14	0	150	56.9	—	323	0	33.6	6.4	22.5	2.9
SD-12	1558.9-1559.5	CHn	Tac2	475	8.5	640	4.4	0.1	155	76.1	—	210	41	33	0.4	54	0.7
SD-12	1582.5-1582.7	CHn	Tac2	482	8.5	420	1.2	0.1	97	71.0	—	113	29	17	4.5	27	4.3
SD-12	1600.6–1603.0	CHn	Tac1	488	9.1	550	2.6	0	129	65.7	—	79	90	27.8	2.6	12.6	3.2
SD-12	1636.8-1637.0	CHn	Tacbt	499	9.1	520	3.8	0	129	64.6	—	67	102	15.2	1.7	11.2	5.6
SD-12	1901.4-1901.5	CHn	Tcp2	580	9.1	470	1.3	< 1	122	90.7	—	151	59	22	5.7	9.3	0.2
SD-12	1938.5-1939.0	CHn	Tcp2	591	8.7	650	1.4	0	165	55.0	—	171	66	34	1.0	26.1	5.2
SD-12	1942.2-1942.9	CHn	Tcp2	592	8.9	550	1.3	0	140	60.1	—	134	66	24	3.5	24.4	4.3
UZ-7A	203.3-203.7	PTn	Tpbt4	62	7.3	830	115	20.6	16.6	69.7	5.6	120	0	70	105	140	-1.4
UZ-7A	220.2-220.5	PTn	Tpbt2	67	7.3	820	117	23.1	18.3	67.6	5.5	100	0	87	112	140	-0.7
UZ-7A	241.4-241.7	PTn	Tpbt2	74	6.9	930	116	21.9	39	52.2	10	70	0	60	83	240	2.0
UZ-14	45.0–45.35	PTn	Tpy	14	8.6	1340	19.6	6.1	249.3	59.5	6.1	245	18	245	35	33	-1.2
UZ-14	85.2–85.6	PTn	Tpbt3	26	6.9	630	49.9	13.2	43.5	89.8	—	131	0	60	22	66	-0.9
UZ-14	91.0–91.25	PTn	Tpbt3	28	7.6	530	40.7	10.1	37.1	80.6	—	87	0	47	26	81	-4.1
UZ-14	95.5–95.9	PTn	Tpbt3	29	7.2	600	53.3	13.2	38.1	81.5	—	73	0	79	29	83	-1.9
UZ-14	96.2–96.6	PTn	Tpbt3	29	6.9	550	46.9	12.7	33.6	79.6	—	79	0	59	26	75	-0.9
UZ-14	100.4–100.8	PTn	Tpbt3	31	7.0	600	51.1	13.8	41.3	91.8	—	128	0	44	23	83	0.4

Table 6. Chemical Composition of Unsaturated-zone Pore-water Samples from Surface-based Boreholes at Yucca Mountain

Bore hole	Depth Interval (ft)	Hydro-Geologic unit[2]	Litho-stratigra-phic unit[2]	Ave. depth (m)	pH	Spec. cond. (:S/cm)	Concentration (mg/L)										Charge balance[1]
							Ca	Mg	Na	SiO_2	K	HCO_3	CO_3	Cl	NO_3	SO_4	
UZ-14	114.75–115.0	PTn	Tpp	35	6.6	540	49.0	10.5	35.9	93.9	—	67	0	61	25	90	-2.2
UZ-14	135.5–135.8	PTn	Tpp	41	6.9	690	68.5	14.3	56.2	92.0	—	105	0	83	23	96	4.5
UZ-14	144.8–145.2	PTn	Tpp	44	7.7	650	65.5	12.0	48.2	81.5	—	118	0	77	22	102	-1.8
UZ-14	147.79–148.1	PTn	Tpp	45	6.9	640	54.8	11.5	51.6	77.3	—	79	0	83	22	102	-1.5
UZ-14	177.6–177.9	PTn	Tpp	54	6.5	730	67.8	11.3	48.7	77.5	—	49	0	100	23	130	-2.0
UZ-14	178.1–178.4	PTn	Tpp	54	6.8	740	64.0	10.6	49.1	93.1	—	62	0	97	21	120	-3.0
UZ-14	215.72–216.1	PTn	Tpp	66	6.8	670	65.5	10.7	39.4	97.8	—	55	0	85	14	130	-3.0
UZ-14	225.9–226.2	PTn	Tpp	69	7.9	640	58.6	10.4	48.4	91.2	—	55	0	93	16	116	-2.5
UZ-14	235.1–235.4	PTn	Tpp	72	7.1	630	67	10.5	29	63	—	96	N/S	84	15	94	-5.7
UZ-14	240.8–241.12	PTn	Tpbt2	73	7.6	810	32	1	103	61	—	162	N/S	99	17	100	-11.8
UZ-14	245.5–245.8	PTn	Tpbt2	75	6.8	580	65	12	9	46	—	66	N/S	77	12	79	-4.8
UZ-14	1258.5–1258.8	TSw	Tptpln	384	—	—	43	3.7	67	35	—	170	N/S	88	16	19	-4.9
UZ-14	1277.4–1277.7	TSw	Tptpln	389	—	—	62	4.5	49	44	—	170	N/S	87	17	45	-7.1
UZ-14	1277.7–1278.0	TSw	Tptpln	389	—	—	74	5.1	45	38	—	170	N/S	130	15	38	-10.4
UZ-14	1409.4–1409.8	CHn	Tpbt1	430	7.8	720	30	0.7	88	57	—	160	0	75	5	106	-13.2
UZ-14	1419.5–1419.8	CHn	Tpbt1	433	8.3	410	20	0.6	68	60	—	166	0	24	6	21	0.9
UZ-14	1461.9–1462.1	CHn	Tac3	446	7.6	570	9.2	0.1	128	68.7	—	265	0	24.2	6.2	37.3	1.1
UZ-14	1495.8–1496.0	CHn	Tac2	456	8.4	500	2.1	0	122	56.7	—	228	0	28.0	10.8	14.3	3.9
UZ-14	1524.55–1524.75	CHn	Tac2	465	7.7	560	1.1	0.1	137	54.8	—	232	0	26.2	12.5	22.3	7.2
UZ-14	1542.3–1542.8	CHn	Tac2	470	—	—	3.6	0.5	207	143	—	384	46	20	4	28	1.0
UZ-14	1563.6–1563.8	CHn	Tac2	477	8.7	660	1.2	0.2	155	72.0	—	160	97	16	4	14	1.1
UZ-14	1564.6–1564.75	CHn	Tac2	477	—	—	1.3	0.2	129	140.4	—	61	113	16	4	17	0.5
UZ-14	1564.9–1565.0	CHn	Tac2	477	8.3	690	1.7	0.5	169	54.0	—	376	0	23	1	30	0.1
UZ-14	1585.0–1585.15	CHn	Tac2	483	9.7	560	0.9	0.3	106.8	74.5	—	98	67	14	7	10	1.7
UZ-14	1585.3–1585.6	CHn	Tac2	483	9.3	400	1.2	0.5	85	75.0	—	148	18	11	6	9	2.4
UZ-14	1605.9–1606.1	CHn	Tac2	490	—	—	1.0	0.3	87.8	67.2	—	178	0	18	6	9	2.4
UZ-14	1644.3–1644.5	CHn	Tac2	501	8.8	420	2.2	0.7	110	74.0	—	74	79	14	0	9	5.6
UZ-14	1674.8–1675.05	CHn	Tac1	511	—	—	1.8	0.6	58	64.6	—	104	0	10	4	9	8.6
UZ-14	1695.4–1695.6	CHn	Tabt1	517	—	—	1.4	1.1	115.8	55.9	—	203	18	21	5	26	0.5
UZ-14	1715.0–1715.3	CHn	Tabt1	523	7.3	390	0.2	0	88	52.9	—	168	0	11.9	3.1	16.0	5.0
UZ-14	1734.5–1734.7	CHn	Tabt1	529	8.7	750	2.0	0.3	184	50.7	—	211	79	39.4	5.6	17.5	3.0

Table 6. Chemical Composition of Unsaturated-zone Pore-water Samples from Surface-based Boreholes at Yucca Mountain

Bore hole	Depth Interval (ft)	Hydro-Geologic unit[2]	Litho-stratigra-phic unit[2]	Ave. depth (m)	pH	Spec. cond. (:S/cm)	Concentration (mg/L)										Charge balance[1]
							Ca	Mg	Na	SiO_2	K	HCO_3	CO_3	Cl	NO_3	SO_4	
UZ-14	1735.3–1735.53	CHn	Tabt1	529	9.0	700	1.7	0	158	46.9	—	288	18	37.4	3.4	15.4	1.5
UZ-14	1804.5–1804.8	CHn	Tcp4	550	8.0	480	0.5	0.2	111	43.0	—	181	12	25.1	15.3	14.9	2.5
UZ-14	1825.8–1826.0	CHn	Tcp3	557	9.4	590	0.6	0.1	138	47.9	—	42	112	23.5	11.8	12.9	4.3
UZ-14	1854.9–1855.1	CHn	Tcp3	565	8.0	460	0.5	0.2	107	34.5	—	181	23	18.8	13.7	15.9	-1.3
UZ-14	1865.7–1865.9	CHn	Tcp3	569	8.6	480	0.3	0	115	30.4	—	204	18	17.3	11.7	12.6	1.3
UZ-14	2014.7–2014.9	CHn	Tcp1	614	9.3	1520	3.2	0.2	392	37.7	—	409	219	32.1	1.8	22.2	5.6
UZ-14	2015.2–2025.7	CHn	Tcp1	616	9.4	1290	0.9	0	312.7	68.6	—	339	176	23.2	0.5	21.7	4.2
UZ-14	2025.1–2025.3	CHn	Tcp1	617	9.1	1550	4.0	0.2	414	54.8	—	493	189	36.5	6.9	26.3	6.3
UZ-14	2095.1–2095.8	Cfu	Tcb	639	8.8	540	0	0	112.8	63.0	—	143	29	30	0.3	29	1.3
UZ#16	163.5–163.85	PTn	Tpbt4	50	6.8	420	42.5	13.4	21.5	77.5	—	94	45	32.4	23.1	72.3	-16.7
UZ#16	180.9–181.27	PTn	Tpbt3	55	7.3	450	55	11	20	83	3	120	0	38	33	38	2.7
UZ#16	952.6-952.9	TSw	Tptpln	290	8.2	—	2.2	13.7	99.5	31.7	—	179	---	81	30	34	-7.1
UZ#16	1166.19–1166.47	CHn	Tptpv1	355	8.1	710	28.9	13.7	83.6	57.1	—	196	0	82	17	28	-1.4
UZ#16	1206.33-1206.67	CHn	Tptpv1	368	7.2	540	39.8	11.7	48.5	61.6	—	105	---	43	28.4	31.1	11.2
UZ#16	1227.35–1227.7	CHn	Tac4	374	8.1	430	26.5	6.2	47.9	62.2	—	137	0	24	23	26	1.1
UZ#16	1235.1–1235.4	CHn	Tac4	377	7.7	480	33.5	7.9	51.3	52.9	—	154	0	52	26	29	-4.8
UZ#16	1269.6–1269.95	CHn	Tac3	387	8.5	430	14.1	2.4	67.5	57.1	—	139	13	27	18	14	-2.8
UZ#16	1280.37–1280.75	CHn	Tac3	390	8.3	530	20.5	3.7	92.0	71.8	—	192	0	28	19	19	6.9
UZ#16	1296.8–1297.06	CHn	Tac3	395	7.5	950	32.4	19.7	98.2	46.7	—	324	12	50	19	18	-1.9
UZ#16	1317.86–1318.24	CHn	Tac3	402	7.2	430	20.6	5.1	60.1	131.6	—	171	0	32	20	18	-4.0
UZ#16	1358.05–1358.4	CHn	Tac2	414	7.5	550	3.4	0.3	76.7	47.9	—	115	0	22.8	16.1	18.7	5.2
UZ#16	1389.36–1389.64	CHn	Tac2	424	9.4	480	3.6	0.9	114.6	62.5	—	100	36	23.5	18.5	23.8	9.9
UZ#16	1395.5–1395.7	CHn	Tac2	425	8.4	710	5.4	0.3	155	88.0	—	216	24	17	16	22	11.9
UZ#16	1398.5–1398.7	CHn	Tac2	427	—	—	5.0	0.4	145	123	—	237	31	14	16	20	4.8
UZ#16	1412.9–1413.2	CHn	Tac2	431	8.7	450	1.2	0.1	101	75.9	—	165	0	26	24	30	0.1
UZ#16	1428.1–1428.4	CHn	Tac2	435	8.8	570	1.9	0.1	134	80.5	—	160	43	23	19	23	3.8
UZ#16	1442.89–1443.22	CHn	Tac2	440	9.5	410	1.7	0.8	79.9	68.9	—	15	87.6	18.9	11.3	13.7	-7.0
UZ#16	1486.9–1487.3	CHn	Tcp4	453	8.9	370	6.3	0.8	79.5	233.3	—	137	0	38	6	11	2.6
UZ#16	1601.1–1601.5	CHn	Tcp3	488	9.0	580	10	0.3	100	36	—	181	0	53	13	27	-3.6
UZ#16	1607.7–1608.05	CHn	Tcp3	490	8.9	670	25	0.3	108	34	—	170	0	71	10	33	2.9
UZ#16	1643.4–1647.2	CHn	Tcp3	501	9.0	490	91	12	34	70	—	162	0	70	8	28	13.5
UZ#16	1651.6–1651.7	CHn	Tcp3	503	8.3	430	17.3	0.3	66	47.4	—	87	19	27	6	20	6.0
UZ-N55	166.1-166.42	TCw	Tpcplnc	51	7.8	845	28.7	7.6	126.9	47.7	—	136.6	---	106.8	97.7	74.9	-5.1

Table 6. Chemical Composition of Unsaturated-zone Pore-water Samples from Surface-based Boreholes at Yucca Mountain

Bore hole	Depth Interval (ft)	Hydro-Geologic unit[2]	Litho-stratigra-phic unit[2]	Ave. depth (m)	pH	Spec. cond. (:S/cm)	Concentration (mg/L)										Charge balance[1]
							Ca	Mg	Na	SiO_2	K	HCO_3	CO_3	Cl	NO_3	SO_4	
UZ-N55	195.27-195.47	PTn	Tpcpv1	60	6.7	630	91.8	8.6	18.4	71.5	—	69.5	---	77.1	93.3	80.7	-3.2
UZ-N55	198.97-199.45	PTn	Tpcpv1	61	6.7	765	91.2	9.5	39.9	76.4	—	35.4	---	76.6	101.7	101	4.4
WT#24	1734.3-1735.1	CHn	Tptpv1	529	8.2	420	4.9	0	96	81.1	8.4	172	0	34	1.7	14	6.1
WT#24	1744.2-1744.5	CHn	Tptpv1	532	7.9	500	5.5	0.1	121	69.5	9.5	242	0	31	2.3	18	4.8
WT#24	1744.5-1745.0	CHn	Tptpv1	532	8.3	440	4.2	0	103	72.7	7.7	210	19	16	2.7	14	0.2

Table 6. Chemical Composition of Unsaturated-zone Pore-water Samples from Surface-based Boreholes at Yucca Mountain

Source for chemical data: DTN: GS950608312272.001, GS961108312271.002, GS000608312271.001, GS970908312271.003, GS981008312272.004 and GS990208312272.001. For 7 samples, data for more than one aliquot are reported in DTN: GS950608312272.001 (UZ-14: top depths 85.2 and 100.4; UZ#16: top depths 1227.35, 1269.6, 1280.37, 1412.9, and 1442.89). For these samples, it is assumed that the data considered to be most representative of the sample are those reported in Yang et al. (1996, Tables 2 and 3).

Relevant assumptions from Table 2: 1 and 2 (TBV)

Notes: "—" data not available.

"0" values below detection limit

"No core" No core available for stratigraphic examination

[1] Charge balance calculated from data shown using the following formula: [(meq cation/L - meq anion/L) / (meq cation/L + meq anion/L)] x 100

[2] Hydrogeologic unit and lithostratigraphic unit nomenclature from Table 1. The stratigraphic interval from which each sample was collected was determined using the appropriate references listed in Table 4.

Table 7. Chemical Composition of Precipitation and Transient Shallow Perched-water at Yucca Mountain

Bore Hole*	Date	Concentration (mg/L)									Charge balance †
		Ca	Mg	Na	SiO_2	HCO_3	CO_3	Cl	NO_3	SO_4	
Precipitation samples											
NTS Area 25[1]	02-23-98	0.14	0.013	0.32	0.10	2.8	0	<0.1	---	0.41	---
UZN#2[2]	08-18-89	14	2.3	51	18	112	0	10	0	29	---
Shallow transient perched-water samples											
UZN#2	04-09-91	---	---	---	---	---	---	19.9	---	40.7	---
UZN#2	02-14-92	1.4	0.5	1.7	0	11.7	0	12	8.2	7.8	-63.4
UZN#2	03-16-92	14	3.9	25	5.8	58.2	0	10	27.3	21	-0.1
UZN#2	03-31-92	25	4.7	16	11.8	128	0	5.8	19.7	15.6	-10.9
UZ-N46	02-14-92	0.8	0.5	1.6	0.2	23.3	0	3.3	1.6	4.7	-59.8

Data sources: DTN: MO0012WTRIONCO.000 for UZN#2 precipitation, UZN#2 perched water for 1992, and UZ-N46 perched water; DTN: MO0012MAJIONIS.000 for NTS Area 25 precipitation; and DTN: LAJF831222AN98.013 for UZN#2 water from 1991 and UZN#91 perched water. These data are only used for corroborative purposes because of incomplete analyses and inadequate charge balances.

Notes:

"—" data not available.

"0" values below detection limit.

*Sampling depths for perched water: UZN#2, 15.8 m; UZ-N46, 30.1 m (Yang et al. 1996, Table 2)

†Charge balance calculated from data shown using the formula: [(meq cation/L - meq anion/L) / (meq cation/L + meq anion/L)] x 100

[1] Sample from behind service station; pH 7.2, specific conductivity 4.5 μS/cm (DTN:MO0012MAJIONIS.000)

[2] pH 7.7, specific conductivity 308 μS/cm (DTN: MO0012WTRIONCO.000

Table 8. Chemical Composition of Deep Perched Water at Yucca Mountain

Sample Identifier	Ave. Depth (m)	Date	Temp. (°C)	pH	Spec. cond. (:S/cm)	Concentration (mg/L)											Charge balance *
						Al	Ca	Mg	K	Na	SiO_2	HCO_3	CO_3	Cl	NO_3	SO_4	
NRG-7A	460.25	03-07-94	—	8.7	224	0.0	3	0	6.8	42	9	114	—	7	1	4	-0.4
SD-9/TS	453.85	07-17-94	27.0	8.6	445	2.1	2.9	0.2	9.8	98	64.2	197	10	5.6	3.3	27.6	7.6
UZ-14 A	384.60	08-02-93	27.1	7.6	312	0.7	23	1.8	5.6	39	34.2	150	0	7.9	8.6	14.3	0.3
UZ-14 A2	384.60	08-02-93	27.1	7.8	308	1.0	24	1.8	3.9	38	36.4	148.8	0	9.1	12.5	13.8	-1.4
UZ-14 B	387.68	08-03-93	23.8	8.1	335	6.1	31	2.7	4.4	40	51.4	147.6	0	8.3	16.9	16.3	5.2
UZ-14 C	390.75	08-05-93	24.2	8.3	518	0.0	45	4.1	5.8	88	7.7	106.1	0	15.5	0	223	-1.9
UZ-14 PT-1	390.75	08-17-93	—	—	—	0.0	37	3.1	6.3	40	21.4	144	0	7.2	12.7	57.3	0.5
UZ-14 PT-2	390.75	08-19-93	—	—	—	0.0	30	2.4	3.3	35	25.7	144	0	7.0	15.4	22.9	0.3
UZ-14 PT-4	390.75	08-27-93	—	—	—	0.0	27	2.1	1.8	34	32.1	141.5	0	6.7	14.5	14.1	0.2
UZ-14 D	390.75	08-31-93	—	7.8	—	0.0	31	2.5	4.1	35	40.7	146.4	0.	7.0	17.1	24.2	0.1
SD-7(3/8)	479.76	03-08-95	—	—	—	0.28	14.2	0.13	5.3	45.5	62.3	112	0	4.4	33.8	9.1	2.5
SD-7(3/16)	488.29	03-16-95	21.8	8.1	239	0.44	13.3	0.13	5.3	45.3	57.4	128	0	4.1	33.8	9.1	-2.9
SD-7(3/17)	488.29	03-17-95	22.6	8.2	285	0	12.8	0.08	5.5	45.8	50.9	130	0	4.1	22.8	8.6	-0.3
SD-7(3/20)	488.29	03-20-95	23.3	8.0	265	0	12.9	0.07	5.4	45.5	55	127	0	4.1	13.4	8.5	3.3
SD-7(3/21)	488.29	03-21-95	23.2	8.2	259	0	13.5	0.08	5.5	44.6	55.9	128	0	4.1	13.2	10.3	2.2

Data source: DTN: MO0012WTRIONCO.000.

Relevant assumptions from Table 2: 1 and 2

Notes:

"—" data not available.
"0" values below detection limit.
*Charge balance calculated from data shown using the following formula: [(meq cation/L - meq anion/L) / (meq cation/L + meq anion/L)] x 100.

Table 9. Isotopic Composition of Perched Water at Yucca Mountain

Water sample	Depth (m)	**Date**	$\delta^{13}C$ (‰)	^{14}C (pmc)	^{14}C age[1] (yr)	^{3}H (TU)	$\delta^{2}H$ (‰)	$\delta^{18}O$ (‰)	$^{234}U/^{238}U$ Activity ratio	$\delta^{87}Sr$ (‰)	$^{36}Cl/Cl$ (x 10^{-15})
SD-7	479.76	03-08-95	-10.4	34.4	8798	6.2	-99.8	-13.4	—	—	511
	488.29	03-16-95	-9.4	28.6	10321	—	-99.7	-13.3	—	—	—
	488.29	03-17-95	-9.5	28.4	10379	—	-99.6	-13.4	3.50	—	657
	488.29	03-20-95	-9.5	27.9	10525	—	-99.6	-13.4	3.58	—	—
	488.29	03-21-95	-9.5	28.4	10379	—	-99.6	-13.3	3.69	—	609 635
SD-9	—	03-07-94	-14.4	41.8	7192	0	-97.8	-13.3	—	—	—
	—	07-07-94	—	—		—	—	—	2.42 (c)	—	—
	453.85	07-17-94	-14.4	41.8	7192	0	-97.8	-13.3	—	—	449
	—	09-12-94	—	—		—	—	—	—	5.92	—
UZ-14 A	384.60	08-02-93	-10.2	41.7	7212	0.3	-98.6	-13.8	—	4.51	559
UZ-14 A2	384.60	08-02-93	-10.1	40.6	7432	3.1	-97.5	-13.5	—	4.47	538
UZ-14 B	387.68	08-03-93	-9.5	36.6	8287	0	-97.1	-13.4	—	4.34	566
UZ-14 C	390.75	08-05-93	-9.2	66.8	3327	0.4	-87.4	-12.1	—	4.37	389
UZ-14 PT-1	390.75	08-17-93	-9.8	32.3	9318	1.8	-97.8	-13.3	—	3.91– 4.30	644
UZ-14 PT-2	390.75	08-19-93	—	28.9	10235	3.1	-97.9	-13.4	—	3.51– 4.19	656
UZ-14 PT-4	390.75	08-27-93	-9.6	27.2	10735	0	-97.3	-13.4	7.55	4.45– 4.49	675
UZ-14 D	390.75	08-31-93	-11.3	29.2	10150	0	-97.6	-13.1	—	—	690
WT-24	—	10-06-97	—	—	—	—	—	—	4.36 (c)	4.08	—
		10-16-97	—	—	—	—	—	—	6.58 (c)	2.61	—
		10-17-97	—	—	—	—	—	—	8.33	3.88	—
		10-22-97	—	—	—	—	—	—	8.37	4.00	586
NRG-7a	—	03-04-94	—	—	—	—	—	—	5.17 (c)	4.94	518
	460.25	03-07-94	-16.6	66.9	3314	10.4	-93.9	-12.8	—	2.54– 2.91	474
	—	03-08-94	—	—	—	—	—	—	—	11.68	—
UZ-1[2]	382	07-07-83 to 07-21-83	-12.1	64.0	3680	1.0	-102	-13	—	—	999
UZN#91	28.7	03-05-92	—	—	—	—	—	—	—	—	880
UZN#2	15.2	04-09-91	—	—	—	—	—	—	—	—	2012[2]
		02-22-95	—	—	—	—	—	—	—	—	3150

Data sources: DTN: MO0012CARB1314.001 for $\delta^{13}C$, ^{14}C, MO0007GNDWTRIS.013, GS980108312322.004 ($\delta^{87}Sr$), LAJF831222AQ98.011 ($^{36}Cl/Cl$), LAJF831222AN98.013 ($^{36}Cl/Cl$ for UZ-1 and UZN#2), MO0012TRITUNSZ.000 for tritium, GS010808312322.004, and GS010608315215.002 ($^{234}U/^{238}U$ activity ratios).

Relevant assumptions from Table 2: 4 to 16

Notes:
(c) This result is not representative of *in situ* conditions due to sample contamination
"—" not available

[1] Uncorrected ^{14}C age calculated using the radioactive decay equation: $t = (t_{1/2} / \ln 2) \ln (A/A_0)$, where $t_{1/2}$ is the half-life for ^{14}C (5715 yr), A is the measured ^{14}C activity, and A_0 is the initial ^{14}C activity (100 pmc). See assumption 10 in Table 2.

[2] Unqualified data because samples were collected prior to the establishment of a formal quality assurance program.

Table 10. Summary of Tritium Analyses in Unsaturated-zone Pore Waters at Yucca Mountain

ESF or borehole location	Geomorphic Location	Collar elevation (ft)	TCw and above		PTn		TSw		CHn above Tcp		Tcp and below		Total	
			Above 25 TU	Total	Above 25 TU	Total	Above 25 TU	Total	Above 25 TU	Total	Above 25 TU	Total	Above 25 TU	Total
ESF Alcove 2	Bow Ridge fault zone	---	8	9	---	---	---	---	---	---	---	---	8	9
ESF Alcove 3	---	---	---	---	---	3	---	7	---	---	---	---	---	10
ESF Alcove 5	---	---	---	---	---	---	---	7	---	---	---	---	---	7
ESF Alcove 6	Ghost Dance fault zone	---	---	---	---	---	---	7	---	---	---	---	---	7
ESF North Ramp	---	---	---	3	---	---	---	2	---	---	---	---	---	5
ESF Main Drift	---	---	---	---	---	---	---	4	---	---	---	---	---	4
Subtotals, ESF			8	12	---	3	---	27	---	---	---	---	8	42
UZ#16	Terrace, large wash	4000	---	4	1	4	11	51	2	27	---	13	14	99
NRG-6	Hillslope	4092	---	---	6	13	---	---	---	---	---	---	6	13
NRG-7A	Hillslope	4207	---	4	---	9	1	22	---	9	---	---	1	44
UZ-7a	Small wash bottom	4228	---	---	---	1	---	13	---	---	---	---	---	14
SD-9	Small wash bottom	4273	---	2	---	15	---	22	---	26	---	3	---	68
SD-12	Small wash bottom	4343	---	13	---	10	---	27	---	18	1	7	1	75
UZ-1	Large channel (Drillhole Wash)	4425	---	1	---	5	1	9	---	---	---	---	1	15
UZ-14	Large channel (Drillhole Wash)	4425	---	---	1	35	---	53	---	35	---	14	1	137
SD-7	Ridgetop	4472	---	10	---	7	---	15	---	18	---	---	---	50
WT-24	Ridgetop	4900	---	---	---	---	7	10	---	---	5	58	12	68
SD-6	Small wash bottom	4905	---	6	---	17	3	22	---	11	4	37	7	93
Subtotals, boreholes			---	40	8	116	23	244	2	144	10	132	43	676
Total, all samples			8	52	8	119	23	271	2	144	10	132	51	718

Data sources: Tritium compositions of pore waters are from DTN: GS961108312271.002 (excluding data for UZ#16), MO0012TRITUNSZ.000 (for UZ#16 data), GS991108312272.004, GS961108312261.006, GS970108312232.001, GS000608312271.001, GS970283122410.002, GS970608312272.005, and GS970908312271.003.

Relevant assumption from Table 2: 4

Notes:

1. Borehole elevations from DTN: MO9906GPS98410.000. These values are listed so as to provide a rough surrogate for average annual precipitation, which typically increases as a function of elevation (Hevesi et al. 1992, Fig. 7 on p. 685).
2. The threshold for indicating the unambiguous presence bomb-pulse or post-bomb tritium is 25 TU, based on the application of Chauvenet's criterion as described in the text (Section 6.6.2). This statistical test was applied to the 803 samples listed in the above DTNs, including 75 duplicate analyses but excluding ESF data that were reported more than once in DTN: GS970608312272.005, GS961108312261.006 and GS961108312271.002. Where duplicate analyses exist, the sample results were only tallied once in the summary table above.
3. The stratigraphic interval from which each sample was collected was determined using the appropriate references listed in Table 4.

Table 11. Tritium Levels above 25 TU in Unsaturated-zone Pore Waters at Yucca Mountain

Sampling location[1]	Top of Sampled Interval (ft)	Hydrologic unit[3]	Stratigraphic unit[3]	Tritium (TU)
ESF-AL#2-HPF#1	34.3	TCw	Tpcpmn	28.8
	47.2	TCw	Tpcpll	30.9
	50.5	TCw	Tpcpll	118.3
	55.4	Bow Ridge fault zone	---	128.1
	58.9	TCw	Tmbt1	78.6
	61.2	TCw	Tmbt1	65.3
	68.6	TCw	Tmbt1	154.6
	83.6	TCw	Tmbt1	32.9
NRG-6	175.6	PTn	Tpp	30.9
	175.6	PTn	Tpp	39.1
	210.4	PTn	Tpp	117.3
	210.4	PTn	Tpp	139.9
	229.4	PTn	Tpbt2	(23.1)
	229.4	PTn	Tpbt2	30.2
NRG-7a	356.7	TSw	Tptrv1	46.8
UZ-1	621	TSw	Tptprl+Tptpul	28.0
UZ-14	135.5	PTn	Tpp	32.0
UZ#16	158.4	PTn	Tpcpv2	142.2
	158.4	PTn	Tpcpv2	148.5
	262.8	PTn	Tptrn	27.0
	262.8	PTn	Tptrn	31.2
	583.0	TSw	Tptpmn	95.8
	583.0	TSw	Tptpmn	105.9
	669.0	TSw	Tptpmn	(25.0)
	669.0	TSw	Tptpmn	28.7
	945.0	TSw	Tptpln	48.2
	945.0	TSw	Tptpln	59.1
	1041.2	TSw	Tptpln	44.4
	1041.2	TSw	Tptpln	56.1
	1041.9	TSw	Tptpln	28.7
	1090.6	TSw	Tptpln	(11.1)
	1090.6	TSw	Tptpln	40.7
	1110.6	TSw	Tptpln	(21.3)
	1110.6	TSw	Tptpln	30.2
	1113.2	TSw	Tptpv3	35.0
	1113.2	TSw	Tptpv3	42.7
	1113.2	TSw	Tptpv3	51.5
	1113.6	TSw	Tptpv3	42.8
	1122.2	TSw	Tptpv3	26.1
	1122.2	TSw	Tptpv3	26.2
	1122.2	TSw	Tptpv3	35.7
	1129.5	TSw	Tptpv3	58.7
	1397.7	CHn	Tac2	41.3
	1397.7	CHn	Tac2	44.4
	1434.3	CHn	Tac2	98.1
	1434.3	CHn	Tac2	108.8
SD-6	1437.5	TSw	Tptpln	26.7
	1440.0	TSw	Tptpln	27.9

Table 11. Tritium Levels above 25 TU in Unsaturated-zone Pore Waters at Yucca Mountain

Sampling location[1]	Top of Sampled Interval (ft)	Hydrologic unit[3]	Stratigraphic unit[3]	Tritium (TU)
	1440.7	TSw	Tptpln	29.7
	1749.3	CHn	Tcpuc	29.7
	1749.3	CHn	Tcpuc	29.9
	1751.0	CHn	Tcpuc	43.2
	1752.1	CHn	Tcpuc	32.7
	1752.1	CHn	Tcpuc	41.6
	1754.1	CHn	Tcpuc	36.6
SD-12	1722.5	CHn	Tcp3	39.2
WT-24	1688.8	TSw	Tptpv3	37.6
	1689.3	TSw	Tptpv3	35.6
	1690.5	TSw	Tptpv3	28.3
	1690.5	TSw	Tptpv3	29.1
	1694.4	TSw	Tptpv3	25.8
	1694.4	TSw	Tptpv3	29.9
	1697.6	TSw	Tptpv3	42.8
	1697.6	TSw	Tptpv3	50.0
	1699.7	TSw	Tptpv3	29.7
	1699.7	TSw	Tptpv3	30.7
	1702.9	TSw	Tptpv3	45.1
	2515.9	CHn	not available	28.3
	2515.9	CHn	not available	31.2
	2515.9	CHn	not available	34.3
	2519.1	CHn	not available	30.2
	2522.2	CHn	not available	25.7
	2522.2	CHn	not available	32.6
	2525.3	CHn	not available	29.0
	2526.0	CHn	not available	33.0

Data sources for tritium levels: DTN: GS961108312271.002 (excluding UZ#16 data), MO0012TRITUNSZ.000 for UZ#16 data), GS991108312272.004, and GS961108312261.006.

Relevant assumption from Table 2: 4

Notes:
[1] Data listed in parentheses lie below the threshold for indicating the unambiguous presence of bomb-pulse or post-bomb tritium, but are included in this table because they are duplicate analyses for samples with tritium concentrations above the threshold.
[2] Distance from borehole collar for ESF boreholes, and depth from surface for surface-based boreholes
[3] Hydrogeologic unit and lithostratigraphic unit nomenclature from Table 1. The stratigraphic interval from which each sample was collected was determined using the appropriate references listed in Table 4.

Table 12. Tritium Profiles in UZ#4 and UZ#5

Sampling location	Depth (m)		Hydrologic Unit[1]	Stratigraphic Unit[1]	Tritium (TU)[2]
UZ#4	1.0	2.3	Alluvium	Alluvium	19
	2.5	4.5	Alluvium	Alluvium	22
	5.5	6.5	Alluvium	Alluvium	7
	8.8	10.3	Alluvium	Alluvium	2
	11.0	11.8	Alluvium	Alluvium	3
	24.7	24.8	TCw	TCw	28
	25.5	25.6	TCw	TCw	3
	33.5	33.6	PTn	Tpy	22
	41.8	41.9	PTn	Tpy	24
	44.8	44.9	PTn	Tpy	41
	44.9	45.0	PTn	Tpy	38
	46.3	47.9	PTn	Tpy/Tpbt3	45
	49.4	49.5	PTn	Tpbt3	45
	95.6	95.7	PTn	Tpbt2	0
UZ#5	28.3	28.4	TCw	TCw	60
	28.8	28.9	TCw	TCw	49
	29.8	30.0	TCw	TCw	65
	30.4	30.6	TCw	TCw	51
	31.4	31.5	TCw	TCw	11
	32.6	32.8	TCw	TCw	75
	33.6	33.7	TCw	TCw	39
	34.0	34.1	TCw	TCw	22
	34.8	34.9	TCw	TCw	42
	36.0	36.1	PTn	Tpbt4	66
	36.5	36.6	PTn	Tpbt4	15
	36.6	36.7	PTn	Tpbt4	36
	37.2	37.3	PTn	Tpy	4
	37.6	37.7	PTn	Tpy	13
	44.8	44.9	PTn	Tpy	6
	68.6	68.8	PTn	Tpp	10
	70.1	70.2	PTn	Tpp	1
	72.4	72.5	PTn	Tpp	0
	72.5	72.7	PTn	Tpp	7
	75.3	75.5	PTn	Tpp	0
	78.7	78.9	PTn	Tpp	0
	82.4	82.6	PTn	Tpp	4
	90.1	90.2	PTn	Tpp	1
	94.1	94.3	PTn	Tpp	6
	94.3	94.5	PTn	Tpp	0
	98.3	98.4	PTn	Tpbt2	1

Data source: DTN: GS920408312272.002

Relevant assumption from Table 2: 4

Notes:
These data are used to corroborate the limited penetration of infiltrating water into thick (13-m) alluvium (UZ#4), as contrasted with the deeper penetration of infiltrating water into a setting with negligible soil cover over densely welded fractured bedrock (UZ#5) (soil cover thickness described in Yang 1992, p. 733). The data also support an interpretation of lateral flow at the bedrock/alluvial interface in order to account for bomb-pulse tritium underlying pre-bomb tritium in UZ#4.

[1] Hydrogeologic unit and lithostratigraphic unit nomenclature from Table 1. The stratigraphic interval from which each sample was collected was determined using the appropriate references listed in Table 4.

[2] Typical uncertainties (one-sigma) for these sample data are ±4 to ±5 TU (Yang 1992, Table 1).

Table 13. Summary of the Distribution of ^{36}Cl in the Unsaturated Zone at Yucca Mountain

Location	Relevant sample sets	Observed ^{36}Cl distribution
Soil	Surface soils[1] Surface runoff Soil profiles Alluvial profiles for UZ-N37, UZ-N39, UZ-N54, UZ-N61, UZ-14, UZ#16	In areas with sufficiently thick soil cover, bomb-pulse ^{36}Cl is almost completely retained within the uppermost 2-3 m of soil. For thinner soils, some fraction of the bomb-pulse signal has moved down into the underlying bedrock. Elevated $^{36}Cl/Cl$ ratios in shallow soils and surface runoff show that residual bomb-pulse ^{36}Cl is still present on the surface.
TCw	Bomb-pulse in TCw: UZ-N11, UZ-N15, UZ-N16, UZ-N17, UZ-N27, UZ-N36, UZ-N38, UZ-N53, UZ-N55, UZ-N64 No bomb-pulse in TCw: UZ-N37, UZ-N54, UZ#16 ESF North Ramp ESF South Ramp	Based on borehole data, bomb-pulse ^{36}Cl appears to be widely present in the fractured welded TCw unit where it is overlain by thin soil cover (ridgetops and sideslopes) and absent where the soil thickness is at least 3 m. Fracture transport is also indicated by UZ-N53 neutron logging data which have shown changes in moisture content down to a depth of 12 m, well into the TCw (Flint and Flint, 1995, p. 29). The North Ramp data provide evidence of transport of bomb-pulse ^{36}Cl through the TCw.
PTn	Bomb-pulse in PTn: UZ-N11, UZ-N53; UZ-N55; ESF North Ramp[2]	Evidence for fast transport of water into the PTn is shown by elevated $^{36}Cl/Cl$ ratios from this interval in boreholes with thin soil cover. Bomb-pulse ^{36}Cl has also been measured in the PTn unit in several ESF samples from the North Ramp.[2]
	No bomb-pulse in PTn: most of PTn in UZ-N37, UZ-N53, UZ-N54, UZ#16, UZ-14 ESF North Ramp ESF South Ramp	No unambiguous evidence of bomb-pulse ^{36}Cl is seen in the South Ramp despite infiltration rates and soil thicknesses that are similar to those over the North Ramp.
TSw	ESF Main Drift, Alcove #6, ESF Niche#1 Cross Drift UE-25 NRG#4 UE-25 NRG#5 USW NRG-7a Perched water: UZ-14, NRG-7A, SD-7, SD-9	Bomb-pulse ^{36}Cl has been observed at several locations in the ESF and Cross Drift, and appears to be associated with faults.[2] No unambiguous levels of bomb-pulse ^{36}Cl are observed in any of the perched water bodies at the base of this unit or at the top of the CHn; values for these samples are at or slightly above present-day background. Borehole ^{36}Cl data (from ream-bit cuttings) for this unit are usually too diluted by rock Cl to provide a reliable indication of the presence or lack of bomb-pulse ^{36}Cl.
CHn	UZ-14 UZ#16 SD-12	No unambiguous levels of bomb-pulse ^{36}Cl have been observed in the CHn in surface-based boreholes. Measured $^{36}Cl/Cl$ ratios are generally at or somewhat above present-day background. The highest ratios have been measured in SD-12, to a maximum value of 843×10^{-15}.
Saturated zone	C#3, G-2, SD-7, J-13, SD-9, WT-10, WT-12	The $^{36}Cl/Cl$ ratio is uniformly at present-day background in the aquifer underlying the site, independent of location or depth

Data sources: The above table is based on a review of data in the following DTNs: LA000000000062.002, LA9909JF831222.003, LA9909JF831222.005, LA9909JF831222.010, LAJF831222AQ95.005, LAJF831222AQ95.006, LAJF831222AQ95.007, LAJF831222AQ96.005, LAJF831222AQ96.006, LAJF831222AQ96.008, LAJF831222AQ96.009, LAJF831222AQ96.010, LAJF831222AQ96.011, LAJF831222AQ96.012, LAJF831222AQ96.013, LAJF831222AQ96.014, LAJF831222AQ96.015, LAJF831222AQ97.002, LAJF831222AQ97.006, LAJF831222AQ97.007, LAJF831222AQ98.003, LAJF831222AQ98.004, LAJF831222AQ98.005, LAJF831222AQ98.009, LAJF831222AQ98.011, LA9912JF831222.001. The stratigraphic interval from which each borehole sample was collected was determined using the appropriate references listed in Table 4.

Relevant assumptions from Table 2: 5, 6 and 7
Corroborative data:

1 Numerous analyses of ^{36}Cl in surface soil samples from Yucca Mountain confirm the continued presence of the bomb-pulse signal (DTN: LAJF831222AN97.012 and LAJF831222AN98.013).

2 Numerous analyses of ^{36}Cl in tunnel construction water confirm that this potential source of contamination cannot be the source of the elevated $^{36}Cl/Cl$ used to identify the presence of bomb pulse (DTN: LAJF831222AN97.008).

Table 14. Chlorine-36 in Faults and Fault Zones in the Cross Drift

Cross Drift station (m)	Sampling criterion	Description of sampled feature	$^{36}Cl/Cl \times 10^{-15}$ (See note)	
CS1135.5	Systematic fault transect	Breccia from Sundance fault zone zone	347 ±	16
CS1137	Systematic fault transect	Fractured wallrock adjacent to Sundance fault zone	1206 ±	98
CS1317	Systematic fault transect	Breccia	587 ±	42
CS1318	Systematic fault transect	Breccia in fault zone	342 ±	29
CS2154	Systematic fault transect	Breccia in fault zone	918 ±	49
CS2154.5	Systematic fault transect	Breccia in fault zone	4890 ±	174
CS2238	Other through-going fault	Breccia in fault zone	2361 ±	106
CS2348	Other through-going fault	Fault with 3 m offset	1052 ±	38
CS2530.5	Systematic fault transect	Fractured rock between 2 faults	1122 ±	45
CS2545	Opportunistic	Highly fractured bedrock within Solitario Canyon fault zone	854 ±	43
CS2550	Opportunistic	Fractured rock and gouge within Solitario Canyon fault zone	324 ±	24
CS2570	Systematic fault transect	Solitario Canyon fault zone	2158 ±	87
CS2580	Systematic fault transect	Solitario Canyon fault zone	890 ±	55
CS2585	Other through-going fault	Brecciated footwall of fault	2460 ±	103
CS2586.5	Other through-going fault	Brecciated hanging wall of fault	1233 ±	41
CS2590	Systematic fault transect	Solitario Canyon fault zone	1379 ±	58
CS2621	Other through-going fault	Solitario Canyon fault zone	974 ±	50

Data source: DTN: LA9909JF831222.003.

Relevant assumptions from Table 2: 5, 6 and 7

Note: Measured $^{36}Cl/Cl$ ratios have been adjusted to correct for the presence of construction water, as estimated from the measured Br/Cl ratio.

Table 15. Carbon Isotopes in Unsaturated-zone Pore Waters from Surface-based Boreholes at Yucca Mountain

Drill Hole	Depth interval (ft)		Processed length of core[1] (ft)	Hydrologic Unit[2]	Lithostratigraphic unit[2]	d ^{13}C (‰)[3]	^{14}C (pmc)[3]	Uncorrected ^{14}C age (yr)[4]
ESF-AL#3-RBT#4	72.0	74.2	2.2	TCw	Tpcplnc	-12.2	89	961
ESF rubble from CS07+57.3	---	---	---	TCw	---	-16.2	84.7	1369
NRG-6	219.9	256.1	1.2	PTn	Tpbt2	-14.9	92.1	679
NRG-7a	166.2	167.0	0.8	PTn	Tpbt3	-12.9	92.6	634
	258.0	259.4	1.4	PTn	Tpp/Tpbt2	---	74.3	2449
	1492.7	1498.9	6.2	CHn	Tpbt1	-18.6	58.4	4435
SD-12	265.8	277.8	12.0	PTn	Tpbt4	-14	80.3	1809
	1517.0	1517.9	0.9	CHn	Tac3	-17.4	69.9	2953
	1637.4	1640.0	2.6	CHn	Tacbt	-16.9	66.5	3364
	1901.6	1901.8	0.2	CHn	Tcp2	-12.2	63.7	3718
	1940.0	1942.6	2.6	CHn	Tcp2	-16.3	59.2	4322
SD-7	338.3	340.8	2.5	PTn	Tpbt3	-18.1	74.1	2471
	1498.2	1498.9	0.7	CHn	Tac2	-15.1	73.5	2539
	1524.6	1525.0	0.4	CHn	Tac1	-17.5	62.8	3836
	1558.1	1558.9	0.8	CHn	Tac1	-27.4	60.6	4130
SD-9	1452.6	1453.0	0.4	CHn	Tptpv1	-14.1	85.9	1253
	1535.2	1535.7	0.5	CHn	Tac3	-15.3	88.9	970
	1619.7	1661.4	41.7	CHn	Tac2	-14.5	95.3	397
	1800.7	1801.6	0.9	CHn	Tacbt	-16.4	82.3	1606
UZ#16	158.1	158.4	0.3	PTn	Tpcpv1	-9.3	87	1148
	180.9	---	---	PTn	Tpbt3	-9.0	89.8	887
	219.4	219.6	0.2	PTn	Tptrv3	-9.4	87.3	1120
	1344.1	1344.3	0.2	CHn	Tac2	---	87	1148
	1343.7	1379.9	0.6	CHn	Tac2	-17.5	58.2	4463
	1380.0	1380.5	0.5	CHn	Tac2	-23.3	71.8	2731
	1395.5	1398.7	0.6	CHn	Tac2	-12.6	97.7	192
	1398.1	1398.3	0.2	CHn	Tac2	---	88.3	1026
	1408.2	1434.6	0.6	CHn	Tac2	-16.6	53.1	5219
	1442.8	1443.2	0.4	CHn	Tac2	-10.3	61.5	4008
UZ-14	85.2	86.1	0.7	PTn	Tpbt3	-17.1	83.2	1516
	91.0	100.8	1.45	PTn	Tpbt3	-15.0	83.3	1507
	114.7	115.5	0.8	PTn	Tpp	---	86.9	1158
	144.8	148.1	1.2	PTn	Tpp	---	84.9	1350
	148.2	148.5	0.3	PTn	Tpp	-13.0	---	---
	215.7	226.2	10.5	PTn	Tpp	-25.0	96.2	319
	235.1	246.4	6.9	PTn	Tpbt2	-10.5	89.6	905
	254.9	255.7	0.8	PTn	Tpbt2	-13.0	---	---
	1409.35	1420.9	1.0	CHn	Tpbt1	-12.4	81.8	1656
	1429.87	1430.15	0.28	CHn	Tac3	-11.1	69.9	2953
	1460.8	1462.1	0.6	CHn	Tac3	-13.4	96.3	311
	1524.55	1526.2	0.6	CHn	Tac2	-11.8	93.4	563
	1563.6	1564.3	0.7	CHn	Tac2	-15.8	76.8	2176
	1563.9	1565.1	1.2	CHn	Tac2	-15.2	80	1840
	1585.0	1585.8	0.8	CHn	Tac2	-11.3	93.7	537
	1605.6	1606.4	0.8	CHn	Tac2	-14.6	81.1	1727
	1644.3	1645.2	0.8	CHn	Tac2	-16.0	86.3	1215
	1674.3	1675.3	1.0	CHn	Tac1	-13.7	91.3	750
	1694.9	1696.0	1.1	CHn	Tacbt	-10.3	92.3	661
	1714.5	1715.8	1.4	CHn	Tacbt	-11.6	96.3	311
	2014.5	2025.7	11.2	CHn	Tcp1	-14.7	94.0	510
	2095.1	2096.0	0.9	CHn	Tcb	-15.7	84.6	1379

Data sources: DTN: MO0012CARB1314.001 (for NRG-6, NRG-7A, UZ-14, UZ#16), GS961108312271.002 (NRG-7a, SD-7, SD-9, SD-12, UZ-14), GS961108312261.006 (ESF samples), and GS000608312271.001 (SD-12).

Assumptions from Table 2: 8, 9 (TBV) and 10

Notes:
[1] Total length of core processed is estimated from the lengths of individual core listed for each composite sample in the source DTNs.
[2] Hydrogeologic unit and lithostratigraphic unit nomenclature from Table 1. The stratigraphic interval from which each sample was collected was determined using the appropriate references listed in Table 4.
[3] Typical uncertainties (one-sigma) for these data are ±0.3 to ±0.7 pmc for ^{14}C, and ±0.2‰ for $\delta\ ^{13}C$ (Section 6.2.5).
[4] Uncorrected ^{14}C age calculated using the radioactive decay equation: $t = (t_{1/2} / \ln 2) \ln (A/A_0)$, where $t_{1/2}$ is the half-life for ^{14}C (5715 yr), A is the measured ^{14}C activity, and A_0 is the initial ^{14}C activity (100 pmc). See assumption 10 in Table 2.

Table 16. Carbon Isotopes in Unsaturated-zone Pore Waters from UZ#4 and UZ#5

Drill hole	Hydrogeologic and lithostratigraphic unit[1]		Depth (m)	Processed length of core (m)	d ^{13}C (‰)	^{14}C (pmc)	Uncorrected ^{14}C age (yr)
UZ#4	PTn	Tpbt2	96.0 – 100.6	4.6	-20.0	88.6	998
UZ#5	PTn	Tpbt2	103.6 – 105.2	1.6	-26.7	55.1	4914

Data source: DTN: GS920408312272.002

Relevant assumptions from Table 2: 8, 9 (TBV) and 10

Notes:
[1] Hydrogeologic unit and lithostratigraphic unit nomenclature from Table 1. The stratigraphic interval from which each sample was collected was determined using the appropriate references listed in Table 4.
[2] Typical uncertainties (one-sigma) for these data are ±0.3 to ±0.7 pmc for ^{14}C, and ±0.2‰ for δ ^{13}C (Section 6.2.5).
[3] Uncorrected ^{14}C age calculated using the radioactive decay equation: $t = (t_{1/2} / \ln 2) \ln (A/A_0)$, where $t_{1/2}$ is the half-life for ^{14}C (5715 yr), A is the measured ^{14}C activity, and A_0 is the initial ^{14}C activity (100 pmc). See assumption 10 in Table 2.

Table 17. Carbon Isotopes in Unsaturated-zone Gases from the Atmosphere and Shallow Boreholes at Yucca Mountain

Borehole	Location of gas collection	Collection date	^{14}C (pmc)	d ^{13}C (‰)
UZ-1	Atmosphere	Apr-84	125.6	-8.9
UZ-1	Atmosphere	Apr/May-85	124.4	-8.6
UZ-13	Atmosphere	21-Mar-95	106.2	---
UZ-13	Atmosphere	26 & 29-Mar-95	115.4	-8.7
UZ-N75	Atmosphere	15-Mar-94	114.6	---
UZ-1	Surface	Apr-84	124.3	-16.6
UZ-1	Surface	Apr/May-85	123.4	-14.6
UZ-6	Annulus	15-Mar-94	90.4	---
UZ-6	Annulus	21-Mar-95	93.0	---
UZ-6	Annulus	26 & 29-Mar-95	94.2	-17.4
UZ-N93	Annulus	15-Mar-94	113.5	---
UZ-N93	Annulus	26 & 29-Mar-95	114.0	-17.4
UZ-N94	Annulus	15-Mar-94	114.0	---
UZ-N94	Annulus	26 & 29-Mar-95	109.8	-17.6
UZ-N95	Annulus	15-Mar-94	106.0	---
UZ-N95	Annulus	26 & 29-Mar-95	109.4	-17.2

Data sources: DTN: GS930508312271.021, GS941208312261.008, GS950808312261.004, and GS960208312261.002

Relevant assumptions from Table 2: 8 and 9

Notes:
These data are used to corroborate the present-day elevated ^{14}C activity in the atmosphere due to global fallout, and that this activity is not greatly diluted by processes in shallow soil or bedrock although the effects of microbial activity and plant respiration on surface and subsurface samples result in a shift in $\delta^{13}C$ to more negative values.

Table 18. Carbon Isotopes in Unsaturated-zone Gases from Deep Open Surface-based Boreholes at Yucca Mountain (NRG#5, NRG-6, NRG-7, SD-7, SD-9, SD-12, UZ-14 and UZ#16)

Bore-Hole	Depth	Hydrogeologic and lithostratigraphic unit[1]		Collection date	CO_2 (vol. %)[2]	d ^{13}C (‰)[3,4]	^{14}C (pmc)[3,4]	Uncorrected ^{14}C age (yr)[5]
NRG#5	133 ft	TCw	Tpcpln	14&15-Aug-96	—	-16.7	88.82	978
					—	-14.6	—	—
					—	-14.6	—	—
	243 ft	PTn	Tpp	14&15-Aug-96	—	-16.7	68.56	3112
					—	-14.9	—	—
					—	-14.8	—	—
					—	-9.7	—	—
	298 ft	PTn	Tpbt2	14&15-Aug-96	—	-15.5	69.57	2992
					—	-14.6	—	—
					—	-14.6	—	—
	354 ft	TSw	Tptrn	14&15-Aug-96	—	-15.3	54.19	5051
					—	-14.4	—	—
					—	-14.4	—	—
	410 ft	TSw	Tptrn	23-Aug-95	—	-14.9	—	—
	(Zone 5)			14&15-Aug-96	—	-15.7	65.77	3455
					—	-14.6	—	—
					—	-14.4	—	—
					—	-13.1	—	—
					—	-12.1	—	—
	466 ft	TSw	Tptrn	14&15-Aug-96	—	-16.4	77.47	2105
					—	-15.6	—	—
					—	-15.6	—	—
	475 ft	TSw	Tptrn	Mar-94	—	-16.1	51.3	5503
	521 ft	TSw	Tptprl or Tptpul	14&15-Aug-96	—	-16.8	69.95	2947
					—	-15.2	—	—
					—	-15.2	—	—
	572 ft	TSw	Tptprl or	23-Aug-95	—	-15.4	—	—
	(Zone 9)		Tptpul	14&15-Aug-96	—	-14.5	57.27	4596
					—	-14.3	—	—
					—	-14.1	—	—
					—	-14.0	—	—
					—	-11.3	—	—
					—	-14.0	—	—
	633 ft	TSw	Tptprl or Tptpul	14&15-Aug-96	—	-14.3	—	—
					—	-14.4	—	—
					—	-15.7	61.31	4034
	744 ft	TSw	Tptpul	14&15-Aug-96	—	-15.7	58.41	4433
	799 ft	TSw	Tptpmn	14&15-Aug-96	—	-14.6	59.00	4350
					—	-13.0	—	—
					—	-13.0	—	—
	1225 ft	TSw	Tptpln	Mar-94	—	-15.0	93.1	589
	(Zone 13)			23-Aug-95	—	-15.0	—	—
NRG-6	20 ft	TCw	Tpcpll	3-May-94	0.07	-15.2	—	—

Table 18. Carbon Isotopes in Unsaturated-zone Gases from Deep Open Surface-based Boreholes at Yucca Mountain (NRG#5, NRG-6, NRG-7, SD-7, SD-9, SD-12, UZ-14 and UZ#16)

Bore-Hole	Depth	Hydrogeologic and lithostratigraphic unit[1]		Collection date	CO_2 (vol. %)[2]	d ^{13}C (‰)[3,4]	^{14}C (pmc)[3,4]	Uncorrected ^{14}C age (yr)[5]
	80 ft	TCw	Tpcpln	Mar-94	—	-15.2	92.1	679
				24-May-94	0.11	-14.3	—	—
	200 ft	PTn	Tpp	Mar-94	—	-14.9	91.0	778
				24-May-94	0.115	-14.3	—	—
	275 ft	TSw	Tptrn	3-May-94	0.06	—	—	—
				24-May-94	—	-15.1	—	—
	600 ft	TSw	Tptpul	Mar-94	—	-15.5	83.2	1516
				24-May-94	0.115	-14.1	—	—
	725 ft	TSw	Tptpmn	3-May-94	0.06	—	—	—
				24-May-94	—	-14.8	—	—
	925 ft	TSw	Tptpll	Mar-94	—	-16.1	94.2	493
				24-May-94	0.11	-14.2	—	—
	1000 ft	TSw	Tptpll	3-May-94	0.07	-14.5	—	—
NRG-7	140 ft	PTn	Tpcpv2	Mar-94	—	-16.8	108.0	Modern
				29-Jun-94	0.12	-17.35	—	—
	490 ft	TSw	Tptrl	Mar-94	—	-18.2	111.7	Modern
				29-Jun-94	0.19	-17.8	—	—
	890 ft	TSw	Tptpll	Mar-94	0.15	-19.0	111.0	Modern
				29-Jun-94	0.15	-17.8	—	—
	1215 ft	TSw	Tptpll	Mar-94	—	-18.0	—	—
				29-Jun-94	0.19	-17.7	—	—
SD-7	300 ft	PTn	Tpcpv2	15-Aug-96	—	-17.6	100.27	Modern
					—	-16.4	—	—
					—	-16.3	—	—
	350 ft	PTn	Tpp	15-Aug-96	—	-16.4	91.38	743
					—	-15.1	—	—
					—	-14.1	—	—
	400 ft	TSw	Tptrn	15-Aug-96	—	-16.2	83.78	1459
					—	-14.6	—	—
					—	-14.5	—	—
	500 ft	TSw	Tptpul	15-Aug-96	—	-16.9	72.18	2688
					—	-13.0	—	—
					—	-13.0	—	—
	550 ft	TSw	Tptpul	15-Aug-96	—	-14.6	92.43	649
					—	-12.3	—	—
					—	-12.1	—	—
	600 ft	TSw	Tptpul	15-Aug-96	—	-14.6	79.40	1902
					—	-12.7	—	—
					—	-12.6	—	—
	650 ft	TSw	Tptpul	15-Aug-96	—	-9.1	—	—
					—	-8.9	—	—
	700 ft	TSw	Tptpmn	15-Aug-96	—	-16.0	86.78	1169
					—	-13.3	—	—
					—	-13.3	—	—

Table 18. Carbon Isotopes in Unsaturated-zone Gases from Deep Open Surface-based Boreholes at Yucca Mountain (NRG#5, NRG-6, NRG-7, SD-7, SD-9, SD-12, UZ-14 and UZ#16)

Bore-Hole	Depth	Hydrogeologic and lithostratigraphic unit[1]		Collection date	CO_2 (vol. %)[2]	d ^{13}C (‰)[3,4]	^{14}C (pmc)[3,4]	Uncorrected ^{14}C age (yr)[5]
	800 ft	TSw	Tptpmn	15-Aug-96	—	-15.6	84.18	1420
					—	-12.3	—	—
					—	-12.3	—	—
	508 – 633 m	TSw	Tptpul	Not specified	—	-25.0	41.52	7247
SD-9	0 – 454 m (Zone 1)	TCw-CHn	Tpcplnc/ Tac3	Not specified	—	-16.1	96.70	277
				2/01/95	0.27	-13.7	—	—
				8/23/95	—	-15.2	—	—
	454 – 560 m (Zone 2)	CHn	Tac3-Tcp4	Not specified	—	-19.1	51.04	5545
				2/01/95	0.092	-19.6	—	—
				8/23/95	—	-19.8	—	—
UZ-14	1445 ft	CHn	Tac3	1997	0.05	-15.1	99.17	Modern
	1490 ft	CHn	Tac3	1997	0.06	-19.4	50.42	5646
	1540 ft	CHn	Tac2	1997	1.0	-8.4	48.76	5922
	1590 ft	CHn	Tac2	1997	0.04	-9.3	99.2*	Modern
	1640 ft	CHn	Tac2	1997	0.06	-9.2	100.9*	Modern
	1690 ft	CHn	Tac1	1997	1.2	-20.9	67.8	3204
	1738 ft	CHn	Tacbs	1997	1.1	-20.0	80.1	1830

Data sources: DTN: GS941208312261.008 (NRG#5, NRG-6, NRG-7), GS950808312261.004 (SD-9), GS960208312261.002 (NRG#5, SD-9), GS961108312271.002 (SD-7, SD-9), GS970283122410.002 (NRG#5, SD-7), and GS970908312271.003 (UZ-14). Only the average CO_2 concentrations and ^{13}C values are reported in the above table when replicate analyses are available. Data have been rounded to make it easier to compare them, although ^{14}C ages have been calculated from the unrounded values reported in the DTNs.

Relevant assumptions from Table 2: 8, 9 (TBV), 10, 17 and 18

Notes:

"—" data not available

"No report" collection date not reported

* Contamination with atmospheric air is suspected as indicated by ^{13}C data, although there were no known leaks present during sample collection (DTN: GS970908312271.003, SEP Table S97576.003)

[1] Hydrogeologic unit and lithostratigraphic unit nomenclature from Table 1. The stratigraphic interval from which each sample was collected was determined using the appropriate references listed in Table 4.

[2] In open boreholes, CO_2 gas concentrations are often quite variable from one collection time to another, even when the samples are collected from the same packed-off borehole interval within 24 hours of one another (e.g., CO_2 data in DTN: GS941208312261.008). Thus, the CO2 values reported in this table should only be used as an approximate indication of *in situ* conditions.

[3] Yang, Yu et al. (1998, p. 16) warn that samples collected for SD-7, SD-9 and SD-12 by the whole-gas balloon method varied from –10 to –25 ‰ for replicate samples (USGS data), probably due to problems with the balloon nozzle, and hence these data are not reported here. The values reported above were obtained by the Desert Research Institute (DRI); these were less variable than the USGS data although they also tend to be more negative by a few units per mil when collected with the molecular sieve.

[4] Typical uncertainties (one-sigma) for these data are ±0.3 to ±0.7 pmc for ^{14}C, and ±0.2‰ for $\delta\ ^{13}C$ (Section 6.2.5).

[5] Uncorrected ^{14}C age calculated using the radioactive decay equation: $t = (t_{1/2} / \ln 2) \ln (A/A_0)$, where $t_{1/2}$ is the half-life for ^{14}C (5715 yr), A is the measured ^{14}C activity, and A_0 is the initial ^{14}C activity (100 pmc). See assumption 10 in Table 2.

Table 19. Carbon Isotopes in Unsaturated-zone Gases from Boreholes UZ-6 and UZ-6s

Bore-Hole	Depth (ft)	Hydrogeologic unit[4]	d ^{13}C (‰)[1]	^{14}C (pmc)[1]			Uncorrected ^{14}C age (yr)[3]
			26-Mar-95 WGM[2]	15-Mar-94 WGM[2]	21-Mar-95 Mole. Sieve[2]	29-Mar-95 KOH[2]	29-Mar-95
UZ-6	200	TCw	-17.40	---	88.47	88.15	1040
	800	TSw	-17.14	---	83.27	84.91	1349
	1195	TSw	-17.18	---	84.74	86.09	1235
	1800	CHn	-16.62	---	50.36	40.98	7355
UZ-6s	20	TCw	-16.68	107.90	90.67	106.81	Modern
	40	TCw	-16.59	107.33	100.93	106.75	Modern
	60	TCw	-16.90	106.09	96.17	105.24	Modern
	100	TCw	-16.45	107.90	109.53	105.62	Modern
	200	TCw	-16.42	109.07	102.03	107.82	Modern
	350	TCw	-16.34	107.79	107.61	107.32	Modern
	400	TCw	-15.16	100.73	101.90	99.45	Modern
	430	PTn	-16.42	---	95.00	94.72	447

Data sources: DTN: GS950808312261.004 and GS960208312261.002.

Relevant assumptions from Table 2: 8, 9 (TBV), and 10

Notes:

[1] Typical uncertainties (one-sigma) for these data are ±0.3 to ±0.7 pmc for ^{14}C, and ±0.2‰ for $\delta\ ^{13}C$ (Section 6.2.5).

[2] Gas collection methods: WGM, whole gas balloon method; Mole. Sieve, molecular sieve method; KOH, gas bubbled through potassium hydroxide solution

[3] Uncorrected ^{14}C age calculated using the radioactive decay equation: $t = (t_{1/2} / \ln 2) \ln (A/A_0)$, where $t_{1/2}$ is the half-life for ^{14}C (5715 yr), A is the measured ^{14}C activity, and A_0 is the initial ^{14}C activity (100 pmc). See assumption 10 in Table 2.

[4] Hydrogeologic unit nomenclature from Table 1. The stratigraphic interval from which each sample was collected was determined using the appropriate references listed in Table 4.

Table 20. CO_2 and Carbon Isotope Profiles in Unsaturated-zone Gases from Instrumented Boreholes UZ-1 and SD-12

Bore hole	Depth	Probe or station	Hydrogeologic and lithostratigraphic unit[1]		CO_2 (vol. %)[2]	d ^{13}C (‰)	^{14}C (pmc)	Uncorrected ^{14}C age[2] (yr)
UZ-1	42 ft	1	Qtac	UO	0.535	-18.9	108.5	Modern
	62 ft	2	PTn	Tpy	0.581	-20.4	104.3	Modern
	93 ft	3	PTn	Tpbt3	0.307	-20.8	96.2	319
	131 ft	4	PTn	Tpp	0.428	-19.9	89.4	924
	201 ft	5	PTn	Tpp	0.230	-20.3	67.2	3277
	266 ft	6	PTn	Tptrv3	0.205	-17.4	64.7	3590
	348 ft	7	TSw	Tptrn	0.104	-16.2	63.3	3770
	421 ft	8	TSw	Tptrn	0.092	-15.7	61.1	4062
	501 ft	9	TSw	Tptpul	0.082	-16.2	47.4	6155
	621 ft	10	TSw	Tptpul	0.051	-16.1	42.6	7036
	747 ft	11	TSw	Tptpmn	0.094	-14.6	47.2	6190
	871 ft	12	TSw	Tptpll	0.121	-15.7	37.1	8175
	998 ft	13	TSw	Tptpll	0.042	-16.9	—	—
	1100 ft	14	TSw	Tptpll	0.091	-15.0	38.8	7806
	1207 ft	15	TSw	Tptpll	0.216	-19.7	14.5	15921
SD-12	24.7 m	P	TCw	Tpcpmn/Tpcpll	—	-22.55	90.98	779
	43.9 m	O	TCw	Tpcplnh	—	-20.20	49.17	5853
	65.2 m	N	TCw	Tpcplnc	—	-21.99	87.39	1111
	91.7 m	L	PTn	Tptrv1	—	-16.41	82.71	1565
	107.0 m	K	TSw	Tptrn	—	-20.98	77.75	2075
						-15.58	94.91	431
	128.9 m	J	TSw	Tptrn	—	-22.11	57.95	4498
	171.0 m	I	TSw	Tptpul	—	-23.57	38.95	7774
	208.2 m	H	TSw	Tptpmn	—	-24.71	36.92	8215
	236.8 m	G	TSw	Tptpmn	—	-25.57	31.57	9506
	256.6 m	F	TSw	Tptpll	—	-24.40	34.13	8863
	285.0 m	E	TSw	Tptpll	—	-21.89	52.41	5327
	322.5 m	D	TSw	Tptpln	—	-21.79	46.65	6287
						-23.83	34.43	8791
	385.6 m	C	TSw	Tptpln	—	-22.86	88.69	990
	407.2 m	B	CHn	Tptpv2	—	-24.63	24.43	11620
						-23.65	26.89	10829
	435.9 m	A	CHn	Tac4	—	-17.17	84.47	1392

Data sources: DTN: MO0012CARB1314.000 (UZ-1 samples collected February 1995) , MO0012CO2UNSZO.004 and GS961108312271.002 (SD-12 samples collected October 1996)
Relevant assumptions from Table 2: 8, 9 (TBV), 10, 17 and 18
Note: "— " not available

[1] Hydrologic and lithographic nomenclature from Table 1. The stratigraphic interval from which each sample was collected was determined using the appropriate references listed in Table 4. UZ-1 stratigraphy and UZ-1 probe depths from DTN: GS930508312271.021.

[2] Uncorrected ^{14}C age calculated using the radioactive decay equation: $t = (t_{1/2} / \ln 2) \ln (A/A_0)$, where $t_{1/2}$ is the half-life for ^{14}C (5715 yr), A is the measured ^{14}C activity, and A_0 is the initial ^{14}C activity (100 pmc). See assumption 10 in Table 2.

Table 21. Carbon Isotopes in Unsaturated-zone Gases from Boreholes in ESF Alcoves

Borehole	Sampled interval (m)	Hydro-geologic unit[1]	Lithostrati-graphic unit[1]	^{14}C (pmc)	$\delta^{13}C$ (‰)
Alcove #1 air	NA	---	---	---	-9.13
					-9.07
ESF-AL#1-RBT#1	30 – 32	TCw	Tpcpul	101.35	-15.61
	35 – 42.5	TCw	Tpcpul	---	-13.49
	44 – 48	TCw	Tpcpul	---	-16.40
	49 – 55	TCw	Tpcpul	---	-13.60
	55.75 – 59	TCw	Tpcpul	---	-14.49
	60 – 73	TCw	Tpcpul	---	-14.42
ESF-AL#1-RBT#2	6.5 – 9	TCw	Tpcpul	---	-18.35
	28 – 38	TCw	Tpcpul	---	-13.46
	62 – 65	TCw	Tpcpul	---	-16.20
	62 – 83	TCw	Tpcpul	92.76	-14.69
	86 – 105	TCw	Tpcpul	---	-16.23
					-15.80
ESF-AL#1-RBT#3	50.75 – 62.5	TCw	Tpcpul	107.35	-15.79
					-10.22
	64 – 66.5	TCw	Tpcpul	---	-17.86
	85.5 – 92.8	TCw	Tpcpul	---	-15.83
ESF-AL#6 ZONE 1 WGM	4.7	TSw	Tptpmn	69.24	-14.14
ESF-AL#6 ZONE 2 WGM	7.8	TSw	Tptpmn	75.09	-14.06
ESF-AL#6 ZONE 3 WGM	9.3	TSw	Tptpmn	71.58	-14.11
ESF-AL#6 ZONE 4 WGM	10.8	TSw	Tptpmn	63.74	-15.08
ESF-AL#6 ZONE 5 WGM	12.4	TSw	Tptpmn	66.77	-15.45
ESF-AL#6 ZONE 6 WGM	13.9	TSw	Tptpmn	68.23	-15.38
ESF-AL#6 ZONE 7 WGM	15.4	TSw	Tptpmn	70.76	-15.55
ESF-AL#6 ZONE 8 WGM	16.9	TSw	Tptpmn	61.37	-14.78
ESF-AL#6 ZONE 9 WGM	18.5	TSw	Tptpmn	58.14	-16.17
ESF-AL#6 ZONE 10 WGM	21.5	TSw	Tptpmn	66.01	-15.89

Data sources: DTN: GS960208312261.002 (ESF Alcove #1), GS970283122410.002 ($\delta^{13}C$ in ESF Alcove #6), and GS990983122410.003 (^{14}C in ESF Alcove #6). The $\delta^{13}C$ values in this table are the averages of those reported for each zone in the Alcove #6 borehole.

Relevant assumptions from Table 2: 8 and 9 (TBV)

[1] Hydrologic and lithographic nomenclature from Table 1.

Table 22. Comparison of Carbon Isotopes in Pore-water and Gas Samples Collected from Similar Borehole Intervals

Borehole	Pore-water results					Gas results				
	Stratigraphic unit		Depth (m)	$\delta^{13}C$ (‰)	^{14}C (pmc)	Stratigraphic unit		Depth (m)	$\delta^{13}C$ (‰)	^{14}C (pmc)
NRG-6	PTn	Tpbt2	71.6	-14.9	92.1	PTn	Tpp	61	-14.1 to -14.9	91.0
SD-7	PTn	Tpbt3	103	-18.1	74.1	PTn	Tpp	107	-14.1 to -16.4	91.4
SD-9	CHn	Tac3	468	-15.3	88.9	CHn	Tac3 to Tcp4	454 to 560	-19.1 to -19.8	51.0
	CHn	Tac2	494 to 506	-14.5	95.3					
	CHn	Tacbt	549	-16.4	82.3					
SD-12	PTn	Tpbt4	82	-14	80.3	PTn	Tptrv1	92	-16.4	82.7
	CHn	Tac3	462	-17.4	69.9	CHn	Tac4	436	-17.2	84.5
UZ-14	CHn	Tac3	436	-11.1	69.9	CHn	Tac3	440	Variable	99.2
	CHn	Tac3	445	-13.4	96.3	CHn	Tac3	454	-19.45	50.4
	CHn	Tac2	465	-11.8	93.4	CHn	Tac2	469	-8.42	48.8
	CHn	Tac2	477	-15.8	76.8					
	CHn	Tac2	477	-15.2	80.0					
	CHn	Tac2	483	-11.3	93.7	CHn	Tac2	485	-9.3	99.2
	CHn	Tac2	490	-14.6	81.1					
	CHn	Tac2	501	-16	86.3	CHn	Tac2	500	-9.24	100.9
	CHn	Tac1	510	-13.7	91.3	CHn	Tac1	515	-20.89	67.8
	CHn	Tacbt	517	-10.3	92.3	CHn	Tacbs	530	-20.05	80.1
	CHn	Tacbt	523	-11.6	96.3					
UZ-14 pore water (compared with UZ-1 gas from similar depth)	PTn	Tpbt3	26	-17.1	83.2	PTn	Tpbt3	28	-20.8	96.2
	PTn	Tpbt3	29	-15.0	83.3					
	PTn	Tpp	45	-13.0	84.9	PTn	Tpp	40	-19.9	89.4
	PTn	Tpp	67	-25.0	96.2	PTn	Tpp	61	-20.3	67.2

Data sources: Based upon a comparison of sampled intervals listed in Tables 15, 18 and 20, data were selected from DTN: MO0012CARB1314.001 (for UZ-14 and NRG-6 pore waters), MO0012CARB1314.000 (for UZ-1 gas), GS941208312261.008 (NRG-6 gas), GS970283122410.002 (SD-7 gas), GS970908312271.003 (UZ-14 gas), and GS961108312271.002 (SD-7, SD-9, and SD-12 pore waters; SD-9 and SD-12 gas).

Relevant assumptions from Table 2: 8 and 9 (TBV)

Table 23. Uranium Isotopic Data for Ephemeral Stream Flow in the Vicinity of Yucca Mountain

Location	Sample Name	Collection Date	Concentration		Activity Ratios	
			U µg/l	±2F	$^{234}U/^{238}U$	±2F
Fortymile Wash runoff	CSS950106FMOV.4	01/06/95	0.0473	0.0002	3.670	0.081
Pah Canyon	SPC00009734 HOH	01/26/95	0.1111	0.0003	1.833	0.015
Fortymile Canyon	SPC00009805 HOH	01/25/95	0.2613	0.0007	1.497	0.015
Upper Split Wash	SPC00009732 HOH	01/25/95	0.3880	0.0010	1.501	0.009
Yucca Wash near mouth	SPC00009733 HOH	01/26/95	0.1086	0.0003	1.623	0.016
Upper reach, Wren Wash	SPC00009806 HOH	01/25/95	0.4868	0.0012	1.525	0.006
Wren Wash	SPC00529907-Wren Wash	02/20/98	0.2224	0.0007	1.543	0.005
Pagany Wash	SPC00529917-Pagany Wash	02/24/98	0.3766	0.0013	1.528	0.006
Yucca Wash	SPC00529927-Yucca Wash	02/24/98	0.1705	0.0005	1.721	0.01

Data sources: DTN: GS010608315215.002 and GS980908312322.009

Uranium isotopic data obtained by mass spectrometry at U.S. Geological Survey, Denver, Colorado. All errors are reported at the 95 percent confidence level.

Table 24. Locations and Other Physical Characteristics of Wells Sampled for Chemical and Isotopic Analyses of Groundwater in the Vicinity of Yucca Mountain.

Site name	UTM-x (m)	UTM-y (m)	Site elevation (m)	Well depth (m)	Water table depth (m)	Aquifer[1]
15S/49E-13dda	553312.5	4055302	796	174	90	Qal
15S/49E-22a1	550086.3	4054974	796	174	90	Qal
15S/49E-22dcc	549672.5	4053523	784	148	78	Qtal
15S/49E-27acc	549552.9	4052722	777	467	73	Qal
15S/50E-18ccc	553710.0	4055273	812	120	105	Qal
15S/50E-18cdc	553934.3	4055151	812	120	105	Qal
15S/50E-19b1	553862.5	4054720	---	110	103	Qal
16S/49E-05acc	546664.5	4049439	746	87	21	Qal
Airport Well	553289.0	4055086	804	229	76	Qal
BGMW-11	534410.9	4062631	786	---	72	Qal
Cind-R-Lite Well	544027.0	4059809	831	140	101	Tv
Cowboy Joe's	554132.4	4055245	---	---	---	Qal
Gexa Well 4	534068.9	4086110	1198	488	188	Tv
JF-3	554498.3	4067974	944	347	216	Tv
NDOT well	554132.4	4055245	810	151	105	Qal
TW-5	562605.0	4054686	931	244	207	Qal
UE-25 b#1 (0-1220 m)	549954.5	4078422	1201	1220	470	Th/Tct
UE-25 b#1 (853-914 m)	549954.5	4078422	1201	1220	470	Tcb
UE-25 c#1	550957.7	4075943	1131	914	401	Tcb/Tct
UE-25 c#2	550944.0	4075867	1132	914	401	Tcb
UE-25 c#3	550919.8	4075886	1132	914	402	Tcb/Tct
UE-25 J-11	563816.0	4071049	1050	405	317	Tb
UE-25 J-12	554435.8	4068767	953	347	226	Tv
UE-25 J-13	554004.4	4073550	1011	1063	283	Tpt
UE-25 ONC-1	550479.9	4076608	1163	469	433	Th/Tcp
UE-25 p#1 (0-1200 m)	551508.7	4075663	1114	1805	382	Tcp
UE-25 p#1 (1300-1800 m)	551508.7	4075663	1114	1805	382	DSlm
UE-25 WT#12	550162.9	4070647	1075	399	345	Tpt/Th
UE-25 WT#14	552638.0	4077337	1076	399	346	Th
UE-25 WT#15	554033.7	4078702	1083	415	354	Tpt
UE-25 WT#4	550445.9	4079420	1169	482	438	Th
UE-25 WT-7	546148.2	4075461	1197	491	421	Tv
UE-29 a#2 (250-355 m)	555753.3	4088351	1215	422	29	Th
UE-29 a#2 (87-213 m)	555753.3	4088351	1215	422	28	Th
USW G-2	548138.6	4082554	1554	1831	534	Th/Tct
USW G-4	548938.0	4078590	1270	915	541	Tct
USW H-1 (572-687 m)	548721.8	4079944	1303	1829	572	Tcp
USW H-1 (687-1829 m)	548721.8	4079944	1303	1829	572	Tcb
USW H-3	547537.0	4075762	1483	1219	751	Tct
USW H-4	549195.0	4077322	1249	1219	519	Tcb/Tct
USW H-5	547665.5	4078838	1477	1219	704	Tcb/Tct
USW H-6 (525-1220 m)	546196.1	4077816	1302	1220	526	Tcb/Tct
USW H-6 (600-650 m)	546196.1	4077816	1302	1220	526	Tcb/Tct
USW H-6 (753-835 m)	546196.1	4077816	1302	1220	526	Tcb/Tct
USW VH-1	539986.2	4071718	963	762	184	Tcb
USW VH-2	537737.6	4073222	974	1219	164	Tv
USW WT-10	545976.0	4073389	1123	431	347	Tpt

Data source: Oliver and Root (1997, attached file yucca.xls)

Table 24 continued

[1] Aquifer – Geologic unit from which water was obtained (Oliver and Root 1997, p. 5)

Qal	Quaternary alluvium
Qtal	Quaternary-Tertiary alluvium
Tv	Tertiary volcanic rocks
Tpt	Tertiary Topopah Spring Member of Paintbrush Tuff
Tct	Tertiary Crater Flat Tuff
Th	Tertiary Tuffaceous beds of Calico Hills
Tcb	Tertiary Bullfrog Member of Crater Flat Tuff

Table 25. Background $^{36}Cl/Cl$ in Precipitation at Yucca Mountain

Field site	Sample identifier	Depth or age	$^{36}Cl/Cl \times 10^{-15}$
Midway Valley soil pits		*Depth (m)*	
UE-25 MWV-P2	ST033	1.9	494 ± 16
	ST034	2.0	470 ± 16
	ST035	2.1	490 ± 10
UE-25 MWV-P6	ST078	3.1	458 ± 12
	ST079	2.75	462 ± 7
UE-25 MWV-P13	ST080	3.0	459 ± 15
	ST081	2.55	475 ± 14
UE-25 MWV-P23	ST084	2.6	483 ± 11
	ST085	2.3	459 ± 11
UE-25 MWV-P24	ST086	2.9	466 ± 11
	ST087	2.5	524 ± 10
UE-25 NRSF-TP-16	ST088	2.4	466 ± 9
	ST089	2.2	468 ± 13
Alluvium from boreholes		*Depth (m)*	
UZN#39	R502	12.5	515 ± 24
	R504	18.1	557 ± 29
UZ-N54	R006	4.9	526 ± 22
	R007	5.9	501 ± 21
	R008	7.3	507 ± 14
	R009	8.0	474 ± 13
UZ-14	R413	3.7	497 ± 16
	R414	4.2	526 ± 13
	R415	5.5	549 ± 18
	R417	7.6	429 ± 16
	R418	9.1	479 ± 11
UZ#16	R167	3.7	526 ± 16
	R168	4.2	500 ± 15
	R169	5.0	528 ± 24
	R170	5.5	750 ± 35
	R171	6.1	494 ± 21
	R172	6.6	538 ± 24
	R173	7.1	601 ± 26
	R174	7.7	507 ± 26
Fossil packrat urine		*^{14}C age (ka)*	
Owl Canyon	PM-035	0.69	514 ± 16
	PM-039	1.65	518 ± 43
	PM-038	3.12	443 ± 21
	PM-034	3.96	442 ± 15
	PM-040	4.00	438 ± 15
	PM-036	6.70	505 ± 31
	PM-037	9.31	510 ± 48
Unweighted average, 39 samples			*501 ± 54*

Data sources: DTN: LAJF831222AQ95.006 (Midway Valley soil pits), LAJF831222AQ96.006 (MWV-P2), LAJF831222AQ96.008 (UZ-N39), LAJF831222AQ96.010 (UZ-N37), LAJF831222AQ96.012 (UZ-N54), LAJF831222AQ96.014 (UZ#16), LAJF831222AQ96.015 (UZ-14), LAJF831222AQ97.002 (packrat middens), and GS960308315131.001 (^{14}C dates for Owl Canyon samples).

Note: Corroborative data provided by Little Skull Mountain fossil packrat urine samples: PM-002, ^{14}C age = 1.09 ka, $^{36}Cl/Cl$ = 516 (± 19) x 10^{-15}; PM004, ^{14}C age = 6.68 ka, $^{36}Cl/Cl$ = 509 (± 16) x 10^{-15} (DTN: GS950708315131.003 and LAJF831222AQ97.002)
ka – thousand years

Table 26. Chloride Concentrations and Infiltration Rates calculated for Tunnel Pore Waters by the Chloride Mass Balance Method

Borehole	Tunnel	Tunnel distance (m)	Hydrologic unit[1]	Stratigraphic unit[1]	mg/L Cl	Apparent infiltration rate[2], mm/yr	
						Rate 1	Rate 2
ECRB-SYS-CS150	Cross Drift	150	TSw	Tptpul	25.0	2.4	4.1
ECRB-SYS-CS200	Cross Drift	200	TSw	Tptpul	19.1	3.1	5.3
ECRB-SYS-CS200	Cross Drift	200	TSw	Tptpul	19.2	3.1	5.3
ECRB-SYS-CS400	Cross Drift	400	TSw	Tptpul	11.8	5.0	8.6
ECRB-SYS-CS450	Cross Drift	450	TSw	Tptpul	33.6	1.8	3.0
ECRB-SYS-CS550	Cross Drift	550	TSw	Tptpul	20.2	2.9	5.0
ECRB-SYS-CS600	Cross Drift	600	TSw	Tptpul	17.9	3.3	5.7
ECRB-SYS-CS650	Cross Drift	650	TSw	Tptpul	16.0	3.7	6.4
ECRB-SYS-CS750	Cross Drift	750	TSw	Tptpul	24.6	2.4	4.2
ECRB-SYS-CS800	Cross Drift	800	TSw	Tptpul	15.0	4.0	6.8
ECRB-SYS-CS850	Cross Drift	850	TSw	Tptpul	26.3	2.3	3.9
ECRB-SYS-CS900	Cross Drift	900	TSw	Tptpul	24.9	2.4	4.1
ECRB-SYS-CS950	Cross Drift	950	TSw	Tptpul	24.9	2.4	4.1
ECRB-SYS-CS1000	Cross Drift	1000	TSw	Tptpul	36.6	1.6	2.8
ECRB-SYS-CS1050	Cross Drift	1050	TSw	Tptpmn	16.6	3.6	6.1
ECRB-SYS-CS1550	Cross Drift	1550	TSw	Tptpll	37.7	1.6	2.7
ECRB-SYS-CS1600	Cross Drift	1600	TSw	Tptpll	31.3	1.9	3.3
ECRB-SYS-CS1650	Cross Drift	1650	TSw	Tptpll	16.5	3.6	6.2
ECRB-SYS-CS1750	Cross Drift	1750	TSw	Tptpll	12.9	4.6	7.9
ECRB-SYS-CS1950	Cross Drift	1950	TSw	Tptpll	14.3	4.2	7.1
ECRB-SYS-CS2000	Cross Drift	2000	TSw	Tptpll	22.4	2.7	4.6
ECRB-SYS-CS2100	Cross Drift	2100	TSw	Tptpll	17.0	3.5	6.0
ECRB-SYS-CS2150	Cross Drift	2150	TSw	Tptpll	16.4	3.6	6.2
ECRB-SYS-CS2300	Cross Drift	2300	TSw	Tptpll	21.0	2.8	4.9
ESF-NR-MOISTSTDY#1a	ESF	727	TCw	Tpcplnc	19.7	3.0	5.2
ESF-NR-MOISTSTDY#2	ESF	750	TCw	Tpcplnc/mw	18.4	3.2	5.5
ESF/CS/07+57.53	ESF	758	PTn	Unknown	34.2	1.7	3.0
ESF-AL#3-RBT#1 32.1/UP	ESF Alcove 3	758	PTn	Unknown	40.9	1.5	2.5
ESF-NR-MOISTSTDY#3	ESF	770	TCw	Tpcplnc/mw	40.3	1.5	2.5
ESF-NR-MOISTSTDY#4	ESF	772	PTn	Tpcpv2	47.1	1.3	2.2
ESF-NR-MOISTSTDY#5	ESF	783	PTn	Tpcpv2	27.9	2.1	3.7
ESF-NR-MOISTSTDY#6	ESF	821	PTn	Tpcpv1	69.2	0.9	1.5
ESF-NR-MOISTSTDY#7	ESF	867	PTn	Tpbt4	15.1	3.9	6.8
ESF-NR-MOISTSTDY#8	ESF	870	PTn	Tpy	15.7	3.8	6.5
ESF-NR-MOISTSTDY#9	ESF	873	PTn	Tpbt3	5.7	10.4	17.9
ESF-NR-MOISTSTDY#10	ESF	880	PTn	Tpbt3	15.0	4.0	6.8
ESF-NR-MOISTSTDY#11	ESF	892	PTn	Tpp	6.7	8.9	15.2
ESF-NR-MOISTSTDY#13	ESF	1008	PTn	Tpbt2	12.0	5.0	8.5
ESF-NR-MOISTSTDY#15	ESF	1054	PTn	Tptrv3/rv2	20.8	2.9	4.9
ESF-NR-MOISTSTDY#16	ESF	1069	TSw	Tptrv2	12.9	4.6	7.9
ESF-LPCA-MOISTSTDY#2	ESF Alcove 4	1130	PTn	Tpbt2/argillic	17.7	3.4	5.8
ESF-LPCA-MOISTSTDY#3	ESF Alcove 4	1130	PTn	Tpbt2	17.5	3.4	5.8
ESF-HD-PERM-3	ESF Alcove 5	~2800	TSw	Unknown	111.0	0.5	0.9
ESF-HD-PERM-3	ESF Alcove 5	~2800	TSw	Unknown	133.0	0.4	0.8
ESF-MD-NICHE3566#1	ESF	3566	TSw	Tptpmn	15.7	3.8	6.5
ESF-MD-NICHE3566LT#1	ESF	3566	TSw	Tptpmn	27.5	2.2	3.7

Table 26. Chloride Concentrations and Infiltration Rates calculated for Tunnel Pore Waters by the Chloride Mass Balance Method

Borehole	Tunnel	Tunnel distance (m)	Hydrologic unit[1]	Stratigraphic unit[1]	mg/L Cl	Apparent infiltration rate[2], mm/yr	
						Rate 1	Rate 2
ESF-MD-NICHE3650#6	ESF	3650	TSw	Tptpmn	15.9	3.7	6.4
ESF-MD-NICHE3650#7	ESF	3650	TSw	Tptpmn	32.3	1.8	3.2
ESF-SR-MOISTSTDY#10	ESF	6648	TSw	Tptrv2	15.3	3.9	6.7
ESF-SR-MOISTSTDY#11	ESF	6658	PTn	Tptrv3	26.5	2.2	3.8
ESF-SR-MOISTSTDY#12	ESF	6668	PTn	Tpbt2	29.7	2.0	3.4
ESF-SR-MOISTSTDY#13	ESF	6679	PTn	Tpbt2	32.2	1.8	3.2
ESF-SR-MOISTSTDY#14	ESF	6696	PTn	Tpbt4	33.0	1.8	3.1
ESF-SR-MOISTSTDY#15	ESF	6704	PTn	Tpcpv1	26.8	2.2	3.8
ESF-SR-MOISTSTDY#16	ESF	6721	PTn	Tpcpv1	39.1	1.5	2.6
ESF-SR-MOISTSTDY#17	ESF	6729	TCw/PTn	Tpcplnc/Tpcpv1	55.3	1.1	1.8
ESF-SR-MOISTSTDY#19	ESF	6826	TSw	Tptpul	17.1	3.5	6.0
ESF-SR-MOISTSTDY#21	ESF	7054	PTn	Tpbt2	80.9	0.7	1.3
ESF-SR-MOISTSTDY#22	ESF	7056	PTn	Tpbt2	103.0	0.6	1.0
ESF-SR-MOISTSTDY#22r	ESF	7056	PTn	Tpbt2	96.1	0.6	1.1
ESF-SR-MOISTSTDY#27	ESF	7444	TSw	Tptrv1	38.9	1.5	2.6
ESF-SR-MOISTSTDY#28	ESF	7446	TSw	Tptrv2	43.2	1.4	2.4
ESF-SR-MOISTSTDY#29	ESF	7453	PTn	Tptrv3	63.2	0.9	1.6
ESF-SR-MOISTSTDY#30	ESF	7460	PTn	Tpbt2	107.6	0.6	0.9
ESF-SR-MOISTSTDY#31	ESF	7465	PTn	Tpbt2	97.6	0.6	1.0
ESF-SR-MOISTSTDY#32	ESF	7472	PTn	Tpbt2	72.4	0.8	1.4
ESF-SR-MOISTSTDY#33	ESF	7477	PTn	Tpbt2	87.3	0.7	1.2
ESF-SR-MOISTSTDY#34	ESF	7481	PTn	Tpp	85.1	0.7	1.2
ESF-SR-MOISTSTDY#35	ESF	7488	PTn	Tpbt3	72.2	0.8	1.4
ESF-SR-MOISTSTDY#36	ESF	7490	PTn	Tpbt3	54.0	1.1	1.9
ESF-SR-MOISTSTDY#37	ESF	7498	PTn	Tpbt4	83.4	0.7	1.2
ESF-SR-MOISTSTDY#38	ESF	7503	PTn	Tpbt4	74.6	0.8	1.4
ESF-SR-MOISTSTDY#39	ESF	7504	PTn	Tpcpv1	85.0	0.7	1.2
UZTT-BB-PH1-2	Busted Butte	NA	CHn	Below Tptpv1/Tac	70.6	0.8	1.4
UZTT-BB-PH1-3	Busted Butte	NA	CHn	Tptpv1	51.2	1.2	2.0
UZTT-BB-PH1-4	Busted Butte	NA	CHn	Tac	64.6	0.9	1.6
UZTT-BB-PH1-6	Busted Butte	NA	CHn	Tptpv2/pv1	36.7	1.6	2.8
UZTT-BB-PH1-7	Busted Butte	NA	CHn	Tptpv2	25.6	2.3	4.0

Source for pore-water chloride data: DTN: GS961108312261.006, LA9909JF831222.004, LA9909JF831222.010, and LA9909JF831222.012.

Relevant assumptions from Table 2: 1, 2 (TBV), 3, 19 (TBV), 20 (TBV) and 21 (TBV).

[1] Hydrogeologic unit and lithostratigraphic unit nomenclature from Table 1. Cross Drift lithostratigraphic contacts from DTN: GS981108314224.005.

[2] The CMB method for estimating infiltration is discussed in section 6.9.1. Rates 1 and 2 assume average annual precipitation of 170 mm with average chloride concentrations of 0.35 mg/L and 0.6 mg/L, respectively.

Table 27. Apparent Infiltration Rates Calculated From Pore-water Chloride Concentrations at Yucca Mountain

Borehole location	Topographic category[1]	Sample stratigraphy	Average chloride concentration[2], mg/L	Apparent infiltration rate[3], mm/yr	
				Rate 1	Rate 2
UZ#4	A	PTn	104	0.6	1.0
UZ#5	A	PTn	42	1.4	2.4
UZ-N37	A	Alluvium	133	0.4	0.8
UZ-N54	A	Alluvium	7400	0.01	0.01
UZ-14	A	Alluvium	520	0.1	0.2
UZ-14	A	PTn	245	0.2	0.4
UZ#16	A	Alluvium	3700	0.02	0.03
UZ#16	A	PTn	32	1.8	3.1
NRG-6	A	PTn	185	0.3	0.6
SD-9	A	PTn	170	0.4	0.6
NRG-7a	B	PTn	39	1.5	2.6
SD-12	B	PTn	50	1.2	2.1
SD-7	C	PTn	77	0.8	1.3
ESF North Ramp (16 samples)	C	PTn	23	8	14
ESF South Ramp (31 samples)	C	PTn	64	1.2	2.1
ESF Main Drift (6 samples)	C	TSw	20	7	12
Cross Drift (24 samples)	C	TSw	22	5	9

Sources for chloride data: DTN: LA0002JF831222.001 (alluvial samples), LA0002JF831222.002 (PTn samples), and Table 26 (ESF and Cross Drift samples)

Relevant assumptions from Table 2: 1, 2 (TBV), 3, 19 (TBV), 20 (TBV) and 21 (TBV).

[1] Topographic categories for borehole locations
A - Beneath deep alluvium (center of large wash, soil > 3 m thick)
B - Terrace (side of large wash or near base of sideslope, soil 0.5 to 3 m)
C - Beneath thin alluvium (ridgetop or sideslope, soil < 0.5 m thick)

[2] The average concentration for alluvial samples includes data only for samples below 5 meters, in order to ensure that the samples lie below the zone of evapotranspiration. Concentrations for PTn samples from surface-based boreholes are reported for the shallowmost PTn sample in each borehole because this sample is more likely to be representative of vertical infiltration at the borehole location than are deeper PTn samples, which are more likely to be affected by mixing with water transported laterally from adjacent zones.

[3] The CMB method for estimating infiltration is discussed in section 6.9.1. Rates 1 and 2 assume average annual precipitation of 170 mm with average chloride concentrations of 0.35 mg/L and 0.6 mg/L, respectively.

Table 28. Estimates of Growth Rates For Opal Hemispheres On Calcite Blade Tips From Sample HD2074 (ESF station 30+50.7)[1]

Measured ^{230}Th/U age, in Ma	Total duration of growth[2], in Ma	Estimated thickness[3], in mm	Growth rate[4], in mm/Ma
Microdigestions			
0.004	0.008	0.01	1.3
0.004	0.008	0.05	6.3
0.012	0.024	0.01	0.4
0.012	0.024	0.05	2.1
Whole hemispheres			
0.15	0.3	0.7	2.3
0.15	0.3	1.3	4.3
0.23	0.46	0.7	1.5
0.23	0.46	1.3	2.8

Data sources: DTN: GS960908315215.014 and GS980908315215.015

Relevant assumption from Table 2: 25

Notes:
[1] Rates are based on ranges of measured ages and ranges in estimated layer thicknesses from both whole hemispheres and microdigestions of hemisphere outer layers.
[2] Total duration of growth equals twice the measured age. Assumes the measured age represents an average between the oldest and youngest layers with a zero-age outermost layer.
[3] Thicknesses are not available for individual analyses. Values represent the typical range expected.
[4] Growth rates represent estimated thickness divided by total duration of growth.

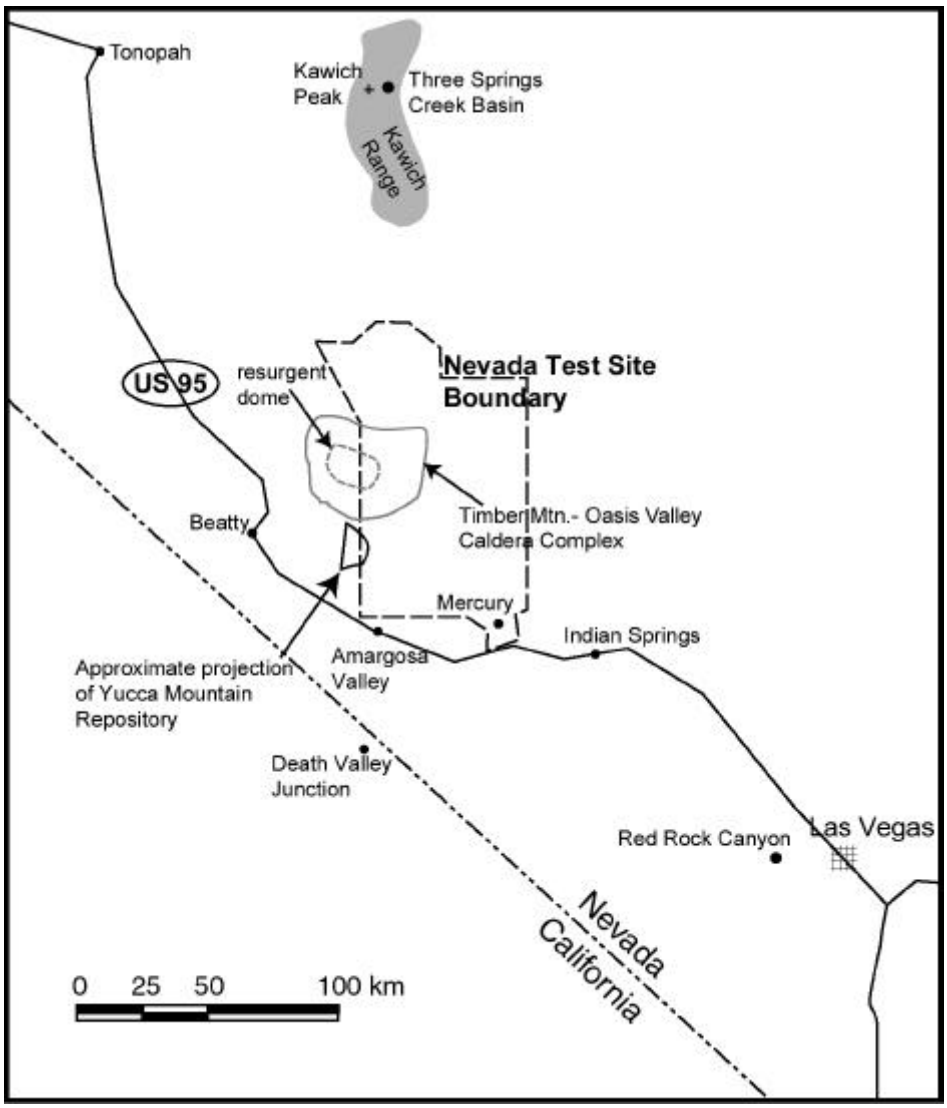

Figure 1. Regional map showing Yucca Mountain and vicinity

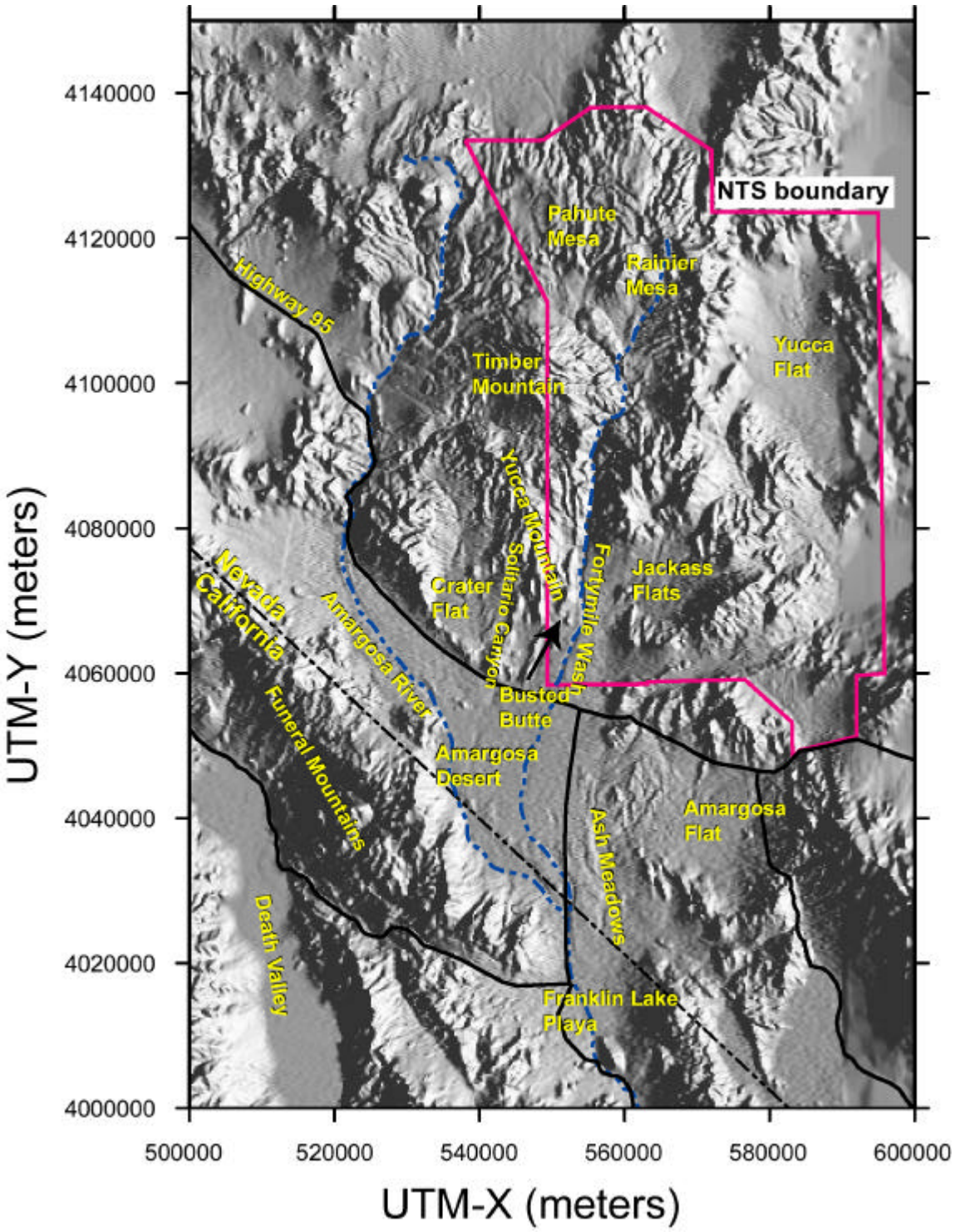

Figure 2. Regional map showing important physiographic features

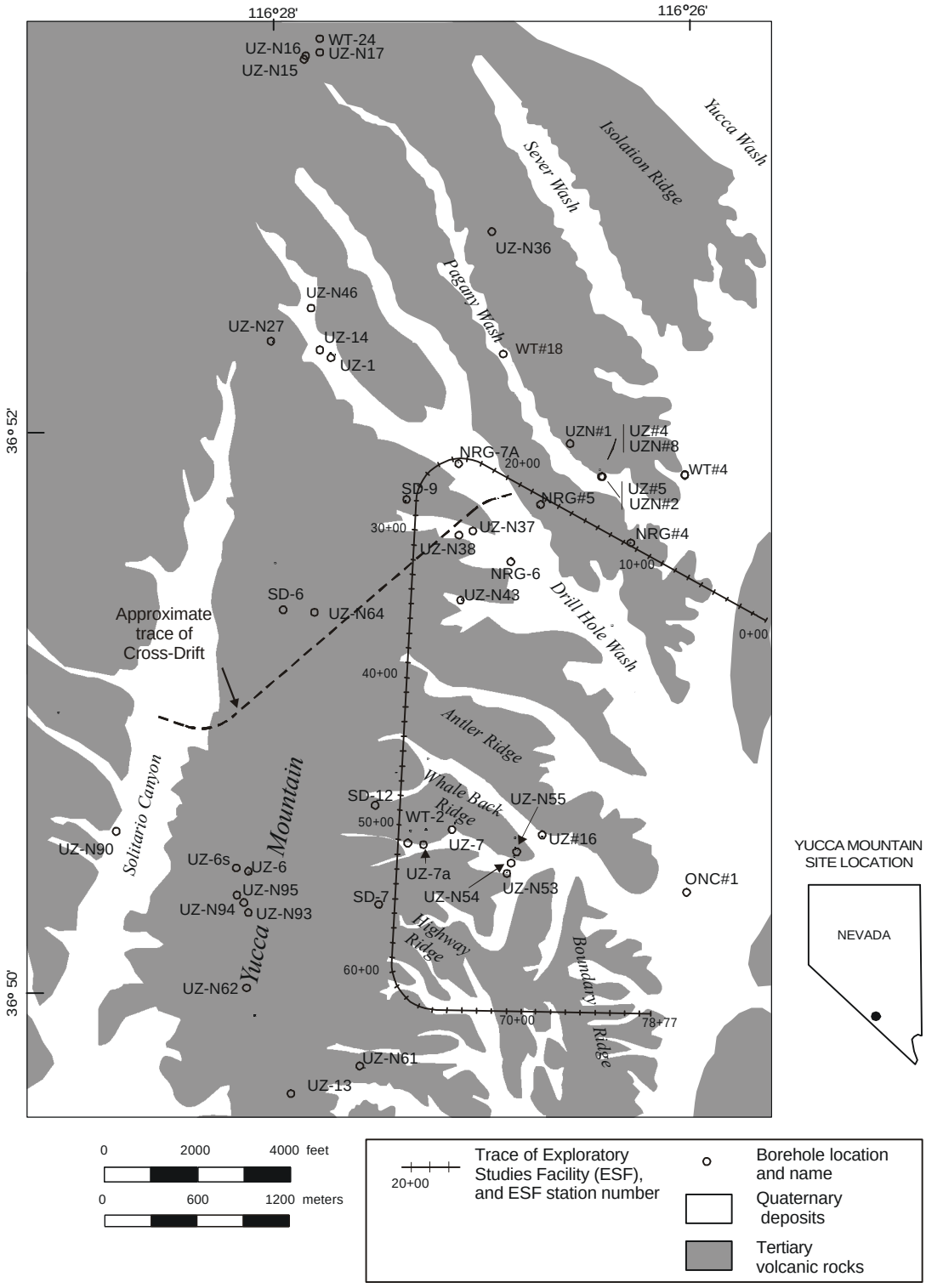

Figure 3. YMP boreholes.

Note: This map shows the locations of surface-based boreholes for which isotopic and geochemical data are available for water and gas samples (Table 3). Boreholes that are not shown because they are outside the map area are UZ-N11, UZN#39 and UZN#91.

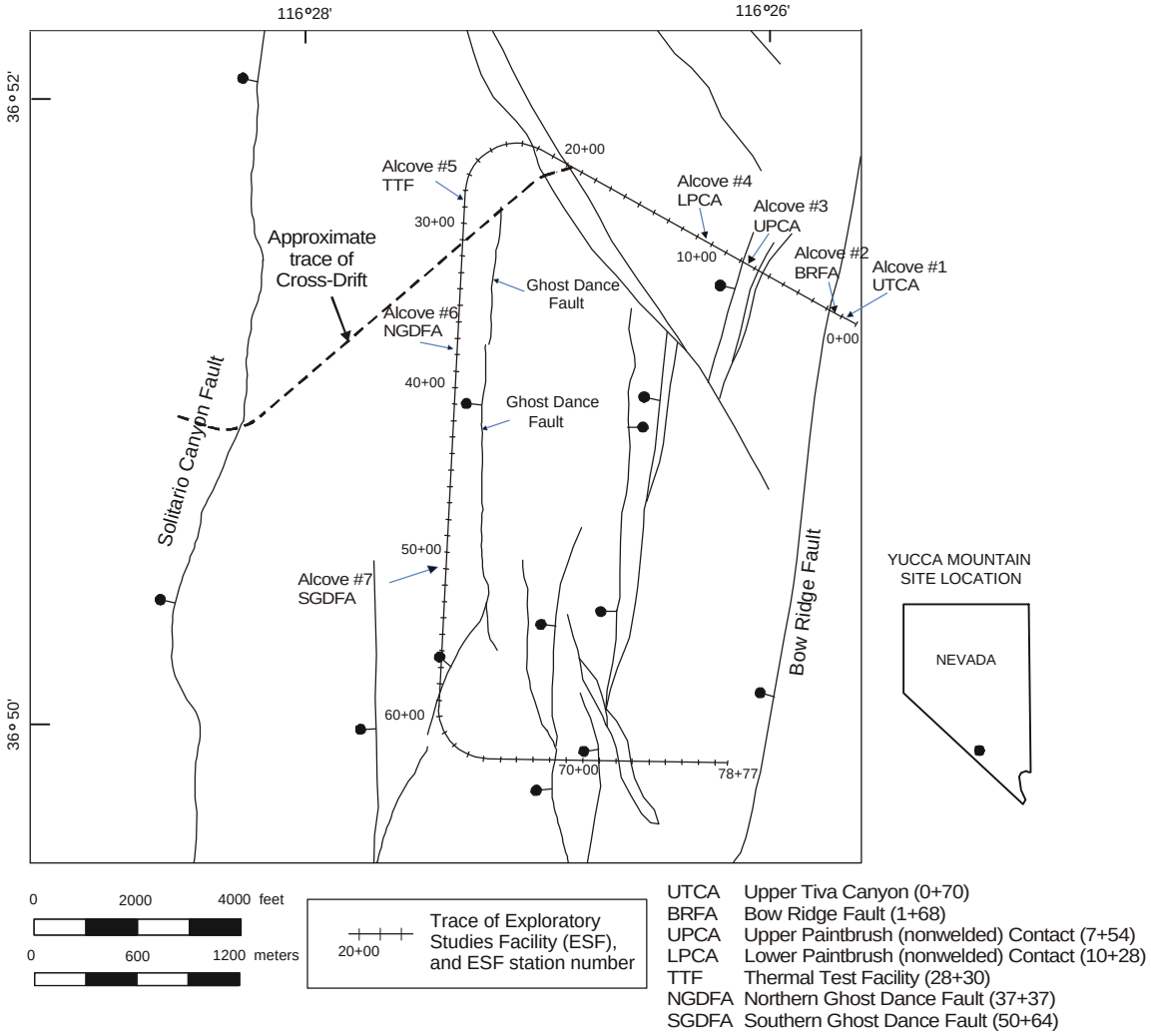

Figure 4. Locations of ESF test alcoves

Note: Alcove locations are shown relative to faults mapped at the surface by Day et al. (1996, Plate 1). Not all faults on that map are shown here.

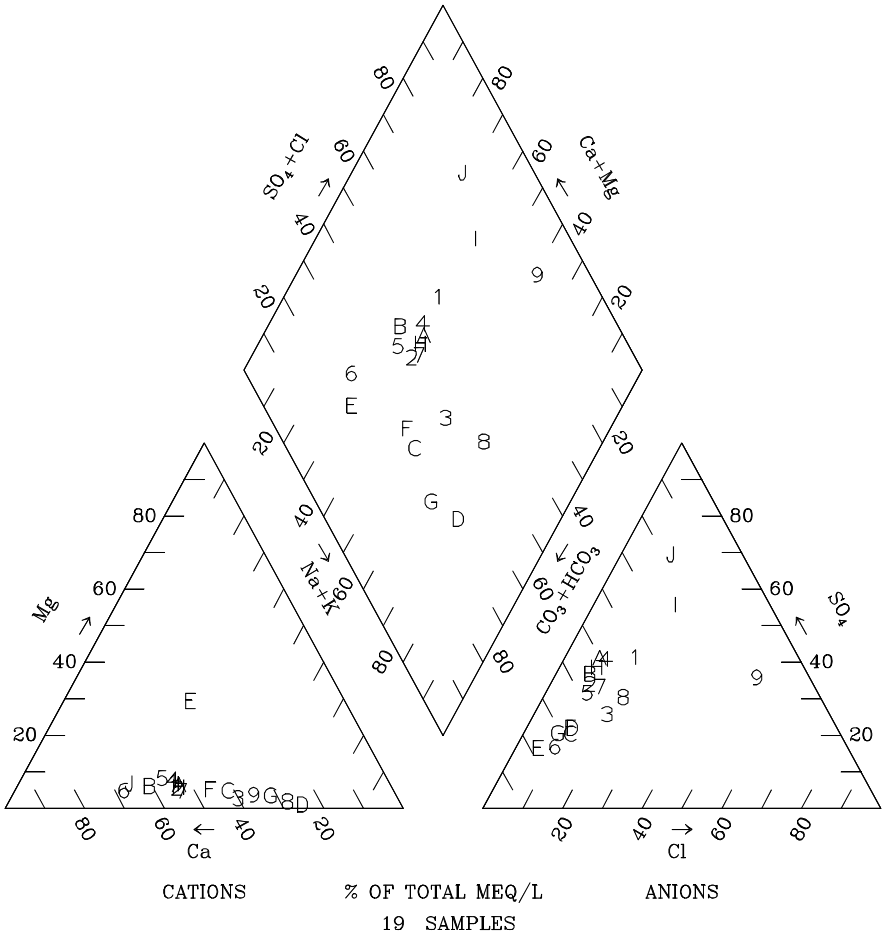

Legend	
Points	**Sample Location**
1-9, A-B	3 Springs Creek
C-J	Kawich Peak

Figure 5. Trilinear diagram for precipitation from the Kawich Range, Nevada.

Note: Data sources are DTN: MO0005CL3SPRGS.000, MO0005CLKAWICH.000, GS930108315214.004, and GS930908315214.030.

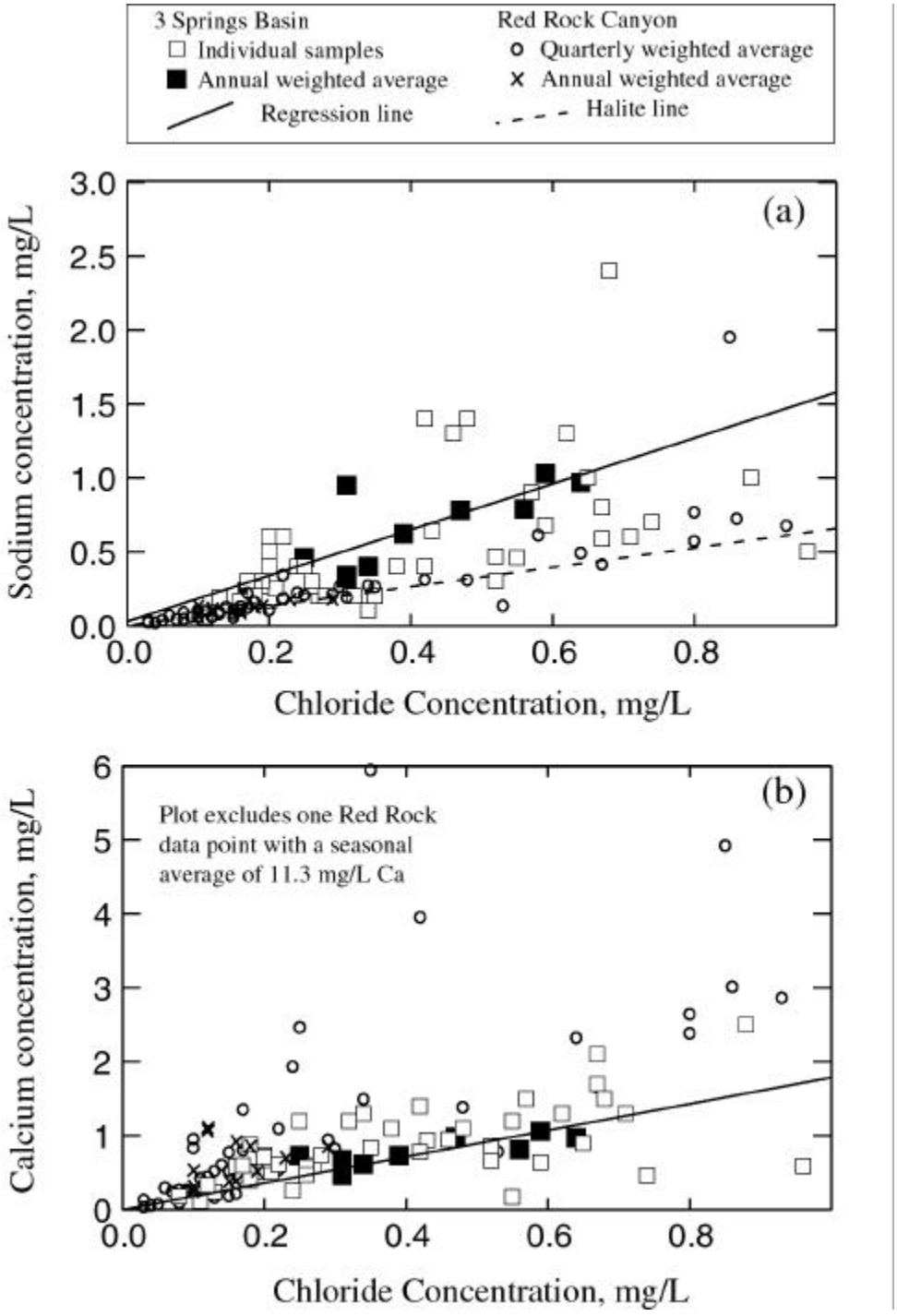

Figure 6. Constituents Plotted versus Chloride for Precipitation Samples.

Note: Samples are from 3 Springs Basin and Red Rock Canyon, Nevada. Chloride versus: (a) Sodium, (b) calcium, (c) sulfate, (d) bicarbonate, and (e) silica. Data for 3 Springs Basin are from DTN: MO0005CL3SPRGS.000, MO0005CLKAWICH.000, GS930108315214.004, and GS930908315214.030. Data for Red Rock Canyon are reported in DTN: LA0003JF12213U.001. Only data with Cl concentrations less than 1 mg/L have been included in this figure. Regression lines for 3 Springs Basin data are from Table 5. The "halite line" on plot (a) is based on a 1:1 molar ratio of sodium to chloride in order to show the trend for halite dissolution.

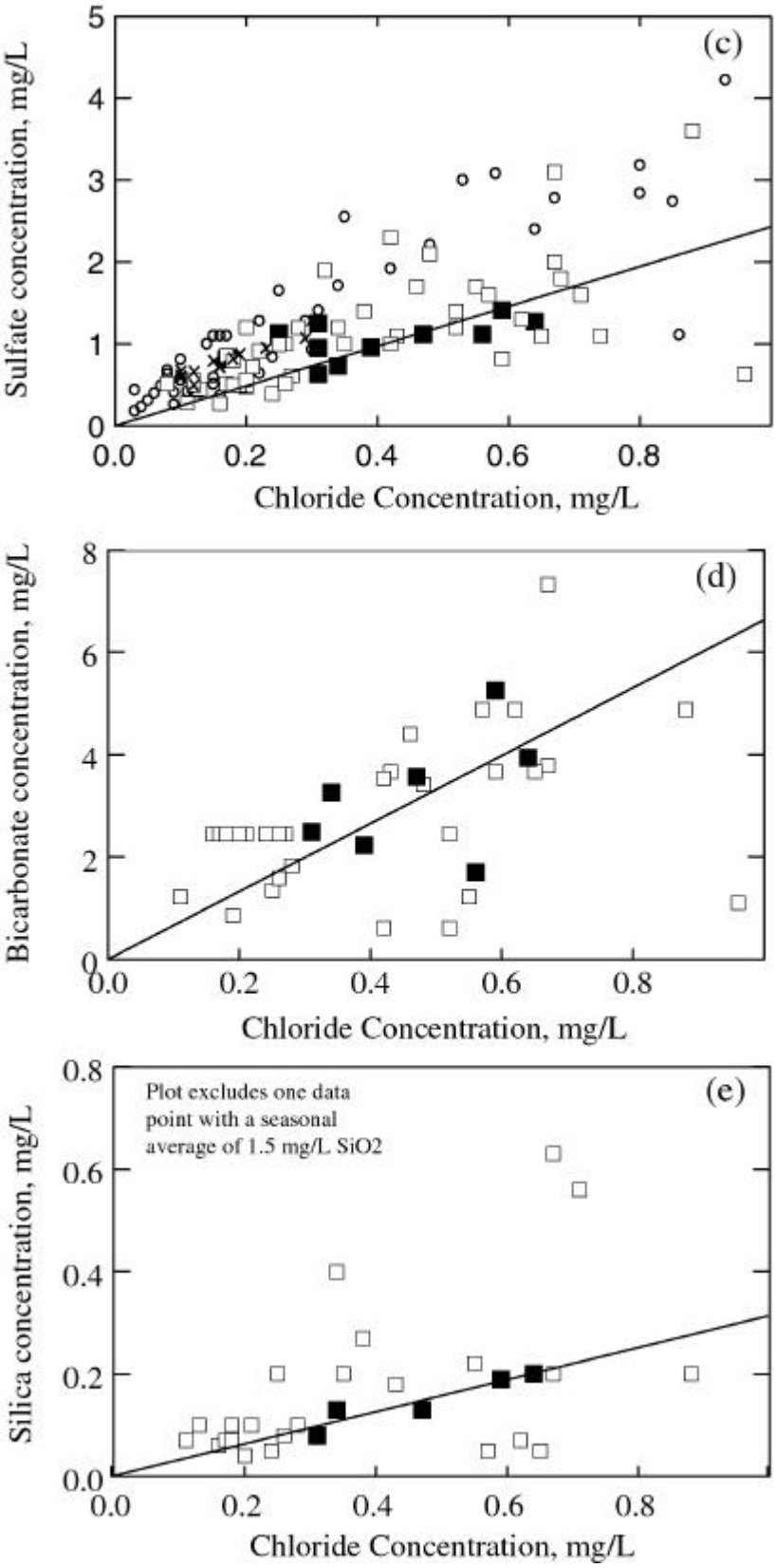

Figure 6. (continued)

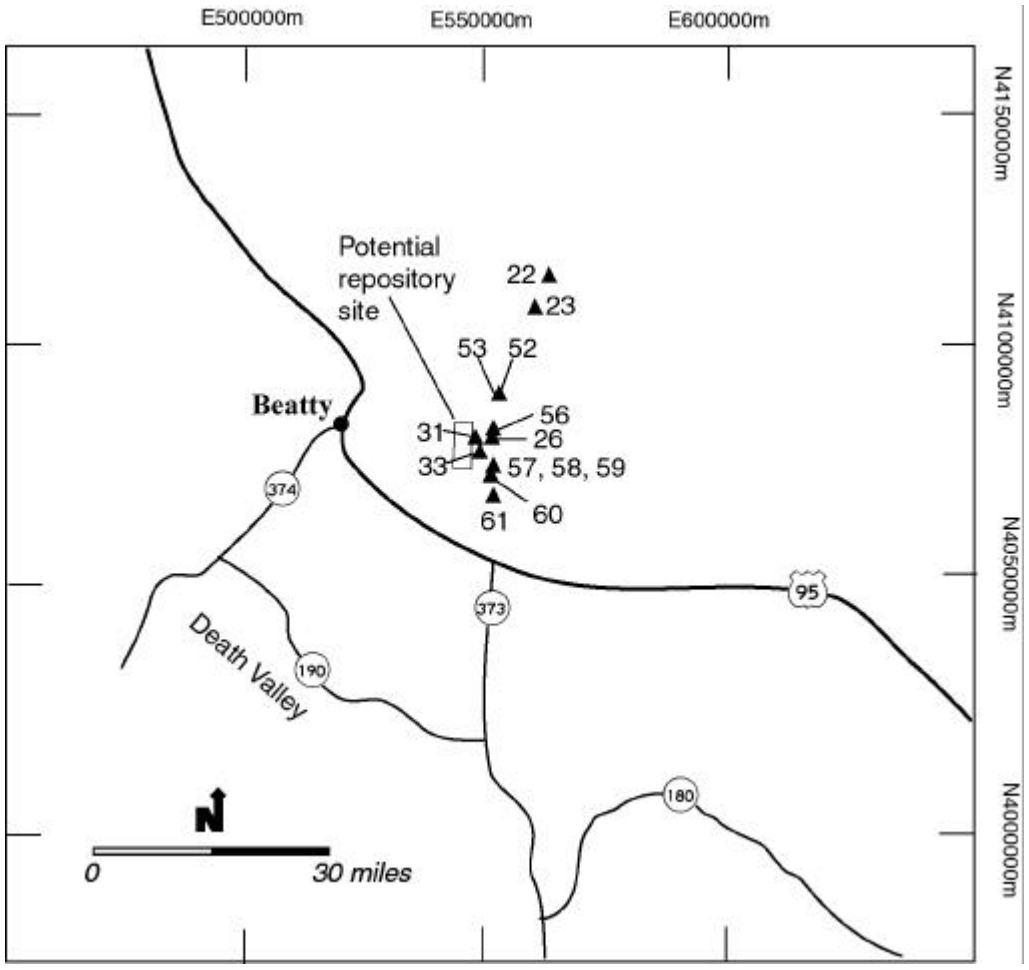

Figure 7. Surface Water Collection Sites.

Note: Surface water quality data collection sites in the vicinity of Yucca Mountain, Mountain, Nevada. Site numbers are identified on the legend of Figure 8.

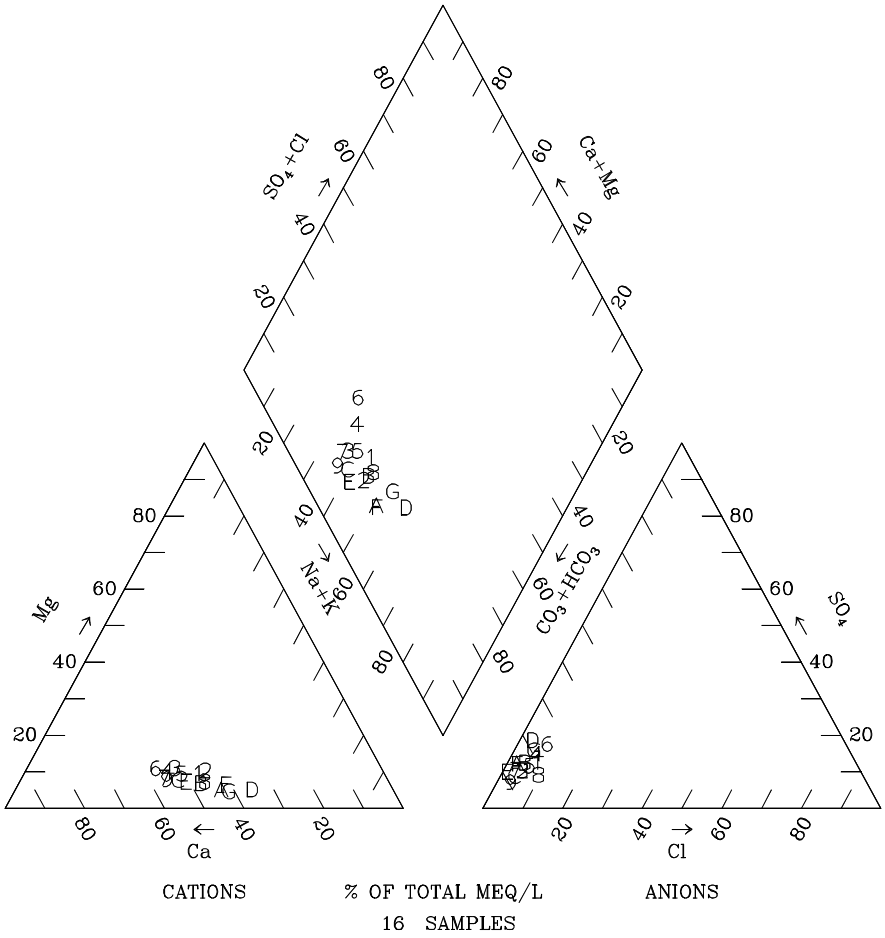

Legend			
List of Plotted Points, Sample Locations and Site Numbers as Listed on Figure 7			
1-2	Tributary to Stockade Wash (22)	B	Wren Wash (31)
3	Stockade Wash (23)	C	Split Wash (33)
4-5	Pah Canyon (52)	D	Drillhole Wash (58)
6	Overland flow near Pah Canyon (53)	E	Fortymile Wash at H-Road (59)
7	Overland flow in Fortymile Canyon (56)	F	Busted Butte Wash (60)
8-9	Yucca Wash (26)	G	Fortymile Wash at J-12 (61)
A	Fortymile Wash above Drillhole Wash (57)		

Figure 8. Trilinear Diagram for Surface Runoff from the Yucca Mountain Area.

Note: Sampling locations shown on Figure 7. Data sources for the plotted points are DTN: GS940308312133.002 (sample 4) and GS960308312133.001 (samples 5, 6, 7, 9, B and C); Emett et al. 1994, p. 550 (samples 1, 2, 3 and 8); and Perfect et al. 1995, file dataedit.wk1 (samples A, D, E, F, and G).

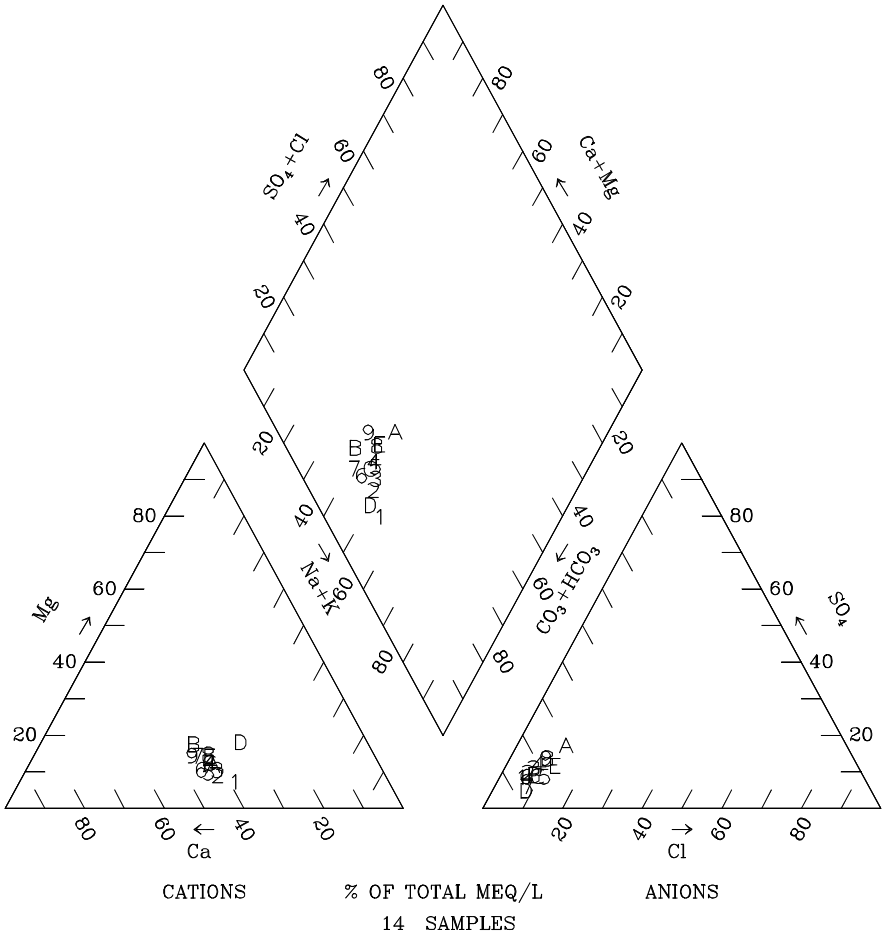

Legend			
List of Plotted Points and Sample Locations			
Stewart Basin, Toiyabe Range		*3 Springs Basin, Kawich Range*	
1-2	Veg Spring	7-8	3 Springs Creek near 3 Spring #3
3-4	East Stewart Creek	9, A	3 Springs Creek near Warm Springs
5-6	Hellebore Spring	B-C	3 Springs Creek near 3 Spring #2
		D-E	3 Springs Creek near Ledge Spring

Figure 9. Trilinear diagram for surface waters from 3 Springs Basin and Stewart Basin, Nevada.

Note: Data from DTN: MO0005CL3SPRGS.000, MO0005CLESTWRT.000, MO0005CLKAWICH.000, GS930108315214.004, and GS930908315214.030. Because of the relative constancy of the chemical compositions, only two data points are plotted for each location.

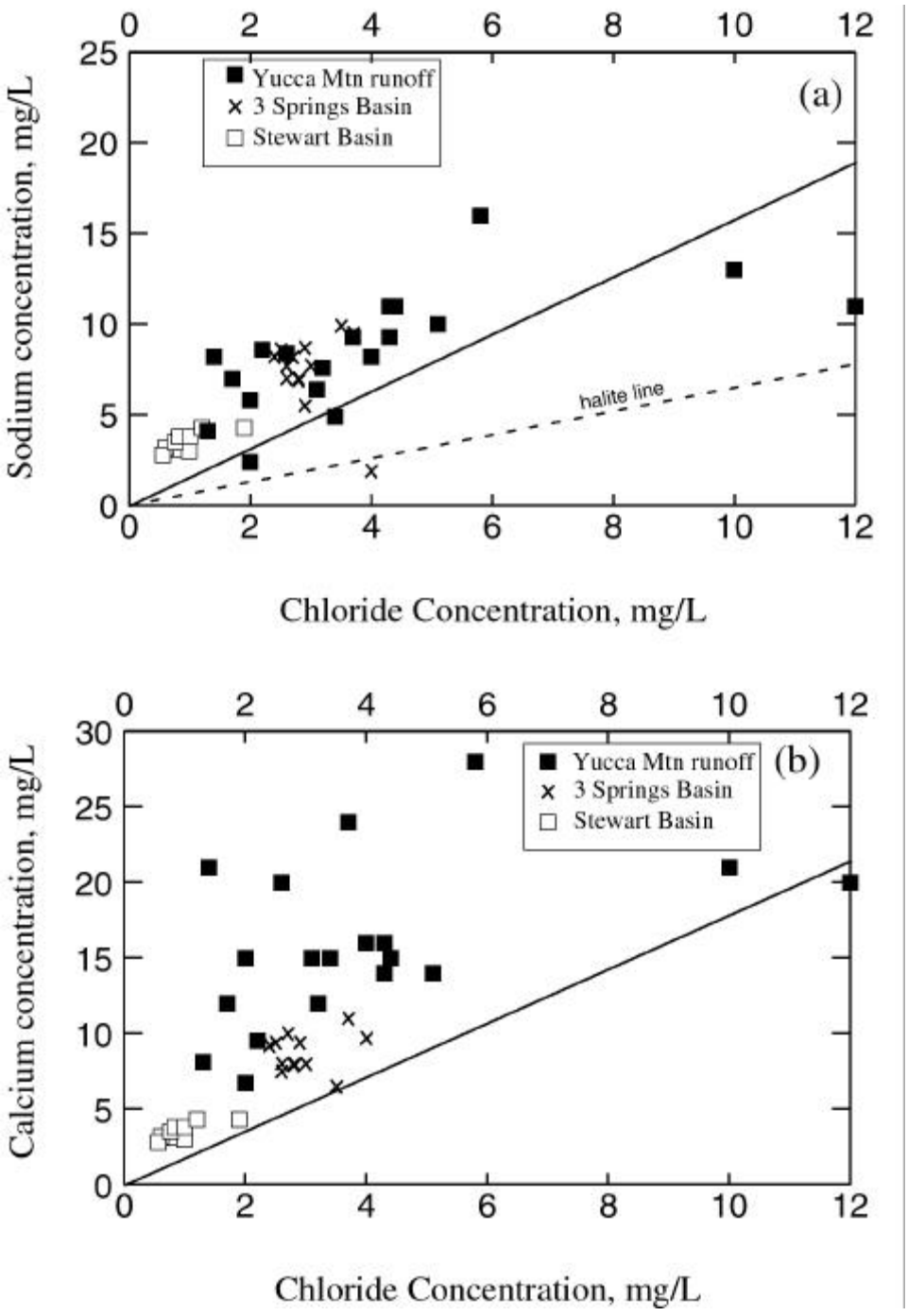

Figure 10. Constituents Plotted versus Chloride for Surface-Water and Runoff Samples.

Note: Surface-water and runoff samples are from Yucca Mountain, 3 Springs Basin, and Stewart Basin, Nevada. Chloride versus: (a) Sodium, (b) calcium, (c) sulfate, (d) bicarbonate, and (e) silica as SiO_2. Data from DTN: MO0005CL3SPRGS.000, MO0005CLESTWRT.000, MO0005CLKAWICH.000, GS930108315214.004, and GS930908315214.030, GS940308312133.002, and GS960308312133.001. Because of the constancy of their composition, only 3 data points are shown for each surface-water sampling location in 3 Springs Basin and Stewart Basin. Also shown are lines of best-fit to the 3 Springs Basin precipitation data, from Table 5. The "halite line" on plot (a) is based on a 1:1 molar ratio of sodium to chloride in order to show the trend for halite dissolution.

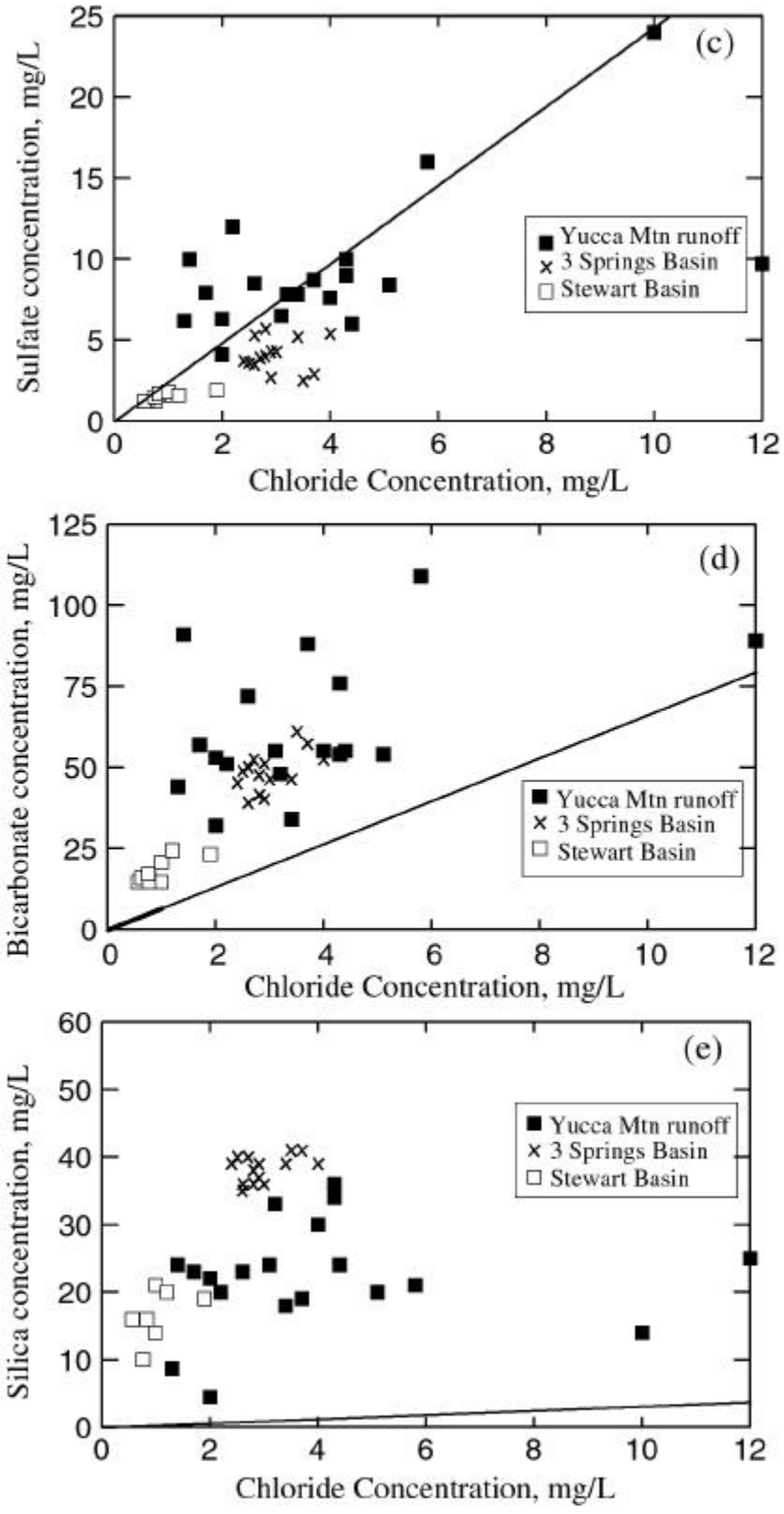

Figure 10. (continued)

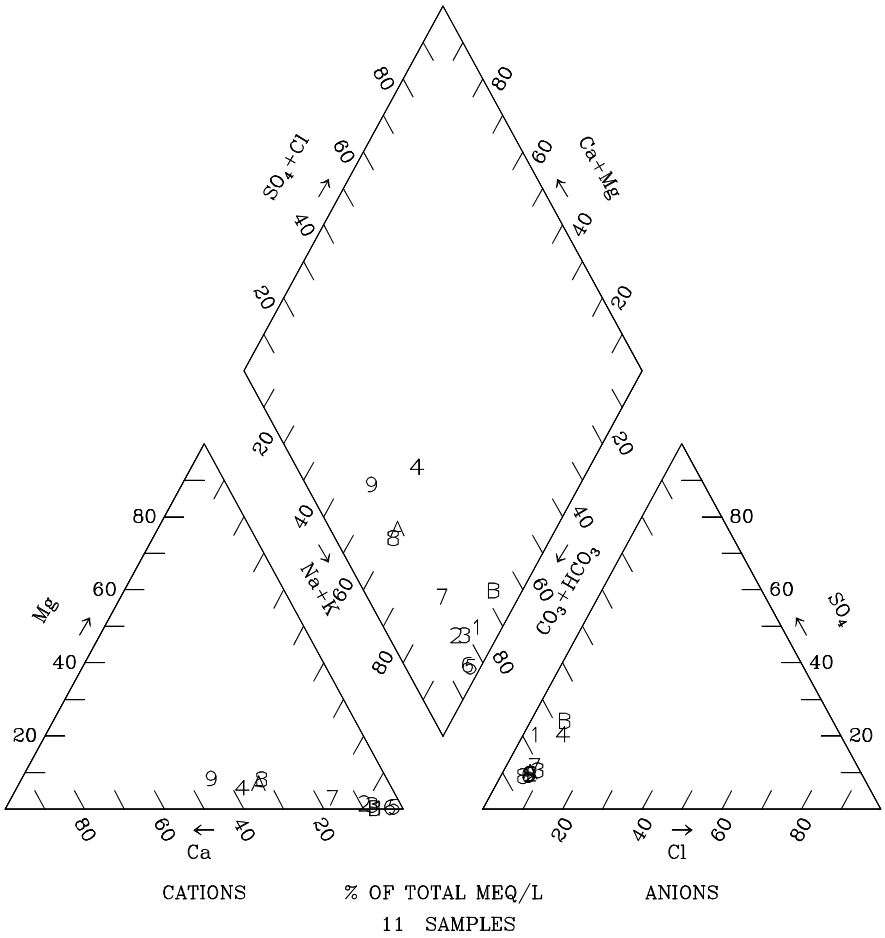

Legend

List of Plotted Points, Sample Identifiers as Listed on Figure 45, and Sample Site Names

1	131	Captain Jack Spring	7	143	Tunnel Seep, U-12t.03
2	132	Rainier Spring	8	144	Tunnel Seep, U-12t.03
3	133	Tunnel Seep, U-12e.06	9	145	Tunnel Seep, U-12t.03
4	134	Tunnel Seep, U-12n	A	146	Tunnel Seep, U-12t.04
5	135	Tunnel Seep, U-12n.03	B	206	Whiterock Spring
6	136	Tunnel Seep, U-12t			

Figure 11. Trilinear diagram for springs and seeps, Rainier Mesa, Nevada.

Note: Data from McKinley et al. (1991, Table 6). Location of sampling sites shown on Figure 45.

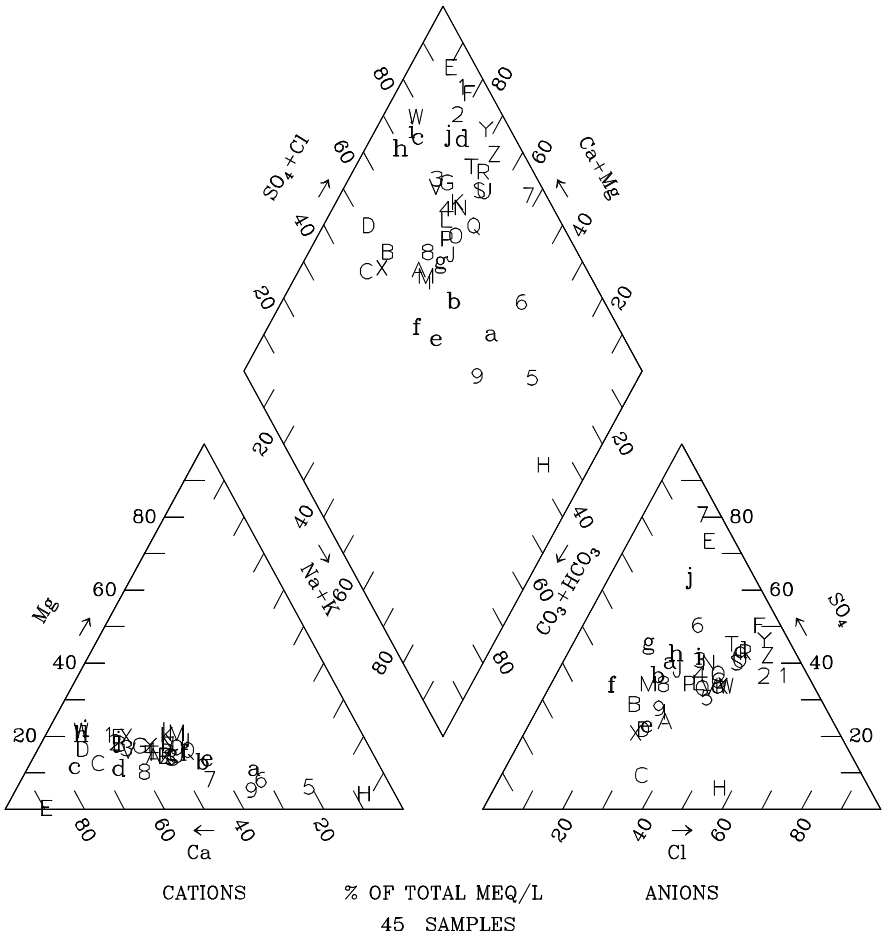

Legend

List of Plotted Points, Borehole Identifiers, and Tops of Sampled Intervals (feet)

1	NRG6-158.2	A	SD12-265.8	J	UZ14-91	S	UZ14-178.1	b	SD9-251.8
2	NRG6-160.8	B	SD12-278.6	K	UZ14-95.5	T	UZ14-215.7	c	UZN55-195.3
3	NRG6-171	C	SD12-296.1	L	UZ14-96.2	U	UZ14-225.9	d	UZN55-199.0
4	NRG6-175.6	D	SD7-339.7	M	UZ14-100.4	V	UZ14-235.1	e	SD6-430.3
5	NRG6-219.9	E	SD7-370.3	N	UZ14-114.8	W	UZ14-245.5	f	SD6-443.2
6	NRG6-244.6	F	SD9-94.2	O	UZ14-135.5	X	UZ#16-180.9	g	SD6-443.5
7	NRG6-255.9	G	SD9-154	P	UZ14-144.8	Y	SD9-114.1	h	UZ7a-203.3
8	NRG7A-165.8	H	UZ14-45	Q	UZ14-147.8	Z	SD9-135.1	i	UZ7a-220.2
9	NRG7A-258	I	UZ14-85.2	R	UZ14-177.6	a	SD9-176.2	j	UZ7a-241.4
								k	UZ14-240.8
								l	UZ#16-163.5

Figure 12. Trilinear Diagram for Pore Waters from the Nonwelded Paintbrush Tuff (PTn) Hydrogeologic Unit.

Note: The plotted data are listed in Table 6, and are reported in DTN: GS950608312272.001, GS961108312271.002, GS000608312271.001, GS970908312271.003, and GS981008312272.004.

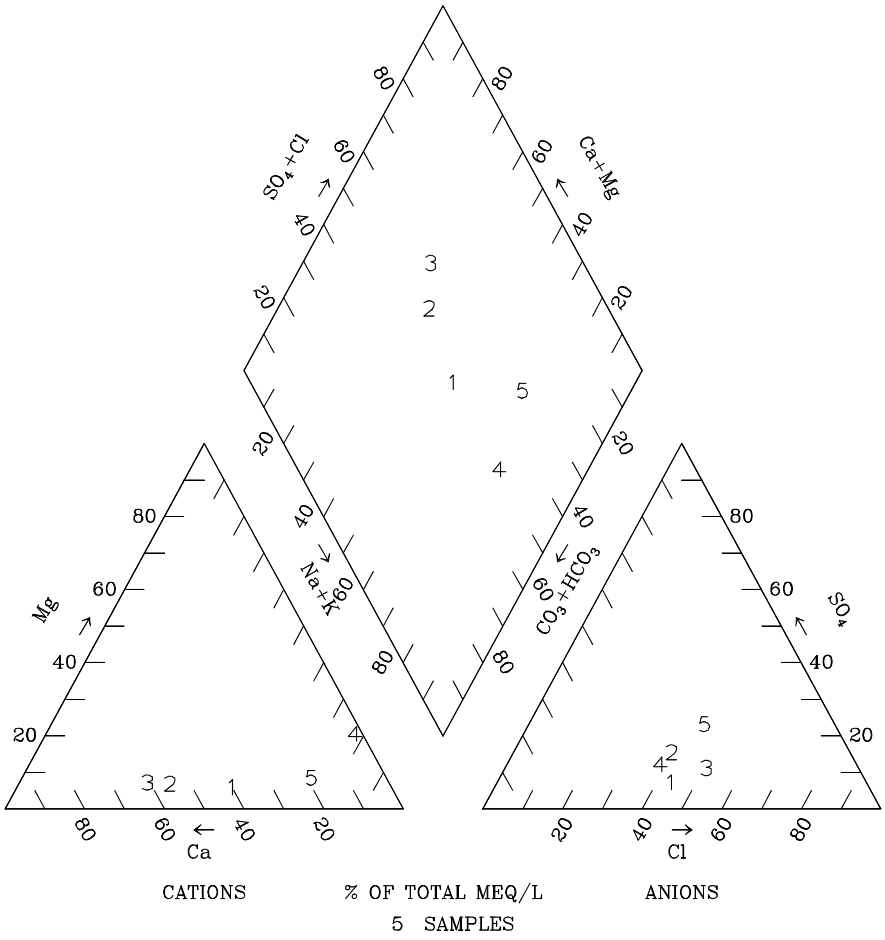

Legend	
List of Plotted Points, Borehole Identifiers, and Tops of Sampled Intervals (feet)	
1 UZ-14 – 1258.5	4 UZ#16 – 952.6
2 UZ-14 – 1277.4	5 UZN55 – 166.1
3 UZ-14 – 1277.7	

Figure 13. Trilinear Diagram for Pore Waters from the Tiva Canyon welded (TCw) and Topopah Spring welded (TSw) Hydrogeologic Units.

Note: Sample UZN55 – 166.1 is from the TCw; all other samples are from the TSw. The plotted data are listed in Table 6, and are reported in DTN: GS950608312272.001.

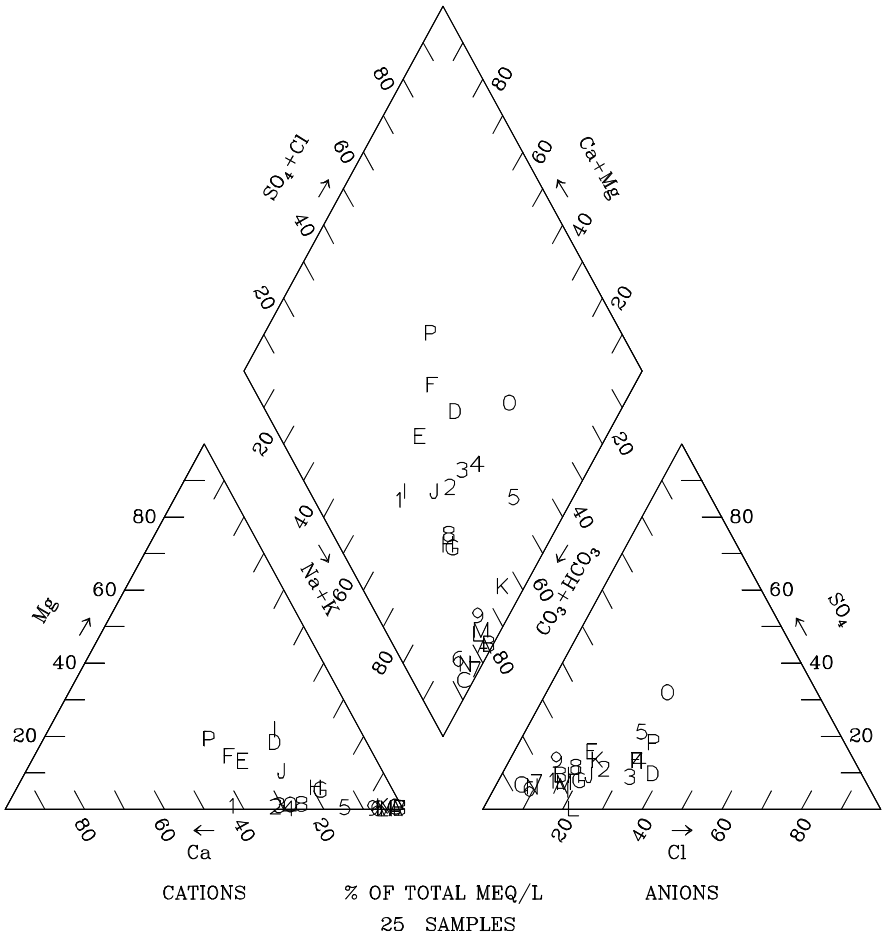

Legend

List of Plotted Points, Borehole Identifiers, and Tops of Sampled Intervals (feet)

1	NRG7A – 1483.5	7	SD9 – 1535.2	D	UZ#16 – 1166.2	J	UZ#16 – 1317.9
2	NRG7A – 1492.7	8	UZ14 – 1419.5	E	UZ#16 – 1227.4	K	UZ#16 – 1358.1
3	NRG7A – 1498.6	9	UZ14 – 1461.9	F	UZ#16 – 1235.1	L	WT24 – 1734.3
4	SD12 – 1460.7	A	UZ14 – 1495.8	G	UZ#16 – 1269.6	M	WT24 – 1744.2
5	SD12 – 1495.5	B	UZ14 – 1524.6	H	UZ#16 – 1280.4	N	WT24 – 1744.5
6	SD9 – 1452.6	C	UZ14 – 1542.3	I	UZ#16 – 1296.8	O	UZ14-1409.4
						P	UZ#16-1206.3

Figure 14. Trilinear Diagram for Pore Waters from the Top 200 feet of the Calico Hills Nonwelded (CHn) Hydrogeologic Unit.

Note: The plotted data are listed in Table 6, and are reported in DTN: GS950608312272.001, GS961108312271.002, GS970908312271.003, GS981008312272.004 and GS990208312272.001.

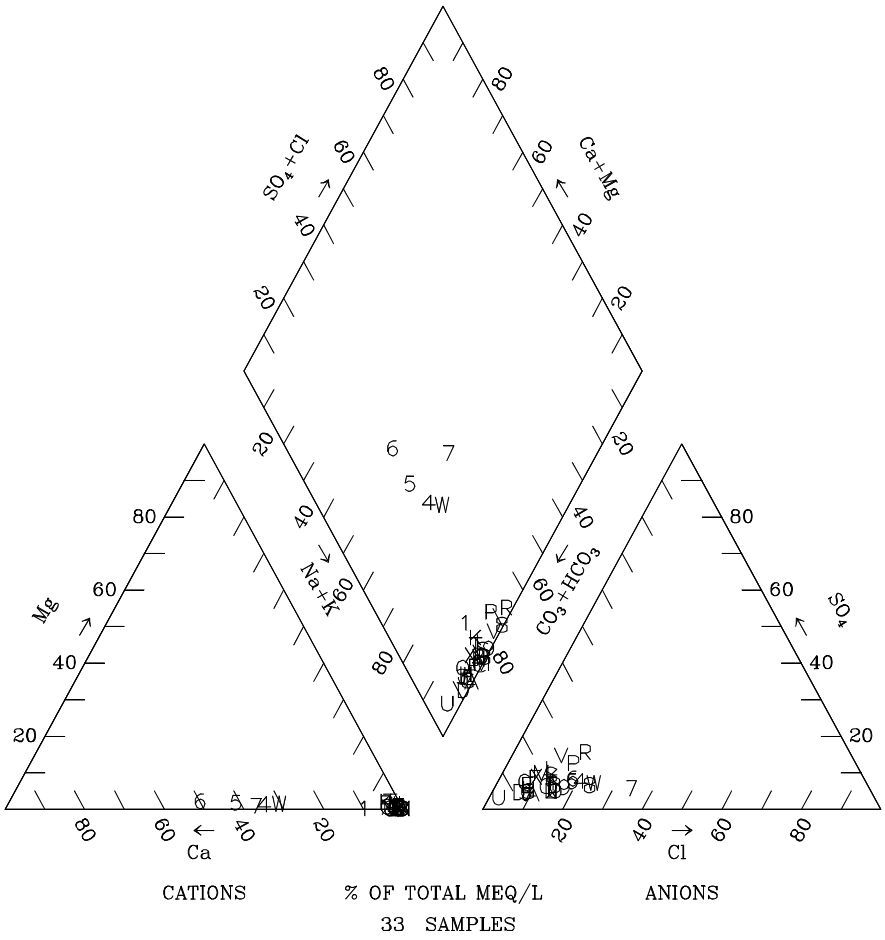

Legend							
List of Plotted Points, Borehole Identifiers, and Tops of Sampled Intervals (feet)							
1	SD12-1517	9	SD9-1661.1	H	UZ14-1585.3	P	UZ#16-1389.4
2	SD12-1600.6	A	SD9-1741	I	UZ14-1605.9	Q	UZ#16-1398.5
3	SD12-1636.8	B	SD9-1741.7	J	UZ14-1644.3	R	UZ#16-1412.9
4	SD7-1498.4	C	SD9-1800.7	K	UZ14-1674.8	S	UZ#16-1428.1
5	SD7-1524.6	D	UZ14-1563.6	L	UZ14-1695.4	T	UZ#16-1442.8
6	SD7-1558.4	E	UZ14-1564.6	M	UZ14-1715	U	SD12 – 1558.9
7	SD7-1617	F	UZ14-1564.9	N	UZ14-1734.5	V	SD12 – 1582.5
8	SD9-1619.9	G	UZ14-1585	O	UZ14-1735.3	W	SD7 – 1600.1
						X	UZ#16–1395.5

Figure 15. Trilinear Diagram for Pore Waters Below the Top 200 Feet of the Calico Hills Nonwelded (CHn) Hydrogeologic Unit, and Above the Prow Pass Lithostratigraphic Unit.

Note: The plotted data are listed in Table 6, and are reported in DTN: GS950608312272.001, GS961108312271.002, GS000608312271.001, GS981008312272.004 and GS990208312272.001.

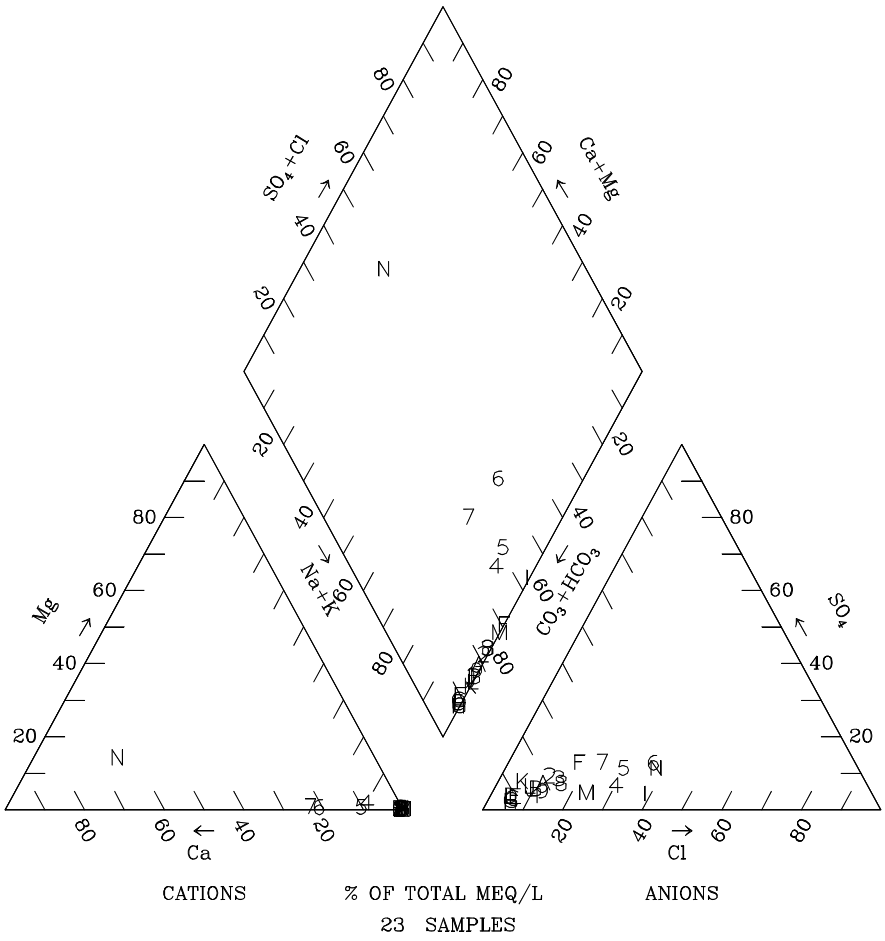

Legend

List of Plotted Points, Borehole Identifiers, and Tops of Sampled Intervals (feet)

1	SD12-1901.5	7	UZ#16-1651.6	D	UZ14-2015.2	J	SD7-2598.3
2	SD12-1942.4	8	UZ14-1804.5	E	UZ14-2025.1	K	SD7-2088.2
3	SD12-1938.8	9	UZ14-1825.8	F	UZ14-2095.6	L	SD7-2170.1
4	UZ#16-1486.9	A	UZ14-1854.9	G	SD7-1890.7	M	SD7-2596.5
5	UZ#16-1601.1	B	UZ14-1865.7	H	SD7-1952.4	N	UZ#16-1643.4
6	UZ#16-1607.7	C	UZ14-2014.7	I	SD7-2596.1		

Figure 16. Trilinear Diagram for Pore Waters from the Prow Pass, Bullfrog and Tram Lithostratigraphic Units

Note: The plotted data are listed in Table 6, and are reported in DTN: GS950608312272.001, GS961108312271.002, GS000608312271.001, and GS970908312271.003.

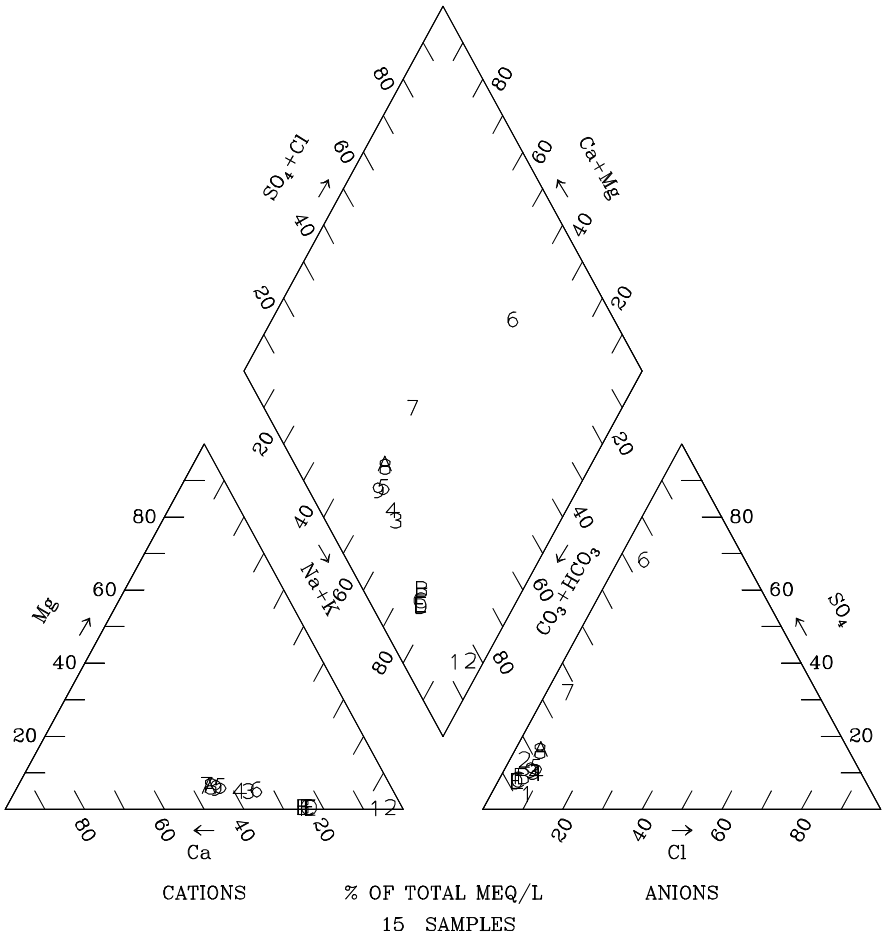

Legend

List of Plotted Points, Borehole Identifiers, and Sampled Depths (feet)

1	NRG7A	460.25	6	UZ14 C	390.75	B	SD7 (3/8/95)	479.76
2	SD9/TS	453.85	7	UZ14 PT1	390.75	C	SD7 (3/16/95)	488.29
3	UZ14 A	384.6	8	UZ14 PT2	390.75	D	SD7 (3/17/95)	488.29
4	UZ14 A2	384.6	9	UZ14 PT4	390.75	E	SD7 (3/20/95)	488.29
5	UZ14 B	387.68	A	UZ14 D	390.75	F	SD7 (3/21/95)	488.29

Figure 17. Trilinear Diagram for Perched Water.

Note: Data are listed in Table 8 and are reported inMO0012WTRIONCO.000.

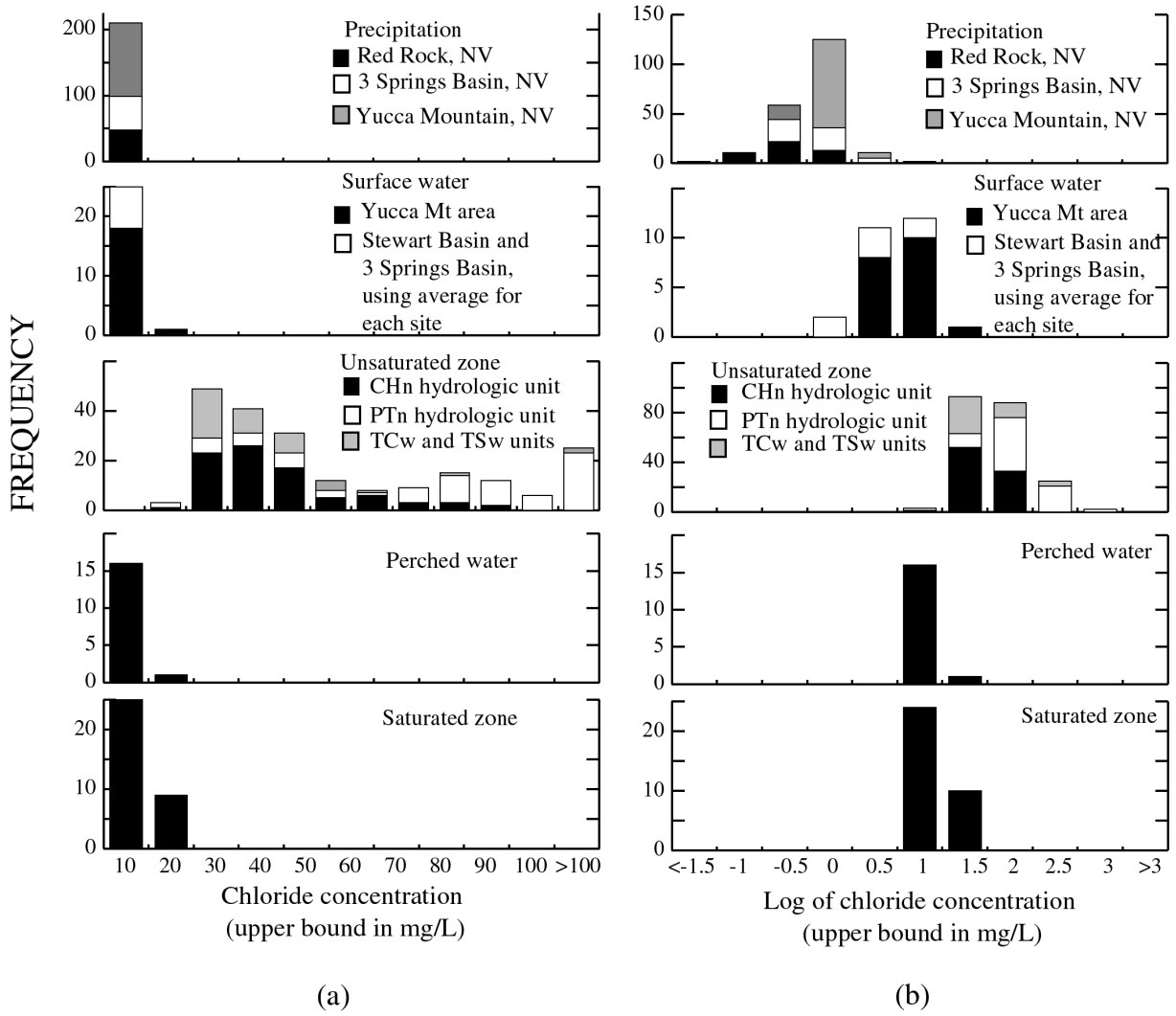

Figure 18. Histograms of chloride concentrations.

Note: Histograms of chloride concentrations in precipitation, surface water, unsaturated zone porewater, perched water, and saturated-zone groundwater. (a) Chloride concentrations. (b) Log of chloride concentrations. Data are from DTN: MO0005CL3SPRGS.000, MO0005CLESTWRT.000, MO0005CLKAWICH.000, GS930108315214.004, and GS930908315214.030 (3 Springs Basin precipitation and surface water); LA0003JF12213U.001 (NADP/NTN data for Red Rock precipitation) and LAJF831222AQ95.003 (Yucca Mountain precipitation); GS940308312133.002, GS960308312133.001, Emett et al. 1994 (p. 550), and Perfect et al. (1995, file dataedit.wk1) (surface water); GS950608312272.001, GS961108312271.002, GS000608312271.001, and GS970908312271.003 (unsaturated zone porewater); GS981008312272.004 and GS990208312272.001 (for unsaturated zone porewater), and MO0012WTRIONCO.000 (for perched water); and Oliver and Root (1997, attached file yucca.xls) (saturated zone).

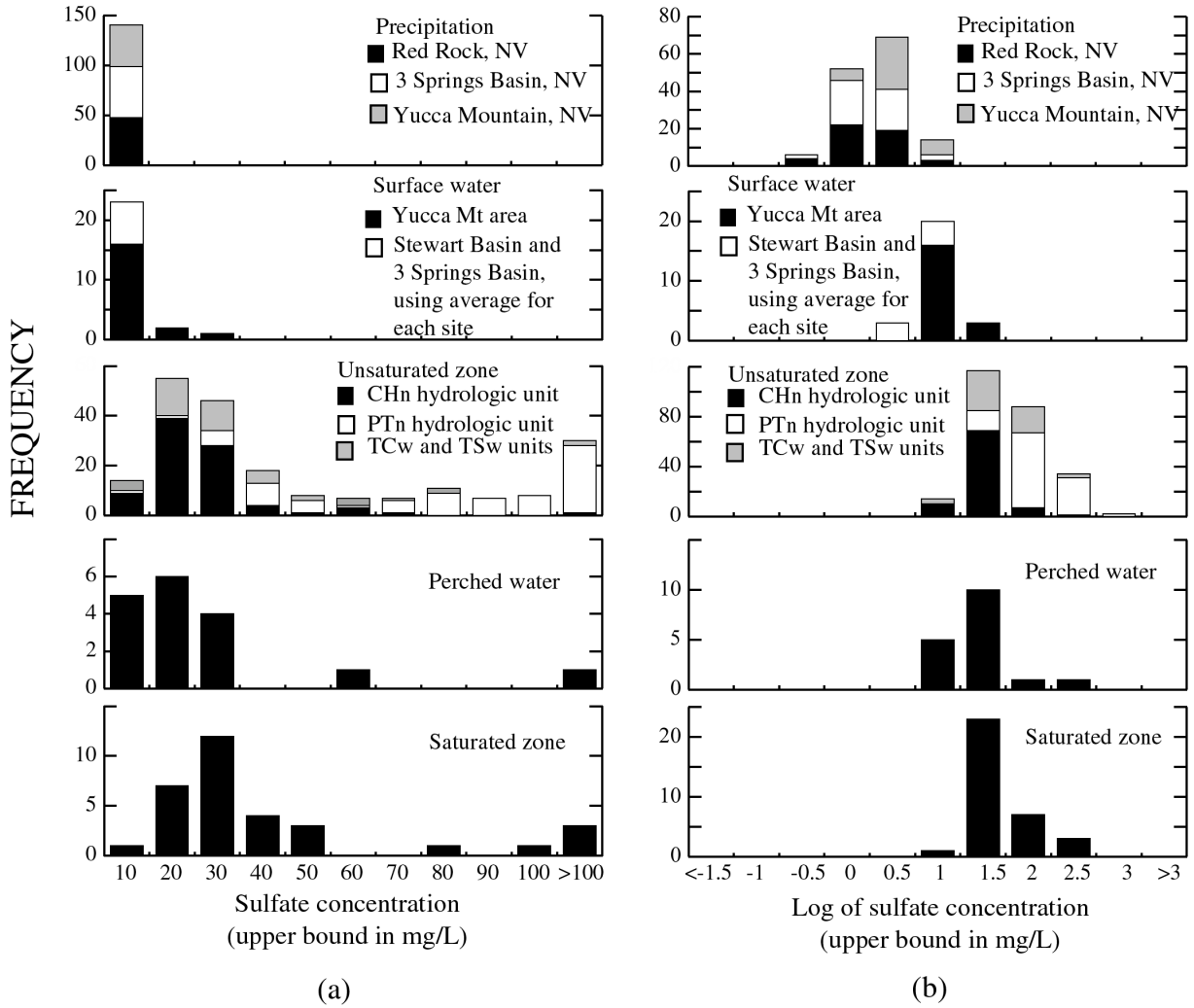

Figure 19. Histograms of sulfate concentrations.

Note: Histograms of sulfate concentrations in precipitation, surface water, unsaturated zone porewater, perched water, and saturated-zone groundwater. (a) Sulfate concentrations. (b) Log of sulfate concentrations. Data are from DTN: MO0005CL3SPRGS.000, MO0005CLESTWRT.000, MO0005CLKAWICH.000, GS930108315214.004, and GS930908315214.030 (3 Springs Basin precipitation and surface water); LA0003JF12213U.001 (NADP/NTN data for Red Rock precipitation) and GS940308312133.002, GS960308312133.001, Emett et al. 1994 (p. 550), and Perfect et al. (1995, file dataedit.wk1) (surface water); GS950608312272.001, GS961108312271.002, GS000608312271.001, and GS970908312271.003 (unsaturated zone porewater); GS981008312272.004 and GS990208312272.001 (for unsaturated zone porewater), and MO0012WTRIONCO.000 (for perched water); and Oliver and Root (1997, attached file yucca.xls) (saturated zone).

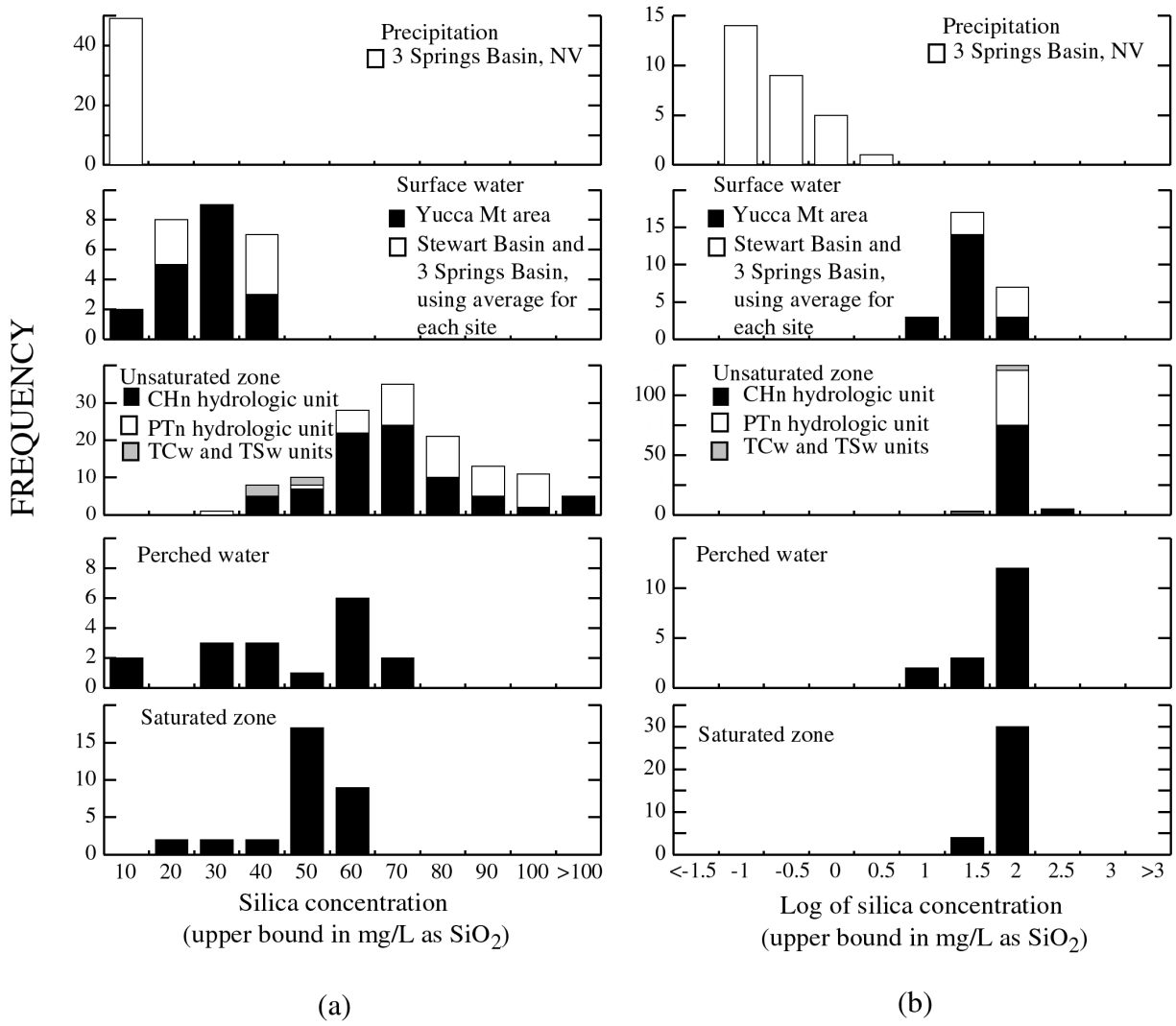

Figure 20. Histograms of silica concentrations.

Note: Histograms of silica concentrations in precipitation, surface water, unsaturated zone porewater, perched water, and saturated-zone groundwater. (a) Silica concentrations. (b) Log of silica concentrations. Data are from DTN: MO0005CL3SPRGS.000, MO0005CLESTWRT.000, MO0005CLKAWICH.000, GS930108315214.004, and GS930908315214.030 (3 Springs Basin precipitation and surface water); GS940308312133.002, GS960308312133.001, Emett et al. 1994 (p. 550), and Perfect et al. (1995, file dataedit.wk1) (surface water); GS950608312272.001, GS961108312271.002, GS000608312271.001, and GS970908312271.003 (unsaturated zone porewater); GS981008312272.004 and GS990208312272.001 (for unsaturated zone porewater), and MO0012WTRIONCO.000 (for perched water); and Oliver and Root (1997, attached file yucca.xls) (saturated zone).

.

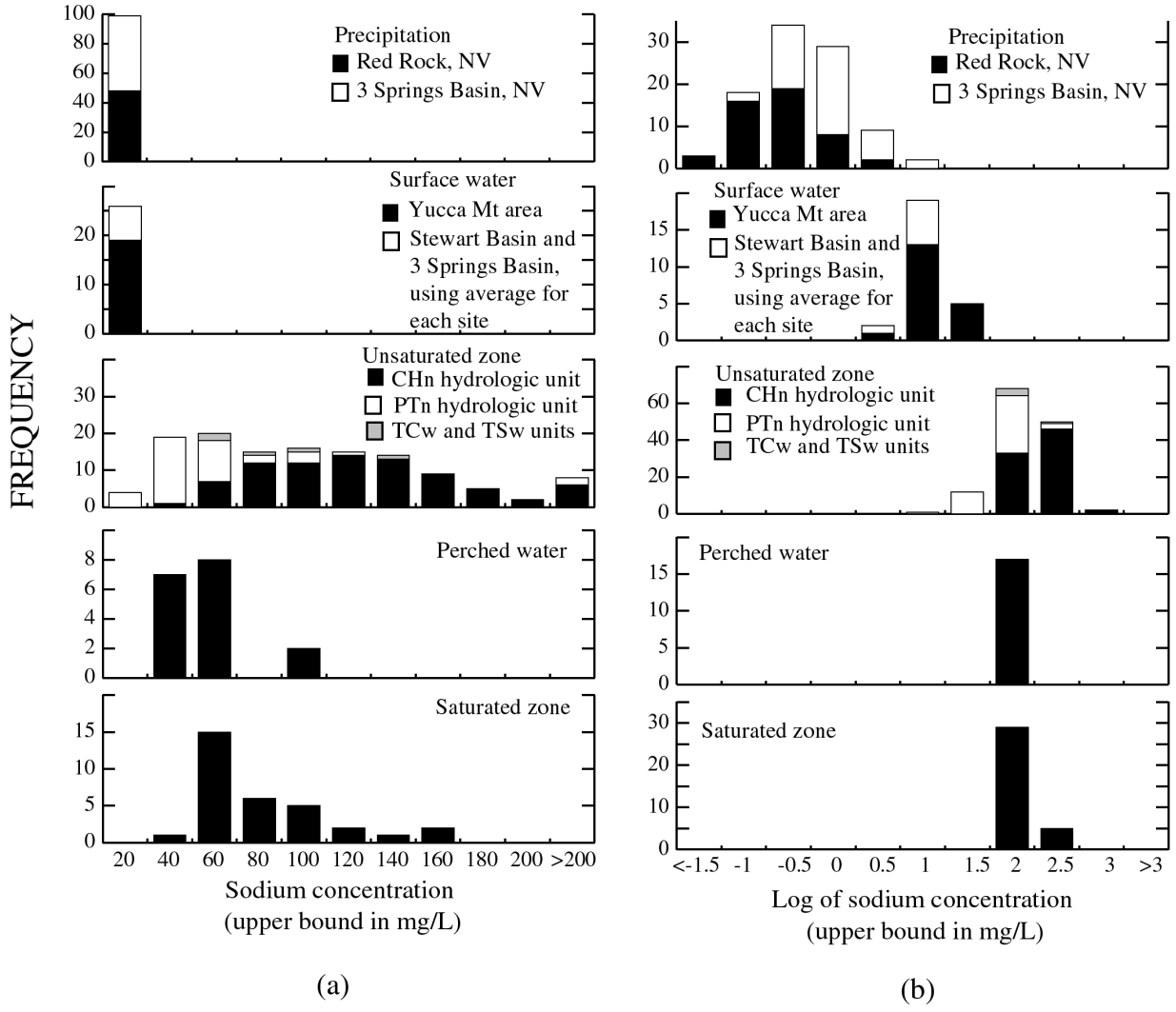

Figure 21. Histograms of sodium concentrations.

Note: Histograms of sodium concentrations in precipitation, surface water, unsaturated zone porewater, perched water, and saturated-zone groundwater. (a) Sodium concentrations. (b) Log of sodium concentrations. Data are from DTN: MO0005CL#SPRGS.000, MO0005CLESTWRT.000, MO0005CLKAWICH.000, GS930108315214.004, and GS930908315214.030 (3 Springs Basin precipitation and surface water); LA0003JF12213U.001 (NADP/NTN data for Red Rock precipitation); GS940308312133.002, GS960308312133.001, Emett et al. 1994 (p. 550), and Perfect et al. (1995, file dataedit.wk1) (surface water); GS950608312272.001, GS961108312271.002, GS000608312271.001, and GS970908312271.003 (unsaturated zone porewater); GS981008312272.004 and GS990208312272.001 (for unsaturated zone porewater), and MO0012WTRIONCO.000 (for perched water); and Oliver and Root (1997, attached file yucca.xls) (saturated zone).

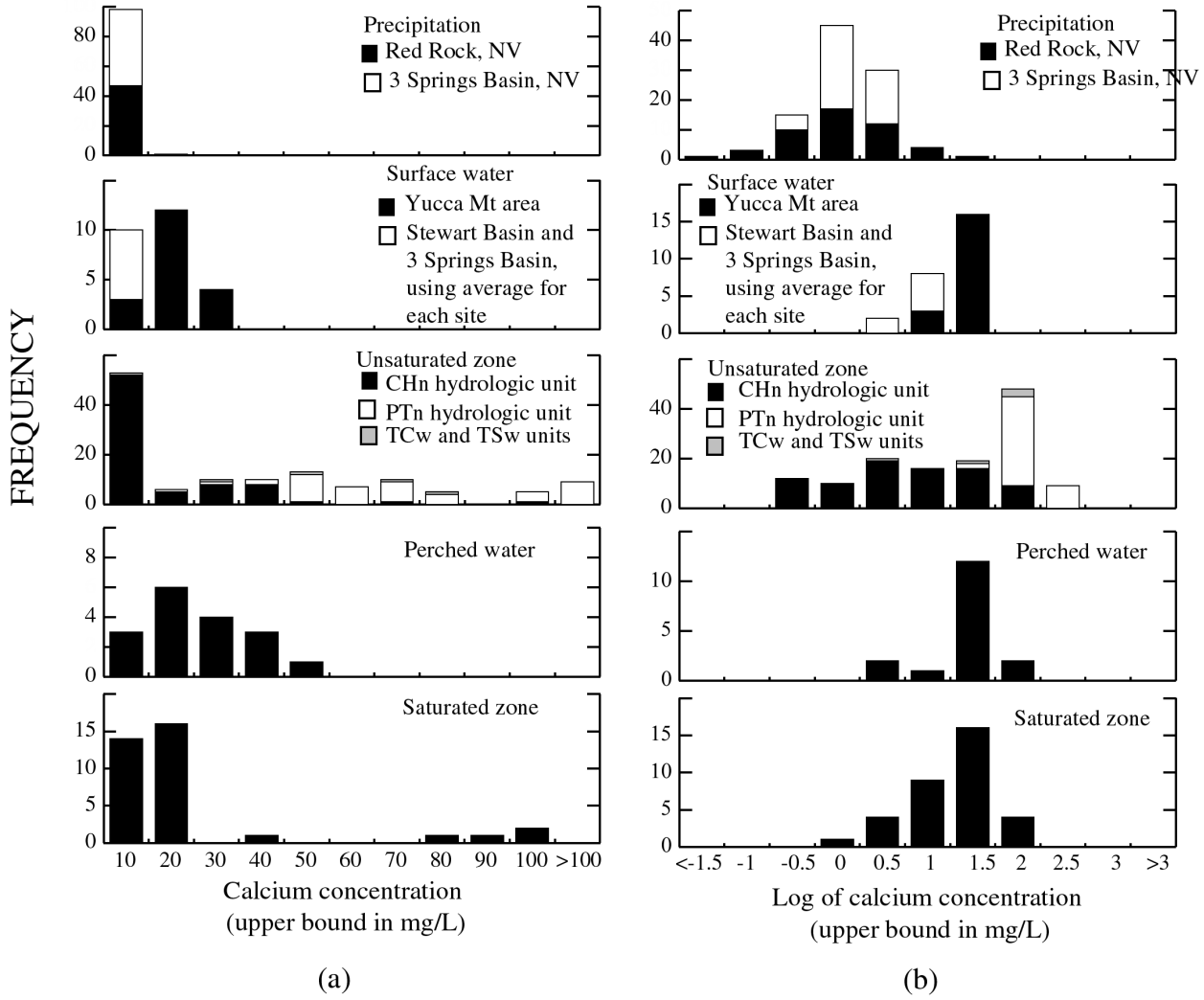

Figure 22. Histograms of calcium concentrations.

Note: Histograms of calcium concentrations in precipitation, surface water, unsaturated zone porewater, perched water, and saturated-zone groundwater. (a) Calcium concentrations. (b) Log of calcium concentrations. Data are from DTN: MO0005CL3SPRGS.000, MO0005CLESTWRT.000, MO0005CLKAWICH.000, GS930108315214.004, and GS930908315214.030 (3 Springs Basin precipitation and surface water); LA0003JF12213U.001 (NADP/NTN data for Red Rock precipitation); GS940308312133.002, GS960308312133.001, Emett et al. 1994 (p. 550), and Perfect et al. (1995, file dataedit.wk1) (surface water); GS950608312272.001, GS961108312271.002, GS000608312271.001, and GS970908312271.003 (unsaturated zone porewater); GS981008312272.004 and GS990208312272.001 (for unsaturated zone porewater), and MO0012WTRIONCO.000 (for perched water); and Oliver and Root (1997, attached file yucca.xls) (saturated zone).

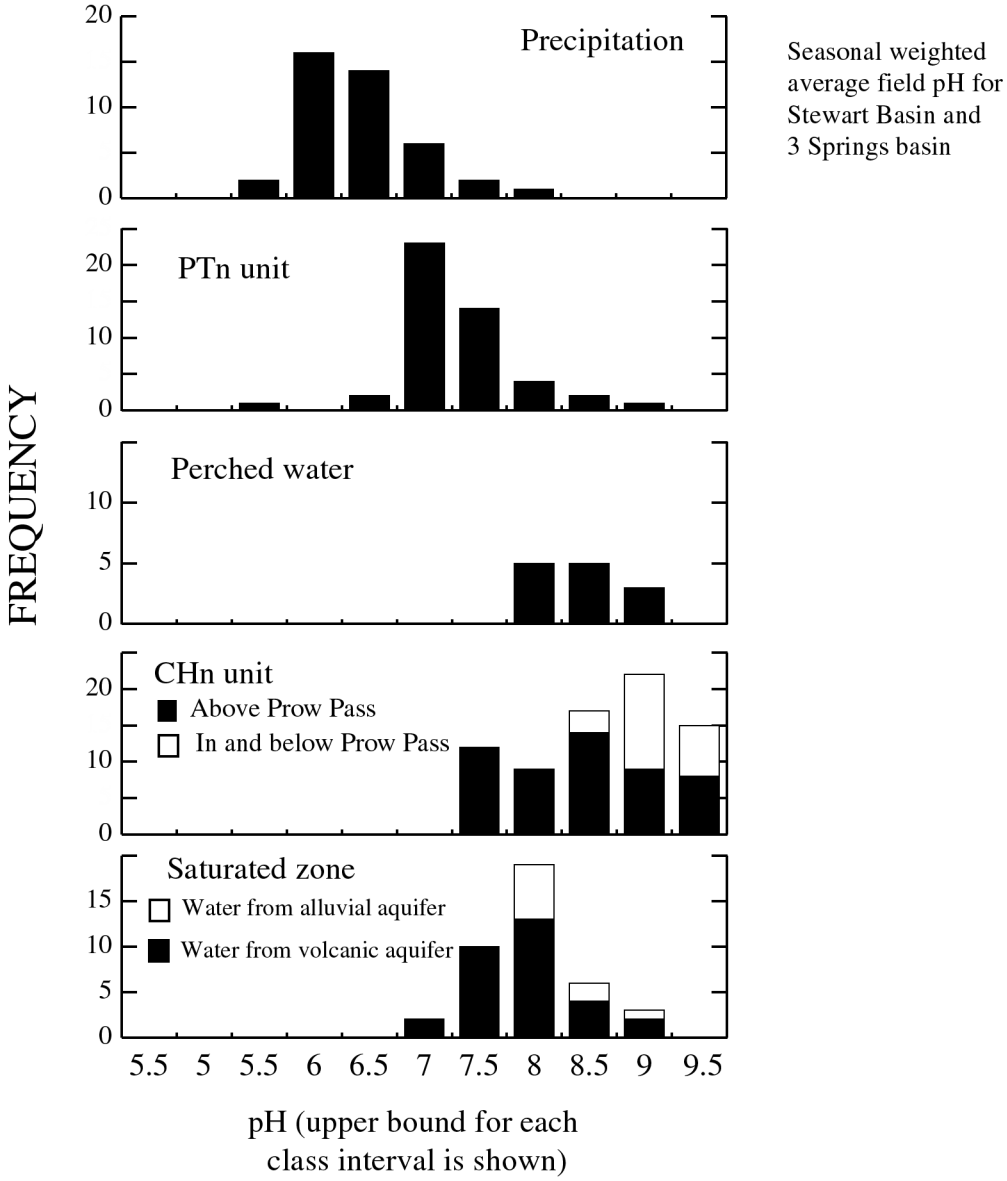

Figure 23. Histograms of pH values.

Note: Histograms of pH values in precipitation, surface water, unsaturated zone porewater, perched water, and saturated-zone groundwater. Data are from DTN: MO0005CL3SPRGS.000, MO0005CLESTWRT.000, MO0005CLKAWICH.000, GS930108315214.004, and GS930908315214.030 (3 Springs Basin precipitation and surface water); LA0003JF12213U.001 (NADP/NTN data for Red Rock precipitation); GS940308312133.002, GS960308312133.001, Emett et al. 1994 (p. 550), and Perfect et al. (1995, file dataedit.wk1) (surface water); GS950608312272.001, GS961108312271.002, GS000608312271.001, and GS970908312271.003 (unsaturated zone porewater); GS981008312272.004 and GS990208312272.001 (for unsaturated zone porewater), and MO0012WTRIONCO.000 (for perched water); and Oliver and Root (1997, attached file yucca.xls) (saturated zone).

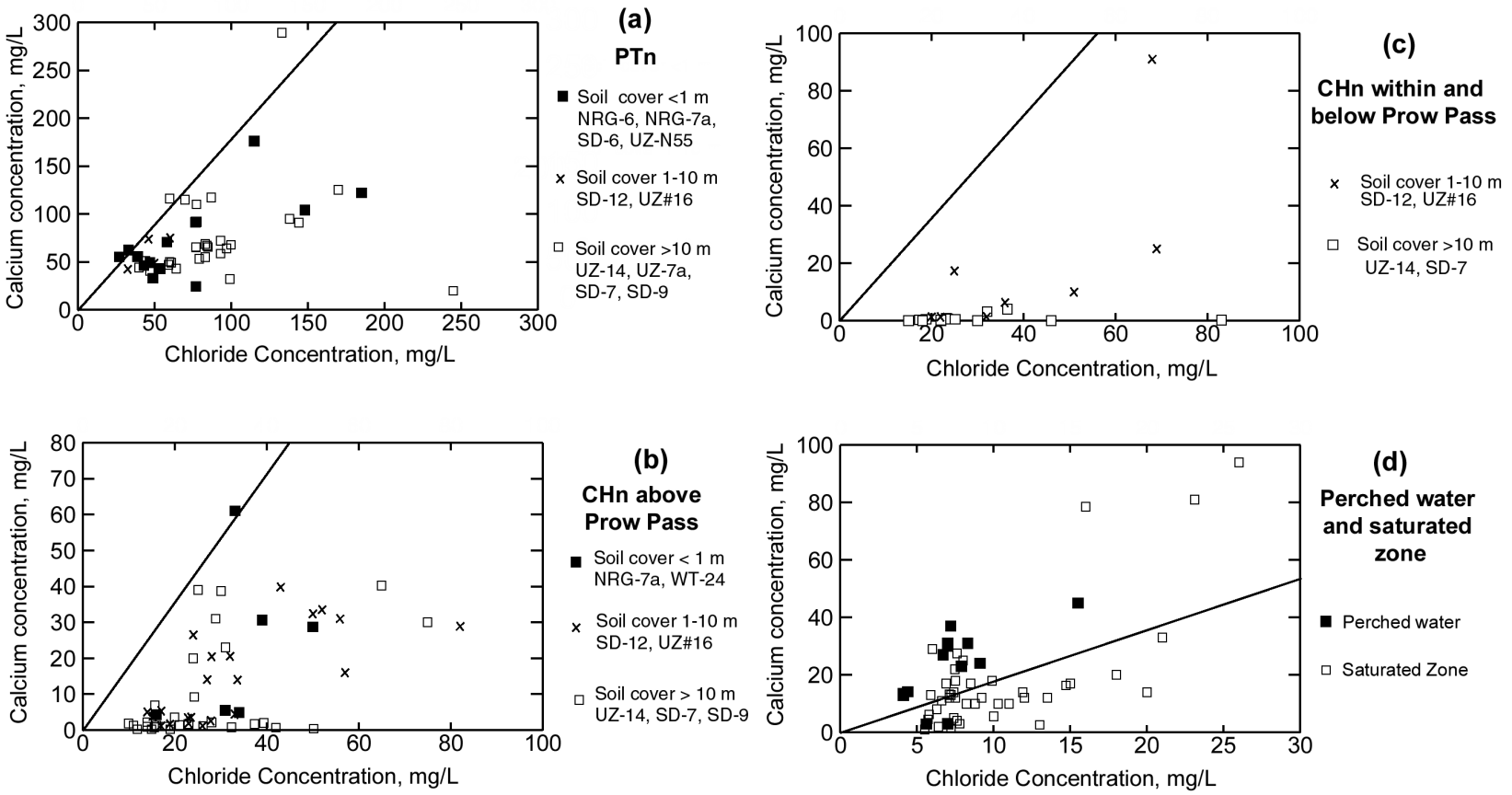

Figure 24. Calcium versus chloride.

Calcium versus chloride in unsaturated-zone porewaters (a) from the PTn hydrogeologic unit, (b) from the Calico Hills hydrogeologic unit above the lithostratigraphic Prow Pass unit, (c) from the Calico Hills hydrogeologic unit within and below the lithostratigraphic Prow Pass unit, and (d) in perched water and from the saturated zone. Porewater data are shown in Table 6, and perched water data are shown in Table 8. Data are from DTNs GS950608312272.001, GS961108312271.002, GS000608312271.001, GS970908312271.003, GS981008312272.004, and GS990208312272.001 (unsaturated zone porewater); and Oliver and Root (1997, attached file yucca.xls) (saturated zone). The solid line on each plot is the best-fit regression line for the precipitation data, from Table 5.

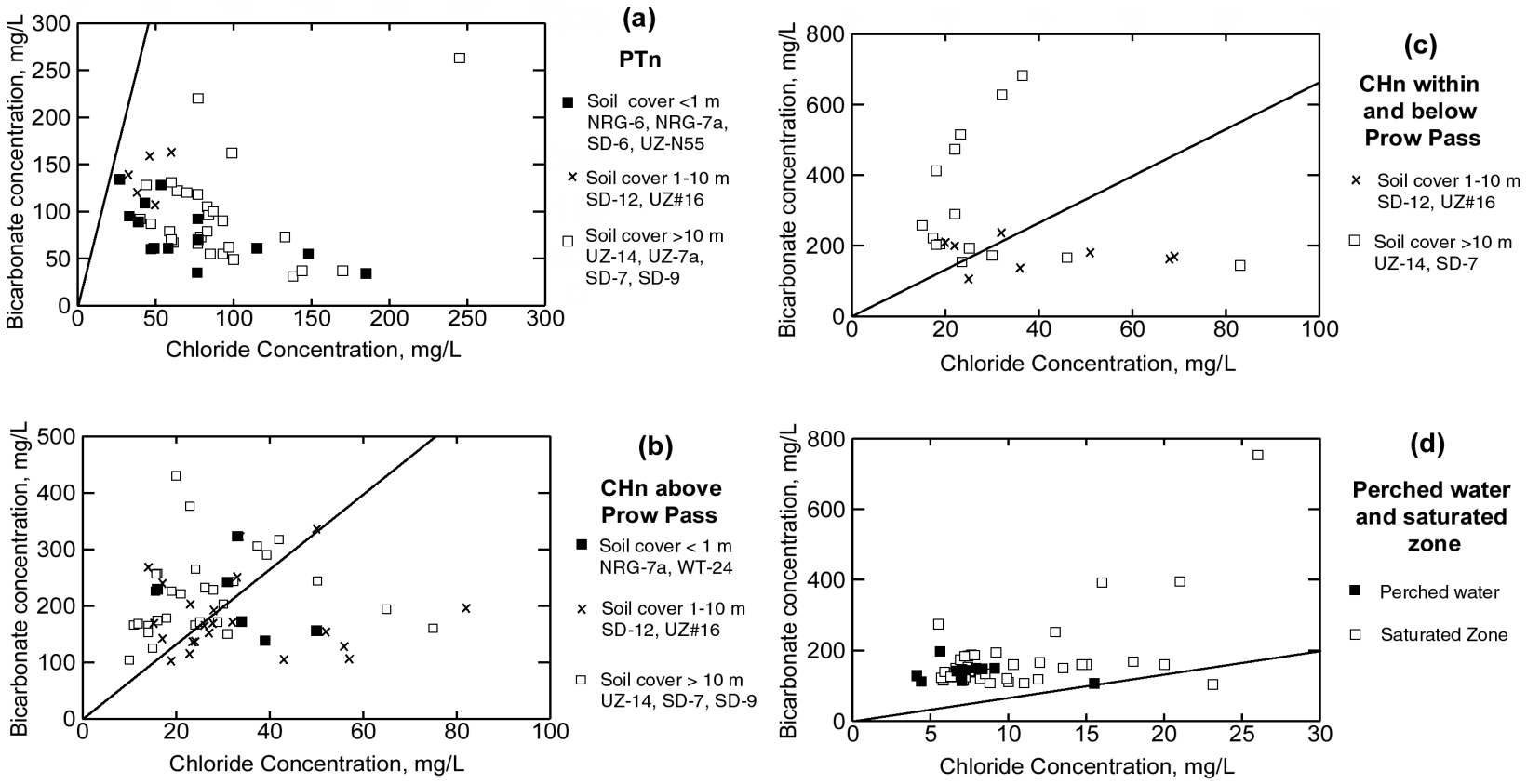

Figure 25. Bicarbonate versus chloride.

Bicarbonate versus chloride in unsaturated-zone porewaters (a) from the PTn hydrogeologic unit, (b) from the Calico Hills hydrogeologic unit above the lithostratigraphic Prow Pass unit, (c) from the Calico Hills hydrogeologic unit within and below the lithostratigraphic Prow Pass unit, and (d) in perched water and from the saturated zone. Porewater data are from Table 6, and perched water data are from Table 8. Data sources are DTN: GS950608312272.001, GS961108312271.002, GS000608312271.001, GS970908312271.003, MO0012WTRIONCO.000, and GS981008312272.004, and GS990208312272.001 (unsaturated zone porewater and perched water); and Oliver and Root (1997, attached file yucca.xls) (saturated zone). The solid line on each plot is the best-fit regression line for the precipitation data, from Table 5.

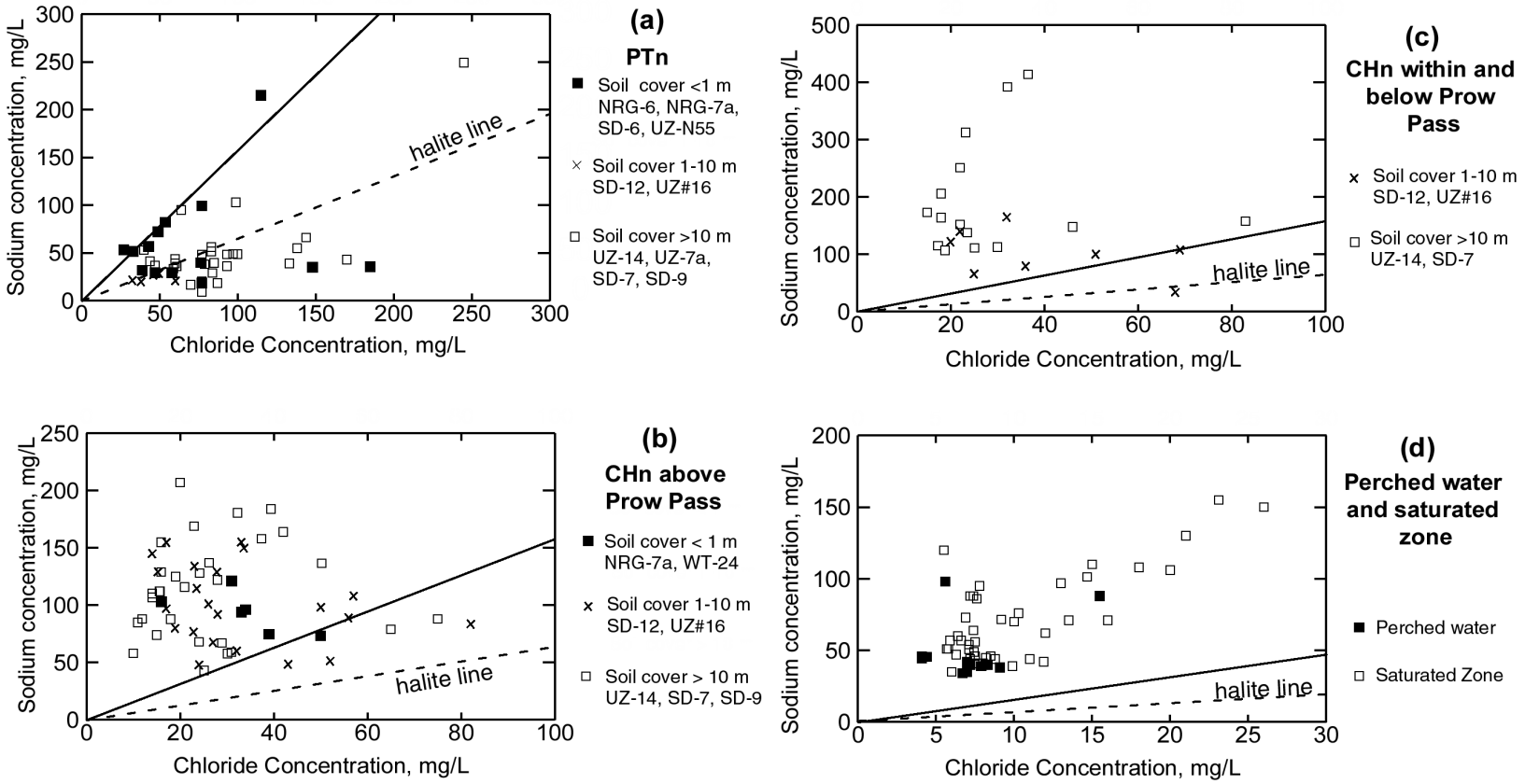

Figure 26. Sodium versus chloride.

Sodium versus chloride in unsaturated-zone porewaters (a) from the PTn hydrogeologic unit, (b) from the Calico Hills hydrogeologic unit above the lithostratigraphic Prow Pass unit, (c) from the Calico Hills hydrogeologic unit within and below the lithostratigraphic Prow Pass unit, and (d) in perched water and from the saturated zone. Porewater data are from Table 6, and perched water data are from Table 8. Data sources are DTN: GS950608312272.001, GS961108312271.002, GS000608312271.001, GS970908312271.003, MO0012WTRIONCO.000, and GS981008312272.004, and GS990208312272.001 (unsaturated zone porewater and perched water); and Oliver and Root (1997, attached Excel file yucca.xls) (saturated zone). The solid line on each plot is the best-fit regression line for the precipitation data, from Table 5. The "halite line" on these plots is based on a 1:1 molar ratio of sodium to chloride in order to show the trend for halite dissolution.

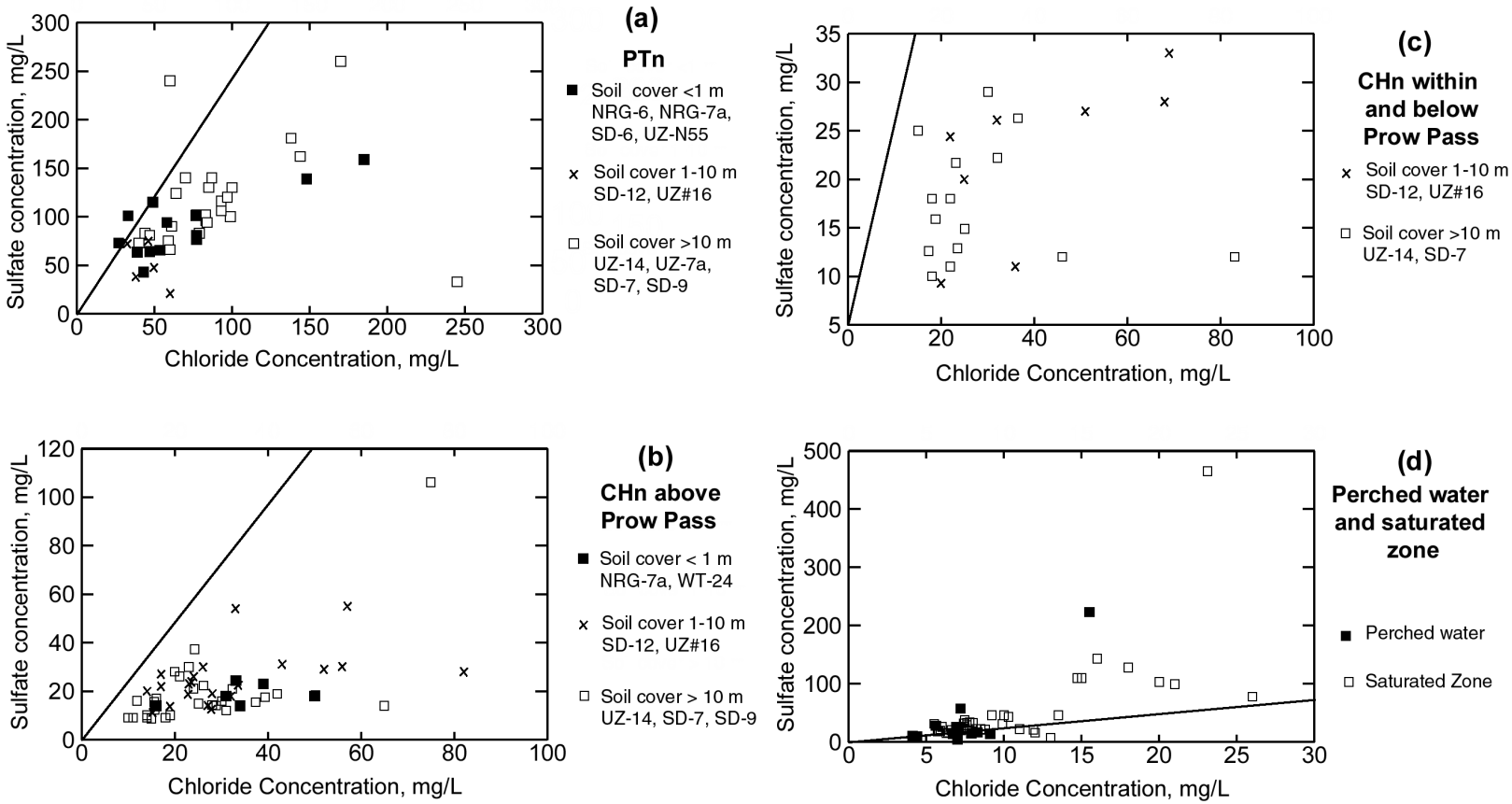

Figure 27. Sulfate versus chloride.

Sulfate versus chloride in unsaturated-zone porewaters (a) from the PTn hydrogeologic unit, (b) from the Calico Hills hydrogeologic unit above the lithostratigraphic Prow Pass unit, (c) from the Calico Hills hydrogeologic unit within and below the lithostratigraphic Prow Pass unit, and (d) in perched water and from the saturated zone. Porewater data are from Table 6, and perched water data are from Table 8. Data sources are DTN: GS950608312272.001, GS961108312271.002, GS000608312271.001, GS970908312271.003, MO0012WTRIONCO.000, and GS981008312272.004, and GS990208312272.001 (unsaturated zone porewater and perched water); and Oliver and Root (1997, attached file yucca.xls) (saturated zone). The solid line on each plot is the best-fit regression line for the precipitation data, from Table 5.

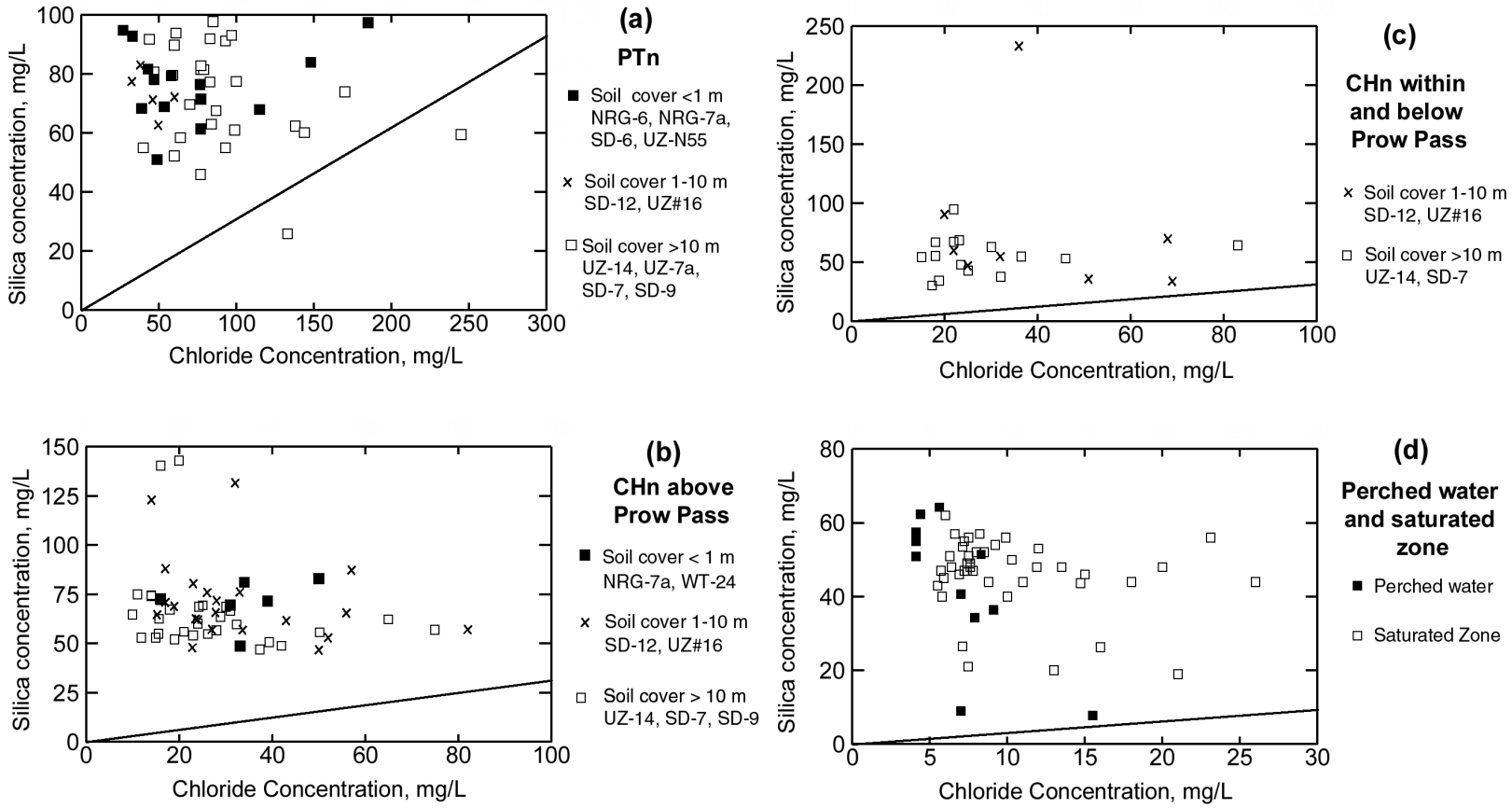

Figure 28. Silica versus chloride.

Silica versus chloride in unsaturated-zone porewaters (a) from the PTn hydrogeologic unit, (b) from the Calico Hills hydrogeologic unit above the lithostratigraphic Prow Pass unit, (c) from the Calico Hills hydrogeologic unit within and below the lithostratigraphic Prow Pass unit, and (d) in perched water and from the saturated zone. Porewater data are from Table 6, and perched water data are from Table 8. Data sources are DTN: GS950608312272.001, GS961108312271.002, GS000608312271.001, GS970908312271.003, MO0012WTRIONCO.000, and GS981008312272.004, and GS990208312272.001 (unsaturated zone porewater and perched water); and Oliver and Root (1997, attached file yucca.xls) (saturated zone). The solid line on each plot is the best-fit regression line for the precipitation data, from Table 5.

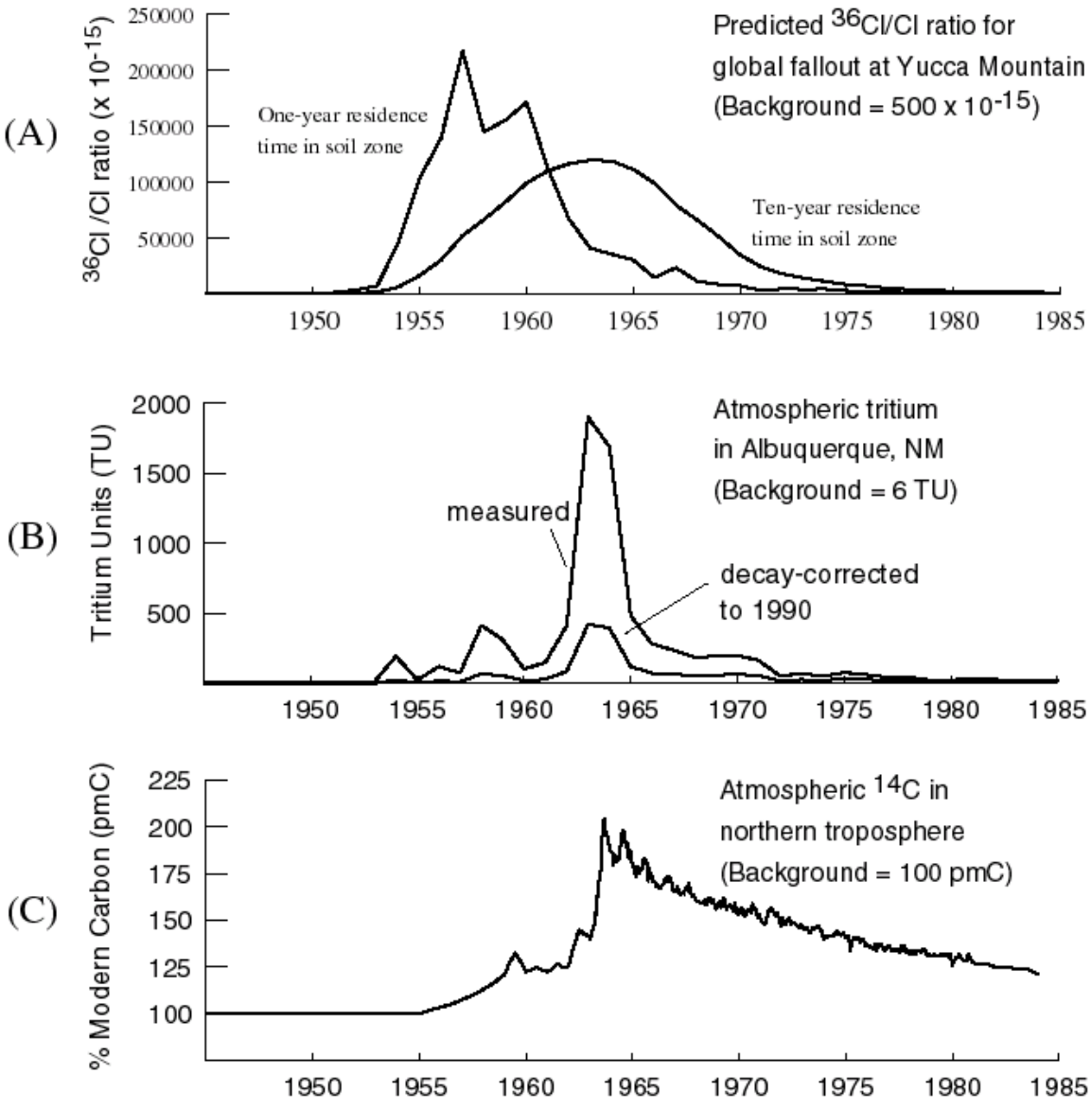

Figure 29. Input functions for bomb-pulse nuclides.

Note: (A) Estimated ^{36}Cl/Cl ratio for global fallout at Yucca Mountain, as a function of average residence time in the soil zone, (B) tritium in atmospheric moisture in Albuquerque, NM, and (C) atmospheric concentrations of bomb-pulse ^{14}C for the northern hemisphere. Reconstructed atmospheric tritium data from DTN: LA0001JF12213U.001; reconstructed ^{14}C and ^{36}Cl data from Fabryka-Martin, Turin et al. (1996, Appendix Tables C1 and C2).

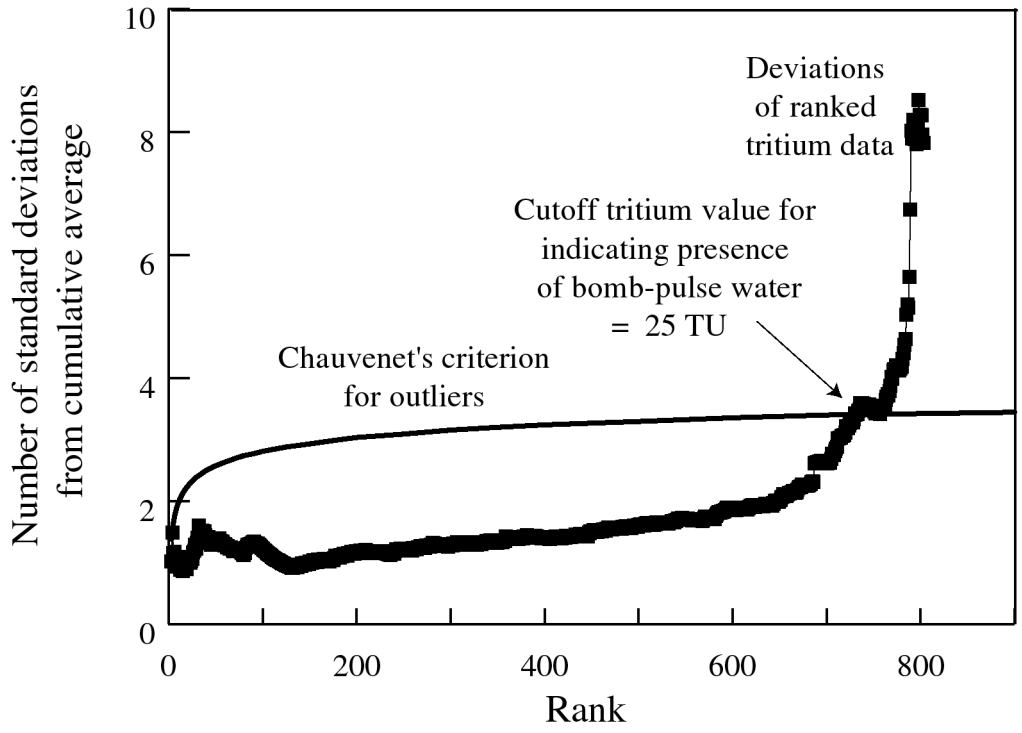

Figure 30. Cutoff tritium value for the presence of bomb-pulse tritium

Note: The plot illustrates the statistical determination of the cutoff tritium value for the presence of bomb-pulse tritium in unsaturated-zone fluid samples, using Chauvenet's criterion. Analyses conducted using tritium composition of porewater from DTN: GS961108312271.002 (excluding data for UZ#16), GS961108312261.006, GS970108312232.001, GS970283122410.002, GS970608312272.005, GS000608312271.001, MO0012TRITUNSZ.000 and GS991108312272.004. Chauvenet's criterion is discussed in Bevington and Robinson (1992, p.58).

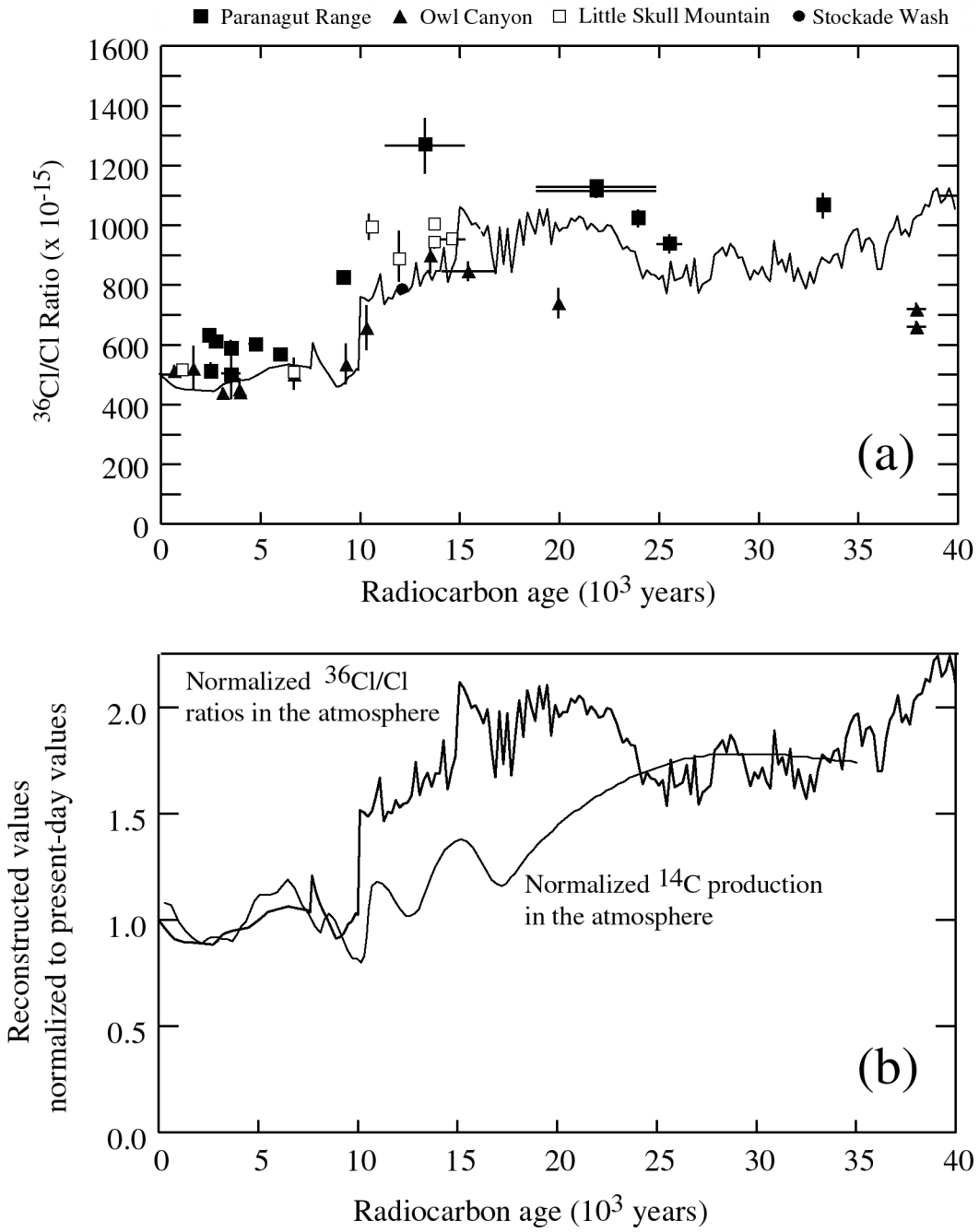

Figure 31. Reconstructed atmospheric ^{36}Cl/Cl ratio.

Note: The top plot compares the reconstructed ^{36}Cl/Cl ratio to measured ^{36}Cl/Cl ratios for fossilized packrat urine from southern Nevada (based on Plummer et al. 1997, Figure 2). The bottom plot compares the reconstructed ^{36}Cl/Cl ratio (normalized to a present-day value of 500 x 10^{-15}) to the reconstructed ^{14}C activity of Plummer et al. (1997, Figure 3B). ^{36}Cl data from DTN: LAJF831222AQ97.002. Radiocarbon ages from DTN: GS950708315131.003 and GS960308315131.001 for top figure and DTN: GS950708315131.001 and GS950708315131.002, GS950708315131.003 and GS960308315131.001 for bottom figure.

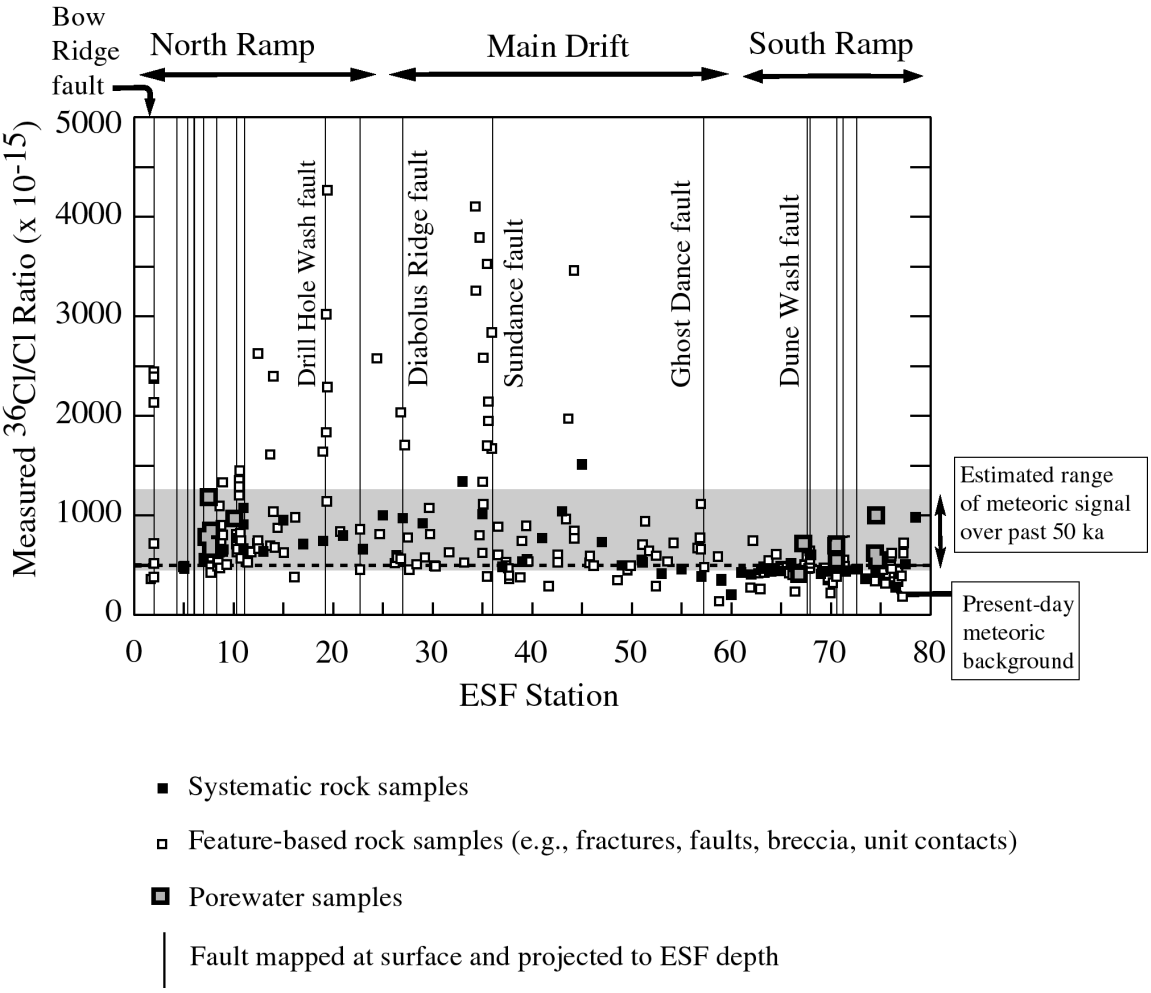

Figure 32. Distribution of ^{36}Cl/Cl in the ESF

Note: This plot shows the distribution of ^{36}Cl/Cl ratios measured for rock samples in the ESF. Faults in the ESF that correlate with mapped faults at surface are shown. ESF stations are labeled in 100-m increments. Analytical uncertainties are less than 10%. Data are from DTN: LAJF831222AQ98.004, LA9909JF831222.005 and LA9909JF831222.010.

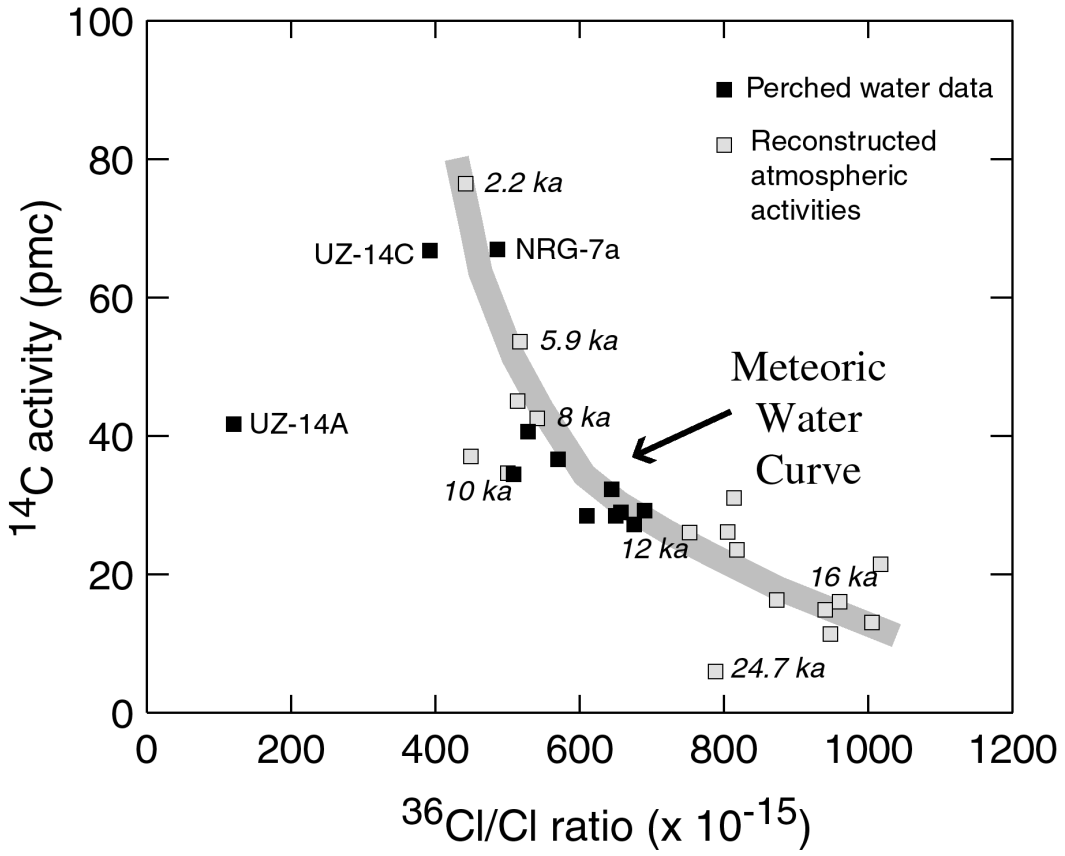

Figure 33. Meteoric and atmospheric Carbon-14 and Chlorine-36 activities.

Note: Reconstructed ^{14}C and ^{36}Cl activities in the atmosphere for the last 20 ka, compared with activities measured in perched water from UZ-14, SD-7, and NRG-7a. Perched water data are plotted with black squares, using ^{14}C and ^{36}Cl data shown in Table 9 and taken from DTN: MO0102UNSZHYCM.000, LAJF831222AQ98.011 and MO0012CARB1314.001. Reconstructed activities (gray squares) are plotted in the lower part of Figure 31. Key perched water data points are identified by borehole and sample identifier, and key reconstruction points are identified by age (ka is the abbreviation for thousand years).

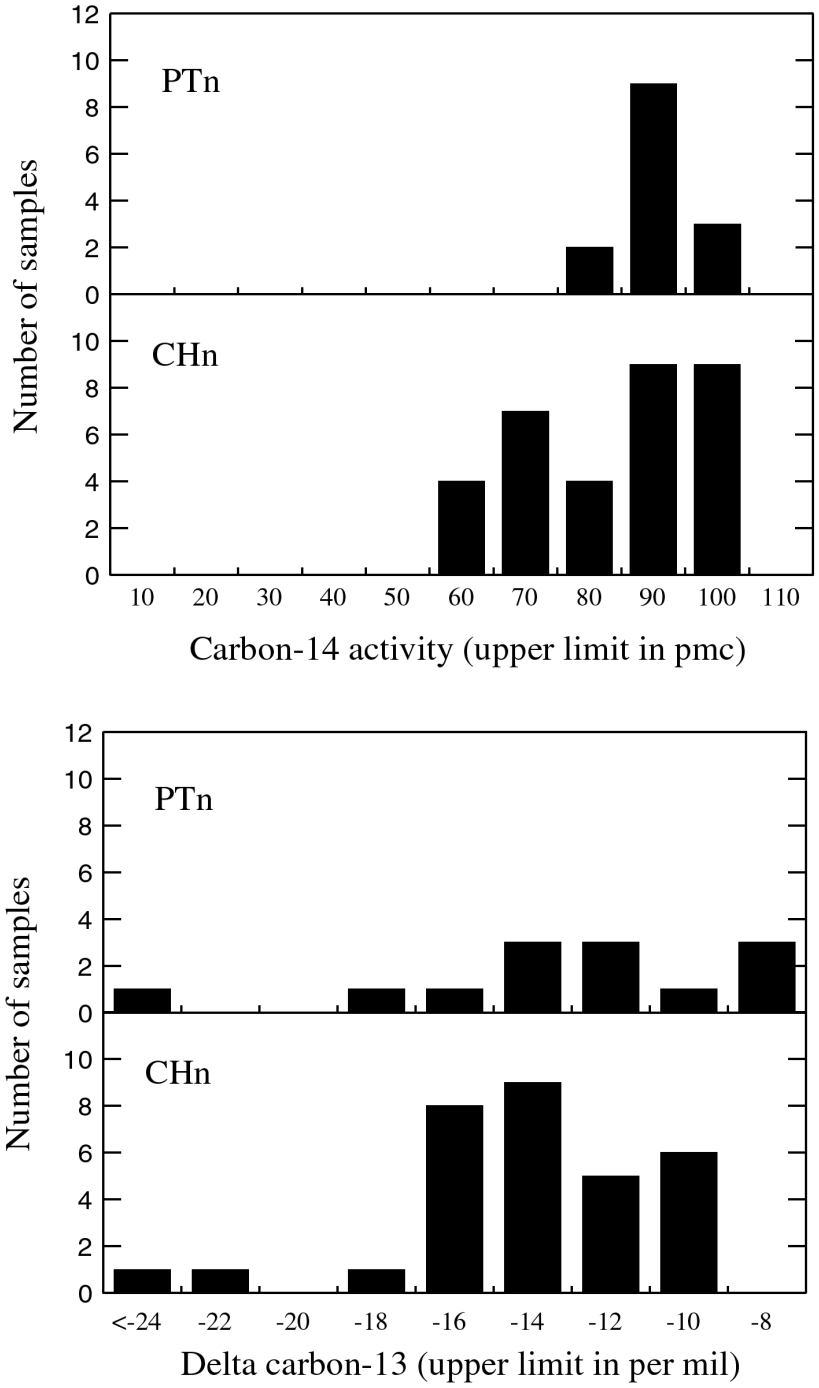

Figure 34. Histogram of Carbon Isotopes in Pore Waters.

Note: Frequency histograms comparing the distribution of carbon-14 activities and stable carbon isotope rations of unsaturated-zone porewaters in the PTn and CHn hydrogeologic units, Yucca Mountain. Data are shown in Table 15 and are from DTN: MO0012CARB1314.001, MO0102UNSZHYCM.000, GS961108312271.002, GS000608312271.001 and MO0012CARBON13.000.

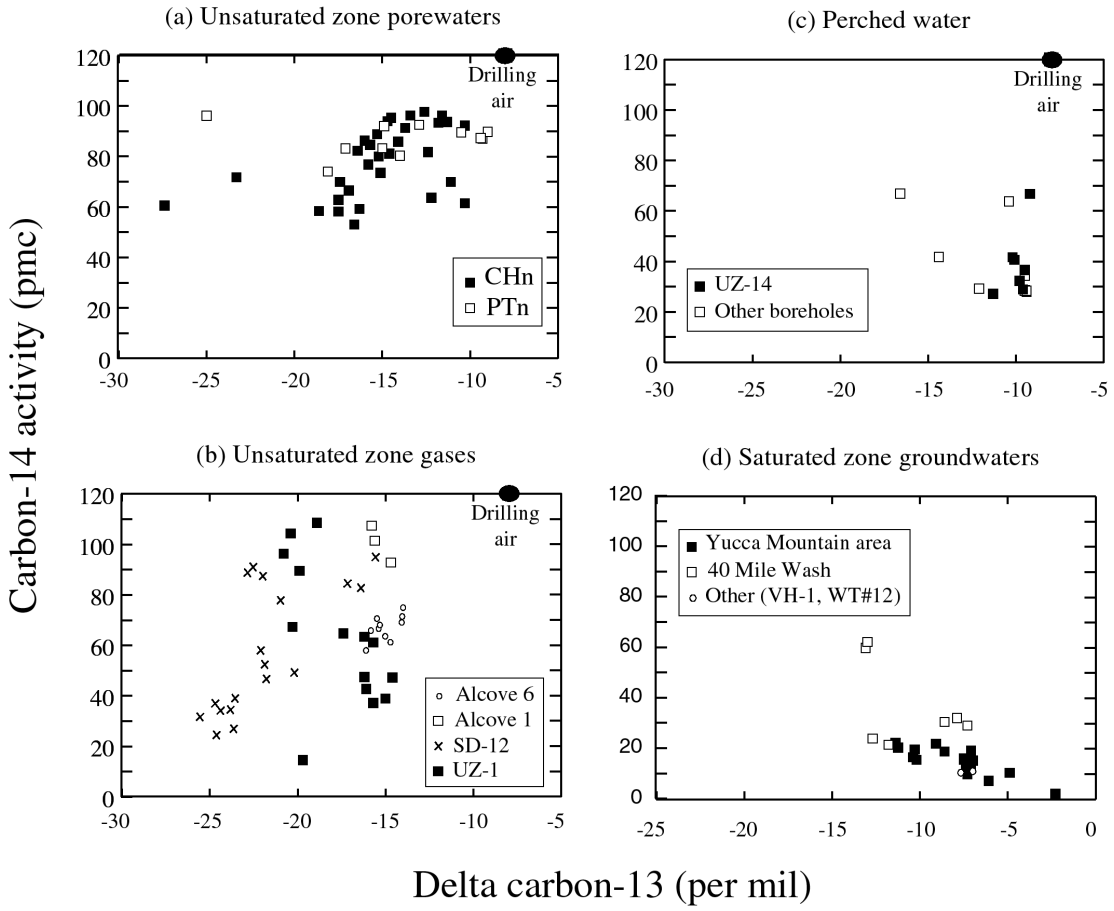

Figure 35. Carbon-14 versus Stable Carbon for Yucca Mountain Waters and Gases.

Note: Plot of carbon-14 activity versus stable carbon isotopic ratio for (a) porewaters from the unsaturated zone, (b) gas from the unsaturated zone, (c) perched water, and (d) groundwaters. Data from DTN: MO0012CARB1314.001, MO0102UNSZHYCM.000, GS961108312271.002, GS000608312271.001 and MO0012CARBON13.000 (unsaturated zone porewaters); MO0012CARB1314.000, GS961108312271.002, GS960208312261.002, GS970283122410.002 and GS990983122410.003 (unsaturated zone gases from instrumented boreholes); GS930308312323.001 and Oliver and Root (1997, attached Excel file yucca.xls) (groundwater).

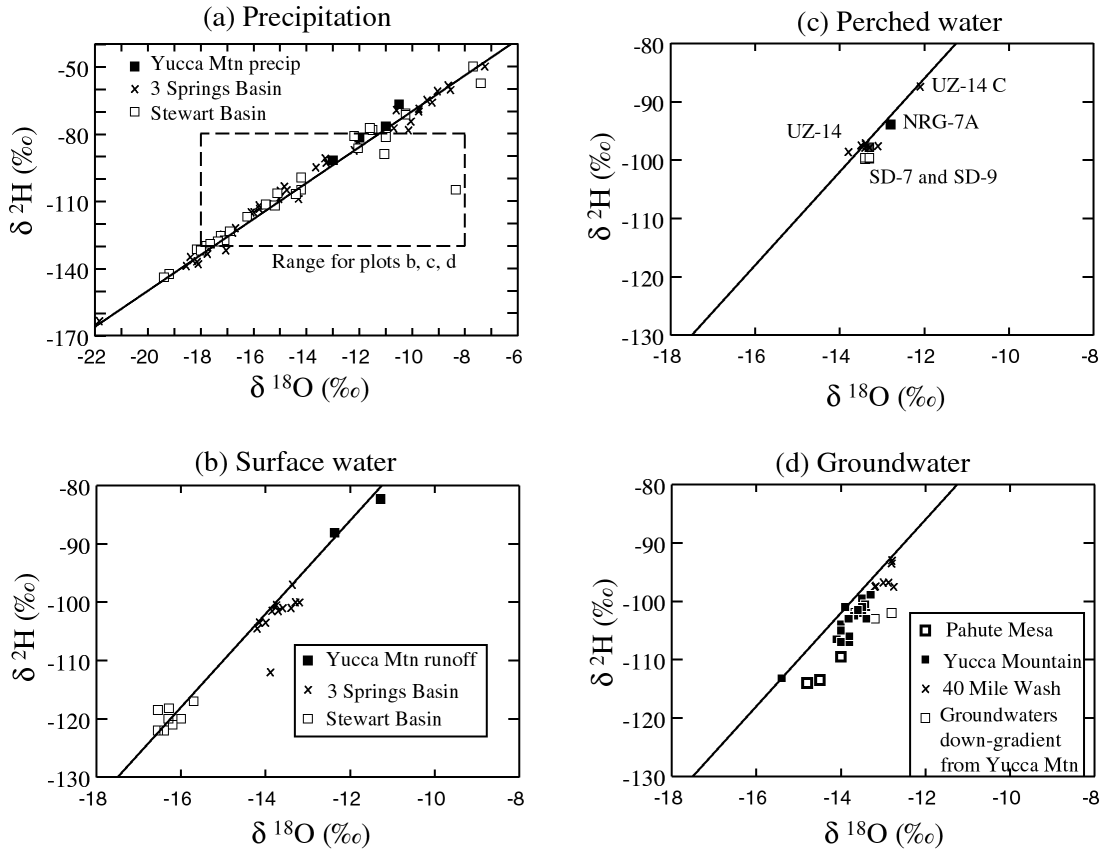

Figure 36. $\delta^{2}H$ and $\delta^{18}O$ Compositions of Yucca Mountain Waters

Note: This plot shows $\delta^{2}H$ and $\delta^{18}O$ compositions of: (a) local precipitation, (b) local surface water, (c) perched water, and (d) Yucca Mountain ground waters. Data from DTN: MO0005CL3SPRGS.000, MO0005CLESTWRT.000, MO0005CLKAWICH.000, GS930108315214.004, and GS930908315214.030 (3 Springs Basin precipitation and surface waters); Yang, Yu et al. (1998, Figure 18) (1984 storms; corroborative data); DTN: GS940308312133.002 (surface water); MO0007GNDWTRIS.013; GS930308312323.001, GS970708312323.001 and Oliver and Root (1997, attached Excel file Yucca.xls) (groundwater); and Benson and Klieforth (1989, Table 3) (groundwater in the Amargosa Desert).

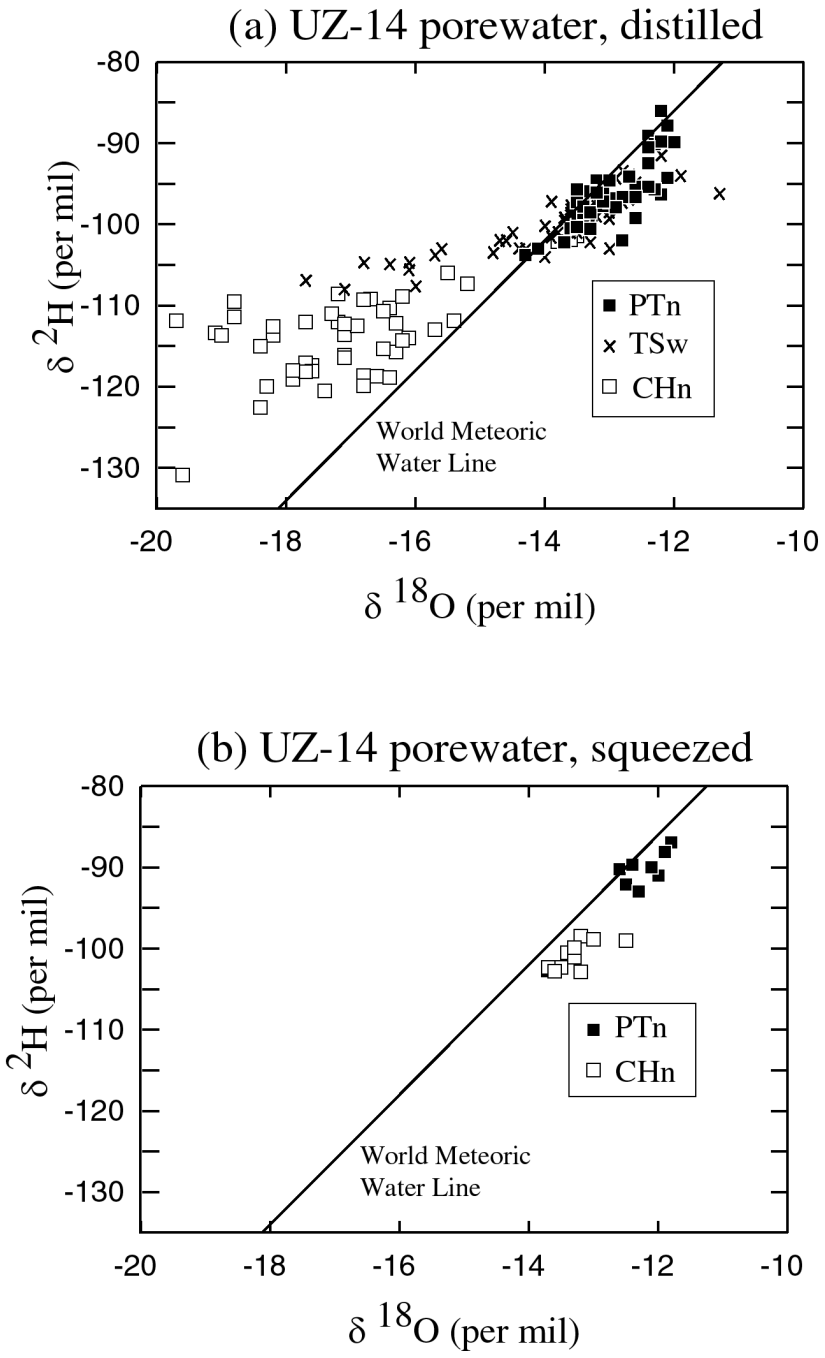

Figure 37. Plot of $\delta^{2}H$ versus $\delta^{18}O$ showing porewater compositions in UZ-14

Note: This plot contrasts the stable isotopic signatures obtained for porewaters extracted using two different methods of extraction. (a) Porewater extracted by distillation. (b) Porewater extracted by squeezing (based on data shown in Yang, Yu et al. 1998, Figures 15 and 16). Data are from DTN: MO0102UNSZHYCM.000 (data set 9903----2272.002).

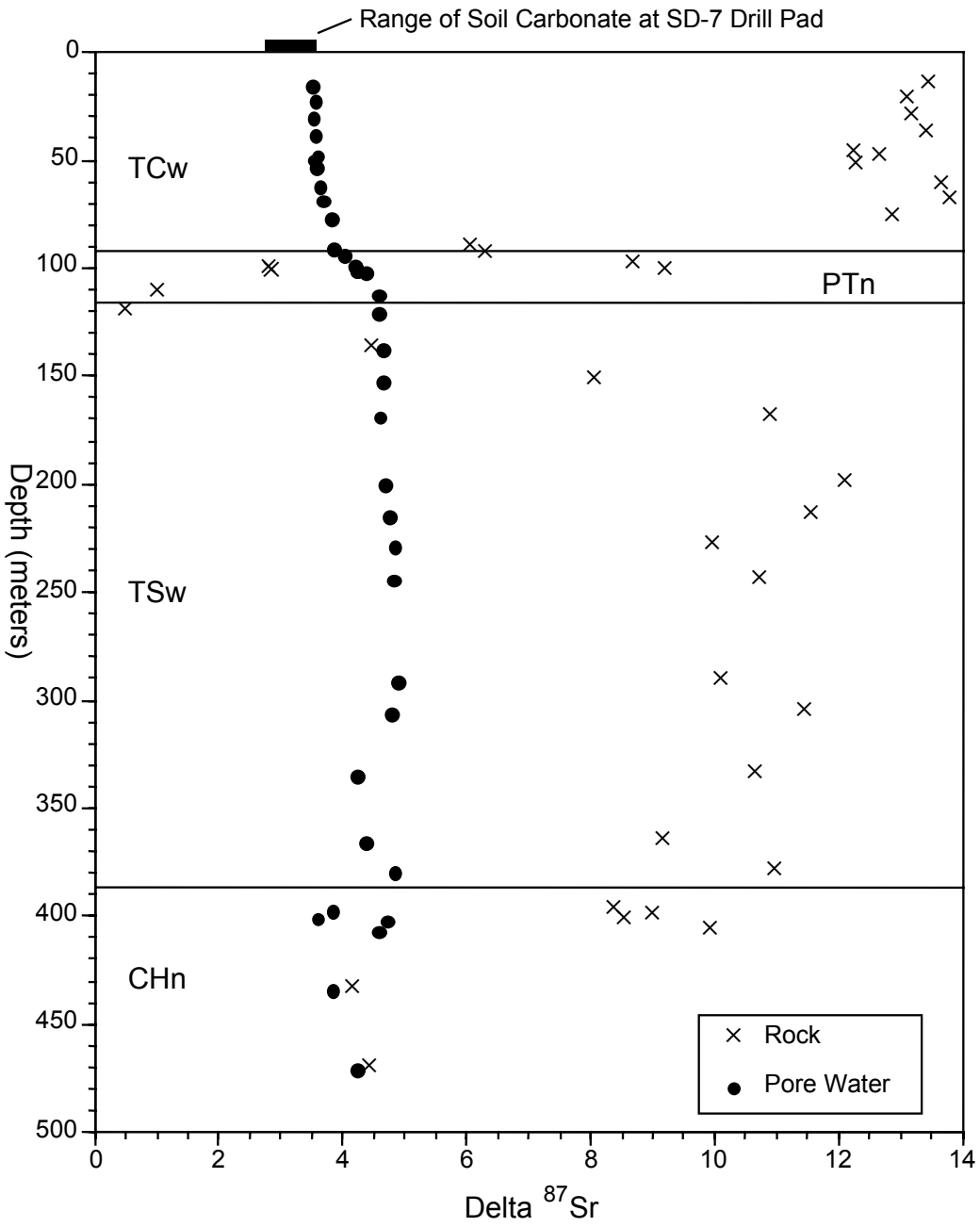

Figure 38. $\delta^{87}Sr$ in SD-7 Pore Waters and Rocks.

Note: $\delta^{87}Sr$ (per mil) of pore waters (black dots) and calcite fracture coatings (X's) in SD-7 as a function of depth. Pore water Sr isotope compositions in SD-7 vary as a function of depth due to water-rock interaction, especially within the PTn. The range of strontium isotope compositions of calcite collected from soils in the vicinity of the SD-7 drill pad are shown by the bar at top. Sr isotopic ratios are reported in DTN GS970908315215.011, from which $\delta^{87}Sr$ values are calculated using equation (7) in section 6.6.6.

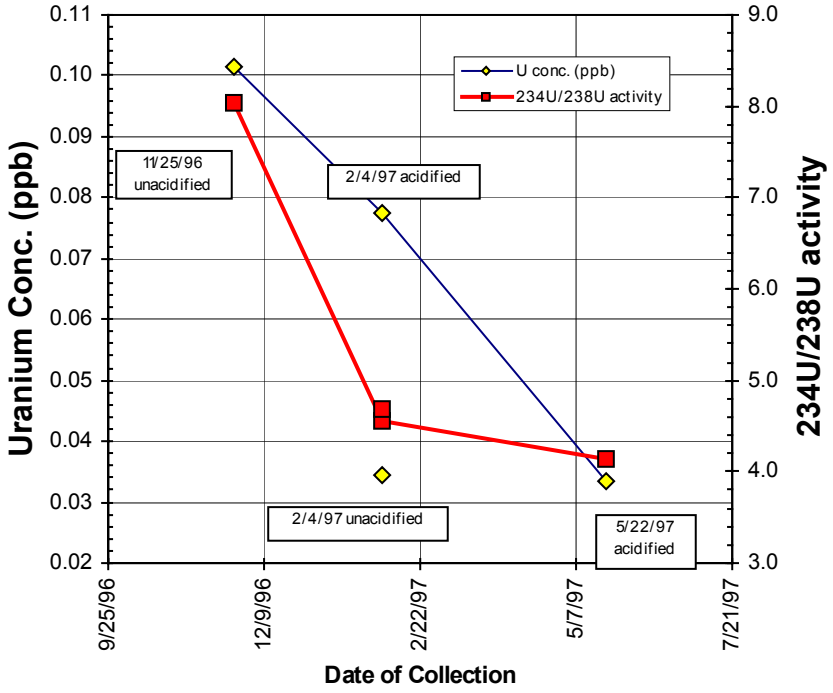

Figure 39. Uranium Concentrations and $^{234}U/^{238}U$ Activity Ratios of Water from the Single Heater Test.

Note: Uranium concentrations and $^{234}U/^{238}U$ activity ratios in water collected from borehole ESF-TMA-NEU2, zone 4, associated with the Single Heater Test, ESF, Alcove #5. Data are from DTNs GS970508312272.001 (11/25/96 sample) and GS980908312322.009 (2/4/97 and 5/22/97 samples).

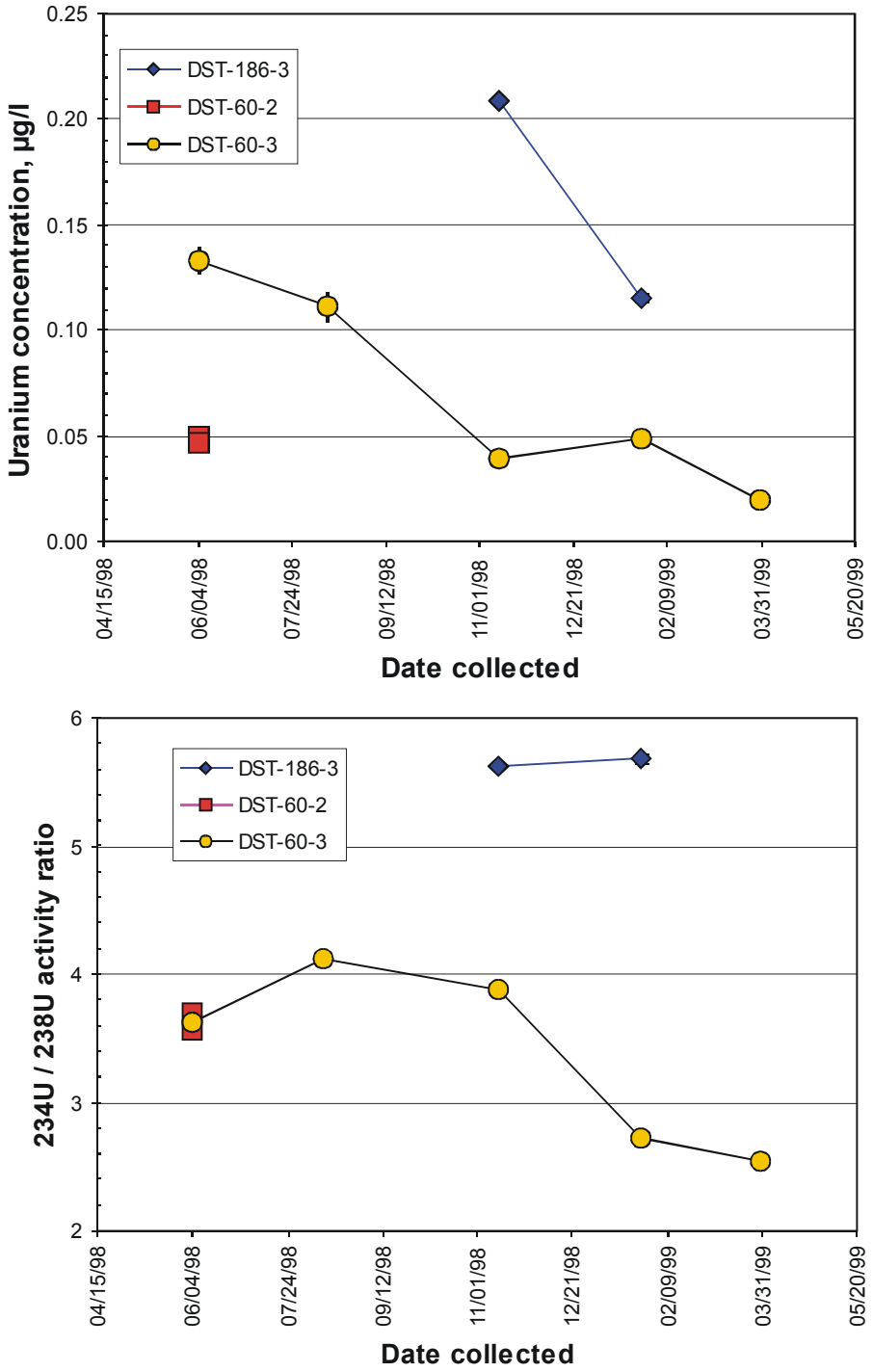

Figure 40. Uranium concentrations and $^{234}U/^{238}U$ activity ratios in water from the Drift-Scale Heater Test

Note: Uranium concentrations and $^{234}U/^{238}U$ activity ratios in water collected from boreholes associated with the Drift-Scale Heater Test, ESF, Alcove #5. Data are reported in DTN: MO0012URANISOT.000.

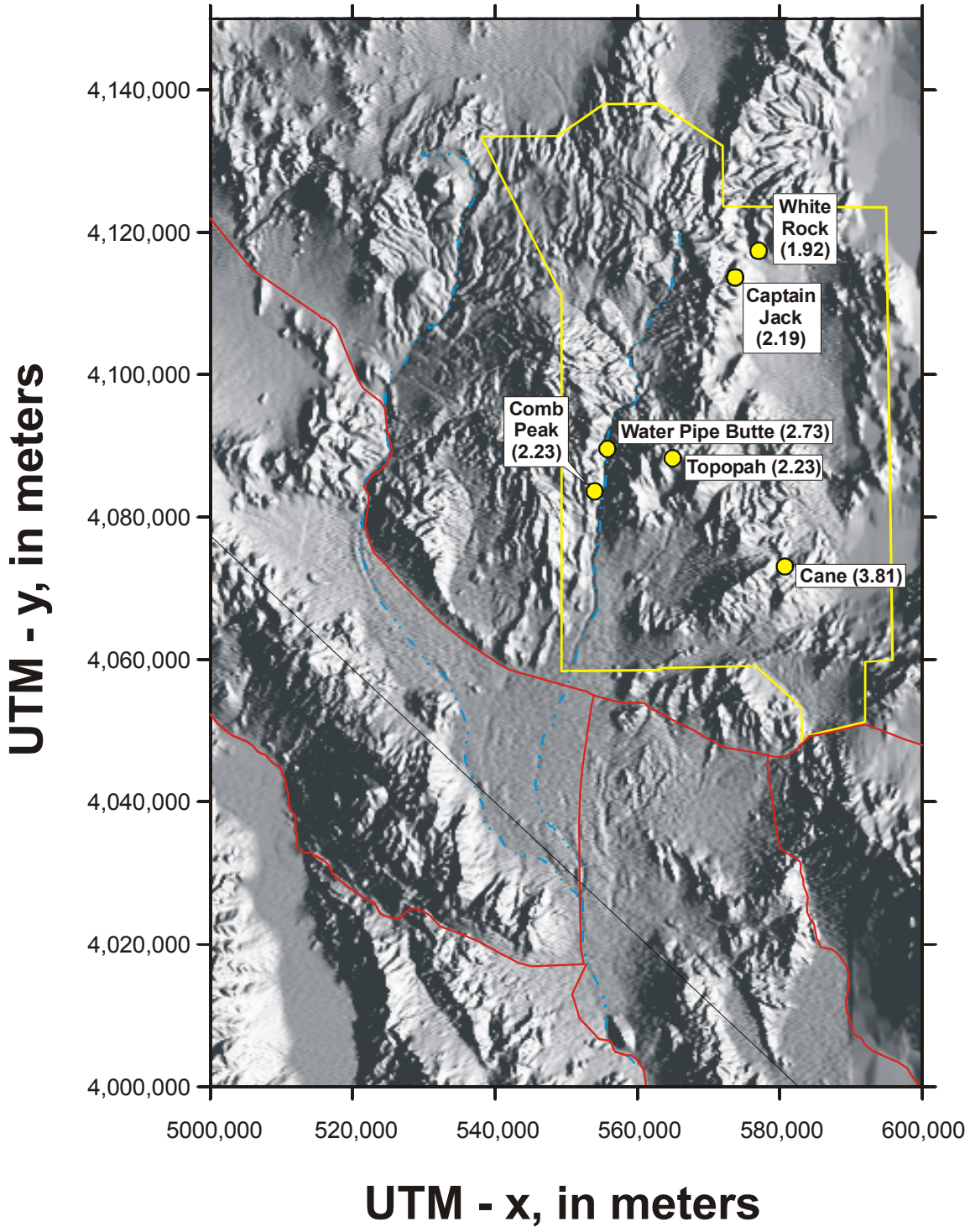

Figure 41. $^{234}U/^{238}U$ activity ratios of water from perched springs

Note: This map shows the locations of perched springs on the Nevada Test Site as well as the $^{234}U/^{238}U$ activity ratios of the discharge. Yucca Mountain straddles the lower western boundary of the Nevada Test Site (boundary shown as yellow line). Data are from GS010608315215.002, GS010808312322.004, GS980908312322.009, and MO0012URANISOT.000.

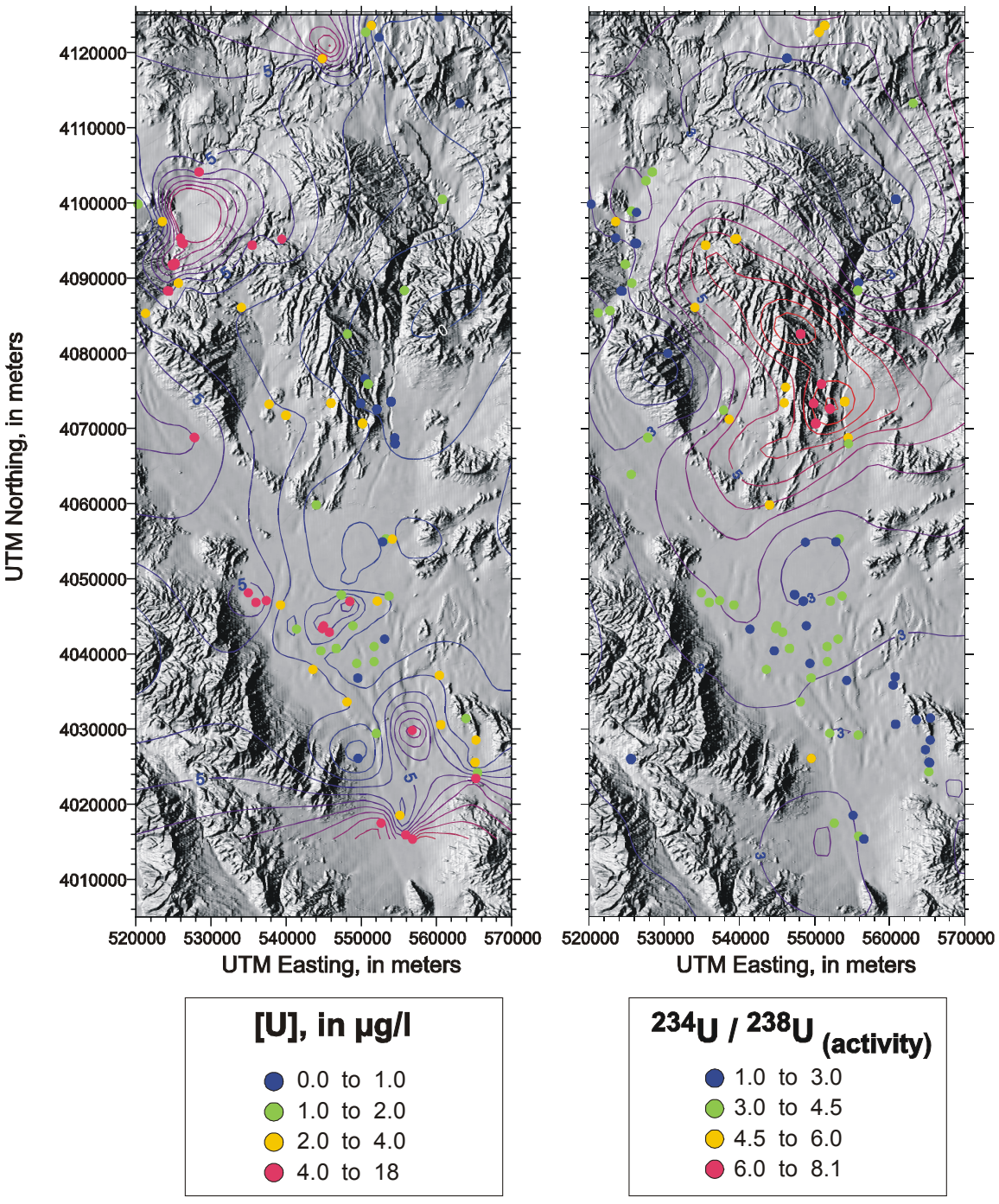

Figure 42. Uranium concentrations and $^{234}U/^{238}U$ activity ratios in regional ground water samples

Note: Uranium concentrations and $^{234}U/^{238}U$ activity ratios of saturated-zone ground water samples from the vicinity of the Nevada Test Site. The highest activity ratios (right-hand figure) are beneath and slightly east of Yucca Mountain. Data are from DTNs GS930108315213.004, GS010608315215.002, GS010808312322.004, GS980208312322.006, GS980908312322.009, and Assumption 26. Total uranium values in DTN GS980208312322.006 may not be representative of the groundwater because of sample handling issues (CRWMS M&O 2000b, Section 3.2).

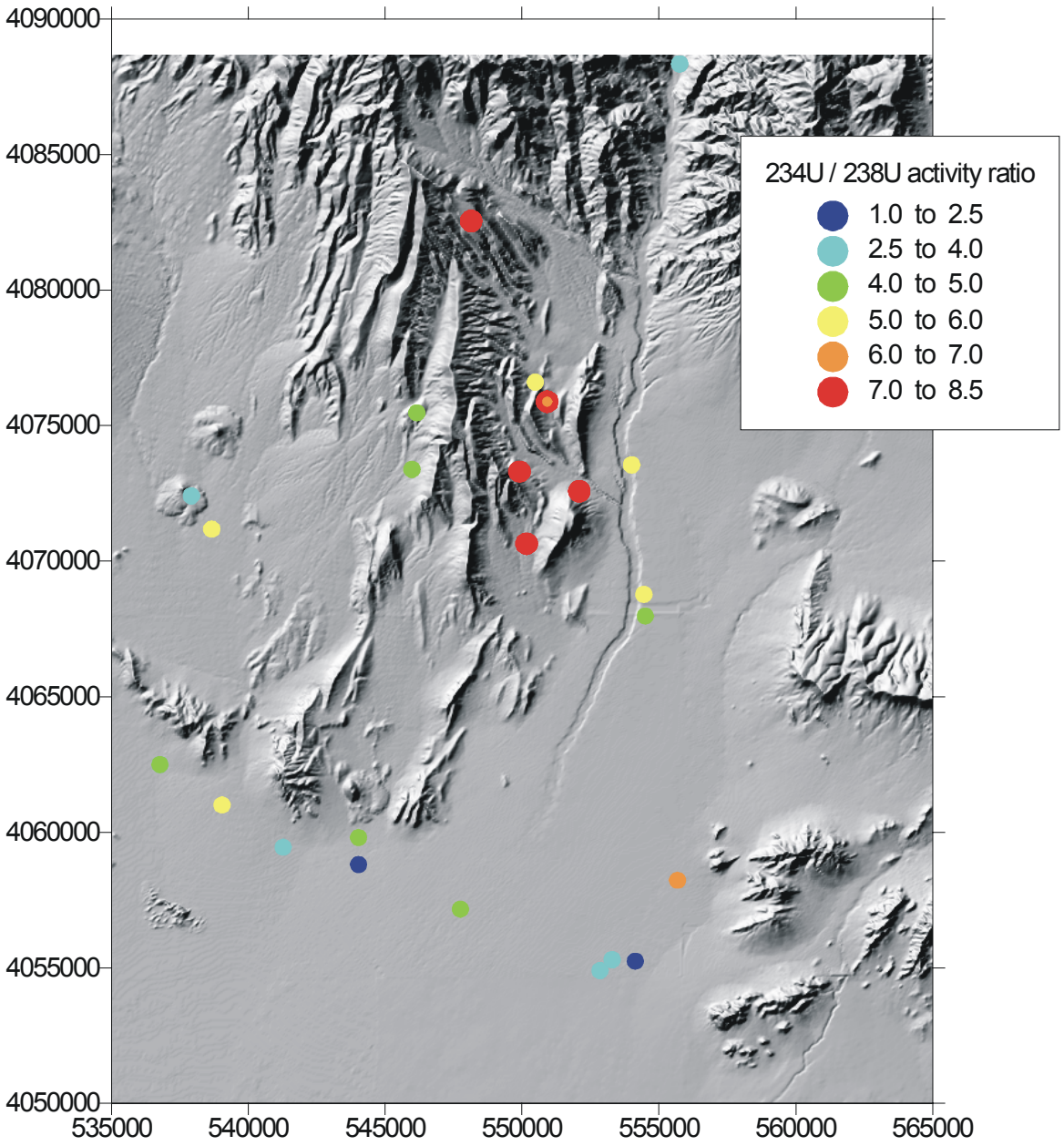

Figure 43. $^{234}U/^{238}U$ activity ratios of ground water in the Yucca Mountain vicinity.

Note: Uranium isotopic compositions of regional saturated zone ground water samples from the Yucca Mountain vicinity. Yucca Mountain is the long ridge slightly west of the cluster of samples with the highest activity ratios on this map. Data from DTNs GS930108315213.004, GS010608315215.002, GS010808312322.004, GS980208312322.006, GS980908312322.009, MO0012URANISOT.000, and Assumption 26.

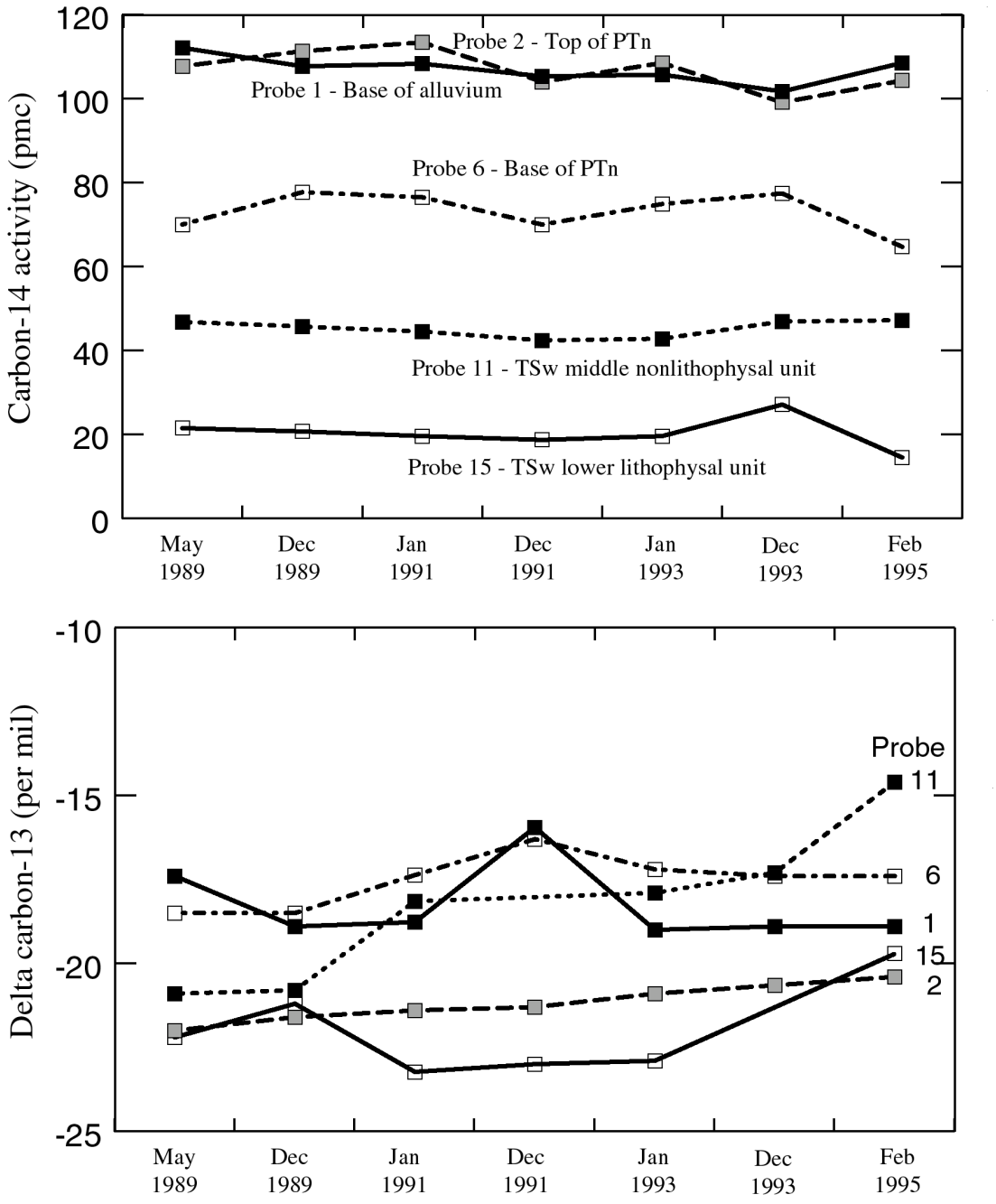

Figure 44. Carbon isotopes in UZ-1 gases

Note: Isotopic data are from DTN: MO0012CO13UNSZ.003, MO0012CO13UNSZ.000, MO0012CO13UNSZ.001, MO0012CO14UNSZ.002, MO0012CO13UNSZ.002, MO0012CO2UNSZO.004, MO0012CARB1314.000, GS940408312271.005 and MO0102UNSZHYCM.000

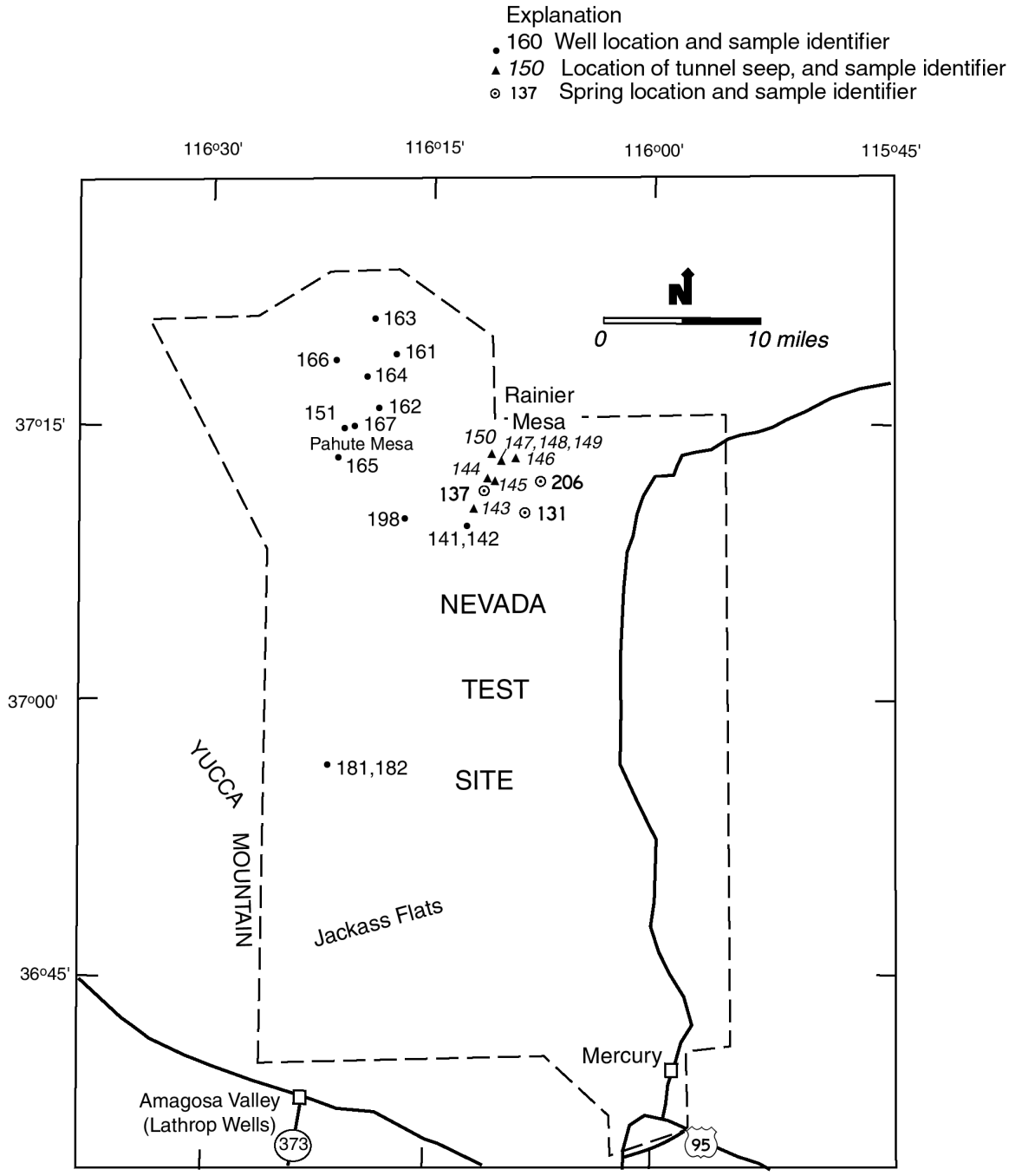

Figure 45. Nevada Test Site Wells and Springs.

Note: Location of selected wells and springs in the Nevada Test Site area, for which isotopic and geochemical data for water samples are available (Figure 4 and Table 5 in McKinley et al. 1991). Identifiers for these samples are given in Figures 11 (for springs and seeps) and 47 (for wells).

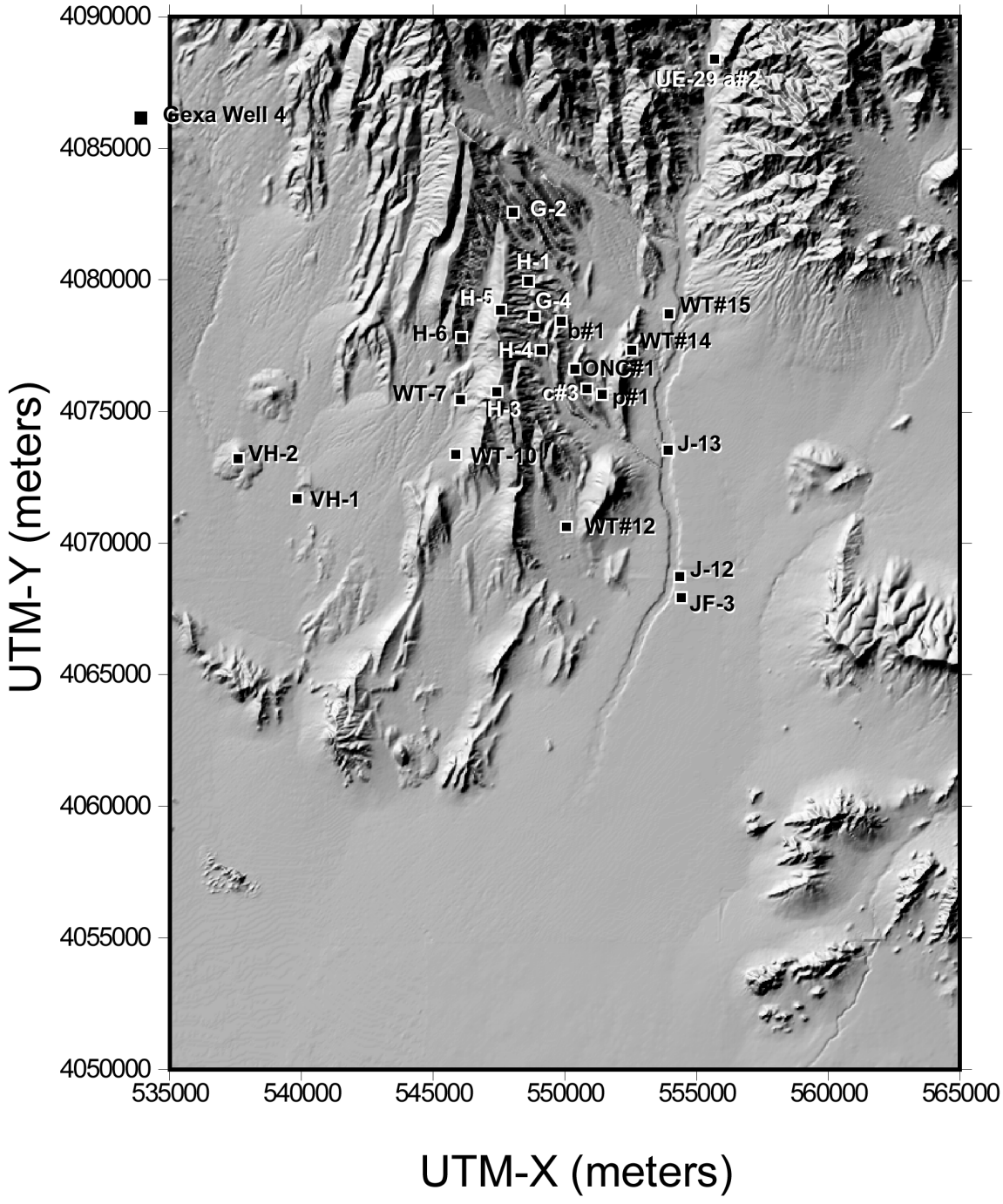

Figure 46. Location of selected wells in the vicinity of Yucca Mountain

Note: This map shows the location of selected wells in the vicinity of Yucca Mountain, for which geochemical data for groundwater samples are available. Well coordinates are from Table 24. H-5 and H-3 mark the ridgeline of Yucca Mountain.

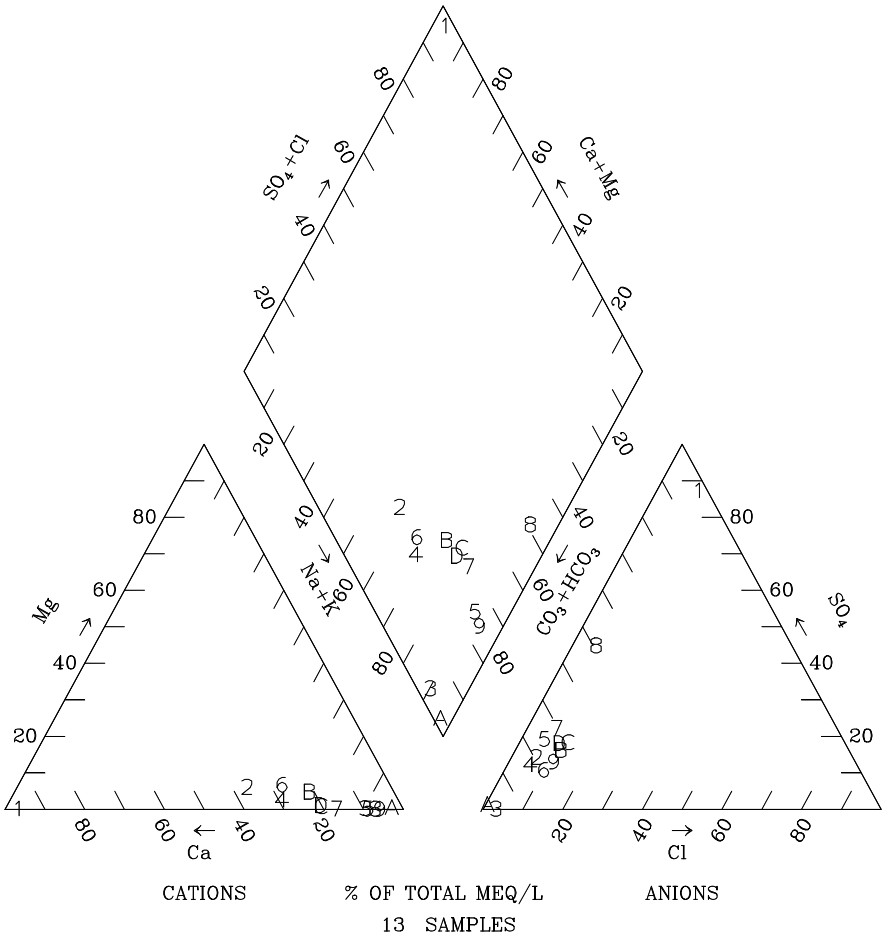

Legend					
List of Plotted Points, Site Numbers as Listed on Figure 45, and Borehole Identifiers					
1	152: U-20a#2	6	165: UE-19fs	B	198: Water Well 8
2	161: UE-19b#1	7	166: UE-19gs	C	181: UE-29 a#2 (250-355 m)
3	162: UE-19c	8	167: UE-19i	D	182: UE-29 a#2 (87-213 m)
4	163: UE-19d	9	141: TW-1 (0-171 m)		
5	164: UE-19e	A	142: TW-1 (0-1282 m)		

Figure 47. Trilinear Diagram for Up-gradient Groundwaters.

Note: This trilinear diagram is for groundwaters up-gradient of Yucca Mountain, for Pahute Mesa and Rainier Mesa, Nevada. Data from DTN: GS930308312323.001 (UE-29 a#2) and McKinley et al. (1991, Table 6).

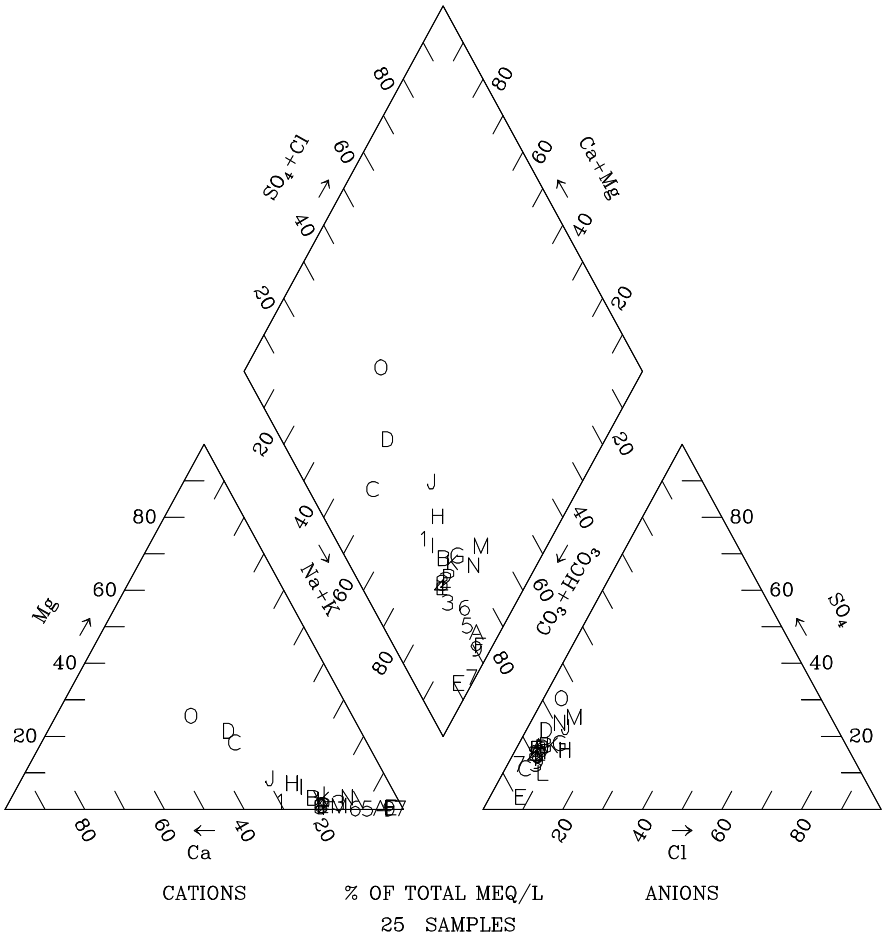

Legend

List of Plotted Points and Borehole Identifiers (locations shown in Figure 46)

Yucca Mountain area				*40 Mile Wash*		*Other*	
1	b#1	9	H-5	G	a#2 (87-213 m)	M	Gexa
2	c#2	A	H-6	H	J-12	N	VH-1
3	G-2	B	ONC#1	I	J-13	O	VH-2
4	G-4	C	p#1 (0-1200 m)	J	JF-3	P	WT#12
5	H-1 (572-6887 m)	D	p#1 (1300-1800 m)	K	WT#14		
6	H-1 (687-1829 m)	E	WT-7	L	WT#15		
7	H-3	F	WT-10				
8	H-4						

Figure 48. Trilinear Diagram for Yucca Mountain Groundwaters

Note: This trilinear diagram is for groundwaters from the vicinity of Yucca Mountain. Full identifiers for wells are given in Table 24. Well locations are shown in Figure 46. Data are from DTN: GS930308312323.001 (b#1, a#2, G-4, H-1, H-4, H-5, H-6, VH-1, J-12, J-13), MO0012MAJIONIS.000 (c#2), GS990608312133.001 (WT#12, WT-10, and G-2), and Oliver and Root (1997, attached file yucca.xls).

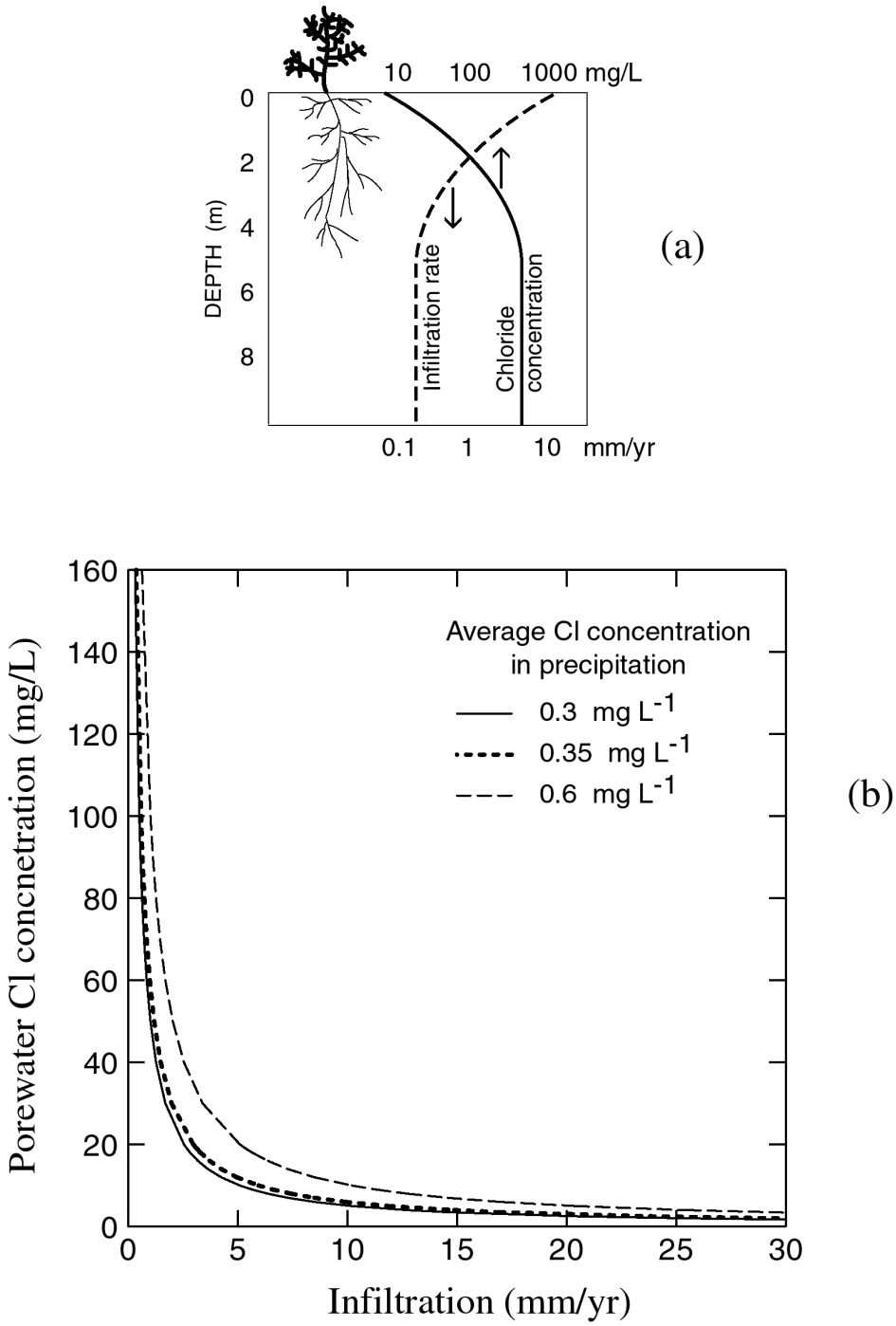

Figure 49. Chloride Mass Balance (CMB) Method for Estimating Infiltration.

Note: (a) Schematic diagram illustrating the underlying basis of the CMB method. (b) Plot showing Cl concentrations as a function of infiltration, assuming a range of average chloride concentrations for local precipitation and an average annual precipitation rate of 170 mm. See text in section 6.9.1 for discussion of the model, its assumptions, and the basis for these parameter values.

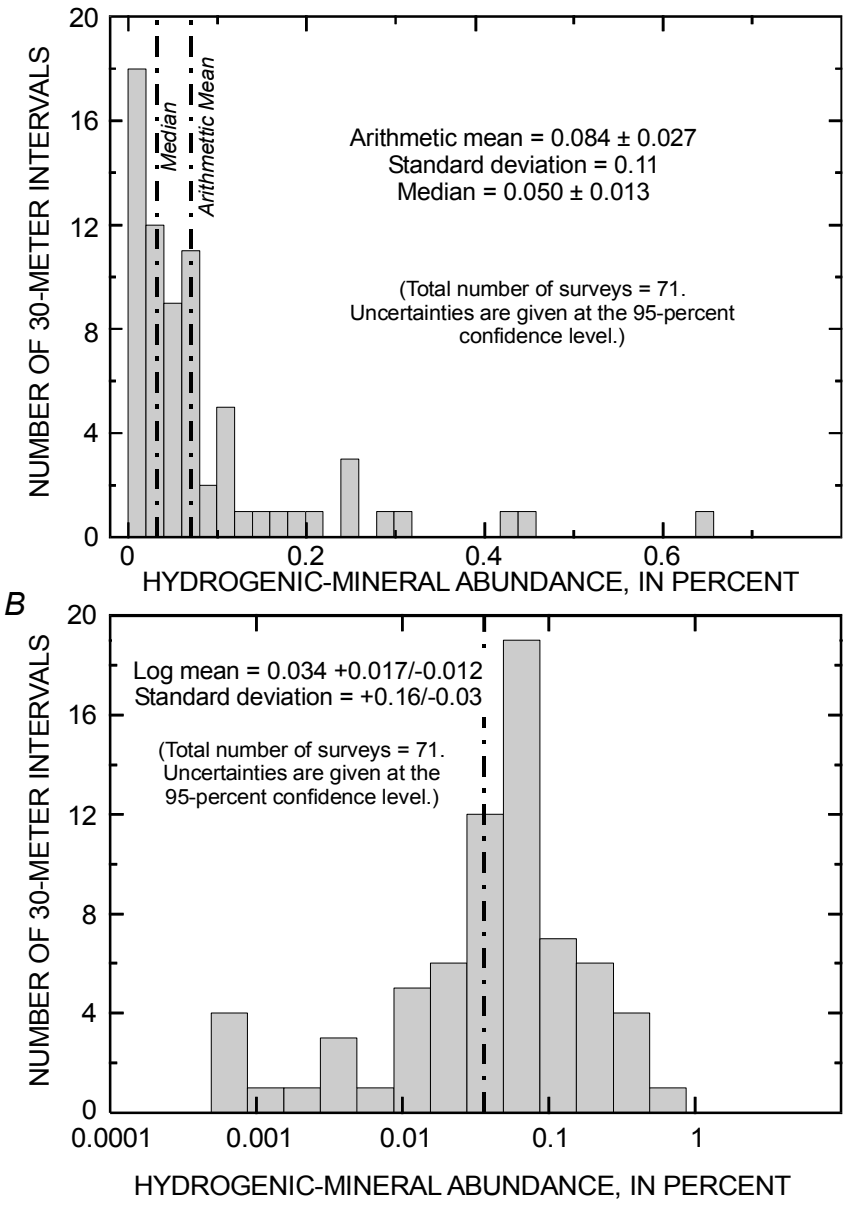

Figure 50. Hydrogenic-mineral abundances.

Note: Histograms showing hydrogenic-mineral abundances in welded tuffs in the Exploratory Studies Facility on A, linear, and B, log scales. Data are from DTN: GS980308315215.008.

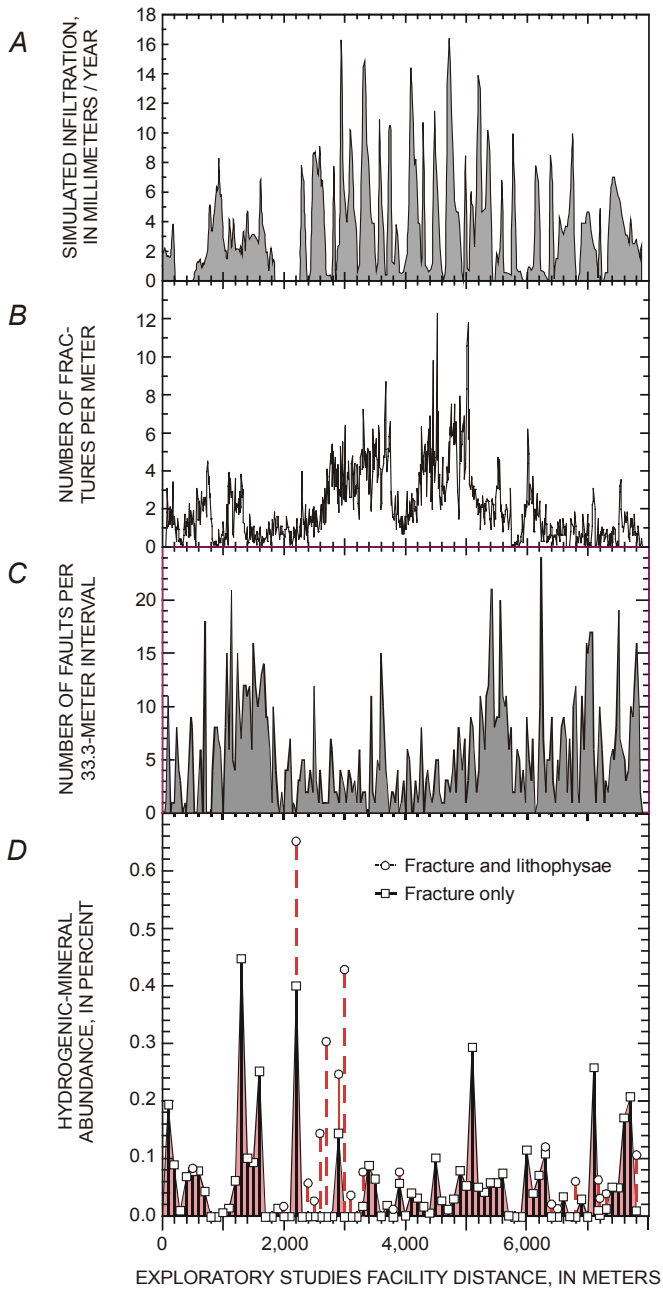

Figure 51. Infiltration, fracture, fault and shear densities, and hydrogenic-mineral abundances

Notes: Estimates of A, simulated infiltration; B, fracture density; C, fault and shear; and D, hydrogenic-mineral abundance; plotted against distance from the north portal of the Exploratory Studies Facility. Data are from DTN: GS960908312211.003 (for plot A); DTN: GS960708314224.008, GS960708314224.010, GS960908314224.014, GS970208314224.003, GS971108314224.022, GS971108314224.023, GS971108314224.024, GS971108314224.025, GS971108314224.026, GS971108314224.028, GS970808314224.008, GS970808314224.010, GS970808314224.012, GS971108314224.020, GS000608314224.004, and GS971108314224.021 (for plots B and C) and DTN: GS980308315215.008 (for plot D).

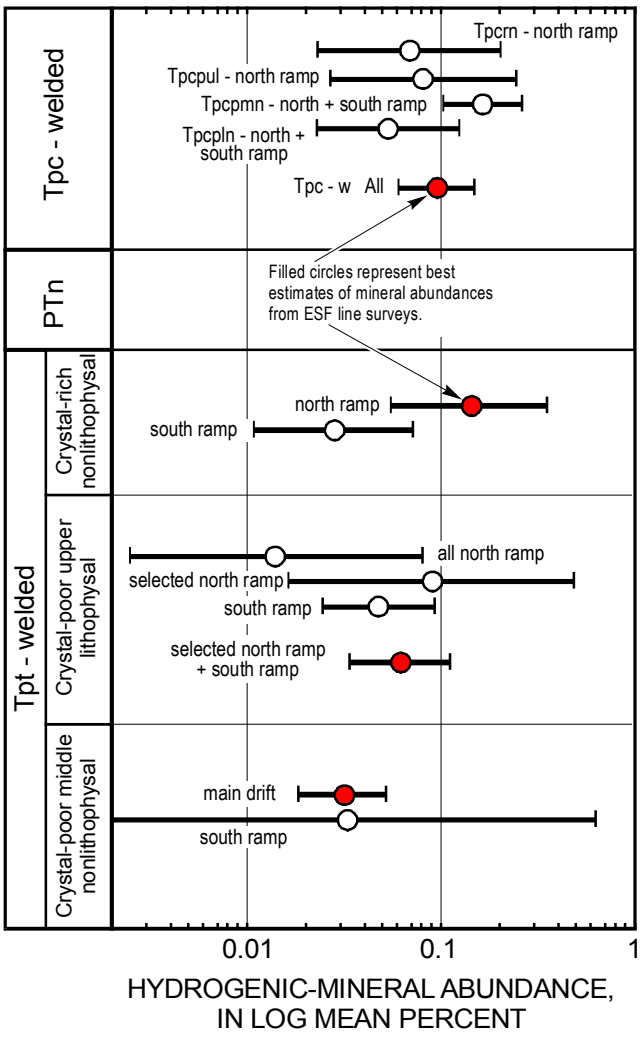

Figure 52. Hydrogenic-mineral abundances in welded tuffs.

Note: Summary of hydrogenic-mineral abundances in welded tuffs in the Exploratory Studies Facility. Stratigraphic units from Buesch et al. (1996). Data are from DTN: GS980308315215.008.

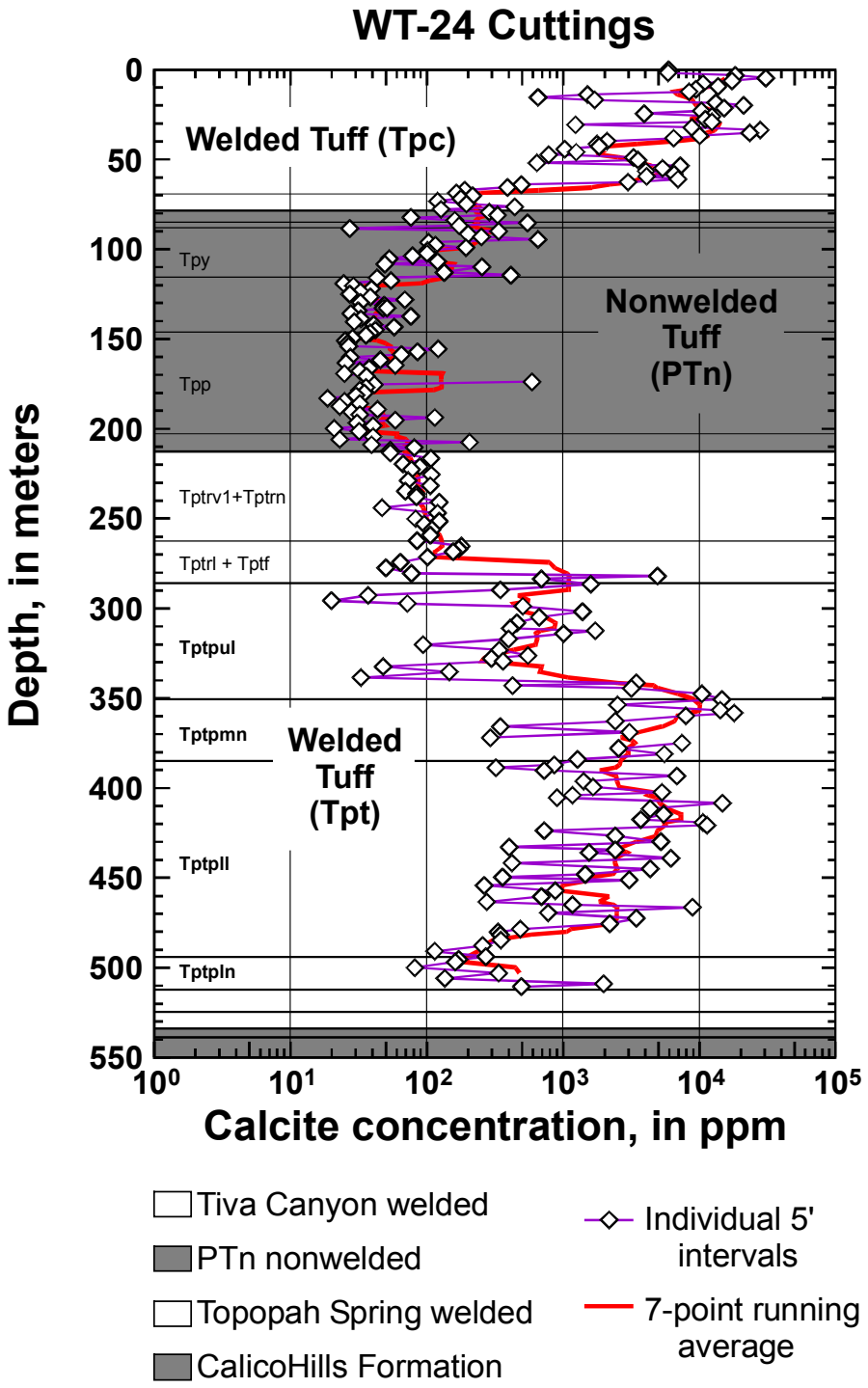

Figure 53. Calcite concentrations in cuttings from borehole WT-24.

Note: Data are reported in DTN: MO0012WTRCAC02.000. See assumption 22 in Table 2.

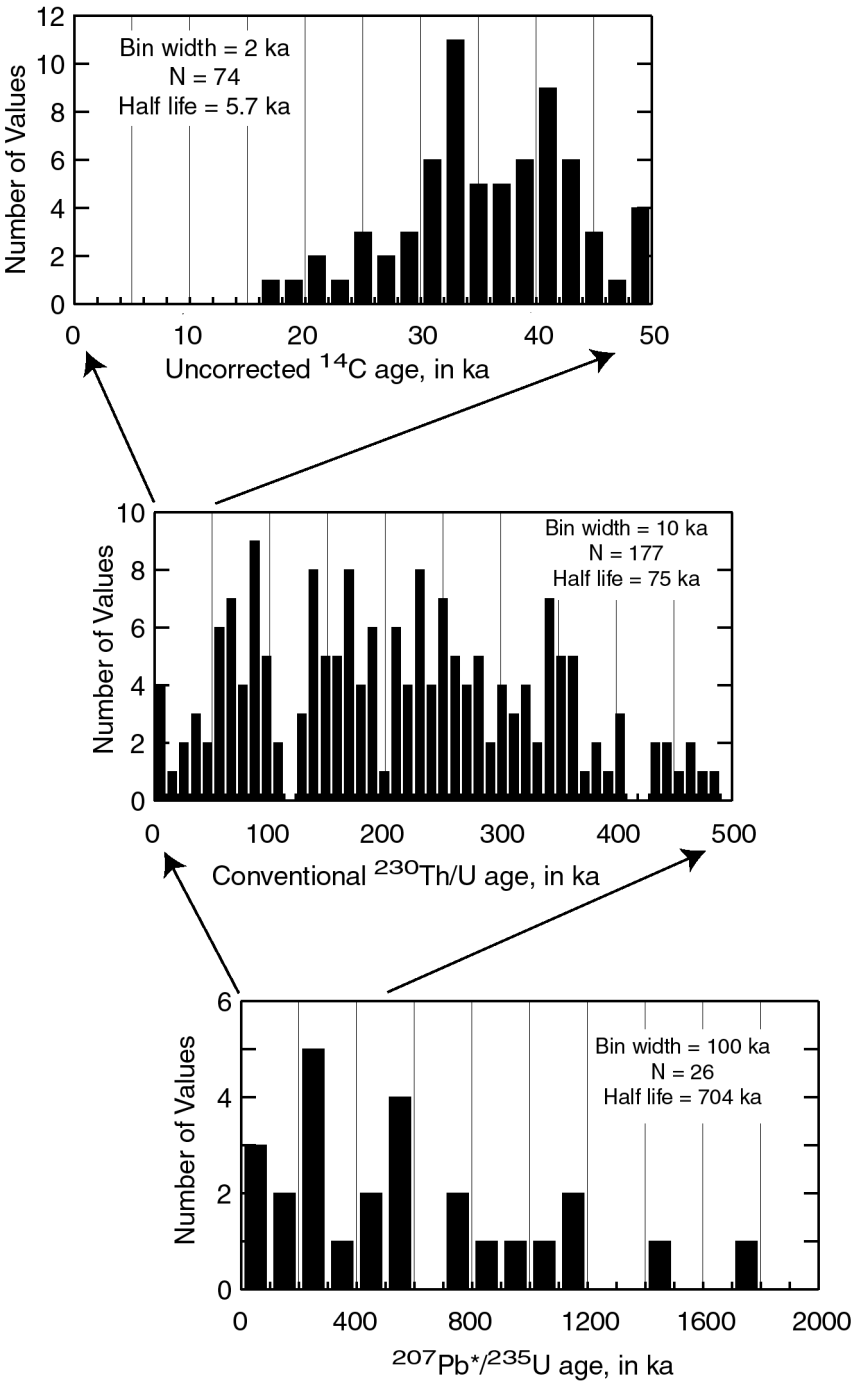

Figure 54. Radiometric ages for calcite and opal.

Note: The frequency diagrams summarize the results of dating the outer surfaces of calcite and opal mineral coatings within the ESF. Data are from DTN: GS970208315215.003, GS960808315215.006 (^{14}C ages); GS960908315215.014, GS970808315215.012 (^{230}Th/U ages); GS970208315215.002 and GS970908315215.013 (^{207}Pb*/^{235}U ages). See assumptions 24 and 25 in Table 2.

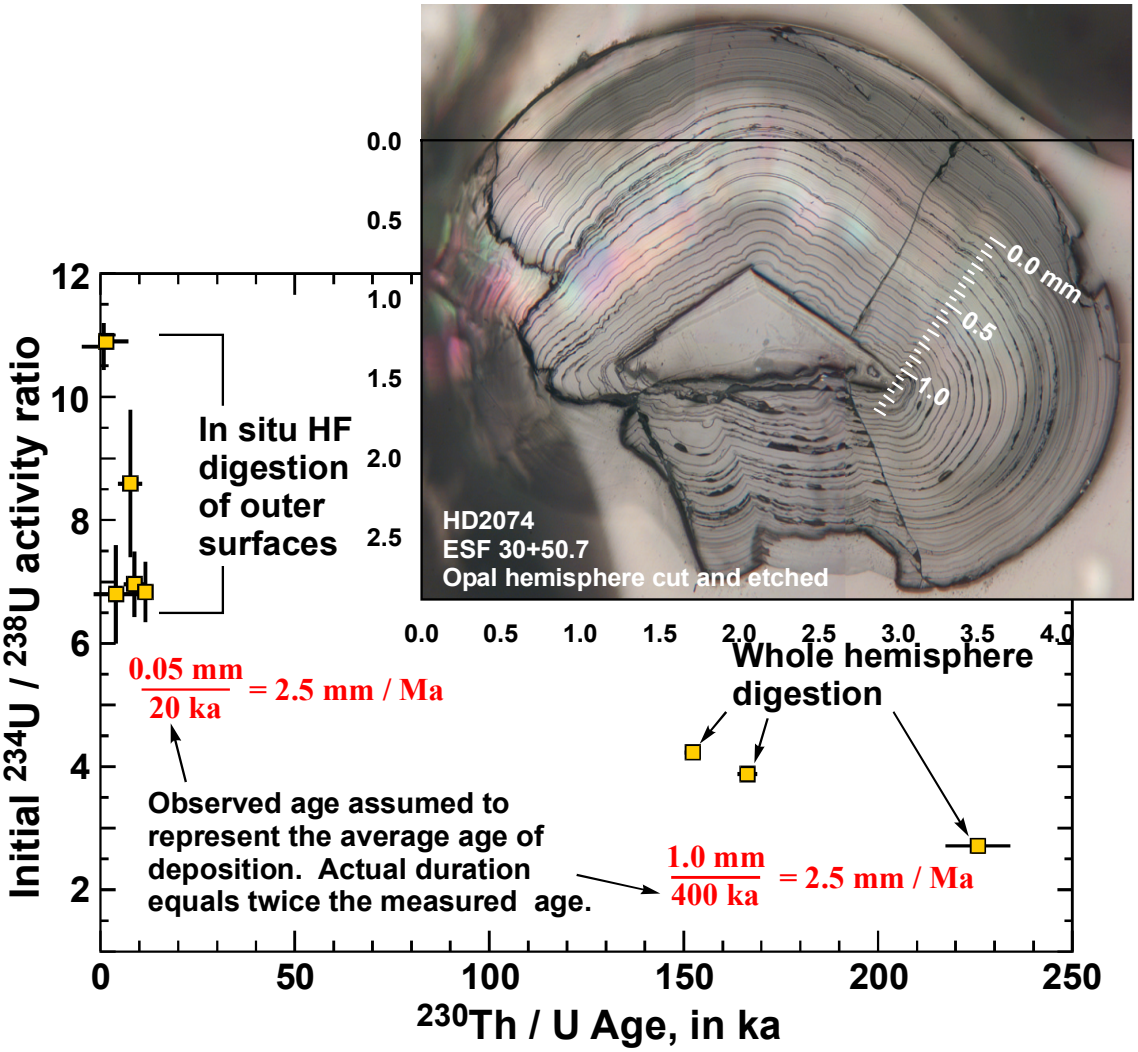

Figure 55. Dating of whole opal hemispheres and outer surfaces.

Note: Results of ^{230}Th / U dating of whole opal hemispheres and of selective removal of outer surfaces only. Data are from DTN: GS980908315215.015 and GS960908315215.014. See assumption 25 in Table 2.

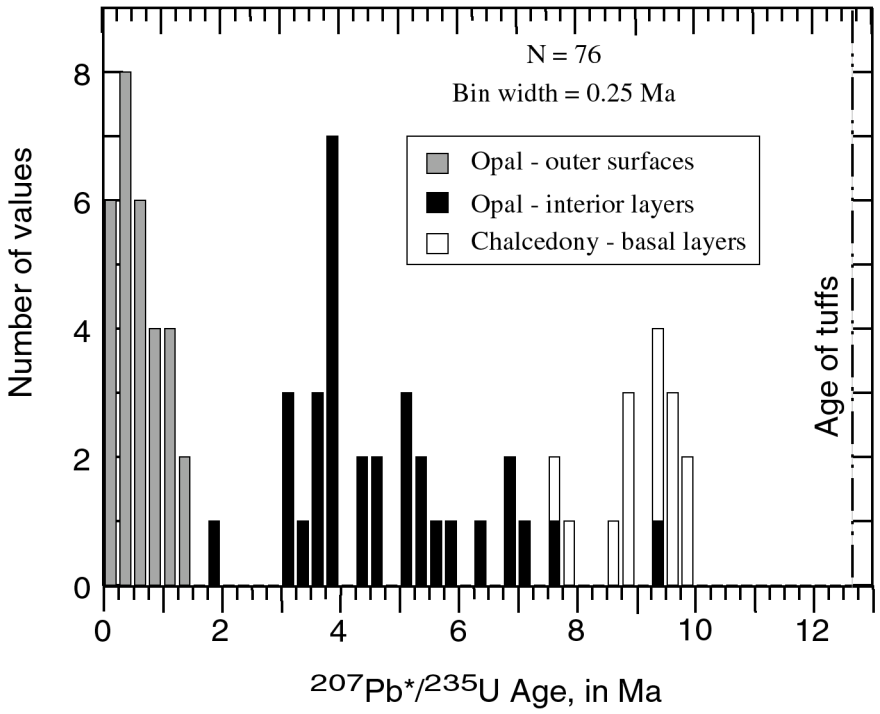

Figure 56. Histogram of ^{207}Pb / ^{235}U ages for ESF mineral coatings.

Note: Histogram of ^{207}Pb / ^{235}U ages for outer and interior layers of opal and basal chalcedony layers from ESF mineral coatings. Data are from DTN: GS970208315215.002 and GS970908315215.013. See assumption 25 in Table 2.

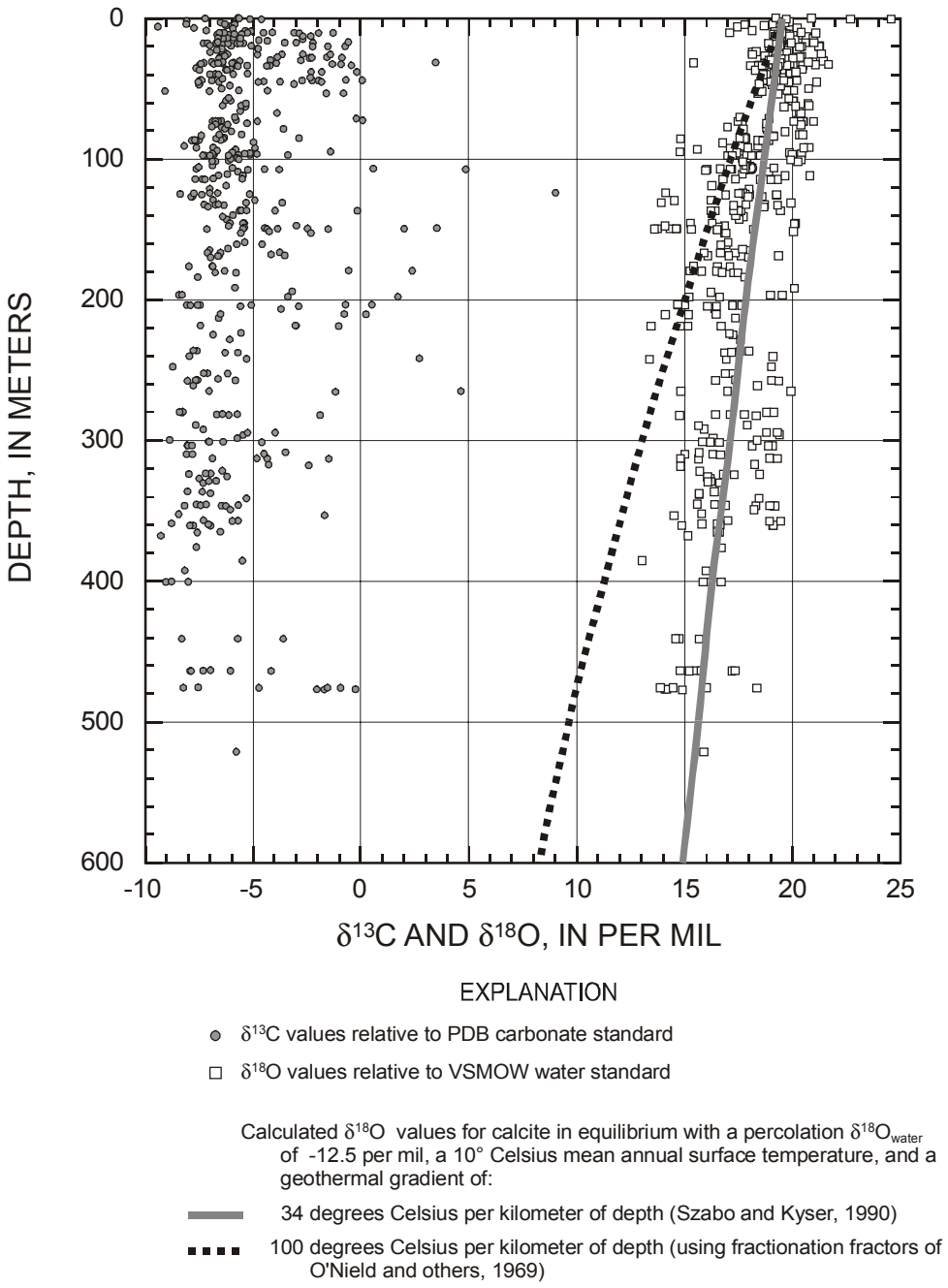

Figure 57. Stable carbon and oxygen isotopic compositions of unsaturated-zone calcite

Note: Stable carbon and oxygen isotopic compositions of subsamples of unsaturated-zone calcite from drill core at Yucca Mountain (modified from Whelan et al. 1998, Figure 5). Data from DTN: GS920708315215.017, GS950708315215.005, GS960408315215.002, GS970208315215.004, GS970808315215.010, and GS980408315215.010. Geothermal gradients shown in figure are based on Szabo and Kyser (1990, p. 1718) and O'Neil et al. (1969, p. 5552).

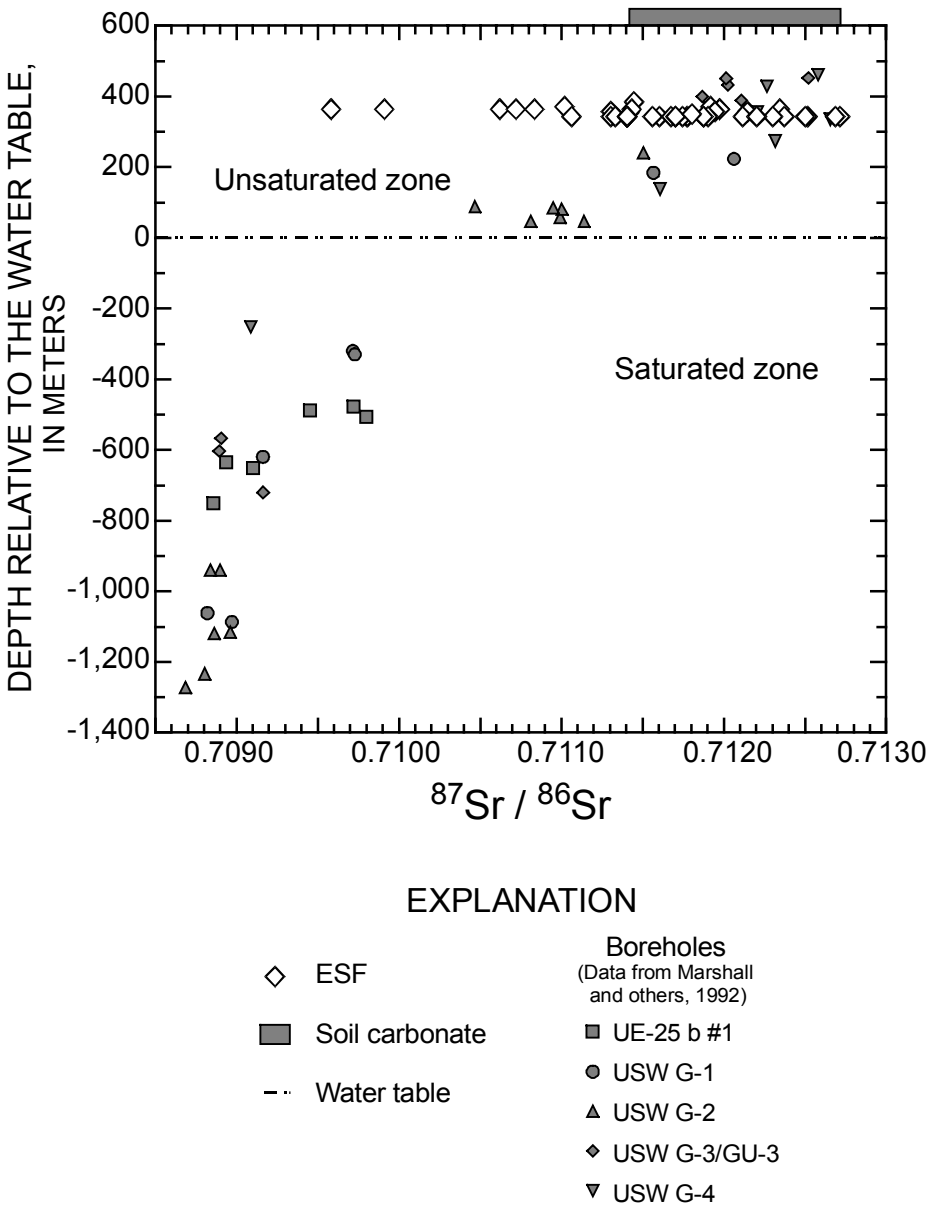

Figure 58. Strontium isotopic compositions of calcite

Note: Strontium isotopic compositions of calcite subsamples from drill core and the Exploratory Studies Facility as a function of depth relative to the water table. Data are from DTN: GS930908315215.027, GS970908315215.011 and MO0012STRIONIS.000.

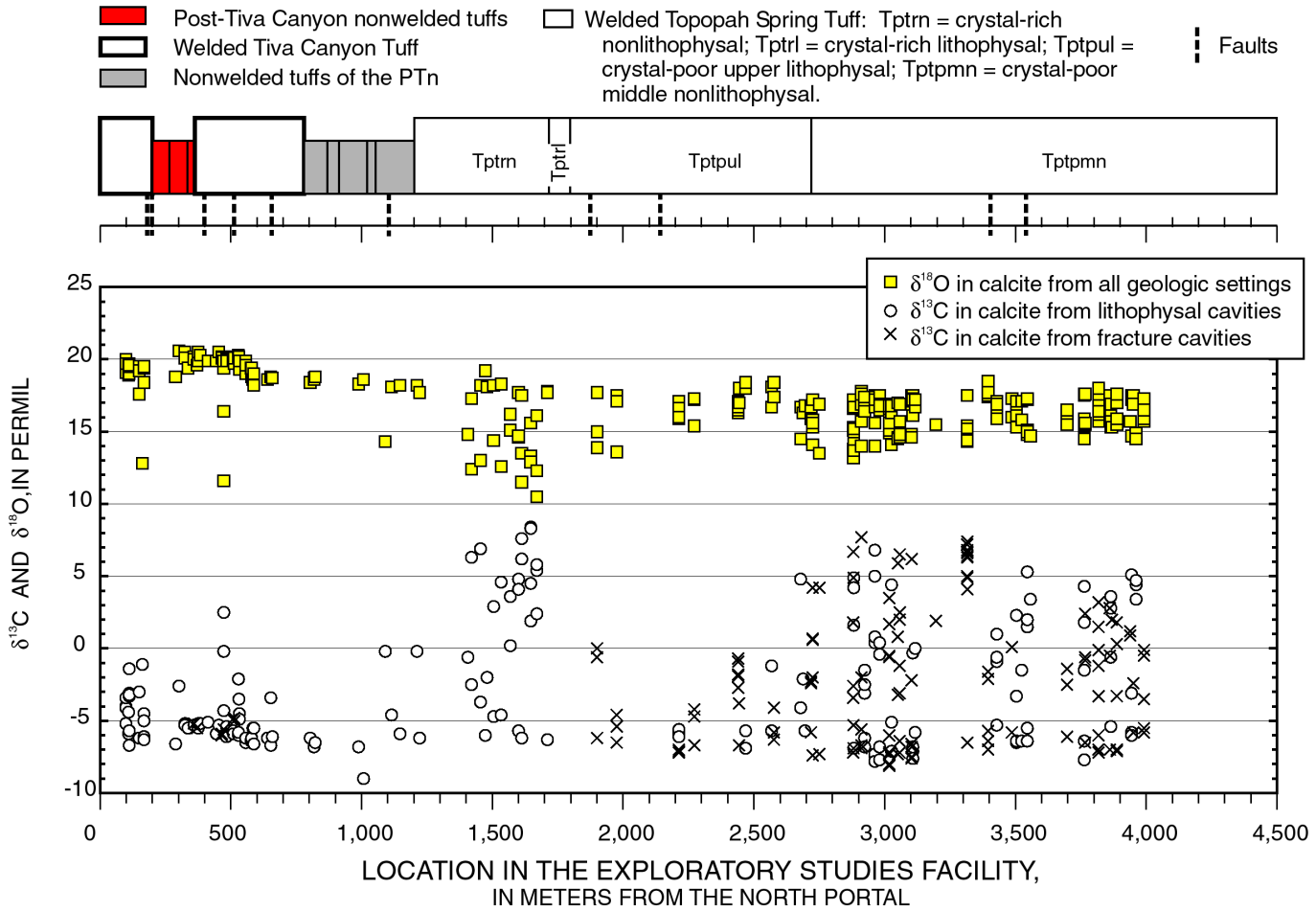

Figure 59. Carbon and oxygen isotopic compositions of calcite from the Exploratory Studies Facility

Note: The figure shows profiles of the carbon and oxygen isotopic compositions of subsamples of calcite from the Exploratory Studies Facility, as a function of distance from the north portal. Data are from DTN: GS970208315215.005 and GS960908315215.010.

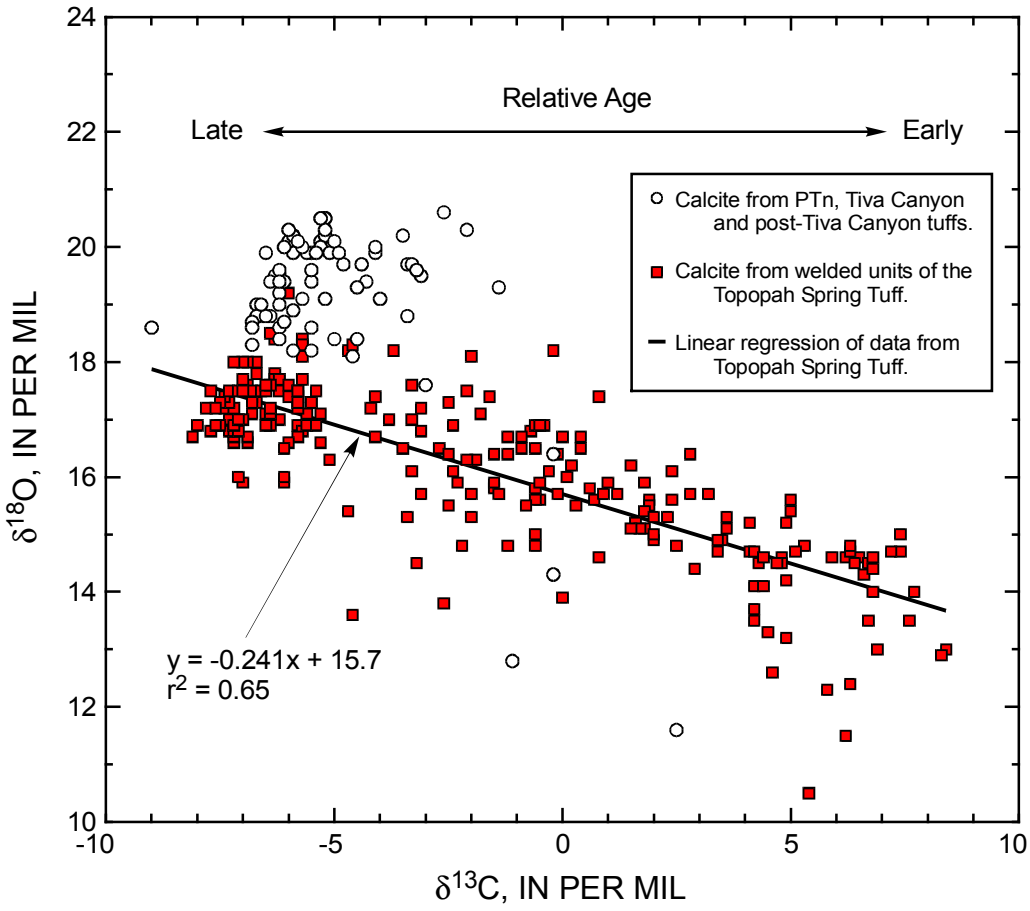

Figure 60. Scatterplot of stable carbon and oxygen isotopic compositions in calcite from the ESF

Note: Isotopic compositions of carbon and oxygen in subsamples of calcite from the Exploratory Studies Facility (Whelan et al. 1998, Appendix 2). Data are from DTN: GS960908315215.010.

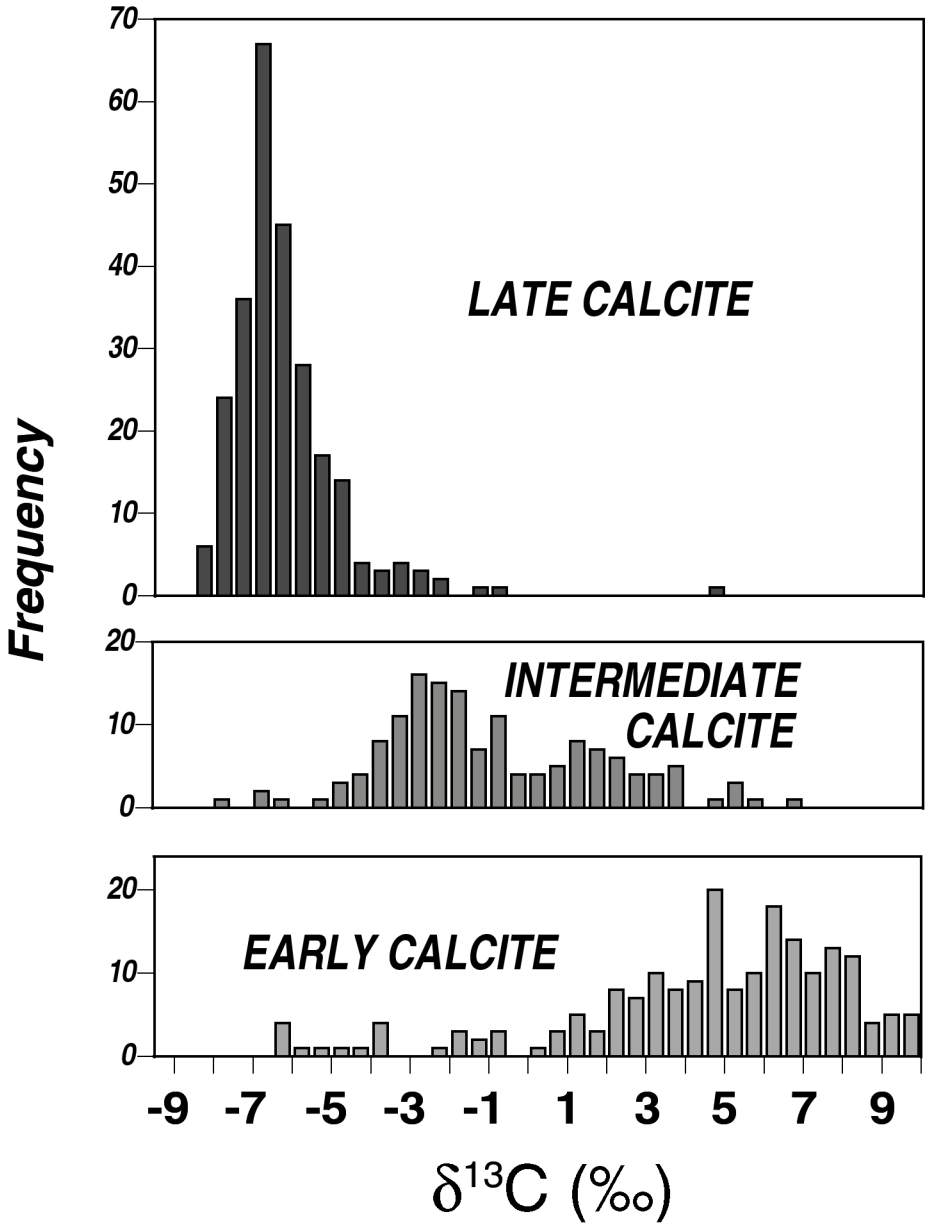

Figure 61. Histograms showing the distribution of $\delta^{13}C$ values.

Note: Histograms showing the distribution of $\delta^{13}C$ values for microsamples of calcite from the Exploratory Studies Facility, classified by relative age determined by visual examination. Data from DTN: GS960908315215.010, GS970208315215.005, GS980908315213.002, and GS990908315213.001.

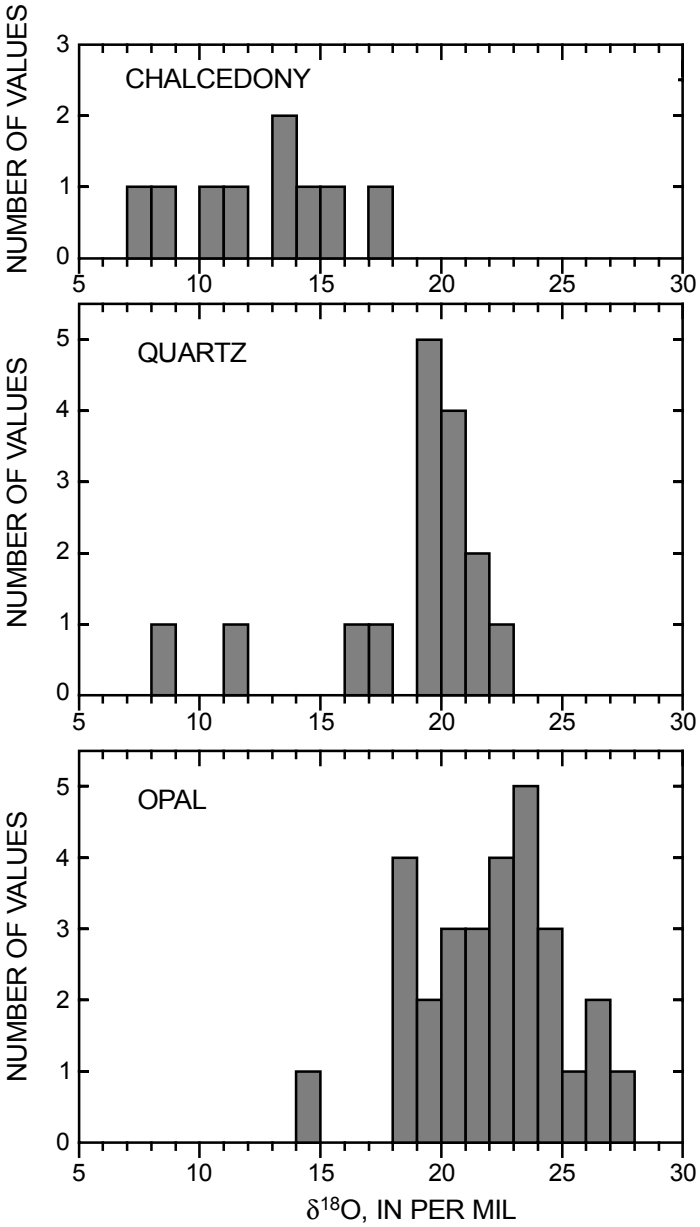

Figure 62. $\delta^{18}O$ values for chalcedony, quartz and opal from the unsaturated zone

Note: Histograms showing the distribution of $\delta^{18}O$ values for subsamples of unsaturated-zone chalcedony, quartz and opal from drill core and the Exploratory Studies Facility (Moscati and Whelan, 1996, Table 1; Whelan et al., 1998, Appendix 3). Data are from DTN: GS931108315215.035, GS940608315215.006, and GS960408315215.003.

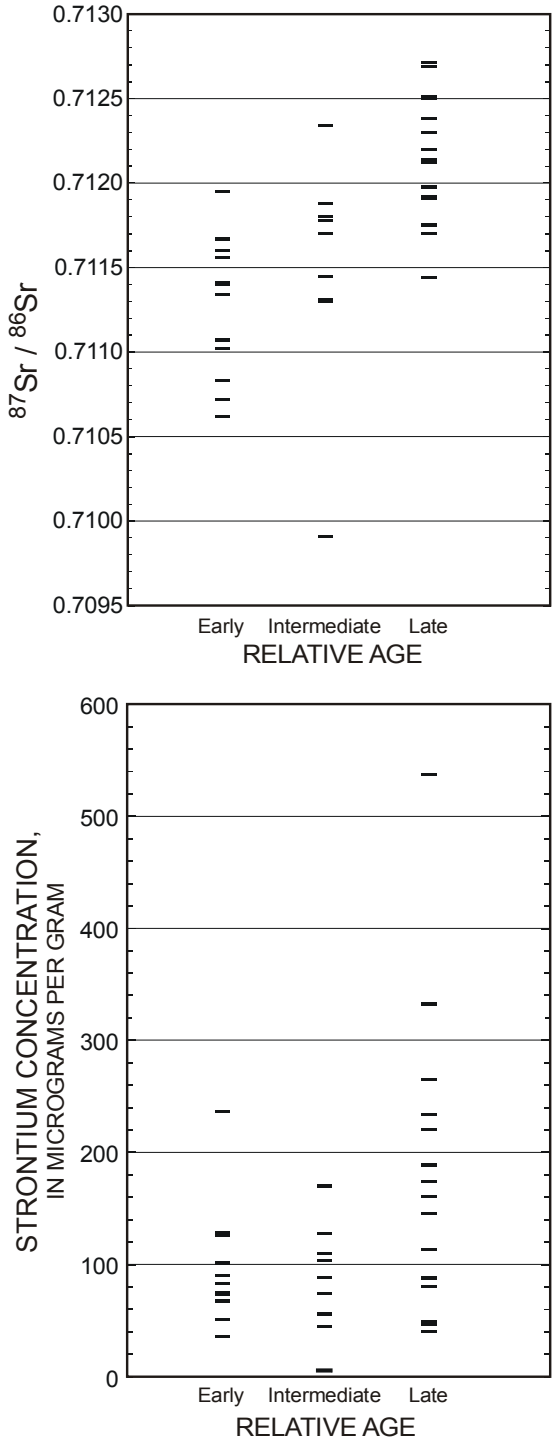

Figure 63. Strontium isotopic compositions and concentrations for ESF calcite.

Note: Strontium isotopic compositions and concentrations for subsamples of calcite from the Exploratory Studies Facility, classified by relative age. Data are from DTN: GS970908315215.011 and MO0012STRIONIS.000.

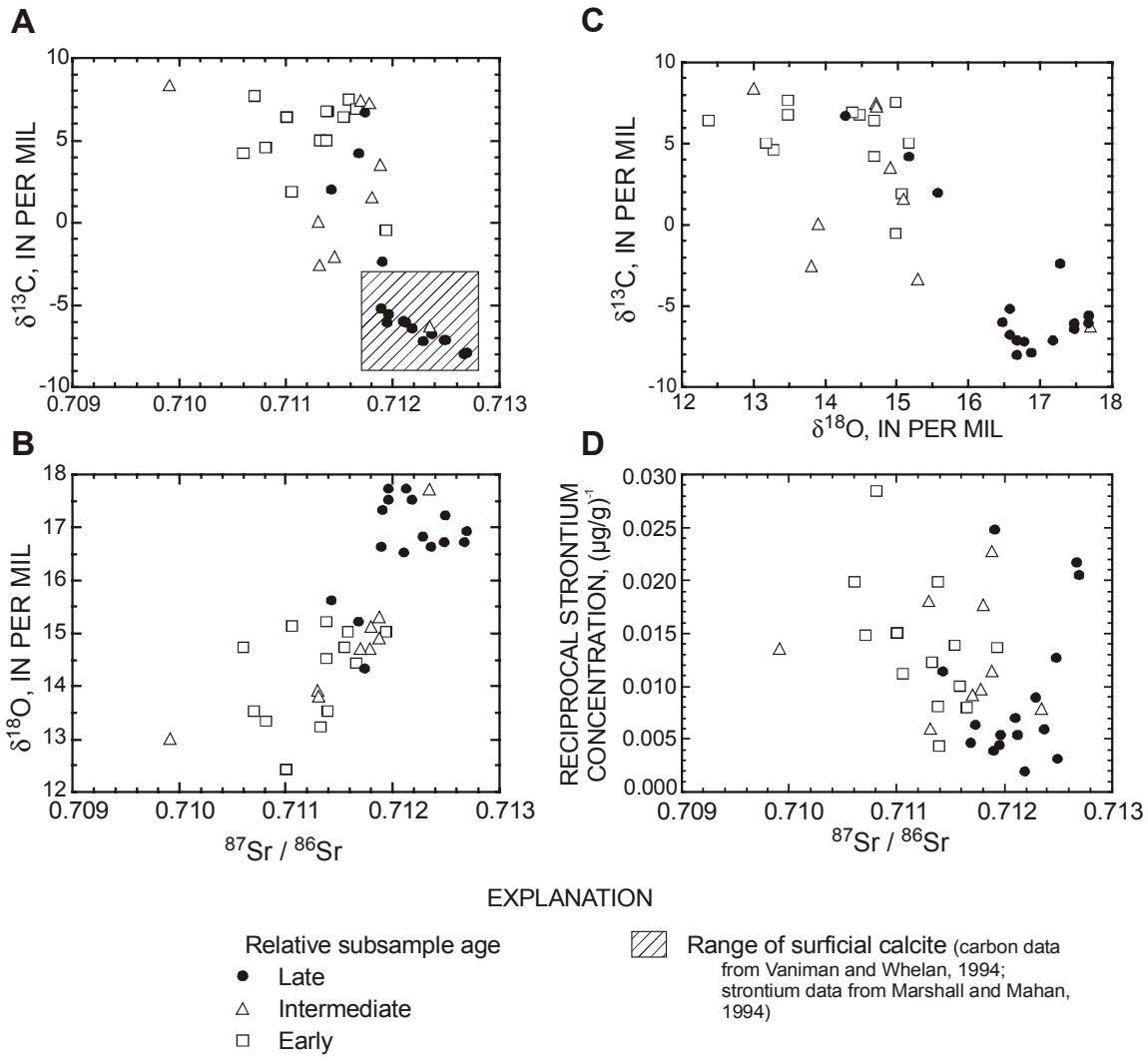

Figure 64. Carbon, oxygen and strontium isotopic compositions in ESF calcites

Note: Relations between carbon, oxygen and strontium isotopic composition and reciprocal strontium concentration for subsamples of calcite from the Exploratory Studies Facility (modified from Figure 4.11 in Paces, Neymark, et al., 1996). Data are from DTN: GS910508315215.005, GS920208315215.008, GS920208315215.012, GS930908315215.027, GS931008315215.029, GS931008315215.030, GS941108315215.010, GS950608315215.002, GS960908315215.010, GS970908315215.011, GS960908315215.010, and MO0012STRIONIS.000.

.

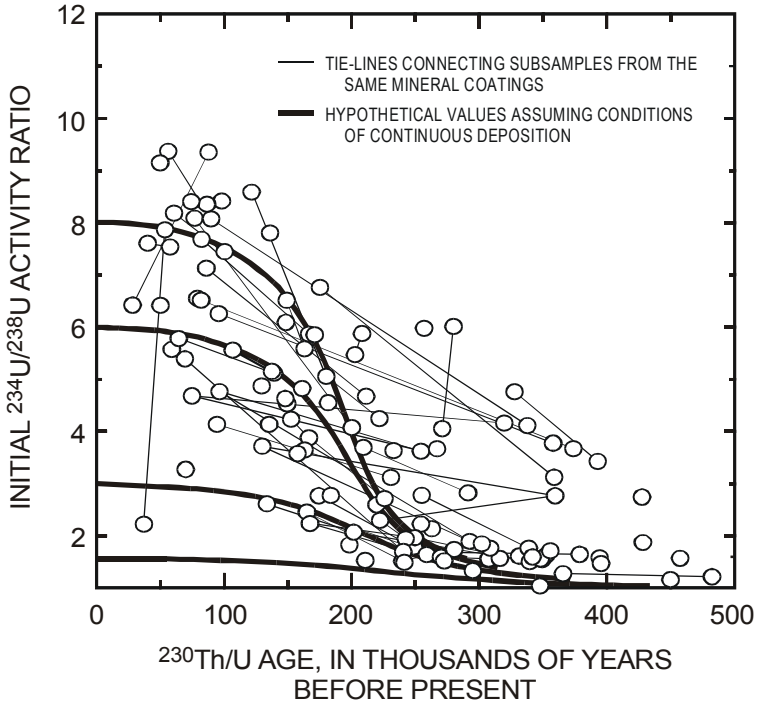

Figure 65. Covariance between initial $^{234}U/^{238}U$ activity ratios and $^{230}Th/U$ ages for calcite and opal deposits

Note: Covariance between initial uranium-234/uranium-238 ($^{234}U/^{238}U$) activity ratios and thorium-230/uranium ($^{230}Th/U$) ages for calcite and opal deposits in the Exploratory Studies Facility. Data are from DTN: GS960908315215.014, GS970208315215.001, and GS970808315215.012. See assumption 25 in Table 2.

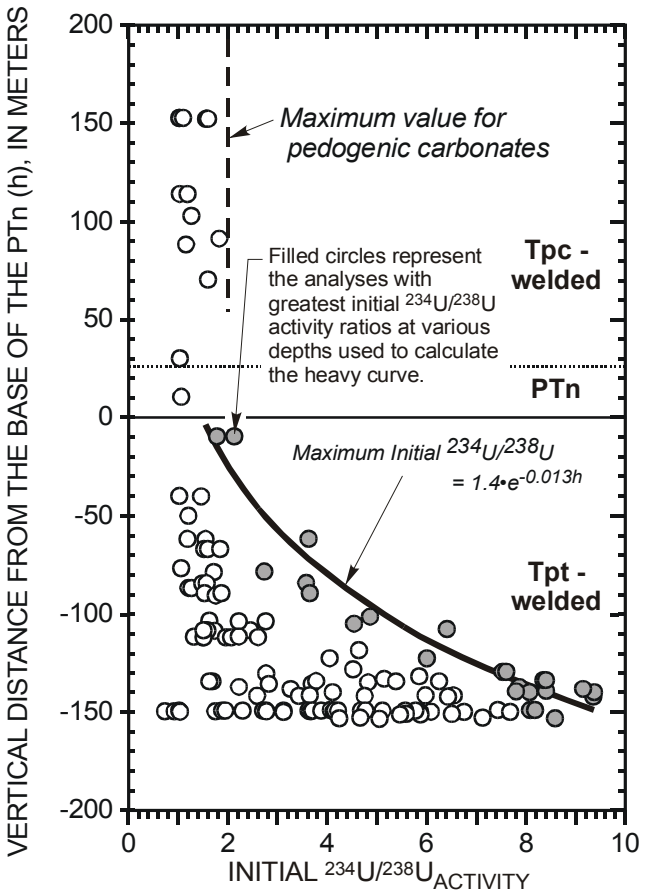

Figure 66. Initial $^{234}U/^{238}U$ activity ratios for hydrogenic minerals

Note: Initial uranium-234/uranium-238 ($^{234}U/^{238}U$) activity ratios for hydrogenic minerals from the Exploratory Studies Facility plotted against vertical distance from the base of the Paintbrush Tuff nonwelded hydrogeologic unit. Stratigraphic units from Buesch et al. (1996). Data are from DTN: GS960908315215.014, GS970208315215.001 and GS970808315215.012.

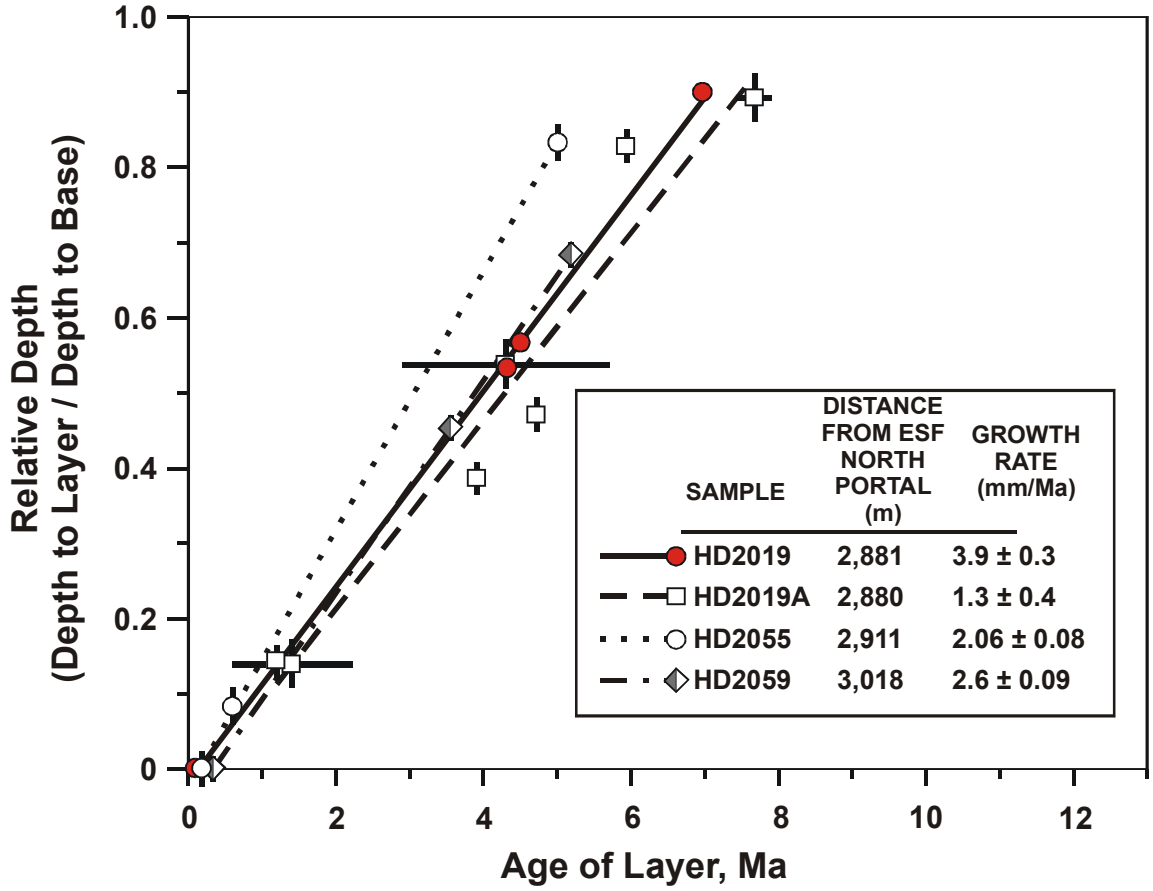

Figure 67. Growth rates of mineral coatings in the unsaturated zone

Note: Growth rates determined from uranium-series and uranium-lead ages from individual mineral coatings in the densely welded, crystal-poor, middle nonlithophysal zone of the Topopah Spring Tuff. Analytical data are from DTN: GS970208315215.002, GS970908315215.013 and MO0012WTRSAMPC.000. Ages were calculated from the measured $^{207}Pb/^{235}U$ ratios reported in the DTNs. See assumption 25 in Table 2.

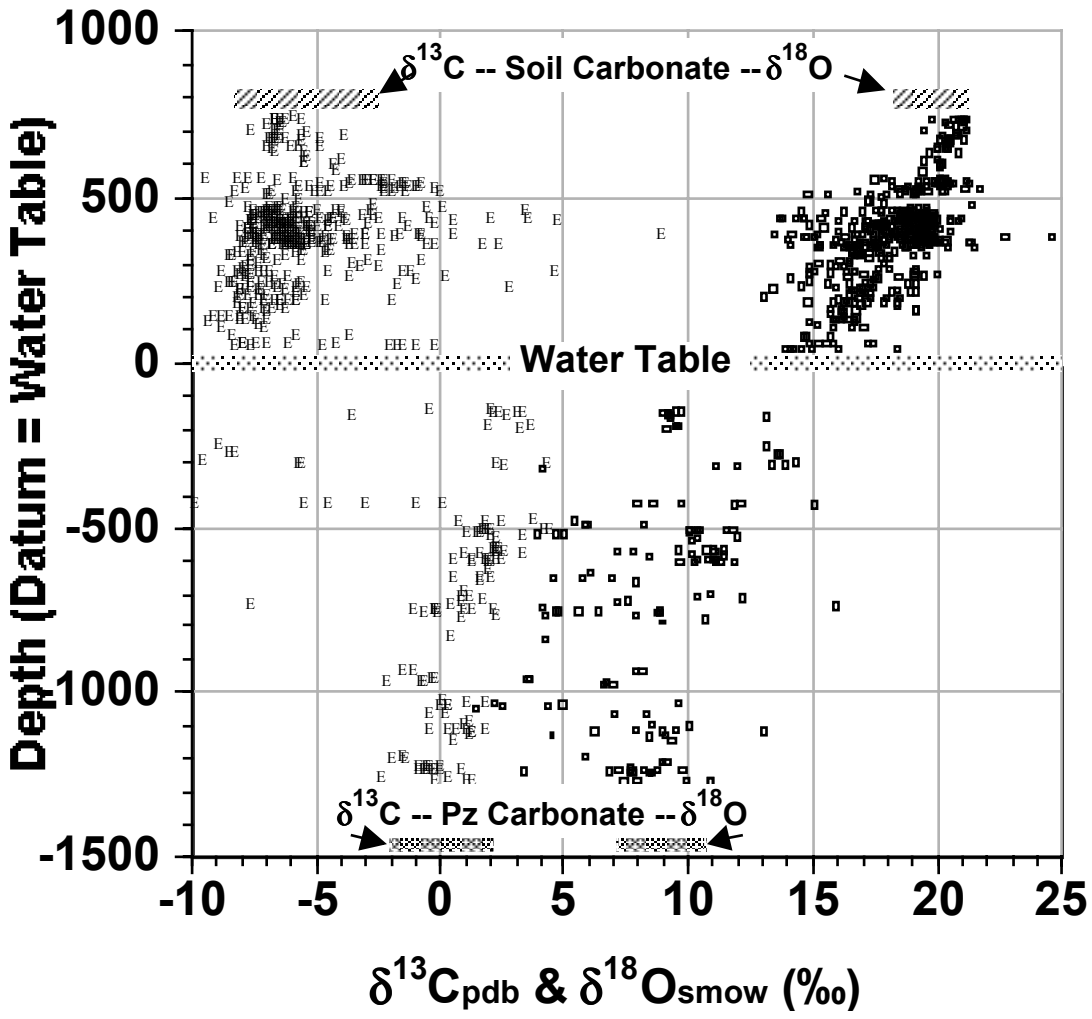

Figure 68. The $\delta^{13}C$ and $\delta^{18}0$ values of unsaturated-zone calcite from boreholes at Yucca Mountain.

Note: The $\delta^{13}C$ and $\delta^{18}0$ values of unsaturated-zone calcite sampled from boreholes at Yucca Mountain, plotted versus height above or below the water table. Ranges of $\delta^{13}C$ and $\delta^{18}0$ values encountered in the pedogenic carbonates of the overlying soils and the calcite that would precipitate from waters of the regional Paleozoic carbonate aquifer are also plotted. Data are from DTN: GS920708315215.017, GS931008315215.030, GS950708315215.005, GS950708315215.006, GS960408315215.002, GS970208315215.004, GS970808315215.010, and GS980408315215.010. Sample depths are part of the sample identifiers in these DTNs.

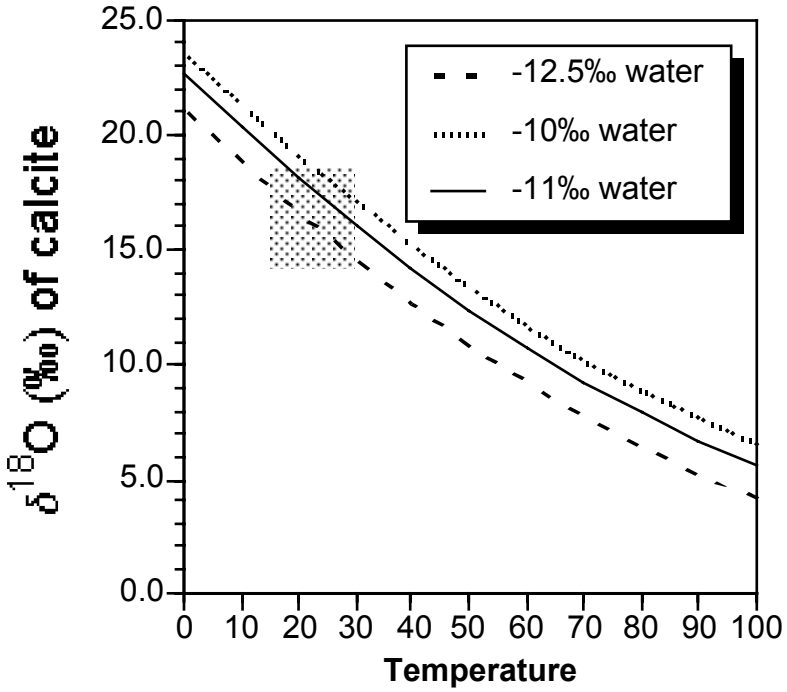

Figure 69. Temperature dependence of the $\delta^{18}0$ value of calcite

Note: Temperature dependence of the $\delta^{18}0$ value of calcite in equilibrium with waters having $\delta^{18}0$ values of – 12.5, -11.0, and –10.0‰ (based on information from O'Neil et al. 1969, p. 5552; Kim and O'Neil 1997, p. 3467). Shaded field is for typical late stage temperature of 15 to 30°C and $\delta^{18}0$ values of 15 to 19‰.

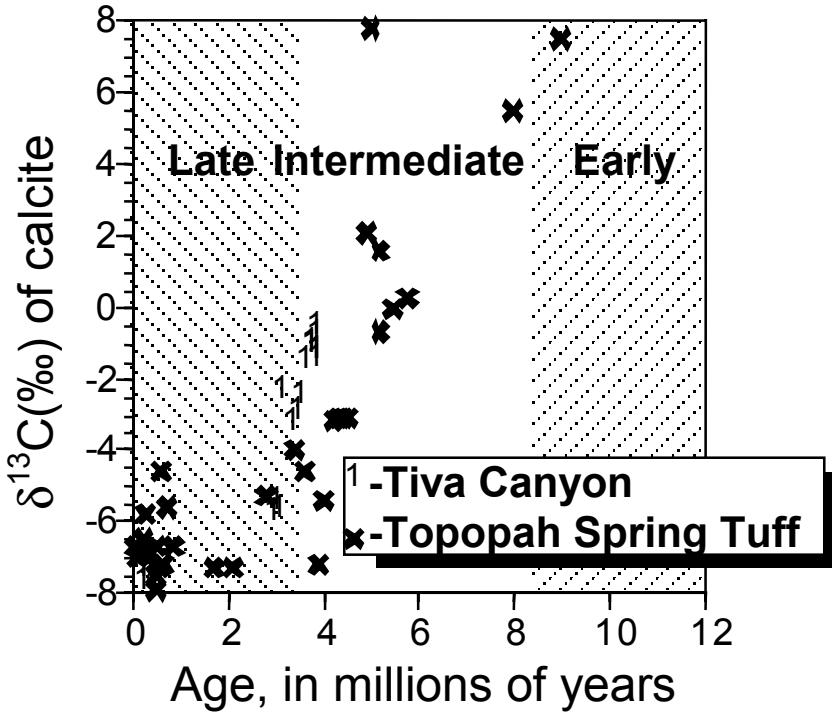

Figure 70. $\delta^{13}C$ value of calcite versus its age

Note: Plot of the $\delta^{13}C$ value of calcite versus age for those samples with U-Pb age control. Ages were calculated based on measured $^{207}Pb/^{235}U$ ratios, using equation 11 in section 6.10.1. See section 6.10 for a discussion of geochronology. Data are from DTN: GS960408315215.002, GS970208315215.004, GS970808315215.010, GS980908315215.016, GS970908315215.013, GS970208315215.002, GS980908315215.015, GS970808315215.012, GS970208315215.001, GS960908315215.014, and GS960208315215.001. See assumption 25 in Table 2.

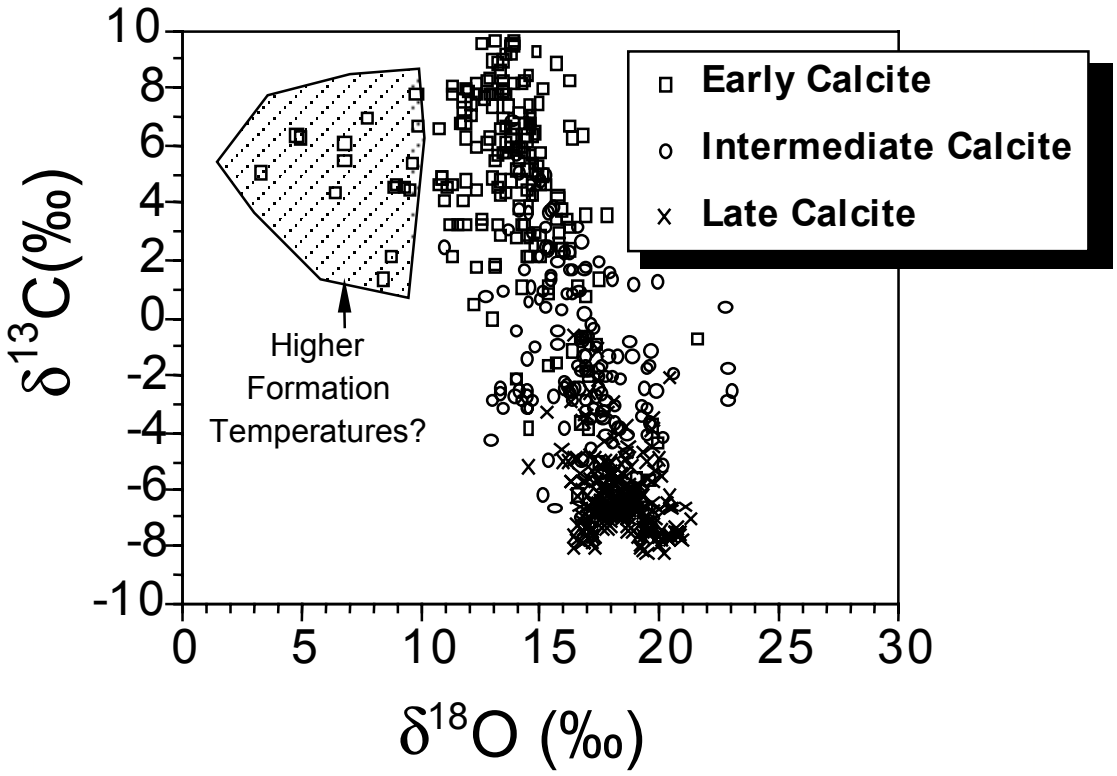

Figure 71. $\delta^{13}C$ versus $\delta^{18}O$ for the ESF calcite microsamples.

Note: Stages are distinguished by different symbols. In general, calcite $\delta^{13}C$ values decrease and $\delta^{18}O$ values increase with time. Microsamples of early stages calcite with anomalously low $\delta^{18}O$ values are shown in the shaded field. Data are from DTN: GS96098315215.010, GS970208315215.005, GS980908315213.002, and GS990908315213.001.

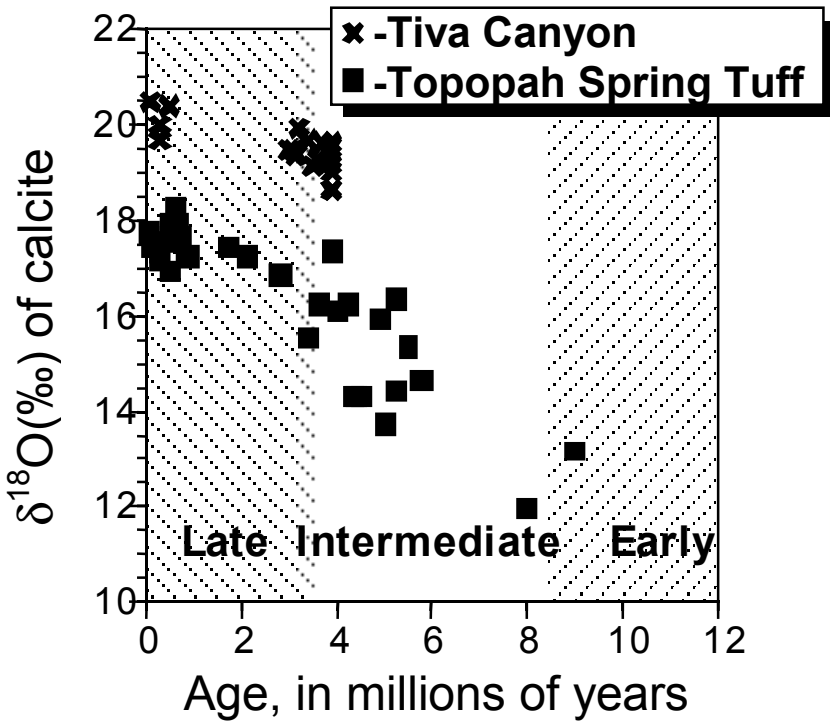

Figure 72. $\delta^{18}O$ value of calcite versus its age.

Note: Plot of the $\delta^{18}O$ value of calcite versus age for those samples with U-Pb age control. Ages were calculated based on measured $^{207}Pb/^{235}U$ ratios, using equation 11 in section 6.10.1. See section 6.10 for discussion of calcite geochronology. Data are from DTN: GS960408315215.002, GS970208315215.004, GS970808315215.010, GS980908315215.016, GS970908315215.013, GS970208315215.002, GS980908315215.015, GS970808315215.012, GS970208315215.001, GS960908315215.014, and GS960208315215.001. See assumption 25 in Table 2.

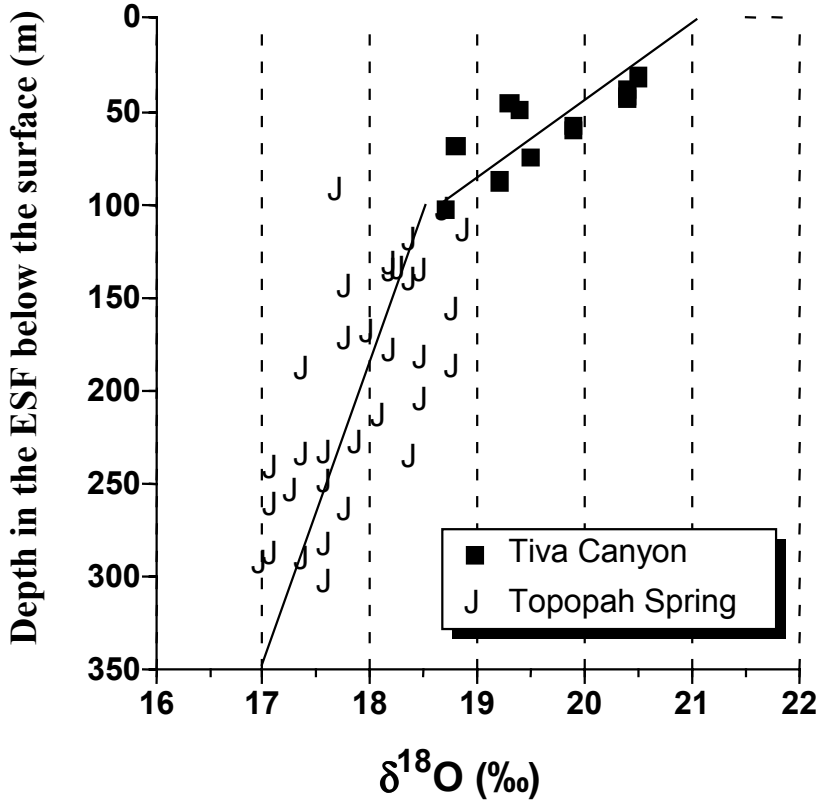

Figure 73. Late-stage calcite $\delta^{18}O$ values plotted by depth below the surface.

Note: Late-stage calcite $\delta^{18}O$ values from the ESF plotted by depth below the surface. Data are from DTN: GS960908315215.010, GS970208315215.005, GS98098315213.002, and GS990908315213.001.

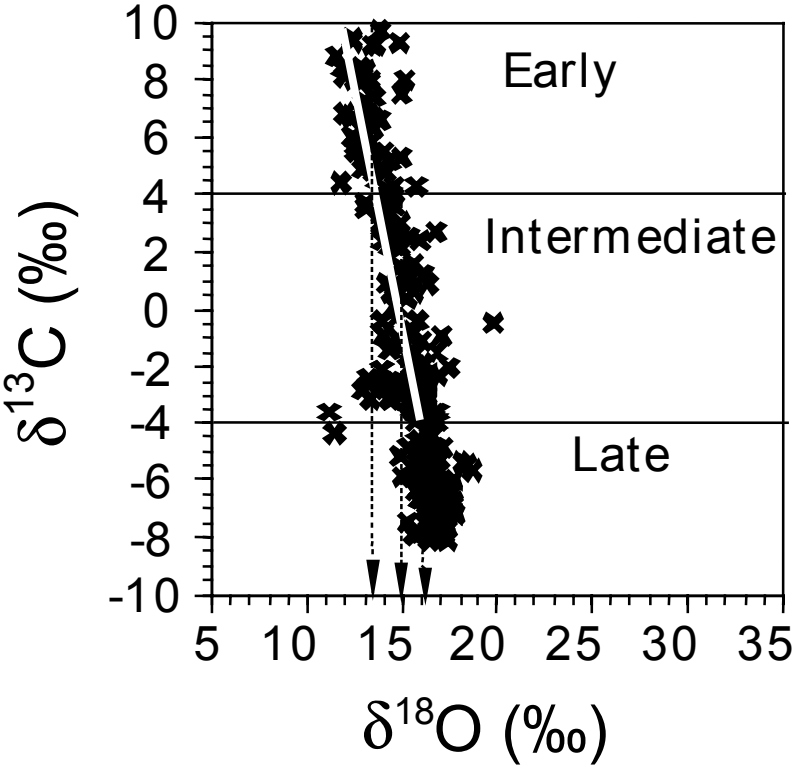

Figure 74. Plot of $\delta^{13}C$ versus $\delta^{18}O$ for calcite from the Tptpmn unit

Note: Plot of $\delta^{13}C$ versus $\delta^{18}O$ for calcite microsamples from the middle nonlithophysal unit (Tptpmn) of the Topopah Spring Tuff, as exposed in the ESF between Stations 2634 and 6018 (station distances in meters). Approximate trends of increasing $\delta^{18}O$ values from earliest to latest calcite are also shown (white line). Data are from DTN: GS960908315215.010, GS970208315215.005, GS980908315213.002, and GS990908315213.001

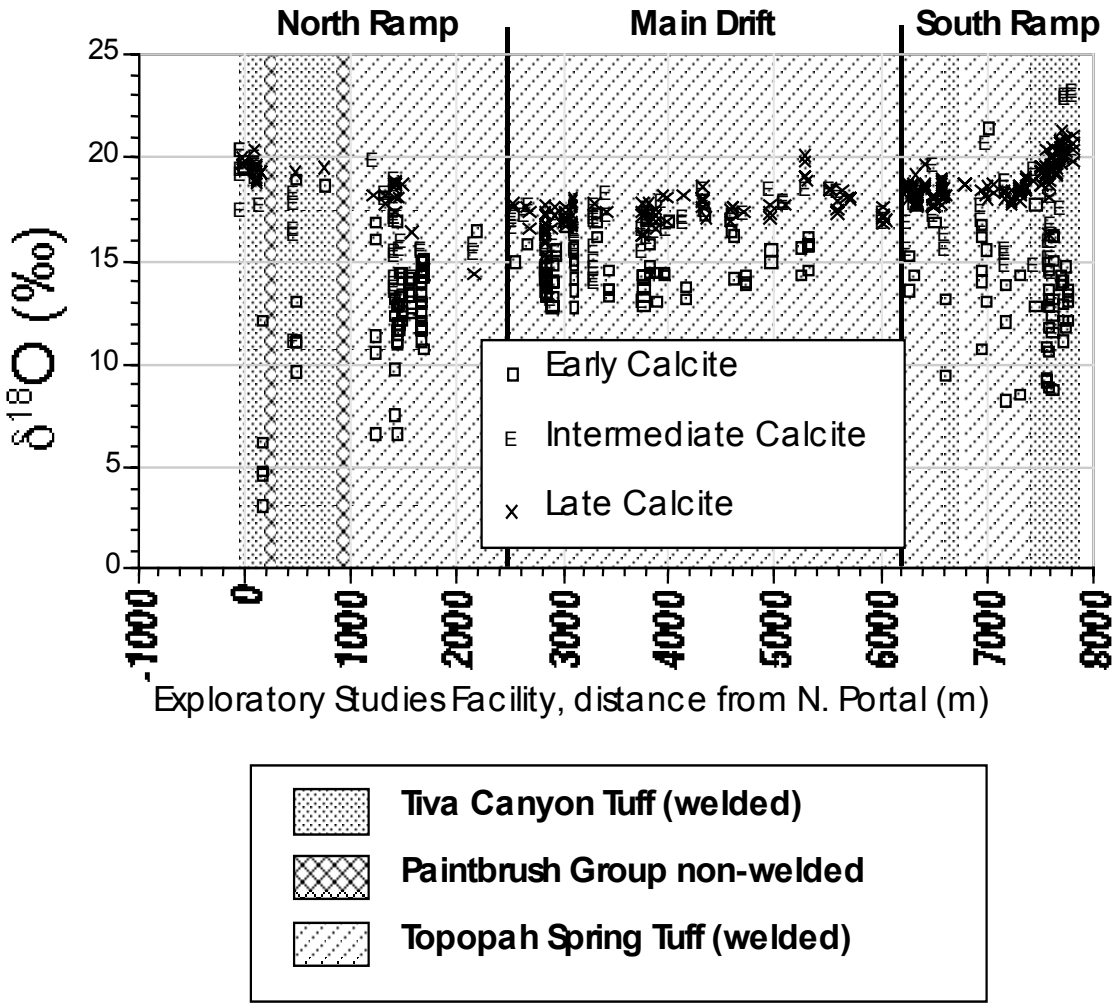

Figure 75. $\delta^{18}O$ values of calcite versus distance from the ESF North Portal

Notes: The $\delta^{18}O$ values of ESF calcite microsamples plotted against distance from the North Portal of the ESF. Stratigraphic contacts and bends in the tunnel are shown. Data are from DTN: GS960908315215.010, GS970208315215.002, GS980908315213.002, and GS990908315213.001